the ENERGY lab

NETL

Office of Fossil Energy
Hydrogen Turbine Program

2012 Portfolio

Turbines for Coal Based Systems that Capture Carbon

Siemens' advanced trailing edge design
Image copyright Siemens Energy 2012
Page 29

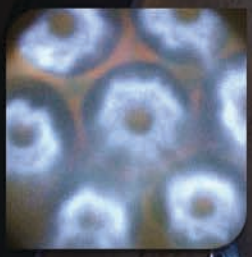

Hydrogen Turbines
GE's hydrogen turbine combustion system
Page 25

Advanced Research
Ames'/Purdue's perpendicular planes for the jet-impingement configuration
Page 41

University Turbine Systems Research
U. Texas' deposition image of an ideal trench configuration
Page 132

Small Business Innovative Research
UES' thermal barrier coating microstructure
Page 231

ENERGY

DOE/NETL-2012/1587

Office of Fossil Energy
Hydrogen Turbine Program

2012 Portfolio

Turbines for Coal Based Systems that Capture Carbon

October 2012

Table of Contents

I. INTRODUCTION

I. Introduction

On behalf of the U.S. Department of Energy (DOE) Office of Fossil Energy (FE), the Hydrogen Turbine Program is pleased to present the Fiscal Year (FY) 2012 Hydrogen Turbine Program Portfolio. This report summarizes current progress towards developing turbines that help to meet the goal of power production from coal that is clean, efficient, less costly, and minimizes carbon dioxide (CO_2) emissions.

Background and Technology Status

Turbines are a proven technology for power generation, which is typified by the sheer number of turbines in use today. Turbines find use in a variety of applications, ranging from turbines for propulsion in the aviation industry to steam turbines in pulverized coal combustion boilers. Turbine technology is responsible for the vast majority of power production in the U.S. and the world. Integration of a steam turbine and advanced gas turbine forms the combined cycle (CC) electric power generation module in the integrated gasification combined cycle (IGCC) power plant. For the past 25 years, increases in power generation capacity have been dominated by natural gas turbines in the CC configuration due to excellent performance in terms of cost, efficiency, emissions, and power density. This trend has become more apparent as the cost of natural gas has declined.

DOE is committed to using coal in ways that are cleaner, more efficient, and that reduce CO_2 emissions. Advancing hydrogen turbine performance in the IGCC power plant offers the most significant near-term performance benefit for reducing emissions and cost while increasing efficiency. Hydrogen turbines in an IGCC application are one of the cleanest and lowest cost ways to capture carbon dioxide in a coal based power plant. The ultimate goal of the Hydrogen Turbine Program is to facilitate the development of advanced components and technology for turbines that provide tangible benefits to the public: lower cost of electricity, reduced emissions of criteria pollutants, and carbon capture options.

Scientific and engineering challenges are being met through cost-shared research and development (R&D) partnerships between industry, academia, and the government. The Hydrogen Turbine Program strives to meet these challenges through R&D on hydrogen combustion, aerodynamics, heat transfer and cooling, leakage control, and material systems development. Examples of technical approaches being undertaken within the Hydrogen Turbine Program to address these challenges include the following:

- **Combustor Design**—Design and develop the combustion portion of the turbine to leverage the best current and advanced technologies to meet strategic system-level goals of an advanced syngas- or hydrogen-fueled gas turbine. Efforts are focused on the measurement and assessment of the fundamental properties of hydrogen combustion and the use of these properties to design and develop low-NOx combustion systems. Several combustion technologies are under evaluation, including, but not limited to, high- and low-swirl pre-mixed, diffusion, hybrid forms of premixed and diffusion, axial staging, and rich-lean catalytic.
- **Thermal Barrier Coatings (TBCs)**—Assess and develop TBCs that can provide the performance and durability required for use in syngas- and hydrogen-fueled advanced gas turbines. Efforts are focused on identifying candidate TBC architectures and material compositions with the proper thermal, mechanical, and chemical properties for use in reducing heat flux to combustor transition pieces, stationary nozzles, and rotating airfoils. Advanced TBC and bond coat architectures are being developed to improve durability and thermal performance in the harsh environment found in the IGCC gas turbine.
- **Aero-Thermo-Mechanical Design**—Assess the unique aero-thermo-mechanical operational conditions associated with hydrogen turbines and investigate design improvements for addressing these unique design spaces. Efforts are focused on reducing cooling flows, reducing sealing and leakage flow rates, reducing rotating blade count, increasing expansion stage areas and increasing airfoil length. The goal of these efforts is to develop machines that are more efficient with a higher power output.

Resolving the scientific and engineering design challenges using the approaches outlined above will allow hydrogen-fueled turbines to be used in IGCC power systems with carbon capture, utilization, and storage (CCUS).

Office of Fossil Energy and Hydrogen Turbine Program Goals

DOE FE manages a portfolio of research programs directed to demonstrate advanced coal-based electric power generation with near-zero emissions. The figure below shows programs managed by FE's Office of Clean Coal under the Clean Coal Research Program and where the Hydrogen Turbines R&D is situated in the portfolio. These programs are designed to provide low-cost technological solutions to high-level Presidential initiatives.

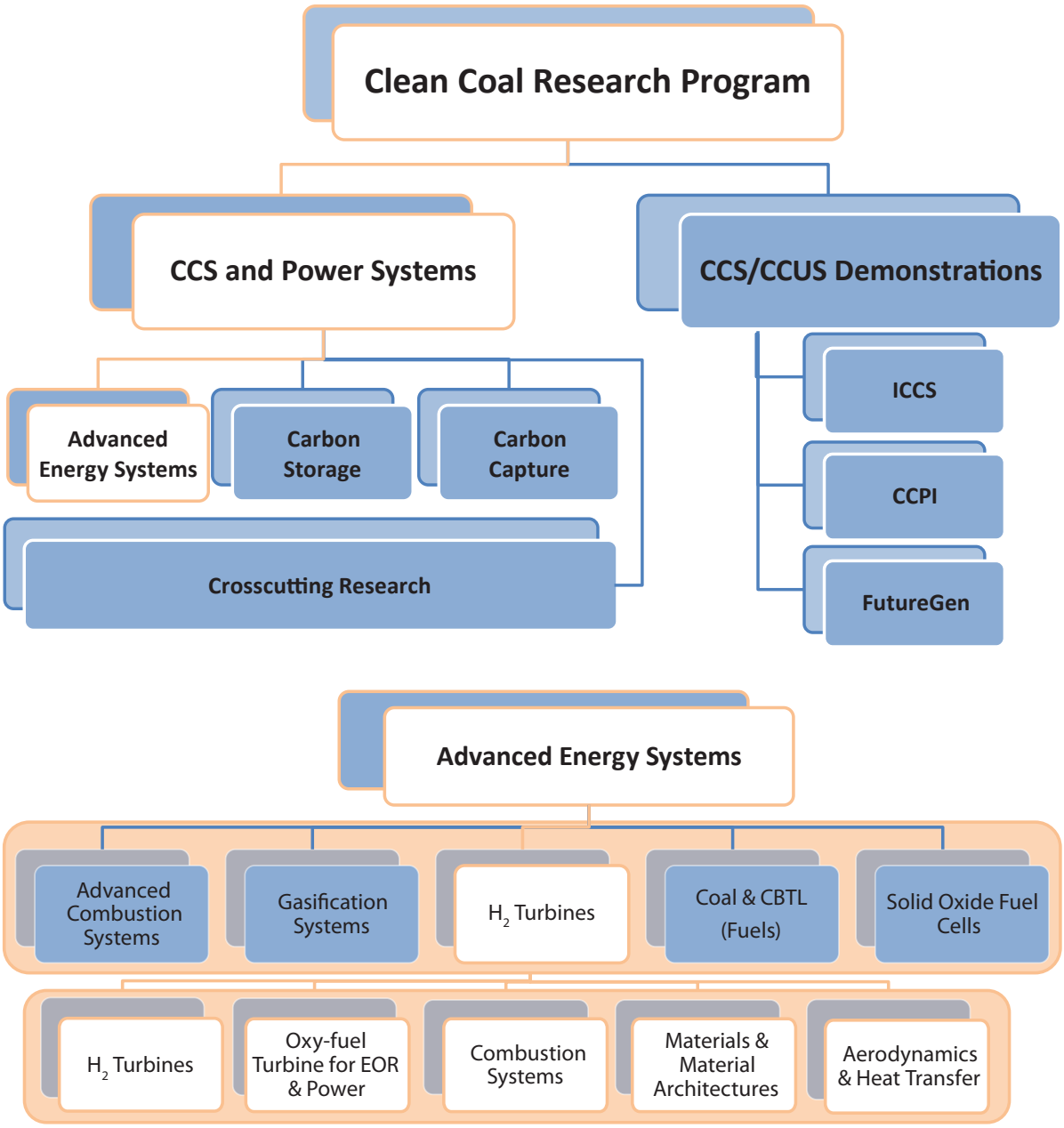

CCS = carbon capture and storage
ICCS = industrial carbon capture and storage
CCPI = Clean Coal Power Initiative

One of these Presidential initiatives establishes a greenhouse gas reduction target of >80% from 1990 levels by 2050. In response to this target and other drivers, the FE program is focused on:

- Research, development, and demonstration to enable CCUS deployment in the post-2020 timeframe.
- Sufficient demonstrations of first generation CCUS and power plant technologies to provide confidence that these technologies can be safely and reliably integrated into power plant and industrial plant operations.
- Development and demonstration of new, advanced second generation CCUS and power plant technologies for deployment in the post-2020 timeframe.

To realize this initiative and provide program area priorities, the following best practice performance targets have been established:

- <10% increase in cost of electricity (COE) with CCUS at 90% capture (pre-combustion for IGCC).
- <35% increase in COE with CCUS at 90% capture (post- and oxy-combustion for pulverized coal power plants).
- <$700/kW fuel cell power blocks (2007$).
- 50% plant efficiency, up to 60% with fuel cells.
- 90% CO_2 capture.
- 99% CO_2 storage permanence.
- +/-30% storage capacity accuracy.

In response to these targets, the Hydrogen Turbine Program has laid out goals to deliver hydrogen-fueled CC power modules for the 2020 time horizon that demonstrate the following achievements:

- Efficiency
  - 2–3 percentage points improvement in CC efficiency (2010) and 3–5 percentage points by 2015 above the baseline.
  - 4 percentage points improvement in overall IGCC plant efficiency with CCUS by 2015.
- Cost Reduction
  - 20–30% reduction in CC capital costs.
  - 25% reduction (>$943/kW) in total overnight capital cost for IGCC with CCUS.
  - 25% reduction (>$88/MWh) in COE for IGCC with CCUS.
- Emissions
  - Turbine NOx emissions in single digits (@15% O_2).
  - IGCC plant optimized for firing temperature with 2 ppm NOx at the stack (includes selective catalytic reduction).

Hydrogen Turbine Program's Objectives

The Hydrogen Turbine Program is organized into three key areas: hydrogen-fueled turbines for IGCC applications with CCUS, advanced research, and the University Turbine Systems Research (UTSR) Program. The program is augmented by a portfolio of Small Business Innovation Research (SBIR) projects, American Recovery and Reinvestment Act (ARRA) funding for advancing industrial application of CCUS, and the National Energy Technology Laboratory (NETL) Regional University Alliance (RUA) collaboration that utilizes the extensive expertise and facilities available at NETL and five nationally recognized regional universities. The following map illustrates Hydrogen Turbine Program project distribution across the U.S., and a listing of the projects by state is given in the table included at the end of this introduction.

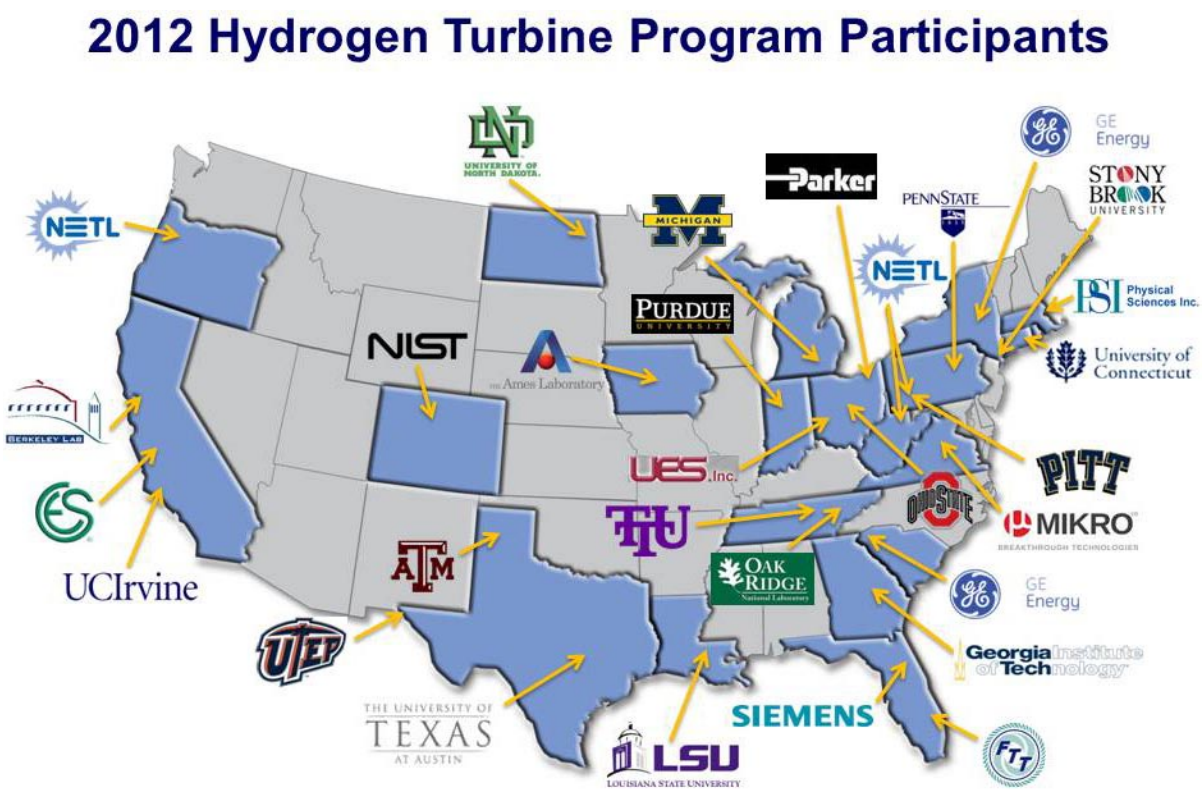

The Hydrogen Turbine Program has contributed to the performance targets and best practices outlined above by meeting and pursuing the following objectives:

- Demonstration of a hydrogen-fueled combined cycle gas turbine (previously fueled with syngas) that maintains the same CC efficiency performance improvement realized in 2010 (2–3 percentage points above the baseline[1]), realizes 3-5 percentage points improvement by 2015, and realizes 4 percentage points improvement in overall IGCC plant efficiency with CCUS.
- Cost reduction of 20–30% (below the baseline) in CC capital cost, plus enhanced value for lower cost of electricity through reduction of total capital costs and total cost of electricity generation.
- Emissions reduction to 2 ppm NOx from the power plant exhaust and single-digit NOx emissions in the simple cycle exhaust (at 15% O_2).

System studies indicate that the 2012 objectives described above have been met through the R&D sponsored by the program to date. The continued achievement of the objectives will be demonstrated by incorporating the latest technological advances in a gas turbine power plant. It is envisioned that this turbine could be installed with a pre-planned technology improvement philosophy. This approach would allow the machine to be optimized in the field for hydrogen combustion, aerodynamics, heat transfer and cooling, leakage control, and other performance-enhancing components or subsystems. This approach would also allow for a machine fueled with 100% hydrogen to operate with the highest efficiency and lowest NOx emissions.

[1] Baseline efficiency is defined in "Development of Baseline Performance Values for Turbines in Existing IGCC Applications," Richard A. Dennis, Walter W. Shelton, and Patrick Le, Proceedings of GT2007, May, 2007.

The Hydrogen Turbine Program is now focused on further advancements to turbine technology to attain the ultimate performance targets for IGCC power plants with CCUS. Thus, by 2015, the program plans to demonstrate:

- Hydrogen-fueled turbines with 3 to 5 percentage points improvement in CC efficiency (total above baseline).
- At least 4 percentage points improvement to the overall IGCC plant performance with CCUS.
- Competitive cost of electricity for near-zero emission systems.
- Hydrogen-fueled IGCC with 2 ppm NOx at the power plant exhaust.

The following chart lists Hydrogen Turbine Program projects by focus area.

2012 Hydrogen Turbine Program Portfolio

36 Projects

(excluding NETL Site Support)

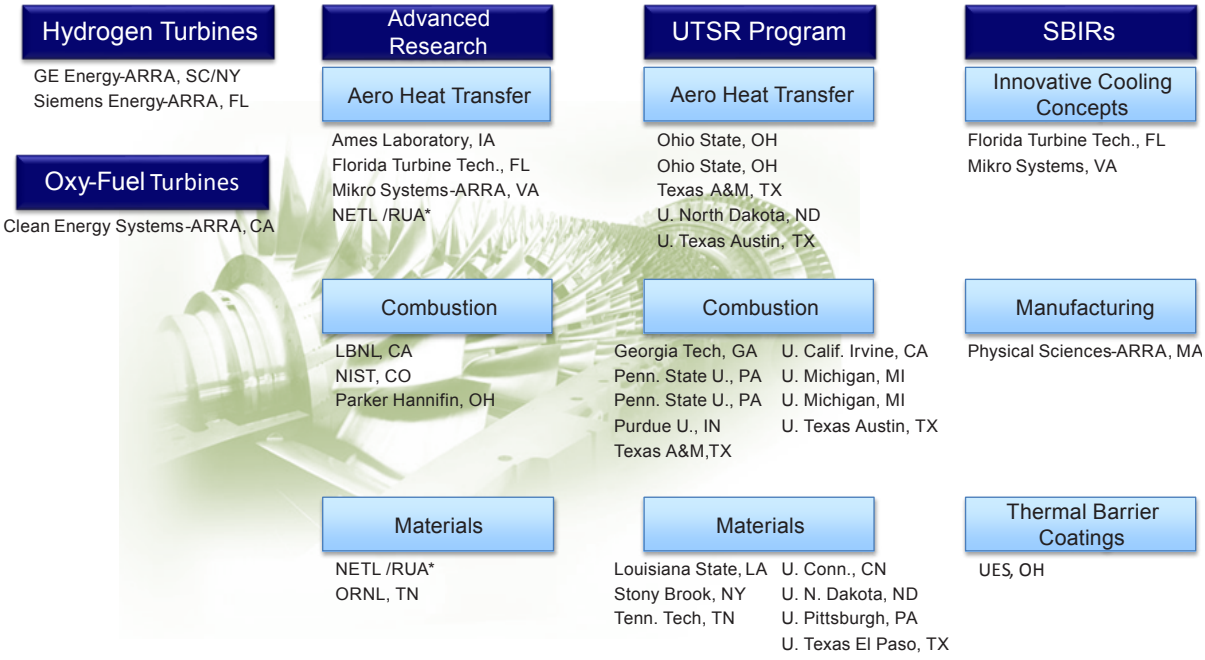

*= single project with multiple activities; ARRA = American Recovery and Reinvestment Act; UTSR = University Turbine Systems Research; SBIR = Small Business Innovative Research; LBNL = Lawrence Berkeley National Laboratory; NIST = National Institute of Standards and Technology; ORNL = Oak Ridge National Laboratory

2012 Annual Accomplishments

System Studies Confirm That Goals Can Be Achieved. At the inception of the Hydrogen Turbine Program, system studies were used to baseline turbine and IGCC performance. Power plants with hydrogen turbines have since been modeled by hydrogen turbine developers General Electric and Siemens Energy, holding the balance of plant (BOP) constant between the baseline plant and the advanced plant unless there was an obvious change required to make the BOP compatible with the hydrogen turbine. The results of these studies have been substantiated with system studies conducted by NETL, and they show that the Program's efficiency and cost goals are attainable, assuming that the R&D pathways (combustion, materials, aerodynamics, heat transfer, and systems) being pursued by the Program are successfully

implemented. The project highlights below and 2012 accomplishments outlined in the body of this report present the key results accomplished along these R&D pathways.

Advanced Energy Systems Peer Review Demonstrates Strength and Success. Seven hydrogen turbine projects were evaluated during the FY 2012 Advanced Energy Systems Peer Review on April 23–24, 2012, in Morgantown, West Virginia. The peer review team of eight reviewers from industry and academia, assembled and led by ASME (American Society of Mechanical Engineers), evaluated the projects across nine criteria grouped into three major categories: (1) Project Overview (a) scientific and technical merit, (b) existence of clear, measurable milestones, and (c) utilization of government resources; (2) Technical Discussion (a) technical approach, (b) rate of progress, (c) potential technology risks considered, and (d) performance and economic factors; and (3) Technology Benefits (a) anticipated benefits if successful and (b) technology development pathways. Reviewers were expected to provide a rating and substantive comments which support that rating for each criteria including strengths, weaknesses, recommendations, and action items.

These formal peer reviews are rigorous, documented evaluations by qualified independent reviewers using objective criteria to make judgments on a project's technical/scientific/business merit, actual or anticipated results, and productivity and management effectiveness of the project. In addition to the numerical scoring described above, reviewers are asked to provide comments on each project in four areas: (1) strengths, identified relative to the evaluation criteria; (2) weaknesses, project items or issues which might hinder a project's success, relative to the evaluation criteria; (3) recommendations, actions or direction that could add value to a particular project related task and/or help achieve a program goal; and (4) action items, deficiencies identified by the Peer Review Panel and proposed mitigations to preclude the project from missing its stated project objectives or program goals. The comments from this year's Peer Review Panel indicate strong pursuit of relevant R&D to ensure that ambitious goals are achievable in the Hydrogen Turbine Program.

SBIR Projects Awarded. In FY 2012, four new Phase I projects were selected under SBIR solicitations:

- *HiFunda* (Salt Lake City, UT) will develop ultra-high temperature TBCs.
- *Powdermet* (Euclid, OH) will develop a multilayered yttria stabilized zirconia coating for improved thermal abrasion resistance.
- *Florida Turbine Technologies* (Jupiter, FL) will develop an innovative design approach to provide a highly durable "contactless" air riding rotating-to-static seal.
- *Mikro Systems* (Charlottesville, VA) will develop ceramic filters that will optimize filtration performance while enabling directional flow of molten alloy during the single crystal casting process.

The NETL-RUA Advances Technology Development Critical to Manufacturer Efforts for Achieving DOE FE's Hydrogen Turbine Program Goals. The NETL-RUA Turbine Thermal Management projects are being conducted to develop advanced technology designs, components and equipment that contribute to achieving the Hydrogen Turbine Program goal of 3–5% plant efficiency gain by permitting higher turbine firing temperatures as a result of realizing more effective cooling, development and utilization of extreme temperature thermal barrier coating protection systems, and secondary flow leakage reduction.

FY 2012 focused on development and performance assessment of novel internal airfoil cooling channels, trailing edge cooling architectures, film cooling hole configurations, and design and construction of a secondary flow rotating rig to assess advanced cooling improvement strategies for the turbine blade platform.

2012 UTSR Workshop to Be Held at University of California, Irvine. The UTSR program will hold its annual workshop October 2–4, 2012, at University of California, Irvine (UCI) in Irvine, California. The workshop, co-organized by NETL and UCI, is open to the public and will bring together experts from academia, industry and government to present and discuss ongoing turbine research in the areas of

combustion, materials, and aerodynamics/heat transfer, with a focus on advanced syngas and hydrogen turbine systems. The agenda will include invited talks, technical presentations, panel discussions, poster presentations, and laboratory tours. Principal Investigators of DOE-funded projects will present their latest results. The findings and recommendations will be used by DOE to guide future work and to make programmatic and funding decisions for the upcoming fiscal years. The 2012 workshop proceedings will be posted on the NETL website.

Project Highlights

Hydrogen Turbines

GE Energy Continues to Demonstrate Low NOx Emissions with Robustness on Hydrogen Fuel in Its Advanced Combustor. In FY 2012, a prime path for manufacturing the advanced high-hydrogen premixing fuel nozzles was identified, and work was started to mature the fabrication to a production-ready state. A set of "pre-production" fuel nozzles using the down-selected manufacturing method and including many of the previously-mentioned improvements was built and tested. In addition to exhibiting high operability on hydrogen fuel, the new fuel nozzles delivered a further reduction in NOx emissions. Improvements made to the high-hydrogen combustion system in the areas of aerodynamic, thermal, and mechanical design were targeted at further reduction in emissions, robust operability, better part life, and reduced costs. The system continued to be tested in the full chamber combustion test rig in GE Energy's state-of-the-art Gas Turbine Technology Lab in Greenville, South Carolina. The system has now been operated for more than 100 hours in the lab at full gas turbine conditions (in excess of F-class) on H_2 fuels. Additionally, a set of fuel nozzles survived, without damage, an aggressive thermal cycle test, where accelerated startup-shutdown cycles were simulated. During the rest of Phase II of the project, the main focus will be on (1) expanding demonstrated performance to the U.S. DOE 2015 conditions, (2) further reducing NOx emissions, and (3) further addressing requirements such as reliability, manufacturability, and durability.

Prototype Parts Manufactured Using Novel Manufacturing Techniques by Siemens Energy are Moving into Full Scale Engine Testing. Novel manufacturing techniques have matured, and prototype parts are being produced utilizing such techniques. These parts are being tested in a full scale engine at the Siemens Berlin Test Facility. Modular vanes, produced using new manufacturing techniques, are undergoing a two phase test which will be complete this year. Never before possible advanced cooling designs have been successfully manufactured into Row 1 blades and undergone full scale engine testing. Local metal temperature reductions were predicted relative to current production parts.

Oxy-Fuel Turbines

Manufacture of the World's First Industrial-Scale Oxy-Fuel Turbine Completed. Under subcontract to Clean Energy Systems, Inc. (CES), the gas turbine experts from Siemens TurboCare completed the manufacture of the world's first industrial-scale oxy-fuel turbine (OFT) capable of powering approximately 150,000 homes while generating nearly zero emissions. Utilizing the detailed designs created by Florida Turbine Technologies, Inc., TurboCare manufactured and installed six new major engine components necessary to convert an existing industrial gas turbine (SGT-900) into a high-temperature intermediate pressure turbine for use in commercial oxy-fuel (O-F) applications. This approach accelerates commercial OFT deployment at significantly reduced costs. Next year the modified engine will be installed and tested at CES' Kimberlina O-F demonstration facility, located in Bakersfield, California.

Advanced Research: Aero-Heat Transfer

Ames National Laboratory Identifies and Quantifies Errors in Transient Measurements of the Heat-Transfer Coefficient. U.S. Department of Energy and Purdue University identified and quantified errors in the widely used transient technique based on thermochromic liquid-crystal (TLC) to measure the

heat-transfer coefficient. With the TLC technique, surface temperature is measured experimentally as a function of time, and the heat-transfer coefficient is inferred from either the exact solution for the unsteady one dimensional (1D) conduction in a semi-infinite solid or the exact solution for unsteady, effectively zero dimensional (0D) conduction in a solid immersed in a fluid, where the 0D assumption is valid if the Biot number (Bi) for the immersed solid is less than 0.1. For a cooling channel with a staggered array of pin fins for heat-transfer enhancement, the TLC transient technique that used the 1D exact solution was found to give reasonably accurate transient heat-transfer coefficients (<2% relative error) for the walls of the cooling channel, which were made of plexiglass. However, the 0D exact solution was found to produce considerable errors (up to 200% relative error) for the heat-transfer coefficient about the pin fins, which were made of aluminum with Bi much less than 0.1 because the heat-transfer coefficient varies appreciably as a function of position along the pin fin. This study also showed that the heat-transfer coefficient measured by the TLC transient technique differs considerably from the heat-transfer coefficient obtained under steady-state conditions with isothermal walls (up to 20-30% relative error) because the heat-transfer coefficient is a strong function of surface temperature.

Enabling Spar-Shell Cooling Technology to be Demonstrated in a Commercial Gas Turbine. In this Hydrogen Turbine Program-funded Phase III project, Florida Turbine Technologies, Inc., (FTT) engineers are developing and will test, at a pre-commercial prototype scale, spar-shell gas turbine airfoils in a commercial gas turbine engine. The airfoil development is based upon FTT's research and development to date in Phases I and II of Small Business Innovative Research grants. In this project, FTT, in partnership with Siemens Energy, will further the commercialization of this new technology in F-frame and other highly cooled turbine airfoil applications. The market for the spar-shell vane for these machines is extensive. According to Forecast International, 3,211 new gas turbine units (in the >50 MW capacity size range) expect to be ordered in the 10 years from 2007 to 2016. This program will lead to the creation of hundreds of engineering and manufacturing jobs and put the nation at the forefront of a technology that will improve energy efficiencies world-wide.

Mikro Systems Licenses TOMO^{SM} Core Fabrication Technology to Siemens Energy. The low rate initial production facility (LRIP) is complete and fully operational. Employees are trained, process control documentation is in place, and Mikro is producing cores for investment casting daily in the facility. Mikro has achieved the target overall process yield of 50% and is continuing to refine the process and end product. Mikro Systems and Siemens Energy, Inc., (SEI), Orlando, Florida, signed a new collaborative technology license agreement to advance state-of-the-art gas turbine performance. SEI and Mikro Systems are working together to validate and certify Mikro Systems' Tomo-Lithographic Molding (TOMO^{SM}) manufacturing technology for use in commercial production of stationary and moving turbine components. This will include production trials and application-specific component testing. SEI has established a field office near Mikro Systems' Virginia facilities to support Mikro Systems' commercialization efforts and add domestic jobs. The technology will enable more sophisticated airfoil designs with improved cooling characteristics, leading to higher operating temperatures and improved efficiency. In addition to enabling designs that were previously impossible to manufacture, the technology will reduce time-to-market for future design enhancements through reduced tooling costs, reduced production lead times and more efficient manufacturing processes. Mikro Systems has worked closely with SEI over the past year to refine and ready TOMO^{SM} core fabrication technology for full commercial production.

NETL-RUA and Virginia Tech Explores Airfoil Film Cooling with Tripod Hole Pattern. Virginia Polytechnic Institute and State University demonstrated tripod hole film cooling geometry benefits on pressure and suction sides of a typical nozzle guide vane under low speed conditions in a linear cascade wind tunnel, including lower coolant usage and less dependence on the blowing ratio for both the pressure and suction sides, as well as improved film cooling effectiveness for the suction side. Aerodynamic benefits were also demonstrated for the tripod hole film cooling geometry: minimal disruption to the downstream flow pattern at all blowing ratios. The effects of pressure gradients, component curvature, and free-stream turbulence on film cooling hole performance were evaluated and shown to have a more robust performance under a variety of flow conditions. A thermo-mechanical stress analysis of cylindrical and

tripod hole designs showed similar stress magnitude for both cases, indicating that thermal stresses will not limit tripod design. Mikro Systems, Inc., indicated that it can easily produce the new hole geometries and that its manufacturing process creates fewer sharp corners that would result in stress risers/concentrations that typically lead to crack initiation

NETL-RUA and University of Pittsburgh Enhance Internal Airfoil Cooling with NSEMC Pin-Fin Arrays. Internal cooling bench-scale testing was completed at the University of Pittsburgh using triangular, semi-circular, and circular pin-fin arrays as internal turbulators for enhanced internal turbine airfoil heat transfer. Research indicated that the triangular pin-fin array has higher heat transfer than semi-circular and circular pin-fin arrays. Bench-scale, near surface embedded micro-channel (NSEMC) models were designed, constructed, and tested with air cooling jets of comparable diameter. Preliminary testing identifies high heat transfer at the jet impingement zone with decreases in the radial direction. Preliminary fully-bridged pin-fin arrays and NSEMC architectures were designed and evaluated in terms of manufacturing at Mikro Systems, Inc., for production of test coupons that will be subjected to high temperature, pressurized, internal cooling heat transfer.

NETL-RUA and Penn State Develop Secondary Flow Rotating Rig. A secondary flow rotating test facility has been designed at Pennsylvania State University to test representative turbine engine hardware in a continuous, steady-state, high pressure environment. The test rig was designed with an operating envelope well above the capabilities of most continuous duration, rotating turbine test facilities in the U.S. and Europe and will be able to simulate internal air system flow leakages and cavity flow conditions within a turbine. Building renovations have been completed, and large equipment for the facility has been procured with the exception of an active magnetic bearing system, a dynamometer water brake system and torque meter, and a telemetry system.

NETL-RUA and University of Pittsburgh Model Two-Fold Increase in Airfoil Trailing Edge Cooling. ANSYS computational fluid dynamics modeling and experimental testing for trailing edge cooling was initiated at the University of Pittsburgh to identify enhanced heat transfer, zig-zag channel, trailing edge configurations. Designs consisting of 110° turning angle zig-zag passages numerically exhibited the highest heat transfer, *h*, in comparison to 70° and 90° turning angle zig-zag passages. Along the airfoil's trailing edge, rib-turbulators were added to the zig-zag passage. This modification is expected to produce a two-fold increase in heat transfer as well as an increase in pressure.

Advanced Research: Combustion

Design Flexibility Demonstrated for Low-swirl Injector at LBNL. The low-swirl injector (LSI) is a simple advanced combustion concept from the Lawrence Berkeley National Laboratory that is being developed for the combustion turbines in an integrated gasification combined cycle (IGCC) clean coal power plant. For these combustion turbines, fuel-flexibility, i.e. switching from natural gas fuel to high-hydrogen fuel without changing combustor hardware, is a critical requirement. In Fiscal Year 2011, a successful demonstration of a fully functional LSI showed this technology to be a cost-effective option for the IGCC combustion turbines to meet the aggressive operational and emissions goals. To facilitate the adaptation of LSI to gas turbine combustors whose configuration and flow requirements can be quite different, a parametric study of the effect of changing LSI geometry on its operability was carried out. Ten LSI swirlers of different vane sizes, vane shapes, and vane angles were fabricated and evaluated in laboratory experiments. Their performances in terms of flame blow-off and emissions were found to be insensitive to changes in the geometric parameters. Moreover, reduced aerodynamic drag was found for swirlers with larger swirl annulus. The drag reduction is sufficiently significant that it can be exploited to increase gas turbine system efficiency. This investigation shows that the LSI offers a wide and flexible design space for adaptation to IGCC combustion turbines.

New Measurements Underway to Improve Knowledge of CO_2 Properties. At the National Institute of Standards and Technology (NIST), new state-of-the-art measurements have been performed of the thermal conductivity of carbon dioxide in gas, liquid, and supercritical states. These measurements,

and correlation work to follow, will provide data to improve the design and optimization of systems for sequestration and for power generation using supercritical CO_2. Separately, an apparatus, utilizing a one-of-a-kind gravimetric hygrometer designed for humidity standards, has been assembled to measure the water content of saturated CO_2 at temperatures from approximately 10°C to 85°C at pressures up to 7 MPa. This will enhance knowledge of the phase behavior of the CO_2-H_2O system, better defining the requirements for drying captured CO_2 for compression and transportation.

Advanced Research: Materials

More Durable High Temperature Coatings Being Developed at ORNL for Coal-Derived Synthesis Gas/Hydrogen-Fired Turbines. Laboratory evaluations of various types of thermal barrier coating (TBC) specimens in different water vapor levels are being conducted at Oak Ridge National Laboratory. Coatings were furnace cycled in air with water vapor levels from 10-90 vol% at 1,150°C for diffusion bond-coatings and 1,100°C for spray-deposited MCrAlY-type bond coatings. In both cases, increasing the water vapor content did not decrease the coating lifetime. However, the lifetimes in 10% water vapor were 30-50% lower than similar experiments conducted without water vapor. Therefore, water vapor has a significant negative effect on coating lifetime, however, higher water vapor contents due to the combustion of high H_2 fuels does not likely explain a decrease in TBC lifetime in these turbines. Coating performance was increased with the addition of Y and Hf to the sprayed bond coatings. Model NiCrAl alloys are being used to study the effects of other minor alloying additions, and new compositions have shown increased spallation resistance in the presence of water vapor. High-resolution analytical electron microscopy is being used to better understand the effect of water vapor on the thermally grown oxide microstructure.

University Turbine Systems Research: Aero-Heat Transfer

New Deposition Model Validated at OSU for Predicting Turbine Deposition Including Endwall Accumulation. This combined experimental/computational research effort was initiated in October 2008 to explore the possibility of modifying turbine endwall geometries to both increase their aerodynamic performance and reduce the potential for degradation due to deposition. The experimental work is divided between two reacting flow turbine test facilities, one at Brigham Young University (BYU) and the other at Ohio State University (OSU). The facility at BYU was modified for high temperature deposition experiments, up to 1,400°C gas temperature with film cooling capability. A series of tests were conducted to explore the effect of gas temperature on deposit growth for particle concentrations and different surface temperatures. Results show conclusively that deposit growth rate is much more dependent on surface temperature than gas temperature. Higher particulate loading also accelerates deposition. The OSU facility provides the capability to test actual turbine vane flowpaths at operating temperatures with film cooling. The final fabrication and assembly of this facility was completed in June 2009. Deposition testing has been ongoing since that time using actual nozzle guide vane sectors from GE. Deposition sensitivity to gas temperature, particle sizes, and ash type have all been explored in detail. Four different coal ash types were tested at a gas temperature of 1,100°C, and it was determined that deposition rates follow the coal rank with more deposition from lignite and less deposition from bituminous. This trend is directly related to the sintering temperature of the ash. Also, an order of magnitude drop in mean particle Stokes number produced a 65% drop in ash deposition rates due to smaller particles that no longer impact the vane surface. Experimental data from both facilities has provided critical validation for computational models of deposition that have been developed under this same research effort. These models have been successfully implemented in a fully three dimensional vane geometry. Deposition dependency on gas temperature, particle size and composition have been modeled. The model was then used to redesign the turbine endwall in an effort to mitigate endwall deposition. While the model did predict realistic endwall deposition patterns relative to experimental data, the modifications tested thus far have shown little benefit in terms of deposition mitigation.

Hot Streak Deposition Simulation for Uncooled NGV Compares Favorably with Initial Experiments in OSU TuRFR. The critical viscosity deposition model was exercised in conjunction with a Fluent model of the GE E^3 nozzle geometry to introduce hot streaks into the inlet plane of the computational domain. The deposition model results show a strong correlation between the deposition peak and the hot streak for the different clocking position. The lag between hot streak position and deposition peak location is exacerbated with increasing particle size due to the ballistic nature of the larger particle trajectories. To verify that the predicted deposition patterns were realistic, dilution plates were installed in the Ohio State University Turbine Reacting Flow Rig (TuRFR) to permit the creation of non-uniform inlet temperature profiles. Both radial and "hot streak" profiles have been demonstrated. The hot-streak profile was tested with particulate to show the resulting deposition on a nozzle guide vane set. Both the prediction and the experiment indicate a deposition bias to the vanes in-line with the hot streak, as expected. Further testing will help to identify thresholds for deposition and optimal clocking locations. Diagnostics are also being developed to more accurately measure the spatial temperature distribution at the inlet to the TuRFR. This will assist in the model validation process by providing appropriate inlet conditions to the Fluent calculation. Finally, a validation test section has been designed that will provide measurements to calibrate the new elastoviscoplasticity deposition model.

Environmental Considerations and Cooling Strategies for Vane Leading Edges in a Syngas Environment Reviewed at OSU. Ohio State University has investigated the impact of leading edge diameter and turbulence levels on deposition rates in a simulated syngas environment. Initial testing validated the use of a faired cylinder to replace the nozzle guide vane for the study of leading edge heat transfer and deposition. Based on this, faired cylinders with a factor of two difference in leading edge diameter were installed in the TuRFR for deposition testing. Results indicate a reduction in leading edge deposition (per unit area) with increased diameter. This follows the expected trend with Stokes number, since the particles approaching the larger leading edge diameter cylinder have a lower Stokes value and are thus not as likely to impact the leading edge ballistically. Subsequent testing has demonstrated the ability to elevate the inlet flow turbulence level using dilution jets upstream of the inlet plane in the TuRFR. This capability will be used for subsequent investigations into the effect of turbulence level on deposition. University of North Dakota (UND) has documented the response of high intensity turbulence in the presence of large diameter stagnation regions. Unlike smaller stagnation regions where near surface fluid strain rates are intense, the strain off larger diameter leading edge regions is less rapid. The current results are showing that the most intense turbulence is less affected by these more mild strain rates meaning heat transfer augmentation levels are lower than expected. UND has also developed and tested two new innovative internal cooling schemes structured for use in cooling the leading edge region of vanes. Conventional high solidity arrays lose cooling potential as cooling air heats up. These new internal cooling arrays incrementally add cooling air through impingement holes which are effectively integrated within the high solidity array. These incremental impingement arrays provide higher downstream cooling and can allow more prescriptive internal cooling by placement and size of these impingement holes.

University of Texas at Austin Improving Durability of Turbine Components through Trenched Film Cooling and Contoured Endwalls. Gas turbine operation using new coal-derived high hydrogen fuels (syngas) requires design of new cooling configurations for turbine components. To operate with high efficiency, gas turbines must operate at very high temperatures, and cooling of the combustor and turbine components downstream of the combustor is critical. When using syngas, an additional factor that must be addressed is the effects of contaminant particles which will impact and adhere to the turbine components. The deposition of contaminants results in much rougher surfaces and partial blockage of film cooling holes that seriously degrade the cooling performance. In our project we have successfully simulated the deposition of contaminants on simulated turbine vanes and endwalls, and quantified increases in surface roughness, coolant hole blockage, and decreases in cooling performance due to these deposits. Experimental studies during the past year included the determination of the combined effects of TBC and film cooling with and without depositions on the vane model. Results from these studies showed that TBC has a dominating effect on overall cooling effectiveness such that the type of film cooling geometry used

has little impact. Furthermore, measurements showed the deposition of contaminants actually improves overall cooling effectiveness because of insulating effects of the deposits on the external surface.

University Turbine Systems Research: Combustion

Georgia Institute of Technology Increases Understanding of Turbulent Flame Propagation Characteristics of High Hydrogen Content Fuels. The objective of this project is to improve the state-of-the-art understanding of turbulent flame propagation characteristics of high hydrogen content (HHC) fuels. Such HHC fuels offer advantages for reducing the carbon footprint of power generation systems. Turbulent flame propagation influences the flashback and blowoff limits of the combustor, the life of hot section components, combustor emissions, and the operating limits required to prevent harmful combustion dynamics. As such, the data, models, and knowledge achieved in this program will have important practical influences on advanced gas turbine technologies. In the second year of this program, we made significant progress with both the Bunsen burner and low swirl burner (LSB) facility. For the Bunsen burner, we completed a comprehensive velocity field characterization study for pressures and mean flow velocities of 1–20 atm and 10–50 m/s, respectively, using laser Doppler velocimetry. We also obtained turbulent consumption speed, $S_{T,GC}$, data at 5 atm and 10 atm for mean flow velocities of 30 m/s and 50 m/s and H_2/CO ratios of 30/70 to 90/10 by volume over a wide range of turbulence intensities. These studies have demonstrated that the fuel effects found in the atmospheric data also exist at the elevated pressure conditions. In other words, mixtures with different H_2 contents, but the same un-stretched laminar flame speeds, $S_{L,0}$, and exposed to the same turbulent flow field can possess different turbulent consumption speeds. Furthermore, we also demonstrated that for a given H_2/CO mixture the consumption speed at 5 atm and 10 atm were roughly a factor of 1.8 and 2.2 greater than the consumption speed at 1 atm. Note that this is not an $S_{L,0}$ effect, as $S_{L,0}$ is kept fixed across the mixtures and pressures. We also completed the assembly of the LSB facility and performed non-reacting and reacting velocity field characterization studies using particle image velocimetry. We also acquired preliminary local turbulent displacement speed, $S_{T,LD}$, data for CH_4/air mixtures in this configuration. Work is currently underway to obtain $S_{T,GC}$ data in the Bunsen facility for pressures of 10 atm and greater for a wider range of H_2/CO mixtures. Furthermore, atmospheric $S_{T,LD}$ data will be acquired in the LSB facility for the same mixtures investigated in the Bunsen facility.

Syngas Chemical Kinetics Model Includes the Effects of H_2O on Syngas Combustion at High Pressures. Measurements obtained at Princeton University were used to expand the data sets on flame speeds and burning rates for high-pressure, low-flame-temperature syngas flames to cover lean mixtures of more direct interest to typical syngas turbine conditions for pressures of 1 atm to 25 atm, flame temperature from 1,400 K to 1,800 K, and equivalence ratio from 0.3 to 1.0. In particular, measurements of the effects of H_2O on syngas combustion showed that water inhibits the mass burning rate of syngas, which is an important parameter in the design of gas turbine combustors. The in-progress chemical kinetics model being developed as part of this research effort was updated in terms of the reaction rates and kinetic pathways to account for the measured effects of H_2O. The updated model demonstrated improved agreement against the more recent high-pressure, low-flame-temperature flame studies as well as reproducing previous validation targets.

Pennsylvania State University Investigates the Effects of Asymmetry on Flame Response in Multi-Nozzle Combustors. Actual gas turbine combustors for power generation applications employ multi-nozzle combustor configurations. Researchers at Penn State and Georgia Tech have extended previous work on the flame response in single-nozzle combustors to the more realistic case of multi-nozzle combustors. Research at Georgia Tech has shown that asymmetry of both the flow field and the acoustic forcing can have a significant effect on flame response and that such behavior is important in multi-flame configurations. As a result, the structure of the flame and its response to forcing is three dimensional (3D). Research at Penn State has led to the development of a 3D chemiluminescence flame imaging technique that can be used to characterize the unforced (steady) and forced (unsteady) flame structure of multi-nozzle

combustors. Important aspects of the flame response in multi-nozzle combustors which are being studied include flame-flame and flame-wall interactions.

Structure and Dynamics of Fuel Jets Injected into a High-Temperature Subsonic Crossflow Investigated at Purdue University. The primary goal of the project is to investigate the structure and dynamics of the reacting flow field for jets injected into a subsonic crossflow. The jet in crossflow study has practical applications while also serving as an important test case for the development of numerical methods for turbulent reacting flow fields typical of gas turbine combustors. Secondary injection of the fuel, also referred to as distributed combustion, is being studied as a means for reducing NOx emissions while increasing the power output of the gas turbine systems. By utilizing high-speed diagnostics techniques, the enhanced mixing and combustion of the fuel jet will be measured in order to determine the quantitative relationship between the unsteady combustion field and the forced oscillatory field. Successful completion of this project will include the following advancements to be made available within the turbine community.

- Provide insight contributing to improvement of the technology and design development process capabilities for distributed or "late-lean" combustion for the next-generation of higher efficiency, ultra-clean turbine engines burning HHC fuels.
- Validation of next generation combustion models with emphasis on complex turbulent vortical structure including modern advanced models on chemical kinetics, turbulence, and turbulence/chemistry interaction.
- Provide insight into the coupling mechanisms between the secondary fuel jets and a simulated unstable flowfield to yield validation data under simulated unstable conditions, and provide information needed to generate transfer functions used in combustion dynamics analysis.

Effect of Impurities on Syngas Ignition and Flame Speeds Measured at Texas A&M. Synthetic gas, syngas, is a popular alternative fuel for the gas turbine industry, but the composition of syngas can contain different types and amounts of contaminates, such as carbon dioxide, moisture, and nitrogen, depending on the industrial process involved in its manufacturing. The presence of steam in syngas blends is of particular interest from a thermo-chemical perspective as there is limited information available in the literature. Other impurities include CH_4, CO_2, and NH_3. Ignition delay times have been measured behind reflected shock waves at 1.5, 12, and 30 atm for a mixture representative of a syngas produced from biomass in 98% Ar (mol%) and for the same biomass-derived syngas mixture doped with 200 ppm of NH_3. The importance of the various constituents on the ignition delay time was investigated by comparing the results with data from various baseline mixtures ($H_2/O_2/Ar$, $H_2/CO/O_2/Ar$ and $H_2/CO/O_2/Ar$ with one of the other constituent of the syngas, i.e., CO_2, H_2O, CH_4 or NH_3). Results showed that the mixture composition can have an important effect on the ignition delay time, with most of the effect being due to CH_4 addition through the reaction $CH_4+OH \leftrightarrows CH_3+H_2O$. The ammonia impurity had very little effect on the ignition delay time over the range of conditions studied. We have also investigated the effect of moisture content (0–15% by volume), temperature (323–423 K), and pressure (1–10 atm) on syngas mixtures by measuring the laminar flame speed in a recently developed constant-volume, heated experimental facility. The experimental flame speed data are compared to the authors' most recent chemical kinetics model showing good overall agreement, but there are areas that need improvement, particularly around the peak flame speed. A performance sensitivity analysis showed that the syngas composition is the most important factor affecting the laminar flame speed, but there is inconclusive evidence of a dominant factor that affects the mass burning rate and the Markstein length. Generally, mixtures with high levels of carbon monoxide stabilize the flame structure of thermal-diffusive instability. The increase of steam dilution has only a small effect on the laminar flame speed of high carbon monoxide mixtures.

Facility Modifications Underway to Allow Development of Design Guides for Premixer Flameholding Tendencies. University of California, Irvine has nearly completed modifications to a facility to allow detailed measurements and associated analysis to be carried out in order to develop design guides to predict how different geometric features within premixer passages might serve to anchor a

reaction in the event of flashback. While hydrogen-containing fuels are being focused on, the results will also be relevant to natural gas fired systems. Unique attributes of the facility include high optical access and detailed quantification of the test conditions, velocities, and geometry of features. As a result, in addition to provision of design guides, the results can also be used by original equipment manufacturers or others to validate/carry out detailed computational fluid dynamic simulations. Experiments will begin in FY 2013.

Critical Parameter Proposed to Delineate Ignition Regimes for H_2/CO Fuels. Rapid compression facility experiments were conducted at the University of Michigan to study ignition of H_2 and CO fuel blends. The results indicate two ignition regimes: strong and weak. Quantitative characteristics were identified from high speed imaging and pressure time-history data for each regime, including the propagation rates of reaction fronts formed during weak ignition. The experimental data span pressures of P = 7.1 to 26.4 atm, temperatures from T = 855 to 1,051 K, equivalence ratios from φ = 0.1 to 1.0, oxygen mole fractions from χ_{O2} = 15% to 20%, and H_2:CO ratios from H_2:CO = 0.25 to 4.0 (mole basis). The thermophysical parameters associated with the strong and weak ignition regimes were evaluated and appear to be delineated by a critical hydrogen mole fraction of $\chi_{H2,critical}$ = 1.5%. Investigation of the physical nature of the critical hydrogen mole fraction using ignition theory indicates that the limiting condition is governed by competing physical and chemical time scales. Combustion systems in the weak ignition regime will likely experience similar sensitivities leading to complex system responses that are difficult to predict a priori.

Joint Experimental/Computational Study to Advance Gas Turbine Design Process at UT. University of Texas (UT) at Austin applied hierarchical validation to improve large-eddy simulation (LES) models for hydrogen-enriched gas-turbine combustion. A new modeling approach, termed the semi-explicit quadrature method of moments, was developed to describe unsteady flame interactions with the turbulent flow inside gas turbines. The hierarchical validation involves validation against increasingly complex experimental data sets. During Fiscal Year 2012 validation data were acquired in the jet-flame-in-crossflow configuration with hydrogen/methane fuels. Normal injection and pitched injection were tested, and detailed measurements of the velocity field using particle image velocimetry were made. Data were used to test new techniques for validating LES models. Using input from industry, a new swirl combustor for turbulent flame measurement and flashback studies has also been designed. By validating the LES using the swirl-combustor measurements, a robust methodology for designing future gas turbines will be developed. UT Austin researchers are working with industry to transfer the models and measurement data.

University Turbine Systems Research: Materials

Louisiana State University Using High Performance Computing for Thermal Barrier Coating Design. Currently, TBCs are usually developed by the trial-and-error approach, which is very expensive and time consuming. Researchers from Southern University and Louisiana State University are working together on the development and evaluation of a computational materials tool for the identification of new thermal barrier coatings. Using high performance computing facility at Louisiana Optical Network Initiative, ab initio molecular dynamics based design tool is currently being tested to screen and identify TBC systems with desired physical properties for integrated gasification combined cycle environment applications. Experimental validation will be performed to demonstrate the computational design tool.

Stony Brook University Develops Atmospheric Plasma Sprayed $Gd_2Zr_2O_7$ Process Maps to Enable Tailored Multifunctional Thermal Barrier Coating Architectures. A key aspect to the development of a multilayer, multifunctional TBC for integrated gasification combine cycle gas turbines is understanding how processing conditions impact coating microstructure and performance. At the Center for Thermal Spray Research of Stony Brook University, process maps have been developed to link in situ particle and coating states to material properties in thermally sprayed systems. This approach has been applied to atmospheric plasma sprayed $Gd_2Zr_2O_7$ to determine various correlations, including relating particle temperature and velocity in a plasma flame to microstructure. Particle diagnostic tools

and cross-sectional scanning electron microscopy imaging have been used to develop a first order process map. Elastic moduli and nonlinear degrees have been determined using an ex situ coating property sensor developed at Stony Brook University. These properties are crucial for developing a TBC that can withstand the thermo-mechanical stresses on gas turbine components. Thermal conductivity for coatings sprayed with various process conditions was determined using laser flash. A second order map has been created relating the mechanical and thermal properties of various $Gd_2Zr_2O_7$ coatings sprayed with different processing conditions. Using these maps, multifunctional coatings have been designed, fabricated and tested to meet the requirements of thermal cycle durability and erosion resistance. Preliminary results have indicated that this is a promising strategy. Scale-up studies are currently underway with the goal towards development of a multilayer coating that can provide reliable thermal protection to metallic gas turbine engine components.

Thermal Barrier Coating Structures Optimized at University of Connecticut to Achieve Low Thermal Conductivity. Burning of coal by gasification with CO_2 separation and storage is a near-zero carbon footprint method of utilizing America's vast coal reserves. A key goal is to make this attractive option as economical as possible. Using gas turbines and maximizing their efficiency and durability are key elements in making coal gasification plants economically attractive. Improved efficiency lowers the cost of electricity but requires higher firing temperatures. Higher temperatures are enabled by improved ceramic thermal barrier coatings to protect the metal parts; and in addition, such coatings operating at higher temperatures need reduced thermal conductivity and improved resistance to chemical attack from contaminants that are especially aggressive at high temperatures. The purpose of this project is to use unique coating fabrication technology developed at the University of Connecticut to create coatings that have lower thermal conductivity, higher allowable operating temperature, and better resistance to high temperature contaminants. In the first year of the project, coatings were successfully made by our new process with the desired conductivity-lowering microstructure achieving very significant reductions in thermal conductivity. Structures are now being optimized to achieve the lowest possible conductivity. In addition, a method to calculate the thermal conductivity from microstructure photos is being developed, and the method is being validated against more time consuming lab measurements. The important reduced sensitivity to chemical attack and improved maximum use temperature are to be developed in the following two years.

Sampling of Microcontaminants in Combusted Synthesis Gas Begun at UND. The University of North Dakota (UND) team has begun sampling activities to determine what types of trace contaminants may occur in cleaned syngas that could lead to corrosion issues in turbines firing syngas. The Energy & Environmental Research Center at UND has several pilot-scale gasifiers that are continually used in a variety of test configurations. Sampling was done with the entrained-flow gasifier (EFG). Funding for the EFG tests was provided from a separate project. The EFG fired a blend of Powder River Basin coal and ground wood. During those tests, particulate and trace element samples were collected from the thermal oxidizer used to burn the syngas produced. The sampling train used was designed for the U.S. Environmental Protection Agency (EPA) Method 29 sampling, although the typical glass fiber prefilter was replaced with a Nucleopore polycarbonate membrane filter with etched 0.1-µm-diameter pores. The thermal oxidizer contains a premixed air-syngas burner at the top of a refractory lined chamber. The sampling occurs at the bottom of the downfired oxidizer. The gas being sampled is at approximately 750°C. It is quenched as it is pulled through the glass sampling tube to approximately 100°C before reaching the filter. Three sample sets were collected: two while firing the coal-biomass blend and one while no coal or biomass was fed into the EFG but natural gas was fired in the thermal oxidizer. The EPA Method 29 impinger samples will be analyzed by atomic absorption spectroscopy, and the filter samples will be analyzed by scanning electron microscopy.

University of Pittsburg Finds Degradation of TBC Systems in Environments Relevant to Advanced Gas Turbines for IGCC Systems This project will study the fundamental mechanisms whereby integrated gasification combined cycle (IGCC) environments and deposits, which may arise in the use of gasified coal or coal + biomass, degrade TBCs in gas turbines. The degradation of conventional

and advanced TBCs caused by gases rich in H_2O and CO_2 up to 1,100°C and typical fly ash deposits over the same temperature range will be studied. A laboratory-scale apparatus has been established to perform testing of air-plasma sprayed TBCs until failure in the different environments is measured. The first samples to be tested have been obtained, and a clear plan for the research project has been established.

Yttria Stabilized Nanostructured Hafnia Based Thermal Barrier Coating with Low Thermal Conductivity and High Stability in Hot Gas Environment Investigated at University of Texas, El Paso. Thermal conductivity of the yttria stabilized hafnia (YSH) coating grown on various substrates has been investigated using photo-caustic (PA) and time domain thermal-reflectance (TDTR) methods. YSH coating showed the thermal conductivity within the range from 0.89 ± 0.03 to 1.3 ± 0.04 W/m-K, which is lower compared to pure HfO_2 or bulk YSH material. Performance of YSH and yttria stabilized hafnia-zirconia (YSHZ) coating in hot gas environment has been evaluated in a laboratory scale combustor rig. Microstructural analysis of coatings has been performed after exposure to the hot gases produced by the burning of methane with air. The coatings exhibit stability to the hot gas environment. No significant microstructural changes were observed from the XRD patterns. The material does not show any change from the cubic crystal structure. No significant change is visible from surface morphology, however, slight sintering is observed in the high magnification of the sample after nine hours of exposure to hot gas at 1,100°C.

Small Business Innovation Research: Innovative Cooling Concepts

Spar-Shell Turbine Component Development Enables a Disruptive Leap in Gas Turbine Performance. Florida Turbine Technologies, Inc., engineers are developing spar-shell gas turbine components to provide significant efficiency improvements in existing and advanced power systems including proposed turbomachinery using high-hydrogen (H_2) and alternative synthetic fuels. Feasibility of the technology has been demonstrated through conceptual design studies and detailed design of equipment is in progress. This technology promotes our nation's independence from foreign fuel. Spar-shell airfoil technology can be retrofit into existing power plants worldwide to create up to 15% more power from the same plants, one-third of which will be completely carbon-free and requires no additional fuel. Application of this technology to 50% of the existing U.S. gas turbine power plants can generate an additional nine gigawatts of power–enough to offset the equivalent of 13 coal plants. Finally, this program will lead to the creation of hundreds of engineering and manufacturing jobs and put our nation at the forefront of a technology that will improve energy efficiencies world-wide.

Ceramic Cores Produced with Advanced Cooling Geometries. Mikro Systems, Inc. has applied its patented TOMO^{SM} manufacturing process to the production of ceramic cores used in investment casting. The features enabled by TOMO^{SM} provide advanced cooling geometries that are otherwise not producible. Mikro has demonstrated that aspects of the TOMO^{SM} process steps provide several advantages including reduced lead times, lower tooling cost, adaptable designs, and advanced geometries. These advantages, for the first time, offer the heat-transfer design community a platform to rapidly and cost effectively test various cooling geometries; a powerful, and much needed tool for pushing power generation technology in order to realize improved plant efficiency targets set by the U.S. Department of Energy.

Small Business Innovation Research: Manufacturing

PSI Investigates Water Guided Laser Drilling System Process Refinements. Physical Sciences Inc. (PSI) constructed a second generation water guided laser drilling system to develop high speed drilling processes for cooling holes in gas turbine components. The key element of the system is the water guiding component that creates a high pressure stream of water to guide a high power laser to a work surface. During the second year of the program, PSI has been working to refine the water guided laser drilling process to improve reliability for drilling the thousands of holes required in gas turbine combustor components. Cavitation has been identified as a major contributor to reliability issues due to pressure fluctuations in the high pressure water delivery system. Cavitation is believed to be responsible for the creation of bubbles in

the water system that cause refraction of the drilling laser that damage the water stream forming orifice in the drilling head. Pressure dampeners have been used to reduce pressure fluctuations with some improvement in the lifetime of the orifice used to create the high pressure water stream.

Small Business Innovation Research: Thermal Barrier Coatings

Low Thermal Conductivity and Erosion Resistant Thermal Barrier Coatings Developed by UES for High Temperature Applications. In this Phase II DOE Small Business Technology Transfer program, the UES, Inc./Penn State University team has expanded the relevant high temperature data on the TBC architectures that were developed for higher temperature turbine engine applications. The TBC architectures (monolayered, multilayered) were based on selected materials, viz. low k yttria stabilized zirconia (YSZ) and $Gd_2Zr_2O_7$ (GZO). Phase I work clearly demonstrated that the TBCs of the selected materials, fabricated by electron beam physical vapor deposition technique, have lower thermal conductivity than the currently used TBC (std. YSZ). Phase I work also demonstrated that the intrinsically higher erosion rate of GZO TBC can be considerably minimized by utilizing multilayered coating architecture. In the Phase II program, high temperature (>1,300°C) sintering characteristics of the TBCs fabricated in Phase I were determined and compared with that of the std. YSZ. It was found that all the fabricated TBCs have better sintering characteristics than the std. YSZ. Also, in the Phase II program, erosion rates of the TBCs were determined after annealing at higher temperatures. It was found that even for annealed samples the intrinsic high erosion rate of GZO can be lowered by multilayered coating architecture. The data obtained so far indicates the need for manipulation of the coating microstructure, chemistry, and design to achieve optimal TBCs for higher temperature applications. TBCs of varying chemistry, microstructure, and design were fabricated. Relevant characteristics (thermal conductivity, sintering behavior, and erosion rate) will be determined in the near future. Moreover, work has been initiated in the Phase II program to develop cost effective atmospheric pressure plasma spray process for the fabrication of TBCs for higher temperature applications.

Summary

In response to the nation's increasing power supply challenges, NETL is researching next-generation turbine technology with the goal of producing reliable, affordable, diverse, and environmentally friendly energy supplies. With the Hydrogen Turbine Program, NETL is leading the research, development, and demonstration of these technologies to achieve power production from coal that is clean, efficient, and cost-effective; minimizes CO_2 emissions; and will help maintain the nation's leadership in the export of electric power equipment. Efforts are coordinated nationwide through NETL and the Hydrogen Turbine Program. A list of the projects by state is provided in the table at the end of this section.

Critical technologies must be modeled and developed for future gas turbine engines in advanced IGCC systems running on HHC fuels. Either new materials must be developed or coatings with novel chemistries must be engineered to protect engine components and allow further increases in engine temperatures to achieve higher efficiency. The development is limited, in part, by the available materials and manufacturing abilities.

DOE's Hydrogen Turbine Program is striving to show that the U.S. can operate on coal-based hydrogen fuel power, increase combined cycle efficiency by three to five percentage points over the baseline, and reduce CO_2 and other emissions by 2015. Program and project emphasis is on understanding the underlying factors affecting combustion, aero/heat transfer, and materials for current IGCC syngas turbines and using that knowledge to design advanced turbines and conduct the research needed to transition to nearly pure hydrogen fuels.

The following sections summarize the scope, objectives, status, and accomplishments for each Hydrogen Turbine Program project. The Hydrogen Turbine Program is encouraged by the technical progress made this year, and the prospects for continued advancements in the coming year are good, paving the way to achievement of the goals.

2012 Hydrogen Turbines Portfolio Projects by State
New Projects in Italics

STATE	PROJECT TITLE	PERFORMER NAME
California	Development of Criteria for Flameholding Tendencies within Premixer Passages for High Hydrogen Content Fuels	University of California, Irvine
	Low-Swirl Injectors for Hydrogen Gas Turbines in Near-Zero Emissions Coal Power Plants	Lawrence Berkeley National Laboratory - LBNL
	Recovery Act: Oxy-Fuel Turbo Machinery Development for Energy Intensive Industrial Applications	Clean Energy Systems, Inc.
Colorado	Thermophysical Properties of Carbon Dioxide and CO_2-Rich Mixtures	National Institute of Standards & Technology
Connecticut	Low Thermal Conductivity, High Durability Thermal Barrier Coatings for IGCC Environments	University of Connecticut
Florida	Demonstration of Enabling Spar-Shell Cooling Technology in Gas Turbines	Florida Turbine Technologies
	High Temperature Capability and Innovative Cooling with a Spar and Shell Turbine Blade	Florida Turbine Technologies
	Recovery Act: Advanced Hydrogen Turbine Development	Siemens Energy
	Air Riding Seal Technology for Advanced Gas Turbine Engines	*Florida Turbine Technologies*
Georgia	Turbulent Flame Propagation Characteristics of High Hydrogen Content Fuels	Georgia Tech Research Corporation
Indiana	Structure and Dynamics of Fuel Jets Injected into a High-Temperature Subsonic Crossflow	Purdue University
Iowa	Analysis of Gas Turbine Thermal Performance	Ames National Laboratory
Louisiana	Computational Design and Experimental Validation of New Thermal Barrier Systems	Louisiana State University
Massachusetts	Advanced Laser Machining Techniques for Cooling Holes in Gas Turbines	Physical Sciences Inc.
Michigan	Development and Experimental Validation of Large-Eddy Simulation Techniques for the Prediction of Combustion-Dynamic Processes in Syngas Combustion	Regents of the University of Michigan
	Fundamental Studies to Enable Robust, Reliable, Low Emission Gas Turbine Combustion of High Hydrogen Content Fuels	Regents of the University of Michigan
Multiple	Turbine Thermal Management	National Energy Technology Laboratory - Regional University Alliance
New York	Recovery Act: Advanced Hydrogen Turbine Development	GE Energy, Inc.
	Advanced Thermal Barrier Coatings for Operation in High Hydrogen Content Fueled Gas Turbines	The Research Foundation of SUNY at Stony Brook
North Dakota	Cooling Strategies for Vane Leading Edges in a Syngas Environment Including Effects of Deposition and Turbulence	University of North Dakota
	Preparation and Testing of Corrosion- and Spallation-Resistant Coatings	University of North Dakota Energy and Environmental Research Center

Continued on the next page

2012 Hydrogen Turbines Portfolio Projects by State (Continued)
New Projects in Italics

STATE	PROJECT TITLE	PERFORMER NAME
Ohio	Effects of Hot Streak and Phantom Cooling on Heat Transfer in a Cooled Turbine Stage Including Particulate Deposition	Ohio State University
	Designing Turbine Endwalls for Deposition Resistance with 1,400°C Combustor Exit Temperatures and Syngas Water Vapor Levels	Ohio State University
	High-Bandwidth Modulation of H_2 /Syngas Fuel to Control Combustion Dynamics in Micro-Mixing Lean Premix Systems	Parker Hannifin Corporation
	High Temperature Unique Low Thermal Conductivity Thermal Barrier Coating (TBC) Architectures	UES, Inc.
	Multi-layered Yttria-Stabilized-Zirconia Coating for Improved Thermal Barrier Abrasion Resistance	*Powdermet, Inc.*
Pennsylvania	An Experimental and Chemical Kinetics Study of the Combustion of Syngas and High Hydrogen Content Fuels	Pennsylvania State University
	Combustion Dynamics in Multi-Nozzle Combustors Operating on High-Hydrogen Fuels	Pennsylvania State University
	Degradation of TBC Systems in Environments Relevant to Advanced Gas Turbines for IGCC Systems	University of Pittsburgh
Tennessee	An Alternative Low-Cost Process for Deposition of MCrAlY Bond Coats for Advanced Syngas/Hydrogen Turbine Applications	Tennessee Technological University
	Coating Issues in Coal-Derived Synthesis Gas / Hydrogen-Fired Turbines	Oak Ridge National Laboratory - ORNL
Texas	Aerodynamics and Heat Transfer Studies of Parameters Specific to the IGCC Requirements: High Mass Flow Endwall Contouring, Leading Edge Filleting and Blade Tip Ejection under Roating Turbine Condition	Texas Engineering Experiment Station -TAMU
	Hafnia-based Nanostructured Thermal Barrier Coatings for Advanced Hydrogen Turbine Technology	University of Texas at El Paso
	Improving Durability of Turbine Components Through Trenched Film Cooling and Contoured Endwalls	University of Texas at Austin
	LES Modeling of Flashback and Flame Stabilization in Hydrogen-rich Gas Turbines using a Hierarchical Validation Approach	University of Texas at Austin
	Turbulent Flame Speeds and NOx Kinetics of HHC Fuels with Contaminants and High Dilution Levels	Texas Engineering Experiment Station -TAMU
Utah	*Ultra-High Temperature Thermal Barrier Coatings*	*HiFunda LLC*
Virginia	Advanced Cooling for IGCC Turbine Blades	Mikro Systems, Inc.
	Phase III Xlerator Program: Rapid Commercialization of Advanced Turbine Blades for IGCC Power Plants	Mikro Systems, Inc.
	Advanced Filtration to Improve Single Crystal Casting Yield	*Mikro Systems, Inc.*

II. HYDROGEN TURBINES

II.1 Recovery Act: Advanced Hydrogen Turbine Development

Reed Anderson
GE Energy
1 River Road, 55-211
Schenectady, NY 12345
Phone: (518) 385-5689; Fax: (518) 385-8796
Email: reed.anderson@ge.com

DOE Project Manager: Robin Ames
Phone: (304) 285-0978
Email: Robin.Ames@netl.doe.gov

Subcontractors:
- GE Global Research Center, Niskayuna, NY
- GE Aviation, Cincinnati, OH

Contract Number: NT42643

Start Date: October 1, 2005
End Date: September 30, 2014

Fiscal Year (FY) 2012 Objectives

- Develop technology advancements necessary for an advanced integrated gasification combined cycle (IGCC), fuel flexible (coal-derived hydrogen and syngas) gas turbine to meet the U.S. Department of Energy (DOE) program goals.
  - Improve IGCC efficiency (+3-5 pts. combined cycle efficiency),
  - Reduce oxides of nitrogen (NOx) emissions to 2 ppm NOx at 15% O_2,
  - Contribute to capital cost reductions.
- Continue advancement of American Recovery and Reinvestment Act (ARRA) funded activities that expand the scope of, accelerate the pace of, and adapt existing development efforts to benefit gas turbines for industrial applications.

FY 2012 Accomplishments

- Realized emissions and operability benefits from improved versions of the leading pre-mixed high-hydrogen combustion concept during extensive megawatt-scale, full chamber combustion rig testing. Fuel nozzle design concept successfully passed aggressive accelerated thermal cycle tests.
- Performed systems analysis to establish a baseline, targets, and overall benefits of the additional scope focusing on industrial applications. Specifically, benefits in the areas of efficiency, emissions, and economics due to the implementation of the advanced turbine technologies being developed in industrial scenarios were examined.
- Selection criteria was established, and top options for advanced sensors and assemblies for testing these sensors were down-selected for further development.
- Completed testing several advanced wheelspace region concepts aimed at reducing the level of required purge flows to keep components at acceptable temperatures in the new test rig that was designed, fabricated, and installed earlier in the project.
- Evaluated candidate thermal barrier coatings (TBCs) and bond coat (BC) combinations in an integrated rig test to enable selection of the final system for detailed characterization. Testing this year included long term gradient testing on the TBC to better understand the effect of temperature gradient and cycles on TBC life.

Introduction

Coal is this nation's most abundant domestic energy resource and is used to produce about 50% of the nation's electricity needs. Its continued use is an important part of realizing an "energy secure" America. The challenge is to produce electricity in a cleaner and more efficient manner while significantly reducing carbon emissions. The goal of this project is to advance gas turbine technologies, including CO_2 capture, so that future coal-based IGCC industrial application and power generation plants can be operated with higher efficiency, lower cost, and reduced emissions. The gas turbine has a significant influence on the performance of the plant. The inherent performance penalties associated with CO_2 capture are driving a renewed focus on gas turbine technology advancement as a means to minimize the penalty.

In an IGCC plant, syngas produced from the coal is cleanly burned in a heavy-duty gas turbine. With pre-combustion CO_2 capture, the resulting fuel burned in the gas turbine is hydrogen. GE's advanced gas turbine technology project addresses key technology developments required to achieve specific DOE performance goals relative to emissions, efficiency, and capital cost. The project is comprised of two phases. Phase I, which ran from October 2005 to September 2007, was focused on conceptual design and technology identification. The output of Phase I was a down selection of key technologies that are currently being further

applied and developed in Phase II. The Phase II effort started in October 2007 and is focused on technology development and validation at a component level. In 2010, this phase was supplemented with ARRA funding. Using this additional funding, activities were added to the plan to expand the scope of, accelerate the pace of, and adapt existing development efforts to benefit gas turbines for industrial applications in addition to the original focus area of IGCC power plants.

Approach

This gas turbine technology advancement project is comprised of three main technology areas (combustion, turbine/aero, and materials) plus a systems level activity.

- The combustion element of the project is focused on improving combustion technology to achieve the emissions target of 2 ppm NOx at the higher temperatures necessary to achieve the targeted efficiency improvement. Work in this area addresses the challenges of developing a combustion system that can burn both syngas and high hydrogen fuels to produce extremely low NOx emissions while avoiding flameholding, flashback, and dynamics issues.
- The turbine/aero element of the project drives technology improvements to address the efficiency targets. Examples include improved aerodynamic characteristics and better flow management.
- The materials portion of the project is focused on applying materials technology to enable the turbine to operate reliably at higher firing temperatures in the harsher IGCC environment. This includes evaluation of advanced coatings, along with targeted use of ceramic matrix composites with environmental barrier coatings.
- The systems level approach translates the integration of technology improvements into plant performance and investigates the various system trade-offs and their impact on overall plant performance.

In summary, this comprehensive project addresses the technology development needs for advanced gas turbines for IGCC applications while targeting the specific goals identified by the DOE relative to emissions, efficiency, and capital cost.

Results

Government fiscal year (GFY) 2012 was the fifth year of Phase II of the project, and as such, advanced analysis tools and rig testing continued to be used extensively in the process of developing and characterizing performance improvements from each technology area.

Improvements made to the high-hydrogen combustion system in the areas of aerodynamic, thermal, and mechanical design were targeted at further reduction in emissions, robust operability, better part life, and reduced costs. The concept combustion system continued to be tested in the full chamber combustion rig in GE Energy's state-of-the-art Gas Turbine Technology Lab in Greenville, South Carolina. The system has now been operated for more than 100 hours in the lab at full gas turbine conditions with greater than 90% hydrogen in the fuel reactants. Additionally, a set of fuel nozzles survived, without damage, an aggressive thermal cycle test, where accelerated startup-shutdown cycles were simulated.

In GFY 2012, a prime path for manufacturing the advanced high-hydrogen premixing fuel nozzles was identified, and work was started to mature the fabrication to a production-ready state. A set of pre-production fuel nozzles using the down-selected manufacturing method and including many of the previously mentioned improvements was built and tested. In addition to exhibiting excellent operability on hydrogen fuel, the new fuel nozzles delivered a further reduction in NOx emissions. Figure 1 shows NOx emissions as a function of combustor exit temperature for the pre-production nozzles compared to the nozzles that previously showed the best emissions.

A systems study was completed that characterizes the benefits of implementing the turbine technologies being developed in an industrial IGCC gas turbine. The study focused on benefits in the areas of plant efficiency, emissions, and economics. The results for one of the cases studied, implementation into U.S. petroleum refineries, theoretically predicted plant efficiencies more than 60% with the use of carbon capture and sequestration (CCS), an improvement of almost 10%

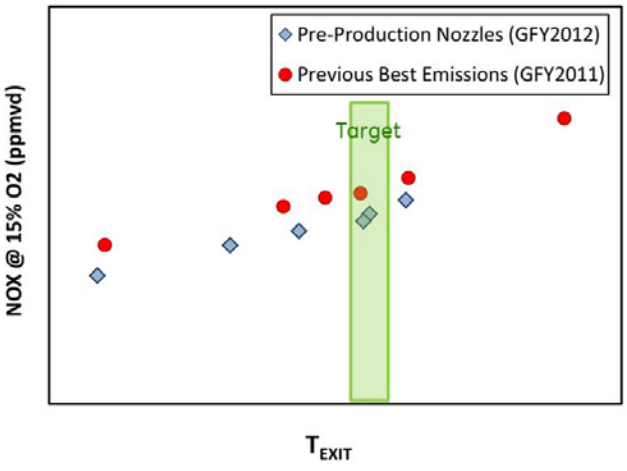

FIGURE 1. Pre-production fuel nozzles with numerous improvements delivered a reduction in NOx emissions during testing in GFY 2012 compared to the previous best hardware

above the baseline. Additionally, it was found that CO_2 emissions could be reduced by 81%, and implementation of the technologies could eliminate the $9.4 billion annual energy purchase expense and replace it with revenues of $4.1 billion annually, with an additional $6.4 billion in revenue if CO_2 credits for CCS are included.

Selection criteria were established and top options for advanced sensors and assemblies for testing these sensors were down-selected for further development. A systematic requirements analysis was conducted to determine the most important requirements for gas turbine sensing needs, especially in the hot gas path. Inputs from various design teams were solicited, and the results were captured using a Six Sigma tool called the Quality Function Deployment tool. It was determined that estimation of access limited, harsh environment parameters (such as metal and gas temperatures, pressures, and flows) for various locations in the hot gas path were of primary interest. Altogether, 19 sensing and estimation technologies were evaluated as part of this process. The result of the process was the down-selection of three key technologies for future development and validation. Development of all three sensor technologies has already been initiated under the project.

Advanced wheelspace region concepts have been developed aimed at reducing the level of required purge flows to keep components at acceptable temperatures. Several of these concepts have been tested using a new Hot Gas Ingestion Rig (HGIR) that was recently fabricated and installed in the GE Global Research Center with additional concept tests planned for the remainder of the year. The culminating task will be test of an optimized concept based on the results of all the previous tests. Figure 2 shows the test rig.

In the materials development area, a series of tests was conducted on integrated candidate TBC/BC systems in the thermal cycling test rig (Figure 3). The results of this testing and metallographic evaluation of the post-test specimens will enable selection of the final TBC/BC system for more detailed characterization that has begun and will continue through the end of the project. Long cycle gradient testing did establish that longer exposure with higher cycles and hotter temperatures decreased erosion performance. As a result of the changes to the corrosion screening testing, two new metallic coatings were down-selected for additional testing.

Conclusions and Future Directions

Phase II (technology development and validation) of this project is a continuation from Phase I (technology identification and conceptual design) which was completed on time, within budget, and with all major milestones achieved. In GFY 2012, the fifth year of the Phase II project was completed, which included additional technology development resulting from the supplemental ARRA funding. Results to date in Phase II have been positive (all major milestones completed on or ahead of schedule) and continue to indicate that project progress is on track relative to available funding. Building on work performed in GFY 2012, future years will continue unfinished efforts from this year and initiate remaining areas of the project. Looking ahead, some of the specific technology areas are:

- The fuel flexibility of the leading high-hydrogen combustion system will be explored, and features may be added to allow low-emissions combustion of startup and backup fuels. The prime manufacturing method for the pre-mixed fuel injectors will be matured to improve performance and durability and reduce cost.
- Potential methods of improving turbine architecture will be studied and leading concepts selected for further evaluation.

FIGURE 2. Hot gas ingestion rig

FIGURE 3. Thermal shock test

- Optimized designs for several more advanced cooling and sealing configurations, including the redesigned wheelspace region, will be completed and their improvement levels validated through rig testing. The next generation airfoils, designed using the improved tools resulting from earlier testing, will also have their efficiency improvement validated via the aerodynamic validation test rig.
- Integrated testing of the new metallic coatings as well as an additional TBC will be completed, and a final down-selection will be made. This will be followed by the process refinement stage and comprehensive performance evaluation/validation tests. Additional processing trials are planned to improve the performance of these new TBCs.
- Applicable technologies from the project will be developed and/or adapted for use in industrial applications, in the process accelerating their maturation schedule, using the added ARRA funding supplement.

Special Recognitions & Awards/Patents Issued

One hundred eleven U.S. patent filings have occurred. To date, seventeen patents have been awarded.

1. 219015 DOE Case #S-110,961; Title-Lean Direct Injection Construction Method; Patent #8042339 B2

2. 219028 DOE Case #S-110,963; Title-Distributed Lean Direct Injection within a Combustor; Patent #7886545

3. 219043 DOE Case #S-110,966; Title-Inlet Flow Conditioner for Reduced Flame Holding; Patent #8117845

4. 220603 DOE Case #S-110,974; Title-Coanda Pilot Nozzle Combustor; Patent #7874157

5. 220605 DOE Case #S-110,975; Title-Coanda Premixing Nozzles for Axially Staged Combustor; Patent #8176739

6. 226221 DOE Case #S-112,380; Title-Flashback Detection via Acoustic Pressure Transducer or Microphone; Patent #7942038

7. 226847 DOE Case #S-113,234; Title-Mini Tube Bundle Premixer - Recessed LDI; Patent #8147121

8. 227319 DOE Case #S-115,534; Title-Adoption of Water Cooling for a Premixed LDI Design to Prevent Flame Holding; Patent #8112999

9. 227444 DOE Case #S-113,313; Title-Axial Staggering of Fuel Vane Pack for Combustion Dynamics Reduction Associated; Patent #7578130

10. 229057 DOE Case #S-115,594; Title-A Vane Design with Suction Side Angled Holes Injection & Pressure Side Trailing Edge Holes Injection; Patent #8104286

11. 229071 DOE Case #S-115-593; Title-A Hybrid Nozzle Design of Swirler Vane and Tube Fuel Injection; Patent #8186166

12. 230282 DOE Case #S-115,804; Title-Vanelets to Improve Flameholding/Syngas Operability; Patent #8113002

13. 230700 DOE Case #S-115,878; Title–A Recessed LDI Design with Premixed Hot Nozzle Extension; Patent #7886991

14. 230905 DOE Case #S-115,876; Title-Passive Extinction Fuel Nozzle; Patent #8007274

15. 234680 DOE Case #S-119,613; Title-Monolithic Construction of Fuel Injector; Patent #8181891

16. 235291 DOE Case #S-117,504; Title-Internal Cooling for PDI Injector; Patent #8157189

17. 243484 DOE Case #S-S-122,490; Title-Inlet Filter for PDI Injectors; Patent #8141334 B2

FY 2012 Publications/Presentations

1. Rahul Bidkar, et al., "Design and Testing Methodology for Motion & Vibration Characterization of Advanced Seals," 47th AIAA/ASME/SAE/ASEE Joint Propulsion Conference, August 2011.

2. Roger Schonewald, "GE Energy's DOE Advanced IGCC/ Hydrogen Gas Turbine Program," UTSR, October 2011.

3. Doug Carper, et al., "Fracture Process in SiC-SiC Fatigue and Creep: Interaction Between Mechanical Damage and Environmental Degradation," 36th Annual Conference on Composites, Materials, and Structures at Cocoa Beach, January 2012.

4. Christine Zemsky, "GE Energy's DOE Advanced IGCC/Hydrogen Gas Turbine Program," ICEPAG 2012, February 2012.

5. William York, et al., "Development and Testing of a Low NOx Hydrogen Combustion System for Heavy Duty Gas Turbines," ASME Turbo Expo 2012, June 2012.

II.2 Recovery Act: Advanced Hydrogen Turbine Development

John Marra (Primary Contact), Tim Bradley
Siemens Energy, Inc.
4400 Alafaya Trail
Orlando, FL 32826
Phone: (407) 736-4190; Fax: (407) 736-5633
Email: john.marra@siemens.com,
tim.bradley@siemens.com

DOE Project Manager: Robin Ames
Phone: (304) 285-0978
Email: Robin.Ames@netl.doe.gov

Subcontractors:
- Florida Turbine Technologies, Jupiter, FL
- Agilis, Jupiter, FL
- Florida Institute of Technology, Melbourne, FL
- University of Florida, Gainesville, FL
- Georgia Institute of Technology, Atlanta GA
- Purdue University, West Lafayette, IN
- Virginia Polytechnic and State University, Blacksburg, VA
- Mikro Systems, Charlottesville, VA

Contract Number: NT42644

Start Date: October 1, 2005
End Date: June 30, 2015

Fiscal Year (FY) 2012 Objectives

- Demonstrate hydrogen operation on a head end combustor and determine required dilution limits.
- Obtain university data to improve the combustion design tools for high hydrogen fuel.
- Continue development of low thermal conductivity, high temperature capable thermal barrier coatings (TBCs). Manufacture components with high temperature TBC for engine demonstration.
- Continue development of high temperature bond coats. Demonstrate that the new bond coats meet target requirements with respect to oxidation resistance and TBC compatibility.
- Continue development of the advanced core manufacturing technology. Cast components with advanced internal cooling features in preparation for engine testing in the Siemens Berlin test facility.
- Develop preliminary turbine airfoil designs for U.S. Department of Energy (DOE) H_2 engine conditions with reduced cooling flow requirements to meet improved performance goals and output requirements.
- Evaluate novel design concepts allowing for incorporation of improved materials, aerodynamic and cooling technologies in turbine airfoils.
- Evaluate high Mach number airfoil designs for a high AN^2 (A = exhaust annulus area, N = shaft rotational speed) fourth stage turbine blade.
- Improve aerodynamic and heat transfer predictive capability to allow for increased design optimization.
- Develop the conceptual design of a polyfunctional emissions reduction catalytic system (PERC) for integrated gasification combined cycle (IGCC) plants with fuel flexibility.
- Perform a 2,000-hour lab reliability test for the PERC system in a high water and sulfur environment.
- Test the new PERC system downstream of a gas turbine to determine NOx and CO removal efficiency in field conditions.

FY 2012 Accomplishments

- The Siemens premixed combustor was modified for multifuel operation on natural gas, syngas and hydrogen fuel. Operation on hydrogen fuel with nitrogen dilution was confirmed in the high pressure test rig. Additional modifications were identified to increase the firing temperature of the design and minimize the dilution flow required to control flashback.
- Turbulent flame speed data was obtained at Georgia Tech for hydrogen mixtures.
- Flame images were obtained at Purdue using OH planar laser-induced fluorescence (PLIF) and coherent anti-Stokes Raman scattering (CARS) processes for computational fluid dynamics (CFD) validation.
- Ten modular vanes have been successfully cast in preparation for engine testing at the Siemens test facility in Berlin.
- TBC limits have increased over the baseline and the new composition is currently undergoing full scale engine testing
- TBC spallation and high temperature oxidation testing has been performed with a new high temperature bond coat showing a 3x increase in oxidation resistance.
- Four turbine blade cooling design variants have been evaluated at current state of the art engine conditions in a production engine. Local metal temperature reductions were predicted relative to the current production parts.

- Tools for the high AN^2 fourth stage blade were manufactured. Prototype Row 4 blade core production is ongoing, and the first pattern with a ceramic core has been produced.
- The first round of testing of last stage turbine blade aerodynamic designs has been completed in a high Mach number test rig. Data will be used for selection of an optimized design to reduce aerodynamic losses on this highly loaded part.
- An optimized first stage turbine blade aerodynamic design has been completed incorporating endwall contouring to reduce losses due to secondary flows. Loss reduction with this technology has been demonstrated in high Mach number rig testing.
- A new PERC is able to reduce emissions of CO to the ultra low levels (95-98%) in the simulated IGCC exhaust in the wide range of GT operating conditions.
- High NOx and CO reduction efficiency of the PERC is accompanied with a very low ammonia slip at the levels below 0.5 ppm.

Introduction

Siemens Energy, Inc. was awarded a contract by the DOE for Phases 1 and 2 of the Advanced Hydrogen Turbine Development Program in October 2005. The DOE Advanced Power System's overall goal is to conduct research and development necessary to produce CO_2 sequestration ready coal-based IGCC power systems with high efficiency, near zero emissions and competitive capital cost.

FY 2012 activities focused on the detailed evaluation of component level technologies and started to move into full scale engine testing. Technologies continued to be verified in subscale tests as well and design tools were updated with fundamental data obtained through laboratory tests at universities. Component manufacturing trials produced prototypes that are now in testing in a full scale engine.

Approach

Siemens has developed an overall program strategy that supports the DOE Program goals and future commercialization. In 2012, Siemens continued with Phase 2 of the program which included advanced technologies development, down-selection and validation, as well as basic component designs and testing. In Phase 3, if awarded, the final product manufacturing specifications will be completed; and, the engine will be manufactured and installed in an IGCC plant for validation testing to demonstrate the project's commercial viability and that the DOE program goals have been achieved.

Results

Significant progress has been made in the development of materials and coatings as well as manufacturing technologies for the advanced hydrogen turbine. A new low thermal conductivity TBC, with a surface temperature limit 10% greater than the baseline composition, has been developed successfully. The new TBC has been applied to first row turbine blades and vanes for engine demonstration at the Siemens test facility in Berlin. TBC spallation and high temperature oxidation testing has been performed with a new high temperature bond coat (Figure 1). The results of the long term oxidation testing indicate that the new bond coat exhibits significantly improved (3x) oxidation resistance compared with the baseline composition (Figure 3). Four cooling designs were developed and manufactured using new techniques that allow for previously impossible designs. The cooling designs were incorporated into row one blades and have undergone testing in a full scale engine (Figure 2). Local metal temperature reductions were demonstrated relative to current production parts.

The Siemens premixed combustor was modified for multifuel operation on natural gas, syngas and hydrogen fuel. Full scale rig testing has been performed operating on undiluted syngas fuel at up to H-Class temperatures. Operation on hydrogen fuel with nitrogen dilution was confirmed in the full scale high pressure test rig. This year, additional modifications were identified to increase the firing temperature of the design and minimize the dilution flow required to control flashback. Testing was

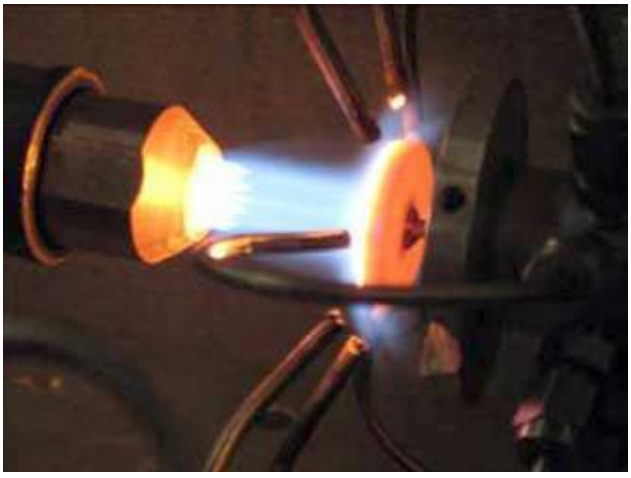

FIGURE 1. Materials test rig

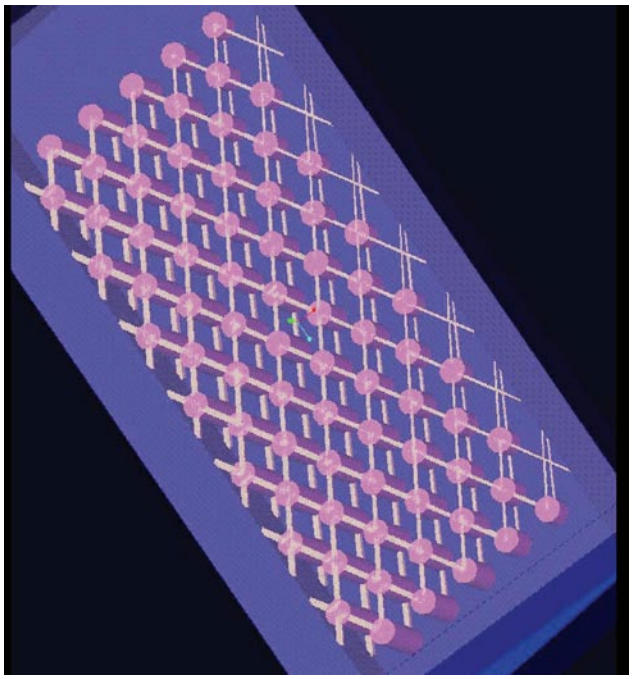

FIGURE 2. Internal cooling feature development

FIGURE 3. Advanced coatings

completed on the modified design which successfully reduced flashback as well as dilution requirements. The goal is premixed operation on hydrogen fuel with no flashback. Additional work was done in partnership with several universities to expedite and expand fundamental high pressure baseline data on hydrogen fuels in regards to turbulent flames, detailed chemical kinetics, laminar flame speed, ignition delay and CFD modeling. Turbulent flame speed data was obtained at Georgia Tech for hydrogen mixtures. Flame images were obtained at Purdue using OH PLIF and CARS processes for CFD validation.

A sizeable amount of activity was performed in the turbine. Areas of focus included manufacturing, heat transfer and aerodynamics. Additionally, several technologies are now moving into full scale engine testing. Ten modular vanes have been successfully cast, machined, and fully assembled. They were delivered to the Berlin Test Facility in preparation for full scale engine testing commencing in late Spring 2012. Because of the large size of the Row 4 blade, new manufacturing techniques are being developed. Tools for the high AN^2 fourth stage blade were manufactured. Prototype Row 4 blade core production is ongoing, and the first pattern with a ceramic core has been produced. Prototype parts will be cast in the third quarter of 2012. Additionally, one full scale engine testing included several cooling designs for the Row 1 blade.

Rig testing was performed and valuable data gathered in the areas of heat transfer and aerodynamics. The first round of testing on the aerodynamic design of the Row 4 blade was completed in a high Mach number rig. Data will be used for selection of an optimized design to reduce aerodynamic losses on this highly loaded part. An optimized first stage turbine blade aerodynamic design has been completed incorporating endwall contouring to reduce losses due to secondary flows. Loss reduction with this technology has been demonstrated in high Mach number rig testing.

The SCR being developed, known as the PERC, made considerable advancements this year. Numerous testing campaigns were completed, and the data gained was used to further refine the catalyst of the PERC. During the test campaigns, stable and durable performance was shown. More precisely, the ability to reduce NOx emissions at integrated gasification combined cycle (IGCC) plant conditions with an efficiency of >95% was demonstrated. The PERC also showed the capability of fuel flexibility (high hydrogen fuel, syngas, natural gas) while operating in the presence of high water and sulfur content in the gas turbine exhaust. Long-term durability testing was also completed in a pilot rig. The testing demonstrated a very good consistency of the pilot rig results with the lab data. Finally, the PERC system was tested in an actual exhaust downstream of a Siemens gas turbine under a wide range of operating conditions. The results have proved the developed concept meets the target values of NOx and CO with negligible ammonia slip. Figure 4 shows a typical commercial scale SCR block.

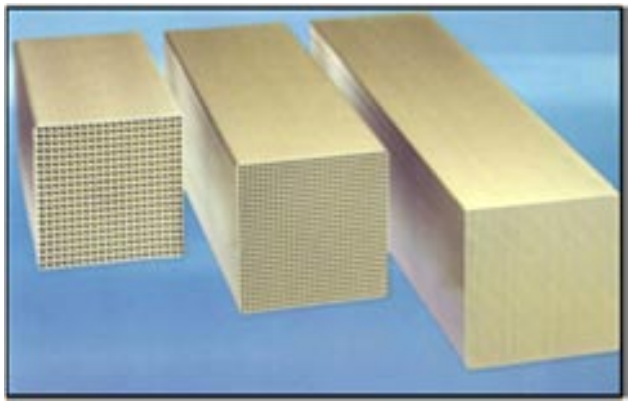

FIGURE 4. Commercial scale SCR blocks

Conclusions and Future Directions

The development effort focus is starting to move into manufacturing development and engine test validation of key enabling technologies such as novel turbine component concepts that improve aerodynamic and cooling efficiency. Engine ready hardware has been successfully produced using the modular technology, advanced cores and advanced thermal barrier coatings. Full scale engine testing has already begun. Material and coating technologies are being developed to enable increased operating temperature and mechanical integrity. The progress made in coatings technology is a key to producing a turbine with the lowest possible cooling flow at elevated temperature. Through advanced manufacturing processes and modular component technology, the feasibility of producing these novel turbine component concepts is made possible. By incorporating these advanced technologies, this gas turbine can significantly improve the efficiency, lower the capital cost, and improve the cost of electricity for IGCC plants with carbon capture.

Down-selected technologies will continue to undergo rigorous testing to fully characterize all design parameters. Improvements to the premix combustor design will continue to be tested at high hydrogen concentrations to verify performance with carbon capture fuels. The combustion program is on track to successfully develop a premixed combustor for IGCC applications capable of high hydrogen operation at elevated temperatures. Early adaptation of technologies to near term applications is planned to accelerate validation and ultimately reduce risk. The technology roadmap to meet the 2015 project objectives is established, and future work will continue towards executing the defined validation plans.

Special Recognitions & Awards/Patents Issued

More than 170 patent disclosures have been submitted on the new technologies being investigated in this project.

FY 2012 Publications/Presentations

1. DOE 11Q4 Quarterly Review Presentation, January 2011.

2. DOE 12Q1 Quarterly Review Presentation, March 2011.

3. ICEPAG Conference Presentation, February 2012.

4. DOE Peer Review Presentation, April 2012.

5. DOE 12Q2 Quarterly Review Presentation, June 2011.

6. 2012 ASME Turbo Expo Presentation, June 2012.

7. Bradley, T., Marra, J., 2012, "Advanced Hydrogen Turbine Development Update," ASME paper GT2012-68169.

III. OXY-FUEL TURBINES

III.1 Recovery Act: Oxy-Fuel Turbo Machinery Development for Energy Intensive Industrial Applications

Rebecca Hollis
Clean Energy Systems, Inc. (CES)
3035 Prospect Park Dr., Suite 150
Rancho Cordova, CA 95670
Phone: (916) 638-7967; Fax: (916) 638-0167
Email: rhollis@CleanEnergySystems.com

DOE Project Manager: Travis Shultz
Phone: (304) 285-1370
Email: Travis.Shultz@netl.doe.gov

Subcontractors:

- Siemens Energy, Inc., Houston, TX
- Florida Turbine Technologies, Inc., Jupiter, FL
- Integrated Engineers & Contractors Co., Sacramento, CA

Contract Number: NT42645

Start Date: October 1, 2005
End Date: September 30, 2014

Fiscal Year (FY) 2012 Objectives

- Disassemble, inspect, and repair all elements of the purchased Siemens gas turbine (SGT) necessary for the conversion to a commercial-scale oxy-fuel turbine (OFT).
- Re-assemble SGT with new engine components to produce a high-temperature intermediate pressure turbine (IPT) for use in industrial oxy-fuel (O-F) applications.
- Complete the detailed design of a test site capable of supporting low-power demonstration testing of an industrial-scale OFT.
- Complete the manufacturing and installation of a pilot-scale O-F reheat combustor and test rig for validation testing of the OFT's combustion system.

FY 2012 Accomplishments

- After arriving at the TurboCare Houston facility in May 2011, all components of a used SGT-900 B12 engine necessary for OFT engine assembly were disassembled, inspected and repaired/refurbished.
- Working with Florida Turbine Technologies, Inc. (FTT), TurboCare completed the manufacture of six new major OFT engine components in March of 2012 and by June had completed the assembly OFT-900, of the world's first industrial-scale OFT. Major build activities included removal of the SGT-900's compressor blades and vanes, installation of a new thrust balance system and repair, rework and high-speed balance of the engine's rotor assembly.
- Clean Energy Systems, Inc., (CES) identified its existing Kimberlina facility as a low-cost solution for OFT-900 demonstration testing. In conjunction with Integrated Engineers and Contractors Co. (IEC), CES completed the detailed engineering designs required to modify and upgrade any and all balance of plant (BOP) equipment and subsystems necessary to support industrial-scale turbine testing. Redesigned systems included natural gas and oxygen supply, electrical transformers and motor control centers, demineralized water makeup and supply and more.
- In late 2011, CES completed the design and manufacture of a single-can reheat combustor capable of raising steam temperatures from approximately 600°F (316°C) to 2,000°F (1,093°C). During this timeframe a test rig, designed to simulate OFT engine operating conditions, was manufactured and installed at CES' Kimberlina test site. By spring 2012 installation and commissioning activities of the pilot-scale OFT combustion system had concluded and validation testing kicked-off. Pilot-scale testing not only reduces risk to engine hardware but also to program cost and schedule by validating and characterizing engine reheater performance well before full-scale manufacture and operation.

Introduction

CES has developed a novel O-F power generation concept that uses proven aerospace technology to enable near-zero emission power generation from fossil fuels. The core of the technology is a high-pressure O-F combustor that burns gaseous fuels with pure oxygen (O_2) in the presence of water to produce a steam/carbon dioxide (CO_2) working fluid for steam turbines or modified gas turbines. This concept was demonstrated in 2005 when CES' 20 MW_t O-F combustor powered an Elliott steam turbine to export more than 2.5 MW of electricity to the grid during over 1,300 hours of operation. The combustor, or gas generator, has also been demonstrated burning multiple fuels including natural gas (NG), simulated coal-derived syngas, hydrogen-

depleted syngas and liquid fuels. With the support of the U.S. Department of Energy (DOE), CES previously completed the design of a commercial-scale, 100 MW_t oxy-syngas combustor, a combustor large enough to power industrial-sized power generation facilities like the one shown in Figure 1. This O-F power cycle utilizes the gas generator to power a turbine chain including high, intermediate, and low-pressure turbines (HPT, IPT and LPT respectively) before capturing the produced CO_2 that can be sequestered or sold for processes such as enhanced oil recovery (EOR).

O-F cycle studies have shown that the overall system performance is greatly enhanced if the inlet temperature of the IPT can be increased to 1,400–2,280ºF (760–1,250ºC) and higher. While the HPT and LPT can be implemented in O-F cycles through use of existing steam turbine technology (as they operate at moderate temperatures), the IPT requires sophisticated materials and cooling technologies to achieve the greater turbine inlet temperatures necessary for higher plant efficiency. Modern gas turbine engines routinely operate within the desired temperature range while demonstrating long life and durability. CES and its development partners have conducted research that shows gas turbine engines can be adapted to operate in the O-F power cycle with minimal modification and effect on turbine life, thus dramatically shortening development time and cost needed to deploy an O-F compatible, high-temperature IPT.

Approach

In September 2010, CES's cooperative agreement with DOE was modified with the goal to design, develop, and test a commercial-scale O-F IPT that can be deployed in industrial O-F plants that capture greater than 99% of the produced CO_2 at competitive cycle efficiencies and cost of electricity. To accomplish this, CES partnered with FTT to complete a detailed design to convert a commercial Siemens SGT-900 gas turbine to an OFT capable of full-load turbine inlet temperatures of approximately 2,000°F (1,093°C). To reduce program costs and time to demonstration, CES has procured a used Siemens gas turbine that was disassembled, inspected, repaired, and modified according to detailed engineering designs created by FTT. The reassembled engine designated the OFT-900, will be demonstrated at an existing CES facility modified to support low-power, short-duration turbine testing.

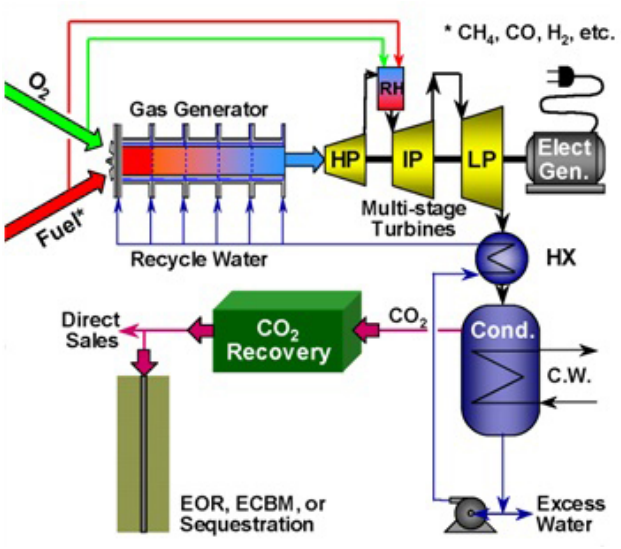

FIGURE 1. Typical oxy-fuel power cycle

Results

Early successes last year led to the completion of major program milestones such as the issuance of all manufacturing and assembly drawings for the OFT-900 and the location and purchase of a used SGT-900 B12 combustion turbine complete with SGT, gearbox, generator, and associated BOP equipment. In May 2011, the purchased SGT-900 B12 arrived at the Siemens TurboCare facility in Houston, Texas. Under sub-contract to CES, the Siemens team completely disassembled the engine and bedplate, identifying all parts to be re-used in the OFT-900. By June 2011 the top half of the SGT-900 turbine casing had been removed (Figure 2). Component inspections took place at three different TurboCare facilities based upon area of expertise: the manufacturing and repair facility located in East Hartford, Connecticut, performed inspections on the turbine ring segments, blades and vanes, while the facility in Rural Hall, North Carolina, performed the inspections on the turbine's inter-stage seals and combustor transition pieces. Larger items, such as the turbine casing, rotor and bearings, remained

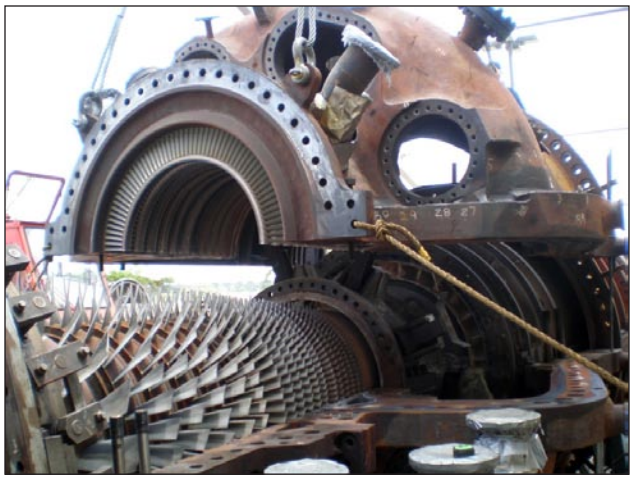

FIGURE 2. Removal of SGT-900 turbine casing

at the TurboCare Houston facility for inspection. All inspection reports were completed and issued for review by October 2011. Final engine assessment concluded that most turbine components were in good condition with only medium to light repairs recommended. By November 2011, CES had kicked-off the Siemens TurboCare team on the refurbishment/repair activities of the SGT components to be reused in the OFT.

In parallel with engine disassembly and inspection, the team also launched manufacturing activities to produce the six new components necessary to convert the SGT to a high-temperature OFT. The new elements included the inlet housing cover, inlet plenum, thrust balance piston, static seal set, inner shaft cover and outer flow guide. Working closely with FTT, the originators of the component designs, and utilizing all American-based Siemens-approved vendors, manufacture of all new components was completed in March 2012. Quality checks were performed on every piece throughout the manufacturing process to ensure the overall engine design intentions were maintained. Utilizing both new O-F elements and refurbished SGT-900 components, engine reassembly was completed in late June 2012 at the Houston TurboCare facility. The OFT was then loaded onto a railcar and shipped to Bakersfield, California, where CES' Kimberlina test facility is located. Figure 3 shows the fully assembled OFT-900 being received at the Bakersfield rail site.

CES partnered with IEC to complete the engineering design of a test facility capable of supporting low-power demonstration of the OFT-900. When operating in near-zero emission power plants the OFT-900 will be capable of producing nearly 150 MW_e with cycle efficiencies of approximately 40%; however, due to funding limitations, initial testing will be limited to 24 MW_e in a simple cycle. Since program kick-off, CES and IEC have worked to (1) characterize the existing equipment and capacities of the CES Kimberlina facility; (2) determine the BOP equipment and support systems required for low-power, short-duration OFT demonstration; and (3) develop detailed plans to modify or upgrade the Kimberlina site to support OFT-900 testing. In March of 2012 test site redesign completed and CES released the Final Design Report for Kimberlina Power Plant upgrades. The report contained over 70 engineering drawings detailing required structural, mechanical and electrical plant upgrades and represented the completion of test site design work. Numerous construction activities have already kicked-off onsite and are expected to continue into early 2013.

To reduce risk, prior to OFT-900 demonstration with reheat combustors, a pilot-scale reheat combustor (RH) test will be conducted at CES' Kimberlina site. Last year CES engineers completed the design of a single-can O-F RH capable of raising steam/CO_2 from 600°F (316°C) to the desired turbine inlet temperature of approximately 2,000°F (1,093°C) at pressures ranging from 25 to 250 psi. Based on CES' patented platelet technology, this RH will replace the existing can-annular combustion system of the SGT-900 and offer improved performance.

The single-can RH and test rig were manufactured and installed at the CES Kimberlina facility in early 2012 (Figure 4). Designed to simulate OFT-900 engine conditions, steam/CO_2 enters the side of the rig, fed by CES' 170 MW_t gas generator. NG and O_2 then enter the front of the rig and are immediately injected into the reheat combustor. A traditional gas turbine spark plug is used to ignite a stoichiometric fuel-O_2 mixture that burns to completion before entering a cool-down section and vertical exhaust stack. Hundreds of instruments continuously monitor pressures, temperatures and flow rates throughout the rig and its feed systems. RH testing began in the Spring 2012 but has since been delayed due malfunctions of test site BOP equipment. Once testing

FIGURE 3. OFT-900 at Bakersfield rail site

FIGURE 4. RH test rig installed at CES Kimberlina

has been completed, the RH performance in a number of areas including combustion efficiency, stability, and controllability will have been characterized.

Conclusions and Future Directions

Excellent progress was made this year toward the demonstration of the world's first industrial-scale O-F turbine. The Siemens TurboCare team worked diligently to complete the disassembly, inspection and repair of an SGT-900 B12 engine, in addition to completing the manufacturing of six new O-F engine components. With the aid of CES contractor FTT the OFT-900 was assembled at the TurboCare Houston facility and shipped to CES' Kimberlina test site. CES worked with IEC to complete the detailed design of a test site capable of supporting low-power, off-grid testing of the OFT. Based upon these designs, construction activities to modify and upgrade CES' Kimberlina facility are underway and are expected to complete in early 2013. Finally, the design, manufacture and commissioning of a pilot-scale O-F reheat combustor and test rig was completed this year. Validation testing of the platelet-style RH was kicked-off but was delayed due to BOP equipment failures.

Next year CES will focus on key activities necessary to reach the program goal of commercial-scale OFT demonstration. These include:

- Completion of Kimberlina site upgrades to support low-power, short-duration OFT demonstration testing.
- Installation and commissioning of the OFT-900 and support systems including lube oil, steam cooling, NG feed, oxygen feed, and engine controls.
- Completion of pilot-scale OFT heat combustor testing.
- Manufacture of a full-annulus of O-F reheat combustors for use in OFT testing.
- Demonstration testing of an industrial-scale OFT-900 with and without reheat combustors.

Special Events/Recognitions

In April 2012, CES participated in a peer review event managed by the DOE's National Energy Technology Laboratory (NETL). Experts from industry traveled to Morgantown, West Virginia, to participate as members of a panel review board. The CES Program (NT42645), as well as many other NETL programs, was reviewed against a standard set of evaluation criteria. Led by the American Society of Mechanical Engineers (ASME) the review panel provides evaluation scores and written comments, i.e., strengths, weaknesses, recommendations, and action items, of the program's scientific and technical approach, and progress to date (setting and achievement milestones). Results are expected in mid-2012.

In May of 2012 an event was held at the TurboCare shop in Houston which focused on the commercial applications of the OFT-900. CES and development partners, Siemens and TurboCare, gave presentations on the engine development to-date and toured site visitors around the OFT-900 assembly that was underway. Representatives from first customer Maersk Oil & Gas discussed several industrial applications and the market potential of the OFT across the globe. Open discussions were held with all participating parties including representatives from NETL and DOE including James Wood, the Deputy Assistant Secretary to the Office of Fossil Energy-Clean Coal.

FY 2012 Publications/Presentations

1. Hollis, R., "Oxy-Fuel Turbo Machinery Development for Energy Intensive Industrial Applications," presentation at the International Colloquium on Environmentally Preferred Advanced Power Generation, Costa Mesa, California, February 2012.

2. Hollis, R., Skutley, P., Ortiz, C., Varkey, V., LePage, D., Brown, B., Davies, D., and Harris, M., Turbo Expo 2012, "Oxy-Fuel Turbomachinery Development for Energy Intensive Applications," ASME Paper No. GT2012-69988.

IV. ADVANCED RESEARCH

A. Aero-Heat Transfer

IV.A.1 Analysis of Gas Turbine Performance

Tom I-P. Shih (Primary Contact),
Kyle Chi, Chien-Shing Li, Christelle Wanko,
Saiprashanth Gomatam Ramachandran
Ames National Laboratory/Purdue University
3317 ARMS, 701 West Stadium Avenue
West Lafayette, IN 47907-2045
Phone: (765) 494-5118; Fax: (765) 494-0307
Email: tomshih@purdue.edu

DOE Project Manager: Robin Ames
Phone: (304) 285-0978
Email: Robin.Ames@netl.doe.gov

Contract Number: AL05205018

Start Date: October 1, 2011
End Date: September 30, 2012

Fiscal Year (FY) 2012 Objectives

- Identify and quantify errors in transient measurements of the heat-transfer coefficient.
- Assess a jet-impingement heat-transfer configuration that does not produce cross flows.
- Assess a triple-impingement configuration for the trailing edge.

FY 2012 Accomplishments

- Identified and quantified errors in a widely used transient technique based on thermochromic liquid crystal (TLC) to measure the heat-transfer coefficient. For a cooling channel with a staggered array of pin fins for heat-transfer enhancement, the TLC technique that uses the 1D exact solution could give reasonably accurate "transient" heat-transfer coefficients. However, the 0D exact solution was shown to give very poor results if the heat-transfer coefficient about the immersed solid—the pin fins in this case —had large variations. This study also showed the heat-transfer coefficient measured by the TLC transient technique to differ considerably from the heat-transfer coefficient obtained under steady-state conditions with isothermal walls. These findings are important because computational fluid dynamics (CFD)-based design tools are validated by these measurements.
- Performed CFD analysis to assess a jet-impingement cooling configuration that do not have cross flows about the impinging jets with and without strategically positioned pin fins for additional heat-transfer enhancement. Results obtained show that adding pin fins on the target wall at locations just below the holes where the coolant exits the impingement configuration reduces the average heat-transfer coefficient on the target wall slightly but increases total heat-transfer rate considerably.
- Performed CFD conjugate analysis to study the flow and heat transfer in a triple-impingement cooling configuration for the trailing edge. Though the configuration was found to produce high heat-transfer rate, it also produces considerable temperature variations within the material—low in regions about jet impingements and high in regions between jet impingements—which induce thermal stress.

Introduction

Developing turbine technologies to operate on coal-derived synthesis gas (syngas), hydrogen fuels, and oxyfuels is critical to the development of advanced power generation technologies, such as the integrated gasification combined cycle (IGCC) for the deployment of near-zero-emission type power plants that can lead to the capture and separation of carbon dioxide (CO_2). Whether the fuel burned is natural gas (the predominant fuel used in current electric power generation gas turbines), syngas, a high hydrogen mixture, or an oxyfuel, the efficiency and service life of the gas turbine engine are strongly affected by the turbine component, where the thermal energy contained in the high-pressure and high-temperature gas is converted into mechanical energy to drive the compressor and the electric generator. The most effective way to increase the efficiency of the turbine component is to raise the temperature of the gas entering the turbine component, which can be as high as the adiabatic flame temperature from the combustion of fuel and oxidizer. Although the temperatures sought today, up to 1,755 K, are still considerably lower than the adiabatic flame temperature (indicating that there is still room to increase efficiency by increasing inlet temperature), 1,755 K already far exceeds the maximum temperature the best superalloys and thermal-barrier coatings (TBC) can withstand and still maintain structural integrity and reliable operation. Thus, cooling—such as internal, film, and impingement—is essential for all parts of the turbine whose surfaces come in contact with the hot gases if a reasonable service life is to be achieved.

Since cooling requires work input (e.g., pressure of cooling flow must be raised high enough to enter the turbine to cool it), effective cooling (i.e., ensure material temperatures to never exceed maximum allowable material temperature) must be accomplished efficiently. This issue deserves increasing attention because of three major reasons. The first is that today's turbines are already designed to operate very close to the material's maximum allowable temperature *based on existing design experience* so that there is little room for mistakes. The second is that industry's current goal is to reduce the cooling flow by 50% to further increase efficiency when it is already extremely difficult to cool effectively with the existing flow rates. This indicates the need for new cooling strategies that can only come about with in-depth understanding of how fluid mechanics affect heat transfer and how external heat transfer with and without film cooling on the hot-gas side is coupled to the internal heat transfer on the cooling side through the superalloy and the TBC. The third is that when the fuel burned is syngas, a hydrogen fuel, or an oxyfuel, the heat transfer characteristics in the turbine on the hot-gas side can increase because of increases in water vapor content, because of increased erosion and deposition tendencies, and because of increases in the hot-gas mass flow rate, making cooling even more difficult. Thus, there is very little room for mistakes in the design of cooling strategies. For example, 10–20 K beyond the maximum allowable temperature could lead to material degradation that terminates service life.

The objective of this project is threefold. The first is to develop and evaluate CFD-based analysis tools that can be used to study heat-transfer issues in the design of the turbine component and to develop guidelines and best practices on their usage. The second is to examine the basis of the experimental methods used to validate CFD design and analysis tools. The third is to apply CFD analysis tools to support the development of turbine technologies for advanced near-zero-emission type coal-based power systems.

Approach

Analysis tools used to design gas-turbine cooling strategies are typically based on quasi-dimensional methods. These analysis tools require inputs on the details of the fluid-flow and heat-transfer processes such as pressure loss coefficients as well as regional or laterally-averaged heat-transfer coefficients. There are two ways to generate the information needed, and they are experimental measurements and CFD simulations. Here, CFD is used, and it is based on the conservation/balance equations of species, continuity, momentum, and energy that govern the three-dimensional flow and heat transfer processes. Depending on the nature of the problem, the effects of turbulence may be modeled by steady Reynolds-averaged Navier-Stokes (RANS), unsteady RANS, detached eddy simulation (DES), or large-eddy simulation (LES).

Results

Transient Measurements of Heat-Transfer Coefficient

In turbine cooling, it is important to know the heat-transfer coefficient from surfaces exposed to convective environments. Transient techniques that use TLC and infrared imaging are widely used to measure the heat-transfer coefficient (h). With these techniques, surface temperature T_{wall} is measured experimentally as a function of time, and that measurement is used with the exact solution for unsteady, zero-dimensional (0D) or one-dimensional (1D) heat conduction into a solid to calculate the local h. In using the 0D or 1D exact solutions, these transient techniques assume h is independent of time, that the free-stream or bulk temperature characterizing the convection environment is a constant, and that the conduction into the solid is 0D or 1D. In this study, CFD conjugate analyses were performed to examine the errors invoked by these assumptions for a problem, where the free-stream/bulk temperature and h vary appreciably along the surface and where conduction into the solid may not be 0D or 1D. The problem selected to assess these errors is a cooling channel with a staggered array of pin fins for heat-transfer enhancement. This conjugate study uses three-dimensional (3D) steady and unsteady RANS closed by the shear-stress transport (SST) turbulence model for the gas phase (wall functions not used) and the Fourier law for the solid phase. The errors are assessed by comparing h predicted by the 3D CFD with those predicted by the 0D and 1D exact solutions, where the surface temperatures needed by the exact solutions were taken from the 3D CFD solution. Results obtained show the 1D exact solution for the semi-infinite wall to give reasonably accurate h (< 2% relative error) for the walls of the cooling channel. However, the 0D exact solution was found to produce considerable errors (up to 200% relative error) for the pin fins because h varies appreciably about each pin fin. This study also showed the h measured by the TLC transient technique to differ considerably from the h obtained under steady-state conditions with isothermal walls (up to 20–30% relative error).

Jet-Impingement Heat Transfer

Computations were performed to study the flow and heat transfer in a jet-impingement configuration (Figure 1) in which there is no cross flow about the impinging cooling jets. The configuration studied

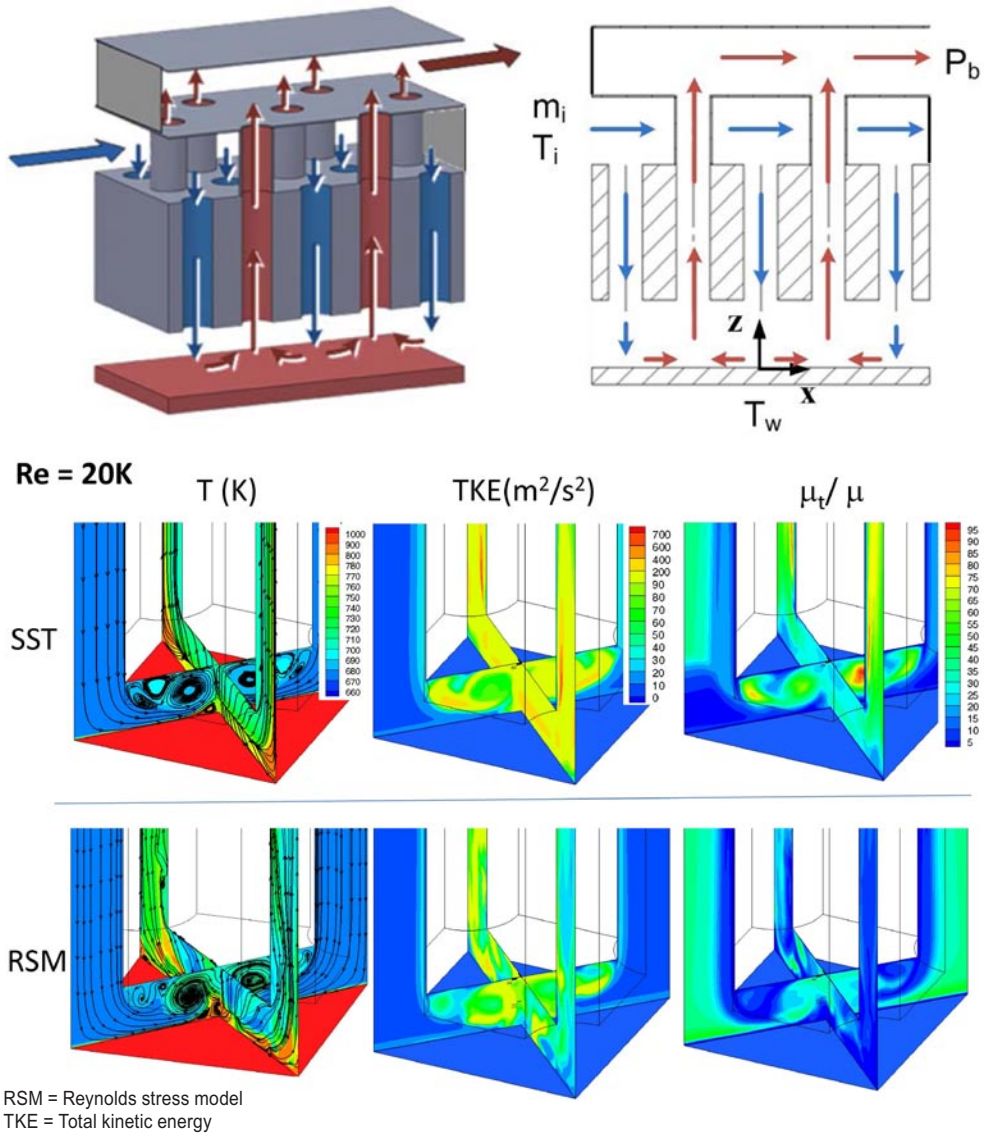

FIGURE 1. Temperature, turbulent kinetic energy, and ratio of turbulent to laminar viscosity in two perpendicular planes that pass through the middle of the impinging and returning jets for the jet-impingement configuration

consists of two sets of staggered arrays of holes with one array of holes for jets to impinge and cool a target wall with or without strategically positioned pin fins and a second array positioned midway relative to the first array of holes for the impinging jets to exit the configuration. For this configuration, the following parameters were investigated: distance between the jet-hole exit and the target surface to be cooled (H/d = 0.5, 1, 4); spacing between jets (S/d = 2, 4); and pin-fin height (H_p/d = 0, 1, 2) on the target surface, where d is the diameter of the holes in the arrays. Also, the jet-impingement velocity was varied to study a range of Reynolds numbers based on the hole diameter d and the mean velocity of the jet in the hole (Re_d = 20,000, 40,000, and 60,000). For all cases studied, the temperature of the coolant air is 673 K; the wall to be cooled is maintained at 1,273 K; and the static pressure at the exit of the jet-impingement array is maintained at 25 bars. This computational study is based on steady RANS with the SST model and the stress-omega full Reynolds stress model. Results obtained show the average Nusselt number on the target wall to increase as the jet Reynolds number (Re_d) increases and as H/d and S/d decrease (Figure 2). Adding pin fins on the target wall at locations just below the holes where the coolant exits the impingement configuration reduces the average heat-transfer coefficient on the target wall by up to 6% and increases pressure loss by up to 4.5%, but increases total heat-transfer rate by up to 67%.

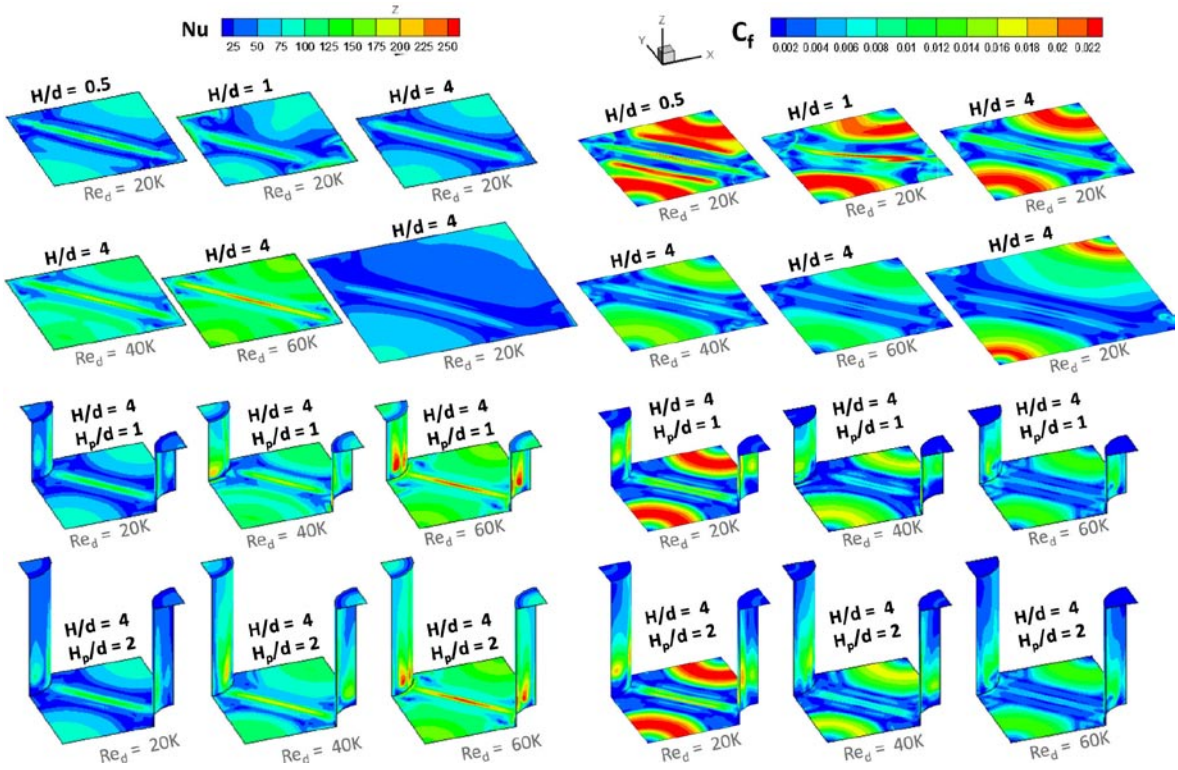

FIGURE 2. Predicted Nusselt number and friction coefficient on the target surface on the jet-impingement configuration

Triple-Impingement Heat Transfer for the Trailing Edge

CFD conjugate analysis based on steady RANS with the SST model was performed to study the flow and heat transfer in a triple-impingement cooling configuration for the trailing edge. Parameters studied include the pressure drop across the configuration (1, 2, 3, 4, and 5 bars) and the heat transfer coefficient on the hot-gas side (2,000, 4,000, and 6,000 W/m^2-K). In all cases with conjugate analysis, the temperature of the coolant at the inlet of the cooling passage is 673 K, the external hot-gas temperature is 1,755 K, and the static pressure at the exit of cooling passage is 25 bars. Simulations were also performed in which the temperature of the cooling-passage wall is kept constant at 1,173 K. Results obtained show the triple-impingement configuration to produce high heat-transfer rate but also considerable temperature variations with valleys and peaks in the turbine material, low in regions about jet impingements and high in regions between jet impingements. This temperature variations within the material creates thermal stress.

Conclusions and Future Directions

Since CFD-based design tools are validated by experimental measurements, it is important to examine the assumptions invoked by the experimental methods of analysis. Future work includes studies on different geometric configurations and operating conditions.

On jet-impingement heat transfer, the results obtained show that the traditional measures such as the average Nusselt number or the Stanton number may not always reveal what is the best heat-enhancement design. Future work includes further exploration on dimensionless parameters that may be more revealing.

On the triple-impingement configuration, the Biot number affects the temperature variation within the turbine material. Future work includes performing analysis on the thermal stresses and the deformations induced by the stresses.

Special Recognitions & Awards/Patents Issued

1. "Momentum Preserving Film-Cooling Shaped Holes," Tom Shih and Sangkwon Na through Iowa State University, Patent Number: 7,997,867, August 11, 2011.

2. "Preventing Hot Gas Ingestion by Film-Cooling Jets via Flow-Aligned Blockers," Tom Shih and Sangkwon Na through Iowa State University, Patent Number: 8,066,478, November 29, 2011.

FY 2012 Publications/Presentations

1. Tchatchouang, C.W., Chi, X., Shih, T.I-P., Bryden, K.M., Ames, R., and Dennis, R.A., "Effects of Turbulence Modeling in Predicting Flow and Heat Transfer in a Duct with Pin Fins," AIAA Paper 2012-0527, January 2012, Nashville, Tennessee.

2. Chi, X. and Shih, T.I-P., "Bulk Temperature, Heat-Transfer Coefficient, and Nusselt Number—Revisited," AIAA Paper 2012-0807, January 2012, Nashville, Tennessee.

3. Shih, Tom I-P., Saiprashanth Gomatam Ramachandran, Ames, R., and Dennis, R.A., "CFD Conjugate Analysis of Transient Measurements of the Heat-Transfer Coefficient in a Duct with Pin Fins," AIAA Paper 2012-0812, January 2012, Nashville, Tennessee.

4. Liu, J., Weaver, A., Lee, C.S., Shih, T.I-P., Klinger, J., Ames, R., and Dennis, R.A., "Flow and Heat Transfer in a Triple-Impingement Configuration for Trailing-Edge Cooling," ASME Paper GT-2012-70075, June 2012, Copenhagen, Denmark.

5. Lee, C.-S., Shih, T.I-P., Bryden, K.M., Ames, R., and Dennis, R.A., "Flow and Heat Transfer in a Jet-Impingement Configuration with No-Cross Flow about Jets," ASME Paper GT-2012-70080, June 2012, Copenhagen, Denmark.

IV.A.2 Demonstration of Enabling Spar-Shell™ Cooling Technology in Gas Turbines

James P. Downs
Florida Turbine Technologies, Inc.
1701 Military Trail, Suite 110
Jupiter, FL 33458-7101
Phone: (561) 427-6250; Fax: (561) 427-6190
Email: jdowns@fttinc.com

DOE Project Manager: Travis Shultz
Phone: (304) 285-1370
Email: Travis.Shultz@netl.doe.gov

Contract Number: FE0006696

Start Date: July 8, 2011
End Date: July 31, 2012

Fiscal Year (FY) 2012 Objectives

- Demonstrate the benefits of Spar-Shell™ technology to provide desired durability in a real gas turbine engine operating environment while cooling flow is reduced by a target of 40%.
- Demonstrate manufacturability and inspectability of the hardware as evidenced by acceptance of the hardware for installation in the defined test article.
- Verify engine efficiency, performance and operability in the presence of the new first stage turbine vane hardware.
- Demonstrate retrofitability of hardware into existing turbomachinery as defined by ease of installation, operation and maintenance.

FY 2012 Accomplishments

- Florida Turbine Technologies, Inc., (FTT) established an agreement with Siemens Energy, Inc., to participate in this project.
- A suitable test vehicle was identified, and a target date for insertion of Spar-Shell™ turbine components into that vehicle was defined.
- The concept design of a Spar-Shell™ vane was completed, and work on the detailed design has progressed to the point where casting details have been released to production.
- Thermal and structural analyses were performed to support the feasibility of the design.
- Fabrication feasibility and cost assessments were facilitated with FTT manufacturing and procurement support.
- Prototype models have been fabricated to demonstrate/illustrate the design concept and to prove the manufacturing feasibility of the concept.

Introduction

Turbine cooling and other technology development that has occurred over the past several decades has enabled the production of highly efficient gas turbine systems that are in common use today. In one example, turbomachinery systems provide the fundamental foundation of aircraft propulsion, which is the backbone of our present aviation industry. In another example, which is of particular interest here, turbomachinery systems are widely used in ground-based industrial applications such as those used for the production of electricity. In the latter case, when combined with a suitable bottoming cycle where exhaust heat is utilized in a Rankine steam cycle, the so-called "combined cycle" system offers an efficient and clean process for producing electricity relative to some of the alternatives such as the direct combustion of fossil fuels to produce the steam needed to drive a turbine-generator set. Further, the combined cycle system can be fueled with a variety of fuel types including oil, gas and coal-derived syngas or hydrogen.

Economics are expected to continue to play a critical role in the development and ultimate selection of future power production systems. Meanwhile, it is clear that new market forces will also play a significant role and have a sizable impact on the industry. Recent concerns, including the production of carbon dioxide and its relationship to global warming, have promoted increased use of gas turbines to produce electricity relative to these other alternatives. In fact, many coal-fired power plants have been cancelled [1] in recent years due to strong public opposition combined with the uncertainty over the future costs of complying with carbon dioxide emission caps and concerns about global warming's environmental and economic impacts. In many of these instances [2], other means of producing electricity, including gas-fired power generation using combined-cycle systems are being pursued as more efficient and cleaner alternatives.

Since the invention of the gas turbine, many technological advancements have been introduced

throughout the machine to increase the power, performance and overall efficiency as well as other attributes such as the cost and longevity of equipment. Many of these advancements have improved the efficiency of specific components, but the most significant improvements have been realized with the development of technologies that permit the temperature and pressure of the turbine working fluid to be increased. To this end, turbine cooling represents an enabling technology that thrusts gas turbines to the forefront as a competitive means of producing power in the modern marketplace.

The fundamental cooling methods permit the turbine components to operate with reduced temperatures relative to the temperature of the hot gases (working fluid) that flow around them. The amount of cooling required by a typical turbine component depends on the material used, the specific environment the component is subjected to and the efficiencies of the convective and film (if applicable) cooling systems.

Despite the use of cooling methods, modern turbines are subject to distress from repeated long-term exposure to the environment of the hot gas flowpath. Information available in the literature [3] shows that turbine and other hot section related issues cause the bulk of major failures in gas turbines. In fact, as shown in Figure 1, turbine-related issues are reported to cause 53% of failures in gas turbines smaller than 170 MW. Larger turbines are reported to be subject to a higher percentage of compressor-related issues, but combined hot section (combustor and turbine) issues still account for over 50% of failures. Turbine components and other hot section hardware are particularly susceptible to distress and deterioration because these parts are subjected to an extremely deleterious environment.

Despite the fact that cooling is successfully used to prolong the serviceability of these parts beyond that which could otherwise be achieved, material limits are routinely approached in the design of cooled turbine components. This is a natural consequence of the need to minimize cooling requirements so that the power and performance of the machine can be optimized. At the same time, this design approach places cooled turbine components in a position of risk. If the cooling system does not work as expected, or is compromised in some way, then material limits can be exceeded, leading to a part that experiences premature distress or failure.

This project supports Spar-Shell™ cooling technology development of a first-stage turbine component that can be installed into an existing F-Class gas turbine system to demonstrate the proof-of-concept, validate the hardware manufacture, performance and operability in the engine and to clear this hurdle toward full scale production and marketing of the product for commercial sale and revenue-producing service within the power sector. To accomplish this task, FTT is working to modify existing F-Class first stage turbine vane hardware to incorporate the sequential impingement cooling system patented by FTT and proposed for Spar-Shell™ turbine vanes. Use of this cooling technology has been shown to be capable of reducing cooling flows by approximately 40%.

Development of the Spar-Shell™ turbine vane has been supported by a U.S. Department of Energy Phase I Small Business Innovative Research (SBIR) titled "Development of Innovative Cooling for Robust Design." Under this SBIR program, FTT has been investigating alternative solutions to problems such as this to make the part more robust but without the need to use excessive quantities of cooling air. To give an example, consider a first stage turbine vane shown in Figure 2 which is typically cooled by the three methods: internal cooling by convection heat transfer, ejection of spent coolant to provide a film cooling effect, and the use of thermal barrier coating (TBC) as a layer of thermal protection. In these parts, the internal cooling by convection heat

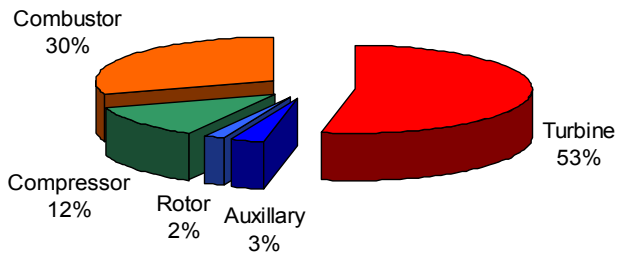

FIGURE 1. Major failures in gas turbines less than 170 MW

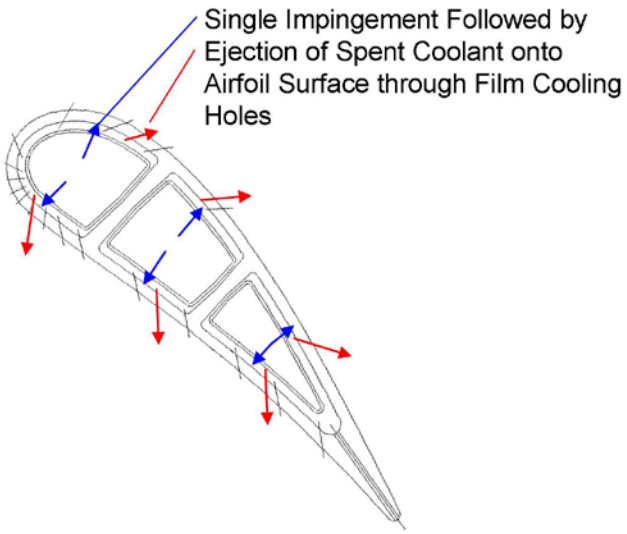

FIGURE 2. Current state-of-the-art first stage turbine vane uses single impingement

transfer is typically accomplished by impingement of cooling air onto the internal surfaces of the component. To facilitate this mechanism, tubes containing a myriad of holes are inserted into the component. Coolant is allowed to flow into the tubes and then into the myriad of holes to form jets which impinge onto the internal surfaces of the airfoil structure. Once the coolant has accomplished the internal cooling by convection heat transfer, it is allowed to enter film cooling holes where it is ejected from the part to form a film cooling effect. In the meantime, the TBC coating provides an insulative barrier which reduces the heat load on the part and further protects it from the hot gases flowing around it.

Realization of significant turbine cooling flow reduction requires the duty of the convective cooling system to be improved relative to the current state-of-the-art. Further, the requirements for film cooling flow must be reduced because reduced cooling flow will have the immediate effect of decreasing the film cooling performance. This is especially true in turbine components located in the first stages of the turbine. To achieve these objectives, turbine designs must be made capable of supporting increasing flows of heat through the walls of the component to provide the desired cooling effects. The material and coating systems must be capable of supporting these increased heat flows without incurring deleterious consequences.

Approach

To improve internal convection heat transfer, FTT has developed an innovative cooling system based on the use of sequential impingement. A schematic representation of such a system from the FTT patent (US8096766) is illustrated in Figure 3. As shown in this figure, coolant flow enters a supply cavity located centrally within the airfoil. The coolant first passes through impingement cooling holes from the supply cavity to impinge directly on a defined heat transfer surface. Second, this flow is returned to return cavities located within the inner structure to be circulated to another region of the part where it again passes through holes to impinge on a second heat transfer surface of interest. The process can be repeated several times within the range of allowable pressure conditions for the coolant. Ideally, the first impingement regions would be directed at surfaces adjoining high gaspath pressures, such as the leading edge and forward pressure side surfaces. Secondary impingement could be directed at surfaces adjacent to lower gaspath pressure regions such as the aft pressure side, and finally, the suction side of the airfoil. Using this system, cooling flow could be leveraged by impinging on separate heat transfer surfaces in a sequential fashion. Further, this approach might be useful to reduce or eliminate the effects of impingement

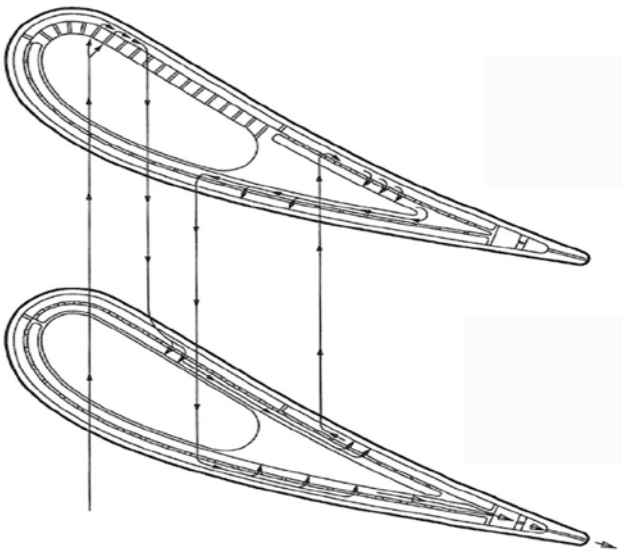

FIGURE 3. Sequential impingement using a spent-flow return system

heat transfer degradation due to cross flow, which are prevalent in existing impingement cooling designs.

Under this program, FTT is pursuing demonstrator application of work that derives from, extends and logically concludes work performed under the aforementioned SBIR programs. The program approach consists of delivering and testing of the first demonstrator turbine vane hardware with the Spar-Shell™ enabling cooling technology incorporated.

Results

This project was put under contract and a kick-off meeting was held on July 25, 2011. Further, agreement was reached with an original equipment manufacturer (OEM), namely Siemens Energy, to participate in this project through (1) identification of a suitable gas turbine engine test article that may be used for the initial test evaluation of Spar-Shell™ vanes in the company's Berlin Test Bed, (2) participation in the design and risk assessment activities, and (3) participation as a proving ground and commercial sales partner.

To date, a suitable gas turbine engine test article has been identified, and a target date for insertion of Spar-Shell™ turbine components into that vehicle has been defined. Also, Siemens Energy has participated in reviews of the design and also in risk analysis activities.

Work was performed to identify a Spar-Shell™ concept design configuration. This work culminated in an evaluation of several concept designs, and down-selection to the configuration to proceed forward into the detailed design phase was completed during a concept design review. This work was supported by

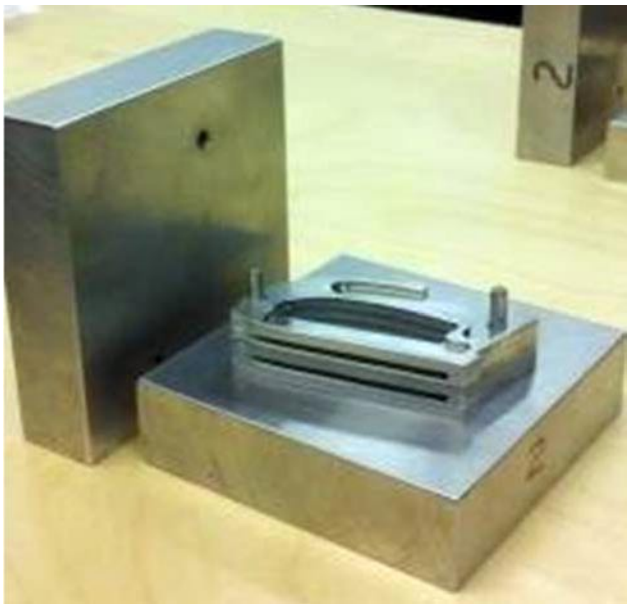

FIGURE 4. Spar-Shell™ vane insert manufacturing trial

mechanical/configuration design, materials selection, heat transfer and structural design and analyses and by manufacturing and procurement. In addition, hardware was manufactured to demonstrate/illustrate the design concept and to prove the manufacturing feasibility of the concept. Risk management continues with evaluation of the possible failure scenarios and identification of mitigation controls that can be put into place. Work on the detailed design of hardware progressed to a release of the casting to production, a milestone which permits manufacturing work on the long lead materials, and in particular the cast parts, to begin.

Prototype models have been fabricated to illustrate the design and to demonstrate the manufacturing feasibility of the concept. One such model of the spar insert arrangement is shown in Figure 4.

Conclusions and Future Directions

The impact of this program is projected to revolutionize the gas turbine industry with the implemention of innovative cooling approaches for robust design. These approaches are needed to provide durable turbines while realizing the future turbine system goals of reduced cooling flow consumption and increased efficiency. Development of these approaches offers several advantages relative to the current state-of-the-art. To provide these designs, innovative cooling design approaches are being developed based on FTT's Spar-Shell™ technology to make turbine hardware capable of performing efficiently and without failure over a wide range of conditions.

The advantages of this technology are compelling. By retrofitting this technology into the installed gas turbine-based electrical power generation capacity, development of the technology has the potential to reduce U.S. dependance on foreign sources of energy with an equivalent oil savings of 84 million barrels of oil per year, which equates to four days of U.S. consumption. The technology will also reduce carbon dioxide emissions by 25 million tons per year.

Development of this technology will maintain the U.S. technological leadership and competitiveness in this important field of gas turbine-based electrical power generation. The innovative nature of the technology will also forge new relationships between industry, academia and government, as these organizations build a new spirit of cooperation and collaboration to understand all of the ramifications of the technology.

Special Recognitions & Awards/Patents Issued

1. US8167537, "Air-Cooled Turbine Airfoil with Sequential Impingement Cooling," William L. Plank, James P. Downs, and John A. Fedock, May 1, 2012.

FY 2012 Publications/Presentations

1. James P. Downs, "Demonstration of Enabling Spar-Shell Cooling Technology in Gas Turbines," Presentation during University Turbine Systems Research (UTSR) workshop, October 27, 2011.

2. James P. Downs, "Perspectives on R&D Needs for Gas Turbine Power Generation," Presentation during University Turbine Systems Research (UTSR) workshop, October 26, 2011.

References

1. "$45.3 Billion in U.S. Coal-Fired Power Plants Cancelled in 2007," Fact Sheet by *Resource Media*, January 8, 2008.

2. "FPL Pursues More Gas-Fired Power Generation in Florida," *EnergyOnline.com News*, December 7, 2007.

3. Boyce, M.P., *Gas Turbine Engineering Handbook*, 3rd Ed., page 895, Gulf Professional Publishing, 2006.

IV.A.3 Phase III Xlerator Program: Rapid Commercialization of Advanced Turbine Blades for IGCC Power Plants

John R. Paulus
Mikro Systems, Inc.
1180 Seminole Trail
Charlottesville, VA 22901
Phone: (434) 244-6480 Ext. 205; Fax: (434) 244-6485
Email: paulus@Mikrosystems.com

DOE Project Manager: Travis Shultz
Phone: (304) 285-1370
Email: Travis.Shultz@netl.doe.gov

Subcontractor:
PCC Airfoils, Mentor, OH

Contract Number: FE0006220

Start Date: October 1, 2010
End Date: October 1, 2012

Fiscal Year (FY) 2012 Objectives

Produce baseline 501F core. The project will focus on an existing original equipment manufacturer (OEM) blade, SEI SGT6-5000F Row 1 blade, as the baseline design. Specific objectives include:

- Produce core tooling for initial set of ceramic cores.
- Produce the first 16 prototype ceramic cores, and run foundry trial.
- Produce 80 cores for a series of pre-production qualification (PPQ) trials at PCC Airfoils (PCC) foundry.

Scale up production. In order to commercialize the production of ceramic cores, Mikro Systems must scale up its current production capabilities. Specific objectives include:

- Increase total core throughput volume. This will be accomplished through the establishment of a low rate initial production (LRIP) facility at Mikro Systems capable of producing approximately 200 fired cores per month, an increase from the current laboratory level of 80 cores per month.
- Improve the overall process yield. This requires a careful study of the nature of part failures, testing and tracking improvements.
- Reduce the required labor to fabricate a part (touch time). To accomplish this, an Initial State Value Stream map of the core fabrication process will be charted to understand where the time is spent and where it can best be reduced. This will have many over-laps with first bullet as the improved process equipment is implemented.

FY 2012 Accomplishments

- Mikro Systems' TOMO^{SM} Lithographic Molding (TOMO^{SM}) technology for producing industrial gas turbine **(**IGT) investment casting turbine blade cores was licensed to Siemens Energy, Inc. (SEI). Mikro Systems, Inc., and SEI signed a collaborative technology license agreement in April 2011. SEI has since established a full-time staff of 10 people in Charlottesville, Virginia, and is working closely with Mikro Systems at the LRIP facility to learn and refine the core fabrication technology. SEI has leased a facility in Charlottesville for producing IGT cores and wax patterns using TOMO^{SM} technology beginning in late 2012.
- Received 501F core tooling. Mikro Systems received the baseline core tooling and has used it to produce the first 16 prototype cores for metal casting trials.
- Completed the LRIP facility expansion. The LRIP facility is fully complete and in production.
- Produced prototype cores and completed metal casting trial. The metal casting trial and results were provided to Mikro Systems.
- SEI/Mikro Systems focus teams formed:
  - Casting improvement
  - Material development
  - Finishing improvement
- All casting automation/improvement equipment and sequences were individually tested for impact on the part and the material quality.
- Rescaled and remade the core tooling to re-compensate for changes from process improvements during the past year.
- During the production run for the first PPQ inspection, Mikro Systems achieved a 50% overall process yield. This achieves the target goal for FY 2012.
- PPQ trials:
  - Defined schedule of PPQ trials with PCC foundry.
  - First lot of 16 PPQ trial cores produced and inspected by PCC.

Introduction

This American Recovery and Reinvestment Act-funded Small Business Innovation Research Phase III Xlerator project addresses the need for rapid, cost-effective manufacturing of advanced turbine airfoils that will improve efficiency through advanced cooling schemes. These overall system improvements could be utilized in the reduction of the forced air cooling budget or the operation at increased temperatures. This will result in fuel savings and reduced turbine firing emissions in integrated gasification combined cycle (IGCC) and natural gas combined cycle (NGCC) power plants. Based on results from Phase I and from other development programs, Mikro Systems has shown that its manufacturing technology, TOMO^{SM}, can enable the production of turbine blades with internal cooling geometries that are beyond current state-of-the-art. During Phase III, we will scale up the TOMO^{SM} process and produce casting cores for an existing OEM production program, SEI SGT6-5000F Row 1 turbine blade (501F blade). The full testing of these blades by SEI will substantially occur after this project has ended and is outside the scope of this project.

Approach

The ability of the TOMO^{SM} process to produce advanced cooling designs for investment cast parts has been established in prior work in small scale production. The commercialization challenge is to advance the core making process from the present laboratory-level fabrication sequence to a more efficient and higher volume production process. To this end, a new LRIP production area has been built at Mikro Systems for the fabrication of IGT cores. The entire core fabrication process is being carefully studied to improve throughput and yield, and reduce touch labor. Process improvements have been identified and implemented from the beginning of the two-year project period; so far the majority of them have been completed and will continue to be implemented through the remainder of the project. This high volume baseline core will make an excellent platform to test advanced cooling features in future work once the basic core has been qualified. This qualification involves a single prototype casting trial of 16 parts, and then a series of PPQ casting trials at the foundry. SEI has provided a statement of support for in-kind contributions of $1.6 million toward this effort. This will be in the form of engineering support, direct funding for tooling, metal casting costs, and testing and analysis services. Mikro Systems is also working with two foundry experts as consultants, Jim Avery, former engineering manager at Howmet, and Dr. Stuart Uram, founder of Certech.

Results

Mikro Systems received the baseline core tooling and has used it to produce the first 16 prototype cores for metal casting trials. The core proved more difficult to fabricate than initially expected, but the necessary troubleshooting and improvements to the process were implemented to produce a successful production run. These and other IGT cores were produced in the fully complete Mikro Systems LRIP facility, designed to produce 200 cores per month and function as a training and testing facility for TOMO^{SM} IGT core production.

The first prototype metal casting trial results were provided to Mikro Systems. Every part experienced a fault of some kind. The dominant failure mode was from "positive metal" resulting from small cracks in the core which allowed metal to enter the cavity. The root causes of this were carefully studied by Mikro Systems and SEI, and corrective actions taken. These included a material improvement which was less prone to developing cracks and had generally improved high temperature performance. In addition, improved patching materials and methodology were developed, so if a defect is repaired, the repair holds properly through metal casting.

Three primary SEI/Mikro Systems focus teams were formed to improve the process and to address the issue uncovered by the first prototype trial. The focus groups and their tasks are summarized in Figure 1. The combined efforts resulted in improved quality and yield, reduced variability, and improved manufacturability. The high temperature stability of the material was improved dramatically as a result of this work. Figure 2 shows "slump tests" of bars at different stages of the material development cycle. The test bar is placed on spaced blocks with a calculated weight on top of it, and run through a rapid temperature profile up to 1,550°C, or 2,822°F, which represents the temperature of the molten metal during casting. The bar should undergo minimal movement during this test. In addition, the number of fired defects was reduced dramatically. Figure 3 shows an X-ray image of the cores made during the prototype trial and cores made after the process improvements were established. The number of patchable defects was reduced by approximately 80%. The results of the focus team efforts are shown in the high overall process yield achieved during the last production run. Mikro Systems and SEI achieved the established goal for FY 2012 of 50% overall process yield. See Table 1.

During the sequence of improvements, several changes were made that affected the compensation factor. The first change was an alteration to the tooling which allowed the flexible liner to better maintain its correct shape through the casting process. The second change was an alteration to the material formulation that reduced

FIGURE 1. Mikro Systems and SEI technical focus groups

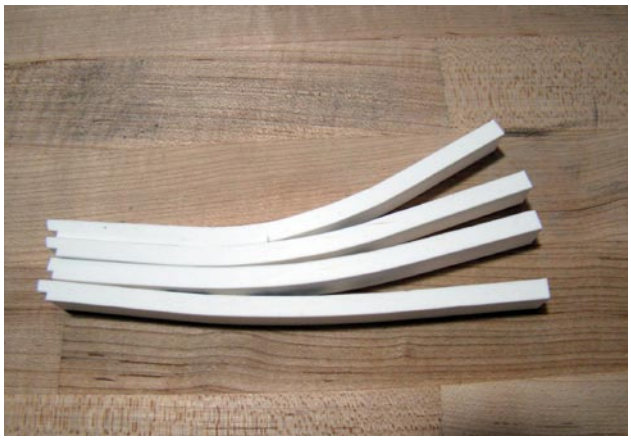

FIGURE 2. High temperature testing of material blends

the fired shrinkage. As a result, parts being produced were of improved contour and material quality but of the wrong general scale. The cores made by the new method were coming out approximately 0.100" oversized overall. This was out of specification and could not be used to continue in pre-production trials. After sufficient data was collected, the core tooling was remade to an adjusted scale. Cores are now being made from this adjusted tooling and are of the correct scale.

Mikro Systems, SEI, and PCC foundry defined a schedule of PPQ trials with PCC foundry. This consists of three trials of 16 parts each followed by another of 32 parts. The schedule is as follows:

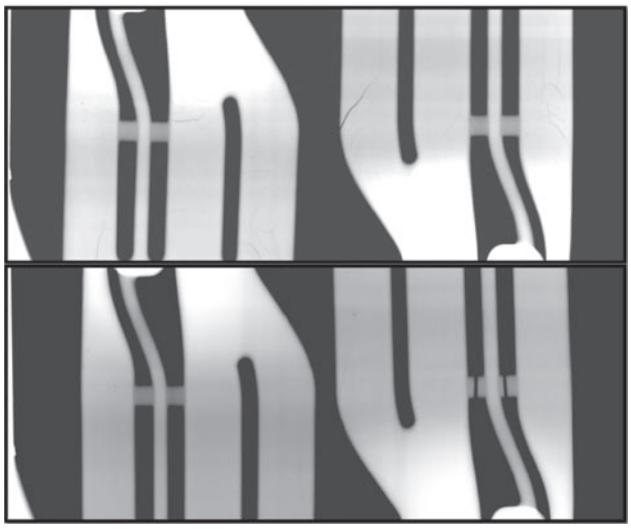

FIGURE 3. Original process cores (top) - show cracks and internal defect lines versus **improved process cores** (bottom) – internal surfaces show a significant improvement

TABLE 1. Yield chart from first production after improvements implemented

Operation	In	Out	Scrap	Yield
Cast	41	41	0	100%
De-Cast	41	37	4	90.20%
Feature Dimension	37	34	3	91.90%
Load	34	34	0	100%
Unload	34	31	3	91.20%
Blue Dye Visual	31	27	4	87.10%
Finish	27	26	1	96.30%
CMM Scan	26	26	0	100%
Quality Review	26	25	1	96.20%
X-Ray	25	22	3	88%
FINAL	**41**	**22**	**19**	**53.70%**

- April 12 Trial 1: 16 cores delivered
- May 24 Trial 2: 16 cores delivered
- July 24 Trial 3: 16 cores delivered
- Sept 24 PPQ: 32 cores delivered

The first lot of 16 PPQ cores were produced and subsequently inspected at the SEI Charlottesville branch office by two members of the PCC foundry quality management group. They found the parts to be vastly improved from the prior shipment. The bulk of their input had to do with hand finishing details which will be easily remedied.

Conclusions and Future Directions

Mikro Systems' TOMO^{SM} core fabrication technology has been licensed by SEI. SEI and Mikro Systems are working closely to bring that technology to full commercial production. Once established, it opens the pathway to bring into the market components with advanced cooling features not previously possible to fabricate. The material improvements and process improvements made during FY 2012 represent important advancements toward commercial viability and are on target with the goals established in the project management plan.

In related work, Mikro Systems is also collaborating with SEI to produce advanced multi-walled cores for Row 1 blades for their new hydrogen engine design. One core design has prototype parts through metal casting, and the other design is ready for wax injection. Mikro Systems is also producing a very large core for Row 4 of the same hydrogen engine. Mikro Systems is able to produce the extreme dimensions of this part through the high strength ceramic binder and the low-pressure de-mold sequence used in the TOMO^{SM} process.

The same TOMO^{SM} technology that is applied to making ceramic cores is also being applied to generating wax patterns. Mikro Systems and SEI are actively using this fabrication platform to produce wax patterns with the same benefits of reduced tooling cost and lead time, and production of advanced features not possible to produce with conventional machining methods. The wax patterns for the 501F cores are being produced in this way.

Mikro Systems is also quoting work for three advanced coupons for the National Energy Technology Laboratory (NETL) Regional University Alliance Turbine Thermal Management project. These various cooling concepts would be tested under pressurized, high temperature combustion gas conditions in NETL's aerothermal test facility in Morgantown, West Virginia.

IV.A.4 Turbine Thermal Management−Aerothermal and Heat Transfer: Airfoil Film Cooling

Mary Anne Alvin (Primary Contact)
U.S. Department of Energy (DOE)
National Energy Technology Laboratory
Regional University Alliance
626 Cochrans Mill Road
Pittsburgh, PA 15236-0940
Phone: (412) 386-5498; Fax: (412) 386-4806
Email: maryanne.alvin@netl.doe.gov

Dr. Srinath Ekkad, Mr. Chris LeBlanc,
Mr. Sridharan Ramesh
Virginia Polytechnic Institute and State University
Department of Mechanical Engineering
100 Randolph Hall
Blacksburg, VA 24061
Phone: (540) 231-7192; Fax: (540) 231-9100
Email: sekkad@vt.edu

Contract Number: 0004000.3.620.243.002

Start Date: October 1, 2011
End Date: September 30, 2012

Fiscal Year (FY) 2012 Objectives

Identify turbine airfoil cooling concepts that provide enhanced heat transfer and reduced coolant flow, and which can be commercially manufactured. Research efforts are focused on development of advanced film cooling concepts that achieve an ~50% reduction in required cooling flow.

FY 2012 Accomplishments

The National Energy Technology Laboratory (NETL)-Regional University Alliance (RUA) Turbine Thermal Management project consists of four research project areas that focus on heat transfer, materials development, and secondary flow control. These projects are being conducted to develop advanced technology designs, components and equipment that contribute to achieving U.S. Department of Energy NETL's Hydrogen Turbine Program goals of three to five percentage point plant efficiency gain by permitting higher turbine firing temperatures as a result of realizing more effective cooling, development and utilization of extreme temperature thermal barrier coating protection systems, and secondary flow leakage reduction.

This report summarizes the FY 2012 research effort scope, approach, and accomplishments with respect to development and performance assessment of novel airfoil film cooling hole configurations. FY 2012 accomplishments follow:

- Virginia Tech demonstrated tripod hole film cooling geometry benefits on pressure and suction side of a typical nozzle guide vane under low speed conditions in a linear cascade wind tunnel. These benefits include lower coolant usage and less dependence on the blowing ratio for both the pressure and suction sides, as well as improved film cooling effectiveness for the suction side.
- Aerodynamic benefits were also demonstrated for the tripod hole film cooling geometry as compared to cylindrical and shaped hole geometries. The tripod holes showed minimal disruption to the downstream flow pattern at all blowing ratios, while the cylindrical and shaped holes disrupted the flow pattern, especially at high blowing ratios.
- The effects of pressure gradients, component curvature and free-stream turbulence effects on film cooling hole performance were evaluated. The tripod hole film cooling geometry, in comparison to the cylindrical and shaped hole geometries, was shown to have a more robust performance under a variety of flow conditions, allowing a potential engine designer more flexibility in the utilization of film cooling holes.
- Tripod hole manufacturability for airfoil geometries was assessed. Mikro Systems, Inc., has indicated that there would be no issues with construction of the new hole geometries, and indicated that their process has the added benefit of fewer sharp corners that would result in stress risers/concentrations that typically lead to crack initiation.
- A thermo-mechanical stress analysis was conducted for the cylindrical and tripod hole designs. The magnitude of the stress was similar for both cases, indicating that thermal stresses will not be the limiting factor of the tripod design.

Introduction

Due to stringent requirements of component life and stress limits, effective airfoil cooling has become an important issue for modern turbine engines. The

next generations of land-based gas turbine engines that are targeted to operate at higher temperatures have an urgent need for innovative film cooling designs that show improved cooling performance with less coolant usage, and which are also less prone to the detrimental effects of thermal barrier coating blockage.

Currently airfoil film cooling holes are arranged with spacing of three hole diameters apart and are typically angled simple or compound with some holes shaped at the exit. Investigators have already shown the benefits and rationale for use of a new tripod hole film cooling design in previous flat plate wind tunnel studies. The tripod hole configuration will use a lesser number of hole inputs but an increased number of exit, and essentially spread more coolant transversely with 50% less coolant. Results have shown that the tripod hole design leads to a 60–70% enhancement in cooling effectiveness with a 50% reduction in coolant mass flow.

Notably, a 50% reduction in film cooling flow with the use of tripod hole designs will directly impact superalloy or single crystal substrate material strength and thermal stress. The reduced cooling flow usage on the film cooling side will also reduce aero losses and improve overall thermal efficiency of the entire engine. With the improved coverage, there is a possibility to use current cooling flow levels to enhance turbine inlet temperatures without further enhanced thermal barrier coatings (TBCs) or material properties.

Approach and Results

Film cooling using tripod holes is being evaluated using flat surfaces, low speed cascades, and testing in NETL's aerothermal test facility. Commercial manufacturability of the tripod hole design is also being addressed, as well as associated local thermal stress, creep and fatigue issues on structural material stability during extended operation in advanced engine gas passages. The technical approach and the results generated for the tripod hole film cooling effort in FY 2012 are described in the following sections.

Assessment of Shaped Hole Geometry for Comparison in Airfoil Applications

Experimental testing at Virginia Tech has shown a clear advantage for the tripod hole design as applied to the GE E^3 first stage vane profile in comparison to the baseline cylindrical hole design. Flat plate testing conducted with variable mass flow rated indicated that the tripod design outperforms the cylindrical and shaped holes on the suction side of the blade, while the shaped hole performs the best on the pressure side. The tripod design also shows less variation due to blowing ratio than the cylindrical and shaped hole designs.

Optimize Tripod Hole Geometry for Airfoil Applications

Having demonstrated the potential for improved performance by using the tripod hole geometry, investigation into variations on the preliminary design was initiated. Parameters that were explored included the spacing between hole groups and the divergence angle of the outside legs of the tripod design (Figure 1). The first alternate tripod hole design utilized a 30° angle of divergence for the outer legs instead of the 15° angle of divergence of the preliminary design, as well as increasing the center-to-center spacing from six diameters to seven and a half diameters. The wall thickness was also lower for this design so that all three legs of the hole set shared the same plenum inlet location. The second alternate tripod hole design utilized the same 15° angle of divergence as the preliminary design, but added a 5° flare and laydown shaping to hole exits. The third alternate tripod hole design again used the 15° angle of divergence as the preliminary design, but added a 10° flare and laydown shaping to the hole exits. The third design's shaping resulted in overlapping sections between adjacent hole sets.

(a) First alternate tripod hole design (b) Second alternate tripod hole design (c) Third alternate tripod hole design

FIGURE 1. Tripod hole designs evaluated in terms of performance and manufacturability

Examination of Aerodynamic Effects in the New Low Speed Cascade with GE E^3 Airfoils

Flat plate experimental results provided adequate motivation to explore the use of tripod holes on a more realistic surface. Virginia Tech constructed a low-speed five-vane cascade using the publicly available GE E^3 airfoil profile. Flow characterization tests on the cascade indicated that the flow is well suited for experimental measurement, with a steady flow distribution spanwise and no detected flow separation along the blade surface. Consisting of a rake of pressure tubes 0.5 axial chord lengths before and after the center vane, testing was conducted using a solid vane, a vane with cylindrical holes on suction and pressure sides, a vane with shaped holes on suction and pressure sides, and a vane with anti-vortex holes on suction and pressure sides. The cylindrical and shaped hole geometries were tested with blowing ratios of 0, 0.5, 1.0, 1.5 and 2.0, and the anti-vortex hole geometry were tested with blowing ratios of 0, 1.0, 2.0, 3.0 and 4.0.

Results indicated that the basic cylindrical holes disrupt the cascade exit flow very little at the lowest blowing ratio, with progressively more disruption as the flow rate is increased. The tripod holes showed almost no disruption of the cascade exit flow until the very highest blowing ratio, at which point a small disruption of the flow was observed. The shaped holes showed some disruption of the cascade exit flow at moderate blowing ratios, and an extreme disruption at the highest studied blowing ratio. This comparison illustrates a clear aerodynamic benefit of the tripod hole design.

Numerical Analysis of Film Cooling Effectiveness

Computational fluid dynamics (CFD) was used to study the effects of cooling hole geometries. The focus of this research effort was to develop a numerical model that can predict film cooling effectiveness, incorporating the flow physics around the cooling holes. Thermo-mechanical stresses resulting from the temperature gradient in the plate material were then studied. Proposed tripod holes (Anti-Vortex 15° and 30°; Figure 2) along with the conventional cylindrical holes were analyzed and numerical results were compared against experimental data.

CFD Fluid Flow Modeling

Commercial CFD package, ANSYS 13.0/14.0, was used to perform these simulations. Geometry included a flat plate test section on a flat plate test rig. The blade (approximated with a flat plate model in this case) was either insulated in order to evaluate adiabatic film cooling effectiveness or ABS (acrylonitrile butadiene styrene, material used to print blades/flat plates which are used for experiments) to find the conduction correction factor. Additional studies included Haynes 230 alloy for the blade material so that the resulting temperature contour would be used for thermo-mechanical analysis.

Coolant (air) enters the plenum chamber at 25°C and forms a uniform mixture inside the chamber before entering cooling holes. Hot gas (air) enters through mainstream inlet at 50°C and flows past the blade surface. The geometry is imported to CFD mesher were tetrahedral meshes (four to five million elements) were applied on the geometry along with inflation layers on the blade. A non-buoyant Navier-Stokes equation was solved, and different turbulence models were tested (k-epsilon, k-omega standard, k-omega shear stress transport). Among these only the k-epsilon model was found to give converging results, and therefore all subsequent CFD simulations, the k-epsilon model was used.

Temperature profiles for different cooling holes were compared at the same blowing ratios (Figure 3a). With almost half the coolant mass flow, the tripod holes proved to have better cooling effectiveness, owing to the fact that both the tripod holes (AV15 and AV30) seemed to have a better lateral diffusion in the near hole region. In the downstream region around x/D ~20, coolant finally diffuses laterally, providing better cooling. The near hole region has the most benefit from tripod holes even though the CFD actually underpredicts the actual effectiveness (Figure 3b). Unlike tripod holes, the CFD results for the cylindrical holes appear almost coincident with the actual experimental result.

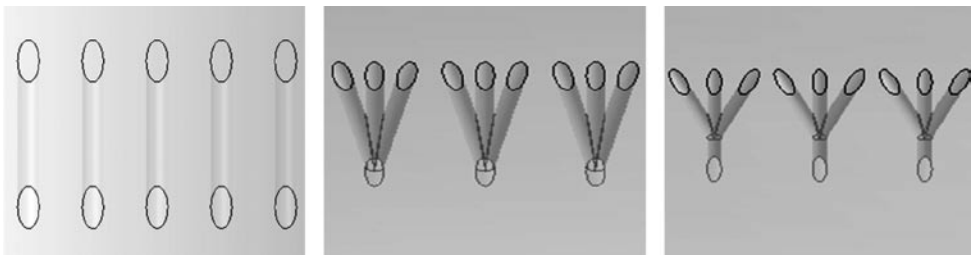

FIGURE 2. Cylindrical and tripod hole configurations

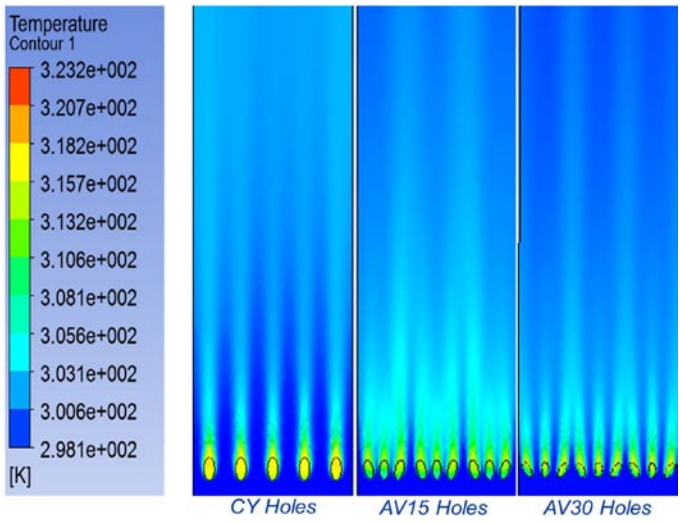

(a) Temperature contours

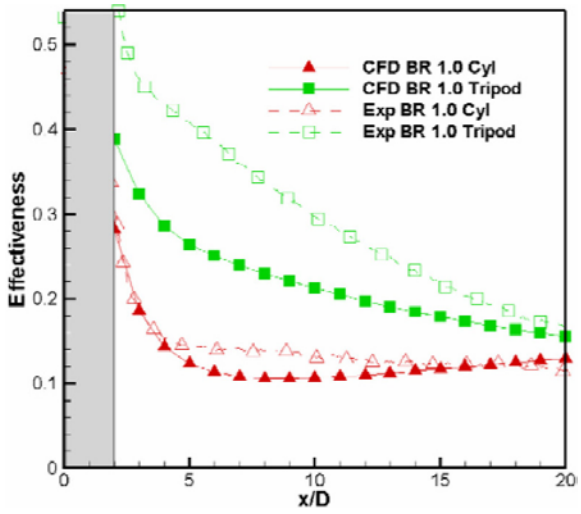

(b) Laterally averaged effectiveness

FIGURE 3. Fluid flow results

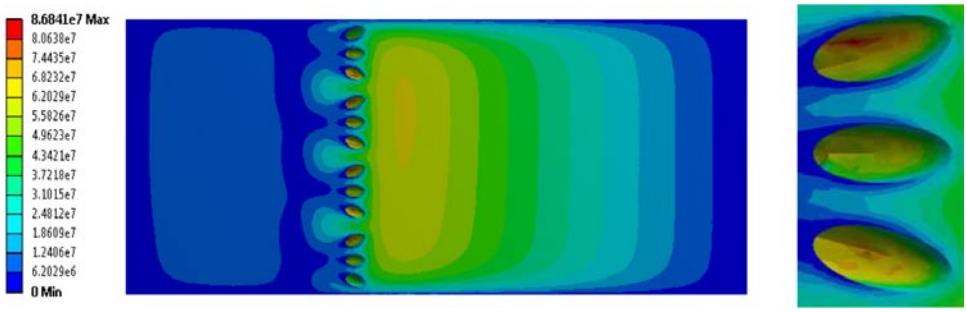

(a) Thermal stress contour

(b) Detail view

FIGURE 4. Thermal stress results

Thermal Stress Analysis

Fluid flow modeling simulations were coupled with a new static structural module which included the material properties for the nickel-based Haynes 230 superalloy. Flat plate temperatures were imported into the model, and all surfaces were made to act as a fixed support. The resulting equivalent (von Mises) stress contour is shown in Figure 4.

The magnitude of von Mises stress that was generated varied from 6 MPa to 87 MPa. The region of high stress concentration (86.841 MPa) was identified to be located inside the tripod holes. The reason can be attributed to a large temperature gradient seen in that region. CFD modeling will also be used to evaluate the cylindrical and/or shaped hole geometry with Haynes 230 alloy, predicting thermal stress.

Conclusions

- Flat plate testing conducted with variable mass flow and coolant density indicates that the tripod design outperforms the cylindrical and shaped holes for a wide range of flow rates.
- Flat plate testing further indicates that a substantial coolant flow savings (~50%) is possible, while increasing the effectiveness of the film cooling (~20% at high flow rates, ~60% at low flow rates) when comparing the tripod hole to the shaped hole.
- Vane cascade testing has shown that the tripod hole geometry outperforms the cylindrical and shaped geometries in all respects on the suction side of the blade, while the shaped hole shows the best film cooling effectiveness on the pressure side. The tripod hole maintains the advantage of lower coolant utilization.

- The tripod design shows less variation due to blowing ratio than the cylindrical and shaped hole designs, allowing designers greater flexibility in their use of film cooling holes.
- Thermo-mechanical stress analysis identifies similar stress levels in the tripod design as in the cylindrical design, indicating that thermal stress will not be the limiting factor of the tripod design. The analysis was conducted without a thermal barrier coating, and therefore the magnitude of stress in an engine application is anticipated to be significantly lower.

Future Directions

- Collaboration will be undertaken with NETL-RUA personnel to determine the effect of internal cooling geometry on film cooling behavior of the tripod hole over the external surface. Efforts will initially utilize a flat plate, and subsequently an airfoil tested in a linear cascade rig.
- Thermal stress and other thermo-mechanical issues, i.e., thermal gradient induced stresses due to changes in internal cooling geometry, and the effect on overall thermal stress, creep and fatigue issues will be experimentally and computationally addressed.
- Commercial manufacture of tripod hole film cooling test coupons will be undertaken with designs developed by the NETL-RUA. These coupons will be subjected to high temperature, pressurized internal cooling-heat transfer testing in NETL's aerothermal test facility in Morgantown, West Virginia.

Acknowledgments

We wish to acknowledge Mr. Richard Dennis and Ms. Patcharin Burke at NETL for their support.

FY 2012 Publications/Conferences/ Presentations

1. J. Lamont, S. Ekkad, and M.A. Alvin, "Detailed Heat Transfer Measurements Inside Rotating Ribbed Channels Using the Transient Liquid Crystal Technique," Accepted: *ASME Journal of Thermal Science & Engineering Applications*, September 2011.

2. J. Lamont, S. Ekkad, and M.A. Alvin, "Heat Transfer Distribution of Various Rib Geometries for Developing Flow at High Rotation Numbers," ASME IMECE, Denver, Colorado, November 2011 (IMECE2011-62610).

3. S. Ramesh, D. Narzary, and S. Ekkad, "Optimization of Low Jet-to-Target Spacing Ratio for Double Wall Impingement Cooling Applications," AIAA 50th Aerospace Sciences Meeting, Nashville, Tennessee, January 9–12 2012.

4. C. LeBlanc, D. Narzary, S. Ekkad, and M.A. Alvin, "Performance of Tripod Anti-Vortex Injection Holes on Vane Film Cooling," ASME Summer Heat Transfer Conference 2012, Puerto Rico, July 7–12, 2012 (HT2012-58135).

5. J. Lamont, S. Ekkad, and M.A. Alvin, "Effect of Rotation on Jet Impingement Heat Transfer for Various Jet Configurations," ASME Summer Heat Transfer Conference, Puerto Rico, July 7–12, 2012 (HT2012-58023).

6. C. Leblanc, D. Narzary, and S. Ekkad, "Film Cooling Performance of an Anti-Vortex Hole on a Flat Plate," Accepted *ASME Journal of Turbomachinery.*

7. J. Lamont and S. Ekkad, "Effect of Rotation on Jet Impingement Heat Transfer," Accepted *ASME Journal of Heat Transfer.*

IV.A.5 Turbine Thermal Management−Aerothermal and Heat Transfer: Internal Airfoil Cooling

Mary Anne Alvin (Primary Contact)
U.S. Department of Energy (DOE)
National Energy Technology Laboratory
Regional University Alliance
626 Cochrans Mill Road
Pittsburgh, PA 15236-0940
Phone: (412) 386-5498; Fax: (412) 386-4806
Email: maryanne.alvin@netl.doe.gov

Dr. Minking Chyu, Mr. Sean Siw,
Mr. Nick Miller, and Dr. Pavin Ganmol
University of Pittsburgh
Department of Mechanical Engineering and
Material Science
Swanson School of Engineering
648 Benedum Hall
Pittsburgh, PA 15261
Phone: (412) 624-9783; Fax: (412) 624-4846
Email: mkchyu@pitt.edu

Contract Number: 0004000.3.620.243.002

Start Date: October 1, 2011
End Date: September 30, 2012

Fiscal Year (FY) 2012 Objectives

Identify turbine airfoil cooling concepts that provide enhanced heat transfer and reduced coolant flow, and which can be commercially manufactured. Research efforts are focused on development of novel internal cooling technology concepts that achieve a cooling enhancement factor of approximately five.

FY 2012 Accomplishments

The National Energy Technology (NETL)-Regional University Alliance (RUA) Turbine Thermal Management project consists of four research project areas that focus on heat transfer, materials development, and secondary flow control. These projects are being conducted to develop advanced technology designs, components and equipment that contribute to achieving U.S. Department of Energy NETL's Turbine Program goals of three to five percentage point plant efficiency gain by permitting higher turbine firing temperatures as a result of realizing more effective cooling, development and utilization of extreme temperature thermal barrier coating protection systems, and secondary flow leakage reduction.

This report summarizes the FY 2012 research effort scope, approach, and accomplishments with respect to development and performance assessment of novel internal airfoil cooling channels. FY 2012 accomplishments follow:

- Bench-scale testing was completed at the University of Pittsburgh using triangular, semi-circular, and circular pin-fin arrays as internal turbulators for enhanced internal turbine airfoil heat transfer enhancement. Based on an overall comparison of the research efforts conducted, testing indicates that the triangular pin-fin array has higher heat transfer on both pin-fins and endwalls in comparison to semi-circular and circular pin-fin arrays. This is mainly due to the presence of sharp edges that generate additional wake, resulting in better flow mixing, thus enhancing the overall heat transfer performance within the triangular pin-fin array.
- Bench-scale, near surface embedded micro-channel (NSEMC) models have been designed and constructed, with initial testing conducted with air cooling jets of comparable diameter. Preliminary testing identifies high heat transfer at the jet impingement zone with decreases in the radial direction. Continued testing will address modification of the inlet jet hole diameter size to establish uniform heat transfer throughout the micro-channel.
- Preliminary fully-bridged pin-fin arrays and NSEMC architectures have been designed and evaluated in terms of manufacturing at Mikro Systems, Inc., for production of test coupons that will be subjected to high temperature, i.e., 1,000ºC, pressurized, internal cooling heat transfer testing in NETL's aerothermal test facility in Morgantown, West Virginia.

Introduction

While typical two-dimensional airfoil rib turbulators or pin-fin pedestals provide an ~2–3 fold heat transfer enhancement compared to the smooth channel baselines, further advances in internal cooling technology with an elevated enhancement factor to approximately five can substantially reduce the level of coolant flow rate and dependence on film cooling. As a result of advances in investment casting processes, future internal cooling configurations are likely to embed

narrow passages extremely close to the airfoil skin as the "multiple-walled" or "skin-cooled" concepts. Existing designs of skin-cooled concepts include Lamilloy® (Rolls Royce), Microcircuit (Pratt & Whitney), and CastCool, where the cooling structure uses two or more layers of bonded metal with coolant flows through the channel space. To enhance the heat transfer performance in the flow passage, surface protrusions, typically three dimensional (3D) short pin-fins, are features on the surfaces of bonded metals. Although the multiple-walled cooling approach has had some successes in cooling of combustor and rocket liners, its applications for turbine hot-section protection continue to suffer from durability issues and extremely low yield in manufacturing.

Approach and Results

NETL-RUA internal airfoil cooling research efforts are focused on development of novel internal cooling concepts as pin-fin arrays, as well as NETL-RUA's NSEMC configuration. Laboratory bench-scale testing of these concepts and commercial manufacturing of coupon samples for exposure to high temperature combustion gas environments in NETL's aerothermal test facility are additional aspects of NETL-RUA's internal cooling aerothermal and heat transfer research efforts. The technical approach taken in each of these areas, and the results generated in FY 2012 are described in the following sections.

Internal Cooling with Multiple Wall Configurations

The main objective of this effort is to explore and develop innovative internal pin-fin cooling concepts that lead to reduction in external cooling. Achieving this goal will reduce coolant consumption, ultimately improving the efficiency of the entire gas turbine system.

Experimental testing at the University of Pittsburgh is being conducted in a newly developed operational open loop test rig that is capable of supplying air at Re ~100,000. All experiments were performed with either the transient liquid crystal imaging or the infrared thermography. Commercially available software, ANSYS CFX, was used to project heat transfer behavior within these architectures.

Table 1 summarizes the test cases conducted during FY 2012. Figures 1 and 2 respectively, illustrate the top view of the experimental test plate which contained triangular, semi-circular and circular pin-fin arrays, and the geometry of pin-fin elements. All pin-fins are fully bridged between both top and bottom endwalls, which is the same as the channel's height, and have the same width, i.e., H = 25.4 mm; D = 6.25 mm. The ratio of pin-fin height-to-length, H/D is equal to four. As previously identified in the literature, staggered arrays out-perform in-line arrays, and therefore only staggered pin-fin configurations were used in this effort.

TABLE 1. Pin-fin configurations

Test Case	Test Identification	Pin-Fin Shape	S_L/D	S_T/D
1	TRI1	Triangular	2.5	2.5
2	TRI2	Triangular	2.5	3.5
3	TRI3	Triangular	2.0	3.5
4	Semi-C	Semi-Circular	2.5	2.5
5	Cir	Circular	2.5	2.5

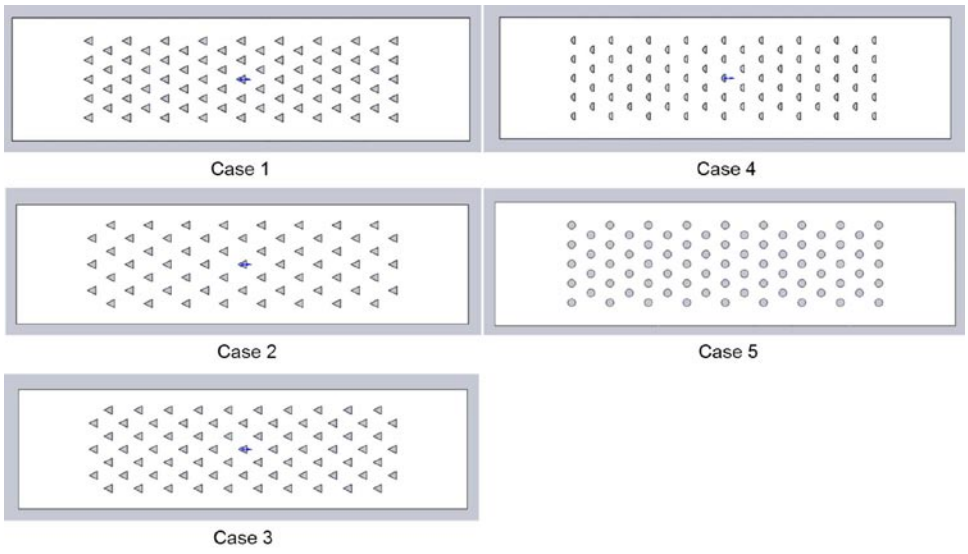

FIGURE 1. Top view of test plate with different pin-fin configurations

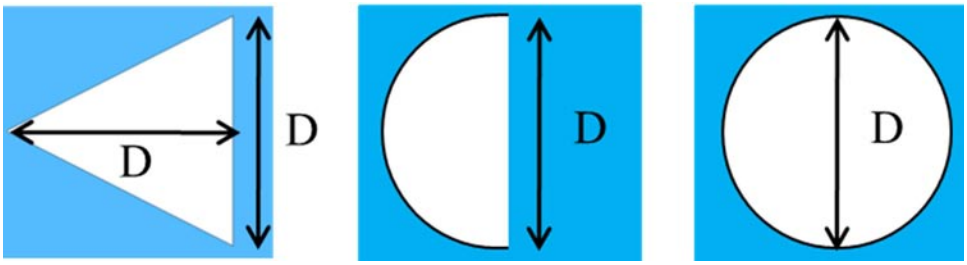

FIGURE 2. Figure pin-fin element

For triangular pin-fin arrays, three configurations corresponding to different inter-pin spacing were used. Larger transverse pitch is introduced into the TRI2 and TRI3 cases based on the numerical findings that triangular pin-fins are capable of generating wider wakes that contribute to higher heat transfer in the lateral region of the channel in comparison to the circular and semi-circular pin-fin cases. Note that TRI1 and TRI3 cases utilize a comparable number of pin-fins, i.e., 77 and 73, while the TRI2 case has the least number of pin-fins, i.e., 59, and the largest pitch in both streamwise and transverse directions. Both the semi-circular and circular pin-fin arrays are based on typical inter-pin spacing of 2.5 times the pin diameter in both transverse pitch and longitudinal pitch, i.e., $S_T/D = S_L/D = 2.5$. The circular pin-fin array, Case 5, is used as the baseline for comparison of all test results.

Testing indicated that similar heat transfer trends result for all triangular pin-fin arrays (Figures 3–5). Heat transfer coefficient (h) increases from the first row and reaches a peak value before decreasing towards a periodic level when the temperature and flow field satisfy the fully developed condition. For the circular shaped pin-fin array, peak heat transfer is achieved at the third or the fourth row (Figure 6). Unlike the circular pin-fin array, significant improvement for the triangular pin-fin arrays results as h continues to increase after the fourth row. Peak h values are attained between the sixth and eighth row. Further downstream, h in the triangular pin-fin arrays remains fairly constant throughout the entire domain. Further comparison shows that the TRI3 case with the largest transverse pitch, i.e., $S_T/D = 3.5$, and smallest longitudinal pitch, i.e., $S_L/D = 2.0$, has higher h on the pin-fins compared to TRI1 and TRI2 cases.

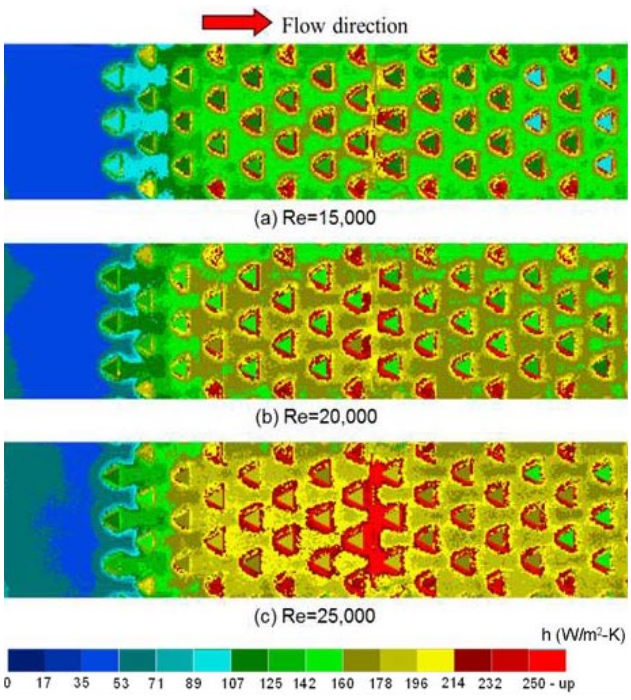

FIGURE 3. TRI1 local heat transfer coefficient distribution

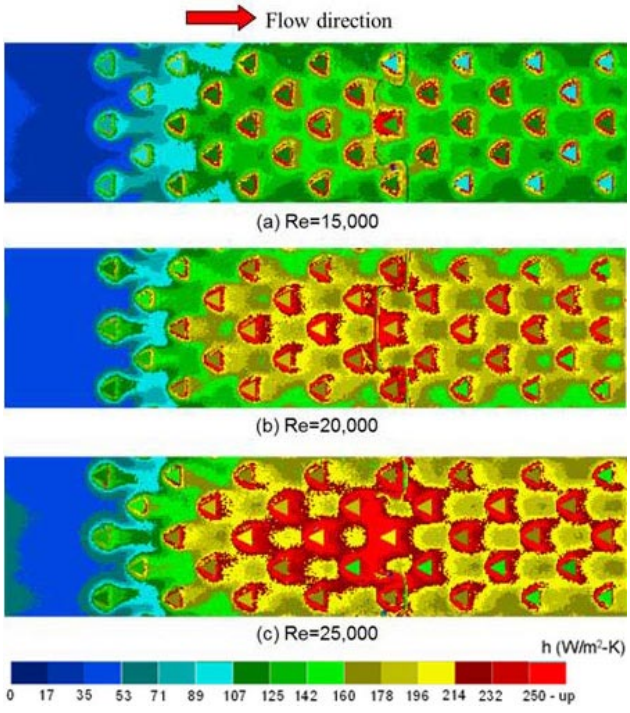

FIGURE 4. TRI2 local heat transfer coefficient distribution

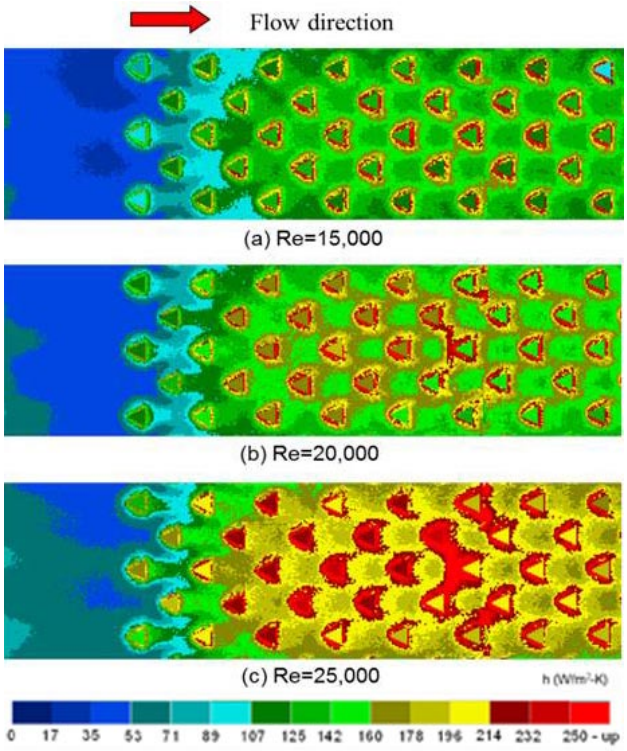

FIGURE 5. TR13 local heat transfer coefficient distribution

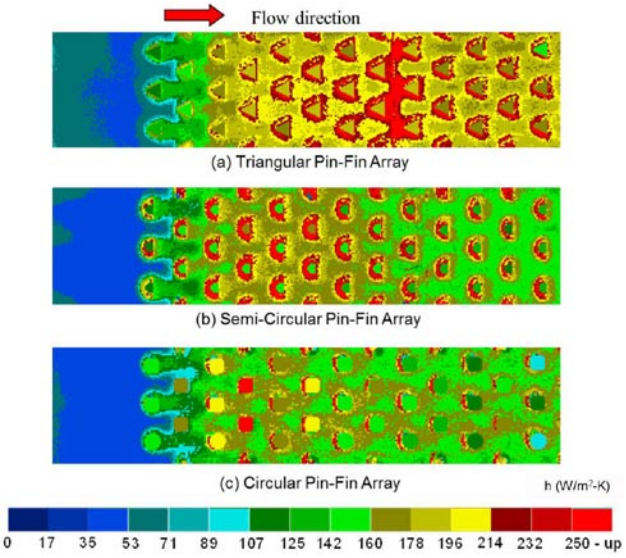

FIGURE 6. Local heat transfer coefficient distribution of triangular, semi-circular and circular shaped pin-fin arrays

However, the TRI1 case has a more uniform *h* than the TRI2 and TRI3 cases. Even though triangular pin-fins have sharp edges that are capable of generating wakes in a wider spanwise direction, having larger transverse pitch causes non-uniformity in heat transfer distribution within the same test domain. Also, the heat transfer at the endwall for all triangular pin-fin arrays is higher than the neighboring pin-fins. In addition, heat transfer at the endwall appears to be fairly uniform after the eighth row.

When plotted at Re = 25,000 (Figure 6), the semi-circular and circular shaped pin-fin arrays have a similar heat transfer pattern, with the peak *h*-value at the third or fourth row before decreasing towards a fully developed value. Due to the presence of horseshoe vortices in the circular and semi-circular pin-fin arrays, the first few rows of both arrays, *h* values of these pin-fins are higher than those of triangular pin-fin array. However, this trend is reversed as the flow progresses downstream. The triangular pin-fin array with a more streamlined profile has lower *h*-value at the leading region in comparison to the circular and semi-circular pin-fin arrays. In addition, one significant advantage of the triangular pin-fin array is that *h* on the endwall is higher than that of circular and semi-circular pin-fin arrays.

Based on this effort, an overall comparison indicates that triangular pin-fin array has higher *h* on both pin-fins and endwalls than that of semi-circular and circular pin-fin arrays. This is mainly due to the presence of sharp edges that generate additional wake, resulting in better flow mixing, thus enhancing the overall heat transfer performance. In addition, the triangular pin-fin array has more uniform *h* at the endwall throughout the entire test domain. Heat transfer enhancement contributed by only the endwall with varying Re for all arrays are shown in Figure 7. Based on the heat transfer enhancement on the endwall, TRI1 outperforms all arrays, with a heat transfer enhancement ranging from 4.0–4.8 which is ~20% higher than that of the circular pin-fin array. The results in Figure 7 indicate that with ~20% fewer pin-fins than the TRI3 case, the TRI2 case exhibits slightly higher heat transfer enhancement than the TRI3 pin-fin case. The semi-circular pin-fin array has the lowest heat transfer enhancement, up to ~10% lower than the baseline case. Heat transfer for the TRI2 and TRI3 cases is slightly lower in comparison to the TRI1 case, but is ~5–10% higher than the circular pin-fin array baseline case.

The total heat transfer enhancement for each pin-fin array, Nu_T, was determined based on the heat transfer contributed by all participating surfaces , i.e., pin-fins and endwall, weighted by the wetted area and normalized by the heat transfer of a fully developed channel as calculated from the Dittus-Boelter correlation. Figure 8 illustrates the overall heat transfer enhancement by considering the magnitude of heat transfer and total effective heat transfer area for all arrays. The TRI3 has the highest overall heat transfer enhancement among all arrays tested, ranging from 3.5 to 3.8. All triangular pin-fin arrays outperform the baseline case by approximately 5-15%. With almost the same total number of pin-fin elements, the results shown in Figure 8 indicate that

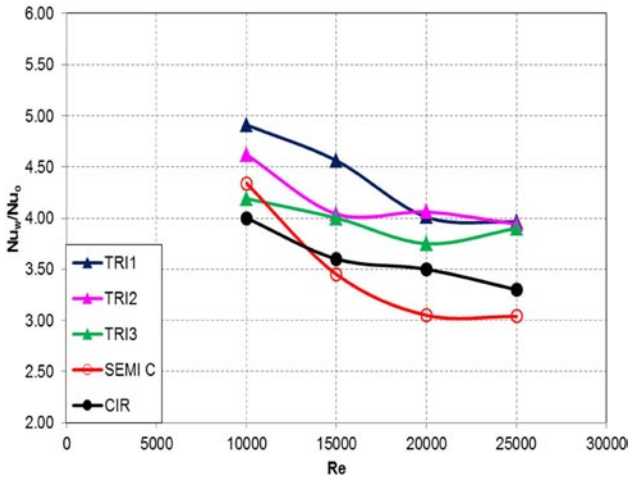

FIGURE 7. Endwall heat transfer enhancement vs. Re

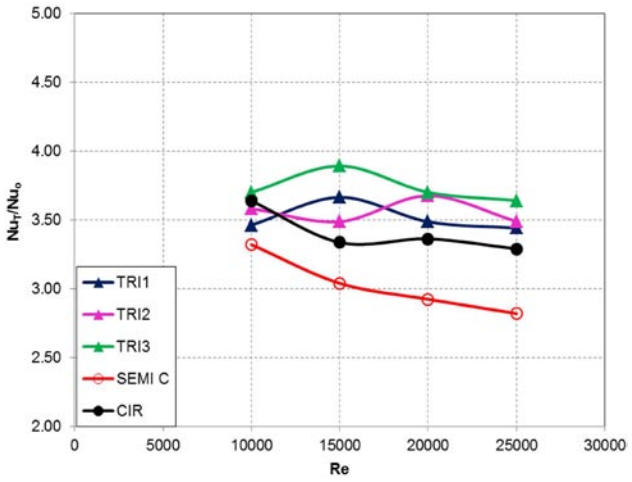

FIGURE 8. Total heat transfer enhancement vs. Re

there is no substantial difference in terms of overall heat transfer performance between the TRI1 and TRI2 cases. As the TRI1 and TRI2 cases have the same longitudinal pitch, i.e., $S_L/D = 2.5$, this ultimately suggests that the overall heat transfer is insensitive to different transverse pitch. Note that when compared to TRI1 case, heat transfer enhancement of the TRI2 case is preserved while having an array with ~20% fewer pin-fins. The semi-circular pin-fin array has the lowest heat transfer enhancement, up to ~10% lower than the baseline case.

The parameter dP/dx represents the pressure drop across the test section by measuring the streamwise static pressure distribution upstream and downstream of the test section. Figure 9 shows the pressure loss of the test cases with varying Re. The TRI1 and TRI3 cases have the largest pressure loss due to the friction and form drag induced by the triangular pin-fins. Larger surface area from each triangular pin-fin together with sharp edges

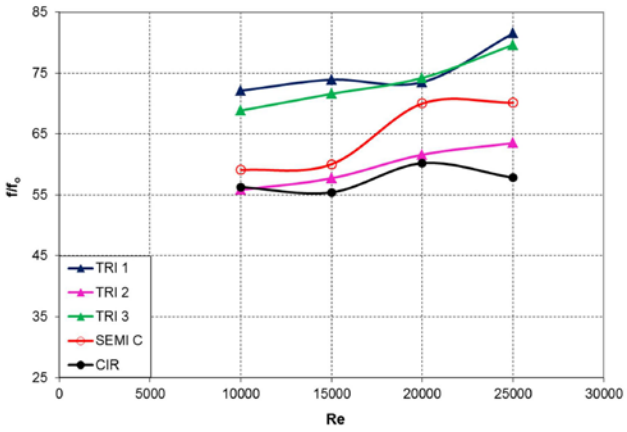

FIGURE 9. Pressure drop vs. Re

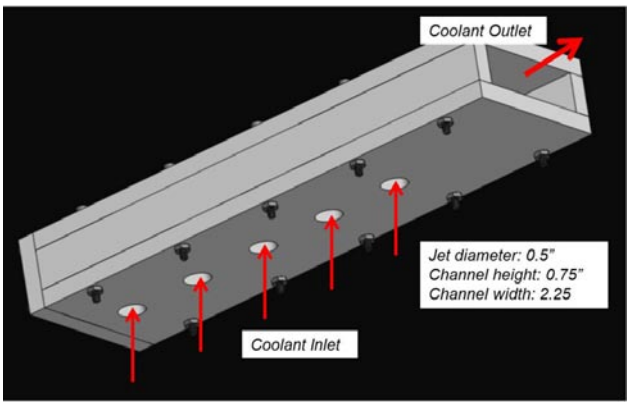

FIGURE 10. 3D schematic view of test section based on NSEMC concept

generate larger friction and form drag in comparison to the other pin-fin elements. Semi-circular pin-fin array has a higher pressure loss compared to the baseline case. With more pin-fin elements, the semi-circular pin-fin array exhibits higher pressure loss than the TRI2 case. The TRI2 case, which has approximately 20% fewer pin-fins than TRI1 and TRI3 cases, exhibits slightly higher heat transfer enhancement than TRI3.

Near Surface Embedded Micro-Channel

One of the advanced, novel, internal airfoil cooling designs being developed by the NETL-RUA is the NSEMC concept which places micro-cooling passages toward or directly adjacent to the external airfoil surface. As part of NETL-RUA's initial research effort, a bench-scale experimental model was designed and constructed (Figure 10) to assess heat transfer within the micro-channel passage. Air jets enter this section through fixed and uniform hole diameters (Table 2), with air flow controlled and metered upstream by individual valves and flow meters (Figure 11).

TABLE 2. Test cases addressing performance of the NSEMC concept

Test Number	Reynolds Number (x1000)				
	Jet 1	Jet 2	Jet 3	Jet 4	Jet 5
1	67	67	67	67	67
2	74	67	47	67	74
3	74	74	67	67	74

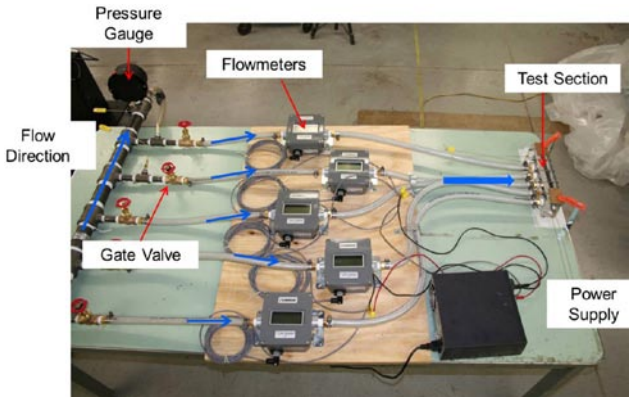

FIGURE 11. NSEMC test facility

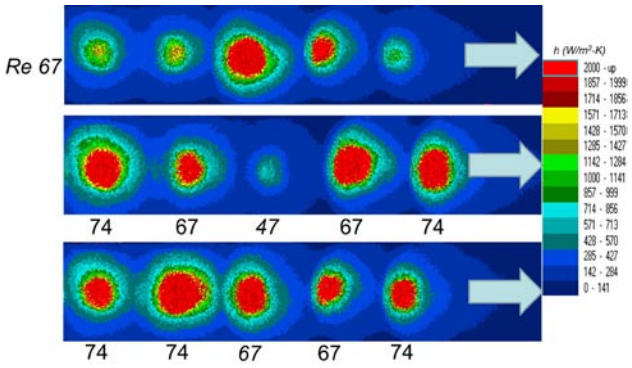

FIGURE 12. Local heat transfer coefficient distribution at varying Re

Using the test parameters shown in Table 2, Figure 12 illustrates the local heat transfer coefficient distribution at baseline Re and varying Re. All test cases show similar trends with high heat transfer at the impingement zone and decreases in the radial direction. Low heat transfer is observed upstream of the first jet, which is mainly due to the presence of a recirculation zone. Lowest heat transfer occurs at the fifth jet, which is attributed to the strong cross-flow effect. As the cross-flow gains momentum as it moves downstream, it can deflect the jets, causing less mass to impinge on the target plate. These downstream jets can also be subjected to heat transfer between the jet and cross-flow, which reduces the heat transfer on the target plate. Figure 13 illustrates the row-resolved averaged heat transfer in the streamwise direction for each test case. The heat transfer at the impingement zone

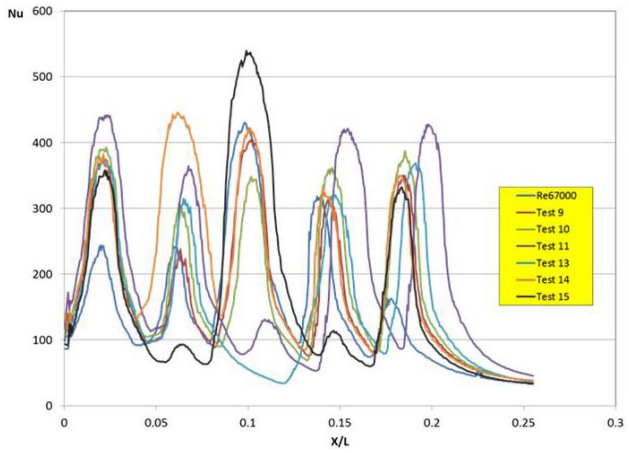

FIGURE 13. Row-resolved heat transfer along the streamwise direction

can reach an ~3–6 fold increase in comparison to the surrounding mid-region between two jets.

Internally Cooled Coupons for NETL Rig Testing

NETL-RUA is collaboratively addressing the appropriate design, methodology and fabrication of internal cooling coupons with Mikro Systems, Inc., for production of test coupons that will be utilized in NETL's high temperature, pressurized, bench-scale aerothermal test facility in Morgantown. Figures 14–15 illustrate the current fully-bridged pin-fin array architecture and the NSEMC design that will be used for testing.

Conclusions

The concept of using triangular and semi-circular shaped pin-fins was used to verify the heat transfer and flow characteristics of both arrays in comparison to circular pin-fin arrays. The following summarizes the major conclusions of this research effort:

- Experimental results of the local heat transfer coefficient distributions suggest that the triangular shaped pin-fin arrays are more uniform in comparison to the semi-circular and circular pin-fin arrays.
- With the greatest number of pin-fins arranged in a dense configuration, the triangular pin-fin array case (TRI3) has the highest overall heat transfer enhancement ranging between 3.5–3.8, which is ~5%–15% higher than that of the circular pin-fin array.
- The semi-circular pin-fin array has the lowest heat transfer performance ranging from 2.7–3.4. However, the semi-circular pin-fin array has only ~50% of the footprint given by the circular pin-fins in the same projected area, the heat transfer performance can be

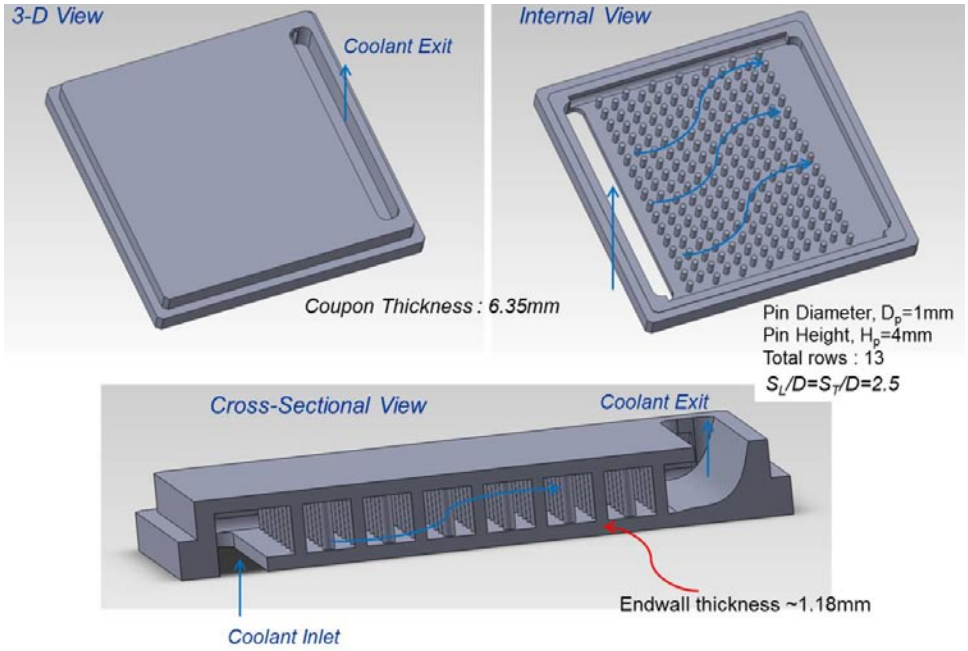

FIGURE 14. Fully-bridged pin-fin array architecture

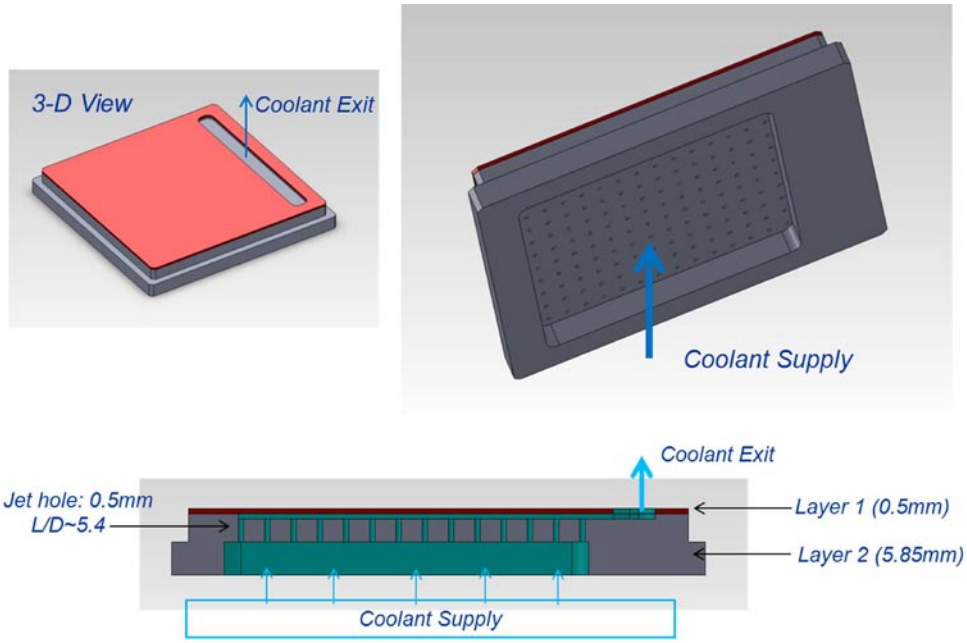

FIGURE 15. Near-surface embedded micro-channel cooling design

increased through the incorporation of additional semi-circular pin-fin elements with tighter inter-pin spacing.

- A higher pressure loss was identified for all triangular pin-fin arrays used in this study, principally as the result of higher friction and form drag.

Future Directions

- Experimental efforts will be continued to further develop and assess the performance of internal cooling configurations to achieve cooling enhancement to nearly or greater than five times that of baseline smooth airfoil channels.

- The effects of NSEMC channel geometry and surface conditions on heat transfer, as well as pressure loss will continue to be assessed in bench-scale laboratory test facilities at the University of Pittsburgh.
- Commercial manufacture of pin-fin and NSEMC test coupons will be undertaken with designs developed by the NETL-RUA. These coupons will be subjected to high temperature, pressurized internal cooling-heat transfer testing in NETL's aerothermal test facility in Morgantown.

Acknowledgments

We wish to acknowledge Mr. Richard Dennis and Ms. Patcharin Burke at NETL for their support.

FY 2012 Publications/Conferences/ Presentations

1. S. Siw, M. Chyu, and M.A. Alvin, "Heat Transfer Enhancement of Internal Cooling Passage with Triangular and Semi-Circular Shaped Pin-Fin Arrays," ASME Turbo Expo, Copenhagen, Denmark, June 11–15, 2012 (GT2012-69266).

2. Revised manuscript: S. Siw, M. Chyu, T. Shih, and M.A. Alvin, "Effects of Pin Detached Space on Heat Transfer and Pin Fin Arrays," from ASME Turbo Expo 2011 was submitted to the *Journal of Heat Transfer.*

3. Revised manuscript: S. Siw, M. Chyu, T. Shih, and M.A. Alvin, *Effects of Pin Detached Space on Heat Transfer in a Rib Roughened Channel,* from ASME Turbo Expo 2011 was submitted to the Journal of Turbomachinery.

4. Manuscript preparation: P. Ganmol, M. Chyu, and M.A. Alvin, *Heat Transfer in Tip-Turn Region of Two-Pass Channel with a 180-Degree Turn*, from ASME Turbo Expo 2011, Journal of Heat Transfer.

IV.A.6 Turbine Thermal Management−Aerothermal and Heat Transfer: Secondary Flow Rotating Rig

Mary Anne Alvin
U.S. Department of Energy (DOE)
National Energy Technology Laboratory
Regional University Alliance
626 Cochrans Mill Road
Pittsburgh, PA 15236-0940
Phone: (412) 386-5498; Fax: (412) 386-4806
Email: maryanne.alvin@netl.doe.gov

Dr. Karen Thole and Dr. Michael Barringer
Pennsylvania State University
Mechanical and Nuclear Engineering Department
137 Reber Building
University Park, PA 16802
Phone: (814) 865-2519; Fax: (814) 865-1280
Email: kthole@psu.edu, mbarringer@psu.edu

Contract Number: 0004000.3.620.243.002

Start Date: October 1, 2011
End Date: September 30, 2012

Fiscal Year (FY) 2012 Objectives

Design and construct a world-class test facility for testing new cooling improvement strategies for the turbine rotating blade platform. The primary focus of the turbine test facility is to increase turbine efficiencies by using disruptive new designs in sealing the interfaces between stationary and rotating airfoil components. The main driver of this effort is to develop new designs that will lead to reduction in fuel usage by an order of magnitude or more. The facility will include a section of a turbine including a vane/blade/vane, which is referred to as a 1.5-stage turbine that will operate at conditions replicating a modern gas turbine engine.

FY 2012 Accomplishments

The National Energy Technology Laboratory (NETL)-Regional University Alliance (RUA) Turbine Thermal Management project consists of four research project areas that focus on heat transfer, materials development, and secondary flow control. These projects are being conducted to develop advanced technology designs, components and equipment that contribute to achieving U.S. Department of Energy NETL's Turbine Program goals of three to five percentage point plant efficiency gain by permitting higher turbine firing temperatures as a result of realizing more effective cooling, development and utilization of extreme temperature thermal barrier coating protection systems, and secondary flow leakage reduction.

This report summarizes the FY 2012 research effort scope, approach, and accomplishments with respect to design and construction of a secondary flow rotating rig to assess advanced cooling improvement strategies for the turbine blade platform. FY 2012 accomplishments follow:

- A secondary flow rotating test facility has been designed at Pennsylvania State University (Penn State) to test representative turbine engine hardware in a continuous, steady-state, high pressure environment. The test rig was designed with an operating envelope well above the capabilities of most continuous duration, rotating turbine test facilities in the U.S. and Europe. The test rig design includes the means to simulate internal air system flow leakages and cavity flow conditions within the turbine. A series of test campaigns were developed to meet the project's research objectives.
- The procurement of large facility equipment including a 1,500 HP compressor system has been completed, and procurement of a facility-wide cooling system is in progress. Vendors have been identified for the remaining large facility items, and discussions related to procurement of the following are on-going: an active magnetic bearing system that will support the turbine shaft, reduce wear, and allow for turbine shaft micro-positioning; a dynamometer water brake system and torque meter to measure the turbine shaft power and torque; and a telemetry system for acquiring instrumentation signals from sensors mounted on the rotating turbine disc and airfoils.
- The building renovation and modifications have been completed that will house the secondary flow rotating test facility. This included construction of three rooms within a large building on the Penn State campus, as well as installing the necessary electrical power to operate the secondary flow rotating test facility.

Introduction

The hardware architecture within existing gas turbine engines, both aircraft and land-based power generation, is one in which significant secondary flow

leakages and cooling requirements limit the firing temperatures and ultimately the fuel burn of the engine. Approximately 25% of the total air flow through a gas turbine engine bypasses the combustor and is used for cooling turbine airfoils, disks, internal rim cavities, and other turbine hardware. Of that 25% cooling flow, 5–10% is associated with non-airfoil cooling. Industry analyses and predictions from proprietary performance codes show that by eliminating 3.3% from the 25% total turbine cooling and leakage air (TCLA), thus resulting in 21.7% TCLA, this would result in a reduction in the fuel burn by 2.0%. This TCLA reduction is consistent with the elimination of unintended leakage paths, but requires understanding of the effects of the individual leak paths to ensure design requirements for engine life and performance are not violated. Not only is fuel burn reduced, but the valuable, high pressure, secondary flow can be used to further cool components thereby allowing higher firing temperatures. Higher firing temperatures lead to higher efficiencies with cooling being integral to maintain part life longevity.

The rotating turbine rig project that is being conducted at Penn State is focused on the development of a new facility that would provide a radical change in the design philosophy of secondary air and cooling supply systems to reduce leakage flows by an order of magnitude, therefore creating essentially a "zero-leakage" secondary air system. Reducing these leakage flows would lead to overall improved usage of coolant flows. The research aims at developing and validating tools for the performance prediction of novel designs that would reduce the overall fuel burn in land-based turbines. In state-of-the-art gas turbines, leakage flows are introduced into the hot gas path through interfaces defined by the stationary and rotating bounding hardware, as well as functional requirements such as supply pressures for the turbine cooling air. No attempt is made to design towards the most effective component/module interaction. A notional secondary flow system study has shown that engine leakage rates could improve a number of key technical areas:

- Redistribution of purge flow supply and egress at the High Pressure Turbine (HPT) rotor/stator interfaces (rim seals and cavities).
- Redesign of rim seals to accommodate the desired purge flow redistribution that will involve transitioning to novel configurations.
- Balancing of turbine cooling air supply pressures with those in surrounding air system cavities.
- Optimization of High Pressure Compressor (HPC) rear hub purge flows for reduced windage losses.
- Reuse of cooling air as sealing air.

While all of these items need to be pursued in order to meet the goal of substantial fuel burn reductions (higher efficiencies), the overall objective is to define a secondary air system configuration based upon a fundamentally different design philosophy. The new facility will provide a means for studying these effects. Studies using the new facility will also include internal cooling of airfoils to encompass a full array of cooling design considerations.

The goal of the secondary flow rotating rig project is to design, construct, and operate a world-class turbine test facility to demonstrate increased turbine efficiency by reducing cooling flow to the turbine through the systematic study of dedicated purge, leakage, and primary core flow interaction.

Simulating interactions between the hot gas path and the secondary air system at relevant scaling parameters translates into significant facility requirements of continuous air flow rates up to 12.5 lbm/s, supply pressures at maximum flow rate of about 60 psia, and power requirements between one and two megawatts. Furthermore, the new facility is being designed for a 1.5-stage model turbine, which will require a turbine shaft brake system in order to be able to operate at desired ratios of axial to circumferential flow velocities and to provide the proper safety infrastructure to operate a disk of about 20 inches diameter at 10,000 RPM. Such a facility and test rig for secondary air system research is currently not available in the United States, which represents a competitive disadvantage of the U.S. industry and research community when compared with the European Union. The secondary flow rotating rig test facility is being designed to promote collaborative interactions between academia, government agencies, and industry to advance land-based gas turbine sealing concept technology development. Additionally the test facility provides a means for training of our nation's future scientists and engineers.

Approach and Results

Effort in this research project provides the Turbine Program with a world-class test facility for testing new cooling improvement strategies for the turbine rotating blade platform and performance data relevant to initial concept designs and/or platform modifications. Research tasks that were undertaken in FY 2012 focus on design and construction of the 1.5-stage turbine test facility. This includes facility design and large item procurement, rig and test section design and construction, and building modifications. A description of the FY 2012 research efforts follows.

Design of the Secondary Flow Rotating Test Facility

The aerothermal rotating turbine rig facility has been designed and is located within an existing research building at Penn State in State College Pennsylvania. The facility consists of three primary rooms, shown in Figure 1, including a compressor room, test bay rig room, and a control room. The facility rig includes a large capacity 1,500 hp (1.1 MW) centrifugal compressor system that will deliver approximately 11,000 standard cubic feet per minute (SCFM) (12.5 lb_m/s) of compressed air at 60 psia and 250°F to a 1.5-stage, true scale, test turbine. The rig also includes the means to deliver a secondary air flow stream to the internal cavity of the test turbines, both upstream and downstream of the turbine rotor disk. The rig allows the pressure and temperature of the primary and secondary flow to be controlled.

Isolated concrete slabs ~3 ft thick were designed to support the compressor and the turbine test section. The intent was to create very large strong slab masses that are de-coupled from the building concrete floor to completely eliminate any vibration transmission to and from the slabs. Vibration isolation foam was also designed to be placed along all four vertical faces of each slab. A compacted stone layer approximately one foot thick was installed underneath each concrete slab. The total combined isolated slab thickness was ~4 ft to ensure the depth was below the locality soil freeze depth.

Plans also include the option for a future facility upgrade that would include a second identical compressor system that would operate in parallel with the first compressor system. The parallel mode of compressor operation would allow testing of turbines at even higher mass flow rates (and thus higher non-dimensional flow parameters) and potentially multiple turbine stages. The second compressor system would not be incorporated until after the research facility is fully benchmarked. Cost estimates for a second compressor system have been obtained and discussed. The installation of the electrical infrastructure required to operate two compressors simultaneously is currently being pursued including the primary power transformer, switchgear, load interrupt switches, and overload relays.

An overhead crane system was designed into the facility within the test bay rig room. The crane system has a 5 ton lifting capacity and will be used during rig construction, as well as during testing to make modifications to the turbine test section. A smaller capacity chain hoist is designed into the crane system to allow very

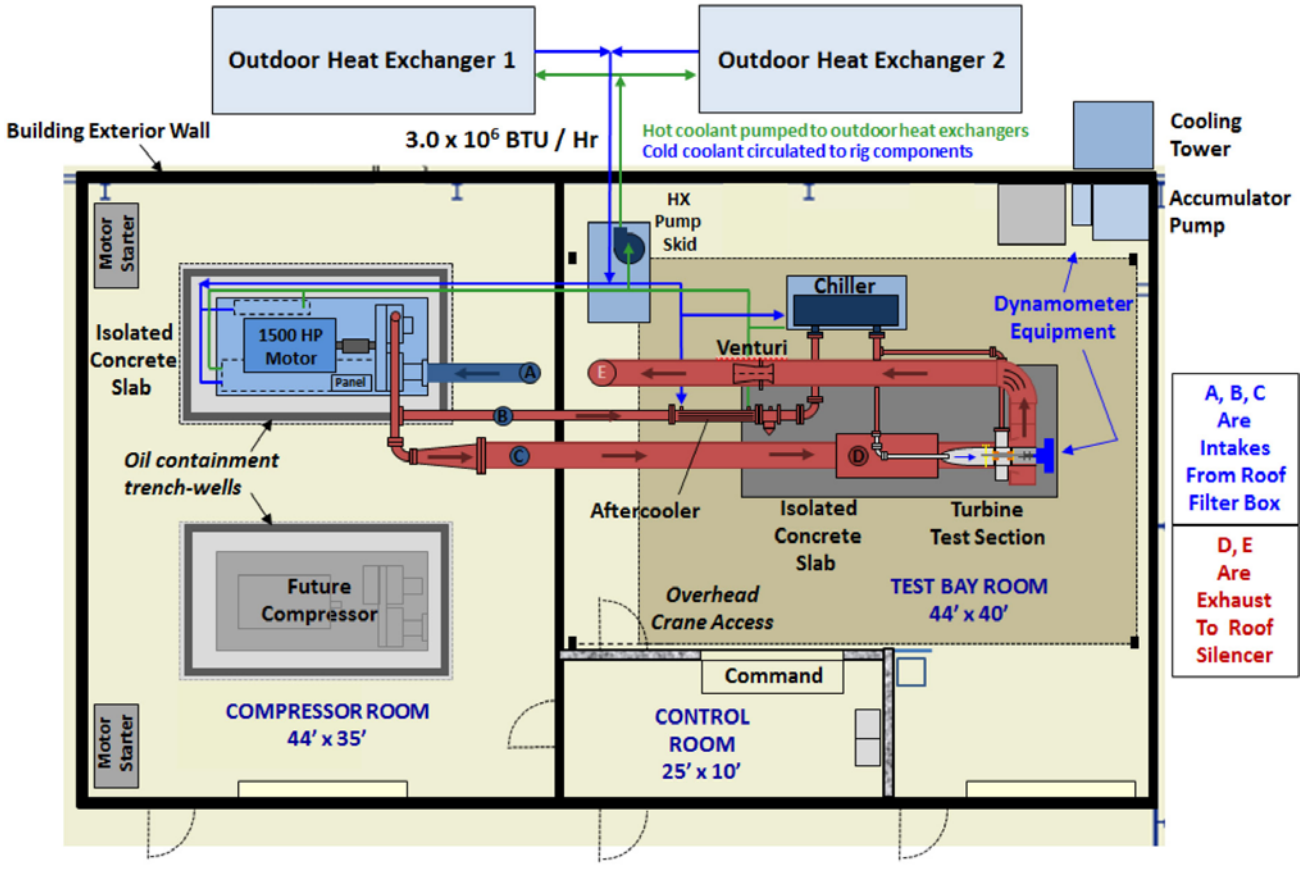

FIGURE 1. Design of the secondary flow rotating turbine rig facility at Penn State

precise lifting and lowering movements related to the turbine test section assembly. In addition, a steel platform was designed above the compressor room on the building roof to support a large inlet filter and weather hood, as well as a large industrial grade exhaust silencer that is suitable for reducing compressed air flow exhaust noise down to appropriate levels (100 dBA down to 72 dBA). The inlet filter and weather hood will remove dirt and moisture from the air and will be piped directly to the inlet of the compressor. The exhaust silencer will be piped directly to the rig downstream of the turbine test section.

Additional facility design considerations include a steel laboratory safety shield designed to surround the turbine test section and the control room ballistic grade windows. In addition, multiple compressed air outlets rated at 125 psig have been placed within the compressor room and test bay room to allow use of pneumatic tooling during rig construction and various other applications including an air buffer seal for the compressor and a thrust balance piston system for the turbine test section. Exhaust fans were designed into the compressor room to aid in removing the significant radiant heat generated during the compressor operation.

Exhaust fans were designed into the compressor room to aid in removing the significant radiant heat generated during the compressor operation. Approximately 5% of the total 1.1 MW operating power, or 55–60 kW, will need to be removed from the compressor room during compressor operation to maintain the room temperature within acceptable machine limits. A drain was designed into the test bay rig room, and oil containment trench wells were designed into each concrete slab to prevent water and oil spills/leaks from propagating through the facility. The control room was designed to have a raised floor to allow wires/cables/chords to be cleanly and efficiently routed to and from equipment, controllers, computers, and data acquisition systems.

Large Item Procurement

Large item procurement includes the compressor system, a facility cooling system, a water brake dynamometer system, and an active magnetic bearing system, facility programmable logical controller (PLC) system, and telemetry system. To date, the compressor has been purchased and installed at the Penn State's test facility.

Compressor

A two-stage Polaris F700 F.S. Elliott centrifugal compressor system was procured through C.H. Reed, Inc., a compressed air equipment supplier. The compressor will supply a steady compressed air flow to the test turbines. The compressor capacity and operating conditions were chosen to provide the flow rate and pressure required to meet the research goals.

A witness test of the compressor operation was successfully performed at the F.S. Elliott factory site in Export, Pennsylvania, during April 2012. The witness test included operating the compressor at several different discharge pressures and flow rates while monitoring instrumentation installed within the compressor that is integrated into the machine's user control panel. In addition, an F.S. Elliott performance prediction code was run for several different inlet air temperatures, pressures, percent relative humidity levels, and inlet guide vane settings. The predicted performance operating curves have been incorporated into a Penn State computational code that will be used to predict operating conditions through the facility rig ductwork system and will be verified during facility operation.

In May 2012, the compressor was delivered to Penn State (Figure 2). Routine monthly service/maintenance on the compressor when it is not running will be performed by a certified F.S. Elliott/C.H. Reed compressor technician. Piping, fittings, and valves to be located upstream and downstream of the compressor are being designed and will be installed according to the manufacturer's recommendations and guidelines that are provided in the machine's user manual. The compressor's plumbing and instrumentation diagram is currently being examined for integration into the facility's PLC system.

FIGURE 2. 1,500 hp centrifugal compressor system

Facility Cooling System

Two independent cooling systems are currently being procured that are capable of rejecting large heat loads to atmospheric outdoor conditions. The first cooling system is the compressor cooling system which is a dry-type closed-loop cooling system with a heat rejection capacity of 2.7 x 10^6 BTU/Hr and will be used to supply the necessary coolant to the compressor's inter-cooler heat exchanger and oil cooler heat exchanger. The compressor cooling system includes a large outdoor air-cooled heat exchanger as well as an indoor pump and control skid. The second cooling system is the turbine cooling system which includes an industrial process chiller with a heat rejection capacity of 685,000 BTU/hr and will be used to supply the necessary coolant to a passive aftercooler heat exchanger that will be installed within the pipe duct that supplies cooling air to the test turbines. Provisions for placing the heat exchanger and process chiller outside of the facility building have been coordinated.

The aftercooler is a passive heat exchanger device that will be installed within the pipe duct that supplies air flow to the internal cavity of the turbine test section. The water/glycol coolant from the cooling system will be circulated to and from this aftercooler. The goal is to reduce the temperature of the secondary purge air flow prior to the air flow reaching the test turbine internal cavity. The reduced temperature of the purge and leakage air flow will allow turbine testing to be performed with an air density ratio (purge flow to main core flow) at the turbine blade inlet near 2.0, which is engine representative. This aftercooler will be the first of two devices used to accomplish this air flow temperature reduction. The aftercooler will reduce the ~250ºF air flow temperature from the compressor discharge temperature to ~100ºF. The second device will be an active refrigerated air chiller which will also be installed within the same pipe duct and will be located downstream of the aftercooler. The chiller system will include advanced control features to allow precise control of the exiting air flow temperature at a variety of air flow rates, pressures, and inlet temperatures. Remote control capability and integration into the facility PLC system will also be included. The chiller will be used to reduce the air flow temperature from ~100ºF to a variety of testing temperatures ranging between 40ºF and 100°F.

The large heat exchangers associated with this facility cooling system will be placed outdoors, ~50 ft away from the building exterior wall to allow for sufficient air flow circulation. The heat exchangers will be mounted on concrete sonotubes in gravel. Piping and electrical cables will be tunneled underneath the driveway in the rear of the building to connect the heat exchangers with the indoor pump and control skid.

A detailed pipe network analysis was performed that included all pipe components (straight pipe, elbows, tees, leg branches, etc.) to properly estimate the pump size that is necessary to circulate the coolant to and from all cooling system equipment. A series of gate valves will also be incorporated into the pipe network to allow each rig component being cooled to receive adequate coolant flow. The valves may be electrically actuated and controlled via the facility PLC system.

Magnetic Bearing System

An active magnetic bearing system that includes both radial and axial (thrust) bearings will be used to both support and micro-position (axial offsets, radial offsets, and whirl orbit) the shaft of the test turbine in both the radial and axial direction. Discussions with the companies SKF Magnetic Bearings and Synchrony Magnetic Bearings are currently in progress. The discussions have focused on initial concepts for the turbine shaft and rotor design, quantity of bearings, support structures, load capacity, shaft material, machining, calibration, rotor dynamics analyses, control hardware, and commissioning.

Due to a thrust limit on the magnetic thrust bearings and the elevated operating air pressure at the turbine inlet (60 psia), a secondary means of absorbing the additional thrust produced by the turbine airfoils and rotor disk is being designed. The total thrust that must be absorbed is ~7,000 lb. A compressed-air controlled thrust balance piston system is also being designed to accommodate the additional thrust load. Discussions of bearing controller/amplifier technology, timelines, budgeting, and technical support have occurred.

Dynamometer

Official quote packages were obtained for three dynamometer water brake systems from both the Kahn company and the Froude-Hoffman company. The dynamometer will be needed to measure and control the rotational speed and torque of the turbines being tested in the facility. The systems include the dynamometer, control system, calibration system, hydraulic power supply unit, water circulation and cooling system, test stand structure, and on-site commissioning. The quote packages were evaluated and a summary spreadsheet was made to compare the six systems against one another based on the range of power absorption, torque, and accuracy, as well as lubrication type, water requirements, test stand features, control system features, commissioning, pricing, and lead times. Off-design operation of the test turbines, for which the shaft rotational speed and torque are significantly reduced, will be needed at times, and therefore to minimize

uncertainty from a measurement perspective, highly accurate speed and torque control systems are required.

A wet type closed-loop water system was investigated for supplying the water necessary to operate the dynamometer water brake system. This system includes a large cooling tower that will be positioned outside the facility building, a large pump rated to ~135 gpm, a large accumulator, and a large back pressure regulation valve.

The coupling between the turbine shaft and the dynamometer water brake is being designed, and failure scenarios are being assessed. If for example, a turbine overspeed condition arises due to a coupling failure, an emergency fast acting valve will be activated to divert all air flow away from the turbine test section and up to the building roof to the exhaust silencer.

Facility PLC System

A recommendation was obtained for the company ARM EnerTech to design and implement the facility PLC system that sends and receives signals to and from rig components, instrumentation, etc., to allow rig operation and testing to be performed smoothly. An example of the required PLC system would be an Allen-Bradley system from Rockwell Automation. The PLC system would monitor compressor settings/operation/alarms and flow meters, temperatures, pressures, turbine speed, etc., and provide the researcher with a visual display computer program with touch buttons to fully interact with the rig during start-up, testing, and shut-down.

Telemetry System

Example telemetry system designs from the companies RotaData and DataTel were obtained. Meetings with both companies have occurred and are still in progress regarding the design and integration of a telemetry system within the turbine test section. Discussions between Penn State and Pratt & Whitney have focused on the pros and cons of telemetry systems versus slip ring systems for acquiring data signals from instrumentation mounted on the rotating turbine disc and airfoils. The turbine test section is currently being designed to accommodate both types of systems for increased flexibility.

Design of the Aerothermal Rotating Rig

A three dimensional layout of the facility, components, systems, and rig ductwork is being performed using the software package AutoCAD. A recommended piping manufacturer and metal fabrication company has been identified and contacted to discuss constructing all of the steel pipe and ductwork. The settling/mixing chamber located upstream of the turbine test section is being designed as a cylindrical shaped pass-through duct. This chamber will be a pressure-vessel, most likely with a clamshell design. The chamber will include a baffle splash plate and access panel. The baffle plate is being designed to serve two purposes including (1) slow the duct flow-down that enters the mixing chamber in order to minimize pressure loss and (2) mechanically support the pipe that will connect to the nosecone of the 1.5-stage test section. The pipe that connects to the nosecone will deliver the turbine purge flow air to the inner cavity of the 1.5-stage test section. The access panel will allow access to the inside of the mixing chamber which in turn will allow pipe installation connections to be made, sealing, and instrumentation.

The steel ductwork will need to be insulated from the compressor discharge all the way to the turbine test section to minimize air flow heat loss. Penn State is designing the support structures for the facility ductwork. Ductwork that is relatively close to the floor (within 5 ft) will be supported using steel braces and bearing blocks bolted to the floor, while ductwork at elevated heights away from the floor (~5 ft) will be supported using steel columns and braces. The pressure rating of all duct piping is being designed to a 150 psig classification for possible future facility upgrades.

Design of the Aerothermal Rotating Rig 1.5-Stage Test Section

Design operating points of the two primary test turbines have been established which include a short span airfoil to be used for studying rotor disk cooling and leakage flow egress, and a tall/full span airfoil to be used for studying airfoil internal cooling with leakage flow egress. The torque and power of the two test turbines have been estimated over a range of turbine operating conditions using realistic blade metal and flow angles as well as realistic pressure ratios (2.0) and total-to-total adiabatic efficiencies (0.9). The range of conditions includes realistic values for both aero and industrial gas turbine engines including (1) non-dimensional rotational Reynolds number associated with the disk cavity purge flow ($Re_\phi = \rho \cdot \Omega \cdot R^2/\mu$) , (2) non-dimensional main gas path flow parameter (C_x/U), and (3) blade inlet axial Reynolds number. The air flow density ratio (DR) associated with the test turbine purge flow relative to the main gas path flow are also being included in the analyses between DR = 1.0 to 2.0.

An interface control document was developed by Penn State and Pratt & Whitney to clearly identify what parts of the rig 1.5-stage test section will be designed internally by Pratt & Whitney and which will be designed by Penn State.

A large venturi flow meter will be positioned downstream of the turbine test section. Smaller venturi flow meters located in the ductwork associated with the test turbine purge flow will also be used. Plans include installing several static pressure taps in the ductwork upstream of the turbine test section, and calibrating them with the venturi that will be located downstream of the turbine test section. This will allow the mixing chamber to be in close proximity to the test turbine.

Example instrumentation probes are currently being constructed in-house at Penn State for future measurement of total temperature and total pressure within the primary main flow path annulus, and within the purge flow cavities (upstream and downstream of the turbine disk). This instrumentation construction process will permit evaluation of capabilities related to miniature probe manufacturing and installation. Thermocouple types will include type K and E. Ultimately thermocouples that have a bead size in the range of 0.0005 to 0.030 in (0.5 to 30 mils) will be needed for testing. Practicing in-house manufacturing techniques and investigating outside methods will be required for making these very small thermocouples. Tubing made from stainless steel and aluminum will first be attempted.

Test Section Component Procurement

Once the turbine test section design is complete, the components will be machined. TurboCAM has been contacted to perform the turbine machining. This segment of the project is planned to be performed and completed during Fall 2012.

Building Renovation and Modifications

In 2011-2012 it was decided to utilize an existing building at Penn State to house the secondary flow rotating rig test facility. The building renovation began January 30, 2012, which was completed at the end of May 2012.

Conclusions

Significant effort has been undertaken at Penn State with respect to design, development, and construction of the secondary flow test facility that will test turbine engine representative hardware in a continuous, steady-state, high pressure environment. The test rig was designed with an operating envelope well above the capabilities of most continuous duration, rotating turbine test facilities in the U.S. and Europe.

Future Directions

- The design of the aerothermal rotating rig facility is in-progress with plans for completion during the summer of 2012. Similarly, the design of the aerothermal rotating rig 1.5-stage test section is in progress with plans for completion during Fall 2012.
- The procurement of test section components will begin in the fall of 2012.
- The construction of the secondary flow rotating test rig is planned to begin the summer of 2012. This will include ductwork and support structures, installation of flow control valves, flow meters, intakes and exhausts, outdoor subsystems, and all subsystem piping.
- The bench-top test section assembly will begin during the fall of 2012. All test section hardware will be trial fitted to verify clearance, tolerances and stack-up. All instrumentation and traversing systems will be trial fitted.
- All control room hardware will be installed including DAQ systems, video monitoring, digitally controlled electronic relays, and instrumentation routing, wiring, connections
- The turbine test section will be assembled and undergo shakedown and debugging. This will include the magnetic bearing system, trust balance piston system, water brake and dynamometer, and instrumentation.
- The entire rig and facility will undergo shakedown. The PLC will be set-up, integrated into the facility and debugged. All rig pressure sealing, as well as secondary purge and cooling flow delivery will be debugged. Standard protocols for startup, operation and shutdown will be established. Emergency shutdown procedures (i.e., manual and PLC controlled) for risk mitigation of all identified failure scenarios will be developed.

Acknowledgments

We wish to acknowledge Mr. Richard Dennis and Ms. Rin Burke at NETL for their support.

FY 2012 Publications/Conferences/ Presentations

1. "Development of a Rotating Turbine Rig at Penn State to Study Secondary Flow Leakages and Aerothermal Cooling," UTSR Meeting, Columbus, Ohio, October 25–27, 2011.

IV.A.7 Turbine Thermal Management−Aerothermal and Heat Transfer: Airfoil Trailing Edge Cooling

Mary Anne Alvin
U.S. Department of Energy (DOE)
National Energy Technology Laboratory
Regional University Alliance
626 Cochrans Mill Road
Pittsburgh, PA 15236-0940
Phone: (412) 386-5498; Fax: (412) 386-4806
Email: maryanne.alvin@netl.doe.gov

Dr. Minking Chyu, Mr. Sean Siw,
Mr. Nick Miller, and Dr. Pavin Ganmol
University of Pittsburgh
Department of Mechanical Engineering and
Material Science
Swanson School of Engineering
648 Benedum Hall
Pittsburgh, PA 15261
Phone: (412) 624-9783; Fax: (412) 624-4846
Email: mkchyu@pitt.edu

Contract Number: 0004000.3.620.243.002

Start Date: October 1, 2011
End Date: September 30, 2012

This report summarizes the FY 2012 research effort scope, approach, and accomplishments with respect to development and performance assessment of novel trailing edge cooling architectures. FY 2012 accomplishments follow:

- ANSYS computational fluid dynamics (CFD) modeling and experimental testing was initiated at the University of Pittsburgh to identify enhanced heat transfer, zig-zag channel, trailing edge configurations. Designs consisting of 110° turning angle zig-zag passages numerically exhibited the highest heat transfer, *h*, in comparison to 70° and 90° turning angle zig-zag passages. When tested in bench-scale models, the resulting experimental data were generally consistent with the ANSYS numerical results.
- To further enhance heat transfer along the airfoil's trailing edge, rib-turbulators were added to the zig-zag passage. By having rib-turbulators throughout the entire zig-zag channel, heat transfer enhancement is predicted to increase approximately two-fold in comparison to smooth zig-zag channel passages. Pressure increases within the airfoil with the inclusion of rib-turbulators.

Fiscal Year (FY) 2012 Objectives

Identify turbine airfoil cooling concepts that provide enhanced heat transfer and reduced coolant flow, and which can be commercially manufactured. Research efforts are focused on development and evaluation of novel airfoil trailing edge cooling designs.

FY 2012 Accomplishments

The National Energy Technology Laboratory (NETL)-Regional University Alliance (RUA) Turbine Thermal Management project consists of four research project areas that focus on heat transfer, materials development, and secondary flow control. These projects are being conducted to develop advanced technology designs, components and equipment that contribute to achieving U.S. Department of Energy NETL's Hydrogen Turbine Program goals of three to five percentage point plant efficiency gain by permitting higher turbine firing temperatures as a result of realizing more effective cooling, development and utilization of extreme temperature thermal barrier coating protection systems, and secondary flow leakage reduction.

Introduction

Due to its limited space and footprint, the trailing edge of a turbine airfoil is one of the most difficult regions to cool. Virtually all trailing edge cooling strategies adopt a passive approach with heat transfer enhancement induced primarily by surface protrusions—pin-fins or pedestals which also provide structural integrity, and block elements. Since the internal cooling flow when reaching the trailing edge usually is fairly warm, its cooling capacity is rather limited. As a result, research emphasis to further enhance advanced trailing edge cooling technology has been directed to development of innovative surface features for heat transfer enhancement, and increasing coolant-to-surface contact area and residence time so that heat removal in the cooling channel can be optimized.

Approach and Results

NETL-RUA trailing edge cooling research efforts are focused on development and bench-scale

laboratory assessment of novel airfoil designs. This effort is being conducted in conjunction with major land-based gas turbine manufacturers, and commercial equipment manufacturers. Fabrication of novel trailing edge concepts is being undertaken, with production of prototype test coupons that will subjected to heat transfer performance evaluation in NETL's high temperature, pressurized aerothermal testing facility in Morgantown, West Virginia. The technical approach and the results generated for the trailing edge cooling effort in FY 2012 are described in the following sections.

Numerical Methodology

The ANSYS CFX k-epsilon model with scalable wall function was used to initially numerical assess the heat transfer and flow field characteristics of three trailing edge zig-zag channels with different turning angles ranging from 70°, 90°, and 110° (Figure 1). Additional experimental testing was conducted using the zig-zag channel with the optimally identified ANSYS geometry.

The zig-zag test channel configuration that was used in this effort had a cross-section of 63.5 mm x 25.4 mm, corresponding to an aspect ratio of 2.5:1. The operating conditions for all cases maintained the inlet air temperature, T_{in}, at 300 K, and both top and bottom walls at 400 K. All sidewall temperatures throughout the entire test domain were set at adiabatic conditions. With the bulk mean velocity at the inlet of 7m/s, the Reynolds number based on hydraulic diameter was 12,500. The pressure at the exit is set to be atmospheric pressure.

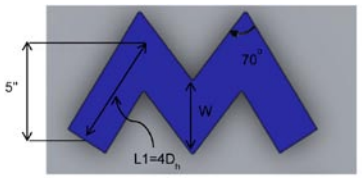

a) Zig-zag channel with 70° turns

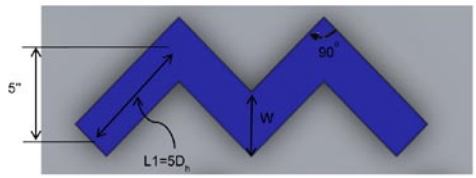

b) Zig-zag channel with 90° turns

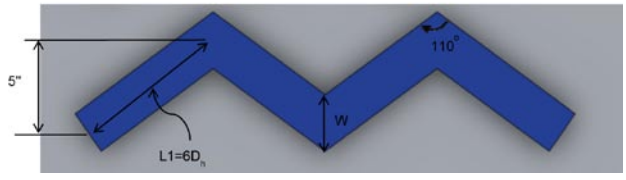

c) Zig-zag channel with 110° turns

FIGURE 1. Zig-zag channel configurations

The mesh for each test case consisted of approximately 4.0 million grids. The y^+ values for each case was within the range of 0.5–2.0 to insure proper usage of the wall functions. The growth from the wall was set at a ratio of 1.2.

Based on the ANSYS CFX modeling, the streamlines and velocity profile at the first pass for all zig-zag channels are generally similar (Figure 2). For the zig-zag channel with 70° turning angle, due to smaller radii of curvature and an unfavorable pressure gradient, gas flow is expected to separate from the main flow. Therefore, a recirculation zone is formed at the corner of the first turning region. Such phenomenon is not observed in other test domains. At the post-turn region of the first pass, flow impinges on the outer wall, that later progresses downstream. At the second pass, flow impinges on the inner wall of the third pass. A recirculation zone is created at the corner of each turn that may extend up to approximately half the size of each pass. In addition, the presence of the turn increases the magnitude of velocity throughout the channel. The zig-zag channel with 70° turning angle has the shortest total flow length, and experiences the greatest velocity increment, followed by the zig-zag channel with 90° and 110° turning angles. Separation occurs when the pressure gradient is lower than the surrounding pressure. The size of the separation zone at the second and third turns is quite substantial, covering ~30–50% of the second and third passages.

Since there are no protruding elements or roughness in the channels, heat transfer characteristics are mainly governed by the impingement and secondary flow induced by the turns. Before the turn, heat transfer, *h*, at the first passage for all test cases is fairly comparable and uniform. This implies that the *h* in the first passage is unaffected by the presence of upstream turn. Heat transfer distribution begins to change drastically after the first turn due to impingement, separation and the presence of secondary flows. Low heat transfer is observed at each corner inside the recirculation zone which later contributes to spatial non-uniformity in heat transfer in each passage through the entire test domain. This is more evident in the third and fourth passages. Overall, *h* is enhanced after every turn.

Heat transfer enhancement is determined based on the total average heat transfer normalized by the fully developed smooth channel obtained from the Dittus-Boelter correlation, $Nu_o = 0.023Re^{0.8}Pr^{0.4}$. As heat transfer enhancement for each case is relatively comparable, i.e., ranging between 2.4–2.6, the overall heat transfer enhancement was shown to be insensitive to the turning angles and total flow length of the zig-zag channels that were used in this study. While the three zig-zag channels exhibit comparable heat transfer performance,

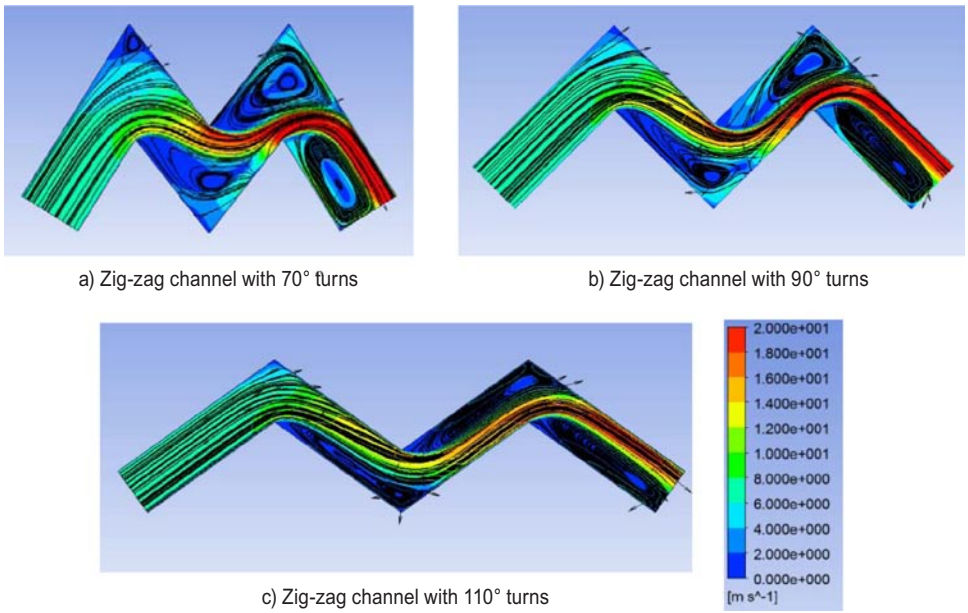

FIGURE 2. Velocity profile and streamlines of zig-zag channels with varying turning angles

the pressure loss in these cases can vary substantially with different turning angles. As shown in Table 1, the zig-zag channel with 70° turning angles has the highest pressure loss, followed by the zig-zag channels with 90° and 110° turn angles. The pressure loss for the zig-zag channel with 70° turning angle is approximately three times higher than that of the 110° case. Therefore, the zig-zag channel with 110° turns was selected for further experimental testing.

TABLE 1. Heat Transfer Performance and Pressure Drop

Zig-Zag Channel	Nu_T	Nu_T/Nu_o	f/fo
110°	72.80	2.47	30.59
90°	78.73	2.62	23.48
70°	74.09	2.43	11.31

f/fo: pressure change
Nu_T/Nu_o: heat transfer enhancement

Experimental Testing

The experimental test section that was used to assess zig-zag heat transfer enhancement characteristics was constructed of low thermal conductivity Plexiglas® and had a cross-sectional area of 63.5 mm x 25.4 mm. Figure 3 illustrates the experimental results for the local heat transfer coefficient, *h* distribution for the zig-zag channel with 110° turning angles for varying Reynolds number, Re. Generally, heat transfer appears to increase with the number of turns. Heat transfer distribution at the first passage is quite uniform with varying Re. Heat transfer distribution changes significantly after the first turn. At the first turn, heat transfer is higher towards the outer wall which is subjected to flow impingement. After passing two turns at the upstream, the flow seems to be more uniformly mixed at the third passage, contributing to a more even heat transfer distribution with a peak at the central region. Heat transfer distribution in the third passage is, however not consistent with the numerical results that were presented in the previous section.

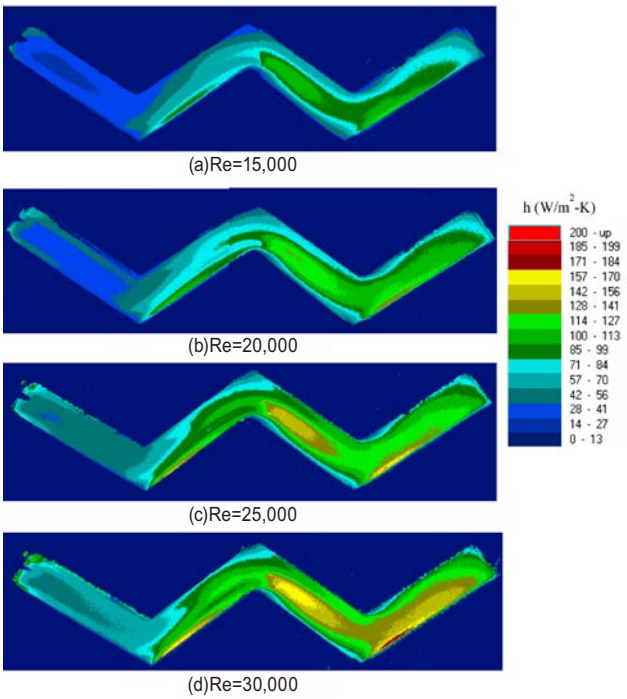

FIGURE 3. Local heat transfer coefficient, *h* (W/m²-K) distribution

Numerically, heat transfer appears to be higher at the inner wall region than the outer wall. The experimental result also indicated that there is no flow impingement effect in the third passage. At the fourth passage, due to the presence of third turn, flow tends to impinge on the outer wall. Therefore, heat transfer at the region closer to the outer wall tends to be higher than the region towards the inner wall. Qualitatively, the experimental results in the first, second, and fourth passages shown in Figure 3 correspond quite well with the numerical results. The deviation of heat transfer pattern in the third passage between the numerical and experimental results may be due to the limitation of the turbulence model and wall function that are incapable of qualitatively predicting the heat transfer and flow field with sufficient accuracy in the zig-zag channel that involves several turns.

Figure 4 illustrates the heat transfer enhancement while varying Re at different passages normalized by the fully developed smooth channel. Based on the results shown in Figure 4, Nu/Nu_o shows similar trends for all test cases. That is heat transfer increases with the number of channel passages. With the heat transfer enhancement close to unity, the heat transfer at the first passage seems to be insensitive to the presence of the downstream turn. However, after the first turn, heat transfer at the second passage is enhanced substantially by ~50%. This is mainly attributed to the secondary flows induced by the turn. Further downstream, heat transfer at the third and fourth pass is enhanced approximately two-fold and begins to be reduced to the fully developed condition. Two main mechanisms that govern heat transfer in the channel include turbulence generated in the channel, and driving potential difference between the wall and bulk flow temperatures. Towards the downstream section of the channel, both effects tend to decrease. However, as the flow length of each passage is rather short, the heat transfer in the subsequent passage appears to be dominated by the secondary flows induced by the upstream turn.

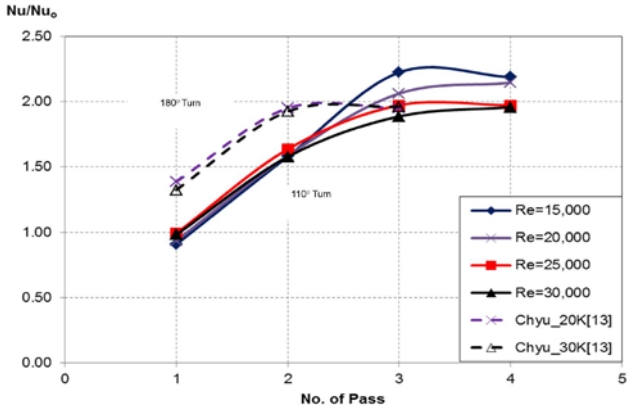

FIGURE 4. Averaged heat transfer enhancement at different passages

Enhanced Trailing Edge Cooling Designs

Two rib-turbulator designs designated as ZZ_Rib1 and ZZ_Rib2 were evaluated as options for overall heat transfer enhancement of the zig-zag channel (Figure 5). The width, r_w and height, r_h of the ribs used in this study are 1.59 mm, with the ribs being positioned vertically at 54.5° to the flow direction (highlighted by 'red' arrow), extending from both side walls. The rib-pitch, P/r_h is equal to 10, which is based on an optimal rib spacing reported by the turbine community. For the ZZ_Rib1 case, rib-turbulators are placed in all four passes. In contrast, for the ZZ_Rib2 case, rib-turbulators are placed in only the first and second pass. Test results from the ZZ_Rib2 case provide detailed information pertaining to the effects of upstream turbulence generated by the rib-turbulators with respect to the smooth downstream region in the third and fourth pass.

Towards the end of the trailing edge region, the cross-sectional area of internal cooling passages becomes thinner and smaller due to the geometry of the airfoil, which imposes a great challenge of having vortex generators, i.e., pin-fins, on both endwalls. Additionally, the pin-fin array features are often subjected to concentrated thermally induced stress. For the geometry and span across the internal zig-zag channel used in this study, the rib-turbulators are preferred in comparison to the pin-fin array as thermal stress is alleviated.

The local heat transfer coefficient, *h* distribution for the ZZ_Rib1 case at varying Re indicates that even with the presence of rib-turbulators, the impingement zones that appear in the smooth zig-zag counterpart are

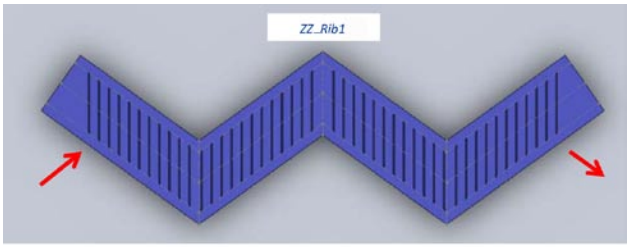

(a) Zig-zag channel with rib turbulators in all four passes

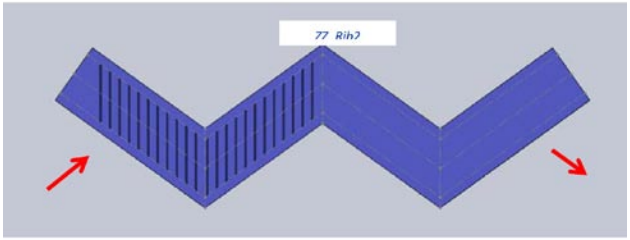

(b) Zig-zag channel with rib-turbulators in first and second passes(ZZ_Rib2)

FIGURE 5. Zig-zag channels with rib-turbulators (top view)

preserved in each passage. This implies that the flow in the channel is still dominated by the secondary flow induced by the turns (Figure 6). Locally, heat transfer is substantially enhanced due to the rib-induced secondary flow moving in the rib angle direction. Depending on the rib-turbulators orientation and location, flow tends to move along the rib-turbulators surface towards the opposite end. In the first pass, the enhanced heat transfer at the endwall is governed by the secondary flow orientation induced by the rib-turbulators. The heat transfer close to the pressure side is higher than that of the suction side. Heat transfer in the downstream is enhanced by the secondary flows induced by both the turn and rib-turbulators. Besides the region between two consecutive rib-turbulators, heat transfer at the impingement zone of the second, third, and fourth passages is significantly enhanced. However, the recirculation zones at each corner of the turn remain lower than that of the smooth zig-zag counterpart.

The local heat transfer coefficient distribution of the ZZ_Rib2 case was shown to decrease substantially without the presence of rib turbulators in the smooth third and fourth passages (Figure 7). However, compared to the smooth zig-zag counterpart, the heat transfer at the third passage is enhanced due to the turbulence and wakes generated by the upstream turns and rib-

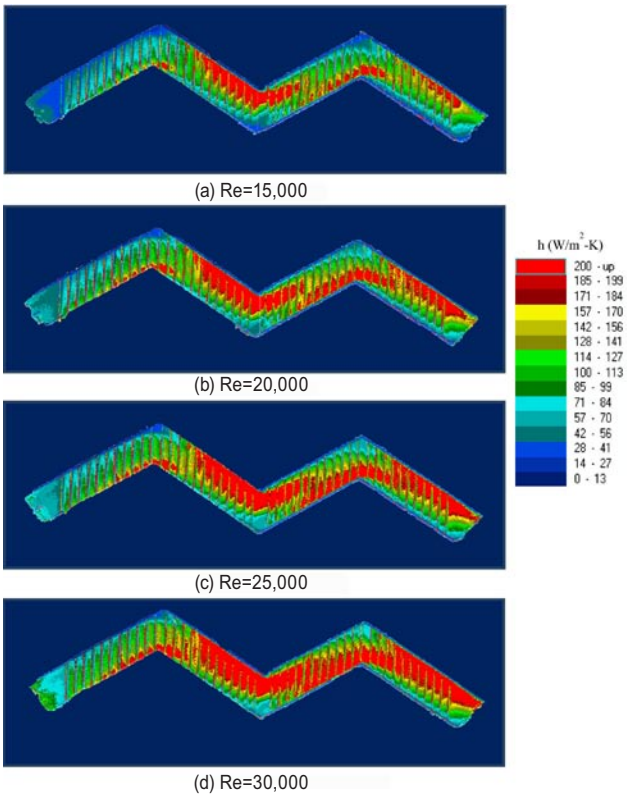

FIGURE 6. Local heat transfer coefficient, h (W/m^2-K) distribution (ZZ_Rib1)

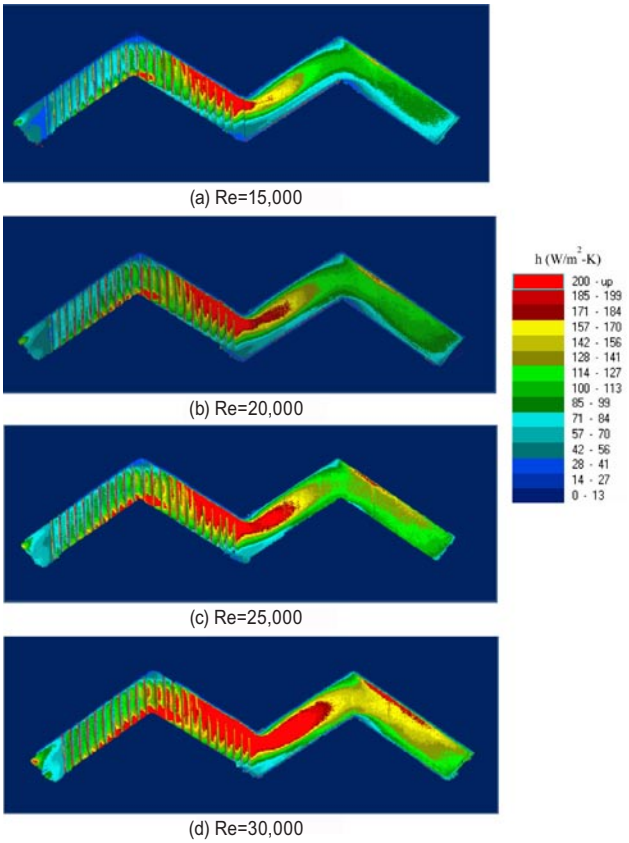

FIGURE 7. Local heat transfer coefficient, h (W/m^2-K) distribution (ZZ_Rib2)

turbulators. Comparison between test results of the smooth zig-zag channel and the ZZ_Rib2 case indicates that there is virtually very little improvement in heat transfer at the fourth passage which implies that the strength of turbulence and wakes generated at the first and second passages are only effective towards the heat transfer enhancement at the third passage.

The overall heat transfer enhancement of the entire channel for all zig-zag channels normalized by the fully developed smooth channel is shown in Figure 8. The results are compared with the limiting case, two-pass and three-pass channels with 180° turns. The smooth zig-zag channel has the lowest heat transfer enhancement and which is relatively constant, i.e., ranging from 1.6–1.7, given the Re values used in this study. The ZZ_Rib1 case with rib-turbulators throughout the entire zig-zag channel has the highest heat transfer enhancement which is approximately 3.0–3.6 fold higher in comparison to the fully developed smooth channel. With the presence of rib-turbulators, the heat transfer in the zig-zag channel is further enhanced approximately 2-fold in comparison to the smooth zig-zag channel. With similar heat transfer trend that is ~20% lower than that of ZZ_Rib1 case, the ZZ_Rib2 has heat transfer enhancement ranging from

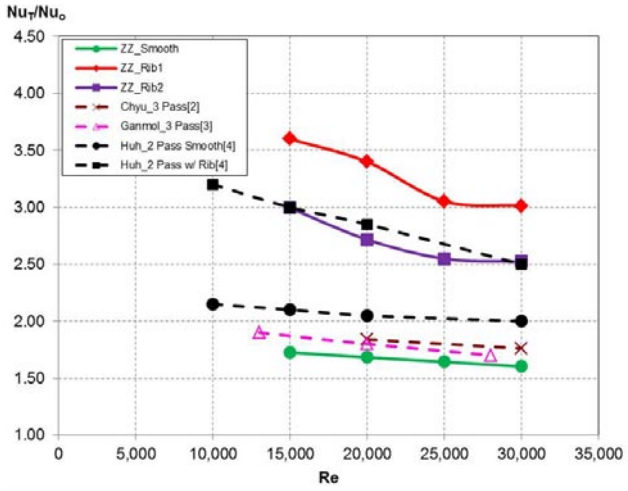

FIGURE 8. Total heat transfer enhancement at varying Re

2.5–3.0. The smooth two-pass and three-pass channels [1–3] has higher heat transfer enhancement than the smooth zig-zag channel. This is mainly attributed to the secondary flow created by the 180° turning angle that substantially enhanced heat transfer in the downstream region. By introducing rib-turbulators in the first and second pass, the overall heat transfer performance of the zig-zag channel, i.e., ZZ_Rib2, is further enhanced and comparable to the two-pass channel with rib-turbulators as reported by Huh [3].

Conclusions

Experimental and numerical studies of airfoil trailing edge zig-zag channels with different turning angles indicate:

- The heat transfer performance in the zig-zag channel is enhanced after every turn within the flow domain. This is mainly attributed to the additional turbulence and better flow mixing induced by each turn.
- Overall heat transfer enhancement in the zig-zag channel is enhanced by ~1.7 times in comparison to the fully developed smooth channel.
- The pressure loss of the zig-zag channel seems to be insensitive to the Reynolds number (Re = 15,000–30,000) that was used in this effort.

Detailed experimental testing of the zig-zag channels that consist of smooth and rib-turbulated surfaces indicate that

- Rib-turbulators significantly impact heat transfer enhancement in the zig-zag channel. By having rib-turbulators throughout the entire zig-zag channel, heat transfer enhancement is increased by approximately two-fold in comparison to the smooth zig-zag channel.
- Overall, the pressure loss in zig-zag channels where all passages contain rib-turbulators is ~30–90% higher than that of the zig-zag smooth counterpart. The pressure loss in zig-zag channels that contain rib-turbulators in the initial passage sections is ~10–60% higher than that of the zig-zag smooth counterpart.

Future Directions

- Innovative cooling channel configurations and surface features for heat transfer enhancement along the thin airfoil trailing edge will continue to be developed. Experimental efforts will be directed to increasing coolant-to-surface contact area and residence time in order to improve heat removal and optimize cooling in the channel. Surface features will be experimentally addressed in bench-scale laboratory testing at the University of Pittsburgh to demonstrate heat transfer enhancement.
- Commercial manufacture of internal trailing edge test coupons will be undertaken with designs developed by the NETL-RUA. These coupons will be subjected to high temperature, pressurized internal cooling-heat transfer testing in NETL's aerothermal test facility in Morgantown, West Virginia.

Acknowledgments

We wish to acknowledge Mr. Richard Dennis and Ms. Patcharin Burke at NETL for their support.

FY 2012 Publications/Conferences/ Presentations

1. S. Siw, M. Chyu, and M.A. Alvin, "Investigation of Heat Transfer Enhancement and Pressure Characteristics of Zig-Zag Channel," ASME Turbo Expo, Copenhagen, Denmark, June 11–15, 2012 (GT2012-69268). Acceptance notification was received on December 19, 2011.

2. Manuscript preparation: S. Siw, M. Chyu, C. Lee, and M.A. Alvin, "Heat Transfer Enhancement and Pressure Characterization of Zig-Zag Channels," *Journal of Heat Transfer.*

3. Revised manuscript: S. Siw, M. Chyu, and M.A. Alvin, "Heat Transfer Enhancement and Pressure Loss Characteristics of Zig-Zag Channel," from ASME Turbo Expo 2012, in preparation for submission to *Journal of Heat Transfer.*

References

1. Chyu, M.K., 1991, "Regional Heat Transfer in Two-Pass and Three-Pass Passages with 180-Deg Sharp Turns," *Journal of Heat Transfer*, Vol. 113, pp. 63–70.

2. Ganmol, P., "2010, Heat Transfer in Two-Pass with Vortex Generators," PhD Thesis Dissertation, University of Pittsburgh, Pennslyvania, USA.

3. Huh, M., Liu, Y.H., Han, J.C. and Chopra, S., 2008, "Effect of Rib Spacing on Heat Transfer in a Two-Pass Rectangular Channel (AR=1:4) with a Sharp Entrance at High Rotation Numbers," ASME Turbo Expo GT2008-50311, Berlin, Germany.

IV. ADVANCED RESEARCH

B. Combustion

IV.B.1 Low-Swirl Injectors for Hydrogen Gas Turbines in Near-Zero Emissions Clean Coal Power Plants

Robert K. Cheng
Lawrence Berkeley National Laboratory
MS 70-108B, 1 Cyclotron Road
Berkeley, CA 94720
Phone: (510) 486-5438
Email: RKCheng@lbl.gov

DOE Project Manager: Robin Ames
Phone: (304) 285-0978
Email: Robin.Ames@netl.doe.gov

Collaborators:
- United Technologies Research Center, East Hartford, CT
- University of California, Irvine, CA
- Georgia Institute of Technology, GA

Contract Number: FWP 7-678402

Start Date: October 1, 2011
End Date: September 30, 2012

Fiscal Year (FY) 2012 Objectives

- Characterize the impact of low-swirl injector (LSI) geometric configuration on its performance.
- Improve characterization of H_2 flame oscillations.
- Characterize turbulent lean H flame structures and the implications on modeling development.

FY 2012 Accomplishments

- Demonstrated that the LSI performance is insensitive to variations in its geometric configurations and showed that the size of the swirl annulus can be increased to lower aerodynamic drag.
- Found that the differences in the flame shapes of CH_4 and high hydrogen fuels (HHF) flames are the causes of their different combustion oscillation characteristics. Such insights can be used in the development of models that predict the combustion oscillation characteristics in gas turbine systems.

Introduction

The goal of this project is to develop a cost-effective and robust combustion system for the gas turbines in near-zero emissions integrated gasification combined cycle (IGCC) coal power plants that burn high hydrogen fuel (80%+) and syngas derived from coal gasification. U.S. Department of Energy (DOE) Fossil Energy Advanced Turbine Program (ATP) sets a very aggressive emissions goal of less than 2 ppm NOx for these turbines. Current dry low-NOx (DLN) combustion technologies developed for natural gas may not be readily adaptable to accommodate the highly reactive and dynamic characteristics of the HHF flames. Some gas turbine original equipment manufacturers (OEMs) are re-evaluating the option of using conventional and more polluting combustion methods for operating with HHF and treating the exhaust stream with expensive "tail-pipe" catalytic cleanup methods to reduce NOx to the targeted level.

All contemporary DLN gas turbines employ lean premixed combustion as their operating principle to mitigate NOx emissions by burning highly diluted lean fuel/air mixtures. Lean turbulent premixed flames are dynamic in nature and behave as self-propelling waves. They burn faster or slower according to the fluid mechanical, chemical, and thermodynamic properties of the system. These include fuel type, initial temperature and pressure, flow velocities, and turbulence intensities. The complex coupling of the flame with turbulence dictates its dynamic behaviors and is the crux of the challenges in designing and engineering DLN combustion systems for gas turbines. The conventional DLN approach is to hold the dynamic premixed turbulent flames within the recirculation zones of intensely swirling flows. The LSI concept takes an opposite approach. It enables the premixed flame to propagate freely and burn in a divergent flow generated at the core of a weakly swirling flow.

Approach

The LSI concept was originally conceived at Lawrence Berkeley National Laboratory for basic research. Laboratory studies and analysis have provided the scientific foundation to facilitate the transfer of this combustion method to gas turbines. To adapt the LSI for

the large-frame 200 mW+ hydrogen fueled engines, the strategy is to optimize the basic LSI nozzle developed for a 7 mW natural gas engine to burn hydrogen and collaborate with a gas turbine manufacturer to scale the design to larger sizes. The heart of the LSI is a patented swirler engineered to produce a turbulent divergent flow. It is capable of supporting stable turbulent lean premixed flames under a wide range of operating conditions. A characteristic signature of the LSI is a lifted flame that does not touch any part of the nozzle. The LSI swirler can be adjusted to accommodate the changes in the combustion properties of various fuels. This is done by reconfiguring the swirler components to change the swirl intensity.

The development of an LSI for IGCC gas turbines started with laboratory studies to optimize the configuration for burning lean hydrogen flames whose NOx emissions are below 2 ppm. The experiments also provided turbulent flame speed data and quantitative information on the LSI flowfield to support the development of an analytical model that can be used to guide the design of LSI hardware for gas turbines. Testing of the LSI at simulated gas turbine conditions had shown its potential to meet the DOE Advanced ATP NOx emissions goals. In collaboration with researchers from national laboratories and universities, laboratory and computational research are being pursued to assist in the development of combustion models and computational design tools for scaling of the LSI to large capacities and adaptation to different engine configurations. The developments of the LSI for HHF gas engines are pursued in collaboration with the OEMs. Prototype hardware will be developed to meet specific engine and system operation requirements and to address issues on combustion intensity, dynamics, emissions, flashback, blowoff and auto-ignition.

Results

Successful development and testing with natural gas and HHF of a fully-functional reduced-scale LSI in FY 2011 have shown this technology to be a cost-effective option for the IGCC combustion turbines to meet the aggressive operational and emissions goals. To refine the engineering guidelines needed for the design of a full-scale prototype, and for the adaptation to gas turbine combustors having different geometric and flow requirements, a parametric study of the effect of changing LSI geometry on its operability was carried out. Ten swirlers were used in the study. The baseline swirler is the one from previous studies shown at the center of Figure 1 and at top left of Figure 2. It has 16 thickened short swirl vanes with vane angle α of 37°. These vanes are attached to a center-channel whose radius is at 67% of the nozzle diameter (i.e., $R = R_c/R_n = 0.67$). When the swirler is fitted inside a cylindrical tube which forms the LSI nozzle, the vanes nest in an annulus between the center-channel and the nozzle. Operation of the LSI relies on controlling the flow-split, i.e., the ratio of the flows passing through the center-channel, and the swirl annulus. To achieve the appropriate flow-split a simple

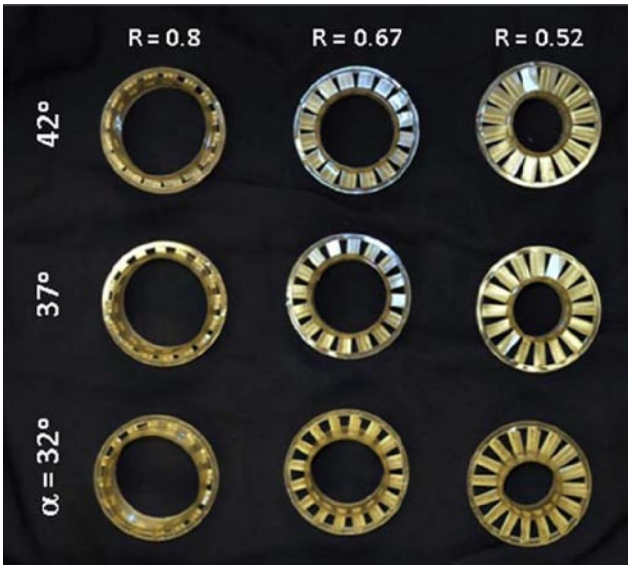

FIGURE 1. Nine LSI swirlers with thickened vanes used for our parametric study. These swirlers are shown before they are fitted with the perforated plate for the center opening. The baseline swirler is at the center.

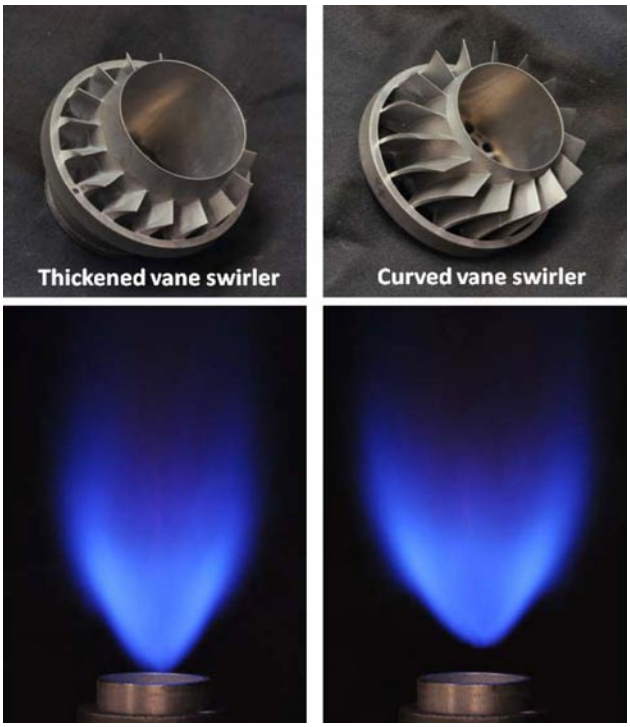

FIGURE 2. Baseline LSI with thickened vanes (left) and its curved vane variant. The CH_4 flames they generate are shown below.

and effective means is to cover the center-channel with a perforated plate. In the case of the baseline swirler, its perforated plate has about 40% openness. Eight variants of the baseline swirler design were fabricated by changing α to 42° and 32°, and R to 0.52 and 0.8 (Figure 1). A tenth swirler with thin vanes was also evaluated (Figure 2 right). It has the same number of blades, the same R and α as the baseline swirler but with a set of thin and longer blades having constant radius curvature (Figure 2 top right). The 10 swirlers were evaluated in the laboratory by comparing their performances in terms of flame blow-off limits, NOx, and CO emissions from methane flames. Also compared are their aerodynamic drags, the similarity features and the normalized axial divergence rates of the flowfields, and positions of the flames they produced.

The results show that all 10 LSI are operable with CH_4. All generated flames of similar shapes and locations. Figure 2 illustrates that the flame positions and flame shapes from the thick and the thin blade LSIs are comparable. The CH_4 flame blow-off limit and NOx and CO emissions are not highly sensitive to the LSI geometric variations. Of the seven LSIs that permitted an examination of the nearfield flow structures, self-similarity features were found. This implies their turndown ranges to be similar. Comparison of the aerodynamic drags showed that the swirlers with smaller center channels, i.e., larger swirl annulus, have lower drag. Using thin vanes instead of thickened vanes further reduced the aerodynamic drag. Therefore, the pressure drop across the LSI, which is proportional to the drag, can be adjusted to match the system requirements of the gas turbine system without compromising performance. More importantly, our result shows that the relatively low aerodynamic drag of the LSI can be exploited in new gas turbine combustion systems to increase the overall system efficiency. Another significant finding of this study is that despite the variations in swirl number, blade shape, and center channel ratio, all 10 LSI share a common feature in that 70% to 80% of the premixture flows through the vane annulus. Therefore, the flow-split can be a very useful engineering design parameter for the LSI because it has a simple design specification of 70%/30% to 80%/20% ratio between the swirled and unswirled flows. Based on these findings and insights from other studies of LSI fuel flexibility, specific design guidelines and recommendations for low-emission and fuel-flexible operations have been developed. These results show that the LSI offers a broad design space with relatively few restrictions for adaptations of the technology to a wide range of gas turbine configurations.

Although the rig-test of a reduced-scale LSI prototype has shown that the LSI remained oscillation free during all the test points, gaining a better understanding of the thermal-acoustic coupling mechanisms that incite combustion oscillations in LSI remains an important aspect of its development for IGCC combustion turbines. As reported in FY 2011, we collaborated with Siemens Energy, Inc., to investigate the thermal-acoustics coupling mechanisms of a CH_4 flame and a 0.9 H_2/0.1 CH_4 flame by a linear general instability model (GIM). It was found that the GIM was suitable for the CH_4 flames because it is lifted and detached from the nozzle (see flames of Figure 3) so that the basic premise of GIM that assumes a time delay between the formation of large scale flow structures such as a vortex and the onset of flame disturbances is satisfied. But for 0.9 H_2/0.1 CH_4 flame, GIM is not appropriate because the high-reactivity of H_2 causes the flame to attach to the rim of the nozzle. Flame attachment means that the large vortices in the outer shear layer develop and burn simultaneously. This process is inconsistent with the basic premise of GIM. To gain insights on the differences in the instability mechanisms of the CH_4 and the 0.9 H_2/0.1 CH_4 flames, we collaborated with United Technology Research Center to investigate the temporal behaviors of the oscillating flame structures by high-speed imaging. The experiments involved the use of two video cameras to capture the oscillating flame structures of twelve flames burning CH_4 and 0.9 H_2/0.1 CH_4.

Our first analysis focused on two thermal-acoustically coupled unstable flames—a CH_4 flame at fuel/air equivalence ratio ϕ = 0.7 (113 kW) and a 0.9 H_2/0.1 CH_4 flame at ϕ = 0.4 (74 kW). Shown in Figure 3 are the flame light images (in grayscale) of the two flames at four phases of an oscillation cycle. To the right of the images are the corresponding mean streamtraces measured by phase-resolved particle image velocimetry (PIV). From the flame light images, it is apparent that the two flames differ not only in their overall flame size, shape, and location, but also in how they evolve through the oscillation cycle. From the locations of the roll-up vortex centers deduced from the spiraling streamtraces, it is also clear that the evolutions of the flame structures in both cases correlate with the formation and convection of the large vortices. The dominance of the large vortices on flame oscillations was verified by performing proper orthogonal decomposition (POD) analysis on the high-speed videos. The POD results show that the flame structures that generate high heat release fluctuations are associated with the traveling roll-up vortices. But due to the differences in the flame size and shape of the CH_4 and the 0.9 H_2/0.1 CH_4 flame, the mechanisms that drive their instabilities are found to be different. This was shown by deducing the time-dependent two dimensional Rayleigh Indices (RI) from the high-speed videos. For the CH_4 flame, thermal-acoustic driving occurs in the region where the trailing edge of the flame impinges on the combustor wall. This causes a phenomenon called flame-folding to create a

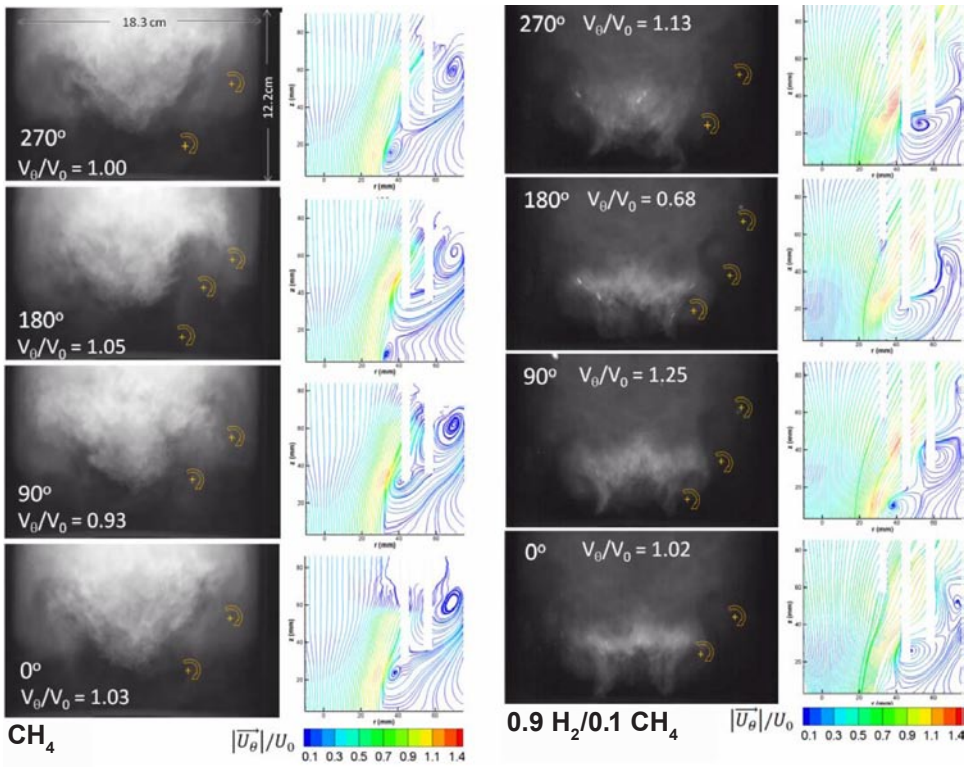

FIGURE 3. Flame light images and streamtraces at four phases of the oscillation cycle. Vortex centers and the rotation direction are marked on photos with "+". V_θ/V_o is the normalized phase resolved volumetric flow rate and U_θ/U_o is the normalized phase resolved velocity magnitude.

small region of localized high heat release rate. However, the flame folding process in the CH_4 is irregular. On the other hand, the driving mechanism of the 0.9 H_2/0.1 CH_4 flame is caused by a regular event involving the roll-up flame in the shear layer vortex merging with the central flame. This resulted in a large region of instantaneous localized high heat release region and a stronger driving mechanism. The differences in the driving mechanism explains why the acoustics emissions of the 0.9 H_2/0.1 CH_4 flame is significantly higher than the CH_4 flame even though the total heat release is lower. The effectiveness of this approach has been demonstrated recently at atmospheric and simulated gas turbine conditions where LSIs fitted with divergent quarls are shown to reduce combustion oscillations.

Conclusions and Future Directions

The study on the sensitivity of LSI performance on operability has shown that it offers a broad design space with relatively few restrictions for adaptations of the technology to a wide range of gas turbine configurations. To reduce the likelihood of combustion instability in a fuel flexible LSI gas turbine combustion, our investigation on flame oscillation mechanisms of CH_4 and 0.9 H_2/0.1 CH_4 showed that the mitigation of flame attachment and/or deferring the formation of the outer shear layer is needed.

Future work will be focused on applying the knowledge gained from these studies for scaling up the design to the capacity of a large-frame utility size gas turbine.

- Investigate the fuel-effects on transition from stable to instable flame.
- Seek opportunity to develop the LSI for gas turbines operating on natural gas.
- Gain insights into the basic properties of hydrogen flames for modeling development.

FY 2012 Publications/Presentations

1. P.L. Therkelsen, J. Enrique Portillo, D. Littlejohn, S.M. Martin, and R.K. Cheng, "Self-induced Unstable Behaviors of CH_4 and H_2/CH_4 Flames in a Model Combustor with a Low-Swirl Injector," to appear, Combustion and Flame (2012).

2. D.W. Davis, P.L. Therkelsen, D. Littlejohn, and R.K. Cheng, "Effects of Hydrogen on the Thermo-Acoustics Coupling Mechanisms of Low-Swirl Injector Flames in a Model Gas Turbine Combustor," to appear, Proceedings of the Combustion Institute (2012).

3. P.L. Therkelsen, D. Littlejohn and R.K. Cheng, "Parametric Study of Low-Swirl Injector Geometry on it Operability," Paper GT2012-68436, ASME TurboExpo, Copenhagen, Denmark, June 10-15, 2012.

4. D. Beerer, V. MeDonnel, P.L. Therkelsen, and R.K. Cheng, "Flashback, Blow out, Emissions and Turbulent Displacement Flame Speed Measurements in a Hydrogen and Methane Fired Low-Swirl Injector at Elevated Temperatures and Pressures," GT2012-68216 ASME TurboExpo, Copenhagen, Denmark, June 10–15, 2012.

IV.B.2 Thermophysical Properties of Carbon Dioxide and CO_2-Rich Mixtures

Dr. Allan H. Harvey (Primary Contact),
Dr. Christopher W. Meyer,
Dr. Richard A. Perkins
National Institute of Standards and Technology
325 Broadway
Boulder, CO 80305
Phone: (303) 497-3555; Fax: (303) 497-5044
Email: aharvey@boulder.nist.gov

DOE Project Manager: Travis Shultz
Phone: (304) 285-1370
Email: Travis.Shultz@netl.doe.gov

Contract Number: FE0003931

Start Date: October 1, 2011
End Date: September 30, 2014

Fiscal Year (FY) 2012 Objectives

- Measure thermal conductivity of pure CO_2 at temperatures up to 340 K and complete analysis of data.
- Complete and validate apparatus for measuring dew point of water in CO_2.

FY 2012 Accomplishments

- Completed thermal conductivity measurements of pure CO_2 at temperatures from 220 K to 340 K in the liquid, vapor, and supercritical gas phases with lower uncertainty than existing literature data at temperatures below 300 K.
- Completed assembly of apparatus to measure dew point of water in CO_2 and validated apparatus by testing with air.

Introduction

Carbon capture and sequestration is of increasing interest for environmentally responsible use of fossil fuels. At many stages of proposed sequestration processes, it is necessary to know properties of both pure CO_2 and mixtures of CO_2 with small amounts of other components. Of particular interest is the equilibrium between liquid water and compressed CO_2; in order to avoid corrosion, pipelines and other equipment should be operated at conditions where no liquid water will condense. Data and thermodynamic modeling are needed to better define these conditions.

In addition, pure carbon dioxide at supercritical conditions is a promising working fluid for achieving higher efficiency in electric power generation. Knowledge of properties such as viscosity and thermal conductivity at the relevant conditions (up to high pressures and temperatures) is needed in order to better design equipment for such power cycles.

Approach

The approach combines high-accuracy experimental work with National Institute of Standards and Technology's (NIST's) expertise in developing models for thermophysical properties. For the CO_2-H_2O system, accurate measurements of the dew point of moist CO_2 will be used to develop a complete thermodynamic model able to describe the phase equilibria and other thermodynamic properties of this mixture at conditions relevant to pipelines and other process equipment. For pure CO_2, new thermal conductivity data at both subcritical and supercritical temperatures, along with new viscosity data taken by collaborators outside this project, will be used to develop reference-quality correlations for these two properties, replacing and improving on the current standard formulations that were developed around 1990.

Results

Measurements have been completed on a pure (99.994 %) sample of carbon dioxide with the cryogenic hot-wire apparatus at NIST. The cryogenic hot-wire cell is shown in Figure 1 and has short and long hot wires that allow compensation for end effects. Measurements of the thermal conductivity of this sample have been made along subcritical liquid and vapor isotherms at temperatures of 220, 235, 250, 265, 280 and 295 K and along supercritical isotherms at temperatures of 310, 315, 325, and 340 K. These measurements are shown in Figure 2 along with lines from the correlation of Vesovic et al., [1] as implemented in the NIST REFPROP 9.0 program [2]. The transient-hot-wire apparatus was operated in the steady-state mode at pressures below 0.5 MPa with subcritical vapor and supercritical gas. The transient mode was used at pressures from 0.5 MPa up to the saturation line for subcritical-vapor isotherms and up to

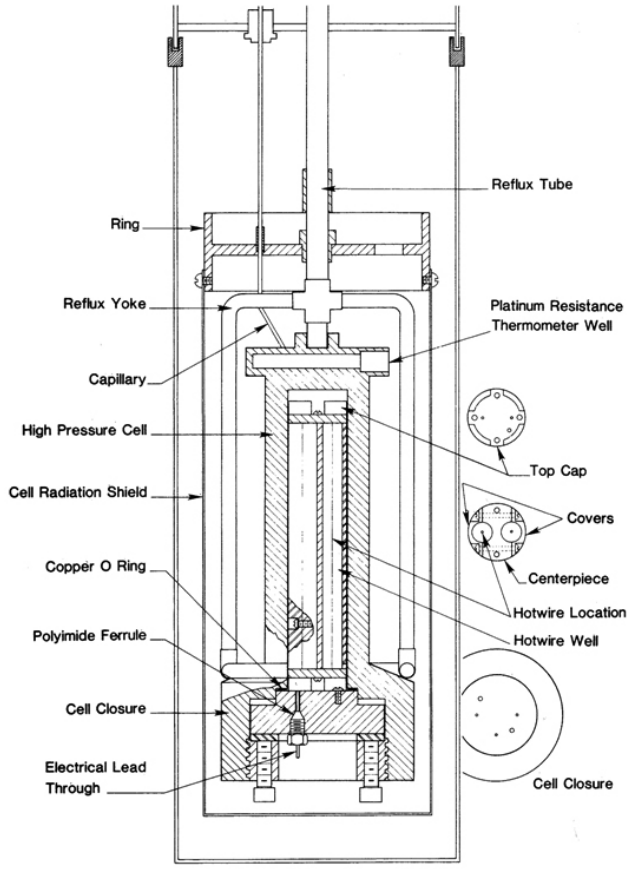

FIGURE 1. Cryogenic hot-wire cell for determination of fluid thermal conductivity at temperatures from 30 K to 340 K at pressures from 0.1 MPa to 70 MPa. Vacuum cryostat is immersed in liquid nitrogen for measurements below 300 K.

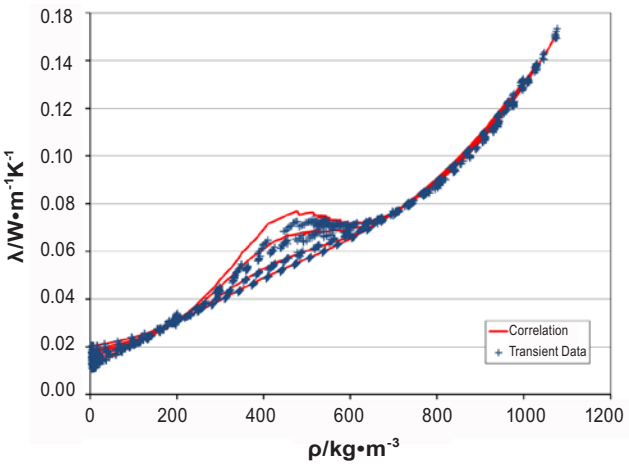

FIGURE 2. Thermal conductivity of CO_2 at temperatures from 220 K to 340 K with pressures up to 68 MPa. Liquid, vapor and supercritical data are shown along with lines from the correlation of Vesovic et al., [1] as implemented in the NIST REFPROP 9.0 database [2].

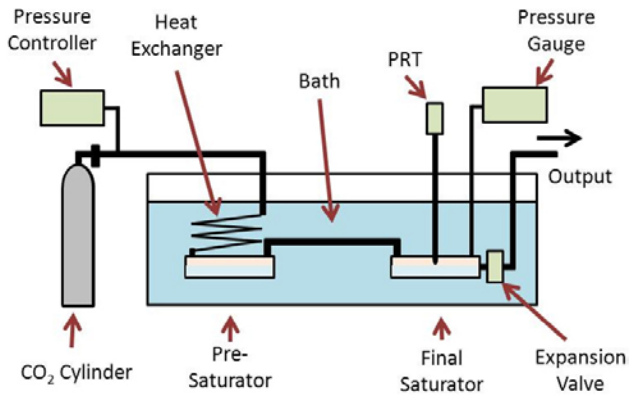

FIGURE 3. Schematic diagram of the dew-point measurement facility.

68 MPa for supercritical gas. The transient mode was also used for the liquid phase at pressures from the saturation line up to 68 MPa. A significant critical enhancement was observed along the supercritical isotherms, which is centered near the critical density. Measurements were made at up to 10 different applied power levels (10 different temperature rises) to verify that natural convection was not a problem during the measurements. The correlation lines shown in Figure 2 were calculated at each measured temperature and pressure so they are not true isotherms and are not smooth in the critical region. These data are in good agreement with other reliable data in the critical region. Final analysis of this data up to 345 K has been completed and reported at the 18th Symposium on Thermophysical Properties in June 2012.

As a preliminary to this work (not funded by this project), a facility (shown schematically in Figure 3) was constructed to be used for measuring the dew point of gases as a function of mole fraction and pressure. The two centerpieces of the facility are (1) a system for saturating CO_2 with water (composed of a pre-saturator and final saturator) at a controlled temperature and pressure; and (2) the NIST gravimetric hygrometer [3]. The hygrometer measures the water mole fraction in a gas stream by separating the water from the dry gas using desiccants and subsequently determining the mass of each. The water is collected in desiccant tubes whose mass is measured before and after the water collection, and the gas is collected in prover tubes (see Figure 4) where its mass is determined using volume, temperature and pressure measurements. A gas-handling system was set up to connect all components of the facility. With this system, a gas flows from its cylinder into the pre-saturator and final saturator at a controlled pressure. The gas then flows out of the final saturator to the gravimetric hygrometer through a metering valve that controls its flow to be about 2 liters/min. The gas handling system also includes tubing that connects the final saturator to

FIGURE 4. Photograph of dry gas collection facility for NIST gravimetric hygrometer.

a pressure gauge. A plumbing station was constructed to connect the reference side of the saturator pressure gauge and the gravimetric-hygrometer pressure gauge to a vacuum; this station includes bypass valves to allow periodic measurement of the zero offset of the gauges. Finally, the saturators were mounted in a temperature-controlled bath constructed with an insulated bath lid with holes that allowed the plumbing tubes to pass through.

After construction of the facility, software was written for controlling the gas flow through the saturator and gravimetric hygrometer and for acquiring the relevant data. Both the facility itself and the data-acquisition protocol were also modified to enable the experiment to provide accurate results without consuming an excessive amount of gas. Preliminary data were taken using air as a carrier gas in order to validate the performance of the system. One set of air data has been taken, in which the air was saturated with water at several different pressures (ranging from 0.5 MPa to 3 MPa) at a temperature of 21.7°C. The results of these preliminary experiments showed good agreement with known values (obtained in the context of NIST humidity standards) for the dew-point/mole-fraction/pressure relations in moist air.

Conclusions and Future Directions

Measurements of the thermal conductivity of pure CO_2 have been completed and analyzed for liquid and vapor isotherms at temperatures of 220, 235, 250, 265, and 295 K and for supercritical isotherms at 310, 315, 325, and 340 K, with pressures up to 68 MPa. Measurements of the thermal conductivity of supercritical CO_2 at temperatures from 340 K to 750 K with pressures up to 70 MPa will be completed in early FY 2013 with final analysis completed by March 2013. A comprehensive model for the thermal conductivity of CO_2 will be developed during 2013-2014.

The apparatus for measuring the dew-point concentration of water saturated in CO_2 has been constructed and tested with air as the carrier gas. Measurements with CO_2 as the carrier gas are commencing late in FY 2012, and the measurements, covering temperatures between 10°C and 85°C and pressures up to 7 MPa, will be completed during FY 2013.

Efforts on other facets of the project, such as the correlation of viscosity data for pure CO_2 and thermodynamic modeling of the H_2O/CO_2 system, are underway, and these tasks will be the focus of extensive efforts during FY 2013.

FY 2012 Publications/Presentations

1. R.A. Perkins, "Thermal Conductivity of Carbon Dioxide at Temperatures below 345 K", presented at 18th Symposium on Thermophysical Properties, Boulder, Colorado, June 24–29, 2012.

References

1. V. Vesovic, W.A. Wakeham, G.A. Olchowy, J.V. Sengers, J.T.R. Watson, J. Millat, "The Transport Properties of Carbon Dioxide," *J. Phys. Chem. Ref. Data* **19**, 763-808 (1990).

2. E.W. Lemmon, M.L. Huber, and M.O. McLinden, "REFPROP: Reference Fluid Thermodynamic and Transport Properties," NIST Standard Reference Database 23, Version 9.0, National Institute of Standards and Technology, Gaithersburg, Maryland, 2010.

3. C.W. Meyer, J.T. Hodges, R.W. Hyland, G.E. Scace, J. Valencia-Rodriguez, and J.R. Whetstone, "The Second-Generation NIST Standard Hydrometer," *Metrologia* **47**, 192-207 (2010).

IV.B.3 High-Bandwidth Modulation of H_2/Syngas Fuel to Control Combustion Dynamics in Micro-Mixing Lean Premix Systems

Dr. Adel Mansour (Primary Contact),
Jeff Melzak, Brian Hollon, Erlendur Steinthorsson
Parker Hannifin
8940 Tyler Boulevard
Mentor, OH 44060
Phone: (440) 266-2300
Email: amansour@parker.com

DOE Project Manager: Robin Ames
Phone: (304) 285-5436
Email: Robin.Ames@netl.doe.gov

Subcontractor:
Georgia Institute of Technology, Atlanta, GA

Contract Number: FE0005508

Start Date: October 1, 2011
End Date: December 31, 2011

Fiscal Year (FY) 2012 Objective

Conduct experimental investigation of H_2/syngas injector and perform combustion dynamics experiments under atmospheric conditions at Georgia Institute of Technology (Georgia Tech).

FY 2012 Accomplishments

The program was successful in meeting its objectives. Specifically, the following was accomplished:

- Demonstrated improvement of lean operability of the Parker multi-point injector through staging of fuel flow and primary zone sheltering
- Tested a piezo valve capable of proportional and high-bandwidth modulation of gaseous fuel flow at frequencies as high as 500 Hz. The valve was shown to be capable of effecting changes to flame dynamics, heat release, and acoustic signature of an atmospheric combustor.

Introduction

This program is focused on the development of fuel injection technologies that will facilitate the development of cost-effective turbine engines for integrated gasification combined cycle power plants, while improving efficiency and reducing emissions. The program involves developing a next generation multi-point injector with enhanced static and dynamic stability performance. Piezo-valve technology is implemented to investigate the potential for enhanced dynamic stability through high-bandwidth modulation of the fuel supply. Demonstration tests have been conducted in an atmospheric combustion facility at Georgia Tech.

Approach

Parker proposed to modify its current micro-mixing hydrogen/syngas fuel injector to enhance its static and dynamic stability. The program made enhancements to the Parker multi-point injector by adopting different fuel staging schemes and implementing high-bandwidth fuel flow modulation to modify combustion dynamics under lean conditions. The effort focused on the impact of fuel staging and operating conditions on the static stability characteristics of hydrogen/syngas combustion. Dynamic stability enhancements and extension of lean blowout performance were made through development and integration of a high-bandwidth piezo valve that modulates fuel flow to the injector for the purpose of attenuating combustion dynamics when the lean stability limit is approached. Detailed atmospheric combustion studies were carried out to elucidate the effects of various operating parameters on injector performance.

Results

A number of injector configurations were tested. Figure 1 shows a representation of these configurations.

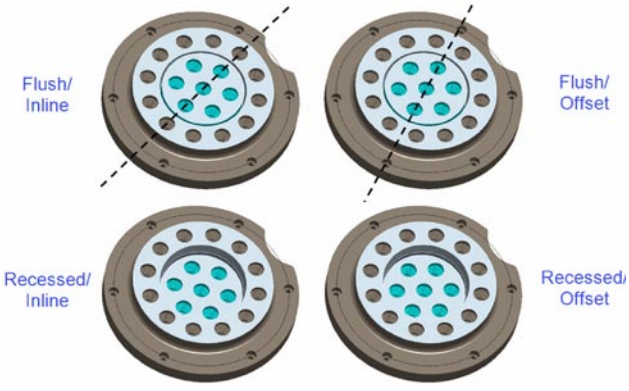

FIGURE 1. Injector configurations tested for operability mapping

The axial position of the primary injector was either flush with the face of the secondary injector or recessed, i.e., sheltered, by 0.5". The rotational position was either "inline" or "offset." For the inline configuration, a given primary cup and the closest secondary cup were aligned at the same clock angle, minimizing the distance between them. For the offset configuration, one primary cup was shared between its two nearest secondary cups.

The combustion experiments were performed in two different sets. The first set was run with the injector operating under steady-state flow conditions, i.e., the valve was not installed. For each configuration described above, the operability range was investigated. Global equivalence ratio was recorded at ignition and lean blowout conditions. In addition, fuel staging was investigated – the injector was operated in three different ways (i) primary circuit only fueled, (ii) secondary only fueled, and (iii) both primary and secondary fueled. Thus, the effects of both fuel staging and injector configuration on ignition and lean blowout were studied. The second set of experiments studied the effects of fuel flow modulation on combustion dynamics and flame response.

Non-Modulated Combustion Testing

Table 1 shows the global equivalence ratios measured at ignition and blowout for each injector configuration in the primary-only cases (note that only global equivalence ratios are reported, so comparison of absolute values should not be made across experiments that were fueled differently). It was observed that the recessed configurations are favored for improved lean blowout by about 7%. This demonstrates improvement of lean operability through staging of fuel flow and primary zone sheltering. For this configuration, combustion occurs predominantly in the recessed zone; sheltering the pilot reduces the interaction between primary flame and the non-fueled secondary air, thereby resulting in minimum dilution of the primary flame.

TABLE 1. Ignition and blowout data with primary-only fueled cases

IGNITION			BLOWOUT	
Inline	Offset		Inline	Offset
.115	.150	**Flush**	.099	.099
.112	.115	**Recessed 0.5"**	.092	.092

Table 2 shows the global equivalence ratios measured at ignition and blowout for each injector configuration in the secondary-only cases. Here the flush configurations are favored for blowout, showing an 18–25% improvement over the recessed cases. For this configuration, recessing the non-fueled pilot results in increased entrainment of the pilot air into the secondary combustion zone, thereby degrading lean operability.

TABLE 2. Ignition and blowout data with secondary-only fueled cases

IGNITION			BLOWOUT	
Inline	Offset		Inline	Offset
.145	.150	**Flush**	.116	.130
.173	.163	**Recessed 0.5"**	.155	.159

Table 3 shows the global equivalence ratios measured at ignition and blowout for each injector configuration with both circuits fueled. Lean blowout is independent of configuration. It is believed the effects of the primary-only and secondary-only cases described above counteract each other when the fuel is not staged.

TABLE 3. Ignition and blowout data with primary- and secondary- fueled cases

IGNITION			BLOWOUT	
Inline	Offset		Inline	Offset
.227	.168	**Flush**	.162	.162
.166	.176	**Recessed 0.5"**	.159	.162

Modulated Combustion Testing

Modulated combustion tests were performed with the Parker piezo valve in operation (sinusoidal drive) to study the effects of fuel modulation on heat release and combustor pressure oscillations. The injector configuration that demonstrated the best lean operability during the non-modulated tests—recessed/inline with primary fuel only – was chosen for all of the modulated combustion tests.

The high-frequency modulation tests were performed following confirmation of valve/actuator performance under steady-state conditions. These tests had two primary objectives: (i) to demonstrate a valve technology capable of proportional and high-bandwidth modulation of gaseous fuel flow at frequencies as high as 500 Hz, and (ii) to determine the valve's ability to impact changes in flame dynamics, heat release, and the acoustic signature of the combustor. Both of these objectives were accomplished by exploring a variety of modulation frequencies and amplitudes. The valve was operated with a sinusoidal waveform at frequencies ranging from 50 Hz to 500 Hz and amplitudes ranging from ±0.002" to ±0.018"; although it should be noted that the maximum achievable amplitude decreased for frequencies above ~225 Hz. Combustor pressure, combustor heat release, and modulated fuel pressure were recorded at each operating condition. The raw data were post-processed with MATLAB to take Fast Fourier Transforms in order to study system response in the frequency domain.

Figure 2 shows a series of fuel line pressure spectra for a 200 Hz valve excitation at various amplitudes. The magnitude of the 200 Hz peak increases monotonically with amplitude, demonstrating the valve's ability to induce oscillations in fuel flow at the driving frequency that are proportional to the valve dither amplitude. This capability was demonstrated for frequencies as high as 500 Hz, thereby meeting the first objective listed above; while a 500 Hz spectra is not presented here, combustor data shown below confirm the valve's ability to successfully modulate flow at this frequency.

Figure 3 shows the corresponding series of combustor pressure spectra (measured simultaneously with those shown in Figure 2). The combustor pressure spectra also show strong peaks at the driving frequency of 200 Hz, along with smaller harmonic peaks, although the harmonics are damped. Furthermore, the same trend in peak height with increasing valve amplitude is observed. These results indicate that the valve is able to directly affect the frequency content of combustor pressure, i.e., that pressure oscillations induced by the valve are "transmitted" to the combustor.

Additional quantitative analysis was performed to investigate the magnitude of the fluctuations in combustor pressure and heat release induced by the valve across the range of frequencies and amplitudes tested. As stated above, for a given valve frequency, the amplitude of the induced oscillations increases linearly with valve amplitude. However, the slope of this increase is not the same for all excitation frequencies. This is evident in the graph shown in Figure 4 for a representative subset of the data including 200 Hz and 300 Hz results. In this case, the vertical axis is the ratio of the heat release variation amplitude (defined as Q') to the mean, i.e., time-averaged, heat release (Qbar). The horizontal axis is valve displacement. The heat release gain at a given frequency is then defined as the slope of the least-squares line fit to this graph. Note that the gain is higher at 300 Hz than it is at 200 Hz.

Combustor pressure gain was calculated in a similar manner, except that it was normalized to atmospheric pressure. Figure 5 shows plots of combustor pressure gain (left) and heat release gain (right) as a function of valve frequency. Note that both gains trend upward

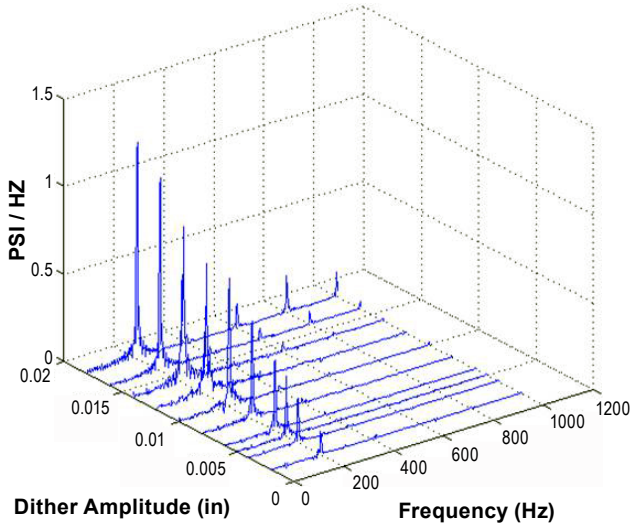

FIGURE 2. Fuel line pressure spectra for varying amplitudes at 200 Hz

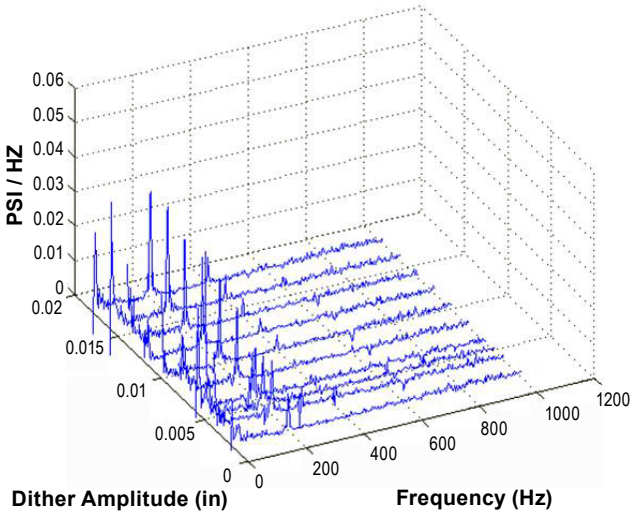

FIGURE 3. Combustor pressure spectra for varying amplitudes at 200 Hz

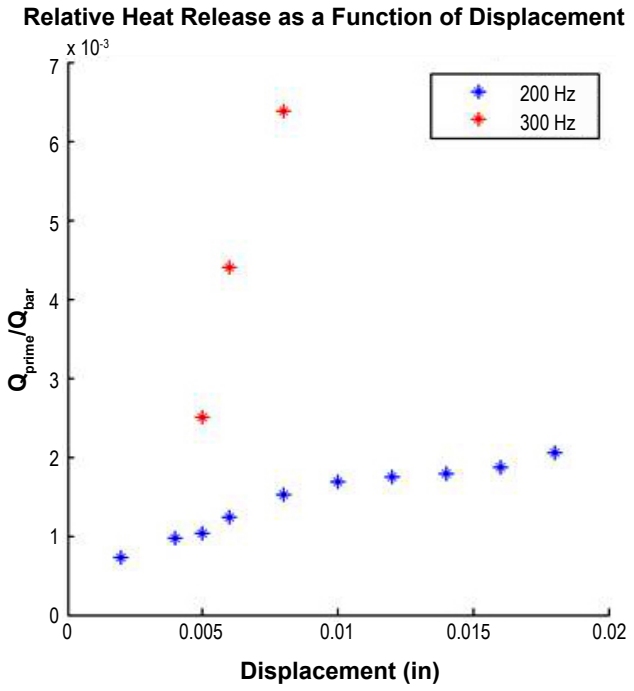

FIGURE 4. Plot of relative heat release variation vs. valve displacement at 200 and 300 Hz

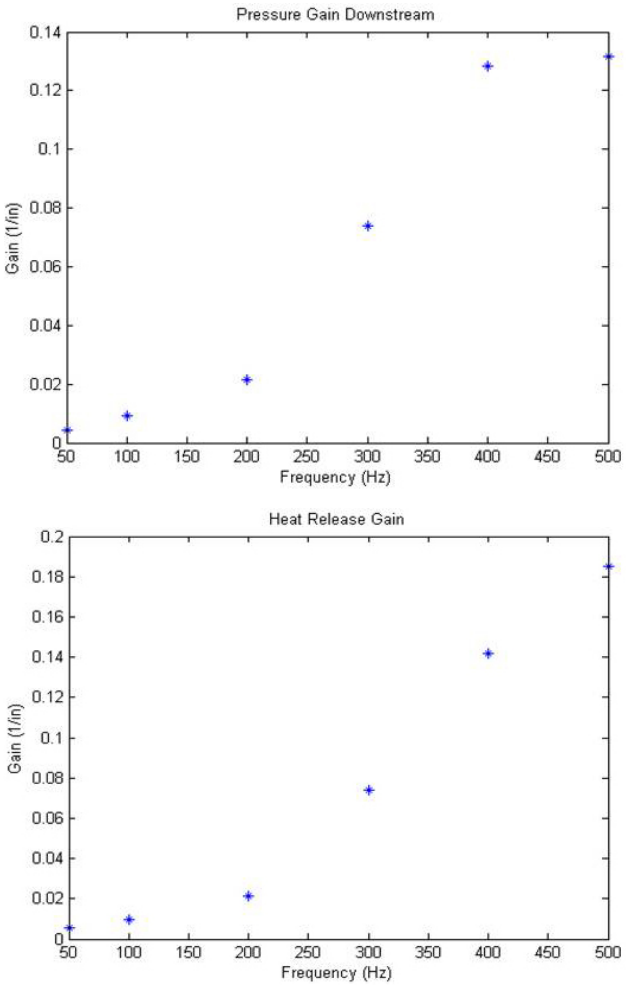

FIGURE 5. Plots of combustor pressure gain (top) and heat release gain (bottom) vs. valve frequency

with modulation frequency, indicating that the valve is capable of inducing relatively large changes in combustor response even at very small dither amplitudes.

Conclusions and Future Directions

Technical progress toward program deliverables has been made during the final quarter of the program. The atmospheric experimental campaign was completed, and valve capability in effecting change to combustion dynamics and heat release fluctuations was demonstrated. The project was completed on December 21, 2011, and the final report was submitted on February 15, 2012.

Special Recognitions & Awards/Patents Issued

1. U.S. Provisional Serial No. 61/474,067; "Distributed Injection with Fuel-Flexible Micro-Mixing Injector," Filed April 11, 2011.

IV. ADVANCED RESEARCH

C. Materials

IV.C.1 Turbine Thermal Management−Coatings and Materials Development

Mary Anne Alvin
U.S. Department of Energy (DOE)
National Energy Technology Laboratory
Regional University Alliance
626 Cochrans Mill Road
Pittsburgh, PA 15236-0940
Phone: (412) 386-5498; Fax: (412) 386-4806
Email: maryanne.alvin@netl.doe.gov

Dr. Brian Gleeson
University of Pittsburgh
Department of Mechanical Engineering and Material Science
Swanson School of Engineering
648 Benedum Hall
Pittsburgh, PA 15261
Phone: (412) 648-1185; Fax: (412) 624-4846
Email: bmg36@pitt.edu

Contract Number: 0004000.3.620.243.002

Start Date: October 1, 2011
End Date: September 30, 2012

Fiscal Year (FY) 2012 Objectives

Development of an advanced, composite, material system architecture that permits operation of turbine airfoils at temperatures >50°C–100ºC higher than current state-of-the-art (SOTA) components. The composite architecture consists of a diffusion barrier coating (DBC), a reduced-cost wet-spray bond coat, and a yttria stabilized zirconia (YSZ) thermal barrier coating (TBC) with an extreme temperature overlay TBC.

FY 2012 Accomplishments

- Fifty hours of bench-scale, thermal cycle testing of nickel-based, single crystal, René N5 coupons coated with National Energy Technology Laboratory (NETL)-Coatings for Industry's (CFI) bond coat system, and NASA Glenn Research Center's (GRC) extreme temperature TBC overlay systems was completed at temperatures of 1,450°C–1,460ºC in steam. At the conclusion of the testing, the coating visually appeared to be intact. Cross-sectional microstructural analyses are currently on-going.
- Rhenium-enriched Cr-Ni DBCs were HVOF (high velocity oxygen fuel) thermal spray deposited along the surface of nickel-based superalloy coupons. Bench-scale isothermal testing at 1,100ºC demonstrated the functional stability of the DBC for periods of up to 100 hrs.

Introduction

Gas turbines are the workhorse of power generation systems, and current land-based engine technology advancements are linked directly to our country's economy and energy security. Technical advancement for any type of gas turbine generally implies better performance, greater efficiency and extended component life. From the standpoint of cycle efficiency and durability, this suggests that a continual goal for higher gas turbine-inlet-temperatures (TITs) with reduced levels of coolant is desirable. Realization of future high-efficiency, near-zero emission turbine power systems depend critically on the advancement of thermal protection of hot sections, such as the first stage vanes and blades, and control of secondary flows. Current technology for protecting such airfoils relies primarily on the combined effects of TBCs and convective cooling. However, SOTA development in both TBC materials and cooling technologies is insufficient to meet the thermal-mechanical demands imposed by the hot gas with elevated TITs. This overall suggests that significant advances in TBC performance and durability and turbine cooling effectiveness must be achieved.

Current coal-fired integrated gasification combined cycle (IGCC) plant operating efficiencies range between 35–45%. The DOE Office of Fossil Energy's (FE's) goals are targeting plant efficiencies of 45–50% at <$1,000/kW, with near zero-emissions including CO_2 with multi-product production, i.e., electricity and hydrogen. DOE FE goals for advanced hydrogen-fired turbines are three to five percentage points above a 7FA engine. Technology developers have performed systems analyses using proprietary data and advanced modeling capabilities, predicting that designs stemming from their research and development (R&D) efforts will exceed this goal [1].

While improvements to turbine efficiencies may be achieved by the use of recuperation to preheat the air entering the combustor, improved sealing and clearance control technology and improved steam cycles, the largest efficiency gains are believed to be achieved by increasing the engine inlet temperature. By using closed-

loop steam cooling in place of compressor discharge air, current H-series gas turbines that were developed under the Advanced Turbine Systems (ATS) program are able to increase inlet operating temperatures from ~1,260ºC to ~1,425ºC, making better use of available compressor air.

Future advanced hydrogen-fired and oxy-fuel turbines that are now being designed to meet DOE FE's goals will experience an enormous level of thermal and mechanical loading as TITs approach ~1,425–1,760°C (Table 1) [2]. Currently there is no commercially available functional metallic-based system that can maintain a reasonable level of compositional and microstructural stability for prolonged exposure above temperatures of ~1,050°C. Alloys for high temperature applications are often protected from surface degradation by either an overlay or a diffusion coating that contains the β-NiAl phase as a primary constituent [3]. Such β-containing coatings have a sufficiently high aluminum content to form a continuous scale layer of the slow growing and highly stable oxide Al_2O_3 at both intermediate (700°C–1,000°C) and high (>1,000°C) temperatures. The thermally grown oxide (TGO) Al_2O_3, serves as an effective barrier, protecting the coated component from the process environment.

TABLE 1. Advanced turbine operating conditions [2]

	Syngas Turbine 2010	Hydrogen Turbine 2015	Oxy-Fuel Turbine 2010	Oxy-Fuel Turbine 2015
Combustor Exhaust Temp, °C	≥1,480	≥1,480		
Turbine Inlet Temp, °C	~1,370	~1,425	~620	~760 (HP) ~1,760 (IP)
Turbine Exhaust Temp, °C	~595	~595		
Turbine Inlet Pressure, psig	~265	~300	~450	~1,500 (HP) ~625 (IP)
Combustor Exhaust Composition, %	CO_2 (9.27) H_2O (8.5) N_2 (72.8) Ar (0.8) O_2 (8.6)	CO_2 (1.4) H_2O (17.3) N_2 (72.2) Ar (0.9) O_2 (8.2)	H_2O (82) CO_2 (17) O_2 (0.1) N_2 (1.1) Ar (1)	H_2O (75-90) CO_2 (25-10) O_2, N_2, Ar (1.7)

HP - high pressure; IP - intermediate pressure

In addition to increased TITs, the advanced hydrogen-fired and oxy-fuel turbines are projected to operate in a combustion gas environment containing >20% moisture (Table 1). Important criteria for structural materials exposed to the combination of high temperature, i.e., above ~1,000°C, and high steam concentrations include sufficient thermal stability, low vapor pressure of the surface materials and/or the reaction product(s) formed, and compatibility of any coating material with the underlying substrate. With regard to this last criterion, surface protection via an oxidation resistant coating is, in reality, a necessity, and will be critically important to maintain the stability of the coating for an extended service, i.e., 8,000–30,000 hrs. This means that there must be minimal interdiffusion between the substrate and the surface-modified region. The constraint of long-term resistance in steam-containing environments at very high temperatures removes surface modifications that are or react to form silica- or chromia-based products. A viable engineering solution is to utilize a metallic Al_2O_3-scale forming surface bond coat with an intermediate diffusion barrier that will essentially preclude coating-substrate interdiffusion and, hence, sustain the protective properties of the coating.

As commercially applied diffusion or overlay bond coat systems are subjected to high temperature for extended periods of time, oxidation, i.e., formation of thick TGOs, and rumpling of the bond coat surface result which induce stress and spallation of the insulating air plasma sprayed (APS) or electron beam physical vapor deposition (EB-PVD), YSZ TBC – ultimately leading to reduced turbine operating life. Mitigating not only bond coat oxidation, but also surface rumpling are essential for extending the operating lifetime of TBC systems.

Incorporating the use of commercially applied YSZ TBCs extends the operating use of current nickel-based superalloy and single crystal substrates to ~1,200°C–1,300ºC. Above these temperatures significant sintering leads to microstructural changes and a reduction of the strain tolerance in combination with an increase of Young's modulus. Additionally phase transformations occur, leading to the formation of tetragonal and cubic phases. Upon cooling, the tetragonal phase further undergoes transformation to the monoclinic phase which is accompanied by a volume change, leading to spallation of the coating. To extend turbine airfoil operation to temperatures >1,300°C, extreme temperature coatings as low thermal conductivity ZrO_2-2mol% Y_2O_3-1mol%Gd_2O_3-1mol%Yb_2O_3 t', and HfO_2-14mol%Y_2O_3-3mol%Gd_2O_3-3mol%Yb_2O_3 are being developed and evaluated.

Approach and Results

In order to maintain the structural integrity of future land-based power generation turbine components under the extreme conditions shown in Table 1, (1) durable TBCs, (2) high temperature creep resistant metal substrates, and (3) effective cooling techniques, will be required. While advances in substrate materials have been limited for the past decades, thermal protection of turbine airfoils for future hydrogen-fired and oxy-fuel turbines will rely primarily on collective advances in

TBCs and aerothermal cooling. To address the DOE FE goals for Advanced Power Systems, NETL-Regional University Alliance (RUA) has developed an integrated materials, heat transfer, and secondary flow team effort whose primary goal is focused on achieving:

- Development of advanced material system architectures that permit operation of turbine airfoils at temperatures ≥50°C–100ºC higher than current SOTA components.
- Development of novel, manufacturable, internal airfoil cooling technology concepts that achieve a cooling enhancement factor of ~5.
- Development of advanced, manufacturable, airfoil film cooling concepts that achieve a 50% reduction in required cooling flow.
- Design, construction and operation of a world-class test secondary flow rig facility for testing new cooling improvement strategies for the turbine rotating blade platform which ultimately reduce fuel burn.

Specific to the area of materials development, efforts at NETL and CFI have been focused on development of a wet spray diffusion bond coat system that can be applied to nickel-based superalloys and single crystal substrates and integrated with either commercially sprayed APS or EB-PVD YSZ TBCs, or with overlay coatings capable of providing thermal insulating properties up to temperatures approaching 1,600°C–1,700ºC (Figure 1). Additionally integration of the reduced-cost diffusion bond coat with DBCs developed at the University of Pittsburgh has been undertaken to mitigate interdiffusion of bond coat systems and the underlying metal substrate, in order to retain a protective alumina scale along the external surface of the bond coat, as well as an aluminum within a reservoir along the surface of the metal substrate during extended high temperature operation.

Bond Coat System Development and Integration with Extreme Temperature Overlays

Commercial bond coatings that are used in the production of TBCs consist of two types: the MCrAlY overlays (M = Ni, Co) and Pt-aluminide diffusion coatings. Overlay coatings are applied by low pressure plasma spray (LPPS), HVOF, or APS thermal spray processes. Diffusion aluminides are manufactured by pack cementation, above the pack techniques, chemical vapor deposition (CVD), or slurry processes. In order to demonstrate the feasibility for development of a reduced-cost, high temperature, oxidation resistant bond coat, NETL has collaboratively worked with CFI to develop bond coat systems targeted for use in advanced hydrogen-fired and oxy-fuel land-based turbine applications. The NETL-CFI bond coats consist primarily of aluminum particles suspended in a binder system that is sprayed onto the surface of single crystal, i.e., René N5, coupons. The coupons are subsequently diffused at temperatures approaching 1,070°C resulting in the formation of a dense surface layer containing primarily β-nickel aluminide (Figure 2). Chromium, cobalt and small amounts of finely dispersed refractory metals, i.e., Ta, W, Mo, and Re, from the underlying metal substrate are present in the coating

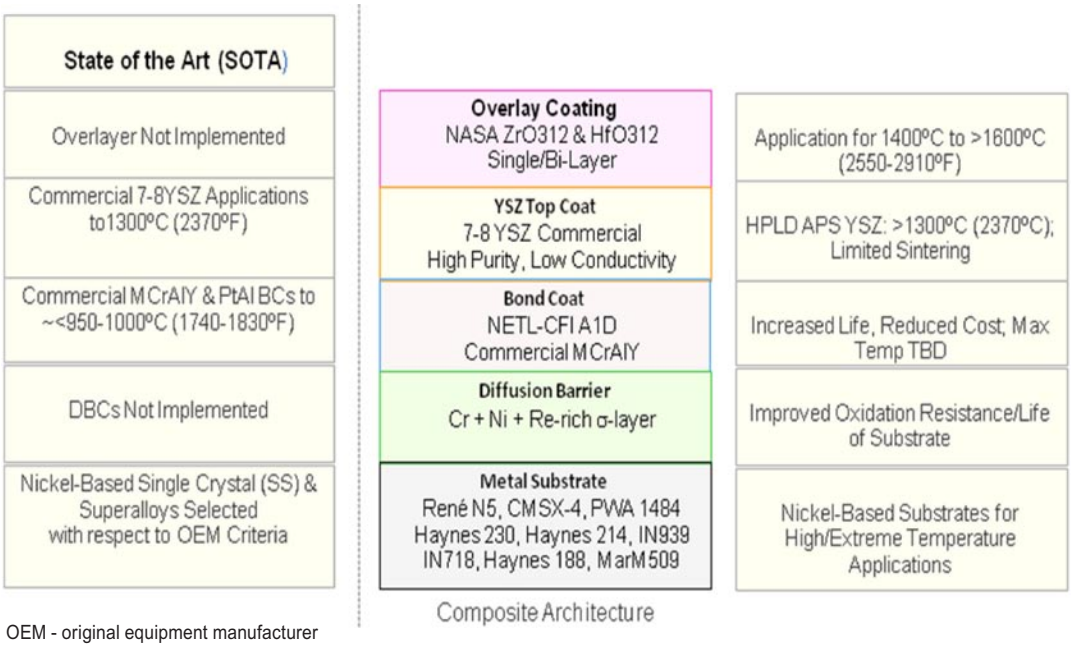

FIGURE 1. NETL TBC composite architecture

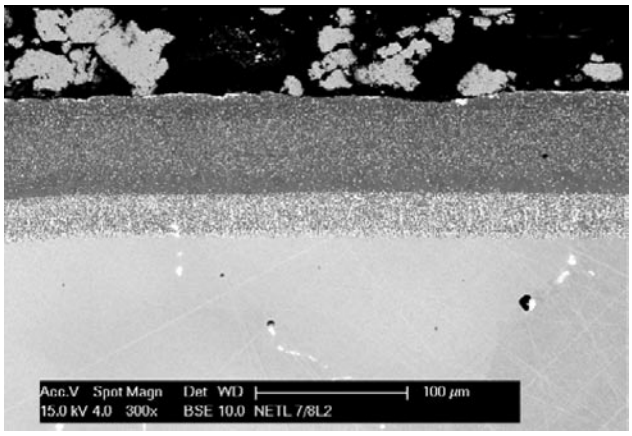

FIGURE 2. Cross-sectional micrograph of the A1D bond coat system

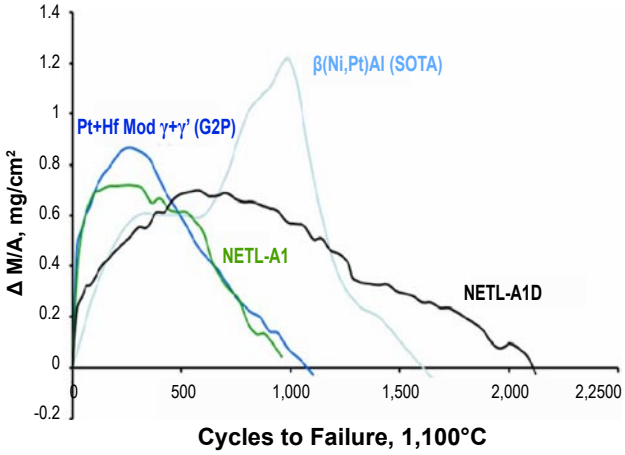

FIGURE 3. Mass change as a function of cyclic oxidation at 1,100°C for diffusion-based bond coat systems

indicating that the high activity bond coat, referred to as A1D, had been inwardly grown. The thickness of the bond coat and interdiffusion zone consistently has been identified as ~50–55 µm and ~25–30 µm, respectively.

In order to address the high temperature oxidative stability of these systems, René N5/A1D coupons were subjected to extended cyclic bottom-loading furnace testing at 1,100°C. The mass change of the coupons was monitored as a function of time, and post-test cross-sectional scanning electron microscopy (SEM) analyses were performed. These data were compared to results obtained for similarly tested commercial SOTA MCrAlY (M=NiCo) and Pt-Al bond coat systems, as well as uncoated René N5/Y. Bench-scale testing indicated that with the addition of the A1D coating along the external surface of René N5/Y, the cyclic oxidative stability of the single crystal substrate was approximately tripled (René N5/Y: 850 cycles vs. René N5/A1D: 2,120 cycles prior to crossing through zero mass change). The René N5/A1D system was shown to exceed the 1,100°C cyclic oxidation life of René N5/SOTA-PtAl and René N5/Pt-Hf Mod γ-γ' G2P (~1,600 and ~1,100 thermal cycles, respectively; Figure 3).

Post-test cross-sectional SEM analyses indicated that the external surface of the A1D bond coat was relatively planar after 2,100 thermal cycles, which implies that enhanced adherence of applied YSZ TBC layers would occur, as ratcheting or rumpling of the bond coat surface is negligible. Internal detrimental secondary reaction zones (SRZ) were not observed after extended high temperature exposure of the A1D bond coat system.

As these materials are projected to experience high steam concentrations (Table 1), and thermal gradients through the thickness of the ceramic-metal architecture as the result of internal cooling that will be required to maintain metal substrate temperatures at <1,100°C, further testing was conducted in NASA GRC's air and

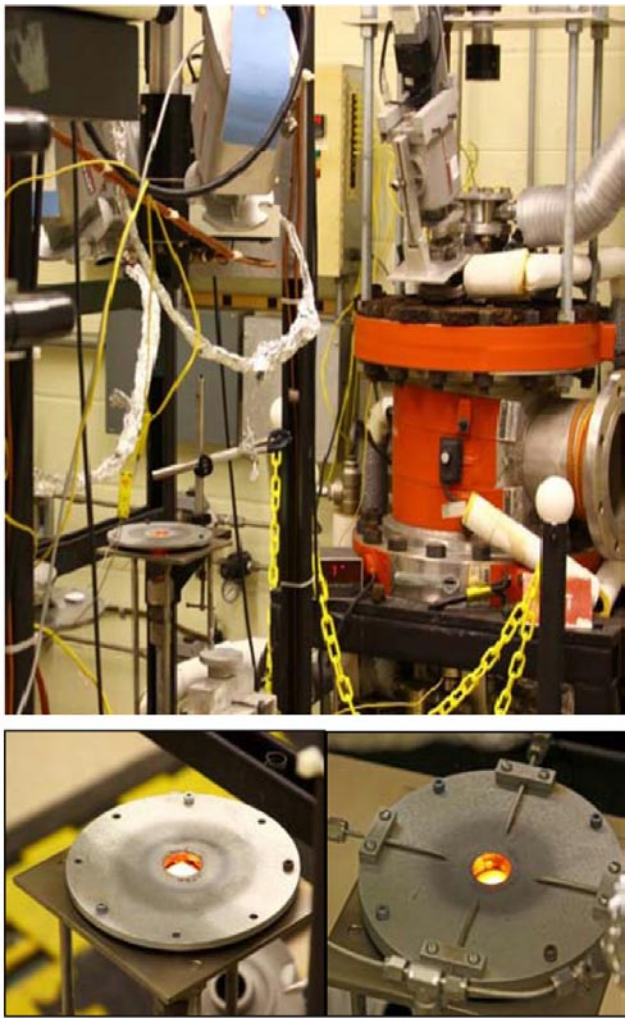

FIGURE 4. NASA GRC laser flux test facility. Bottom left photo: coupon exposure in air at ~1,100°C. Bottom right photo: coupon exposure in air/steam at ~1,100°C.

steam thermal flux test facilities (Figure 4). Two tests were conducted which maintained the bond coat surface temperature at ~1,100°C for 1 hr followed by three minutes at room temperature, with repeated cycling for a total of 50 hours of testing (Table 2: Test No. 1 and 2). With time, the surface temperature of the bond coat increased slightly due to increased laser power absorption from the oxide scale which formed. During testing, slight laser power adjustments were made in order to maintain a constant bond coat surface temperature. After 50 hours of laser flux testing in either air or steam, the surfaces of the René N5/A1D coupons visually appeared to be intact, i.e., absence of material removal or spallation.

Post-test cross-sectional SEM analyses of the René N5/A1D coupons indicated that although cracks were intermittently evident in the bond coat after laser thermal flux exposure, little if any evidence of coating failure had occurred, as there was no indication of aluminum depletion in the coating. The average thickness of the surface oxide that formed after 50 hrs of exposure in air was ~18 µm, while in steam an average ~19.6 µm scale thickness was formed. Surface energy dispersive X-ray analyses (EDAX) identified the presence of alumina with hafnium-rich transient oxides.

Thermal flux testing was additionally conducted in air and in steam using René N5/A1D coupons that were coated with ~250–270 µm commercial 7–8 APS YSZ and ~550 µm NASA GRC's low conductivity ZrO312 coating (ZrO_2-2.8wt%Y_2O_3-3.3wt% Gd_2O_3-3.6wt% Yb_2O_3; Figure 5: Test No. 1-3 and 1-5, respectively). A René N5/LPPS MCrAlY/APS YSZ/ZrO312 coupon (~300 µm MCrAlY) was additionally subjected to laser

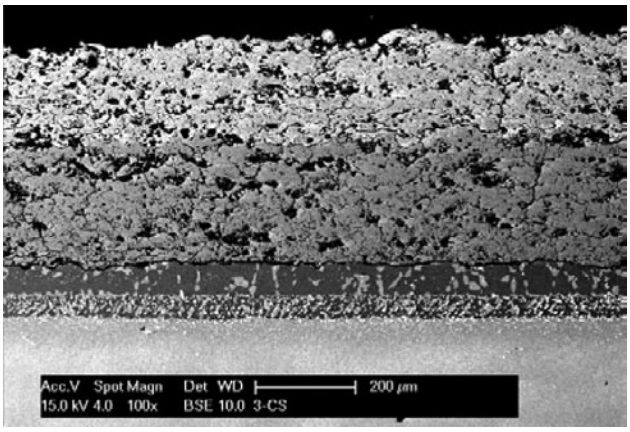

FIGURE 5. Cross-sectional micrograph of the René N5/A1D/YSZ/ZrO312 coupon after 50 hrs of thermal flux testing in air at 1,100°C

flux testing (Test 1–4). The external surface temperature of each coupon was maintained at ~1,480°C, with an interface bond coat temperature of ~1,100°C, and a back surface metal substrate temperature of ~1,000°C. During the first hours of high temperature exposure which were followed by cooling to room temperature, the thermal conductivity of the TBC increased possibly due to sintering and/or porosity reduction within the topcoat overlayer and/or YSZ layers. Thereafter very slight thermal conductivity reduction resulted possibly from defect formation, i.e., gaps; microcracks, within the topcoat or along the TGO interface. At test termination after being subjected to 50 hrs of thermal flux testing in air, the TBC visually appeared to be intact (Figure 6). Very minor edge buckling or spallation was observed

TABLE 2. Laser thermal flux and thermal cyclic testing of TBC material systems

Test No.	Substrate & Coating Composition	Steam	Back Coupon Surface	Bond Coat Surface or Interface	YSZ Surface	Overlayer Surface	Visual Inspection
1	René N5/A1D	—	995-1,090ºC	1,050-1,140ºC	—	—	Intact
2	René N5/A1D	√	1,000-1,094ºC	1,050-1,140ºC	—	—	Intact
APS Composite Coating Architectures							
1-4	René N5/LPPS MCrAlY/APS YSZ/APS ZrO312	—	1,000°C	1,115°C	—	1,482°C	Intact after 50 Cycles
1-3	René N5/A1D/APS YSZ/APS ZrO312	—	1,018°C	1,120°C	—	1,482°C	Intact after 50 Cycles
1-5	René N5/A1D/APS YSZ/APS ZrO312	√	1,050°C	1,135°C	—	1,482°C	Failed after 49 Cycles
EB-PVD Composite Coating Architectures							
2-4	René N5/A1D/P&W EB-PVD YSZ	√	975-1,000°C	1,100-1,140°C	1,300°C	–	Spalled after 20 Cycles
2-5	René N5/A1D/EB-PVD YSZ/ EB-PVD ZrO312	√	900°C	1,120°C	–	1,450-1,460°C	Intact after 50 Cycles
2-3	René N5/A1D/P&W EB-PVD YSZ/HfO_2-14mol%Y_2O_3-3mol% Gd_2O_3-3mol%Yb_2O_3	√	990°C	1,120°C	–	1,500-1,520°C	Spalled after 50 Cycles

FIGURE 6. APS TBC coated coupons after laser flux testing. Left photo: René N5/A1D/APS YSZ/ZrO312; air at ~1,482°C, 50 1-hr cycles (Test 1–3). Middle photo: René N5/LPPS MCrAlY/APS YSZ/ZrO312; air at ~1,482°C, 50 1-hr cycles (Test 1–4). Right photo: René N5/A1D/APS YSZ/ZrO312; steam at ~1,482°C, 49 1-hr cycles (Test 1–5).

for the MCrAlY coupon. In contrast, after 49 cycles in steam, the René N5/A1D/APS YSZ/ZrO312 coupon experienced spallation along half of the coated coupon surface, possibly as the result of exposure to the steam thermal flux environment or from stresses imposed along the edge of the coupon by test fixture clamping.

Post-test microstructural characterization indicted that when the coupons were subjected to thermal flux testing in air, there was little evidence of coating failure. Although there were features of aluminum depletion in both the A1D and MCrAlY bond coats, both maintained a continuous alumina TGO surface scale (~5 μm, and ~5-10 μm, respectively). SEM characterization however indicated that the MCrAlY overlay bond coat had more extensive degradation than the A1D diffusion bond coat, that is, the overlay coating had numerous large internal oxide formations (Figure 7), while the A1D diffusion coating did not. The superior performance of the diffusion coating is considered to be due, at least in part, to a higher aluminum concentration in the silicon-containing β-A1D aluminide coating in comparison to the lower aluminum-containing γ + β MCrAlY coating.

When exposed to steam, failure of the René N5/A1D/APS YSZ/ZrO312 coating occurred as a result of cracking in the TBC adjacent to the ceramic bond coat interface. Investigators in numerous prior studies of plasma sprayed ceramic coatings suggest that this type of failure is the result of thermal mismatch between the bond coat and the TBC. However, if thermal expansion mismatch alone were the cause of the observed failure, then for a given set of cyclic test parameters, all three coupons should have failed, but they did not. Published information on oxidation in air plus water vapor indicates that water vapor increases the growth rate of alumina at high temperature. Post-test characterization of the René N5/A1D coupons identified the formation of a continuous ~2 μm and ~2.5 μm alumina scale after 50 hrs of exposure at 1,100°C in air and steam, respectively. When coated with an external TBC layer, an ~<5 μm and ~3–7 μm scale formed along the A1D surface of the René N5/A1D/APS YSZ/ZrO312 coupons after 50 hours of exposure in air and steam, respectively. The slight

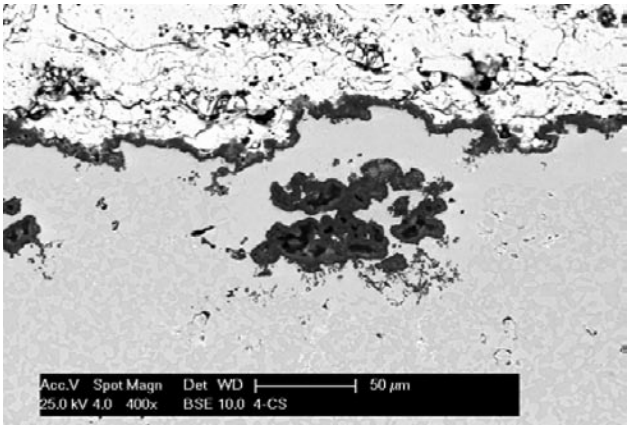

FIGURE 7. SEM cross-sectional micrograph illustrating internal oxidation of the bond coating of the René N5/LPPS MCrAlY/APS/ZrO312 coupon

increase in TGO thickness for coupons with an APS YSZ coating reflects additional exposure time at high temperature during application of the TBC, as well as possible diffusion of oxygen from the YSZ at the bond coat interface. In contrast an ~5-10 μm scale formed along the surface of the René N5/LPPS MCrAlY/ZrO312 coupon after 50 hours of laser flux testing in air. If it were suggested that the internal stress in the TBC increases as alumina forms, then coupons with a faster growing oxide would have greater internal stress after the same thermal exposure time, than coupons with a slower growing scale on the bond coat. If this were the case, then the René N5/LPPS MCrAlY/APS/ZrO312 coating should similarly have failed. A combination of internal stress, reduced through-wall thermal gradient, and possibly stress resulting from test fixture clamping are considered as contributors to failure of the René N5/A1D/APS YSZ/ZrO312 coating during high temperature, thermal flux, steam exposure.

Thermal flux testing was additionally conducted in steam using René N5/A1D coupons that were EB-PVD coated with YSZ (Test 2–4), YSZ-ZrO_2-2mol% Y_2O_3-1mol%Gd_2O_3-1mol%Yb_2O_3 t' (Test 2–5), and YSZ- HfO_2-14mol%Y_2O_3-3mol%Gd_2O_3-3mol%Yb_2O_3 (Test 2–3). During testing of the René N5/A1D/EB-PVD YSZ coupon at 1,300ºC, the surface temperature increased to ~1,400°C at the 20th thermal cycle due to reduced steam flow into the coupon chamber which resulted in interface bond coat/YSZ temperatures of ~1,180°C for two cycles, and subsequent localized spallation and buckling of the coating. Post-test microstructural characterization identified partial detachment of the TBC from the bond coat as a result of TGO fracture (Figure 8). Loss of aluminum from the A1D bond coat was additionally observed which led to the formation of γ' along the metal-oxide interface and grain boundaries, and within the coating grains.

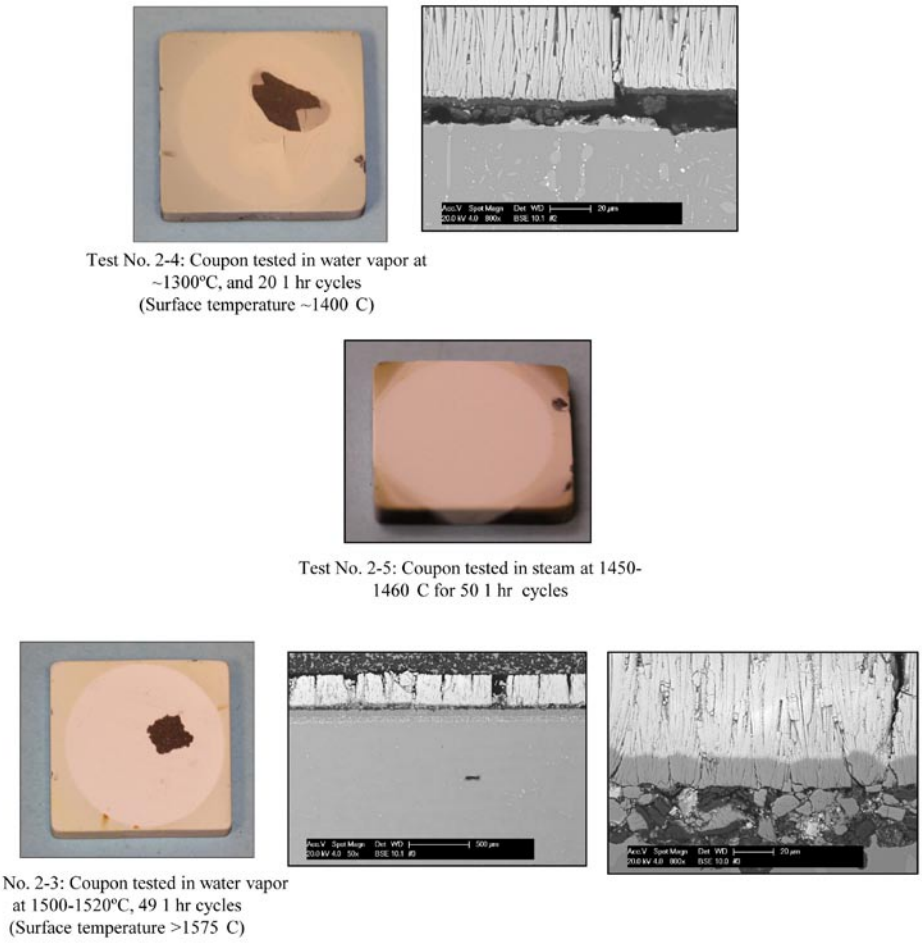

FIGURE 8. EB-PVD TBC coated coupons after laser flux testing

When the René N5/A1D/YSZ-ZrO_2-2mol% Y_2O_3-1mol%Gd_2O_3-1mol%Yb_2O_3 t' coupon was subjected to 50 thermal cycles and 1,450–1,460ºC laser thermal flux in steam, the thermal conductivity of the coating initially increased due to sintering, but subsequently decreased possibly due to minor coating delamination (Figure 8). With continued thermal cycling a very minor reduction in coating's thermal conductivity was observed, indicting the relative stability of the coating.

During extreme temperature thermal flux testing of René N5/A1D/P&W EB-PVD YSZ/HfO_2-14mol%Y_2O_3-3mol%Gd_2O_3-3mol%Yb_2O_3 coupon, the surface temperature of the coating increased to over 1,575°C, i.e., at the 6^{th}-13^{th} cycle, due to a sudden reduction of steam flow into the test chamber. Although the bond coat/YSZ interface temperature was projected to reach ~1,150°C during these eight cycles, no visual coating damage was observed. Continued cycling, however, identified a slight reduction in thermal conductivity indicating interface damage had occurred, Localized spallation of the coating was observed after the 49^{th} thermal cycle exposure (Figure 8). Post-test microstructural characterization of the coupon indentified the segmented structure of the EB-PVD TBC, with evidence of large crack formations in the area where the TBC had been removed. The TGO appeared to be extensively fractured which led to limited to continuous alumina formation along the A1D bond coat. A mixture of alumina and stabilized zirconia grains was observed between the stabilized zirconia and the diffusion aluminide bond coat. TBC failure was attributed to growth and coalescence of the TGO crack formations.

Diffusion Barrier Coating Systems

Recent research on rhenium-base alloys has shown a range of Re-Cr-Ni-based compositions can act as a highly effective diffusion barrier layer between a heat resistant alloy and an Al-reservoir layer, to form and maintain a protective, long lasting alumina scale [4]. Coatings with a two-layer structure comprised of an inner, Re-base alloy layer and an outer β-NiAl layer have been successfully formed on the nickel-base superalloys and even niobium-base alloys.

With respect to NETL-RUA's DBC development, DBC-source powder was prepared at the Ames Laboratory via high-energy mechanical milling (Zoz mill). The σ-DBCs were deposited at the Caterpiller Inc.'s Technical Center via HVOF deposition onto nickel-based Haynes 230 and Haynes 214 substrates which were provided by Haynes International. The Al-reservoir layer was a standard NiCrAl overlay (Ni-343 from Praxair) that was also deposited via HVOF. The advantage of directly depositing the DBC systems by a plasma spray process is that it provides practical tractability and compositional flexibility. The nominal composition of the NiCrAlY overlay coating was 67Ni-22Cr-10Al-1Y (wt%).

DBC layers had thicknesses of ~20 μm and 45 μm (referred to as "thin" and "thick" respectively; Figure 9). For the DBCs, the targeted composition was 40Re-40Cr-20Ni (at%); however, EDAX analysis revealed that the average composition of the thick DBC was 50Re-24Cr-26Ni (at%); while that of the thin DBC was 72Re-14Cr-11Ni. The reason(s) for the thin DBC composition being quite different from the targeted composition is currently not understood, but it is noteworthy that such a Re-rich composition corresponds to an (unwanted) equilibrium σ + δ-Re + γ-Ni phase constitution.

The general performance of the deposited DBC systems was assessed by conducting thermal exposures at 1,100°C and 1,200°C. Of particular interest were the stability and effectiveness (in terms of serving as a diffusion barrier) of the DBCs tested. For the thick DBC deposited on Haynes 214, there was found to be little change in Re content after 100 hrs of thermal exposure at 1,100°C; although, a small amount of a Cr- enriched phase formed at the NiCrAlY/DBC interface (Figure 10). For thin DBCs, some degree of incompatibility between the DBC and the NiCrAlY overlay was evident. Even so, the DBC was effective.

The thick DBC was also found to be reasonably effective for exposures at 1,200°C; although, rhenium was found to have diffused from the DBC to the NiCrAlY coating and aluminum from the coating to the DBC, as well as permeability of constituents from the DBC into the Haynes 214 substrate. As a consequence, there was a measureable change in the DBC composition with increasing exposure time at 1,200°C. For both the

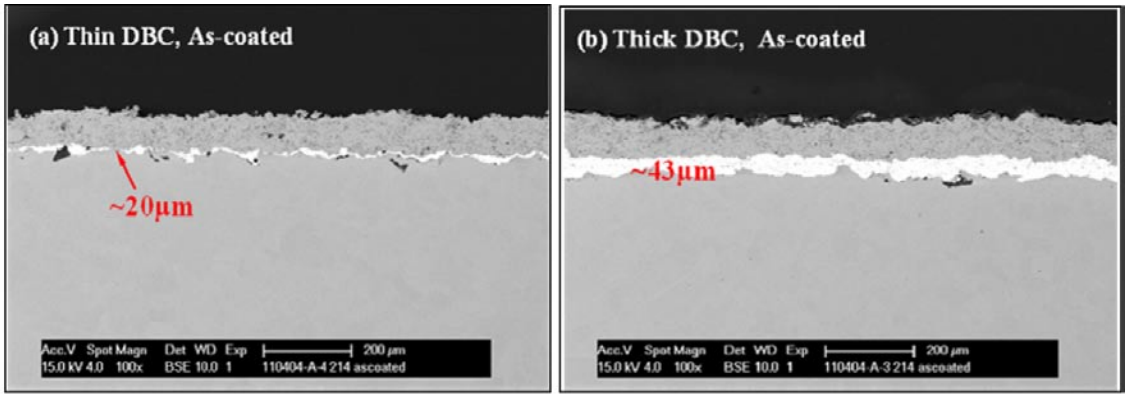

FIGURE 9. Representative cross-sectional micrographs of the as-manufactured (a) thin and (b) thick DBC systems

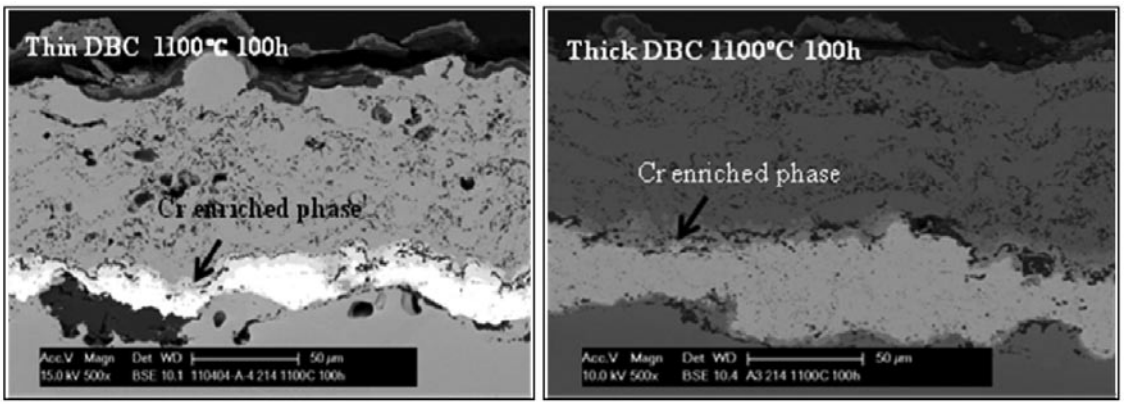

FIGURE 10. Cross-sectional micrographs of the thin and thick DBC systems after 100 hrs exposure at 1,100°C

thin and the thick DBC systems, there was no evidence of interactions that led to the formation of embrittling topologically closed packed (TPC) phases.

Conclusions

- The viability of the reduced-cost, wet spray, NETL-CFI A1D bond coat system was demonstrated during conduct of extreme temperature thermal flux testing in steam environments when bond coat/TBC interface temperatures are maintained at or below 1,100ºC.
- At maximum test exposure temperatures of 1,100ºC, the A1D bond coat was shown to be relatively planar after 2,100 thermal cycles, which implies that enhanced adherence of applied YSZ TBC layers would occur, as ratcheting or rumpling of the bond coat surface is negligible. Internal detrimental SRZ were not observed after extended high temperature exposure of the A1D bond coat system.
- The production thickness and surface roughness of the A1D bond coat diffusion layer formed during wet spray commercial application onto metal substrate coupons were shown to be acceptable for subsequent APS and EB-PVD TBC application.
- Bench-scale testing of low thermal conductivity, extreme temperature TBC overlayers in conjunction with NETL-CFI bond coat systems demonstrated initial use and viability of the composite system at temperatures of 1,450°C–1,460ºC which exceed the SOTA test temperatures of 1,300ºC for commercial 7-8YSZ TBCs.
- When conducted in a controlled fashion, laser flux testing permits thermal/physical/chemical assessment of newly developed coating material systems to temperatures representative of advanced engines, i.e., >1,400ºC. Test equipment and systems malfunctions as reduction of steam and/or air flow into the test coupon chamber, leads to over-temperature conditions along the external surface of the coating, as well as at the bond coat interface, which subsequently leads to localized spallation of the coating architecture.
- The high-energy mill σ-powder fabrication followed by HVOF deposition of the powder is an effective DBC processing route. Moreover, this route provides the latitude to deposit a range of aluminum-reservoir overlays, such as the NiCrAlY.
- Results for tests using Haynes 230 and Haynes 214 substrates suggest that an HVOF-deposited DBC can be effective for a commercial NiCrAlY bond coat overlay. The effectiveness of the DBC, however, decreases with increasing exposure temperature above 1,100°C.
- Based on testing at 1,100°C, the DBC was adequately stable, showing no obvious decrease in thickness, when the primary composition of the DBC is σ-phase. The thick σ-based DBC was effective in limiting coating/substrate interdiffusion.

Future Directions

- Establish processing parameters, materials compositions and coating thicknesses for integrating DBC architectures with the NETL-CFI A1D bond coat system.
- Further enhance oxidation and performance life of the A1D bond coat system through co-doping.

Acknowledgments

In addition to Mr. Richard Dennis and Ms. Patcharin Burke at NETL who provided support for conduct of this project, we wish to acknowledge Mr. Kevin Klotz and Mr. Bruce McMordie at CFI for collaborative development of the A1D bond coat system; Dr. Daniel Sordelet at Caterpillar, Inc., for HVOF DBC deposition; Dr. Bruce Warnes at Corrosion Control Consultants, Inc., and Ms. Xiaodan Wu at the University of Pittsburgh for post-test characterization of the coupons; and Dr. Dongming Zhu for conduct of the laser thermal flux testing at NASA GRC.

FY 2012 Publications/Presentations

1. M.A. Alvin, K. Klotz, B. McMordie, B. Gleeson, N. Mu, D. Zhu, B. Warnes, B. Kang, and J. Tannenbaum, "Development and Assessment of Coatings for Future Power Generation Turbines," ASME Turbo Expo, Copenhagen, Denmark, June 11–15, 2012 (GT2012-69655).

References

1. "Current and Future Technologies for Gasification-Based Power Generation, Volume 2: A Pathway Study Focused on Carbon Capture Advanced Power Systems R&D Using Bituminous Coal," November 25, 2009, DOE/NETL-2009/1389.

2. R.A. Dennis, "FE Research Direction—Thermal Barrier Coatings and Health Monitoring Techniques, Workshop on Advanced Coating Materials and Technology for Extreme Environments, Pennsylvania State University, State College, Pennsylvania, September 12–13, 2006.

3. B. Gleeson, *Journal of Propulsion and Power*, **22**, 375 (2006).

4. Prof. Toshio Narita, Hokkaido University, Japan, communications with Brian Gleeson.

IV.C.2 Coating Issues in Coal-Derived Synthesis Gas/Hydrogen-Fired Turbines

Bruce Pint
Oak Ridge National Laboratory
1 Bethel Valley Rd.
Oak Ridge, TN 37831-6156
Phone: (865) 576-2897
Email: pintba@ornl.gov

DOE Project Manager: Briggs White
Phone: (304) 285-5437
Email: Briggs.White@netl.doe.gov

Contract Number: FEAA070

Start Date: October 1, 2011
End Date: September 30, 2012

Fiscal Year (FY) 2012 Objectives

- Maximize the service lifetime of bond coatings in thermal barrier coatings (TBC) by applying mechanistic understanding of the factors that contribute to their degradation in the environments expected in syngas/hydrogen-fired turbines, initially examining the roles of water vapor and multiple reactive element additions to the superalloy and/or coating.
- Complete testing and characterization of failed TBC specimens from the initial study of the effect of water vapor content and superalloy composition on TBC lifetime in furnace cyclic testing with sprayed MCrAlY and MCrAlYHf bond coatings.
- Complete testing of sprayed MCrAlY-type bond coatings in different cycle frequencies to understand the effect of short (one hour) and long (100 hour) thermal cycles on TBC lifetime.
- Begin testing of model MCrAl cast alloys to develop bond coatings with increased spallation resistance in the presence of water vapor.

FY 2012 Accomplishments

- Demonstrated that TBC lifetime was not affected by increasing the water vapor content from 10% to 50% or 90% in furnace cycling for either sprayed MCrAlY-type bond coatings or Pt-containing diffusion bond coatings.
- Determined that Y and La additions to the Ni-base superalloy did not appear to improve TBC lifetime under these conditions.
- Determined that Y and Hf additions to sprayed MCrAlY-type coatings consistently produced a 15-40% improvement in TBC lifetime in all test conditions compared to the same bond coating without Hf.
- Demonstrated that decreasing the cycle frequency from one hour to 100 hours increased the average TBC lifetime by 3-10X thereby validating the strategy of high frequency testing to induce coating failures at shorter exposure times without further increasing the exposure temperature.
- Completed characterization of the thermally-grown alumina scale formed on various bond coatings with and without water vapor and found that only minor changes were observed in the oxide with the addition of water vapor.

Introduction

Using gas synthesized from coal (i.e., syngas) or hydrogen to fuel land-based gas turbines represents several operational and materials problems compared to burning natural gas. These fuels require different combustion conditions and have more water vapor in the exhaust gas entering the turbine hot section [1]. Also, during the synthesis process, upset conditions in the gas cleanup process can allow sulfur and other contaminants to periodically enter the turbine. Thus, compared to the nominally clean natural gas fuel, these synthetic fuels will likely require more robust materials in the turbine hot section in order to achieve the same performance. To maintain turbine availability with current materials, the turbine inlet temperature may be reduced thereby reducing the turbine efficiency.

Superalloy turbine blades and vanes in the hot section typically are protected by oxidation-resistant coatings including a TBC to reduce the metal temperature in service. There are dozens of different commercial MCrAlYX (M=Ni,Co; X=Hf, Si, Re, etc.) coatings. All TBC systems rely on the formation of a slow-growing, adherent alumina scale between the metallic bond coating and the ceramic yttria-stabilized zirconia (YSZ) top coating. The overall goals of this project are to (1) study

strategies to make the alumina more adherent or slower growing, (2) quantify how the syngas/H_2 environment is more aggressive than a conventional natural gas-fired turbine, and (3) use advanced characterization techniques (e.g., high resolution transmission electron microscopy) to better understand the underlying mechanisms involved in each case.

Approach

The oxidation resistance of the bond coating is a critical weak link determining TBC lifetime because spallation of the thermally grown alumina scale formed on the bond coating will ultimately result in loss of the outer ceramic thermal protection layer. The strategy adopted here is to identify issues that could have a strong near-term impact on coating performance and generate data that could be easily transferred to turbine manufacturers and users. The first target was to quantify the benefit on coating performance of dopants to the superalloy and bond coating. Commercially available Y- and La-doped alloy CMSX-4® has limited experimental evidence showing improvements in TBC lifetime [2], while a combination of Y and Hf is well known to improve alumina scale adhesion [3,4]. For the initial series of experiments, three different variants of CMSX-4® were coated with two different NiCoCrAlY bond coatings (identical except for the addition of 0.07Hf and 0.65Si in one) and an air-plasma sprayed top coat to quantitatively determine if the dopants affected the YSZ lifetime in furnace cycling tests. The bond coatings were deposited at Stonybrook University using high velocity oxygen fuel (HVOF), a common industrial coating process [5].

For understanding the syngas/H_2 environment, it seems clear that these environments will have higher water vapor contents either due to combustion or the use of steam diluents [1]. Therefore, a clear understanding of how higher water vapor contents affect TBC lifetime appears to be necessary to develop improved coatings as well as to design proper experiments. Controlled laboratory experiments with different water vapor contents will yield initial information about the effect of increasing water vapor on TBC lifetime. In order to build on existing knowledge, this task focused on well-characterized Pt diffusion (γ+γ') and Pt-modified aluminide (β) coatings where a baseline already existed. Subsequently, additional experiments were conducted on the same series of MCrAlY bond coatings and CMSX-4® superalloys described above.

In both cases, characterizing the alumina scale microstructure and microchemistry is essential to understanding the role of dopants and water vapor. Since the scale is typically 1-10 µm thick, it is difficult to gain understanding using conventional scanning electron microscopy (SEM) or electron microprobe analysis (EPMA). Therefore, analytical transmission electron microscopy (TEM) characterization is needed to gain a better mechanistic understanding of these effects.

Results

Figure 1 shows the effect of environment on the average (three specimens) TBC lifetime defined as the time to 20% spallation of the low thermal conductivity air plasma spraying (APS) YSZ top coating. An example cross-section of a failed APS YSZ coating is shown in Figure 2. Under these conditions, the addition of 10 vol% water vapor to the furnace cycling test resulted in ~30% drop in the average coating lifetime for both types of NiCoCrAlY bond coatings; however, in both cases the addition of Hf resulted in a 20-25% increase in coating lifetime. In contrast, the addition of yttrium (Y) and lanthanum (La) dopants to the Ni-base superalloy CMSX-4® showed little effect on coating lifetime in air with 10% H_2O (the third variant with 2 ppma Y and 3 ppma La showed similar lifetimes). Finally, to investigate the effect of higher water vapor contents, the same specimens were cycled in air with 50% H_2O but no further decrease in average coating lifetime was observed. As expected [3], the Hf-modified bond coating showed a higher lifetime in all cases. However, characterization of the alumina scale thickness in the failed specimens did not show any significant effect of the Hf dopant, nor did the addition of water vapor or the Y and La doping in the CMSX-4® substrate.

Higher water vapor contents of 50 and 90% also did not further decrease the 1,150°C lifetime of β-phase Pt-modified aluminide coatings on GE second generation single crystal alloy N5 with an ~125 µm

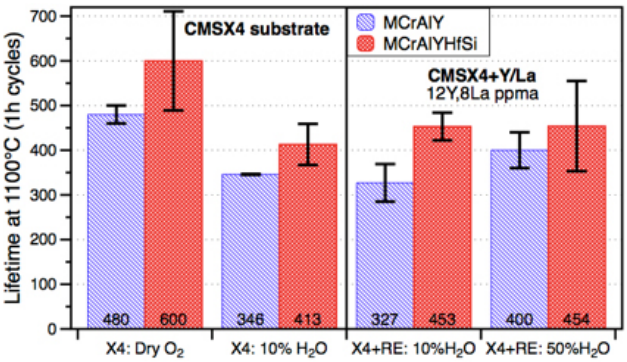

FIGURE 1. Comparison of the effect of environment and HVOF bond coating composition on average APS TBC life of three specimens on two commercial superalloy substrates (with and without Y and La doping) during 1-h furnace cycles at 1,100°C. The standard deviation is shown for each condition.

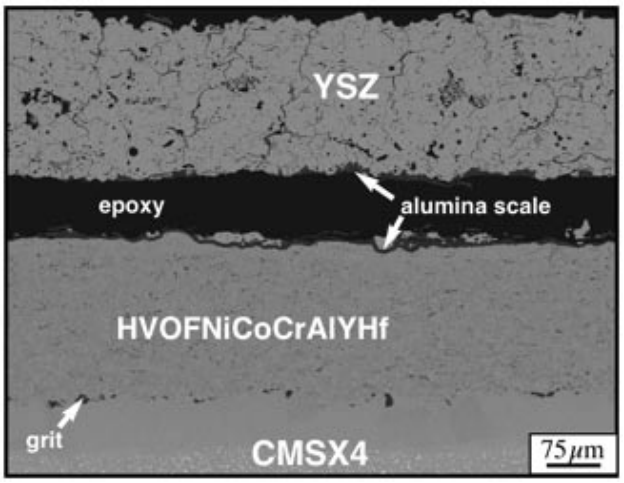

FIGURE 2. Scanning electron microscope back scattered electron image of a failed TBC after 440 1-h cycles at 1,100°C in air with 10% H_2O. Failure occurred along the metal-oxide interface, so, the thermally grown alumina scale is partially attached to both the metallic HVOF NiCoCrAlYHfSi bond coating and the ceramic APS YSZ top coating.

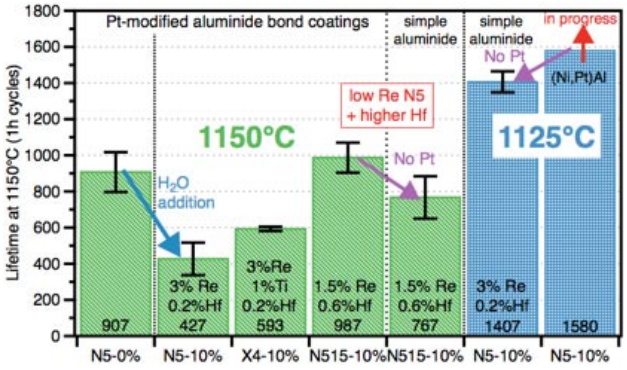

FIGURE 3. Average lifetimes for EB-PVD YSZ-coated superalloy specimens exposed in 1-h cycles at 1,125° or 1,150°C in dry O_2 or wet air. The bars note the standard deviation for three specimens of each type. One group of coatings is still being tested.

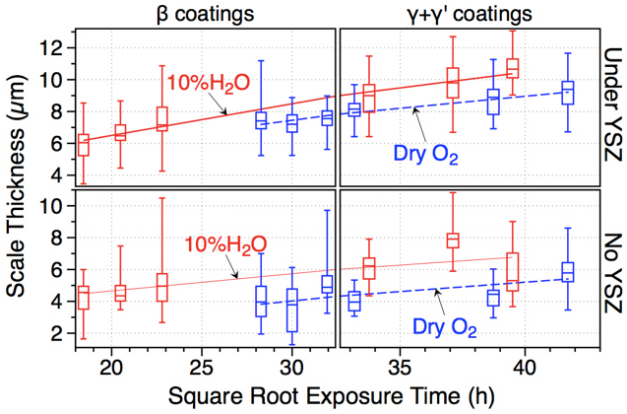

FIGURE 4. Box plots of ~40 alumina scale thickness measurements as a function of the square root of exposure time (1-h cycles to failure) at 1,150°C for the specimens with β and γ+γ' Pt-containing diffusion bond coatings and EB-PVD YSZ on one side. The thickness with and without the YSZ overlayer in two environments is shown. The box plots mark the 25%, median and 75% values and the bars mark the minimum and maximum thicknesses measured.

thick commercially-deposited electron beam (EB-PVD) YSZ top coating [6,7]. The most significant effect was a >50% drop in average coating lifetime when air with 10% H_2O was compared to lifetime in dry O_2 (Figure 3). In contrast, the average EB-PVD YSZ lifetime with γ+γ' Pt-diffusion bond coatings was not affected by the addition of 10%, 50%, or 90% water vapor. To further characterize the effect of water vapor on coating performance, the alumina scale thickness was measured for each of the failed specimens. Figure 4 shows box plots of the measurements as a function of the square root of exposure time (i.e., time to failure) to emphasize the parabolic oxidation relationship. To simplify, only the data for dry O_2 and 10% water vapor are shown. Because of the limited number of specimens in each condition (3 β phase and 3 γ+γ' coatings), all of the specimens were fit to one curve. While the scatter is significant, the median values are lower in dry O_2, and the remaining alumina scale was thicker beneath the YSZ top coating than on the opposite side of the specimen without YSZ (Figure 4). A thicker oxide with greater strain energy per unit volume would be more likely to spall, thus explaining the decreased coating lifetime for the β coating in air with 10% H_2O. However, this argument does not support the similar lifetime for the γ+γ' coatings in these two environments, although there was less difference in the alumina thickness for these specimens.

Additional work is in progress to better understand the effect of 10% H_2O with simple (NiAl) and Pt-modified aluminide bond coatings where the bond coatings are all made by a standard process at Oak Ridge National Laboratory with the assistance of Tennessee Technological University [8,9]. Figure 3 shows coating lifetimes for other superalloy substrates including the same CMSX-4® superalloy shown in Figure 1 and N515, a low (1.5 wt.%) Re version of N5 that also contains higher Hf. These substrates both showed higher average lifetimes than N5 at 1,150°C in air with 10% H_2O. Even without Pt in the coating, the YSZ lifetime was significantly higher on the N515 substrate. This difference is attributed to a beneficial effect of the higher Hf content [10] in N515 compared to N5 or CMSX-4®. An additional comparison also is being made at 1,125°C, where coating rumpling is expected to be decreased [11]. An increased rate of rumpling in the presence of water vapor was attributed to the decreased aluminide coating lifetime [6,7]. The 1,125°C study is still in progress

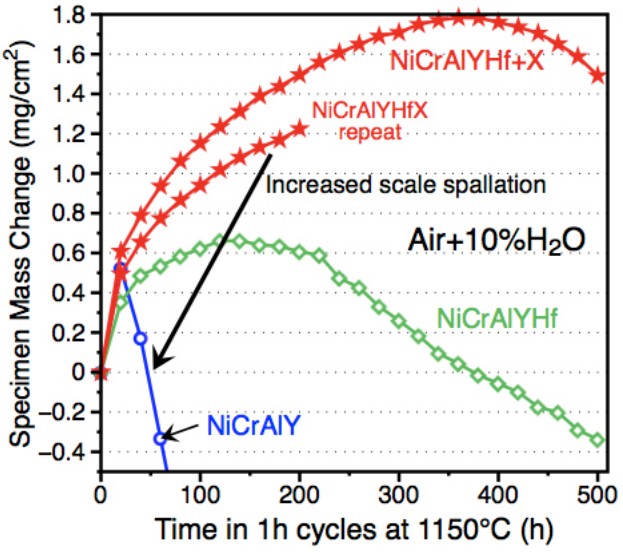

FIGURE 5. Specimen mass change for cast model NiCrAl alloys during 1-h furnace cycles at 1,150°C in air with 10% H_2O. The addition of Hf improved the alumina scale adhesion resulting in less specimen mass loss. Element X (not identified at this time due to intellectual property concerns) further improved the scale adhesion under these conditions.

but currently illustrates why higher temperatures are used to accelerate coating failure. The coating lifetime for Pt-modified coatings is at least 3.5 times higher with only a 25°C decrease in exposure temperature. For these experiments, the characterization not only included roughness measurements but also residual stress measurements using photo-stimulated luminescence spectroscopy.

Finally, Figure 5 shows cyclic oxidation results for cast model NiCrAl alloys that are being used to identify new coating compositions. Similar to the results for NiCoCrAlY bond coatings at 1,100°C (Figure 1) a benefit was observed for the addition of Hf to the casting. In this case at 1,150°C in air with 10% H_2O, the higher mass gain for the Y and Hf containing casting indicates less alumina scale spallation, i.e., better scale adhesion. Figure 5 shows that the addition of a third dopant element further improved scale adhesion in the presence of water vapor. Prior to a decision about intellectual property, this element is only identified as X. If this addition continues to show promise, the next evaluating step will be to make powder for fabricating HVOF coatings to determine TBC lifetime.

Conclusions and Future Directions

The benefit of superalloy and bond coating dopants and the effect of water vapor is being quantified by measuring TBC lifetime in furnace cycling experiments. The results in water vapor suggest that TBC testing in water vapor may be more representative of the turbine environment than results obtained in dry environments; however, higher water vapor contents do not increase TBC degradation. For developing TBC systems with increased durability, Hf-containing bond coatings appear more promising than Y and La additions to the Ni-base superalloy. However, higher Hf contents in the superalloy may be worth investigating. Finally, initial results with cast NiCrAl specimens suggest that further improvements are possible with minor alloying additions.

Future work on this project will include:

- Completing a study of the effect of cycle frequency, which has initially increased average TBC lifetime 3-10 times by increasing the cycle time from one hour to 100 hours at 1,100°C.
- Completing 5,000-10,000 h exposures at 900°C in air with 10% H_2O to better understand the oxidation kinetics and Al interdiffusion at a metal temperature closer to the actual turbine operation.
- Evaluation of coating performance in additional environments containing H_2O and CO_2.
- Complete additional high-resolution TEM characterization work to study the effect of water vapor and superalloy composition on the thermally-grown alumina microstructure and microchemistry.
- Complete work on model MCrAl-type compositions to identify potentially more oxidation resistant compositions. If warranted, alloy powders will be fabricated in order to make HVOF coatings with the new composition.
- Investigate new coatings and processes such as the GE NiAlCr+Zr (or Hf) coatings and suspension plasma spray coatings, which produce more strain tolerant YSZ.

FY 2012 Publications/Presentations

1. B.A. Pint and J.A. Haynes, "Effect of Higher Water Vapor Content on TBC Performance," *Adv. Mater. Proc.*, 170 (5) (2012) 52.

2. J.A. Haynes, K.A. Unocic and B.A. Pint, "Effect of Water Vapor on the 1100°C Oxidation Behavior of Plasma-Sprayed TBCs with HVOF NiCoCrAlX Bond Coats," submitted to *Surf. Coat. Technol.,* and presentation at the International Conference on Metallic Coatings and Thin Films, San Diego, California, May 2012.

3. K.A. Unocic and B.A. Pint, "Effect of Water Vapor on Thermally Grown Alumina Scales on Bond Coatings," submitted to *Surf. Coat. Technol*., and presentation at the International Conference on Metallic Coatings and Thin Films, San Diego, California, May 2012.

4. B.A. Pint and K.A. Unocic, "Ionic Segregation on Grain Boundaries in Thermally Grown Alumina Scales," *Mater. High Temp.* (2012) in press.

5. B.A. Pint, J.A. Haynes, K.A. Unocic and Y. Zhang "The Effect of Water Vapor and Superalloy Composition on Thermal Barrier Coating Lifetime," in E. Huron et al. eds., *Superalloys 2012*, TMS, Warrendale, Pennsylvania, (2012) in press; and presentation at Superalloys 2012, Seven Springs, Pennsylvania, September 2012.

References

1. I.G. Wright and T.B. Gibbons, "Recent Developments in Gas Turbine Materials and Technology and Their Implications for Syngas Firing," *International Journal of Hydrogen Energy*, 32 (2007) 3610-3621.

2. K. Harris and J.B. Wahl, "Improved Single Crystal Superalloys. CMSX-4®(SLS)[La+Y] and CMSX-486®," in K.A. Green, T.M. Pollock, H. Harada, T.E. Howson, R.C. Reed, J. Schirra and S. Walston eds., *Superalloys 2004*, TMS, Warrendale, Pennsylvania, 2004, p. 45-52.

3. D.K. Gupta and D.S. Duvall, "A Silicon and Hafnium Modified Plasma Sprayed MCrAlY Coating for Single Crystal Superalloys," in *Superalloys 1984*, M. Gell, et al. eds., p. 711-20, TMS, Warrendale, Pennslylvania (1984).

4. B.A. Pint, "Optimization of Reactive Element Additions to Improve Oxidation Performance of Alumina-Forming Alloys," *J. Am. Ceram. Soc*., 86 (2003) 686-695.

5. Y. Itoh, M. Saitoh and M. Tamura, "Characteristics of MCrAlY Coatings Sprayed by High Velocity Oxygen-Fuel Spraying System," *J. Eng. Gas Turb. & Power,* 122 (2000) 43-49.

6. B.A. Pint, G.W. Garner, T.M. Lowe, J.A. Haynes and Y. Zhang, "Effect of Increased Water Vapor Levels on TBC Lifetime with Pt-Containing Bond Coatings," *Surf. Coat. Technol*. 206 (2011) 1566-1570.

7. B.A. Pint and J.A. Haynes, "The Effect of Water Vapor Content on TBC Lifetime," in Proceedings of the 8th International Charles Parsons Turbine Conference, G.M. McColvin, et al. eds., *IOM*, 2011, London, Paper G3.3.

8. Y. Zhang, W.Y. Lee, J.A. Haynes, I.G. Wright, B.A. Pint, K.M. Cooley, and P.K. Liaw, "Synthesis and Cyclic Oxidation Behavior of a (Ni,Pt)Al Coating on a Desulfurized Ni-base Superalloy," *Met. Trans*., A 30 (1999) 2679-2687.

9. B. A. Pint, J.A. Haynes, and Y. Zhang, "Effect of Superalloy Substrate and Bond Coating on TBC Lifetime," *Surf. Coat. Technol*., 205 (2010) 1236-1240.

10. V.K. Tolpygo, K.S. Murphy, and D.R. Clarke, "Effect of Hf, Y, C in the Underlying Superalloy on the Rumpling of Diffusion Aluminide Coatings," *Acta Mater*., 56 (2008) 489-499.

11. V.K. Tolpygo and D.R. Clarke, "Temperature and Cycle-Time Dependence of Rumpling in Platinum-Modified Diffusion Aluminide Coatings," *Scripta Mater.* 57 (2007) 563-566.

V. UNIVERSITY TURBINE SYSTEMS RESEARCH

A. Aero-Heat Transfer

V.A.1 Designing Turbine Endwalls for Deposition Resistance with 1,400°C Combustor Exit Temperatures and Syngas Water Vapor Levels

Jeffrey P. Bons (Primary Contact), Ali Ameri
Department of Aerospace Engineering
The Ohio State University
2300 West Case Rd.
Columbus, OH
Phone: (614) 247-8414
Email: bons.2@osu.edu

DOE Project Manager: Mark Freeman
Phone: (412) 386-6094
Email: Mark.Freeman@netl.doe.gov

Subcontractor:
Thomas H. Fletcher,
Brigham Young University, Provo, UT

Contract Number: NT0005055

Start Date: October 1, 2008
End Date: March 31, 2012

Fiscal Year (FY) 2012 Objectives

- Conduct deposition testing in Brigham Young University (BYU) Turbine Accelerated Deposition Facility (TADF) with varying gas and surface temperatures.
- Conduct deposition testing in BYU TADF with augmented water vapor levels.
- Conduct deposition testing in Ohio State University (OSU) Turbine Reacting Flow Rig (TuRFR) with varying particle size.
- Conduct deposition testing in OSU TuRFR with film cooling.
- Perform endwall optimization using computational fluid dynamics (CFD).

FY 2012 Accomplishments

- BYU TADF successfully demonstrated operation up to 1,400°C gas temperature. Studies were conducted varying gas temperature up to 1,400°C and surface temperature up to 1,100°C. Deposition rate is much more dependent on surface temperature than gas temperature over this range.
- BYU TADF deposition experiments indicate that particle loading has a secondary influence on deposition compared with surface temperature.
- Film cooling to casing (vane trailing edge cooling cavity) only reduced deposition substantially on latter half of vane in TuRFR. Critical requirement of holding positive backflow margin for coolant vs. gaspath stagnation pressure duly noted.
- Four ash types tested in TuRFR at 1,100°C. Bituminous coal has highest ash melting temperature and lowest deposition rate. Lignite and sub-bituminous both deposit rapidly on leading edge and pressure surface.
- Drop in particle diameter of 3x (10x in Stokes number) results in 65% reduction in deposition rate for given operating conditions.
- Computational deposition model was successfully implemented in both the GE/NASA E^3 geometry and the CFM56 geometry from GE.
- Simulations predict increased deposition with increasing particulate size and gas temperature, consistent with experimental observations.
- Using CFD, dependency of deposition on Stokes number was identified. Large particles have a more ballistic trajectory, while small particles can navigate the entire vane passage without impacting the surface.
- Endwall flow simulations suggest secondary flows have primary role in deposition on hub and casing endwalls. Redesigns have limited effect on deposition rate.

Introduction

Turbine inlet temperatures for large power generation gas turbines have been steadily increasing over the last several decades due to significant advances in materials and cooling technologies. At the same time, political and economic pressures are pushing utilities to consider fuel flexibility using synfuels that have higher concentrations of trace elements and ash compared to "clean" burning natural gas. Current plans to transition from current syngas to high hydrogen fuels produced from coal syngas and oxy-fuels will only exacerbate these challenges with high water vapor levels. The combination of increased engine operating temperatures and synfuel integration warrant a re-evaluation of current hot gas path design to consider the potential impact of deposition. In the first stage high pressure turbine vane (nozzle), the majority of material system failures occur

at the junction of the vane and the passage endwall. Secondary flows in this region create unique challenges for thermal management and efficient cooling design. Recent initiatives of passage endwall contouring and vane leading edge modifications have been developed for use with natural gas fired turbines, and thus their compatibility with ash-bearing and/or high steam content synfuels at elevated operating temperatures has yet to be assessed. Clearly, there is a critical need to explore innovative endwall designs that could both increase turbine durability and mitigate the adverse effects of deposition in the endwall.

Approach

This research effort addresses this critical turbine operability and maintainability issue in three distinct phases.

- Phase 1—Modeling and Experimental Validation: A deposition model will be developed and incorporated in an existing CFD code capable of handling modern turbine geometries. Validation of this new model will be performed using both the OSU and BYU accelerated deposition facilities. The BYU TADF facility will be modified to accommodate higher firing temperatures (up to H-class engine temperatures 1,400°C) and the addition of water vapor. The OSU facility will be used to investigate deposition patterns around real film-cooled turbine hardware at engine relevant conditions. Hardware will be donated from GE, Siemens, and Pratt through collaborative agreements.
- Phase 2—CFD and Experimental Endwall Design Study: Various endwall design modifications will be evaluated, both experimentally and computationally, to determine their influence on deposition. The objective will be to evaluate each of the design modifications for deposition resistance as well as aerodynamic and heat transfer performance. BYU will perform gas temperature and fuel type test series to determine high temperature extension of deposition data.
- Phase 3—CFD Design Study with Cooling and Experiments with Water Vapor: BYU will explore the effect of water vapor on turbine deposition. Experiments will be conducted with various thermal barrier coatings material systems with water vapor levels up to 15% to simulate levels anticipated with high hydrogen combustion. The effect of film cooling on deposition will also be studied, both at BYU and OSU. Deposition models will be used to determine optimum film flow location to mitigate endwall deposition and improve material system survivability.

Thus, with this aggressive research program, the U.S. Department of Energy and industry will gain valuable insights into factors affecting the safe, efficient operation of modern industrial turbines with alternative fuels as well as new, innovative endwall designs that are tailored for this more adverse operating environment.

Results

Experimental Facility at BYU

The TADF went through a major redesign during the first year of this effort. The objective was to allow high temperature operation up to 1,400°C. Silicon carbide was chosen as the candidate material for the new hot section. These modified components were designed, manufactured and installed successfully. During the second year, a number of facility maintenance issues were resolved that will allow safe, efficient testing for years to come. The test coupon holder was also redesigned with spray water impingement cooling to allow operation at elevated temperatures. A series of tests exploring the dependency of ash deposition on test duration was conducted with subbituminous coal ash of two different particle diameters. Testing parameters during the third year included both gas and surface temperature as well as particulate loading. Figure 1 shows the results of a preliminary test varying both gas and surface temperature. When the gas temperature is varied by 38°C at constant surface temperature, capture efficiency remains relatively constant. By contrast, when

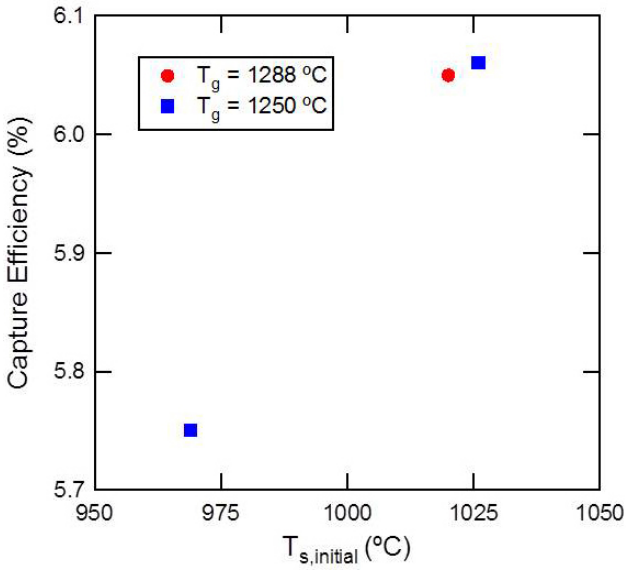

FIGURE 1. Effect of gas and surface temperature on capture efficiency from TADF at BYU

the surface temperature is varied by 60°C at constant gas temperature, the capture efficiency drops by 5%. A similar trend was found in the TuRFR testing at OSU.

Experimental Facility at OSU

The fabrication and initial performance testing of the now fully assembled OSU Turbine Reacting Flow Rig was completed during the first year of this effort. A gas temperature sensitivity study was conducted, varying the temperature from 1,800°F to 2,050°F to determine the effect of temperature on deposition. A dramatic increase in deposit thickness and character was noted around 1,950°F for the lower grade coal ash species (lignite and subbituminous) while bituminous ash did not deposit significantly in the same range. A study was conducted with four different ash types to determine the sensitivity of deposition on ash type. Lignite and two subbituminous ash deposited much more rapidly than bituminous. The bituminous melting temperature was measured and found to be 100°C higher than that of the other ash samples, which partly explains the differences. The subbituminous ash was ground into four mass median diameters from 6 µm to 18 µm. Figure 2 is a spanwise surface trace indicating leading edge deposit thickness for two different particle sizes (large vs. small Stokes) and with/without film cooling. As the figure indicates, the drop in Stokes number resulted in a 60–70% reduction in deposition. This effect is well captured by the computational model. Film cooling was only applied on the back half of the vane, and there is a significant reduction in deposition in this region; however even the leading edge registers a slight reduction in deposition (as shown in Figure 2). Leading edge deposits fall off significantly near the endwall due to secondary flows, as will be discussed below.

Computational Methods at OSU

An initial literature survey covering research efforts centered on alternative (syngas) fuels deposition on turbine blades with film cooling was completed. After consulting the literature, a methodology for particle tracking and deposition was selected where an Eulerian-Lagrangian approach is to be followed, Eulerian approach for continuous phase and Lagrantian approach for discrete phase. After considering various options, it was decided that the particle-tracking and deposition models would be developed and implemented with the use of a commercial CFD code, Fluent. The Fluent based deposition model was successfully validated against both the TADF deposition data and a previous study at VonKarmann Institute during the first year of the grant. During the second year, the team exercised the deposition model in an actual three dimensional (3D) vane geometry with the NASA/GE E^3 design. This architecture is particularly interesting since it actually has derivatives that currently operate in industrial gas turbines. An exhaustive study was conducted using two different deposition models: critical velocity [2] vs. critical viscosity [1]. Despite their limitations (which are many), both models predict the initial phases of deposition reasonably well. During the final year, they were applied to the CFM56 geometry and compared directly to results from the TuRFR. Since one of the objectives of this project is to evaluate endwall deposition mitigation, the model was used to explore multiple geometric modifications as shown in Figure 3. The "extended" and "new" inlet designs in Figure 3 were intended to reduce the abruptness of the acceleration into the nozzle guide vane (NGV), thus reducing the secondary flow and hopefully the endwall deposition. Figure 3 also shows the deposition results for the new inlet configuration.

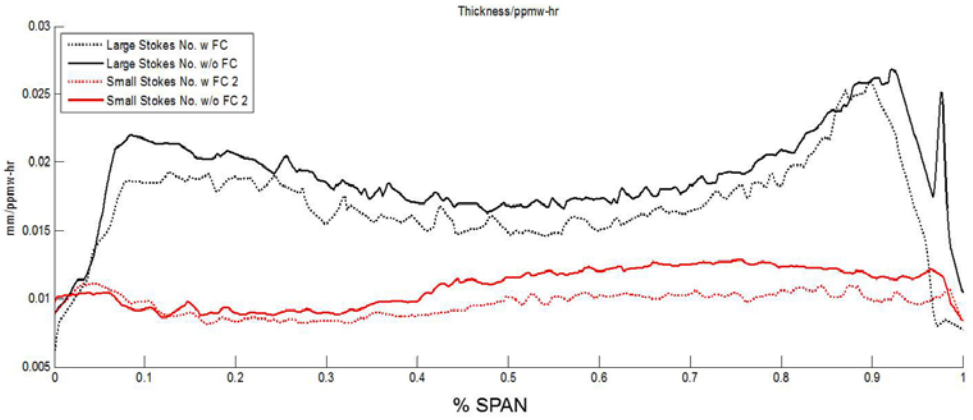

FIGURE 2. Leading edge surface trace of deposit thickness for Large/Small Stokes and with/without film cooling from TuRFR at OSU

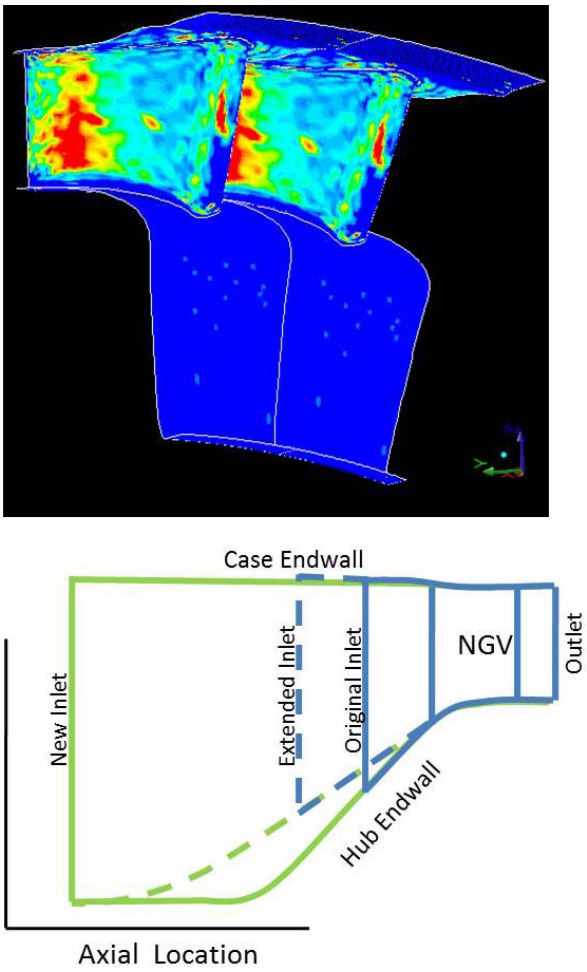

FIGURE 3. Modified inlet geometry used to explore endwall deposition mitigation. CFD result showing deposition prediction on modified endwall model.

Unfortunately, the modification had little effect on the endwall deposition. To study this further, another model was created of a cylinder in cross-flow with flat endwall (simulated NGV leading edge), as shown in Figure 4. Figure 4 also shows the results of an experimental validation, indicating similar deposition patterns near the endwall due to the horseshoe vortex that forms there. This result is encouraging because it indicates that the model is capable of predicting deposition in highly 3D flowfields.

Conclusions

The project is now complete and has achieved a number of significant milestones.

- Controlled deposition up to gas temperatures of 1,400°C.

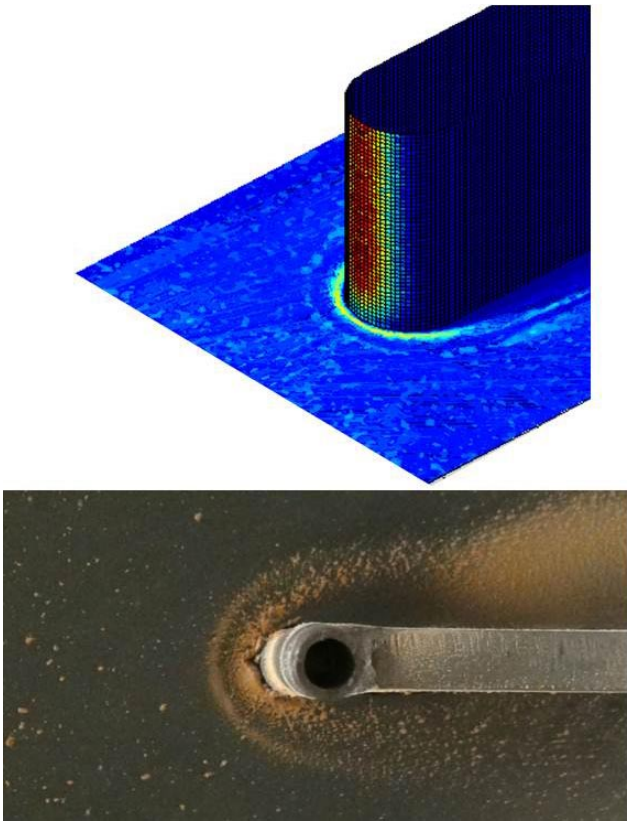

FIGURE 4. Deposition model predictions of endwall deposition pattern compared with experimental validation of same

- Explored deposition sensitivity to ash type, particulate size, and temperature.
- Demonstrated effect of film cooling on deposition rate.
- Developed deposition model coupled with commercial CFD particle tracking code.
- Demonstrated/validated deposition model for a modern, high-performance nozzle guide vane.
- Explored endwall modifications to mitigate deposition.
- Demonstrated/validated deposition model for endwall deposition.

Special Recognitions & Awards/Patents Issued

1. IGTI/ASME Heat Transfer Committee 2011 Best Paper Award for "Coal Ash Deposition on Nozzle Guide Vanes: Part I—Experimental Characteristics of Four Coal Ash Types," by J. Webb, B. Casaday, B. Barker, J.P. Bons, A.D. Gledhill, and N.P. Padture, Presented at ASME Turbo Expo 2011 in Vancouver, Canada, June 2011. (GT2011-45894).

FY 2012 Publications/Presentations

1. Casaday, B.P., Ameri, A., Bons, J.P., 2012, "Effect of Hot Streaks on Ash Deposition in Turbine Vane Passage," presented at AIAA Aerospace Sciences Meeting in Nashville, Tennessee, January 9–12, 2012. Paper #AIAA-2012-0474.

2. Bonilla, C., Webb, J., Clum, C., Casaday, B., Brewer, E., and Bons, J.P., 2012, "The Effect of Particle Size and Film Cooling on Nozzle Guide Vane Deposition," accepted for presentation at ASME Turbo Expo 2012 in Copenhagen, Denmark, June 11–15, 2012. Paper #GT2012-69084.

3. Casaday, B.P., Ameri, A., Bons, J.P., 2012, "Numerical Investigation of Ash Deposition on Nozzle Guide Vane Endwalls," accepted for presentation at ASME Turbo Expo 2012 in Copenhagen, Denmark, June 11–15, 2012. Paper #GT2012-68923.

References

1. Sreedharan, S.S., and Tafti, D.K., 2009. "Effect of Blowing Ratio on Syngas Fly Ash Particle Deposition on a Three Row Leading Edge Film Cooling Geometry Using Large Eddy Simulations," ASME Paper No. GT2009-59326.

2. El-Batsh, H. and Haselbacher, H., "Numerical Investigation of the Effect of Ash Particle Deposition on the Flow Field through Turbine Cascades," IGTI, 2002, Amsterdam, Netherlands, GT-2002-30600.

V.A.2 Effects of Hot Streak and Phantom Cooling on Heat Transfer in a Cooled Turbine Stage Including Particulate Deposition

Jeffrey P. Bons (Primary Contact), Ali Ameri
Department of Aerospace Engineering
The Ohio State University
2300 West Case Rd.
Columbus, OH
Phone: (614) 247-8414
Email: bons.2@osu.edu

DOE Project Manager: Travis Shultz
Phone: (304) 285-1370
Email: Travis.Shultz@netl.doe.gov

Contract Number: FE0007156

Start Date: October 1, 2011
End Date: September 30, 2014

Fiscal Year (FY) 2012 Objectives

- Pursue improvements to Ohio State University's (OSU) existing deposition models, with the goal of more faithfully capturing the fundamental physics of the particle sticking process.
- Use the Turbine Reacting Flow Rig (TuRFR) to measure hot streak migration and surface temperature in nozzle guide vane (NGV) without film cooling.
- Use the TuRFR to measure deposition patterns and rates in uncooled NGV with hot streaks.
- Compare model predictions to TuRFR hot streak and deposition measurements. Adjust model as needed.

FY 2012 Accomplishments

- Incorporated elastoviscoplasticity (EVP) model which incorporates both elastic and plastic particle deformation. Previous models accounted for either elastic (critical velocity model) or plastic (critical viscosity model) deformation only.
- Conducted preliminary hot streak clocking study to determine dependency of deposition on hot streak location, particle size, and hot streak severity.
- Generated hot streaks in TuRFR.
- Conducted hot streak deposition test with uncooled NGV.

Introduction

As energy demands increase, the U.S. must consider clean, high efficiency alternatives to present fuels. The U.S. has an abundance of coal, the proper use of which could reduce our dependency on foreign gas and oil imports. Coal can be utilized in an environmentally responsible manner if it is decarbonized (assuming carbon sequestration) to produce a high hydrogen content fuel through a water-gas shift process. This high hydrogen content (HHC) synthesis (syngas) gas can then be burned in a gas turbine as part of a highly efficient integrated gasification combined cycle (IGCC) plant. To harness the full potential of HHC fuels, the gas turbine will be operated at higher firing temperatures than at present with natural gas. However, localized hot spots, as well as large temperature gradients adversely affect the longevity of turbines. The rise in the turbine inlet temperature must be accommodated by the development of better-suited materials and the design of more efficient and effective cooling schemes. Designing efficient cooling schemes requires a detailed knowledge of the gas temperature field through the nozzle and blade of the first turbine stage so that coolant can be effectively used where it is most needed. Hot streak migration in the turbine blade passage creates hot gas accumulation on the pressure side and accumulation of cooling air (or "phantom cooling") on the suction side. Another important characteristic of the HHC fuels is the particulate content of the fuel. Although much of the ash content of the fuel is extracted in the process of gasification and clean-up, a trace amount of particulates remain. Over time, such particulates can deposit and accumulate on hot surfaces and contribute to the deterioration in aero and heat transfer performance of the affected gas turbine. The particulates can also clog film cooling holes and lead to reduced longevity of the blades. Since the deposition process is most dependent on gas and surface temperatures, particulate is most likely to deposit in the path of the hot streaks emanating from the combustor. Clearly, the ability to accurately predict the path of the combustor exit temperature non-uniformities is critical to determining the areas of highest concern for deposition with HHC fuels.

Approach

This research effort addresses this critical turbine operability and maintainability issue in three distinct phases.

- Phase 1—Model validation with experiments for hot streaks in uncooled vane with deposition. Improvements to existing deposition models will be pursued and implemented in a comprehensive computational fluid dynamics (CFD) model. The model will be validated using experimental data from the TuRFR. Model results will then be compared to experimental measurements in the TuRFR for an uncooled nozzle guide vane.
- Phase 2—Model validation with experiments for hot streaks in cooled vane with deposition. Coolant will be added to both the model and the experiment.
- Phase 3—Model validation for hot streak migration in rotating turbine stage. The model will be exercised in the rotating frame of the first stage turbine rotor as well. Results will be compared to previously obtained experimental results from the University Research, Engineering, and Technology Institutes (URETI) program (conducted at OSU's Gas Turbine Laboratory under NASA sponsorship).

Thus, with this aggressive research program, the U.S. Department of Energy and industry will gain valuable insights into factors affecting the safe, efficient operation of modern industrial turbines with alternative fuels.

Results

Computational Modeling

The methodology used for particle tracking and deposition is the Eulerian-Lagrangian approach: Eulerian approach for the continuous phase and Lagrangian approach for the discrete phase. These models have been developed and implemented in the commercial CFD code, Fluent. Traditionally, two different deposition models have been exercised: critical velocity [2] vs. critical viscosity [1]. The critical velocity model accounts for elastic deformation and a force of adhesion that are functions of particle stiffness (and thus temperature). This model does not account for plastic deformation of the particle upon impact. The critical viscosity model only accounts for plastic deformation, the "flowing" of the particle onto the surface as its viscosity decreases with increasing temperature. In reality, both mechanisms are important. Following an extensive literature search, a model was identified that accounts for both mechanisms. Deposition with this elastoviscoplasticity model is thus dependent on particle temperature *and* velocity. Figure 1

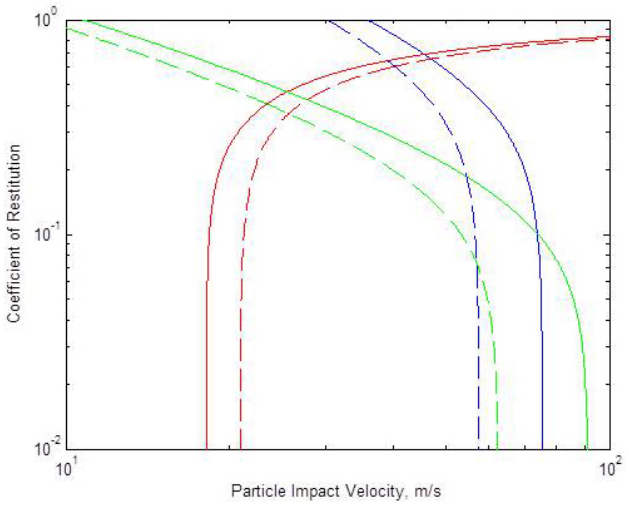

FIGURE 1. Predicted COR vs. particle impact velocity for integration elastoviscoplasticity (green), energy elastoviscoplasticity (blue), and critical velocity (red) models. The dashed line shows the effect of increased temperature for all cases.

compares the variation of coefficient of restitution (COR), where COR = 0 implies no particle rebound, or deposition, with particle velocity for two different EVP models and the critical velocity model. The trends are quite different. Note the critical viscosity model is not shown because it does not account for velocity in the calculation of sticking. Work is underway to calibrate this new, improved deposition model using fundamental particle impingement studies. In the meantime, the critical viscosity model was used in conjunction with a Fluent model of the GE E^3 nozzle geometry; hot streaks were introduced into the inlet plane of the computational domain, as shown in Figure 2. The deposition model results are shown in Figure 3 for four different clocking positions as well as a uniform inlet temperature. As expected, the deposition peak follows the hot streak with the different clocking position.

Experimental

Dilution plates were installed in the OSU TuRFR to permit the creation of non-uniform inlet temperature profiles. Both radial and hot streak profiles have been demonstrated. The hot streak profile was tested with particulate to show the resulting deposition on a nozzle guide vane set. Figure 4 shows the result side-by-side with the Clocking 1 position prediction from Figure 3. In the prediction, the hot streaks are lined up with Vanes 2 and 4, counting from the top of the image, while in the experiment the hot streaks are lined up with Vanes 1 and 3. Both the prediction and the experiment indicate a deposition bias to the vanes in-line with the hot

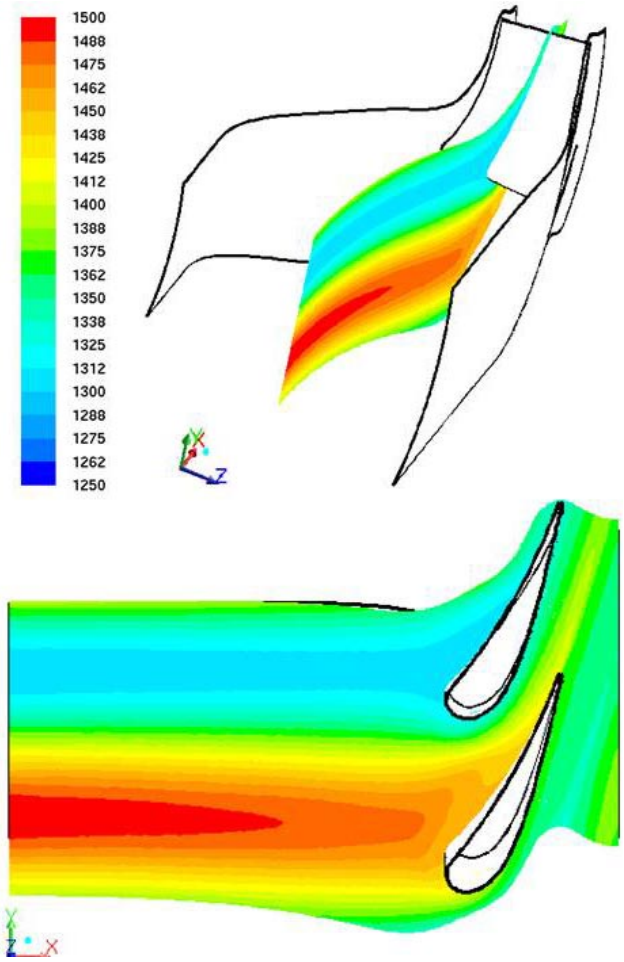

FIGURE 2. Contours of total temperature showing hot streak migration through vane passage for Clocking Position 1

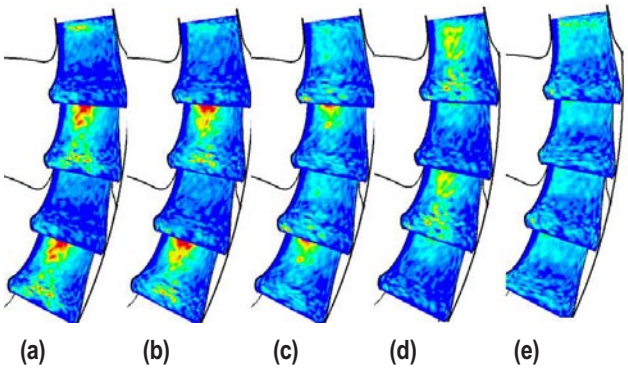

FIGURE 3. Simulation results showing deposition on pressure surface of vanes for 8 μm particles (St_k = 1.2). From left to right: (a) Clock Position 1, (b) Clock Position 4, (c) Clock Position 7, (d) Clock Position 10, (e) Uniform temperature inlet

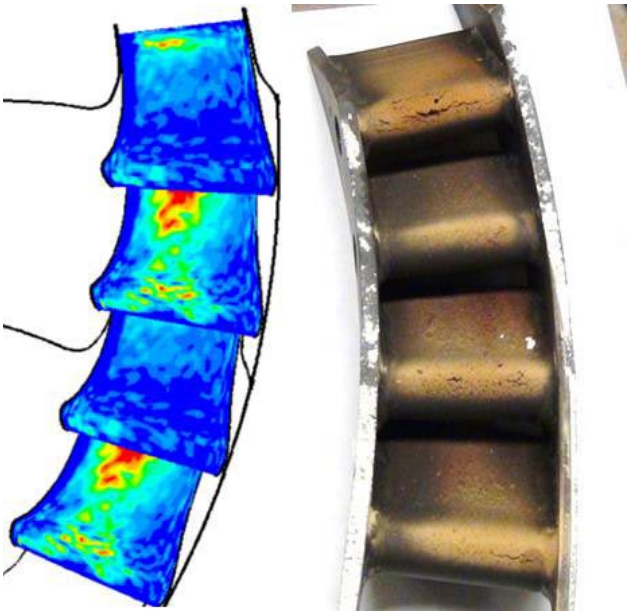

FIGURE 4. Computational deposition patterns for a clock position of one and experimental deposition patterns for a shifted clock position of 13 (one vane over)

streak, as expected. Further testing will help to identify thresholds for deposition and optimal clocking locations. Diagnostics are also being developed to more accurately measure the spatial temperature distribution at the inlet to the TuRFR. This will assist in the model validation process by providing appropriate inlet conditions to the Fluent calculation. Finally, a validation test section has been designed that will provide measurements to calibrate the new EVP deposition model.

Conclusions and Future Directions

Reporting on the first year of the project, progress has been excellent. The Fluent model has been exercised to establish that hot streaks have a significant effect on the uncooled vane and on deposition patterns. Fundamental evaluation of the deposition modeling has yielded a new model that will be calibrated later this year. Preliminary hot streak deposition testing in the TuRFR provides reasonable agreement with current predictions. For the remainder of this year, research will focus on model validation and development as well as additional experimental testing and diagnostics. The second year will introduce cooling into the nozzle cascade. Progress has already been made in developing the flow model for the rotating simulations that will be conducted during the third year.

FY 2012 Publications/Presentations

1. Casaday, B.P., Ameri, A., Bons, J.P., 2012, "Effect of Hot Streaks on Ash Deposition in Turbine Vane Passage," presented at AIAA Aerospace Sciences Meeting in Nashville, Tennessee, January 9–12, 2012. Paper #AIAA-2012-0474.

References

1. Sreedharan, S.S., and Tafti, D.K., 2009, "Effect of Blowing Ratio on Syngas Fly Ash Particle Deposition on a Three Row Leading Edge Film Cooling Geometry Using Large Eddy Simulations," ASME Paper No. GT2009-59326.

2. El-Batsh, H. and Haselbacher, H., "Numerical Investigation of the Effect of Ash Particle Deposition on the Flow Field through Turbine Cascades," IGTI, 2002, Amsterdam, Netherlands, GT-2002-30600.

V.A.3 Aerodynamics and Heat Transfer Studies of Parameters Specific to the IGCC-Requirements: Endwall Contouring, Leading Edge Filleting and Blade Tip Ejection under Rotating Turbine Conditions

Dr. Meinhard, T. Schobeiri (Primary Contact), Dr. Je-Chin Han
Turbomachinery Performance and Flow Research Laboratory (TPFL)
Mechanical Engineering, Texas A&M University
College Station, TX 77843-3123
Phone: (979) 845-0819; Fax: (979) 845-0812
Email: tschobeiri@mengr.tamu.edu

DOE Project Manager: Robin Ames
Phone: (304) 285-5436
Email: Robin.Ames@netl.doe.gov

Contract Number: FE0000753

Start Date: December 1, 2010
End Date: September 30, 2012

Fiscal Year (FY) 2012 Objectives

- Numerically investigate the impact of the purge flow injection on aerodynamics and film cooling effectiveness of the contoured endwall of the first and the second turbine stage and of the non-contoured reference case.
- Complete manufacturing for the first and second turbine stage endwall contouring.
- Complete manufacturing for four sets of turbine blades with different ejection hole geometries and their instrumentation.

FY 2012 Accomplishments

- The new rotor two independent cooling loop, with endwall contouring, purge flow injection, and blade tip ejection film cooling hole, was inserted into the facility.
- Contoured endwall as well as blades with tip ejection holes were instrumented with pressure sensitive paints (PSP).
- A charge-coupled device camera with strobe light and synchronization sensors was installed and tested.
- For performance tests, the turbine was completely instrumented with four inlet rakes, four exit rakes, numerous static pressure sensors, and thermocouples.
- For interstage aerodynamic measurements, the seven-axis traversing system, with each axis instrumented with a five hole probe, was installed.
- Several shakedown tests were performed to ensure the correct and safe operation of the new turbine rotor.
- A full range of performance, interstage, and film cooling experiments are being conducted.

Introduction

Efficiency Improvement Through Endwall Contouring

As reported in [1–3] and summarized in [4], the team introduced a new method for designing non-axisymmetric endwalls. The method is based on a continuous diffusion process and utilizes a prescribed deceleration of the secondary flow velocity from pressure to suction surface. By defining a target pressure and constructing the non-axisymmetric endwall contouring, it was shown that the pressure difference on the hub can be controlled, reducing the secondary flow and increasing the efficiency. This method can equally be applied to high pressure, intermediate pressure, or low pressure (LP) turbines and compressors regardless of the load coefficient, flow coefficient, and degree of reaction. It is strongly physics-based, very straightforward, and easy to use. The method was applied to the second rotor of the Turbomachinery Performance and Flow Research Laboratory (TPFL)-turbine, where on the first attempt an efficiency increase of $\Delta\eta = 0.51\%$ was obtained. This increase is quite remarkable given the fact that the target pressure was defined such that it covers the critical range of 38% of the axial length. Moreover, it has exceeded all the other values delivered by conventional trial and error method. Further efficiency improvement is expected by extending the target pressure upstream of 6% and downstream of 73% of the chord. It is worth noting that, if all three stator and all three rotor rows are contoured, an efficiency improvement of more than 2.5% would result for the existing three-stage turbine.

Influence of Purge Flow and Endwall Contouring on Film Cooling Effectiveness

The first stage of a gas turbine engine is subjected to a high temperature. In order to protect the blade material

and rotor structure from excessive thermal stresses, film cooling is applied to the blades as well as to the hub portion of the rotor. For the hub cooling, a certain amount of compressor air is injected through a circumferential slot into the hub. To understand the complex flow picture associated with the purge flow injection, the three-stage research turbine of TPFL was used. The injection mechanism is shown in Figures 1, 2 and 3. As seen in Figure 1, two independently controlled concentric coolant loops provide the necessary mass flow for all the platform film cooling experiments. The inner loop supplies coolant mass for film cooling experiments on the hub platform through an upstream stator-rotor circumferential gap positioned between the first stage stator and rotor. A concentric jet exits this circumferential gap at an angle of 25° into the mainstream (Figures 2 and 3). The outer loop supplies coolant for the planned blade tip film cooling experiments.

To investigate the effect of endwall contouring on film cooling effectiveness through purge injection, the first rotor hub had to be contoured. This was necessary for mapping the film cooling effectiveness of the first rotor in conjunction with the purge flow ejection through the circumferential gap. While, in the case of the second rotor, the endwall contouring brought substantial reduction in secondary flow losses and thus, efficiency increase, the first rotor shows different behavior due to its immediate exposure to the purge flow injection.

Approach

The endwall design of the first rotor row required particular attention. While in the case of the second rotor (Figure 3 right), the endwall contouring extending upstream has brought substantial reduction in secondary flow losses and, thus, increasing efficiency, the first rotor is directly exposed to the purge flow with no space to extend the contouring upstream of the first rotor blade's leading edge. It is worth noting that the space restriction

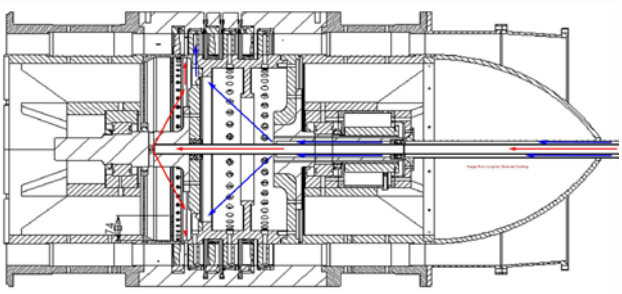

FIGURE 1. Turbine components with two independent cooling loops

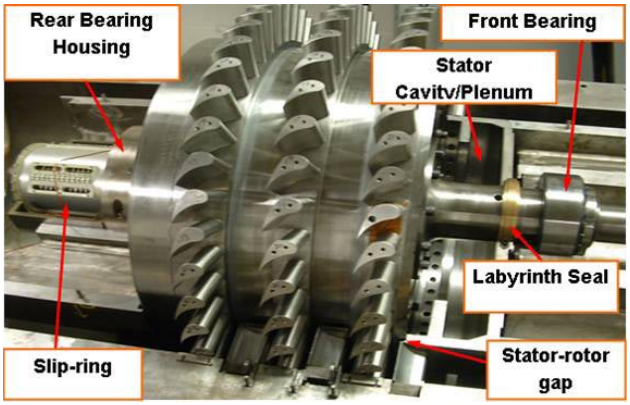

FIGURE 2. Turbine components showing stator cavity and gap

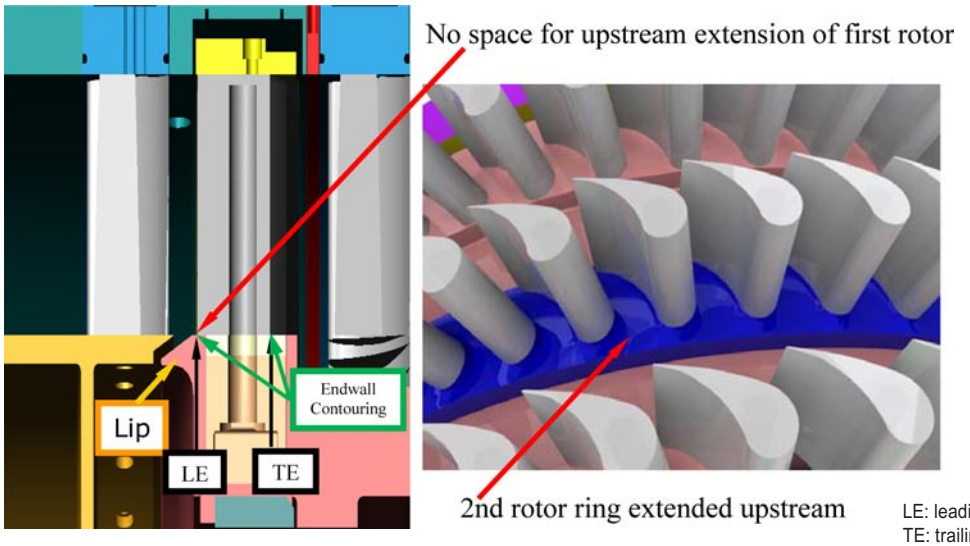

FIGURE 3. Position of the circumferential gap for ejection of purge flow (left), extension of the contouring upstream of second rotor endwall contouring

was dictated by the existing turbine hardware, which was designed to exactly simulate the purge flow situation through a gas turbine engine. This circumstance caused a shortening of the target pressure range to design an optimum endwall contouring for the first rotor. Prior to simulating the interaction of the purge flow with the endwall contouring, extensive numerical simulations were performed.

Results

First Rotor Hub Contouring

To investigate the effect of the gap presence on the efficiency of the reference case, and considering the spatial restrictions mentioned above, the team started with the reference case without contouring and prescribed a target pressure that caused a sharp deceleration rate (Figure 4, Curve R1). This resulted in an efficiency that was just slightly above the reference case without contouring. Apparently, the corresponding diffuser contour experienced some flow separation. By varying the target pressure by increasing Δp_{target} (Figure 5), a moderate deceleration rate was achieved that resulted in a fully attached flow inside the contouring, and thus higher efficiency, as shown in Figure 6. As seen, the new contouring labeled R1-4 has the highest efficiency of 90.81%, compared to 90.47% for the reference case. This efficiency improvement is far below the one obtained for the second rotor, as illustrated in [1–4].

Pressure Distributions

Pressure distributions at 0% span (directly on the hub) for the reference case and contoured endwall are displayed in Figure 7. Mass flow ratio (MFR) is varied from 0.0% to 1.5%. For MFR = 0, a noticeable change in pressure distribution on the suction surface is observed for the contoured case of Figure 7e compared to the non-contoured one 7a. Although this change is not substantial, it does reflect an interesting phenomenon, which does not exist in a cascade flow: at MFR = 0, due to rotation and centrifugation of the boundary layer, fluid discharges from the cavity, leaving behind a temporary vacuum within the cavity. Because of the pitchwise pressure distribution, with lower pressure being predominant on the suction surface, the fluid particles tend to eject toward the suction side of the blades. After the vacuum level has reached a certain threshold, the vacuum breaks down. Fluid from the main stream flows back, filling the cavity, and the periodic process of emptying and re-filling starts all over again. This periodic unsteady process cannot be captured by steady Reynolds-averaged Navier-Stokes (RANS) code, which averages the results. Consequently, to capture the periodic changes of all quantities, the unsteady version, URANS, must be used. As the MFR increases, the changes in pressure distribution pattern become more pronounced. At the ratio MFR = 1.0 (Figure 7c), the first signature of a periodic unsteady ejection appears in the form of a quasi-periodic distribution of LP spots in the pitchwise direction. Finally, at the ratio MFR = 1.5%, a clear manifestation

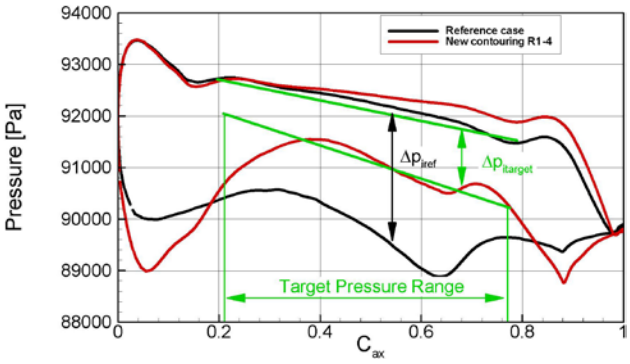

FIGURE 5. Pressure distributions directly at the hub for reference case (black: non-contoured) and contoured case (red) with target pressure to design the contouring using the technique in [1]

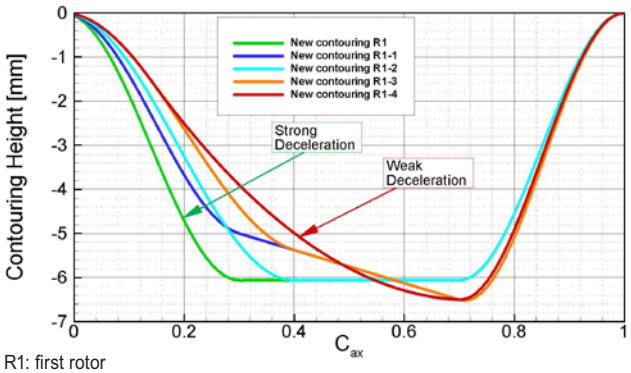

R1: first rotor
C_{ax}: axial chord length of the blade

FIGURE 4. Variation of deceleration rate defined by the diffusion length to obtain the best endwall contouring efficiency

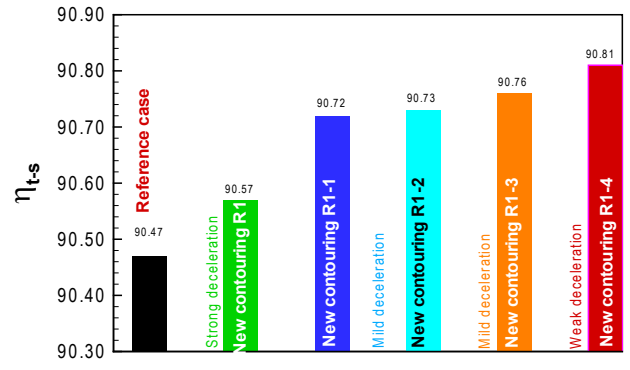

η_{t-s}: total-to-static efficiency

FIGURE 6. First rotor efficiency development varying deceleration rate

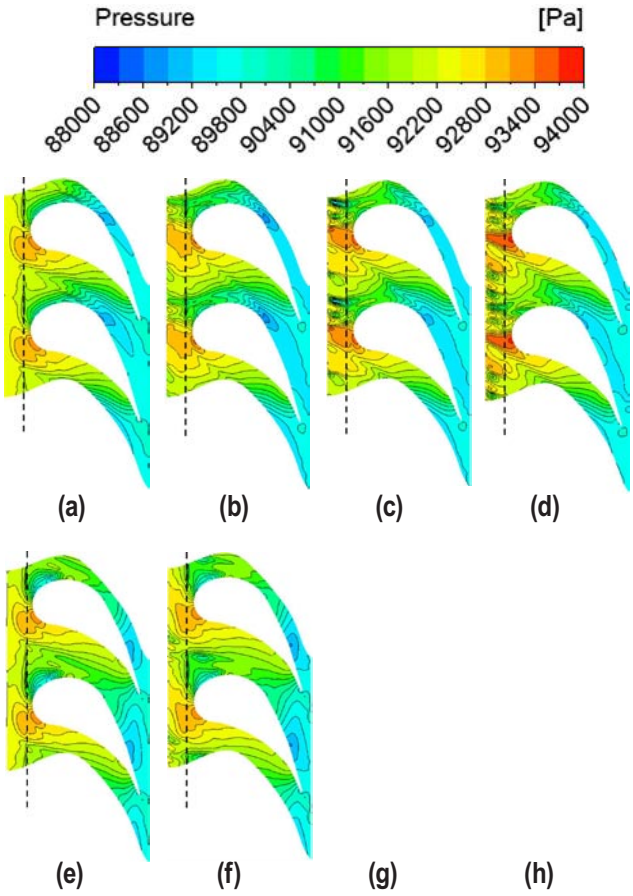

FIGURE 7. Pressure distribution at 0% span: (a) reference case with MFR=0%; (b) reference case with MFR=0.5%; (c) reference case with MFR=1.0%; (d) reference case with MFR=1.5%; (e) new contouring with MFR=0%; (f) new contouring with MFR=0.5%; (g) new contouring with MFR=1.0%; (h) new contouring with MFR=1.5%

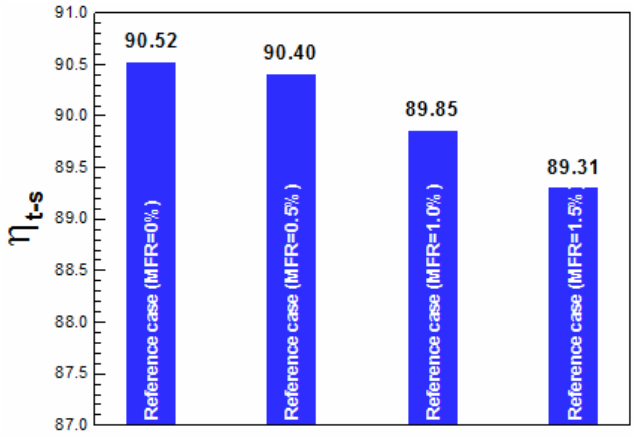

FIGURE 8. Total-to-static efficiency for reference case at different MFRs

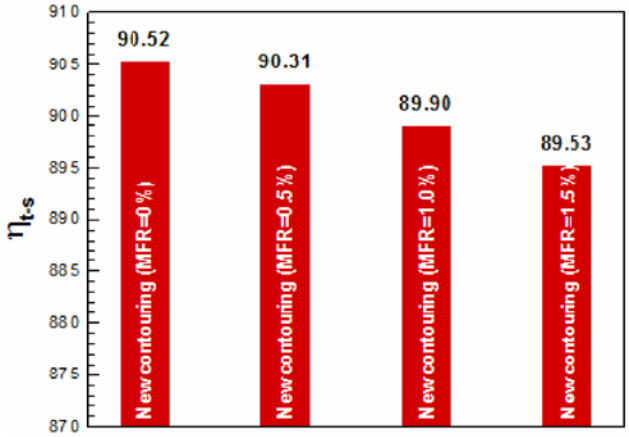

FIGURE 9. Total-to-static efficiency for contoured case at different MFRs

of pitchwise high and LP spots is seen in Figure 7d. In contrast, the pressure patterns of the contoured cases with MFR = 0.5, 1.0 and 1.5% (Figure 7g, 7h) suggest that the presence of contouring exerts a certain control mechanism that forces the flow from the cavity to eject asymmetrically from the gap without noticeable pitchwise periodic signature.

Total-to-Static Efficiencies

The effect of ejection associated with contouring on the total-to-static efficiency is shown in Figures 8 and 9. Generally, the efficiency decreases with increasing mass flow ratio regardless of the presence of contouring. This is directly explained through the energy balance. As seen, for MFR = 0%, efficiency has not experienced any changes. For a small mass flow ratio of MFR = 0.5%, the efficiency of the contoured case is reduced below the reference case with a difference of $\Delta\eta_{t-s}$ = -0.09%, indicating that for relatively small MFRs, contouring not only does not contribute to efficiency improvement, but it also has a detrimental effect on efficiency. The situation reverses at higher MFRs. As seen, for MFR = 1.0%, the contouring brings a very small improvement of $\Delta\eta_{t-s}$ = 0.05%. Increasing MFR to 1.5% results in slightly higher $\Delta\eta_{t-s}$ = 0.22%. These marginal negative and positive changes of efficiency suggest that contouring for the first rotor that is directly exposed to purge flow is not recommendable.

Film Cooling Effectiveness Distributions

The film cooling effectiveness (defined in the nomenclature) is essentially a non-dimensional temperature distribution, with a reference cooling temperature that is chosen based on specific application. Figure 10 shows adiabatic film cooling effectiveness on the rotating platform for the reference case and the new contouring case with MFR = 0.5%, 1.0%, and 1.5%, respectively. For the reference case, it seems that coolant purged from the gap is pushed away from the rotor blade pressure-side towards suction-side due to pressure

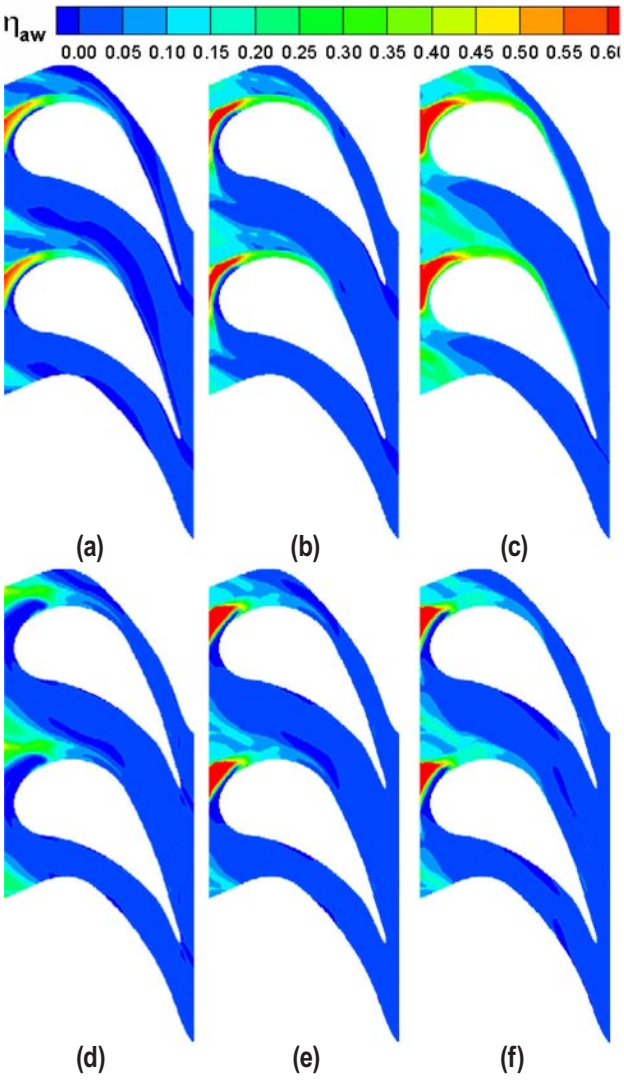

FIGURE 10. Adiabatic film cooling effectiveness: (a) reference case with MFR=0.5%; (b) reference case with MFR=1.0%; (c) reference case with MFR=1.5%; (d) new contouring with MFR=0.5%; (e) new contouring with MFR=1.0%; (f) new contouring with MFR=1.5%

gradient. This results in better film cooling protection from the leading-edge along the suction-side edge region. Meanwhile, the passage vortex, developed from the leading-edge pressure-side leg horseshoes vortex towards the suction-side trailing edge, rolls across the platform passage and tends to mix coolant with mainstream. This leaves the entire platform passage totally unprotected. In addition, coolant purged from the gap is highly non-uniform in the circumferential direction (pitchwise) due to interaction with the upstream passage vortex. As expected, film cooling effectiveness increases with increasing purge MFR from 0.5% to 1.5%. The increased purge flow pushes more coolant further into the platform to provide better film protection, and the stronger purge

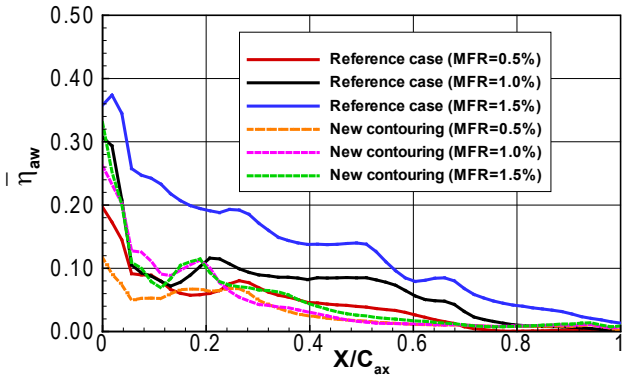

FIGURE 11. Pitchwise averaged adiabatic film-cooling effectiveness along the rotating platform passage (CFD)

flow reduces upstream passage vortex effect to improve purge coolant uniformity in the circumferential direction. Figure 10 also shows the film cooling effectiveness comparison between the reference case and the new contouring. It seems that the new contouring case shows similar trends of film cooling distribution from purge flow. However, with increasing purge flow rate, film cooling effectiveness for the new contouring platform does not improve as seen for the reference platform case. The stronger purge coolant of MFR = 1.5% is not able to reach the lower endwall contour area near the suction-side of the platform. Therefore, film cooling effectiveness near the suction-side platform area is insensitive to the purge flow rate from 0.5% to 1.5%.

Figure 11 shows the pitchwise averaged film cooling effectiveness along the rotating platform passage for the reference case and the new contouring case with MFR = 0.5%, 1.0%, and 1.5%, respectively. Results show that pitchwise averaged film cooling effectiveness decreases along the rotating platform passage for both the reference case and the new contouring case with MFR = 0.5% to 1.5%. In general, the averaged effectiveness increases with increasing purge flow rate; the reference case provides better averaged film effectiveness than the new contouring case. In particular, for the case of higher purge flow with MFR = 1.5%, the difference is significant. Figure 12 shows a comparison of the pitchwise averaged film effectiveness for the reference case and previous experimental data under similar conditions. For purge flow with MFR = 1.0%, the current computational fluid dynamics (CFD) seems to over-predict film cooling effectiveness over most of the rotating platform passage. For purge flow with MFR = 1.5%, the current CFD still over-predicts film effectiveness over most of the platform. This is consistent with earlier observation that CFD tends to over-predict pitchwise averaged film cooling effectiveness on a rotating platform.

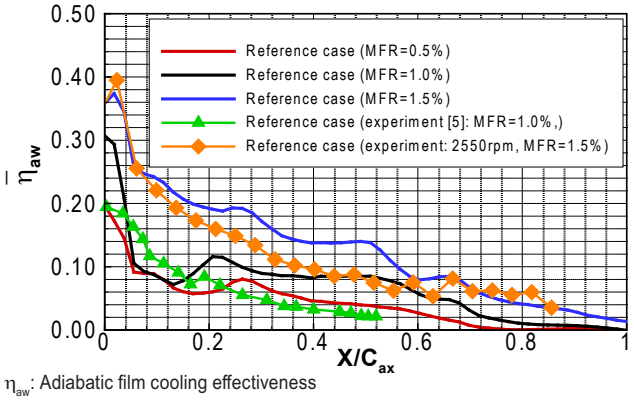

FIGURE 12. Comparison of the pitchwise averaged film effectiveness between reference case and previous experimental data under similar conditions

Conclusions, Ongoing and Future Research Work

Aerodynamics, performance, and heat transfer quantities were calculated using a commercial Navier-Stokes solver. Investigation was focused on the first rotor row, which was contoured and directly exposed to the purge flow. The simulations were performed at a rotational speed of 2,400 rpm and the coolant ejection at MFR = 0.0%, 0.5%, 1.0% and 1.5%. As expected, the first rotor row efficiency decreased as the purge mass flow ratio was increased for both reference (non-contoured) and contoured cases. Comparing the efficiencies of the reference case with those of the contoured one revealed a marginal decrease for MFR <1 and a marginal increase for MFR >1. At MFR = 0, due to rotation and centrifugation of the boundary layer, fluid discharges from the cavity, leaving behind a temporary "vacuum" within the cavity. It was observed that because of lower pressure on the suction surface, the fluid particles of the purge flow tend to eject toward the suction side of the blades. Furthermore, after the vacuum level has reached a certain threshold, the vacuum breaks down. Fluid from the main stream flows back, filling the cavity, and the periodic process of emptying and re-filling starts all over again. This periodic unsteady process cannot be captured by steady RANS code, which averages the results. Consequently, to capture the periodic changes of all quantities, URANS, must be used. The efficiency development for the first stage suggests that contouring does not result in a noticeable improvement whenever the contoured surface is exposed to purge flow. For adiabatic film cooling effectiveness, results show that coolant purged from the gap is pushed away from the rotor blade pressure-side towards suction-side due to pressure gradient. This results in better film cooling protection from the leading edge along the suction-side edge region. Meanwhile, the passage vortex rolls across the platform to further reduce film cooling effectiveness and leave the entire platform passage totally unprotected. Results also show that pitchwise averaged film cooling effectiveness decreases along the rotating platform passage for both the reference case and the new contouring case with MFR = 0.5% to 1.5%. In general, the averaged effectiveness increases with increasing purge flow rate; the reference case provides better averaged film effectiveness than the new contouring case. In particular, for the case of higher purge flow with MFR = 1.5%, the difference is significant.

Ongoing work on this project includes:

- Efficiency and performance measurement to experimentally expedite the efficiency improvement by the new contouring method.
- Measurement of film cooling effectiveness of the first stage rotor endwall surface subjected to the purge flow.
- Interstage flow measurement to obtain the loss distributions of the second stage rotor with endwall contouring.
- Comparison of the experimental findings with CFD-simulation results.

Future work on this project includes measurement of blade tip film cooling for four different hole distribution geometries.

FY 2012 Publications/Presentations

1. M.T. Schobeiri and K. Lu, 2012, "Endwall Contouring Using Continuous Diffusion, A Breakthrough Method and Its Application to a Three-Stage High Pressure Turbine," Presented at ISROMAC-14, the 14th International Symposium on Transport Phenomena and Dynamic of Rotating Machinery Conference, from February 27, until March 2, 2012, Honolulu, Hawaii.

2. M.T. Schobeiri, K. Lu, and J.C. Han, 2012,"Effect of Purge Flow on Aerodynamic Performance and Film Cooling Effectiveness on a Rotating Turbine with Non-Axisymmetric Endwall Contouring," ASME Paper, GT2012-69069. Proceedings of ASME Turbo Expo 2012: Power for Land, Sea and Air, June 11–15, 2012, Copenhagen, Denmark.

3. M.T. Schobeiri and J.C. Han, 2011, FY 2011 Office of Fossil Energy Advanced Turbine Program Annual Report, "V.A.2 Aerodynamics and Heat Transfer Studies of Parameters Specific to the IGCC-Requirements: Endwall Contouring, Leading Edge Filleting and Blade Tip Ejection under Rotating Turbine Conditions."

4. M.T. Schobeiri and K. Lu, 2011, "Endwall Contouring Using Continuous Diffusion, a Breakthrough Method and its Application to a Three-stage High Pressure Turbine," ASME Paper, GT2011-45931.

V.A.4 Environmental Considerations and Cooling Strategies for Vane Leading Edges in a Syngas Environment

Forrest E. Ames
Department of Mechanical Engineering
School of Engineering and Mines
University of North Dakota (UND)
243 Centennial Drive, Stop 8359
Grand Forks, ND 58202-8359
Phone: (701) 777-2095
Email: forrest.ames@engr.und.edu

DOE Project Manager: Robin Ames
Phone: (304) 285-0978
Email: Robin.Ames@netl.doe.gov

Subcontractor:
Jeffrey P. Bons
The Ohio State University (OSU), Columbus, OH

Contract Number: FE0004588

Start Date: October 1, 2010
End Date: September 30, 2013

Fiscal Year (FY) 2012 Objectives

- Since turbulent diffusion is known to be a significant mechanism for deposition in turbines, different freestream turbulence levels will be generated in the Ohio State University (OSU) Turbine Reacting Flow Rig (TuRFR).
- Study deposition rate for various turbulence and leading edge diameter combinations (OSU).
- Measure deposition rate, surface roughness, deposit thickness, and composition (OSU).
- Send deposit surfaces to University of North Dakota (UND) for modeling (OSU).
- Explore use of infrared camera and cylinder-integrated thermocouples to determine the heat load during deposition as well as evolution of deposition under different flow conditions (OSU).
- Develop stereo-lithography models for leading edge deposits and apply to cylinders. (UND).
- Conduct leading edge heat transfer studies with select OSU deposition surfaces (UND).
- Conduct leading edge internal cooling heat transfer study (UND).
- Survey rough cylinder boundary layer development (UND).

FY 2012 Accomplishments

- Developed faired cylinders for deposition testing in TuRFR (OSU).
- Designed, developed, and validated capability to generate elevated inlet turbulence in TuRFR (OSU).
- Designed, manufactured, and tested new nozzle guide vane test section based on Rolls-Royce (now LG Fuel Cell Systems) design without film cooling holes (OSU).
- Generated multiple deposition surfaces for use as scaled models in UND tunnels (OSU).
- Compared deposition for different leading edge diameters using faired cylinders (OSU).
- Developed leading edge internal cooling models for testing (UND).
- Conducted leading edge internal cooling heat transfer study (UND).
- Measured turbulent spectra response to approaching leading edge across turbulence conditions (UND).
- Made preparations to survey cylinder boundary layer development (UND).

Introduction

Cooling the leading edge of a first stage vane of a modern gas turbine offers considerable challenges due to an aggressive heat transfer environment and a very modest pressure difference for cooling. The aggressive environment includes high temperatures, high free-stream turbulence and surface roughness. High free-stream turbulence substantially augments leading edge heat transfer and generally dissipates film cooling protection. Surface roughness, often formed from deposition of fuel and air-bound impurities, promotes early transition and can even produce direct augmentation of heat transfer in the stagnation region. In the past, conventional leading edges were most often cooled using showerhead film cooling arrangements. However, with the use of syngas fuels, the application of showerhead cooling becomes questionable. Compared to natural gas, synfuels have higher levels of impurities which, combined with the higher firing temperatures envisioned for future turbines, increase the risk of vane leading edge deposition. Thus the potential for leading edge film cooling geometries to clog calls into question

their assured reliability. The question then becomes what other approaches can be used to cool the leading edge of vanes in modern power turbines without film cooling protection? One key piece of this answer comes from industry trends for the leading edge of first stage vanes which show growing diameters. While increasing diameters are expected to produce lower peak heat transfer levels in the leading edge region, the complex interactions of diameter, turbulence, and roughness on the resulting heat transfer and deposition rates offer considerable design challenges.

Approach

This research effort generates technology important to the reliability of gas turbines using syngas as fuel. This research is organized into three phases.

Phase 1 Leading Edge Model Development and Experimental Validation

The initial task for OSU's TuRFR facility will be to determine if the deposition mechanism for faired cylinders is similar to deposition for turbine vanes. If this approach works, the relative impact of leading edge diameter on deposition can be investigated using varying diameter cylinders instead of vanes. Next, the deposition measurements will be made and sent to UND for surface modeling. During this Phase 1 period, UND will study the response of turbulence approaching large cylindrical stagnation regions, the associated heat transfer augmentation as well as boundary layer development on the cylinder's surface. Additionally UND will begin the development of candidate internal cooling geometries for cooling a leading edge region.

Phase 2 Experimental Deposition and Roughness Study

During Phase 2 of this experimental study, OSU will use its TuRFR facility, modified to generate higher levels of turbulence, to study the influence of turbulence on deposition rates in turbines. These results will not only be used to improve predictive modeling, but they will also be available to UND for their heat transfer measurements with realistic roughness. UND will use surfaces generated and provided by OSU as part of their leading edge heat transfer and boundary layer studies. UND will also develop and test candidate internal cooling schemes for large leading edge regions.

Phase 3 Mitigation of Deposition Using Downstream Full Coverage Film Cooling

During Phase 3 of this experimental study, OSU will develop faired cylinders to explore various film cooling designs to assess their effectiveness at reducing deposition. Later, an actual turbine vane geometry will be used to explore the influence of select film cooling patterns on deposition. UND will investigate the combined influence of turbulence and realistic roughness on film cooling effectiveness and surface heat transfer. As a basis of comparison, they will initially look at the influence of turbulence on film cooling effectiveness and heat transfer for select full coverage geometries.

Results

Experimental Facility at UND

Over the last year, UND has made upgrades to its facilities and fabricated a number of test surfaces for testing. In order to prepare for testing the new internal cooling geometries, UND has upgraded its bench scale heat transfer rig with a new diffuser, a new flow conditioning section, and several new plenums. In addition, one conventional high-solidity pin-fin internal cooling geometry was designed, fabricated, instrumented and assembled for testing. Two new internal cooling geometries were also designed, fabricated, instrumented and assembled for testing. These three cooling configurations are pictured in Figure 1 showing the cold side plate on the left and the internal cooling channel on the right. These new innovative cooling geometries incorporate incremental impingement to improve the cooling effectiveness of the method in the later rows of the array. Preparations have also been completed for testing the response of turbulence approaching the leading edge region of our 4-inch and 16-inch cylindrical leading edge test surfaces.

Experimental Measurements at UND

The current project includes research to better understand the gas path environment a first stage vane is subjected to as well as methods to cool and otherwise mitigate the influence of this environment on the long term reliability of this vane. In this last year, the research effort at UND has been focused on improved understanding of the response of high intensity turbulence to the larger leading edge regions expected in new vanes. In the last year, testing one conventional and two new internal cooling methods was also done to keep these leading edge regions cool. We have documented the decay of six different elevated levels of turbulence in our test section without the cylindrical leading edge test surfaces and have documented the response of turbulence approaching both the large (16-inch diameter) and smaller (4-inch diameter) cylindrical leading edge test surfaces. The results are generally showing a more significant intensification of the turbulence, with turbulence having a lower dissipation rate. We have also

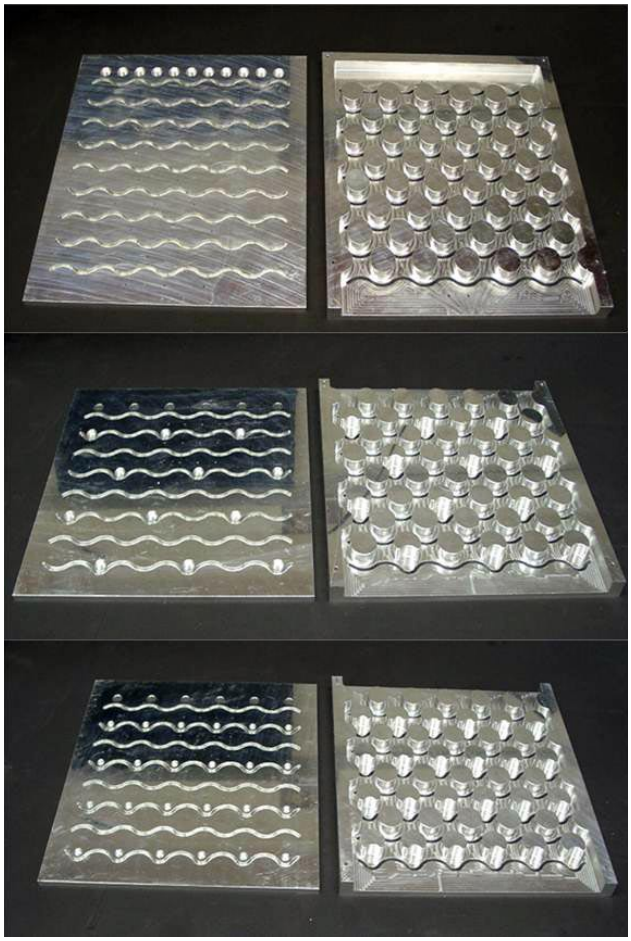

FIGURE 1. Photographs of conventional and incremental impingement high solidity cooling arrays

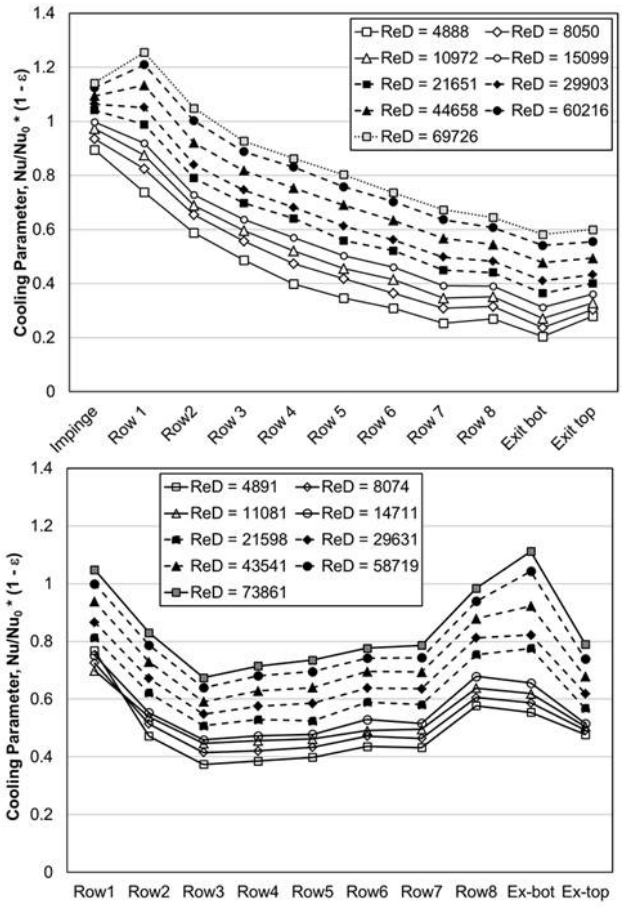

FIGURE 2. Cooling parameter comparison for conventional (top) and incremental impingement (bottom) cooling array which shows improved downstream cooling performance

documented the heat transfer and internal effectiveness of our conventional and incremental impingement cooling arrays. A comparison between the conventional array and one of the incremental impingement arrays is shown in Figure 2. The incremental impingement array shows superior cooling performance in the downstream rows, and it is adaptable to providing higher levels of cooling where they are most needed.

Experimental Facility at OSU

Over the last year, OSU has spent considerable time designing, fabricating, and testing new test pieces for this study. Figure 3 shows the faired cylinder hardware that has been used to simulate leading edge deposition for a variety of leading edge diameters. In most cases, the deposition testing is conducted with different cylinder diameters in each slot (0.25", 0.375", and 0.5" diameter) so that the effects can be compared directly. Also during the last year, OSU designed and fabricated two other test sections: a full nozzle guide vane (NGV) set based on

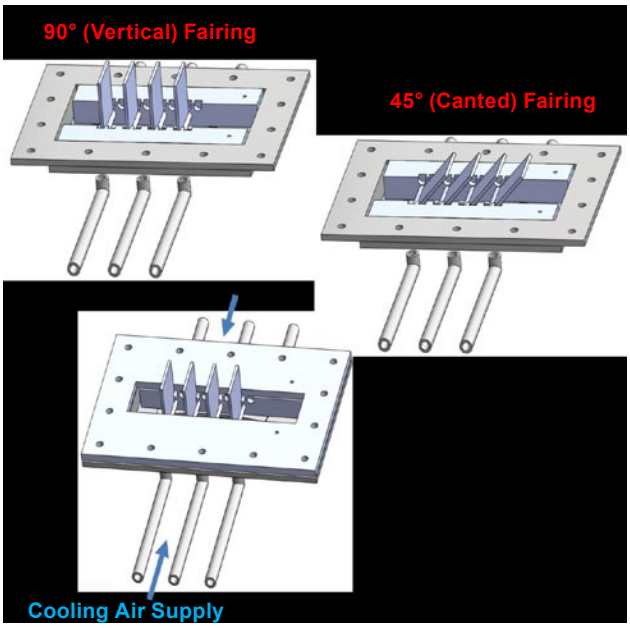

FIGURE 3. Schematic of faired cylinder test section for TuRFR deposition testing with different leading edge diameters

an LG (formerly Rolls-Royce) experimental profile, and a 1" diameter cylinder (without fairing). The LG NGVs have internal but not film cooling while the 1" diameter cylinder is film cooled. The TuRFR facility was also modified to accommodate variable dilution jets upstream of the NGV inlet. These jets produce elevated turbulent mixing in the TuRFR inlet.

Experimental Measurements at OSU

In this last year, the research effort at OSU has been focused on assessing first whether the faired cylinder is a reasonable substitute for a vane leading edge and second what the effect of leading edge diameter is on deposition. Initial results with the cylinders showed similarities between leading edge deposits and NGV deposits taken from the TuRFR testing with the CFM56 nozzles. Since the CFM56 vanes are film cooled and the cylinders are not, the LG vane set was fabricated without cooling holes. The deposit buildup pattern on the LG vane and faired cylinder showed considerable similarity and the testing proceeded with multiple cylinder diameters. Figure 4 shows images of several cylinders both during (top) and after (bottom) deposition testing at 1,950°F. Both during and after the test, the smaller diameter cylinder appears to have a more dense deposit structure. Using the definition of Stokes number shown in Equation 1, where the cylinder diameter is found in the denominator, one can expect that particles approaching the smaller diameter cylinder will have a larger effective Stokes number compared with the same particles approaching the larger cylinder, if all other variables are held constant.

Equation 1.

$$S_t = \frac{\rho_\rho D^2_\rho U_{in}}{18\mu_{in} D_{LE}}$$

A larger Stokes number suggests that the trajectory of the particles is governed more by ballistics rather than fluid dynamics. In other words, the larger cylinder diameter has a greater upstream influence on the flow than the smaller counterpart. This will cause the flow streamlines to begin deviating from their straight-line trajectory further upstream, hence increasing the probability that the particles will miss the leading edge of the cylinder or avoid a direct hit with the surface. The net result is an expected reduction in the probability of sticking. Computational simulations were run to validate this theory using a particulate-laden flow approaching a cylindrical leading edge where the Stokes number was varied.

FIGURE 4. Photographs of deposition on 0.375", 0.5", and 0.25" faired cylinders during test (top) and after testing (bottom)

Conclusions and Future Directions

The joint project between UND and OSU has been developing well over the first six quarters of the project. Experimental measurements have been conducted at both OSU in the TuRFR facilty and at UND in its large scale wind tunnel and its bench scale internal cooling facility. UND is currently beginning boundary layer measurements for its smooth leading edge surfaces and is making preparations to acquire slot and full coverage film cooling measurements over its smooth surfaces. At the same time, UND will be working with Dr. Jeffrey Bons to identify the realistic surfaces generated in the TuRFR facility and the appropriate scaling for understanding the influence of realistic roughness on stagnation heat transfer and downstream film cooling. OSU will continue assessing the influence of cylinder diameter and turbulence level on deposition. OSU is also developing techniques to assess surface temperature distributions using an infrared camera.

FY 2012 Publications and Presentations

1. M.L. Busche, L.P. Moualeu, C. Tang, and F.E. Ames, "Heat Transfer and Pressure Drop Measurements in High Solidity Pin Fin Cooling Arrays with Incremental Replenishment," 2012, ASME Paper No. GT2012-69289. (Accepted for presentation and publication at the 2012 International Gas Turbine Congress and Exhibition, June 13, 2012, Copenhagen, Denmark).

V.A.5 Improving Durability of Turbine Components through Trenched Film Cooling and Contoured Endwalls

David G. Bogard (Primary Contact),
Frederick Todd Davidson,
David A. Kistenmacher
University of Texas at Austin
1 University Station C2200
Austin, TX 78712
Phone: (512) 471-3128; Fax: (512) 471-8727
Email: dbogard@mail.utexas.edu

DOE Project Manager: Robin Ames
Phone: (304) 285-0978
Email: Robin.Ames@netl.doe.gov

Subcontractors:
Karen A. Thole, Amy Mensch
Pennsylvania State University (Penn State)
136 Reber Building
University Park, PA 16802-1412
Phone: (814) 865-2519; Fax: (814) 865-1280
Email: kthole@psu.edu

Contract Number: FE0005540

Start Date: October 1, 2010
End Date: September 30, 2013

Fiscal Year (FY) 2012 Objectives

- Use a high conductivity, matched Biot number, model vane to evaluate the performance of a simulated thermal barrier coating (TBC) with and without film cooling.
- Simulate particulate deposition on matched Biot number, model vane with TBC with varying film cooling hole and trench configurations.
- Use a matched Biot number endwall to evaluate the contribution of internal impingement cooling and external film cooling to overall effectiveness.
- Measure the effect of contaminant depositions on overall effectiveness for the matched Biot number model.

FY 2012 Accomplishments

- Completed experimental simulation of a turbine vane with TBC. Measurements were made with a matched Biot number conducting model to obtain overall effectiveness with and without film cooling on the pressure side of the vane.
- These tests provide important experimental data to evaluate the insulating effects of TBCs without and with film cooling.
- Experiments were completed in which contaminant depositions on the leading edge and pressure side of a turbine vane with TBC were simulated using our unique molten wax spray technique. Results showed that the contaminant deposition acted as an insulating layer on the TBC surface, therefore decreasing the vane metal temperature.
- Matched Biot number model design was completed for flat and contoured endwalls. The six available passages have been divided into three sections with two passages each. The sections are film cooling only, internal impingement cooling plus film cooling, and internal impingement cooling only.
- Auxiliary chiller was installed in the coolant loop to increase the temperature difference between the coolant and the mainstream. This reduced the uncertainty in overall effectiveness to 0.02.
- Preliminary experiments measuring overall effectiveness of a matched Biot number flat endwall model have been conducted for film cooling only, as well as internal impingement cooling plus film cooling.

Introduction

Gas turbine operation using new coal-derived high hydrogen fuels (syngas) requires design of new cooling configurations for turbine components. To operate with high efficiency, gas turbines must generate very high temperatures in the combustion process, and cooling of the combustor and turbine components downstream of the combustor is a critical factor to enable efficient operation. When using syngas an additional factor that must be addressed when designing turbine section cooling is the effects of contaminant particles which will impact and adhere to the turbine components. The deposition of contaminants results in much rougher surfaces and partial blockage of film cooling holes that seriously degrade the cooling performance. Performing full engine tests to determine where these contaminants deposit and how to mitigate the effects of these depositions is costly. However, we have developed techniques to simulate the deposition process in laboratory test facilities which allows us to develop

new turbine cooling designs that reduce depositions of contaminants and/or maintain effective cooling even after contaminants have deposited to the surface.

There are two key technologies used to cool turbine components, TBCs and film cooling. TBC is a low thermal conductivity ceramic material that is applied to the surface of turbine components to insulate them from hot mainstream gases. Film cooling uses high pressure air bled from the gas turbine compressor and injected through small holes along the surface to provide a "film" of relatively low temperature air over the surface of the turbine components. Consequently the heat transfer from the hot mainstream gases to the turbine component walls is reduced. Past studies have shown that film cooling performance can be significantly improved if coolant is directed through shallow trenches on the surface which enhance the distribution of the coolant over the surface. A major goal of this research project is to investigate how these shallow trenches can be formed using TBCs and to develop film cooling designs that mitigate the effects of contaminant depositions. These new cooling designs will lead to reduced costs for the user as a result of longer component life.

Approach

Wind tunnel facilities at Penn State and University of Texas at Austin (UT) have been specifically designed to simulate film cooling of turbine vanes, blades, and endwalls. These facilities incorporate equipment that simulate the deposition of contaminants in the engine by using molten wax particles to simulate the molten contaminant particles that occur at actual engine conditions. The wax particles used in the test facilities are sized appropriately to simulate the inertial behavior of particles that exist in engine conditions. The use of wax also allows for the simulation of the liquid-to-solid phase change that is essential to the primary deposition mechanism.

The performance of shallow trench film cooling configurations for various positions on the suction and pressure sides of a simulated vane with active deposition is being investigated at UT. At Penn State the effect of active deposition on various endwall cooling configurations is being investigated. Preliminary results showed that deposition could be simulated dynamically using wax and that the effects of deposition could be quantified using infrared thermography. New endwall and vane surface film cooling configurations will be developed to minimize deposition and maximize cooling performance under contaminated conditions.

Results

Combined Effects of TBC and Film Cooling

A unique capability for our laboratories is the simulation of conjugate heat transfer effects due to the interaction of the hot gas flow around turbine airfoils and along the turbine endwalls. This is accomplished by carefully designing and constructing the simulated turbine components to have the correct thermal conductivity so that the relative heat transfer for the gas and the solid is matched to engine conditions. This matching of gas and solid heat transfer is referred to as a matched Biot number test. Using matched Biot number testing allows us to study the performance of TBCs, and particularly the combined performance of TBCs and film cooling. When quantifying the cooling performance, the external wall "metal" temperature, $T_{w,e}$, normalized using the coolant temperature, $T_{c,vane\ inlet}$, and the mainstream temperature, T_∞, to obtain the "overall effectiveness", ϕ, defined as: $\phi = (T_\infty - T_{w,e})/(T_\infty - T_{c,vane\ inlet})$. The temperature of the exterior TBC surface is normalized in the same manner as the overall effectiveness; however, $T_{TBC,e}$ is used in place of the wall temperature, $T_{w,e}$. This normalized TBC surface temperature, τ, is defined as: $\tau = (T_\infty - T_{TBC,e})/(T_\infty - T_{c,vane\ inlet})$. The conventional technique for quantifying film cooling performance is to determine the adiabatic wall temperature, T_{aw}, using a very low conductivity model, film cooling hole exit temperature, $T_{c,hole\ exit}$, and defining the film effectiveness as follows: $\eta = (T_\infty - T_{aw})/(T_\infty - T_{c,hole\ exit})$. A method was developed by Davidson (2012) that allows both ϕ and τ to be analytically predicted using a one dimensional heat transfer analysis with reasonable accuracy for configurations with no film cooling using only the geometry and thermal conductivities of the vane, bond coat, and TBC as well as experimental results for film effectiveness, η. This analytical model was verified using experimental results obtained at UT. The key advantage of this analytical tool is in its ability to predict TBC performance using experimental results obtained from adiabatic effectiveness tests rather than more costly and time consuming overall effectiveness tests.

Experiments were conducted to obtain overall effectiveness, normalized TBC surface temperatures, and internal surface temperatures for various film cooling configurations as well as various coolant flow rates defined as the "blowing ratio": $M = \rho_c U_c / \rho_\infty U_\infty$ where ρ_c and ρ_∞ are the coolant and mainstream densities, respectively, and U_c and U_∞ are the coolant and mainstream velocities, respectively. The overall effectiveness, ϕ, is shown in Figure 1 for varying blowing ratios with and without TBC. It is apparent in Figure 1 that the overall effectiveness is greatly increased when TBC is applied to the surface of the vane. It can also be

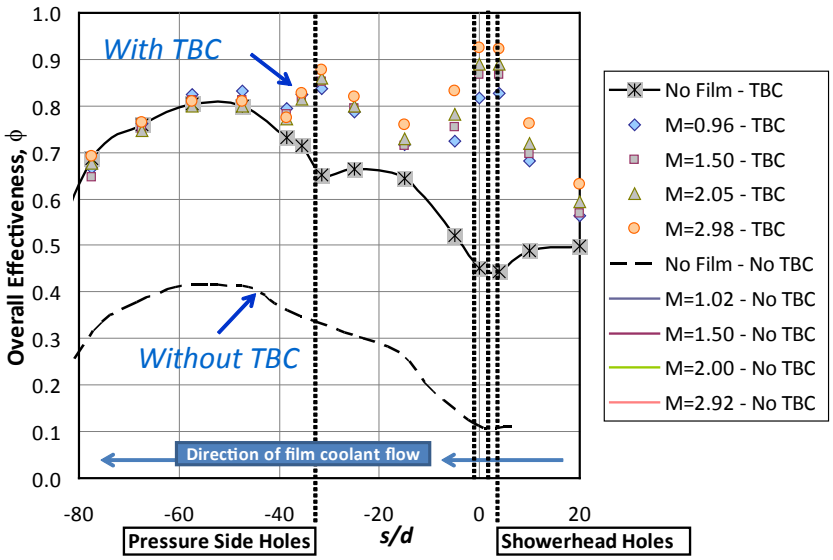

FIGURE 1. Effect of TBC and blowing ratio on ϕ for round film cooling holes

seen that the overall effectiveness with TBC and no film cooling is greater than in the case of film cooling with no TBC downstream of the showerhead holes. This result indicates that TBC cooling dominates over film cooling. Figure 1 indicates that the sensitivity to blowing ratio is reduced when TBC is applied to the vane. Further results show that the sensitivity to different film cooling hole and trench geometries is also reduced when TBC is included on the surface of the vane.

Simulations of contaminant depositions on the pressure side of a turbine vane with TBC and an ideal trench are shown in Figure 2. Depositions grew on both the downstream and upstream lips of the trench and then proceeded to crowd over the trench opening. This result for the ideal trench is similar to results with other cooling configurations. Contaminant deposition acts as an insulator on the surface of the TBC and increases the overall effectiveness of the vane. The deposition also acts to increase surface roughness and therefore detrimentally affect the cooling performance in terms of τ. Further testing is required to determine the deposition's detrimental effect on the aerodynamic performance of the vane due to increased surface roughness.

Flat Endwall Overall Effectiveness

Preliminary measurements of overall effectiveness were made for the flat conjugate endwall. Blade passages incorporating film cooling only and impingement plus film cooling were measured. Important parameters for these experiments were average blowing ratio, $M = \rho_c U_c / \rho_\infty U_\infty \sim 1.0$; average momentum flux ratio, $I = \rho_c U_c^2 / \rho_\infty U_\infty^2 \sim 0.8$; mainstream to coolant temperature difference, $T_\infty - T_c \sim 20$ K to 25 K; and density ratio,

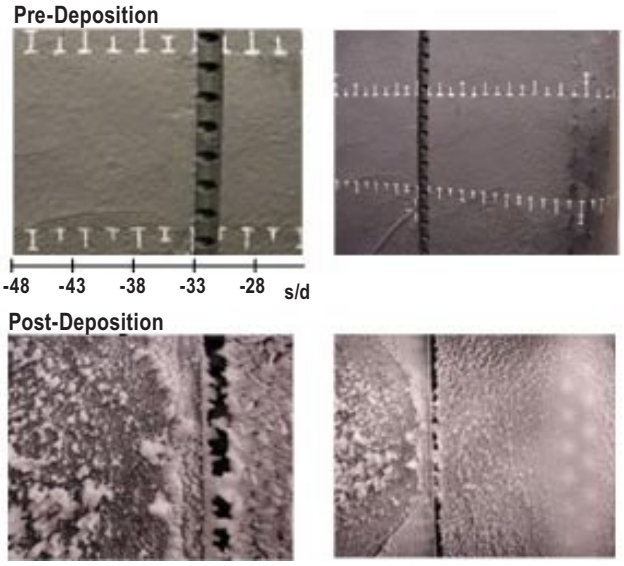

FIGURE 2. Pre and post deposition images of an ideal trench configuration

$DR = \rho_c / \rho_\infty \sim 1.08$. The temperature differential, $T_\infty - T_c$, resulted in an uncertainty of approximately 0.05 in ϕ.

The experiment with only film cooling was performed in one blade passage, shown in Figure 3 (left). The effects of conduction cooling through the endwall were apparent despite the stagnant plenum beneath. Values of ϕ upstream of the film cooling holes were non-zero (0.1 to 0.3), whereas values of adiabatic effectiveness, η, upstream of the holes were almost zero, seen in Figure 3 (right). Upstream of any film cooling on the conducting wall passage (left), the area of non-zero ϕ corresponded closely with the outline of the plenum

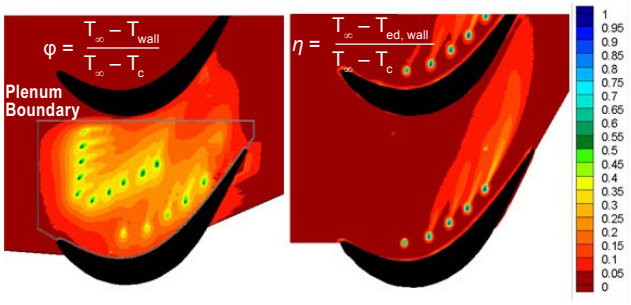

FIGURE 3. Contours of conducting endwall overall effectiveness, φ, (left) with film cooling only (30° holes), *M* = 1.0, *DR* = 1.09, and contours of endwall adiabatic effectiveness, *η*, (right) with film cooling (45° and 40° Holes), *M* = 1.2, *DR* = 1.07 from Lynch et al. (2011)

boundary as marked on Figure 3. Without film cooling, any non-zero effectiveness was a result of conduction cooling through the wall from the coolant plenum. Although ϕ was higher than *η* over most of the passage, peak ϕ was lower than peak *η*. Both of these effects arose from conduction in the endwall, which allowed the effect of the coolant to spread through the endwall instead of being limited to locations next to the coolant jets. For both of the contours presented in Figure 3, it appeared that the coolant jets were not attached to the endwall, as expected when *I* is larger than 0.4.

Overall effectiveness was measured in two passages with impingement plus film cooling and the contours presented in Figure 4. The impingement and film cooling hole locations were shown in order to observe the impact of their locations. As with film cooling only, conduction effects could be seen upstream of the holes and to a larger extent where jets impinged on the surface from underneath. Upstream of the film cooling holes the plenum boundaries surrounded the areas of non-zero ϕ. In general, ϕ with internal impingement was higher than without, except near the row of holes along the pressure side of the blade. Because the coolant had to pass through the impingement holes located in the front and middle of the passage before reaching the endwall, most of the coolant was directed through the two rows of film cooling holes located above the impingement holes. Sufficient coolant was also prevented from reaching the pressure side row of holes because the local pressures along the pressure side of the blade were higher than the local pressures at the other two rows of holes. Both proximity and local pressure of the holes contributed to less coolant going through the pressure side row. In future experiments, the pressure side row of film cooling holes will be removed for proper comparison of the cases with and without impingement cooling.

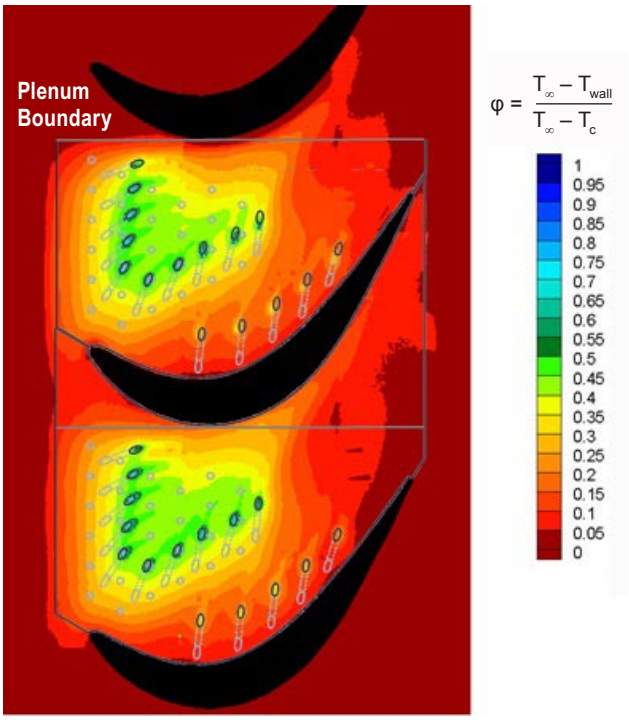

FIGURE 4. Contours of endwall overall effectiveness, φ, with impingement plus film cooling, *M* = 1.0. *DR* = 1.07; note impingement holes are 90° with no extensions indicated

Conclusions and Future Directions

Experiments at UT characterized the thermal effects of simulated TBCs on a conducting, matched Biot number, vane model with and without film cooling. As expected, the addition of the TBC to the surface of the vane significantly improved overall cooling of the vane. An unexpected consequence of using TBC was the overall cooling of the vane was much less sensitive to a decrease in film cooling performance as well as a change in cooling configuration. Another unexpected result is that the vane receives a significant amount of cooling from convection within the film cooling hole. The next phase of the project will investigate the effect of TBC thickness on overall cooling performance, the aerodynamic losses due to deposition, and the aero-thermal boundary layers on the vane surface with simulated TBC.

Overall effectiveness results displayed the effects of conduction in the endwall. Overall effectiveness was more uniform throughout the passage than adiabatic effectiveness, and peak ϕ values were lower than peak η values. The overall effectiveness results quantitatively described the non-dimensional metal temperature for the geometry and conditions tested. The effect of adding internal impingement cooling to the stagnant plenum resulted in increased ϕ. However, the increase was

strongly dependent on the impingement jet locations and was only observed in the upper left area of the passage.

Special Recognitions & Awards/Patents Issued

1. Todd Davidson received the ASME IGTI Young Engineer Travel Award to attend the 2012 IGTI Conference and present his papers: GT2012-70029 and GT2012-70033 (Listed in the FY 2012 Publications/Presentations section).

2. Amy Mensch received the Gabron Family Graduate Fellowship in Mechanical Engineering for Spring 2012.

FY 2012 Publications/Presentations

1. Davidson, F.T., "An Experimental Study of Film Cooling, Thermal Barrier Coatings and Contaminant Deposition on an Internally Cooled Turbine Airfoil Model," Ph.D. Dissertation, University of Texas at Austin, 2012.

2. Davidson, F.T., Kistenmacher, D.A., Bogard, D.G., 2012, "Film Cooling with a Thermal Barrier Coating: Round Holes, Craters, and Trenches," Paper No. GT2012-70029, ASME Turbo Expo, Copenhagen, Denmark.

3. Davidson, F.T., Kistenmacher, D.A., Bogard, D.G., 2012, "A Study of Deposition on a Turbine Vane with a Thermal Barrier Coating and Various Film Cooling Geometries," Paper No. GT2012-70033, ASME Turbo Expo, Copenhagen, Denmark.

4. Lawson, S.A., Lynch, S., and Thole, K.A., 2012, "Simulations of Multi-Phase Particle Deposition on a Non-Axisymmetric Contoured Endwall with Film Cooling," ASME Gas Turbine Expo, paper GT2012-68174, Copenhagen, Denmark.

5. Thrift, A., Thole, K.A., and Hada, S., 2012, "Impact of the Combustor-Turbine Interface Slot Orientation on the Durability of a Nozzle Guide Vane Endwall," ASME Gas Turbine Expo, paper GT2012-68096, Copenhagen, Denmark.

References

1. Davidson, F.T., "An Experimental Study of Film Cooling, Thermal Barrier Coatings and Contaminant Deposition on an Internally Cooled Turbine Airfoil Model," Ph.D. Dissertation, University of Texas at Austin, 2012.

V. UNIVERSITY TURBINE SYSTEMS RESEARCH

B. Combustion

V.B.1 Turbulent Flame Propagation Characteristics of High Hydrogen Content Fuels

Jerry Seitzman (Primary Contact), Tim Lieuwen
Georgia Institute of Technology
School of Aerospace Engineering
270 Ferst Drive
Atlanta, GA 30332
Phone: (404) 894-0013; Fax: (404) 894-2760
Email: jerry.seitzman@ae.gatech.edu

DOE Project Manager: Mark Freeman
Phone: (412) 386-6094
Email: Mark.Freeman@netl.doe.gov

Contract Number: FE0004555

Start Date: October 1, 2010
End Date: September 30, 2013

Fiscal Year (FY) 2012 Objectives

- Characterize the velocity field of the Bunsen burner at pressure conditions using laser Doppler velocimetry (LDV).
- Obtain turbulent consumption speed data for H_2/CO mixtures at elevated pressures.
- Prepare strained flame database.
- Build and install low swirl burner (LSB).
- Acquire local displacement speed data for CH_4/air mixtures using the LSB.

FY 2012 Accomplishments

In the second year of the project the following tasks have been accomplished:

- Performed cold flow velocity field characterization of the Bunsen burner for pressures and mean flow velocities of 1-20 atm and 10-50 m/s respectively using LDV.
- Obtained global turbulent consumption speed data at 5 and 10 atmospheres (atm) for mean flow velocities of 30 and 50 meters per second (m/s) and H_2/CO ratios of 30/70 to 90/10 by volume while investigating a wide range (5-30) of turbulence intensities, $u'_{rms}/S_{L,0}$.
- Assembled and commissioned the LSB facility.
- Modified existing experimental facility to allow for easy interchange between Bunsen and LSB configurations.
- Acquired preliminary local displacement speed data for CH_4/air mixtures using the LSB.

Introduction

The objective of this project is to improve the state-of-the-art understanding of turbulent flame propagation characteristics of high hydrogen content (HHC) fuels. Such HHC fuels offer advantages for reducing the carbon footprint of power generation systems. Turbulent flame propagation influences the flashback and blow-off limits of the combustor, the life of hot section components, combustor emissions, and the operating limits required to prevent harmful combustion dynamics. As such, the data, models, and knowledge achieved in this project will have important practical influences on advanced gas turbine technologies.

Research is needed that will obtain data and develop models of the turbulent burning rate of HHC fuels at *realistic* conditions and in *inhomogeneous* environments, such as in premixer nozzle boundary layers and core flows. The proposed research specifically addresses three of the combustion topic areas identified by the U.S. Department of Energy as of great importance for HHC systems, (1) turbulent burning velocities, (2) flashback, and (3) exhaust gas recirculation (EGR) impacts. Moreover, the results of this effort will enable advances in several other combustion topic areas, e.g., predicting combustion dynamics (which requires flame shape predictions) and improving large eddy simulation (LES) capabilities (by providing turbulent burning rate sub-models for HHC fuels).

Approach

This program will extend current knowledge in several critical areas, all needed to develop predictive tools for utilizing HHC fuels. We will look to extend existing data sets to a broader reactant class more representative of HHC fuels, such as mixtures diluted with CO_2, H_2O, and N_2, at realistic pressures, temperatures, and turbulence intensities. Depending upon the degree of dilution, these mixtures will simulate both gasified fuel blends, as well as systems with extensive levels of EGR. We will obtain measurements of both global consumption speed, $S_{T,GC}$, and local displacement speeds, $S_{T,LD}$, at gas turbine realistic conditions.

We will also develop physics-based models of turbulent burning rates in realistic flows. This will consist of both experimental and theoretical tasks. Experimentally, we will obtain localized turbulence/chemistry interaction measurements, using high repetition rate particle image velocimetry (PIV) and OH-planar laser induced fluorescence (OH-PLIF). These data will be used for both local characterization of instantaneous flame properties, such as flame strain rate, flow fields, and burning rates, as well as time averaged characteristics, such as local turbulent displacement speed. These data can be used as both inputs to and validation of turbulent flame models. This work will be supported by parallel level set computations that will show how to relate the strained flame characteristics of the leading points of the turbulent flame brush to its turbulent burning rate.

Results

This section details the key accomplishments made over the past year. Progress has been made with both the Bunsen burner facility, which is being used to make the $S_{T,GC}$ measurements and the LSB facility, which is being used to make the $S_{T,LD}$ measurements.

For the Bunsen burner, cold flow velocity field characterization was performed over a range of pressures using LDV. $S_{T,GC}$ data were also acquired at high pressures for a variety of flow conditions and H_2/CO fuel mixtures. These data are then correlated using the previously developed leading points scaling law [1].

For the LSB, initial flow characterization was performed and $S_{T,LD}$ data were acquired for CH_4/air mixtures.

Experimental Facility

The facility has been modified to allow for easy switching between the Bunsen burner and the LSB. This has required extensive planning and design since the LSB has the ability to vary swirl numbers on the fly, which is a unique feature of our facility.

Bunsen Burner Velocity Characterization

The performance of the turbulence generator was characterized over a range of pressures, temperatures, and mean flow velocities for burner diameters of 12 and 20 mm. It was found that the turbulence intensity monotonically increases with blockage ratio. We also noted that the 12 mm burner has lower turbulence intensities than the 20 mm burner at the same blockage ratio, because the flow velocity through the blockage plate gaps is lower for the smaller burner (note that the nozzle exit velocity is the fixed parameter, not the velocity through the plates).

Bunsen Burner Experimental Results

During this year, $S_{T,GC}$ data has been obtained at 5 atm and 10 atm to extend the previously obtained database of atmospheric measurements [1]. These measurements were obtained by varying the H_2/CO ratio and equivalence ratios simultaneously to keep the mixture $S_{L,0}$ constant at 34 cm/s. Data were obtained as a function of $u'_{rms}/S_{L,0}$. using the 12 mm diameter burner for mean flow velocities and volumetric H_2/CO ratios of 30 and 50 m/s and 30/70 to 90/10, respectively.

Table 1 below provides a summary of the experimental conditions, along with the color and symbol scheme used to plot the data.

TABLE 1. Color scheme and legend for plotting the $S_{T,GC}$ data; cell colors for ϕ indicate the symbol fill color

U_0 (m/s)	20, 30, 50			
H_2 (%)	30	50	70	90
Symbol	○	◁	▷	◇
ϕ, 1 atm	0.61	0.55	0.51	0.48
ϕ, 5 atm	0.75	0.68	0.63	0.59
ϕ, 10 atm		0.75		
$S_{L,0}$ (m/s)	0.34			

Figure 1a plots $S_{T,GC}/S_{L,0}$ as a function of $u'_{rms}/S_{L,0}$ for the constant $S_{L,0}$ data obtained at 1, 5, and 10 atm.

Several important observations can be made from Figure 1a. First, the "fuel effect" is clearly present at the elevated pressure conditions, i.e., different H_2/CO blends at constant $S_{L,0}$ and u'_{rms} have different turbulent flame speeds. Second, $S_{T,GC}$ at 5 atm and 10 atm is approximately 1.8 and 2.2 times, respectively, its value at 1 atm. Note that this is not an $S_{L,0}$ effect, as $S_{L,0}$ is kept fixed at 34 cm/s.

$S_{L,max}$ Correlation

This section presents the results of correlating the data presented above using Equation 1, which was developed utilizing leading points concepts. A more detailed discussion on the development of this equation is given in Venkateswaran, et al [1].

Equation 1.

$$\frac{S_T}{S_{L,\max}} = 1 + \frac{u'_{LP}}{S_{L,\max}}$$

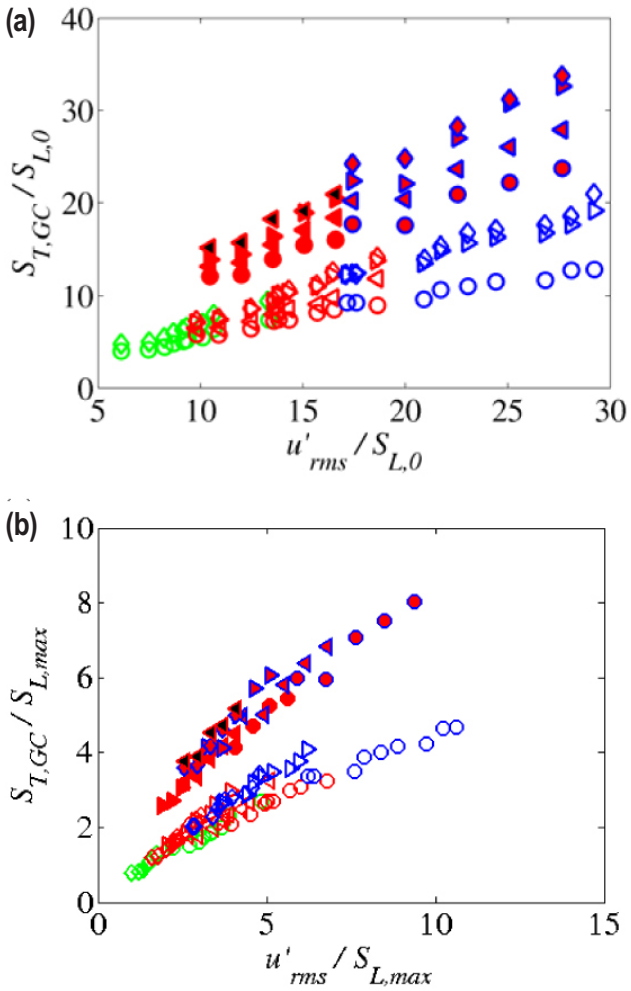

FIGURE 1. $S_{T,GC}$ as function of u'_{rms} normalized by (a) $S_{L,0}$ and (b) $S_{L,max}$ for the constant $S_{L,0}$ studies using the 12 mm diameter burner (see Table 1 for the legend)

Equation 1 is utilized by normalizing the flame speed data using $S_{L,max}$ instead of $S_{L,0}$ as in Figure 1a, where $S_{L,max}$ is the maximum stretched laminar flame speed of a mixture. Figure 1b presents the $S_{L,max}$ normalized 12 mm data, and it is seen that both the 5 atm and 1 atm data sets collapse quite well individually but that there are systematic differences between them. No similar comparison can be made for the 10 atm data set, since only one composition was examined.

Incorporation of Non-Quasi-Steady Effects

The above results show that the $S_{L,max}$ concept provides some interesting prospects for collapsing a range of H_2/CO data, but does not work well in collapsing data taken across different pressures. In starting this discussion of these data, it is important to note that $S_{L,max}$ is itself not a fundamental property of the mixture. Rather, it depends on a variety of other factors such as the type of imposed stretch, the laminar flame speed definition used, the strain rate profile through the flame and the frequency of the imposed stretch rate [2]. In this study, we focus on the frequency dependent nature of $S_{L,max}$ recognizing that the steady-state values used here are only appropriate if the internal structure of the leading point is quasi-steady. Furthermore, the calculations presented in the following discussion suggest that this is the largest effect.

In unsteady opposed-flow calculations, Im and Chen [3] show that the absolute value of the Markstein length and $S_{L,max}$ both decrease as the frequency of the imposed strain rate is increased. This dependency can be incorporated into Equation 1 by replacing $S_{L,max}$ with $S_{L,max}(\omega)$, which is the frequency dependent $S_{L,max}$. The resulting expression can then be divided by the steady-state $S_{L,max}$ to give:

Equation 2.

$$\frac{S_T}{S_{L,\max}} = \frac{S_{L,\max}(\omega)}{S_{L,\max}} + \frac{\langle u'_{rms}\rangle_{LP}}{S_{L,\max}}$$

The degree of non-quasi-steadiness can be determined using the time scale ratio, $\tau_{S_{L,max}}/\tau_{flow}$, where $\tau_{S_{L,max}}$ is a chemical time scale associated with the highly stretched flamelets and τ_{flow} is a characteristic fluid mechanic time scale, i.e., $S_{L,max}(\omega)/S_{L,max} \rightarrow 1$ *as* $\tau_{S_{L,max}}/\tau_{flow} \rightarrow 0$. The chemical time scale, $\tau_{S_{L,max}}$, is given by $\tau_{S_{L,max}} = \delta_F|_{S_{L,max}}/S_{L,max}$, where $\delta_F|_{S_{L,max}}$ is the flame thickness at $S_{L,\max}$ calculated using $\delta_F = (T_b - T_u)/(dT/dx)_{max}$.

It was found that within the H_2/CO mixtures, $\tau_{S_{L,max}}$ increases by about a factor of three as the H_2 content is increased from 30% to 90% at 1 atm. The difference between the CH_4 case and the 90/10 H_2/CO mixture is about a factor of 7.7. In addition, for a fixed H_2 content of 30%, there is a factor of four and eight reduction in $\tau_{S_{L,max}}$ for a pressure increase from 1 atm to 5 atm and 10 atm, respectively. This result shows that pressure variations and changes from H_2/CO to CH_4 leads to the largest chemical time variations.

Figure 2 plots $S_{T,GC}/S_{L,max}$ as a function of $\tau_{S_{L,max}}/\tau_{flow}$, where $\tau_{flow} = D/U_0$, for fixed turbulence intensities, $u'_{rms}/S_{L,max}$, of 3.5, 9.5, and 15.5. Each color denotes a constant $u'_{rms}/S_{L,max}$ grouping. Also shown is the power law fit to these data of the form $S_{T,GC}/S_{L,max} \sim (\tau_{S_{L,max}}/\tau_{flow})^b$.

Note the clear correlation between the turbulent flame speed and critically stretched chemical time scale ratio across the entire range of pressure and fuel composition. Slower chemistry is associated with lower values of the normalized turbulent flame speed, as would be expected, since the effective $S_{L,max}$ value of the non-quasi-steady flame is lower than its quasi-steady value.

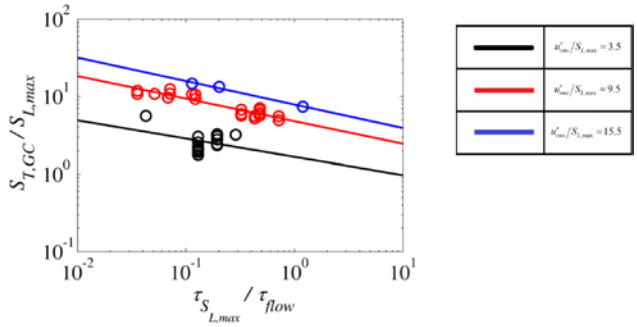

FIGURE 2. Dependence of $S_{T,GC}/S_{L,max}$ upon $\tau_{S_{L,max}}/\tau_{flow}$ at fixed turbulence intensities, $u'_{rms}/S_{L,max}$, of 3.5,9.5 and 15.5 for the 12 mm diameter

While the time scale ratios are much less than unity (indicating that the chemistry is actually quasi-steady with respect to the large scales), the corresponding ratios calculated using Kolmogorov time scales range from 20-95 for the same data. In other words, significant non-quasi-steady chemistry effects would be expected for small flow length scale-flame interactions. Work is currently underway to investigate which turbulent time scale is most pertinent to assess these non-quasi-steady state effects.

Low Swirl Burner Experimental Results

Velocity characteristics of non-reacting and reacting flow fields were obtained using PIV. The data presented in this section were acquired at standard temperature and pressure (STP) for a swirl number $S = 0.57$, bulk flow velocity $U_0 = 20$ m/s, and, for the reacting cases, an equivalence ratio of $\varphi = 0.9$ for pure CH_4.

Figure 3a and Figure 3b compare mean velocity fields obtained in non-reacting and reacting flows. These profiles show the typical features of LSB flow fields. The velocity is higher in the outer swirling region due to the fact that more of the flow (approximately 68%) passes through the swirler. In the central non-swirling portion of the flow, the velocity profile is relatively flat with almost no radial component, an important feature when determining $S_{T,LD}$. The reacting flow field also exhibits increased divergence compared to the non-reacting case. Figure 3c and Figure 3d compares the 2D turbulent kinetic energy, q', defined as $q' = \frac{1}{2}\sqrt{u'^2_{ax} + u'^2_{rad}}$.

The velocity along the centerline of the LSB decays linearly in the near-field, and the flame stabilizes where the local axial flow velocity matches the turbulent displacement speed, $S_{T,LD}$, making determination of the flame speed a relatively simple task.

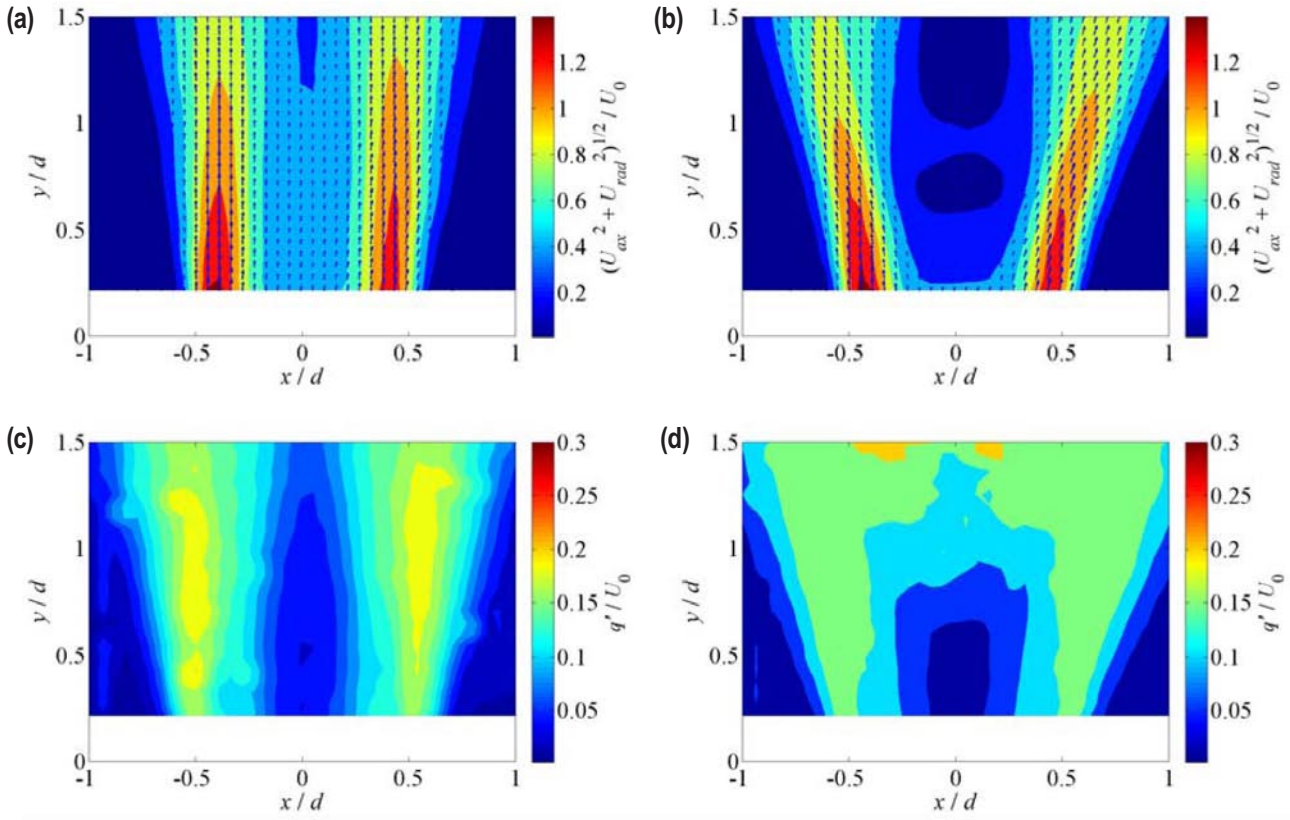

FIGURE 3. Mean velocity normalized by U_0 for (a) non-reacting and (b) reacting (100% CH_4, $\varphi = 0.9$) cases; 2D turbulent kinetic energy, q', normalized by U_0 for (c) non-reacting and (d) reacting (100% CH_4, $\varphi = 0.9$) cases; conditions at STP, $U_0 = 20$ m/s, $S = 0.57$, and $BR = 69\%$

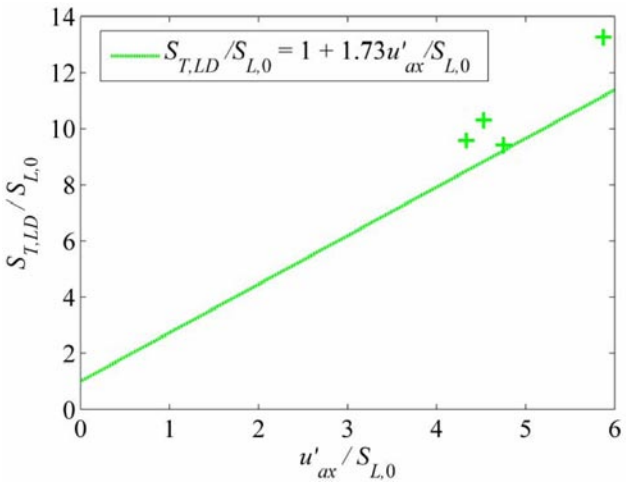

FIGURE 4. Variations of the turbulent local displacement speed, $S_{T,LD}$, with axial turbulence intensity, u'_{ax}, Normalized by $S_{L,0}$ for 100% CH_4, φ = 0.9 cases at STP; U_0 = 20 m/s, S = 0.57, and BR = 69%; the plotted line is the correlation fit found by Cheng et al. [4]

Figure 4 presents the variation of $S_{T,LD}$ with u'_{ax} normalized by $S_{L,0}$ along with a correlation line found by Cheng et al. [4]. The different data points were found by changing the blockage ratio of the turbulence generator. The results show good agreement with the correlation, with the differences being within the scatter of Cheng's data. This agreement will allow for benchmarking future acquired data against other datasets in the literature.

Conclusions and Future Directions

Velocity characterization studies were performed for the Bunsen burner over a wide range of pressures, temperatures, and mean flow velocities. Measurements of $S_{T,GC}$ were obtained for H_2/CO blends ranging from 30/70 to 90/10 by volume for mean flow velocities ranging from 20-50 m/s at 5 atm and 10 atm.

The data were then normalized with $S_{L,max}$ as per the scaling law derived in our earlier work. These data show that, at a given pressure, different fuel compositions and equivalence ratio data collapse. However, systematically different trends are observed with the 5 atm and 10 atm data. There is some evidence that these systematic differences are more fundamentally due to non-quasi-steady effects, as the pressure differences can be reasonably correlated with a computed chemical time scale for the 12 mm burner. Work is currently underway to extend the $S_{T,GC}$ measurements to include data for more mixtures at 10 atm and higher pressures. Work is also in progress to extend the correlation given by Equation 1 to other turbulent flame speed databases found in the literature.

Initial characterization of the LSB has also been performed, including non-reacting and reacting flow field characterization. Reacting data were acquired for CH_4/air mixtures, and $S_{T,LD}$ measurements were obtained as well. The next step is to obtain $S_{T,LD}$ measurements for similar H_2/CO mixtures investigated for the $S_{T,GC}$ measurements, as well to obtain detailed local and instantaneous flame/flow characteristics using high repetition rate PIV and PLIF.

FY 2012 Publications/Presentations

1. A. Marshall, P. Venkateswaran, D. Noble,; J. Seitzman, T. Lieuwen, *Experiments in Fluids,* 51 (3) (2011) 611-620.

2. P. Venkateswaran, A. Marshall, E. Bahous, J. Seitzman, T. Lieuwen, in: *2011 AFRC Combustion Symposium*, Houston, Texas, 2011.

3. P. Venkateswaran, A. Marshall, J. Seitzman, T. Lieuwen, Spring Technical Meeting of the Central States Section of the Combustion Institute, Dayton, Ohio, 2012.

4. A. Marshall, P. Venkateswaran, J. Seitzman, T. Lieuwen, ASME Conference Proceedings 2012 (To Appear) (2012).

References

1. P. Venkateswaran, A. Marshall, D.H. Shin, D. Noble, J. Seitzman, T. Lieuwen, *Combustion and Flame* 158 (8) (2011) 1602-1614.

2. A. Marshall, P. Venkateswaran, J. Seitzman, T. Lieuwen, ASME Conference Proceedings 2012 (To Appear) (2012).

3. H.G. Im, J.H. Chen, Proceedings of the Combustion Institute, 28 (2) (2000) 1833-1840.

4. R.K. Cheng, D. Littlejohn, P.A. Strakey, T. Sidwell, Proceedings of the Combustion Institute, 32 (2) (2009) 3001-3009.

V.B.2 An Experimental and Chemical Kinetics Study of the Combustion of Syngas and High Hydrogen Content Fuels

Dr. Robert J. Santoro (Primary Contact),
Dr. Frederick Dryer, Dr. Yiguang Ju
The Pennsylvania State University
240 Research Building East, Bigler Road
University Park, PA 16802-2321
Phone: (814) 863-1285; Fax: (814) 865-3389
Email: rjs2@psu.edu

DOE Project Manager Mark Freeman
Phone: (412) 386-6094
Email: Mark.Freeman@netl.doe.gov

Subcontractor:
Drs. Frederick Dryer and Yiguang Ju
Princeton University, Princeton, NJ

Contract Number: FE0000752

Start Date: October 1, 2009
End Date: September 30, 2012

Fiscal Year (FY) 2012 Objectives

- Quantify the uncertainty in measurements of the rate coefficient for the reaction $H + O_2 + CO_2 \rightarrow HO_2 + CO_2$.
- Determine the effect of added H_2O on the high pressure mass burning rate of H_2/CO flames.
- Compare the predictions of chemical kinetics model under development in this work (in-progress model) with results of other commonly used chemical kinetics models.
- Measure the autoignition of H_2/air and H_2/CO/air mixtures in the high-pressure, high temperature flow reactor in the temperature and pressure range of 800 K to 900 K and 10 atm to 15 atm, respectively.

FY 2012 Accomplishments

- The in-progress chemical kinetics model now incorporates a new model for the C1 combustion chemistry that is required to accurately predict the combustion of syngas.
- Recent measurements of the reaction rate coefficient of $H + O_2 + CO_2 \rightarrow HO_2 + CO_2$ allowed an improved understanding of the uncertainty in previous measurements of this reaction rate and led to a new suggested rate coefficient for this important reaction.
- Mass burning rate measurements in H_2/CO flames over the pressure range of 1 atm to 10 atm determined the effects of adding H_2O to the reactants. The results showed that water vapor chemically inhibits the mass burning rate of the fuels investigated, with this inhibition becoming stronger with the increase of pressure. For hydrogen flames, water vapor addition reduces the critical pressure above which a negative pressure dependence of the burning rate is observed.
- Measurements of the autoignition time of H_2/air and H_2/CO/air mixtures in the temperature range of 800 K to 900 K at pressures of 10–15 atm showed consistent results that are in much better agreement with chemical kinetic models than measurements previously obtained in earlier studies. These results show the injector design used in previous studies may be the underlying cause for earlier discrepancies between modeling results and experimental measurements.

Introduction

An integrated and collaborative effort involving Pennsylvania State University and Princeton University composed of experiments and complementary chemical kinetic modeling is investigating the effects of major species (H_2O and CO_2) and minor species (CH_4, C_2H_6, etc.) on the ignition and combustion of high hydrogen content (HHC) fuels that are characteristic of syngas. The present research effort specifically addresses broadening the experimental data base for ignition delay, mass burning rate and oxidation kinetics at high pressures, and further refinement of chemical kinetic models so as to develop compositional specifications related to the above major species and minor species. The foundation for the chemical kinetic modeling is the well validated model for hydrogen and carbon monoxide developed by Professor Frederick Dryer and his coworkers at Princeton University over the last 28 years. The goal is to further advance the understanding needed to develop practical guidelines for realistic composition limits and operating characteristics for HHC fuels. To achieve this goal a suite of experiments are ongoing which involve a high pressure laminar flow reactor, a pressure-release type high pressure combustion chamber and a high pressure, high temperature turbulent flow reactor.

The motivation for these studies lies in the recently noted difficulties observed in the ability of existing elementary kinetic models to predict experimental ignition delay, burning rate, and homogenous chemical kinetic oxidation characteristics of hydrogen and hydrogen/carbon monoxide fuels with air and with air diluted with nitrogen and/or carbon dioxide at pressures and compositions in the range of those contemplated for gas turbine applications with low NO_x emissions. This project supports U.S. Department of Energy's Hydrogen Turbine Program, which is striving to show that the U.S. can operate on coal-based hydrogen fuel, increase combined cycle efficiency by two to three percentage points over baseline, and reduce toxic emissions by 2012. The importance of the present project is to further advance the understanding and modeling capabilities needed to develop practical guidelines for realistic composition limits and operating characteristics for HHC fuels. Results from this project will further research leading to the production of hydrogen and other clean fuels from domestic resources in an effort to reduce reliance on petroleum imports and address environmental concerns, including greenhouse gas emissions.

Approach

A combined experimental and chemical kinetics modeling approach is directed at advancing understanding of combustion of HHC fuels. Three experimental facilities are involved in this effort. The first is the high pressure laminar flow reactor (HPLFR) that is used principally as a homogenous kinetic reaction system (uncoupled with wall effects) and can be operated at pressures from 10–30 atm. Simultaneously, the potential coupling of material surfaces with gas phase kinetic properties will also be addressed. The second facility is a pressure-release type high pressure combustion chamber and high speed Schlieren imaging system, which can operate at pressures from 1–30 atm. This apparatus is used to measure flame speeds and mass burning rates of HHC fuels at high pressures and low flame temperatures as well as to characterize OH and O concentrations near the post flame zone region using laser-based techniques to further constrain chemical kinetic model predictions. The final experimental facility is a high-pressure, high-temperature flow reactor that is used to measure ignition delay for HHC fuels. Similar to the other two facilities, high pressure operation capabilities allow studies between 1–30 atm. The complementary measurements obtained from these experimental facilities will provide benchmark data to be compared with the chemical kinetics models.

Results

Significant progress has been made during the past year with respect to the in-progress chemical kinetics model being developed as part of the current research program. In particular, additions to the model have focused on improvements in treating H_2/CO mixtures and inclusion of the effects of H_2O on the oxidation of H_2 and CO. The study on the effects of H_2O supplements previous work on the effects of small hydrocarbons (e.g., CH_4, C_2H_6 and C_2H_4) on syngas combustion.

Specifically with respect to hydrogen oxidation, work has been devoted to revisiting predictions of the in-progress chemical kinetic model in order to compare model predictions with the measurements of Hong et al. [1]. The predictions of the in-progress model are compared to other widely used chemical kinetics models as shown in Figure 1. The in-progress model shows very good agreement with the results of Hong et al. [1] at a temperature of 1,398 K and pressure of 1.91 atm for both H_2O and OH. Agreement with the data of Hong et al. at 1,800 K and 1.74 atm for OH is slightly less good, but is shown to be sensitive to small changes in the H atom concentration (0.7 ppm) and small changes in the temperature. Work will continue to improve agreement between the in-progress model and new data that becomes available based on studies that are a part of the present project as well as those of other researchers.

Laminar burning rates of lean mixtures of H_2, H_2/CO, and C_2H_4 were measured in a spherical bomb at 400 K. Pressures for these experiments ranged from 1–10 atm, while water dilution in the unburned gas compositions varied from 0–15% in volume. A thermal inhibitory effect has been seen previously with water dilution [2,3]; however, our recent experiments were designed to keep a constant flame temperature through dilution adjustments, thus isolating the kinetic effects of added H_2O independent of these thermal inhibition effects. Our experiments are also unique in that they access a higher pressure than previous studies in the literature with water vapor dilution, which enhances the effects of H_2O in the reaction $H + O_2 + M = HO_2 + M$. The results (Figure 2) show that water vapor chemically inhibits the mass burning rate of the three fuels investigated, with this inhibition becoming stronger with the increase of pressure. For hydrogen flames (see Figure 2a), water vapor addition reduces the critical pressure above which a negative pressure dependence of the burning rate is observed. The H_2 flames were accurately predicted by the recent Burke et al. kinetic model [4]. A model composed of the Burke et al. [4] hydrogen model with the Li et al. [5] C_1 reactions produced predictive errors for the H_2/CO flames (Figure 2b). However, these data were more accurately predicted by the in-progress model of Haas et al., which includes a C_1 chemical kinetics model [6].

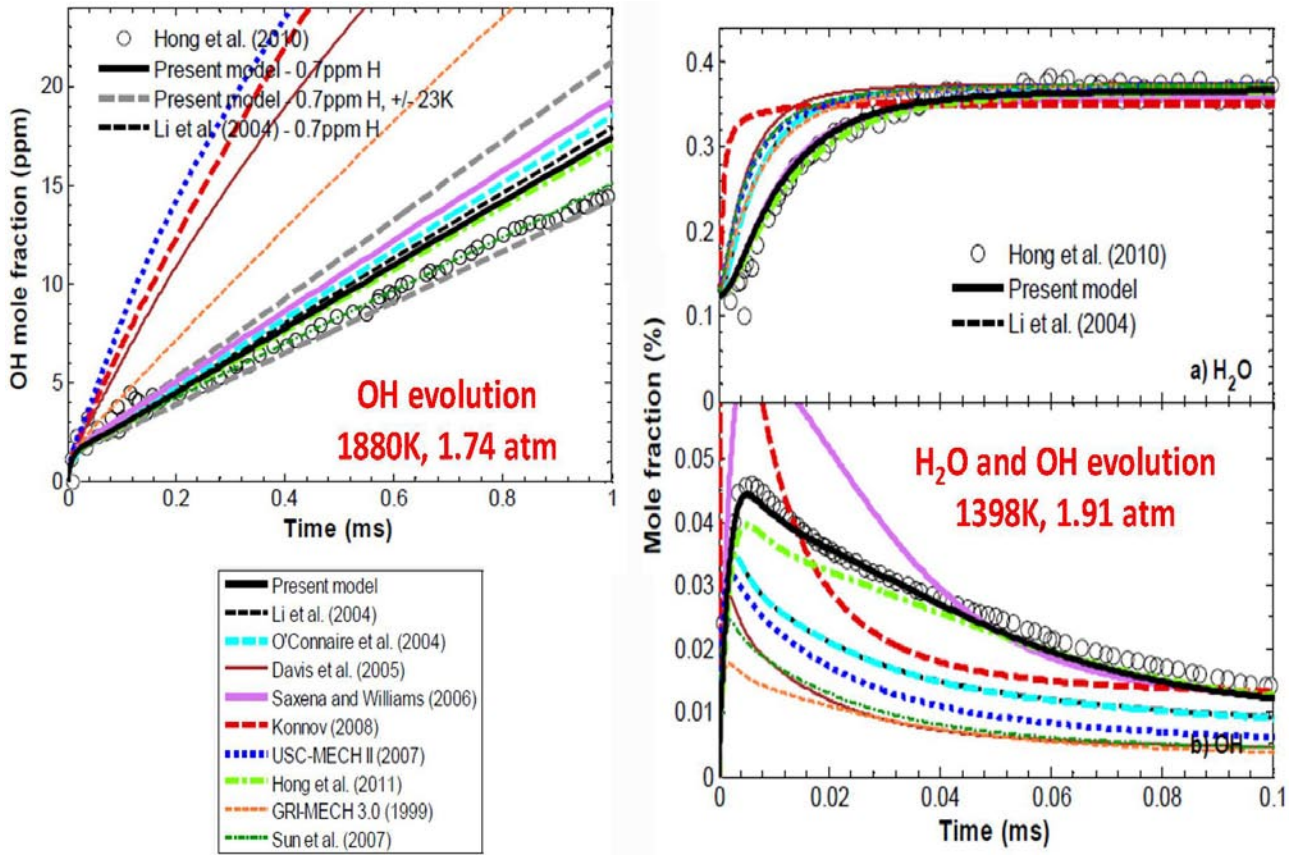

FIGURE 1. Comparisons of various H_2/O_2 models with the measurements of Hong, et al. [1] for OH and H_2O. Results for two temperature and pressure cases are shown: 1,800 K, 1.74 atm in the upper left hand corner and 1,398 K, 1.91 atm in the upper right hand corner.

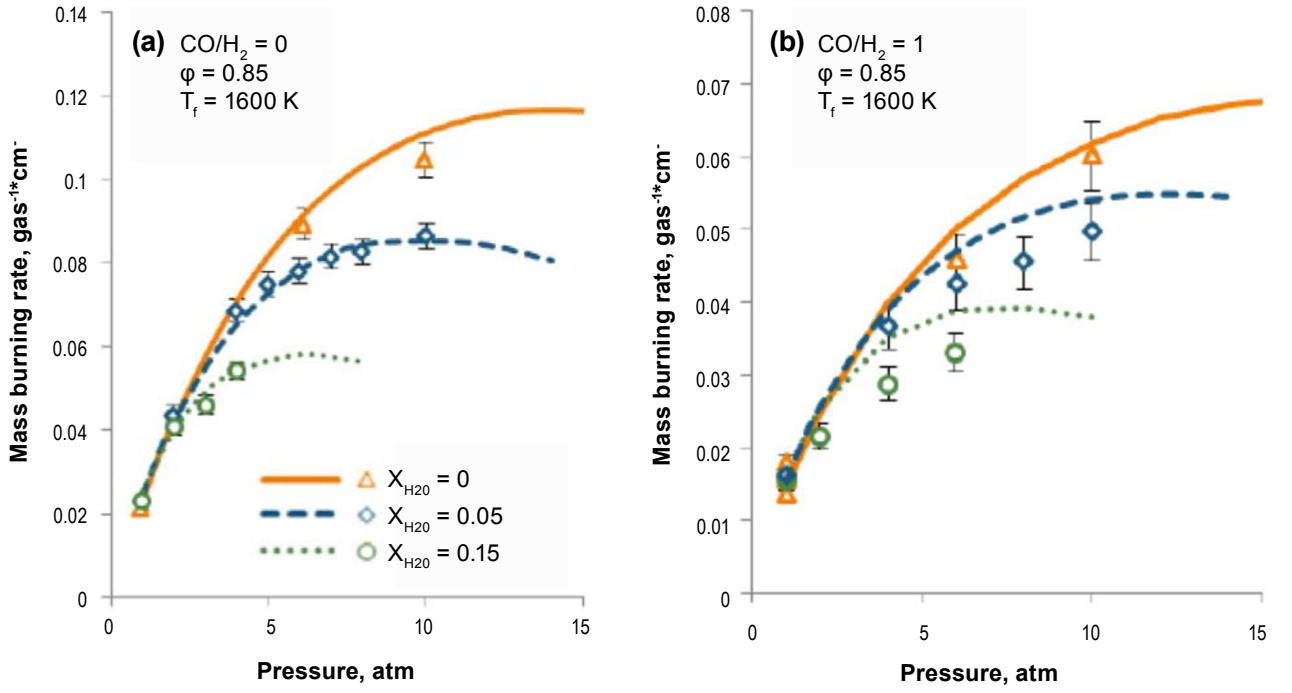

FIGURE 2. Pressure dependence of the mass burning rate. Points represent experimental results; lines represent simulations from a) Burke et al. [4] for H_2 and b) the hybrid model from Burke et al. [4] and Li et al. [5] for H_2/CO fuel blend.

The chemical effects of water addition were caused by a flame structure shift and chemical inhibition. Water addition caused the flame structure to shift into a narrower, higher temperature window, similar to the effects of increased pressure [7]. This shift was caused by the high collisional efficiency of H_2O in $H + O_2 + M = HO_2 + M$, which competes with the major branching reaction $H + O_2 = OH + O$. However, this high collisional efficiency somewhat increases reactivity in the hydrocarbon system by promoting $HCO + M = H + CO + M$ over $HCO + O_2 = HO_2 + CO$, leading to highly active H radicals. Water vapor also increases flux through the reaction $H_2O + O = 2OH$. The net effect of water addition is a general shift in the radical pool composition towards increased concentrations of OH and HO_2 and decreased H and O (Figure 3). This radical pool change causes decreased branching through various pathways, most notably HO_2, H_2, and C_2H_4 consumption pathways.

The Burke et al. H_2/O_2 kinetic model paper [4] has been recently published in the *International Journal of Chemical Kinetics*. Efforts are underway now to extend this foundational chemistry to the CO/syngas hierarchy. Recent experimental and theoretical work on reactions $CO + OH \rightarrow CO_2 + H$, $CO + OH \rightarrow HOCO$, and $CO + HO_2 \rightarrow CO_2 + OH$ since the predecessor Li et al. C1 model [5] necessitates evaluation and validation. Example validations of an interim H_2/CO model against a variety of targets are presented in Figure 4.

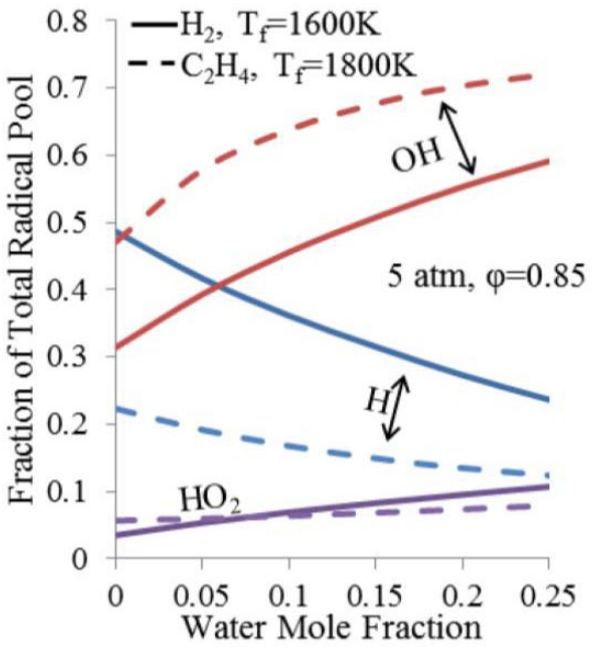

FIGURE 3. Behavior of the composition of the radical pool for H_2 [4] and C_2H_4 [8] flames at 5 atm. For simplicity, O was omitted, although its behavior is similar to that of H.

Conclusions and Future Directions

Significant progress was made over the last year in advancing the understanding of syngas combustion. Some of the important findings include:

- Detailed understanding of the chemical kinetics reaction paths important when H_2O vapor is present in syngas as can be expected under practical conditions. These results showed that H_2O inhibits mass burning, thus affecting the energy release rate in land-based gas turbine combustors used for power generation.
- Improvements in the in-progress chemical kinetics model for syngas combustion were made for specific reaction rate constants as well as initiating the addition of improved C1 chemical kinetics needed to properly treat H_2/CO mixtures.
- Measurements of the autoignition time of H_2/air and H_2/CO/air mixtures in the temperature range of 800 K to 900 K show consistent results that are in much better agreement with chemical kinetic models that previously obtain in earlier studies. These results show the injector design used in previous studies in our laboratory and by other researchers may be the underlying cause for earlier discrepancies between modeling results and experimental measurements.

Special Recognitions & Awards/Patents Issued

1. Prof. Fredrick Dryer received the Aldred C. Egerton Gold medal from the Combustion Institute in recognition of his many contributions to combustion science and technology.

2. Prof. Yiguang Ju received Bessel Research Award from Alexander von Humboldt Foundation (Germany).

FY 2012 Publications/Presentations

Publications

1. M.P. Burke, M. Chaos, Y. Ju, F.L. Dryer, S.J. Klippenstein, "Comprehensive H_2/O_2 Kinetic Model for High-Pressure Combustion," *Int. J. Chem. Kinet.* V 44, n 7, 444-474 (2012).

2. M.P. Burke, F.L. Dryer, Y. Ju, "Assessment of Kinetic Modeling for Lean $H_2/CH_4/O_2$/Diluent Flames at High Pressures," *Proceedings of the Combustion Institute* 33 905-912 (2011).

Presentations

1. J. Santner, Y. Ju, "The Effects of Water Addition on Lean Premixed Hydrogen Flames," Fourth International Forum on Multidisciplinary Education and Research for Energy Sciences, Waikiki, Hawaii, December 2011.

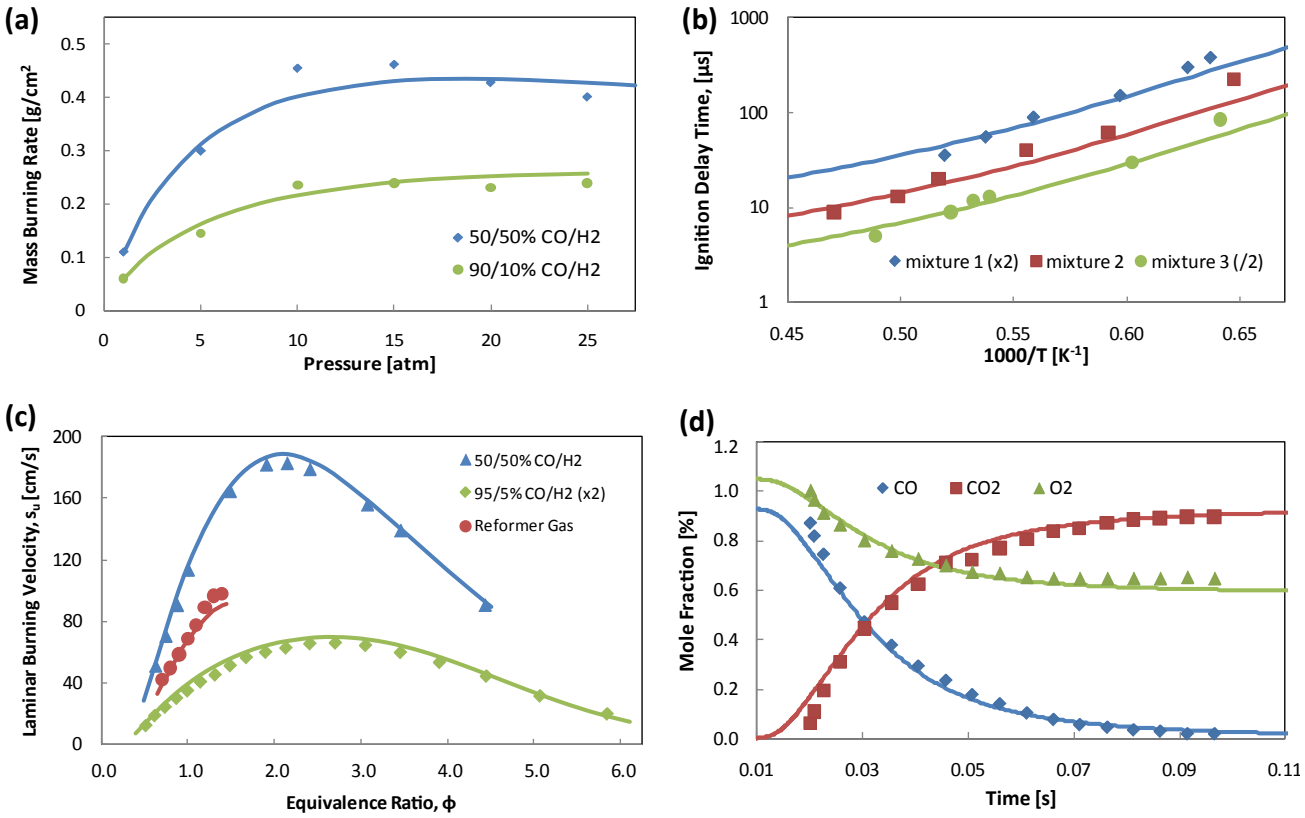

FIGURE 4. (a) Comparison of present model laminar mass burning rate predictions to Burke et al. [4] high pressure mass burning rate measurements of φ = 2.5 H_2/CO mixtures in Ar bath gas. Nominal adiabatic flame temperature is ~1,600 K and unburned gas temperature is 295 K for both cases. (b) Comparison of Bowman [9] shock tube ignition experiments to present model constant U,V ignition delay time predictions (based on ([CO] x [O])max) for φ = 0.75 CH_3OH mixtures at pressures ranging from 1.2–4.5 atm. Methanol mole fractions are 2%, 1%, and 0.75% for Mixtures 1, 2, and 3, respectively. Bath gas is Ar. (c) Comparison of present model laminar burning velocity predictions to atmospheric burning velocity measurements of H_2/CO [10] and typical reformer gas [11] pre-mixtures in air at 298 K. The reformer gas composition is 28/25/46% H_2/CO/N_2. (d) Comparison of Yetter et al. [12] atmospheric pressure flow reactor speciation experiments to present model isobaric, adiabatic species evolution predictions for a mixture of 0.93/0.58/1.05% CO/H_2O/O_2 in balance N_2 at 1,033 K. Predictions have been time shifted to the point of 50% fuel consumption.

2. R.J. Santoro, F.L. Dryer, Y. Ju, "An Experimental and Chemical Kinetics Study of the Combustion of Syngas and High Hydrogen Content Fuels," 2011 University Turbine Systems Research Workshop, The Ohio State University, Columbus, Ohio, October 25–27, 2011.

3. F.M. Haas, S. Vranckx, M. Chaos, R. Fernandes, F.L. Dryer, "An Updated Kinetic Model for Syngas Fuels and C_1 Oxygenates," Fall Technical Meeting of the Eastern States Section of the Combustion Institute, University of Connecticut, Storrs, Connecticut, October 9–12, 2011.

4. F.M. Haas, T.I. Farouk, M. Chaos, M.P. Burke, F.I. Dryer, "Rate Coefficients for H+O_2+CO_2 → HO_2+CO_2 Determined in a New High Pressure Flow Reactor," Fall Technical Meeting of the Eastern States Section of the Combustion Institute, University of Connecticut, Storrs, Connecticut, October 9–12, 2011.

5. F.M. Haas, T.I. Farouk, M. Chaos, M.P. Burke, F.L. Dryer, "Determination of the Rate Coefficient for H+O_2+CO_2 → HO_2+CO_2: Development and Validation of a New High Pressure Flow Reactor Facility and Critical Evaluation of Literature Rate Coefficient Data," 5th Combustion Energy Frontier Research Center Junior Research Associates Teleconference, October 5, 2011.

References

1. Z. Hong, R.D. Cook, D.F. Davidson, R.K. Hanson (2010), R.H. *J. Phys. Chem.* A 114, 5718–5727.

2. A.K. Das, K. Kumar, C. Sung, *Combust. Flame* (2011), 158 345-353.

3. A.N. Mazas, B. Fiorina, D.A. Lacoste, T. Schuller, *Combust. Flame*, (2011) 158 (12) 2428-2440.

4. M.P. Burke, M. Chaos, Y. Ju, F.L. Dryer, S.J. Klippenstein (2012), *Int. J. Chem. Kinet.* V 44, n 7, p 444-474.

5. J. Li, Z. Zhao, A. Kazakov, M. Chaos, F.L. Dryer, J.J. Scire (2007), *Int. J. Chem. Kinet.* 39 109-136.

6. F.M. Haas, S. Vranckx, M. Chaos, R.X. Fernandes, F.L. Dryer, "An Updated Combustion Kinetic Model for Syngas Fuels and C1 Oxygenates," The 2011 Fall Technical Meeting, Eastern States of the Combustion Institute, University of Connecticut, 2011.

7. M.P. Burke, M. Chaos, F.L. Dryer, Y. Ju (2010). *Combust. Flame,* 157:618–631.

8. H. Wang, X You, A.V. Joshi, S.G. Davis, A. Laskin, F. Egolfopoulos, C.K. Law (2007), USC Mech Version II, "High-Temperature Combustion Reaction Model of H2/CO/C1-C4 Compounds," http://ignis.usc.edu/USC_Mech_II.htm.

9. C.T. Bowman (1975), *Combust. Flame,* 25: 343-354.

10. I.C. McLean, D.B. Smith, S.C. Taylor (1994), *Symp. (Int.) on Comb.*, 25 (1): 749-757.

11. Y. Huang, C.J. Sung, J.A. Eng, (2003), *Combust. Flame,* 139(3): 239-251.

12. R.A. Yetter, F.L. Dryer, H. Rabitz, (1991), Comb. Sci. Tech., 79(1): 97-128.

V.B.3 Combustion Dynamics in Multi-Nozzle Combustors Operating on High-Hydrogen Fuels

Dom Santavicca
The Pennsylvania State University
Research Bldg. East, Bigler Road
University Park, PA 16802
Phone: (814) 863-1863; Fax: (814) 865-3389
Email: das8@psu.edu

DOE Project Manager: Mark Freeman
Phone: (412) 386-6094
Email: Mark.Freeman@netl.doe.gov

Subcontractor:
Tim Lieuwen
Georgia Institute of Technology, Atlanta, GA

Contract Number: NT0005054

Start Date: October 1, 2008
End Date: September 30, 2013

Fiscal Year (FY) 2012 Objectives

- Implement phase-synchronized three dimensional (3D) chemiluminescence imaging with high speed intensified camera.
- Develop improved software for processing and display of 3D chemiluminescence data.
- Use the extensive database of velocity-forced flame transfer function results that have been obtained during the first three years of this project to identify specific operating conditions for further study using phase-synchronize 3D chemiluminescence imaging.
- Extend current models of flame response to axisymmetric disturbances to include flame excitation by helical disturbances which are excited during transverse instabilities.
- Develop models of stagnation point stabilized flames to velocity forcing.

FY 2012 Accomplishments

- The high speed intensified camera has been installed on the multi-angle imaging system.
- Phase-synchronized 3D chemiluminescence images have been acquired on the multi-nozzle can combustor using the high speed intensified camera.
- Characterization and relative contribution analysis done for flame wrinkle destruction processes in harmonically forced laminar and turbulent premixed flames.
- High speed particle image velocimetry (PIV) characterization if dominant flow field features of transversely excited flames showed strong presence of helical modes.
- Developed model to predict response of flames to helical flow disturbances.

Introduction

Combustion dynamics [1,2] are a major technical challenge in the development of efficient, low emission gas turbines. Current understanding of the underlying phenomenology of combustion dynamics in lean premixed combustors is almost entirely limited to longitudinal mode instabilities in single-nozzle combustors operating on natural gas. In contrast, current combustors employ multi-nozzle can or annular combustor configurations which exhibit both transverse and longitudinal instabilities and are expected to meet operability requirements using a range of gaseous fuels, such a syngas produced by the gasification of coal and biomass.

The goal of this research is to use a synergistic research approach to understand the underlying physics of the coupling mechanisms between catastrophic acoustic resonances and the flame dynamics that fuel them. The use of a multiple-nozzle experimental facility recreates the flow conditions in an actual gas turbine and allows for specific attention to be paid to the complicated interactions between flames that can aggravate the combustion dynamics problem.

Approach

A physics-based, flexible, and synergistic approach is the key to successfully studying the response of a multi-nozzle combustor to longitudinal and transverse acoustic excitation. Two test rigs have been designed and constructed for use on this project, a multi-nozzle can combustor test rig with longitudinal air-forcing and a multi-nozzle annular combustor test rig with transverse air-forcing. In order to identify and characterize the underlying phenomenology of the flame's response to longitudinal and transverse acoustic oscillations, a number of measurement techniques are employed. This

includes chemiluminescence imaging of the spatial distribution of the flame's heat release rate and PIV measurements of the two dimensional (2D) velocity field [4]. These measurements are phase-synchronized with the acoustic forcing, thereby revealing the periodic phase-averaged flame response and its relationship to the phase-averaged acoustically-forced velocity field. In the later stages of the project, time-resolved PIV measurements will be made in the multi-nozzle annular combustor test rig, which will allow for more detailed inspection of vortex formation, flame movement, and adjacent flame interaction. And lastly, acetone planar laser induced fluorescence and a recently developed 3D chemiluminescence imaging technique will be used to characterize the fluctuations in the flame area and the relationship to the chemiluminescence heat release measurements, as well as the flame-to-flame interactions in the multi-nozzle combustor and their effect on the overall flame response.

Results

Transverse Forcing

The emphasis of this year's work has been to explore the role of asymmetry of both the flow field and the acoustic forcing on the response of flames. This issue of asymmetry is of paramount importance in multi-flame configuration as none of the flames are subject to symmetric boundary conditions, and in transversely forced systems, the acoustic forcing can be asymmetric as well. There were two parts to this study. First, the natural asymmetries in the instability characteristics of the swirl flow were investigated. In particular, this work investigates the response of the vortex breakdown region of a swirling, annular jet. The time-average flow field is shown to exhibit both monotonically varying and abrupt bifurcation features as acoustic forcing amplitude is increased. The unsteady motion in the recirculation zone is dominated by the low frequency precession of the vortex breakdown bubble. In the unforced flow, the azimuthal m = -2 and m = -1 modes, i.e., disturbances rotating in the same direction as the swirl flow, dominate the velocity disturbance field. These modes correspond to large scale deformation of the jet column and two small-scale precessing vortical structures in the recirculation zone, respectively. To visualize this, filtered velocity data in the r-θ plane are shown in Figure 1 as a series of images at progressive instances in time. Here, the velocity data have been low-pass filtered at 200 Hz using a second-order Butterworth filter. This low-order filter captures the pertinent motion in the low frequency range while blocking any motion due to the system resonance near 400 Hz. Filters with cutoff frequencies between 160 Hz and 240 Hz were tested with little change to the results. To highlight the coherent motions in this flow,

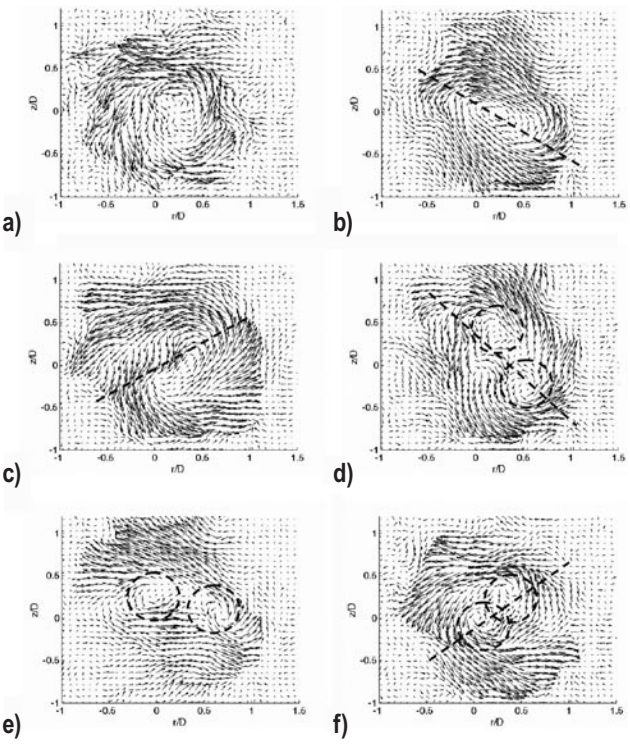

FIGURE 1. Precessing vortex core shown through the filtered velocity field in the r - θ plane at x/D = 1 and a) t = 0.5 ms, b) 4.1 ms, c) 10.1 ms, d) 13.1 ms, e) 17.1 ms, f) 20.1 ms, for a non-reacting, unforced flow at u_o =10 m/s, S = 0.85

dotted lines have been drawn to indicate the major axis of the jet column, and circles have been drawn about the instantaneous flow centers, or locations of zero rotational velocity.

The second portion of this study investigated the response of the flow to both symmetric and asymmetric forcing conditions. The presence of transverse forcing adds an additional degree of freedom to the forced problem because of the non-axisymmetric nature of the forcing. Unforced swirling flows are not generally instantaneously symmetric, e.g., swirl biases the strength of co- and counter-signed helical instabilities. Moreover, non-axisymmetric forcing can preferentially excite certain non-axisymmetric modes in a different manner than they would otherwise naturally manifest themselves. The symmetric versus asymmetric flow response was measured in two ways. First, in the r-x plane where axial and radial components of velocity are measured using high-speed PIV, a helical and ring vortex rollup of the shear layers is evident in the asymmetric and symmetric forcing condition, respectively. Additionally, the swirling motion of the jet is measured in the r-θ plane at two downstream locations and a spatial decomposition is used to calculate the strength of azimuthal modes in radial velocity fluctuations. At the forcing frequency, the

$m = 0$ mode is strongly excited at the nozzle exit with symmetric forcing, while asymmetric forcing results in a strong peak in the $m = 1$ mode, or the first helical mode. The results in this plane of view are congruent with those in the *r*-*x* plane. Further downstream, however, the mode strengths change as the vorticity is realigned and natural asymmetries of the swirling jet set in. This feature can be seen in Figure 2.

Flame Response to Transverse and Helical Modes

This research work describes an analytical approach to modeling the response of premixed swirling flames in non-axisymmetric disturbance fields. Some typical non-axisymmetric disturbance fields include those due to one-dimensional transverse excitation and the presence of non-axisymmetric helical modes in a general helical disturbance field.

In order to model these analytically, the thin flamelet assumption is used so that a level-set based front tracking approach can be used to model the local flame dynamics. A general solution to the 3D flame position (measured vertically along the axial flow direction) in a general 3D disturbance field was derived. When simplified to a general axisymmetric mean flow and mean flame case, the following conclusions were drawn:

- The global flame transfer function is zero for a premixed swirling flame in a bulk transverse excitation field (compact field). This can be intuitively seen from the fact that while one side of the flame is perturbed by its local disturbance, the diametrically opposite side is perturbed in the exact opposite away, hence leading to a cancellation. But, as the flame becomes non-compact, the global flame transfer function becomes non-zero and finite.
- The local flame dynamics are a function of the swirl parameter, but the global flame transfer function is independent of swirl.
- The low frequency limit of the global flame transfer function for longitudinally forced flames is unity due to a finite change in area uniformly across the flame surface azimuth. However, the low frequency limit for the transverse excitation case is zero, due to the cancellation effects mentioned earlier (flame is compact in this limit).

An example flow field was assumed to show the features of the 3D flame surface for different swirl parameters in the presence of a bulk transverse excitation field. For this, a solid body swirl flow with a uniform axial velocity was assumed. The swirl parameter here was the ratio of the acoustic time scale to the swirling time scale (or the ratio of swirling rate, Ω to the angular acoustic frequency, ω), denoted as $\sigma = \Omega/\omega$. Some inferences drawn from this example result were:

- For $\sigma < 1$, the flame surface shows the resulting interference between the flame wrinkling due to the local disturbance field interacting with that due to the transport of wrinkles along the mean flame surface, which occurs both due to the axial flow and the swirl flow. The effective wrinkling wavelength increases with σ.
- For $\sigma = 1$, a limiting case occurs where the interference leads to a global flame surface that rotates in the solid-body rotation field like a cone

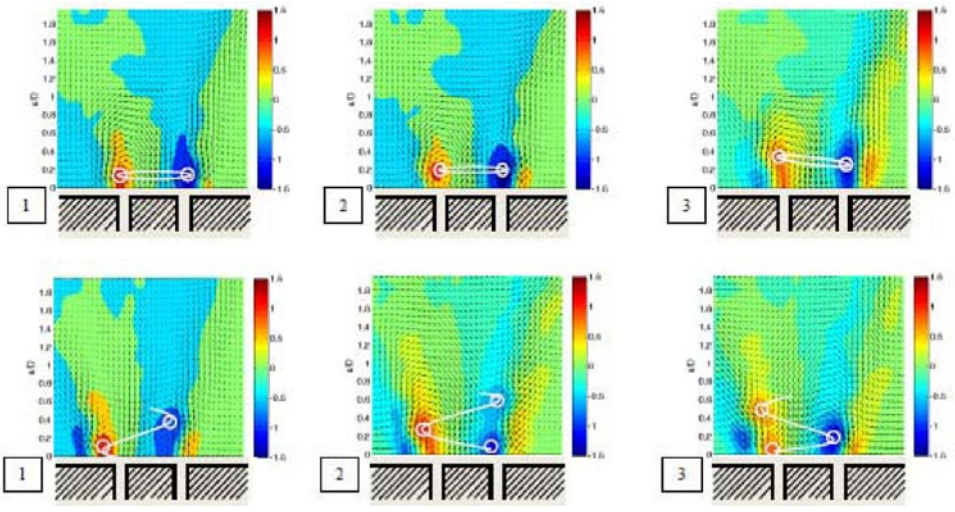

FIGURE 2. Phase-averaged velocity field with in-phase (top) and out-of-phase (bottom) forcing at 400 Hz, non-reacting flow at u_o = 10 m/s, S = 0.85. White lines trace the shear layer vortex created by the different forcing symmetries.

with an axis not aligned with the axial coordinate. This is an effective wrinkling wavelength of infinity.

- For $\sigma > 1$, the wrinkling wavelength becomes finite again and decreases with increasing σ. However, while the phase roll-off in the case of $\sigma < 1$ was negative, indicating wrinkles that move downstream, the case of $\sigma > 1$, shows an apparent upstream motion of wrinkles along the flame surface. This is similar to an aliasing effect, seen for example when the rate of a vehicle's tire rims (as seen in films) has an apparent backward motion, despite the vehicle's forward motion. Note that this apparent backward motion refers to the trace velocity of the wrinkles and not their actual wave velocity. The wrinkles move downstream in this case as given by the tangential velocity along the flame surface.

With the general solution derived and applied to the example case of transverse excitation, this general solution was also reformed for application to flame response in the presence of helical disturbances. The disturbance flow field can be decomposed into its helical modes, m where $m < 0$ for co-swirling modes and $m > 0$ for counter-swirling modes. Note that this notation is for the case where the azimuthal coordinate is counter-clockwise and swirl is along this coordinate. The flame response solution was derived for a general non-axisymmetric flame in a helical disturbance field. This was then simplified for a general axisymmetric case. Some general inferences obtained in this case were:

- The local flame dynamics are dependent on the mode number. The mode number controls both amplitude and phase characteristics.
- The helical mode m in the disturbance flow field leads to a helical mode in the flame response as well. This is not true in the general non-axisymmetric case where the helical modes of the mean flow also pay a role and so helical mode m in the disturbance flow field leads to a helical mode $j \neq m$ in the flame response.
- The global flame response is controlled only by the axisymmetric mode in the flame position solution. Hence, for axisymmetric flames, only the $m = 0$ modes in the disturbance field contribute to the global flame response. For non-axisymmetric flames, since $m \neq 0$ modes in the disturbance flow field can contribute to $j = 0$ modes in the flame position, they ultimately play a role in the global flame transfer function.
- The dominant local flame response mode (m_0) is controlled by a parameter χ_L, which is an interplay of four different time-scales: the axial flow time scale, the swirling flow time scale, the convective time scale of forcing and the acoustic time scale. These result in three different Strouhal numbers (St_c, St_2, $St_{\Omega,2}$). Depending on their values, the dominant mode can be a non-axisymmetric mode. However, despite its dominance for the local flame response characteristics, it still does not contribute to the global flame response and only the $m = 0$ contributes as stated earlier.
- An example calculation was performed using the same mean flow field as earlier, but in the presence of a longitudinal helical disturbance. In this case, these parameters are related as: $m_0 = (St_c - St_2)/St_{\Omega,2}$ and $\chi_L = St_{\Omega,2}(m_0 - m)$. Note that mode that gives χ_L closest to zero, is the dominant mode. Some sample results for the amplitude variations of different modes and the flame surface for different modes are shown in Figure 3, which is a case where $m_0 = 1$ is the dominant mode.

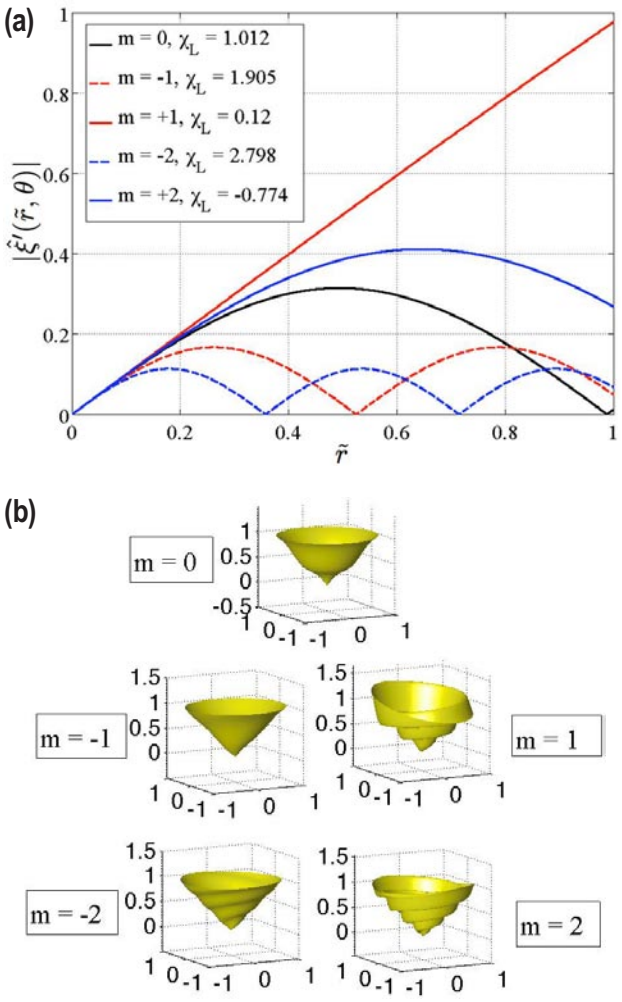

FIGURE 3. (a) Amplitude variations for different modes, and (b) instantaneous flame surface plots showing the wrinkling due to different helical for $s_L = 0.4$, $k_c = 0.5$, $S_t = 1.25$, $\sigma = 0.6$. Surface wrinkling has been exaggerated to highlight features.

This work shall continue to incorporate the helical mode amplitude variations in space for the disturbance flow-field as well the analysis for non-axisymmetric mean flame shapes.

Dynamics of Flame Wrinkles

This research describes numerical and theoretical analyses of the nonlinear dynamics of harmonically forced, turbulent and stretch-sensitive premixed flames. A key objective of this work was to identify the dominant processes involved with flame wrinkle destruction and to analyze their relative contributions.

For stretch-sensitive premixed flames, these wrinkle smoothing processes were kinematic restoration and flame stretch. Kinematic restoration is an intrinsically nonlinear process with a two spatial-zone structure, whose amplitude dependence is fundamentally different near and far from the wrinkle excitation source. Flame stretch processes appear even in the small perturbation limit and smooth out flame wrinkles in thermodiffusively stable mixtures. Which process dominates is a function of the perturbation amplitude, frequency, stretch sensitivity of the mixture, and spatial location. Based on the analysis, the study identified a regime diagram identifying the dominant mechanism based on the operating conditions. This research presents computed results illustrating the solution characteristics, as well as key dimensionless parameters controlling the solution based upon a third order perturbation analysis.

For turbulent flames, the processes which control the rate of wrinkle smoothing/destruction are deterministic and turbulent effects. The study shows that this smoothing action occurs through both kinematic restoration and random phase jitter effects. Numerical simulations were conducted in 3D domain with isotropic turbulence, whose typical simulated flame fronts are shown in Figure 4. Also, a third order perturbation analysis was performed to find key dimensionless parameters describing their relative contributions. It was shown that the dominant contributors vary with perturbation amplitude, turbulence intensity, and spatial location.

Complete Development of 3D Imaging System and Related Image Processing

This task is comprised of the following subtasks: (1) implement high speed intensified camera for phase-synchronized 3D chemiluminecence imaging, (2) develop new software for processing and displaying 3D chemiluminescence data, and (3) identify specific operating conditions for further study using phase-synchronized 3D chemiluminescence imaging. The status of this task follows.

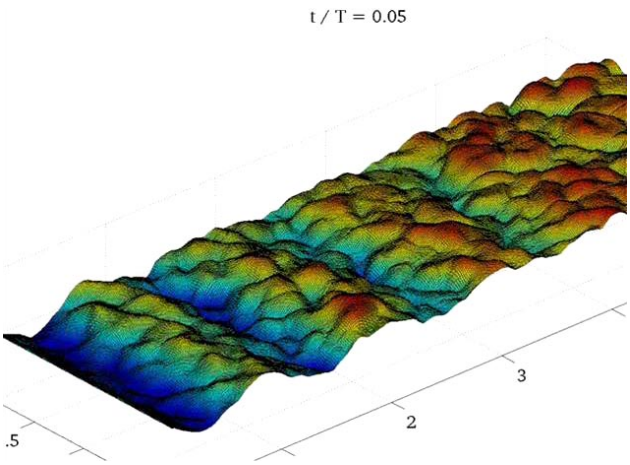

FIGURE 4. Simulated flame front forced by an oscillating flame holder in an isotropic turbulent flow

The chemiluminescence flame imaging technique that had been used previously for characterizing flame structure in a single-nozzle combustor is limited to axisymmetric flame geometries, whereas the flame in the multi-nozzle can combustor is inherently 3D. In order to characterize the 3D flame structure, a multi-angle chemiluminescence imaging technique has been setup. An intensified camera is mounted on a dolly which moves along a 90° section of a 138" diameter circular track. The track is secured to an optical table to ensure that the camera moves along a rigid and fixed plane which is positioned perpendicular to the centerline of the combustor.

In the steady flame case, chemiluminescence images are acquired at each of N equally spaced viewing angles around the 90° section of track. Each image is the average of M images acquired with a camera exposure time of 100 ms. The result is a set of N line-of-sight or projection images, each at a different viewing angle (α). Representative projection images are shown in Figure 5 for the two viewing angles. The chemiluminescence images are presented in pseudo-color where the intensity varies from minimum to maximum as the color varies black to white as illustrated in the color bar shown in Figure 5.

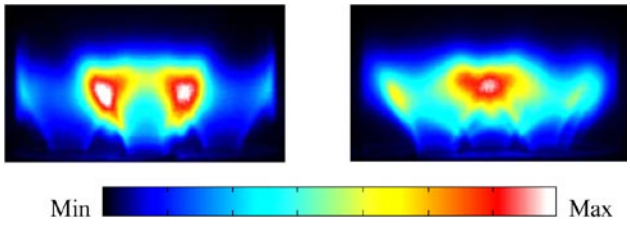

FIGURE 5. Projection images from two different viewing angles

In the forced flame case, the chemiluminescence images acquired at each of N equally spaced viewing angles are phase-synchronized with the velocity fluctuation in phase-angle increments of $\Delta\theta$. Therefore, $360°/\Delta\theta$ phase-synchronized measurements are acquired at each viewing angle, where each phase-synchronized image is the average of M projection images taken at a specific phase-angle (θ) and viewing angle (α).

Each projection image is divided into single-pixel-wide horizontal rows. Horizontal rows corresponding to a fixed axial position (z) in each of the N multi-angle projection images are combined into an N by 500 array, where 500 is the number of pixels along each of the horizontal rows. Assuming that the multi-nozzle flames display 90° symmetry, this array is repeated three more times to get a full 360° range of projection images resulting in a 4N by 500 array.

A filtered back projection algorithm is used to perform the Inverse Radon Transform on the multi-angle projection image slices corresponding to a specific axial position (z). This yields a 2D slice of the 3D image. This is repeated using the horizontal rows of pixels at each axial position (z), and the resulting slices are combined to produce the 3D image. In order to visualize the 3D structure, a transparency map is combined with the colormap such that the opacity is proportional to the chemiluminescence intensity, i.e., high intensity regions are more opaque while low intensity regions are more transparent.

The stable flame tests were performed with natural gas fuel at a combustor pressure of 1 atm, inlet temperature of 200°C, equivalence ratio of 0.6 and inlet velocity of 20 m/s. Projection images were captured at 2° increments around the 90° section of track encircling the combustor, resulting in a total of 46 images. Each projection image was an average of 10 images, each with an exposure time of 100 ms.

Detailed information on the 3D structure of the multi-nozzle flame can be obtained by viewing two-dimensional slices of the 3D image. This is illustrated in Figures 6 and 7, which show a series of vertical and horizontal slices, respectively, of the reconstructed 3D image. The results shown in these figures clearly illustrate the complex 3D structure of this multi-nozzle flame, for example, the flame interaction regions and the effect of swirl on this interaction.

In order to assess the accuracy of the 3D reconstruction, projection images were created from the 3D images and compared to measured projection images. Figure 8 compares the projection images obtained by viewing into the combustor from downstream. Qualitatively, the reconstructed projection images (Figure 8a) include all of dominant features shown in the measured projection image (Figure 8b), giving confidence

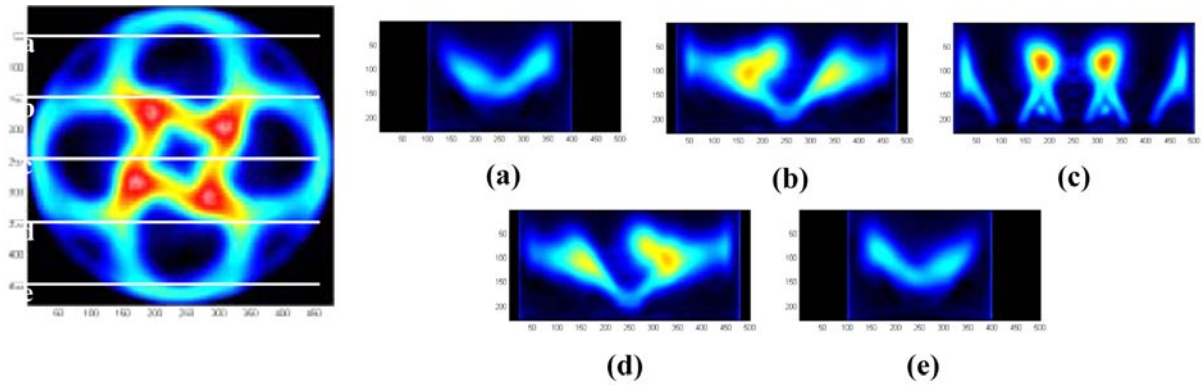

FIGURE 6. Vertical slices at the indicated locations: a, b, c, d and e

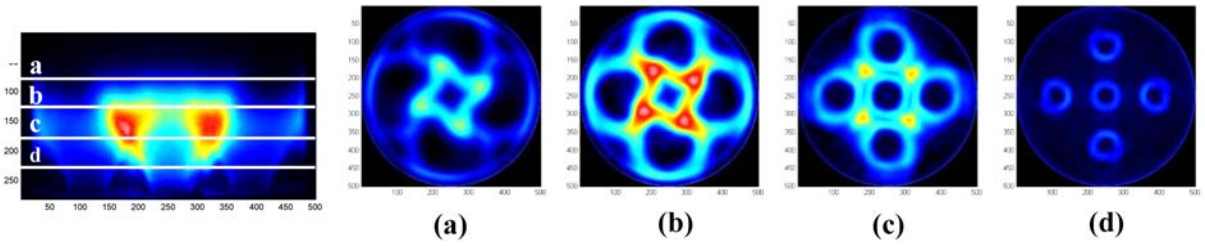

FIGURE 7. Horizontal slices at the indicated locations: a, b, c and d

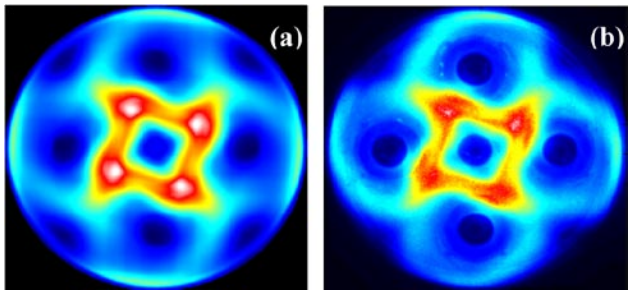

FIGURE 8. Comparison of reconstructed (a) and measured (b) downstream projection images

to the 3D reconstruction results. The difference between the reconstructed and measured projection images can be quantified in terms of a 2D correlation coefficient. A value of $r = 1$ indicates perfect correlation between two images. The 2D correlation coefficient for the downstream comparison was 0.9735.

Velocity forced flame tests were performed at the same operating conditions as the stable flame tests [3]. The flames were forced using a siren device to modulate the flow of premixed fuel and air. The forcing frequency was 100 Hz and the forcing amplitude (u'/u_{mean}) was 5%. Projection images were acquired at 15° increments around the combustor. Twelve images at phase increments of 30° of the forcing cycle were acquired at each location. Two dimensional slices of the forced flames can be generated. The forced flame slices are displayed as a set of images at various phase angles of the cycle or as an animation.

Conclusions and Future Directions

A study of the role of asymmetry of both the flow field and the acoustic forcing on the response of flames has shown that asymmetry is important in multi-flame configurations as none of the flames are subject to symmetric boundary conditions. The presence of transverse forcing adds an additional degree of freedom to the forced problem because of the non-axisymmetric nature of the forcing.

An approach to modeling the response of premixed swirling flames in non-axisymmetric disturbance fields has been developed. This approach is based on a thin flamelet assumption so that a level-set based front tracking approach can be used to model the local flame dynamics. A general solution to the 3D flame position (measured vertically along the axial flow direction) in a general 3D disturbance field was derived and applied to the analysis of a general axisymmetric mean flow and mean flame case, yielding new insights regarding these effects. This work shall continue to incorporate the helical mode amplitude variations in space for the disturbance flow-field as well the analysis for non-axisymmetric mean flame shapes.

Numerical and theoretical analyses were performed of the nonlinear dynamics of harmonically forced, turbulent and stretch-sensitive premixed flames. This study has been used to identify the dominant processes involved with flame wrinkle destruction and their relative contributions. It was shown that the dominant contributors vary with perturbation amplitude, turbulence intensity, and spatial location.

As mentioned above, multi-nozzle flames are inherently asymmetric; therefore measurement techniques are required for characterizing the 3D structure of such flames. A multi-angle chemiluminescence imaging technique capable of such measurements has been developed and successfully demonstrated on the multi-nozzle can combustor. The first measurements were taken with an intensified charge-coupled device camera, however, the recent addition of a high speed intensified camera system has significantly reduced the time required to take the phase-synchronized multi-angle measurements used in the reconstruction of the time varying 3D flame structure. In addition to the successful development of the 3D flame imaging capability, a number of data processing programs have been written and demonstrated for characterizing specific aspects of the flame structure relevant to the current study of flame response in multi-nozzle combustors.

References

1. J. O'Connor, C. Vanatta, J. Mannino, and T. Lieuwen, "Mechanisms for Flame Response in a Transversely Forced Flame," in 7th US National Technical Meeting of the Combustion Institute. 2011: Atlanta, Georgia.

2. J. O'Connor. and T. Lieuwen, "Disturbance Field Characteristics of a Transversely Excited Burner. Combustion Science and Technology," 2011. 183(5): p. 427-443.

3. M. Szedlmayer, B. Quay, J. Samarasinghe, A. De Rosa, J.G. Lee and D. Santavicca, "Forced Flame Response of a Lean Premixed Multi-Nozzle Can Combustor," in Proceedings of ASME Turbo Expo 2011, Vancouver, British Columbia, Canada, 2011.

4. J. O'Connor, and T. Lieuwen, "Further Characterization of the Disturbance Field in a Transversely Excited Swirl-Stabilized Flame," *Journal of Engineering for Gas Turbines and Power*, 2012. 134(1).

V.B.4 Structure and Dynamics of Fuel Jets Injected into a High-Temperature Subsonic Crossflow: High-Data-Rate Laser Diagnostic Investigation under Steady and Oscillatory Conditions

Robert P. Lucht (Primary Contact) and
William E. Anderson
School of Mechanical Engineering, Purdue University
585 Purdue Mall
West Lafayette, IN 47907-2088
Phone: (765) 494-5623
Email: Lucht@purdue.edu

DOE Project Manager: Robin Ames
Phone: (304)285-0978
Email: Robin.Ames@netl.doe.gov

Contract Number: FE0007099

Start Date: October 1, 2011
End Date: September 30, 2014

Fiscal Year (FY) 2012 Objectives

- Development and modification of project management plan (PMP) in collaboration with National Energy and Technology Laboratory (NETL) project manager.
- Modification of the test rig for the reacting jet in crossflow (RJIC) studies. Design and fabrication of test rig components for the RJIC study. The test rig that has been used for previous secondary jet injection studies will be modified for the University Turbine Systems Research (UTSR) reacting jet in crossflow studies.
- Development of test matrix for FY 2012 experiments. A matrix of test operating conditions including but not limited to pressure, composition of the jet fluid, vitiated versus non-vitiated crossflow, temperature of the crossflow, jet-to-crossflow momentum ratio J, and jet-to-crossflow velocity ratio R will be developed.
- Development of particle imaging velocimetry (PIV) particle seeder for the high-pressure test rig.
- Successful implementation of high-data-rate OH planar laser-induced fluorescence (PLIF) imaging in the high-pressure combustion test rig.

FY 2012 Accomplishments

- The PMP was delivered electronically to the NETL federal project manager, Robin Ames.
- The necessary components for the modification of the test rig for the U.S. Department of Energy RJIC studies were designed and fabricated. The major difference between the old and new test rig configurations is that the window dimensions are considerably larger: 98 mm wide x 73 mm high in the new test rig as compared to 63.5 mm wide x 38.1 mm high in the old test rig.
- Performed a series of tests in the new test rig to compare performance and results from the new test rig with the old test rig. These measurements were performed using transverse jet injection nozzles designed in collaboration with Siemens Power Systems.
- A particle seeder for high-speed, high-pressure PIV was designed and fabricated.

Introduction

This project is a detailed investigation of the structure and dynamics of fuel jets injected into a subsonic oxidizing crossflow in order to enhance the fundamental level of understanding of these important flows and to provide a validation database for comparison with detailed numerical models of the reacting jets in crossflow.

Accurate high-resolution spatial and temporal measurements of the resulting turbulent flame structures will provide improved understanding of the complex processes of fuel/air mixing and turbulence-chemistry interaction with attendant impact on operability when using high hydrogen content (HHC) fuels. Additionally, the representative crossflow will be forced into stationary and oscillatory conditions to simulate an unstable condition. The enhanced mixing and combustion of the fuel jet will be measured to quantify the relationship between the unsteady combustion field and the forced oscillatory field. The benchmark quality data sets resulting from these experiments will include comprehensive measurements of mean and fluctuating components of velocity, temperature, and species at high

pressure and with crossflow conditions representative of modern gas turbine engines with practical applications within the turbine industry.

Approach

The primary goal of the project is to investigate the structure and dynamics of the reacting flow field for jets injected into a subsonic crossflow. The jet in crossflow study has practical applications while also serving as an important test case for the development of numerical methods for turbulent reacting flow fields typical of gas turbine combustors. Secondary injection of the fuel, also referred to as distributed combustion, is being studied as a means for reducing NO_x emissions while increasing the power output of the gas turbine systems. By utilizing high-speed diagnostics techniques, the enhanced mixing and combustion of the fuel jet will be measured in order to determine the quantitative relationship between the unsteady combustion field and the forced oscillatory field. Advanced laser diagnostics, including high-speed PIV, high-speed PLIF, and coherent anti-Stokes Raman scattering (CARS) will be used to probe the flow fields in a high-pressure gas turbine combustion facility. PIV and planar laser induced fluorescence of OH radicals (OH PLIF) will be used to visualize fuel/air mixing and combustion at data rates of 5-10 kilohertz (kHz). One kHz CARS will be employed for temperature measurements using femtosecond lasers. The combustion facility will utilize three different fuels, a natural gas (NG) baseline and two high hydrogen content (HHC) fuels.

Results

Most of our effort so far was devoted to the assembly of the new test rig featuring a new window assembly with much improved optical access. The fully assembled test rig with the new window assembly is shown in Figure 1. Some of the main tasks associated with the modification of the test rig assembly included:

1. New water cooling lines had to be fabricated or purchased to attach to the new window combustor. A combination of both flexible and stainless steel tubing had to be adapted to the new rig. New lines were required for both the high pressure water and low pressure water cooling systems. The high pressure water lines had to be modified for the new NOx quench section, the window combustor, the connecting upstream spool, and downstream spool. New low pressure water lines had to be fabricated to attach to the outer window retainers as shown in Figure 1.

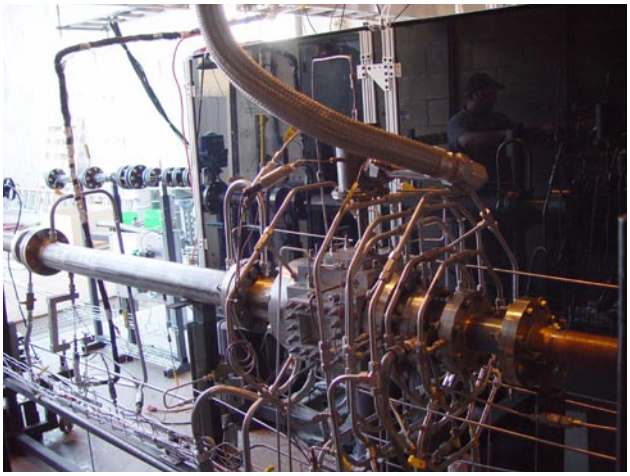

FIGURE 1. Full assembled test rig with new, larger window assembly

2. The secondary air system had to be modified to adapt to the new test rig. The secondary air system was significantly upgraded with new and better insulation and a better electrical heating system to minimize heat losses between the electrical heater and the test rig.
3. The nitrogen flow system for the window film cooling was significantly upgraded. In the old system the nitrogen pressure was set to the same value as for the fuel purging system. In the new system the pressure for the nitrogen film cooling is set using a computer-controlled regulator. New nitrogen film cooling lines were fabricated. The nitrogen film cooling is run from the nitrogen panel and split into four injection points in the new window assembly.

Photographs of the assembled test rig in operation are shown in Figures 2 and 3. A series of shakedown runs were performed in the new test using transverse jet injection nozzles designed in collaboration with Siemens Power Systems. In these initial tests, a straight tube injector was used for the axial jet injection. The axial jet fluid consisted of premixed methane/air with equivalence ratios ranging from 0.8 to 5.0. Emissions sampling was performed to compare with similar cases run with the old window assembly. CH chemiluminescence was detected using an intensified high-speed complementary metal oxide semiconductor camera with a framing rate of 5 kHz. A frame from one of the high-speed CH chemiluminescence movies is shown in Figure 4. The turbulent nature of the RJIC process is clearly evident in Figure 4. The initial results have been very encouraging, and have demonstrated that the system is able to run for up to seven hours without window damage.

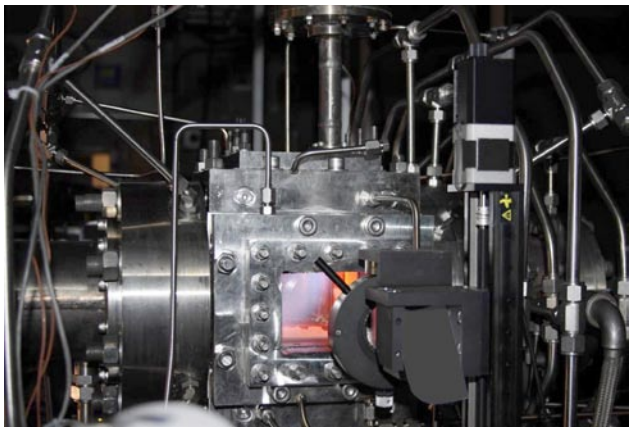

FIGURE 2. High-pressure reacting jet in vitiated crossflow test rig in operation with the new window assembly in place. The blue CH chemiluminescence from the rich premixed natural gas/air jet injection is evident.

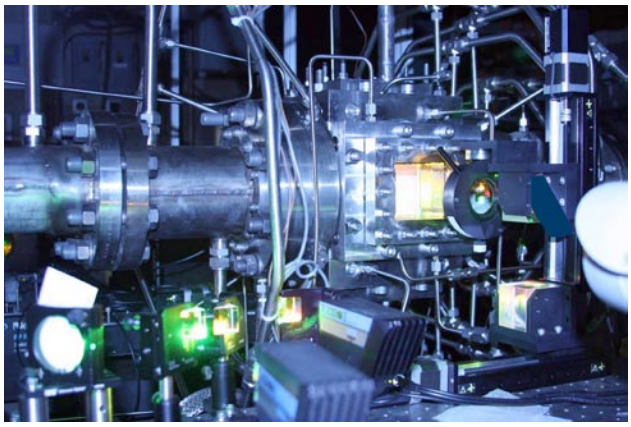

FIGURE 3. High-pressure reacting jet in vitiated crossflow test rig in operation with the new window assembly in place. The laser beams for CARS temperature measurements are directed into the window assembly.

Conclusions and Future Directions

The critical accomplishment for the project thus far is the development, modification, and testing of the RJIC test rig with the new window assembly. After a series of runs with window failures, the root causes of the window failures were identified as (1) inadequate nitrogen shield flow, (2) inadequate allowance for metal expansion, and (3) the pressure rise during ignition was too rapid and the magnitude was too high. All of the issues were addressed and several runs of 5–7 hours at a variety of operating conditions have been made with no window damage. Consequently, the test matrix is ready to be finalized and advanced laser diagnostics to probe the RJIC flow field can begin to be applied.

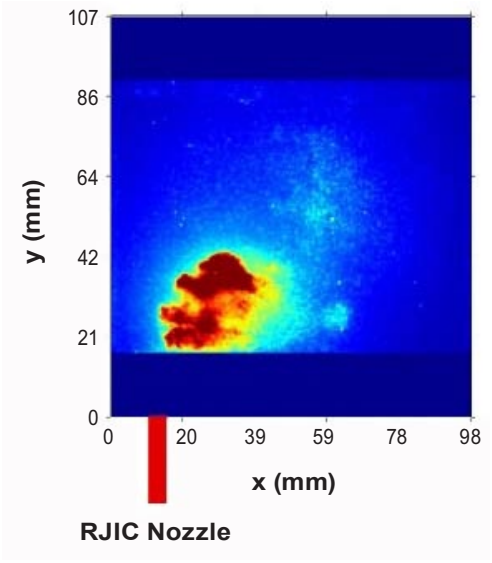

FIGURE 4. Single frame from a high-speed video of CH chemiluminescence from the rich premixed natural gas/air jet injection into a lean vitiated coflow. The vitiated flow direction in the figure is from left to right and the RJIC injection nozzle is indicated by a red tube at the lower left of the image. The vitiated flow was produced by burning premixed NG and air with an equivalence ratio of 0.5. The flow channel is 107 mm high and the viewing area of the window extends to within 17 mm of the top and bottom walls. The window viewing length is 98 mm in the horizontal direction.

Future work on this UTSR project will include:

- The development and testing of a particle seeding system for high-speed PIV.
- High-speed PIV measurements of the RJIC flow field for both NG and HHC gas jet injection.
- High-speed OH PLIF measurements of the RJIC flow field for both NG and HHC gas jet injection.
- Simultaneous high-speed OH PLIF and PIV measurements of the RJIC flow field for both NG and HHC gas jet injection.
- High-speed CARS temperature and species measurements of the RJIC flow field for both NG and HHC gas jet injection.

V.B.5 Turbulent Flame Speeds and NOx Kinetics of HHC Fuels with Contaminants and High Dilution Levels

Eric L. Petersen
Texas A&M University
Department of Mechanical Engineering
3123 TAMU
College Station, TX 77843
Phone: (979) 845-1257; Fax: (979) 845-3081
Email: epetersen@tamu.edu

DOE Project Manager: Mark Freeman
Phone: (412) 386-6094
Email: Mark.Freeman@netl.doe.gov

Contract Number: FE0004679

Start Date: October 1, 2010
End Date: September 30, 2013

Fiscal Year (FY) 2012 Objectives

- Complete the design and fabrication of the turbulent flame speed rig.
- Perform shock-tube experiments on syngas mixtures containing various levels of key impurities.
- Assemble a kinetics submechanism for NOx and ammonia impurities in syngas.
- Conduct shock-tube experiments on mixtures containing hydrogen sulfide.
- Perform laminar flame speed experiments using a statistical matrix for syngas fuel mixtures containing CO, H_2, CO_2, H_2O, and typical impurities.
- Correlate the laminar flame speeds of hydrogen and CO-H_2 mixtures from the chemical kinetics mechanisms.
- Begin laser absorption measurements related to determination of the rate of the key NNH reaction forming NO.

FY 2012 Accomplishments

- A chemical kinetics submechanism for NOx compounds and ammonia was assembled and compared with shock-tube data obtained in this project.
- Correlations of laminar flame speeds of pure-hydrogen and hydrogen-carbon monoxide mixtures were developed, covering a wide range of pressure, initial temperature, and stoichiometry.
- Ignition delay time experiments were performed in a shock tube for a bio-syngas mixture with various levels of contaminants, namely CH_4, NH_3, H_2O, and CO_2.
- A complete series of laminar flame speed experiments were performed with CO-H_2 mixtures containing water vapor.
- Experiments were performed in the mock-up turbulent flame speed rig to characterize the turbulent flow field as a function of fan blade design.
- Turbulent flame speed rig modifications, i.e., fan design, were designed and completed.
- Shock-tube experiments on H_2-O_2 mixtures containing H_2S impurities were performed, and a preliminary kinetics mechanism for H_2S chemistry was identified.

Introduction

Power generation cycles operating on high hydrogen content (HHC) fuels such as syngas offer a promising power source for the near future [1,2]. Syngas can be produced from different solid fuel feedstocks such as coal or biomass, with the main components of the gaseous fuel being H_2 and CO. However, the variability of the source and the synthesis process can result in a wide range of possible fuel blends that can also contain CO_2, H_2O, lower-order hydrocarbons, and impurities in addition to hydrogen and carbon monoxide. The impact of this variation in fuel content on the combustion chemistry and fuel reactivity remains a topic of active research. Flame speeds, ignition behavior, and NOx production are properties that impact the design and operation of power systems utilizing syngas. Much progress has been made recently in understanding the chemical kinetics of the H_2/CO system [3], the chemical kinetics of which is dominated by the presence of hydrogen [4]. However, despite the comprehensiveness of the database and mechanisms, improvements are still needed. For example, modern models have not been calibrated for significant levels of water or other diluents on the laminar flame speeds of syngas-related mixtures, nor have the effects of contaminants such as NOx, H_2S, NH_3, and metal carbonyls been implemented into the mechanisms in any comprehensive manner.

While laminar flame speeds provide valuable data for the validation of the chemical kinetics and provide

some insight into the combustion behavior in real systems, it is the turbulent flame speed that is of practical importance to the design of burners for integrated gasification combined cycle (IGCC) applications [5,6]. Nonetheless, few turbulent flame speed data exist for HHC fuels at gas turbine pressures. In addition, the physics of the relationship between turbulent flame speed and parameters such as turbulence intensity, stretch, and laminar flame speed are complex and not necessarily well understood [7]. Reliable turbulent flame speed data for HHC fuels are therefore needed at practical conditions. To these ends, the present project seeks to undergo a methodical and unique array of experiments and analyses that will lead to deeper and much-needed understanding of the turbulent flame speed behavior and NOx-formation kinetics of HHC fuels for IGCC applications. In addition to a comprehensive database and improved understanding of the basic physics and chemistry of syngas in the presence of impurities and high levels of diluents, the present project aims to offer a validated chemical kinetics model that can be utilized for the design of new systems and the improvement of existing ones.

Approach

The basic approach is best summarized by the six main tasks. Task 1, *Project Management and Program Planning*, includes the submission of regular and required reports to U.S. Department of Energy, in addition to routine management of the Texas A&M University (TAMU) project by the project investigator. This task also includes the specific interaction with the industry consultants. Feedback from General Electric, Siemens, Rolls-Royce, and Alstom is being obtained through face-to-face and telephone meetings.

Task 2, *Turbulent Flame Speed Measurements of Syngas Mixtures*, involves the development and application of a high-pressure, turbulent flame speed facility. The original flame speed vessel at TAMU is being modified with the capability to perform turbulent flame speed measurements. Turbulence is generated with fans, and the experiment and turbulence level is being well characterized prior to performing experiments. Turbulent flame speeds will be measured as a function of turbulence level, mixture composition, and initial pressure. Correlations will be developed that relate the turbulent speed to the equivalent laminar flame speed for the same mixture and initial pressure.

Task 3, *Laminar Flame Speed Measurements with Diluents*, uses a heated flame speed vessel to conduct high-pressure experiments up to 20 atm over a wide range of syngas mixtures. These mixtures will have realistic levels of diluents, with emphasis on high levels of water dilution. The heated facility allows for such mixtures, with initial temperatures as high as 600 K possible. The resulting database is being compared with current chemical kinetics models and is being used as the baseline for the turbulent flame speed measurements.

Task 4, *NOx Mechanism Validation Experiments*, involves shock tubes to obtain data for validation of the NOx submechanism at realistic ranges of mixture composition, stoichiometry, and pressure. Emphasis is placed on two types of experiments, (1) ignition experiments (both dilute and high concentration) containing initial levels of NO_2 and N_2O, to test the mechanisms in a global way, and (2) dilute experiments wherein key intermediate and NOx-related species profiles are measured using laser absorption and ir emission techniques. The resulting database will be compared to the NOx mechanism, and areas for improvement will be identified as needed.

Task 5, *Fundamental NOx Kinetics*, involves the direct measurement of specific rate coefficients to improve the accuracy of the NOx predictions at conditions involving high hydrogen and dilution levels. The principal focus is on the NNH pathway, and the rate measurements are being done in carefully designed shock-tube experiments at controlled conditions.

Finally, Task 6, *Effect of Impurities on Syngas Kinetics*, involves measuring primarily ignition measurements from shock-tube experiments that contain realistic levels of syngas impurities. Flame speed measurements will also be performed to assess the impact of the most important or likely impurities.

Results

Much progress was made toward the design and construction of the turbulent flame speed facility. The main focus was on the design of the fan impellers. Turbulence statistics of three impellers with different geometric features were measured using particle image velocimetry inside a Plexiglas® model (~1:1 scale) of a cylindrical flame speed vessel (12″ ID × 14″ L). Figure 1 shows a schematic of the experimental setup. With four impellers arranged in a central-symmetric configuration, turbulence intensities between 1.2 and 1.7 m/s with negligible mean flow (0.1 u′) were attained at the lowest fan speeds. Acceptable ranges for homogeneity and isotropy ratios of the velocity fields were set within a narrow bandwidth near unity (0.9–1.1). Homogeneity ratio was found to be controlled by the fan placement, and the prototype with higher number of blades caused the flow to become anisotropic. The integral length scale of the flow fields varied between 54 mm and 38 mm, which correlates well with those typically observed inside a gas turbine combustor. The mechanism to independently vary the intensity level and the integral

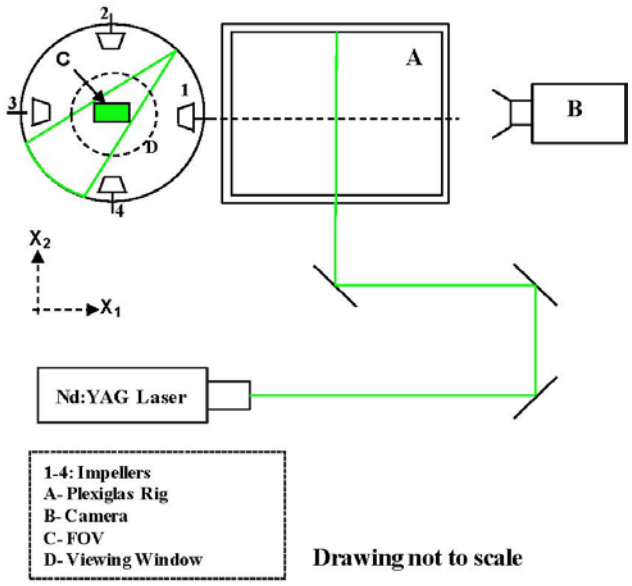

FIGURE 1. Schematic of the Plexiglas® rig and the aligned particle image velocimetry system. The FOV lies in the center of the optical access port of the existing flame speed vessel.

length scale was established, where turbulence intensity level was dependent on the rotational speed of the fan, and the integral length scale decreased with increasing blade pitch angle. The resulting design was drawn up and fabricated, which included the required modifications to the existing flame speed vessel to accommodate the new impellers.

During FY 2012, this project investigated the effect of moisture content (0%–15% by volume), temperature (323 K–423 K), and pressure (1 atm–10 atm) on syngas mixtures by measuring the laminar flame speed in a constant-volume, (newly) heated experimental facility. A design-of-experiments methodology was applied to these conditions to cover the widest range of conditions that are relevant to the gas turbine industry, shown in Table 1. The resulting experimental flame speed data were compared to the authors' most recent chemical kinetics model showing good overall agreement, but there are areas that need improvement, particularly around the peak flame speed. Typical results for three of the combinations in Table 1 are seen in Figure 2. A performance sensitivity analysis showed that the syngas composition is the most important factor affecting the laminar flame speed, but there is inconclusive evidence of a dominant factor that affects the mass burning rate and the Markstein length. Generally, mixtures with high levels of carbon monoxide stabilize the flame structure of thermal-diffusive instability. The increase of steam dilution has only a small effect on the laminar flame speed of high carbon monoxide mixtures.

TABLE 1. Laminar flame speed matrix with nine blends using four factors [temperature (T), pressure (P), steam dilution (χ), and syngas composition (H_2:CO)] at three levels

Exp.	T (K)	P (atm)	χ (% by mole)	H_2:CO
1	323	1	7.5	0.2743056
2	323	5	0	50:50:00
3*	323	1	15	100:00:00
4	373	1	0	100:00:00
5	373	5	15	0.2743056
6	373	10	7.5	50:50:00
7	423	1	15	50:50:00
8	423	5	7.5	100:00:00
9	423	10	0	0.2743056

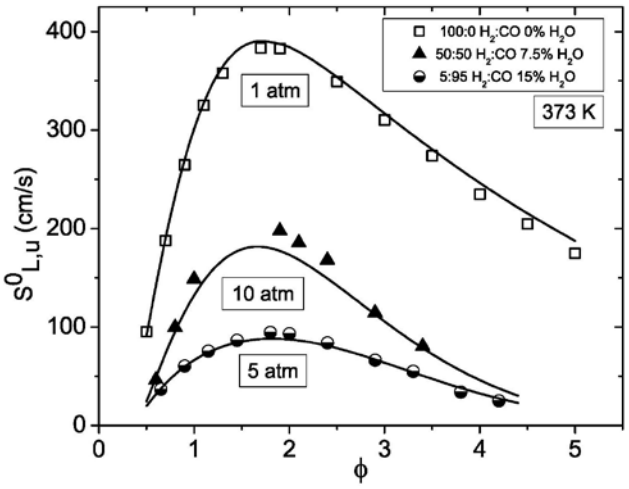

FIGURE 2. Laminar flame speed for three syngas compositions at 1 atm, 5 atm, and 10 atm each at different steam dilutions initially heated to 373 K compared to the chemical kinetics model (Exps. 4, 5, and 6 in Table 1)

Correlations of laminar flame speed are also of use in the combustion community. This fiscal year led to a new set of correlations for the laminar flame speeds of hydrogen-oxygen mixtures with nitrogen (air) and helium as diluents, using a recently updated chemical kinetics mechanism. A wide excursion of equivalence ratios (φ= 0.5–5.0), pressures (1 atm–30 atm) and temperatures (270 K–620 K) was performed. Flame speed correlations were developed at five pressures, namely 1 atm, 5 atm, 10 atm, 20 atm, and 30 atm for the pure-hydrogen case. The disparities between the kinetic model predictions and the correlation estimates, commonly associated with existing correlations, were significantly reduced, and the correlation estimates are within ±13 cm/s of the model predictions. Also, a correlation for lean and HHC syngas blends of H_2+CO+H_2O was developed from the

pure hydrogen correlations. A wide range of pressures (1 atm–30 atm), initial temperatures (323 K–550 K), steam contaminant levels (5%–15%), and hydrogen content in the fuel blend (15%–100%) were simulated. A design of experiments approach was adopted to determine the critical mixtures necessary to develop the correlation. The developed HHC correlation agrees within ±12% of the model predictions.

Ignition delay times were measured behind reflected shock waves at 1.5 atm, 12 atm, and 30 atm for a mixture representative of a syngas produced from biomass (0.29659% CO / 0.29659% H_2 / 0.15748% CO_2 / 0.08924% CH_4 / 0.20997% H_2O / 0.95013% O_2 in 98% Ar [mol.%]) and for the same biomass-derived syngas mixture doped with 200 ppm of NH_3. The importance of the various constituents on the ignition delay time was investigated by comparing the results with data from various baseline mixtures (H_2/O_2/Ar, H_2/CO/O_2/Ar and H_2/CO/O_2/Ar with one of the other constituent of the syngas, i.e., CO_2, H_2O, CH_4 or NH_3). The set of mixtures studied is shown in Table 2. The equivalence ratio was set to 0.5 during this study. Several recent detailed kinetics mechanisms from the literature were computed against these data, with fair agreement. Results showed that the mixture composition can have an important effect on the ignition delay time, with most of the effect being due to CH_4 addition through the reaction $CH_4+OH \rightleftarrows CH_3+H_2O$. The ammonia impurity had very little effect on the ignition delay time over the range of conditions studied. Figure 3 shows some typical results at a pressure near 12 atm, which highlights the noticeable effect of CH_4 and the small effect of NH_3, H_2O, and CO_2.

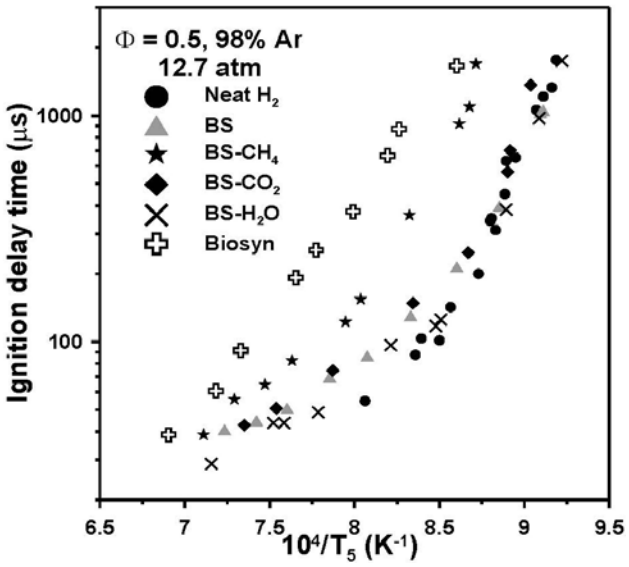

FIGURE 3. Effect of the composition on the ignition delay time for a syngas with a H_2/CO ratio set to 1 at a pressure around 12.5 atm

Conclusions and Future Directions

During FY 2012, significant progress was made in all of the project tasks. For the turbulent flame speed setup, which represents a new capability for the project investigator's group, a mockup vessel was used to perfect the production of the turbulence. These tests led to a final design of the fan blades that will lead to separate control of the turbulent length scale and the fluctuating velocity; the rig modifications were made in the summer of 2012. For the laminar flame speed experiments, the baseline hydrogen and CO-H_2 results were obtained, and a design of experiments approach was used to conduct a complete study of CO-H_2 mixtures with high levels of steam addition over a wide range of pressures and initial temperatures.

For the shock-tube experiments, experiments focused on the effect of impurities on the baseline syngas mixtures, namely CO-H_2, bio-syngas, and coal-syngas. The impurities included ammonia, H_2S, CH_4, and CO_2. The methane impurity had the largest impact on fuel ignition, while the NH_3 and H_2O had minimal impacts. All experiments were compared to the most recent chemical kinetics mechanism, which includes a newly compiled NOx and ammonia submechanism.

TABLE 2. Composition of the mixtures investigated in the shock tube for the syngas impurity study

Mixture name	% H_2	% CO	% O_2	% CH_4	%CO_2	% H_2O	%NH_3	% Ar
Neat H_2	1	0	1	0	0	0	0	98
BS	0.5	0.5	1	0	0	0	0	98
BS-CH_4	0.406	0.406	1.113	0.075	0	0	0	98
BS-CO_2	0,46	0,46	0,93	0	0,15	0	0	98
BS-H_2O	0.444	0.444	0.889	0	0	0.223	0	98
BS-NH_3	0.5	0.5	1	0	0	0	0.02	97.98
Biosyn	0.29659	0.29659	0.95013	0.08924	0.15748	0.20997	0	98
Biosyn-NH_3	0.29659	0.29659	0.95013	0.08924	0.15748	0.20997	0.02	97.98

Future work includes the following:

- Complete the ignition delay time experiments of H_2-O_2 mixtures with H_2S addition.
- Finalize the shock-tube measurements of coal-syngas blends with and without impurties.
- Conduct shock-tube experiments to measure the rate coefficient of the important NNH reaction NNH + O → NO + NH.
- Perform the first turbulent flame speed measurements in the new turbulent flame speed facilty.
- Perform turbulent flame speed measurements for H_2 and syngas mixtures at 1 atm.
- Measure the laminar burning velocities for syngas mixtures with CO_2 dilution and impurities.
- Suggest a final chemical kinetics mechanism for syngas, including modules for NOx chemistry and impurity chemistry.

FY 2012 Publications/Presentations

1. O. Mathieu, A. Levacque, and E.L. Petersen, "Effects of NO_2 Addition on Hydrogen Ignition behind Reflected Shock Waves," *Proceedings of Combustion Institute*, in press.

2. O. Mathieu, M.M. Kopp, and E.L. Petersen, "Shock-Tube Study of the Ignition of Multi-Component Syngas Mixtures with and without Ammonia Impurities," *Proceedings of Combustion Institute*, in press.

3. M. Krejci, O. Mathieu, A. Vissotski, S. Ravi, T. Sikes, E. Petersen, Kéromnès, A., Metcalfe, W., and H. Curran, "Laminar Flame Speed and Ignition Delay Time Data for the Kinetic Modeling of Hydrogen and Syngas Fuel Blends," *Journal of Engineering for Gas Turbines and Power*, in press.

4. M. Krejci, O. Mathieu, A. Vissotski, S. Ravi, T. Sikes, E. Petersen, Kéromnès, A., Metcalfe, W., and H. Curran, "Laminar Flame Speed and Ignition Delay Time Data for the Kinetic Modeling of Hydrogen and Syngas Fuel Blends," ASME Paper GT2012-69290, 57th ASME Turbo Expo, June 11–15, 2012, Copenhagen, Denmark.

5. O. Mathieu, A. Levacque, and E.L. Petersen, "Shock-Tube Study of the Effects of NO_2 Addition on Hydrogen Ignition," Paper 12S-15, Spring Technical Meeting of the Central States Section of the Combustion Institute, April 22–24, 2012, Dayton, Ohio.

6. O. Mathieu, M.M. Kopp, and E.L. Petersen, "Ignition Kinetics of a Multi-Component Syngas Mixture with and without Ammonia Impurities," Paper 12S-23, Spring Technical Meeting of the Central States Section of the Combustion Institute, April 22–24, 2012, Dayton, Ohio.

7. S. Ravi, S.J. Peltier, R.A. Humble, and E.L. Petersen, "Design and Development of a Flame Speed Vessel to Study Flame Propagation in Homogeneous and Isotropic Turbulence," Paper 12S-92, Spring Technical Meeting of the Central States Section of the Combustion Institute, April 22–24, 2012, Dayton, Ohio.

8. M.C. Krejci, A.J .Vissotski, S. Ravi, W.J. Metcalfe, A. Keromnes, H.J. Curran, and E.L. Petersen, "Effect of Steam Dilution on Laminar Flame Speeds of Syngas Fuel Blends at Elevated Pressures and Temperatures," Paper 12S-02, Spring Technical Meeting of the Central States Section of the Combustion Institute, April 22–24, 2012, Dayton, Ohio.

9. A. Levacque, O. Mathieu, and E.L. Petersen, "Effects of N_2O Addition on the Ignition of H_2-O_2 Mixtures: Experimental and Detailed Modeling Study," 2012 Spring Meeting of the Western States Section of the Combustion Institute, March 19–20, 2012, Phoenix, Arizona.

References

1. Dennis, R.A. and Harp, R. (2007) "Overview of the U.S. Department of Energy's Office of Fossil Energy Advanced Turbine Program for Coal Based Power Systems with Carbon Capture," ASME Paper No. GT2007-28338.

2. Richards, G.A. and Casleton, K.H. (2010) "Gasification Technology to Produce Synthesis Gas," in *Synthesis Gas Combustion—Fundamentals and Applications*, Lieuwen, T.C., Yang, V., and Yetter, R. (Ed.), CRC Press, Boca Raton, pp. 1-28.

3. Chaos, M. and Dryer, F.L. (2008) "Syngas Combustion Kinetics and Applications," *Combustion Science and Technology*, Vol. 180, pp. 1053-1096.

4. Kalitan, D.M., Mertens, J.D., Crofton, M.W., and Petersen, E.L. (2007) "Ignition and Oxidation of Lean CO/H_2 Fuel Blends in Air," *Journal of Propulsion and Power*, Vol. 23, No. 6, pp. 1291-1303.

5. Lieuwen, T., McDonell, V., Petersen, E., and Santavicca, D. (2008) "Fuel Flexibility Influences on Premixed-Combustor Blowout, Flashback, Autoignition, and Instability," *Journal of Engineering for Gas Turbines and Power*, Vol. 130, 2008, pp. 011506-10.

6. Lieuwen, T., McDonell, V., Santavicca, D., and Sattelmayer, T. (2010) "Operability Issues Associated with Steady Flowing Combustors," in *Synthesis Gas Combustion—Fundamentals and Applications*, Lieuwen, T., Yang, V., and Yetter, R. (Ed.), CRC Press, Boca Raton, pp. 261-288.

7. Driscoll, J.F. (2008) "Turbulent Premixed Combustion: Flamelet Structure and its Effect on Turbulent Burning Velocities," *Progress in Energy and Combustion Science*, Vol. 34, pp. 91-134.

V.B.6 Development of Criteria for Flameholding Tendencies within Premixer Passages for High Hydrogen Content Fuels

Vincent McDonell
UCI Combustion Laboratory
University of California, Irvine
Irvine, CA 92697-3550
Phone: (949) 824-5950 x11121
Email: mcdonell@ucicl.uci.ed

DOE Project Manager: Joseph Stoffa
Phone: (304) 285-0285
Email: Joseph.Stoffa@netl.doe.gov

Contract Number: FE0007045

Start Date: October 1, 2011
End Date: September 30, 2014

Fiscal Year (FY) 2012 Objectives

- Fuel space selection.
- Premixer passage module selection.
- Fabrication of modules.
- Rig setup/diagnostics.

FY 2012 Accomplishments

- The fuel space has been determined through feedback from U.S. Department of Energy (DOE) and original equipment manufacturers (OEMs).
- The overall test section has been redesigned to overcome condition limitations associated with the previously existing test section that was originally planned for use.
- Initial premixer feature modules have been decided upon.
- Fabrication of the test section and premixer feature modules is 75% complete.

Introduction

Lean-premixed operation of gas turbine engines results in low NOx emissions while minimizing emissions of CO and hydrocarbons. In addition to this, to increase overall cycle efficiency, engines are being operated at higher pressure ratios and higher combustor inlet temperatures. Increasing combustor inlet temperatures and pressures in combination with lean-premixed operation leads to a significant risk of flashback, which can severely damage the engine. Effort is required to curtail flashback on engines operated on hydrocarbon fuels, and challenges are greater when fuels with a high concentration of hydrogen are considered. When flashback occurs with hydrocarbon fuels, the flame is usually disgorged from the premixing section. However, the high reactivity of hydrogen can result in the flame anchoring within the premixer, resulting in engine damage.

In order to design a gas turbine premixer that will not allow a flame to anchor within it, it is necessary to quantify the conditions that promote flameholding. While considerable work has been done to quantify flame stability in the wake of bluff bodies designed to hold flames, little work has been done with incidental wall features that are designed to avoid flameholding. Further, the majority of work has focused on less reactive, hydrocarbon fuels. The goals of this study are to develop design guides that can be used to predict flame holding tendencies within premixer passages as a function of (1) pressure; (2) temperature; (3) fuel composition; and (4) feature geometries found within the passages such as steps, gaps, or struts.

Approach

The aim of this research project is to address questions that are critical for expanding the use of hydrogen in gas turbine power systems and specifically to develop criteria for the flameholding tendencies of high hydrogen content fuels in the wakes of wall disturbances at elevated temperatures and pressures like those seen in gas turbine engines. The experiment will focus on five major factors. Three of these factors, pressure, temperature, and velocity, are systems factors that are controlled by the balance of the engine and are not controlled by a combustion engineer. As a result, experiments will be carried out across a wide range of pressures, temperatures and velocities, in order to provide useful data for the greatest number of engine configurations. Another factor is fuel composition and fuel-air ratio. Often, it is required to design a combustion system that will operate reliably over a range of fuel types and fuel-air ratios; however, this becomes increasingly challenging as hydrogen is introduced to the fuel. In this experiment, hydrogen-natural gas fuel blends will be studied over the entire mixture range, from pure natural gas to pure hydrogen. Finally, the type

of flame-holding feature and its size will be investigated. This is a factor that is entirely within the control of a combustion system engineer. Several types of features will be studied for their flame-holding tendencies. Simple features such as a weld bead, a gap, or a screw head recess will be investigated because often these types of features are unavoidable inside an engine. Additional features to be tested may include airfoils of wall mounted struts. In an engine, these features would provide the necessary turbulence to ensure complete mixing of the fuel and air. Because of this, they are very likely to provide wakes capable of stabilizing a flame.

Results

Analysis of the capabilities of the previously available test section was carried out, and it was concluded that it would limit the conditions of interest too severely. Furthermore, previous issues with that test section were noted, including non-uniform approach velocities and fuel/air mixing. As a result, a modified design was undertaken to mitigate these issues.

A new test section has been designed with the ability to swap the test features as well as have optical access both at the feature, and upstream of it. Sample ports will be included at regular intervals along the test section to allow for extractive sampling. In addition to this, the upstream section of the new/modified test section will be tailored to produce a uniform fuel and velocity distribution. Figure 1 shows the proposed test section. It has a cross section of 1.76" x 0.76", which is representative of current large engines (see Figure 2) and has optical access both at the test section and upstream of the test section. Upstream of the test feature is a port

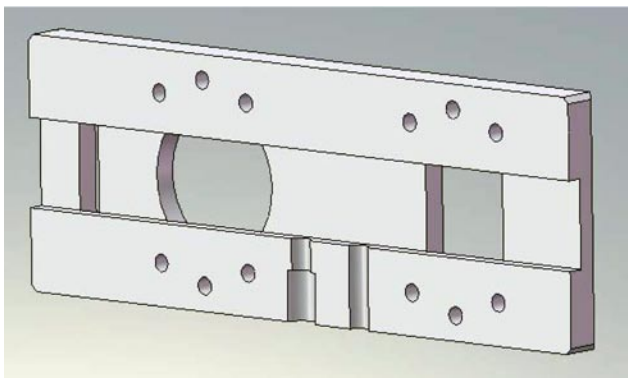

FIGURE 1. Cross section of revised test section

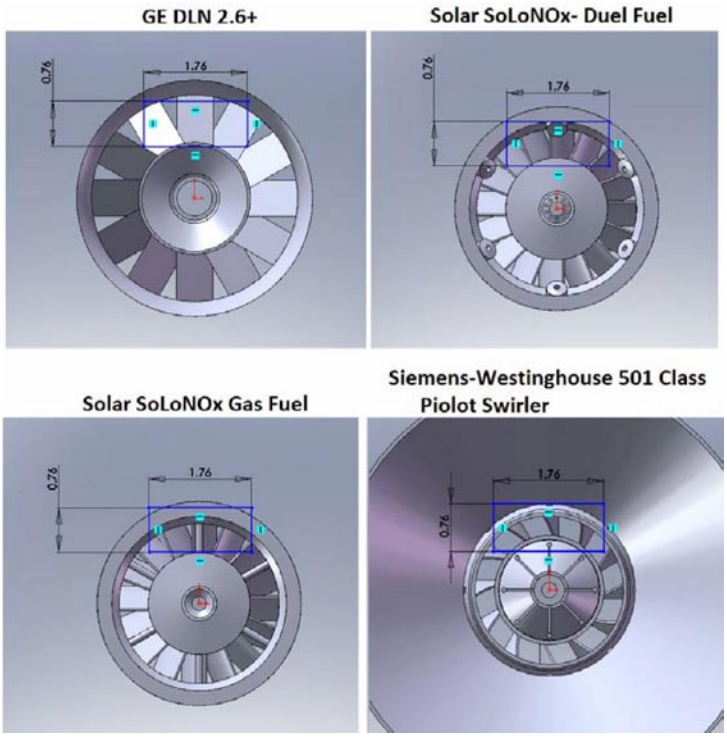

FIGURE 2. Revised approach flow section

for inserting turbulence generating bodies to modify the turbulence intensity of the flow. Optical access will allow for assessments of velocity and fuel distribution with laser Doppler velocimetry and acetone planar laser induced fluorescence.

Figure 3 shows the flow development section upstream of the test section, which was designed to ensure fully developed flow at the test section as well as complete mixing between the fuel and air. The flow development section consists of an annular air passage with an internal channel where fuel is mixed with air. The multiple cross jets of air should provide excellent mixing that will only be improved with the addition of the long flow development channel. The inner channel is 48 inches long and has a rectangular cross section that matches that of the test section. The entire apparatus is contained within three-inch pipe and is flanged to attach to the test section as well as the surrounding facility.

Figure 4 shows renderings of the typical features found in the premixing passage ways of current gas turbine engines. The three features selected for the first round of testing are a reverse step, an exposed bolt/rivet, and a flat vane. These features are common in most premixed engine passage ways and have strong potential for anchoring a flame in their wake. The rivet/bolt test feature can be varied by raising or lowering the height of the exposed profile, and the vane test feature can be

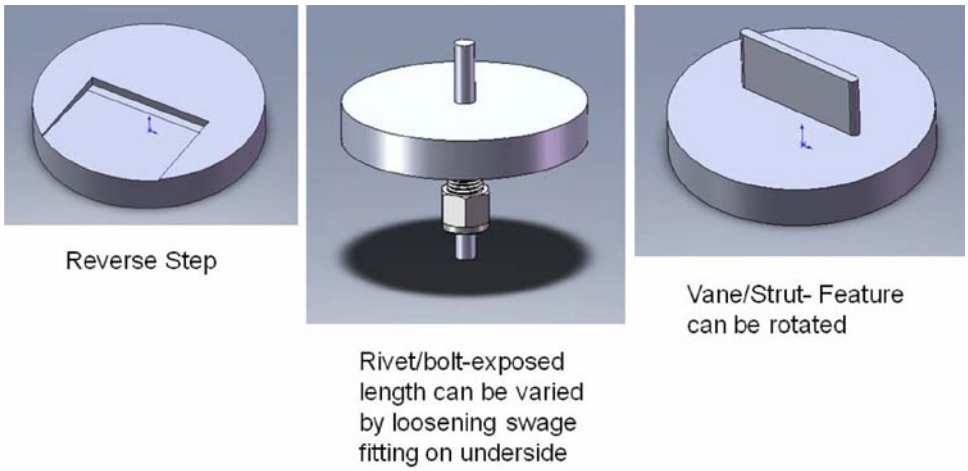

FIGURE 3. Overall integration of the test section and approach flow module with existing high pressure test facility infrastructure

FIGURE 4. Overall integration of the test section and approach flow module with existing high pressure test facility infrastructure

rotated in place to provide different flow patterns. The variability of these two types of test features will make testing more efficient and reduce down time of the test facility.

Conclusions and Future Directions

After detailed consideration of modifications to the available existing test section, it was decided to develop a modified section for increased flexibility as well as span of the conditions of interest in terms of temperature, pressure, and flow velocities. While this has delayed planned progress by 2-3 months, it will pay off by the end of the project. At this point, feedback from OEMs has been incorporated into the overall test planning and geometric features to be studied.

Future work on this project will include:

- Completion of the test section and approach flow module.
- Establishment of the needed diagnostics.
- Initiation of testing.
- Initial analysis towards correlation of the results in form of a design guide.

FY 2012 Publications/Presentation

1. V.G. McDonell, (2011), "Development of Criteria for Flameholding Tendencies within Premixer Passages for High Hydrogen Content Fuels," Presentation at UTSR 2011 Workshop, Ohio State University, October 2011.

2. V.G. McDonell, (2011), "Development of Criteria for Flameholding Tendencies within Premixer Passages for High Hydrogen Content Fuels," Kickoff Webinar with U.S. Department of Energy, November 2011.

3. E. Sullivan-Lewis and V.G. McDonell, (2012), "Development of Criteria for Flameholding Tendencies within Premixer Passages for High Hydrogen Content Fuels," Project Review with GE Energy Personnel, February 2012.

4. E. Sullivan-Lewis, and V.G. McDonell, (2012), "Development of Criteria for Flameholding Tendencies within Premixer Passages for High Hydrogen Content Fuels," Project Review with Siemens Energy Personnel, May 2012.

V.B.7 Development and Validation of Large-Eddy Simulation Techniques for the Prediction of Combustion-Dynamic Process with Syngas

Matthias Ihme
Department of Aerospace Engineering
University of Michigan
Ann Arbor, MI 48105
Email: mihme@umich.edu

DOE Project Manager: Mark Freeman
Phone: (412) 386-6094
Email: Mark.Freeman@netl.doe.gov

Contract Number: FE0007060

Start Date: October 1, 2011
End Date: September 30, 2012

Fiscal Year (FY) 2012 Objectives

The goals of the computational research efforts are:

- Develop improved large-eddy simulation (LES) combustion models for application to unstable gas turbine (GT)-combustion regimes; special emphasis is attributed to the accurate characterization of unsteady combustion processes (such as flash-back, lift-off, and flame extinction), and combustor stability limits.
- Utilizing database of jet-in-cross-flow configurations, perform a priori investigations to assess and improve important modeling components in the LES combustion model.
- Perform detailed LES-calculations in order to identify and characterize facility-induced non-idealities in flow-reactor experiments that are potential sources of observed irregular and stochastic ignition events in flow reactor experiments.

The goals of the experimental investigation of a GT-combustor are:

- Build and operate a generic gas turbine combustor in order to validate the next generation of LES-combustion models for understanding and predicting combustion events such as flashback and acoustically coupled combustion instabilities.
- Conduct fuel flexibility studies using high hydrogen content fuels in the experimental database to understand how the chemistry and large flame speed of hydrogen affects flashback, blowout, and combustion instabilities.
- Record a high-quality database of laser-based measurements of flame flashback, blowout, and combustion instabilities using high hydrogen content (HHC) fuel as well as traditional fuels for comparison purposes.

Introduction

With the rapidly growing energy demand and environmental concerns, the utilization of reformed fuels is gaining increasing attention. Specifically, the operation of HHC-fuels in power-generation applications offers enormous potential for significant reductions in greenhouse-gases, particulate matters, and other harmful and corrosive substances. Syngas contains varying amounts of carbon monoxide (CO) and hydrogen (H_2) as main fuel components and other species such as water (H_2O) and carbon dioxide (CO_2). Syngas can be generated from different sources including coal, biomass, organic waste, and refinery residuals [1]. Other advantages of syngas-technology are its potential for clean utilization of fossil fuel source when combined with carbon-capture and sequestration strategies [2], and the separation of pollutants (sulfur, ammonia, and particulate matter) before combustion [3].

Integrated gasification combined cycle (IGCC) power generation technologies can provide significant improvements in thermal efficiency and dramatic reductions in environmental impact compared to conventional coal-fired power plants. In these and other high-efficiency/low-emission combined cycle power plants, syngas is generated from the partial oxidation of coal with oxygen and steam in high-pressure gasifiers [4]. The subsequent gas turbine cycle utilizes the excess enthalpy of the high-temperature syngas mixture from the gasification process, resulting in a significant increase in overall power plant efficiency.

Although the successful operation of gas turbines using syngas has been demonstrated [6], fundamental scientific and technological challenges must be overcome in order to utilize the full potential of IGCC systems. These challenges are primarily attributed to the low density and higher diffusivity of hydrogen compared

to conventional hydrocarbon fuels. Variations in the thermo-diffusive properties of the mixture can lead to significant modifications in flame speed, flammability limits, and other fundamental combustion characteristics [8,10], which can adversely affect combustion stability and fuel conversion. In addition, high flame temperatures associated with hydrogen combustion make NOx emissions a concern, and dilution strategies are required to reduce these emissions to acceptable levels [11].

Currently, the combustor design is further complicated by uncertainties in the syngas combustion kinetics at gas-turbine-relevant operating conditions. These uncertainties are reflected by large discrepancies between chemical kinetics models and experimental data of syngas mixtures at high pressures ($p_0 > 10$ bar) and intermediate temperatures ($T_0 < 1{,}000$ K). To reconcile these observed discrepancies, experimental studies were conducted in rapid compression machines, shock tubes, and flow reactors. Revised CO/H_2 reaction mechanisms were developed [1,3,12–14,16,18,19,21,23–26], and different hypotheses have been put forward to explain the discrepancies between experiments and predictions, including (i) sensitivity of rate coefficients at high-pressure/low-temperature conditions; (ii) effects of inhomogeneities in mixture composition and flow-field structure on ignition characteristics in experimental facilities; (iii) catalytic effects of syngas mixture due to contaminations with metal carbonyls and nitric oxides; and (iv) significance of induction chemistry related to compressibility, mixing, and surface-catalytic effects.

However, limitations in experimental instrumentation and diagnostics precents the systematic investigation of these hypotheses. Furthermore, the characterization of such facility-induced non-idealities has so far mainly focused on shock tubes and rapid compression machines, and detailed experimental and computational investigations of flow reactors have not been performed. This is partially attributed to the high-Reynolds number flow regimes in flow reactors (with Reynolds numbers in excess of 10^5). To address these issues, a closely coordinated experimental and computational research effort is conducted to obtain an improved understanding about critical combustion-physical processes and to enable the successful implementation of HHC-combustion in GT-systems.

Results

Experimental Setup

The gas turbine model combustor (GTMC) is used to study acoustic behavior and performance. A schematic of the burner is shown in Figure 1. The injector consists of a central air nozzle, an annular fuel nozzle, and a co-annular air nozzle. Both air nozzles supply swirling air

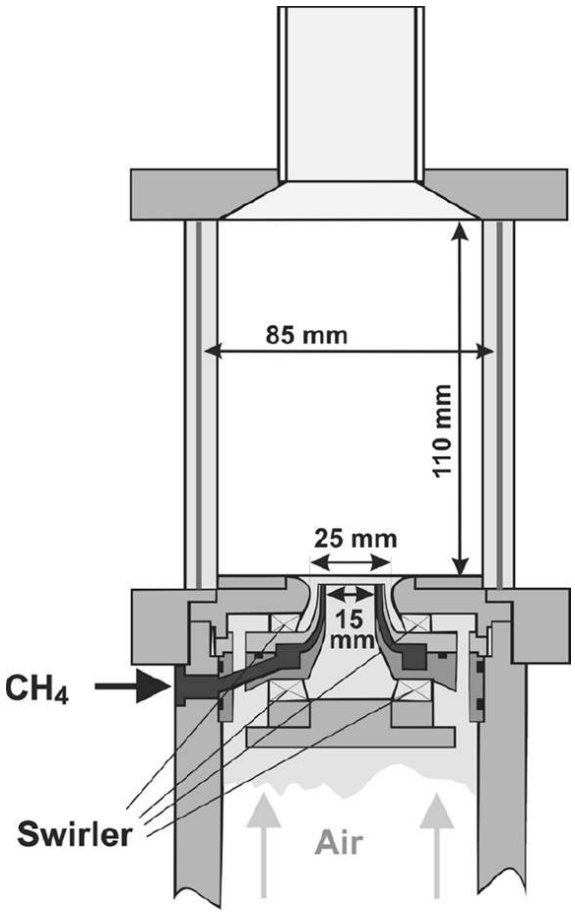

FIGURE 1. GT model combustor experiment [design of Meier at German Aerospace Center (DLR)]

at atmospheric pressure and temperature from a common plenum. The inner air nozzle has an outer diameter of 15 mm, and the annular nozzle has an inner diameter of 17 mm and an outer diameter of 25 mm. The measured swirl number is approximately 0.55. Non-swirling fuel is provided through three exterior ports fed through the annular nozzle which is subdivided into seventy-two 0.5 mm 0.5 mm channels. The exit plane of the central air nozzle and fuel nozzle lies 4.5 mm below the exit plane of the outer air annulus. The exit plane of the outer air annulus will be referred to as the injector face. The combustion chamber has a square cross section of 85 mm in width and 110 mm in height. The following fuel mixtures have so far been considered: methane, propane, syngas (with different H_2-content), and ethylene.

Comparison of Syngas and Hydrocarbon Fuels: Laminar Flame Speed Effects

Laminar flame speeds were varied by changing both fuel type and global equivalence ratio. It is expected that once the gases leave the injector there will be some

degree of premixing over the liftoff height. The frequency response generally increases with equivalence ratio, except for alkanes, which show non-monotonic trends. The highest frequencies occur for the fastest burning fuels (ethylene and syngas) and the maximum values tend to occur for stoichiometric or slightly rich conditions.

Figure 2a shows the relationship between the observed frequency and the flame speed of a given mixture at all studied equivalence ratios for m_a = 282 g/min. The frequency of the instability is nearly linearly proportional to the laminar burning velocity for a wide range of fuels and equivalence ratios. This result is unexpected and is not explained by conventional acoustic concepts. The presence of a flame in a Helmholtz resonator may create a driven state. Helmholtz theory describes a fluid element in the "neck" region which oscillates as a simple harmonic oscillator. This oscillation can be altered by the flame as it is swept downstream and then propagates rapidly upstream, a motion dependent on the laminar burning velocity. Other possible explanations are that the burning velocity affects the flame base liftoff height and the flame shape, both of which may influence the acoustic impedance. It is noted that the adiabatic flame temperature also changes as the fuel type and equivalence ratio are varied, and this can change the speed of sound of the product gases. However, the variation in temperature is not large enough to explain the significant variation in frequencies observed.

Syngas Compositional Variations

The frequency at a given equivalence ratio shows a slight linear dependence on the hydrogen concentration as shown in Figure 3. From this figure, it can be seen that with increasing hydrogen-content, the flame speed increases until a hard cutoff occurs, in which the instability is rendered inactive and the flame becomes non-resonating. The concentration at which this "quit" limit occurs is equivalence-ratio dependent, but the limit is extended for richer flames. Within the range of equivalence ratios considered, the maximum cutoff occurs near 43% H_2. As well, this shift is quasi-stable for syngas, where once the flame is non-resonating, it will not transition back to resonating. Hydrocarbon fuels can display intermittent behavior where resonant transitioning can occur. The amplitude of the dominant pressure signal is not equivalence ratio independent. As the "quiet" limit is approached, the instability strength is reduced until silent. This type of behavior suggests that thermoacoustic instabilities can be reduced by increasing the hydrogen content of the fuel.

Characterization of Non-ideal Effects in Rapid Compression Machines

The role of turbulence on the syngas ignition in rapid compression machines over a wide range of operating conditions was studied [20]. For this, a self-contained model was developed that describes the amplification of small-scale turbulence and mixture fluctuations during the rapid compression machine (RCM) phase and the subsequent ignition process. Rapid distortion theory is utilized to characterize the turbulence amplification during the compression phase. The ignition process is described by a Lagrangian Fokker-Planck model, which considers the micromixing between different ignition environments.

The model reduces to the well-known homogeneous reactor problem in the absence of perturbations in the initial flow field, mixture composition, and temperature.

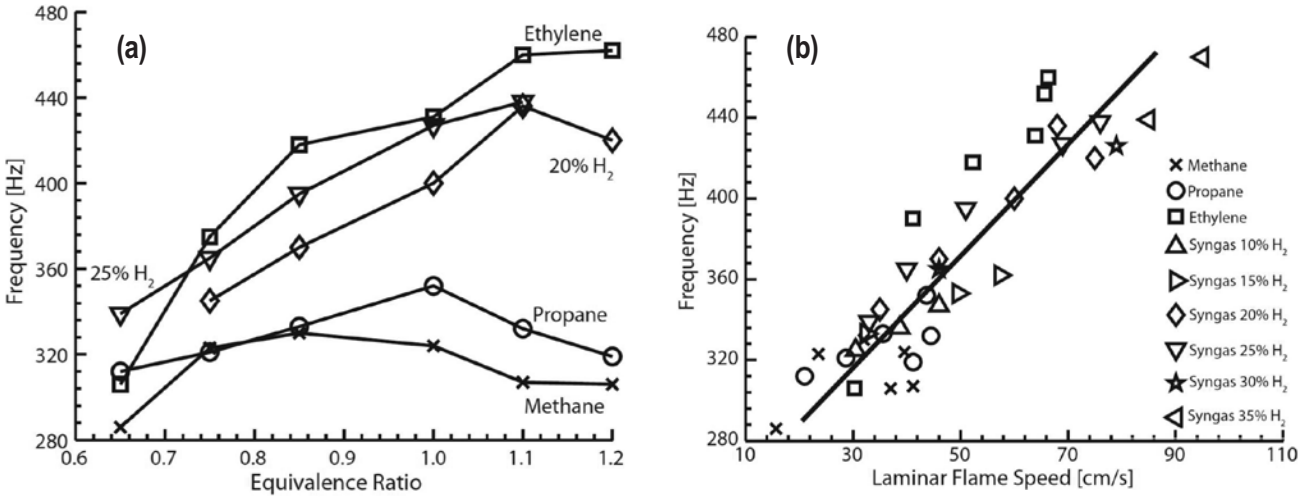

FIGURE 2. Effect of laminar burning velocity on the frequency of the combustion instability. (a) Effect of equivalence ratio; (b) frequency as function of flame speed for all fuels studied at m_a = 282 g/min, for varying φ = 0.65–1.2

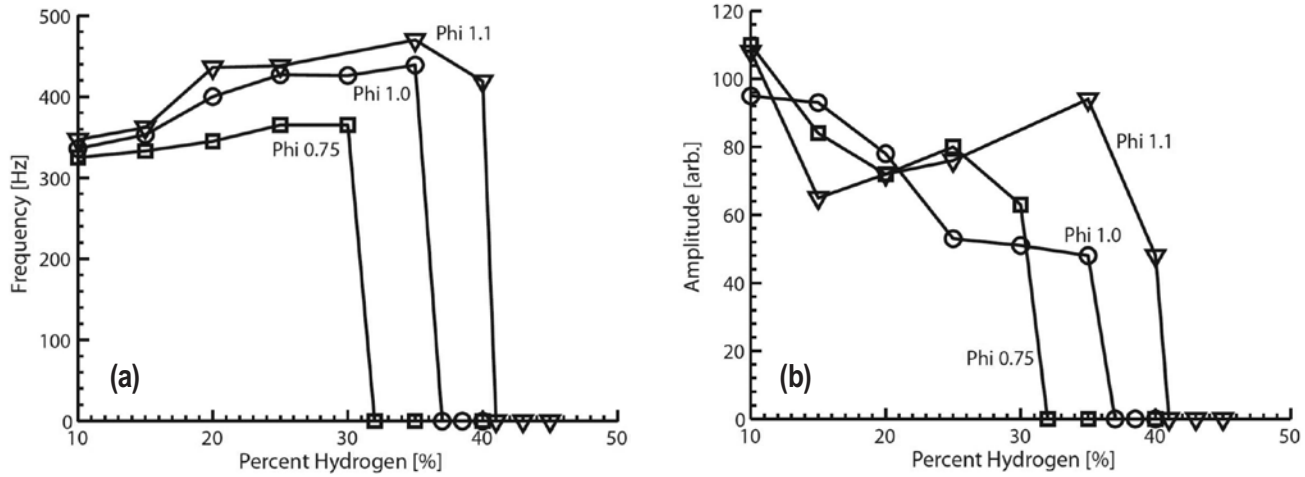

FIGURE 3. (a) Frequency as a function of hydrogen composition, (b) power spectral density amplitude as a function of hydrogen composition for m_a = 282 g/min

The model analysis showed that the turbulence level temperature perturbations, mixture fluctuation, mean mixture stratification and compression ratio are the key parameters that affect the ignition process.

Comparisons with experimental data (see Figure 4a) showed that the model parametrically captures observed trends of retarded reaction progress and reduced ignition delay for increasing levels of turbulence and mixture fluctuations. Parametric studies were conducted for different turbulence and mixture conditions over a wide range of operating conditions. In this study, a Damkoehler criterion was proposed (see Figure 4b) to characterize the sensitivity of the induction chemistry to turbulence and mixture fluctuations in RCMs. Mixtures with Damkoehler numbers below a value of approximately 50 exhibit increasing sensitivities to turbulence fluctuations which is reflected by significant reduction in ignition delay times.

Although this study only considered an idealized RCM-facility and syngas-mixture, based on these modeling results the following recommendations can be made to further assess the relevance of non-idealities in rapid compression machines:

- Parametric studies identified turbulence and fluctuations in temperature and composition as potential sources for systematic errors in RCM-measurements. These errors are presumably dependent on operating conditions and facility-specific, and could exacerbate other non-idealities that arise from heat-transfer, mixture impurities, catalytic effects, among others.
- Different facility-specific sources of inhomogeneities were identified. Detailed measurements of turbulence and flow-field structure throughout the compression stroke and ignition phase are desirable to improve the quantitative understanding about these hydrodynamic processes. Such measurements

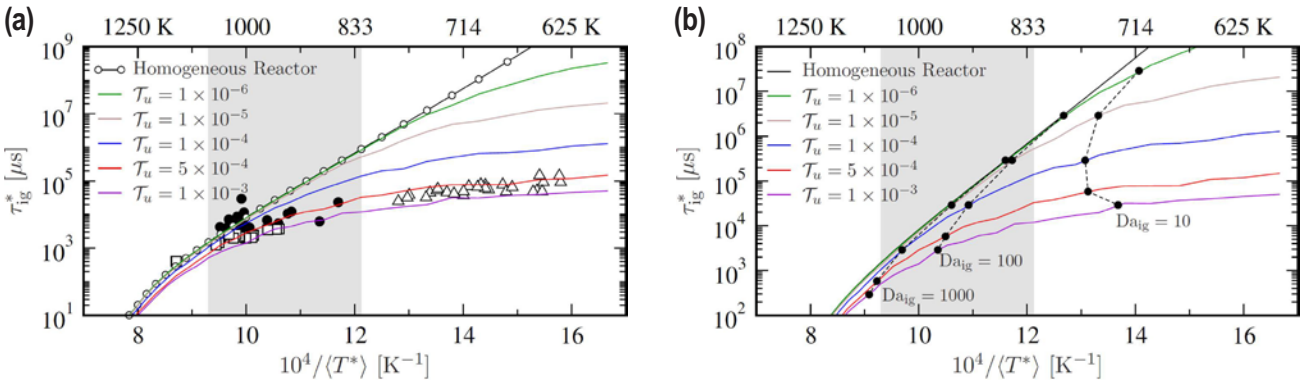

FIGURE 4. Ignition delay time of syngas/air mixtures [20]. (a) Experimental data are corrected to 20 atm. (b) Mixture composition is H_2/CO/CO_2/O_2/N_2 = 7.33/9.71/1.98/17.01/63.97 and φ = 0.5; pressure at the end of the compression phase is 20 atm; gray area illustrates the typical RCM-operating range

are also helpful to further constrain the parameters in the RCM-model.

- Depending on the Damkoehler criterion, the turbulence/chemistry interaction could add a stochastic component to the RCM-ignition process. This would require multiple experiments to obtain statistically significant results and quantify experimental uncertainties.
- Model results suggest that comparisons of global quantities, such as ignition delay and equilibrium composition, remain relatively insensitive to facility-induced perturbations. Therefore, time-resolved measurements for temperature, pressure, speciation, and wall-heat flux would be desirable to enable a systematic comparison with computational models and high-fidelity simulations.

Conclusions and Future Directions

The following conclusions can be drawn from the experimental investigation of the GT-combustion:

- Comprehensive parametric investigations have been conducted to investigate effects of equivalence ratio, air mass flow rate, air temperature, flame speed, and fuel type on acoustic instability. Results indicate that GTMC exhibits a wide range of acoustic behaviors, associated with different active and coupled acoustic modes.
- Syngas exhibits significantly different behavior than hydrocarbon fuels, even when the laminar flame speeds of the fuels were matched; flame speed was found to play an important role in affecting frequency and amplitude of the instability.

Major research findings and conclusions from the computational research effort are:

- Development of low-order model to characterize non-ideal effects, arising from in- homogeneities in temperature, mixture composition, and turbulence on the syngas-ignition dynamics in RCM experiments.
- Parametric investigations identified sensitivities of syngas-ignition to parameters and operating conditions, including RCM-compression ratio, turbulence, level, mixture stratification, and heat-losses.
- A Damkoehler criterion was introduced, comparing the significance of turbulence and inhomogeneities in affecting ignition dynamics. This criterion can be used to provide guidance in identifying the operability range of RCMs; Damkoehler-criterion is applicable to general fuel-mixture.

Future research directions include the following:

- Extend experimental investigations to high-pressure operating environments.
- Develop low-order model to describe observed combustion-dynamical behavior that was observed in our experimental GTMC investigations on the syngas and hydrocarbon fuels.
- Develop model to characterize non-ideal effects in flow-reactor facilities. Preliminary applications of this model to a canonical flow-reactor facility are encouraging, and extended parametric studies will be conducted.

FY 2012 Publications/Presentations

1. M. Ihme, "On the Role of Turbulence and Compositional Fluctuations in Rapid Compression Machines: Autoignition of Syngas Mixtures," *Combust. Flame*, 159, 1592-1604, 2012.

2. P.M. Allison, J.F. Driscoll, and M. Ihme, "Acoustic Characterization of a Partially-Premixed Gas Turbine Model Combustor: Syngas and Hydrocarbon Fuel Comparisons," *Proc. Combust. Inst.*, 34, (in press), 2012.

3. S. Weiher and M. Ihme, "Characterization of Mixing and Ignition Effects in Flow Reactor Facilities Using a Particle Method," AIAA-paper 2012-499, presented at 50th AIAA Aerospace Sciences Meeting including the New Horizons Forum and Aerospace Exposition, Nashville, Tennessee, January 9–12, 2012.

4. P.M. Allison, J.F. Driscoll, and M. Ihme, "Acoustic Behavior of a Partially Premixed Gas Turbine Model Combustor," AIAA-paper 2012-504, presented at 50th AIAA Aerospace Sciences Meeting including the New Horizons Forum and Aerospace Exposition, Nashville, Tennessee, January 9–12, 2012.

References

1. M. Chaos and F.L. Dryer, "Syngas Combustion Kinetics and Applications," *Combust. Sci. Tech.*, 180:1053-1096, 2008.

2. P. Chiesa, S. Consonni, T. Kreutz, and R.H. Williams, "Co-Production of Hydrogen, Electricity and CO_2 from Coal with Commercially Ready Technology. Part A: Performance and Emissions," *Int. J. Hydrogen Energy*, 30:747-767, 2005.

3. C.-J. Sung and C.K. Law, "Fundamental Combustion Properties of H_2/CO Mixtures: Ignition and Flame Propagation at Elevated Pressures," *Combust. Sci. Tech.,* 180:1097-1116, 2008.

4. K.M. Tait and M.M. McDonald, "Recent Developments in IGCC Technology," *CIM Bulletin*, 87(981):27-35, 1994.

5. M.M. Johsi and S.G. Lee, "Integrated Gasification Combined Cycle–A Review of IGCC Technology," *Energy Sources*, 18(5):537-568, 1996.

6. D.M. Todd and R.A. Battista, "Demonstrated Applicability of Hydrogen Fuel for Gas Turbines," In Proc. of the IchemE Gasification 4 Conference. Noordwijk, Netherlands, 2000.

7. P. Chiesa, G. Lozza, and L. Mazzocchi, "Using Hydrogen as Gas Turbine Fuel," *J. Eng. Gas Turbines Power*, 127:73-80, 2005.

8. L. He and P. Clavin, "Premixed Hydrogen-Oxygen Flames. Part I: Flame Structure Near the Flammability Limits," *Combust. Flame*, 93:391-407, 1993.

9. S.D. Tse, D.L. Zhu, and C.K. Law, "Morphology and Burning Fluxes of Expanding Spherical Flames in H_2/O_2 Inert Mixtures up to 60 Atmospheres," *Proc. Combust. Inst.*, 28:1793–1800, 2000.

10. C.K. Law, "Combustion Physics," Cambridge University Press, Cambridge, 2006.

11. N. Shilling and R. Jones, "The Response of Gas Turbines to a CO_2 Constrained Environment," 2003, Gasification Technologies Conference.

12. E.L. Petersen, D.M. Kalitan, A.B. Barrett, S.C. Reehal, J.D. Mertens, D.J. Beerer, R.L. Hack, and V.G. McDonell, "New Syngas/Air Ignition Data at Lower Temperature and Elevated Pressure and Comparison to Current Kinetics Models," *Combust. Flame*, 149:244-247, 2007.

13. S.M. Walton, X. He, B.T. Zigler, and M.S. Wooldridge, "An Experimental Investigation of the Ignition Properties of Hydrogen and Carbon Monoxide Mixtures for Syngas Turbine Applications," *Proc. Combust. Inst.*, 31:3147-3154, 2007.

14. G. Mittal, C.J. Sung, and R.A. Yetter, "Autoignition of H_2/CO at Elevated Pressures in a Rapid Compression Machine," *Int. J. Chem. Kinet.*, 38:516, 2006.

15. G. Mittal, C.-J. Sung, M. Fairweather, A.S. Tomlin, J.F. Griffiths, and K.J. Hughes, "Significance of the HO_2 + CO Reaction During the Combustion of CO + H_2 Mixtures at High Pressures," *Proc. Combust. Inst.*, 31:419-427, 2007.

16. W.C. Gardiner, M. McFarlan, K. Morinaga, T. Takeyama, and B.F. Walker, "Initiation Rate for Shock-Heated Hydrogen-Oxygen-Carbon Monoxide-Argon Mixtures as Determined by {OH} Induction Time Measurements," *J. Phys. Chem.*, 75:1504, 1971.

17. M. Dean, D.C. Steiner, and E.E. Wang, "Shock-Tube Study of H_2/O_2/CO/Ar and H_2/N_2O/CO/Ar Systems: Measurement of Rate Constant for H + N_2O = N_2 + OH," *Combust. Flame,* 32(1):73-83, 1978.

18. G. Fotache, Y.Tan, C.J. Sung, and C.K. Law, "Ignition of $CO/H_2/N_2$ Versus Heated Air in Counterflow: Experimental and Modeling Results," *Combust. Flame*, 120:417-426, 2000.

19. I. Wierzba and V. Kilchyk, "Flammability Limits of Hydrogen-Carbon Monoxide Mixtures at Moderately Elevated Temperatures," *Int. J. Hyd. Energy*, 26:639-643, 2001.

20. M. Ihme, "On the Role of Turbulence and Compositional Fluctuations in Rapid Compression Machines: Autoignition of Syngas Mixtures," *Combust. Flame,* 159, 1592-1604, 2012.

21. M. O'Conaire, H.J. Curran, J.M. Simmie, W.J. Pitz, and C.K. Westbrook, "A Comprehensive Modeling Study of Hydrogen Oxidation," *Int. J. Chem. Kinet.*, 36:603–622, 2004.

22. J. Li, Z. Zhao, A. Kazakov, and F.L. Dryer, "An Updated Comprehensive Kinetic Model of Hydrogen Combustion," *Int. J. Chem. Kinet.*, 36:566-–575, 2004.

23. M.A. Mueller, R.A. Yetter, and F.L. Dryer, "Flow Reactor Studies and Kinetic Modeling of the H_2/O_2/NOx and CO/H_2O/NOx Reactions," *Int. J. Chem. Kin.*, 31:705, 1999.

24. S.G. Davis, A.V. Joshi, H. Wang, and F. Egolfopoulos, "An Optimized Kinetic Model of H_2/CO Combustion," *Proc. Combust. Inst.*, 30:1273–1281, 2005.

25. I. Zsely, J. Zador, and T. Turanyi, "Uncertainty Analysis of Updated Hydrogen and Carbon Monoxide Oxidation Mechanisms," *Proc. Combust. Inst.*, 30:1273–1281, 2005.

26. F.L. Dryer and M. Chaos, "Ignition of Syngas/Air and Hydrogen/Air Mixtures at Low Temperature and High Pressures: Experimental Data Interpretation and Kinetic Modeling Implications," *Combust. Flame*, 152:293–299, 2008.

V.B.8 Robust, Reliable Low Emission Gas Turbine Combustion of High Hydrogen Content Fuels

Margaret S. Wooldridge (Primary Contact)
and Hong G. Im
University of Michigan
2350 Hayward Street
Ann Arbor, Michigan 48109-2125
Phone: (734) 936-0349; Fax: (734) 647-3170
Email: mswool@umich.edu

DOE Project Manager: Mark Freeman
Phone: (412) 386-6094
Email: Mark.Freeman@netl.doe.gov

Contract Number: FE0007465

Start Date: October 1, 2011
End Date: September 30, 2014

Fiscal Year (FY) 2012 Objectives

- To initiate research program with meetings between researchers and industry experts on syngas kinetics and combustion.
- To experimentally and computationally determine diverse combustion benchmarks for high hydrogen content fuels/syngas at the high pressure conditions relevant to gas turbines
- To create and validate a detailed syngas reaction mechanism by cross-validating the experimental measurements and computational models
- To investigate the effects of mixture inhomogeneities using different modeling approaches including direct numerical simulation

FY 2012 Accomplishments

- The co-PIs met with several syngas reaction kinetics and modeling experts during the past fiscal year of funding.
- Results of rapid compression facility experiments on syngas ignition were analyzed to identify conditions of strong and weak ignition.
- Criteria were proposed to predict strong and weak ignition behavior. A critical hydrogen mole fraction of 1.5% was identified for the range of conditions considered, including pressures from P = 7.1 atm to 26.4 atm, temperatures from T = 855 K to 1,051 K, fuel-to-air equivalence ratios from φ = 0.1 to 1.0, oxygen mole fractions from χ_{O2} = 15% to 20%, and H_2:CO ratios from H_2:CO = 0.25 to 4.0 (mole basis).
- Theory was proposed and evaluated to determine the physical and chemical mechanisms responsible for the critical hydrogen mole fraction.
- High fidelity computational models have been developed and configurations to conduct parametric studies have been identified.

Introduction

Researchers at the University of Michigan are performing experimental and computational studies which provide improved and robust understanding of the reaction kinetics and other fundamental characteristics of combustion of high hydrogen content (HHC) fuels that are vital to advancing HHC turbine design and to making coal gasification power plants environmentally sustainable and cost competitive. The scope of work includes rapid compression facility (RCF) studies of HHC ignition delay times and hydroxyl radical (OH) time-histories, flame speeds, and flammability limits. A range of temperatures, pressures, and test gas mixture compositions have been initially investigated experimentally and computationally. The experimental data are analyzed to identify the parameters controlling ignition behavior and to validate and improve detailed combustion mechanisms for HHC fuels. The computational work includes modeling studies of HHC auto-ignition characteristics and flammability limits. The results of the study will provide domain maps which identify conditions where HHC combustion has significant sensitivity to flame and auto-ignition interactions. Such regions of high sensitivity may be a difficult design space for gas turbine operation. The domain maps may also identify conditions for heightened combustor control.

Approach

Previous ignition studies were conducted by Walton et al. [1] using the University of Michigan (UM) rapid compression facility in which ignition delay times for syngas (specifically H_2 and CO) fuel blends were measured. The data from Walton et al. included high speed imaging of chemiluminescence that was recorded during the ignition experiments. During the

past year, the high speed imaging data from Walton et al. were analyzed to characterize the syngas ignition regime (strong or weak) for the specific mixtures and experimental conditions. For cases with weak ignition, the reaction front propagation speeds were determined and compared to the thermophysical parameters of the experiments. Ignition theory was proposed and evaluated to identify distinguishing characteristics of the ignition regimes.

Results

Weak ignition is characterized by spatial non-uniformities with the formation of localized ignition sites and reaction fronts, whereas strong ignition is characterized by spatial uniformity with a single ignition event across the entire volume of the test section of the RCF. Examples of the features of strong and weak ignition are shown in Figure 1.

As seen in the right panel of Figure 1, a reaction front is characterized by a well-defined perimeter to the chemiluminescence with a well-defined central location. Figure 2 shows a series of still images of a weak ignition condition which shows the progress of the reaction front through the UM-RCF reaction chamber. In the case of weak ignition, the reaction front(s) propagates through the reaction chamber for a period of time until strong ignition occurs in the remaining unburned volume of the reaction chamber. The reaction front affects the unburned charge by compression heating and potentially through transport at the reaction front.

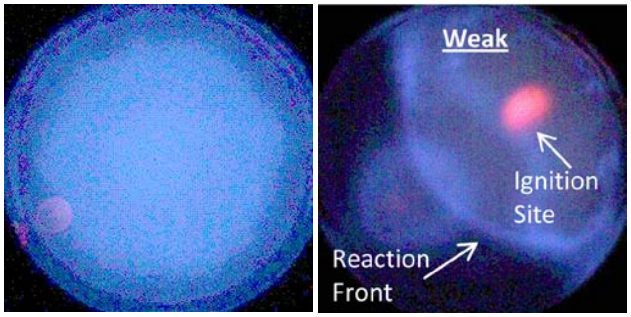

FIGURE 1. Examples of still images of syngas ignition in the UM-RCF reaction chamber for strong and weak behavior. Left: T = 1,028 K, P = 7.6 atm, φ = 0.15, χ_{H2} = 3.6%, χ_{CO} = 2.4%, χ_{O2} = 19.8%, Balance N_2 (mole basis). Right: T = 1,009 K, P = 11.6 atm, φ = 0.4, χ_{H2} = 2.9%, χ_{CO} = 11.5%, χ_{O2} = 18%, Balance N_2 (mole basis).

For each experimental case that yielded weak ignition behavior, the reaction front propagation speed was determined from the high-speed imaging data. This was accomplished by tracking the location of the reaction front through time with a manually imposed series of arcs as illustrated in Figure 2.

A summary of the measured speeds are provided in Figure 3. There is a clear pattern to the data with increasing speeds observed at higher mole fractions of hydrogen. Numerous additional parameters were considered, and the hydrogen mole fraction was the best correlated with the observed trends in ignition regimes. By extrapolating to the intercept of a line fitted to the data shown in Figure 3, the results indicate the ignition regimes for syngas (at the conditions studied) are delineated by a critical hydrogen mole fraction of 1.5%. Investigation of the physical nature of the critical mole fraction using ignition theory (described in detail in Mansfield and Wooldridge [2]) indicates that the limiting condition is governed by the competing time scales of strong ignition and weak ignition events. Theoretical thermal gradients which may govern the reaction front propagation speed were found to be in agreement with known thermal gradient magnitudes in similar experimental equipment. However, the thermophysical properties of the gas mixture suggest that if a global thermal gradient exists, it must be formed by the gas dynamics of the compression process.

Conclusions and Future Directions

The current work demonstrates the existence of two distinct ignition regimes for syngas mixtures at the high pressure, low temperature conditions studied.

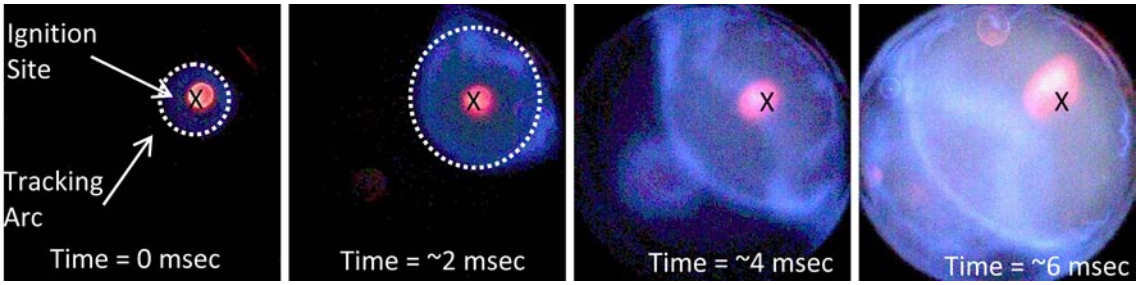

FIGURE 2. Example of method used to determine the propagation rates of reaction fronts observed during weak ignition; a single arc is shown for clarity

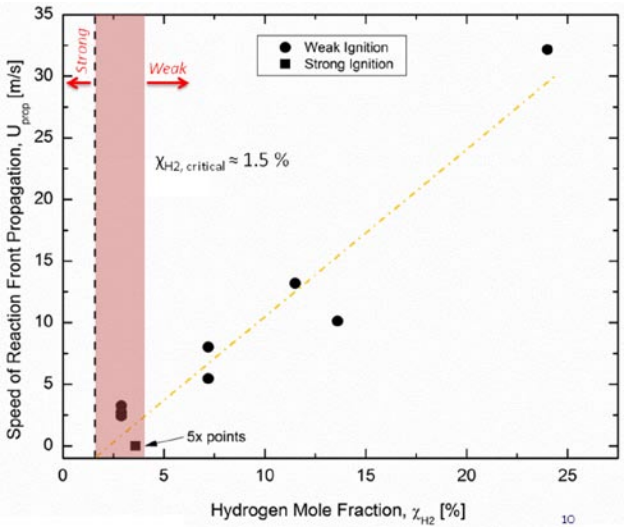

FIGURE 3. Measured reaction front propagation speed as a function of H_2 fuel mole fraction; the critical limit is based on linear extrapolation of the experimental data for weak ignition

The regimes are delineated by a critical hydrogen mole fraction of 1.5%. This critical value is supported by both experimental data and ignition theory. Investigation of the physical nature of the critical mole fraction indicates that this value is governed by the competing time scales of strong ignition and weak ignition events. The weak ignition time scale is determined as the ratio of a characteristic length of the reaction chamber and the reaction front speed, which relate to the volume of fuel consumed during weak ignition behavior. Theoretical thermal gradients which may govern the reaction front propagation speed are in agreement with known thermal gradient magnitudes in similar experimental equipment. However, the thermophysical properties of the gas mixture suggest that if a global thermal gradient exists, it must be formed during the compression process.

Next steps in the research project include additional ignition studies of syngas mixtures to test the ignition theory developed based on the initial experiments. These experiments will also be used to identify conditions well suited for the OH laser absorption studies. The ignition data will be used to refine and validate HHC combustion reaction mechanisms.

Previous computational studies [3,4] have attempted various systematic means to identify distinct ignition regimes of reactant mixture in the presence of thermal and compositional inhomogeneities, in which computational singular perturbation (CSP) was employed as an automatic diagnostic tool to identify ignition and front propagation. Similar parametric studies will be conducted using high fidelity simulation of syngas auto-ignition.

Special Recognitions & Awards/Patents Issued

1. Professor Wooldridge received the 2011, American Society of Mechanical Engineers George Westinghouse Silver Medal for rich contributions to power development.

2. Professor Wooldridge received the 2011-2012 Trudy Huebner Service Excellence Award from the University of Michigan for service contributions to the engineering profession, education, and research.

FY 2012 Publications/Presentations

1. Wooldridge, M.S., "Fundamental Studies to Enable Robust, Reliable, Low Emission Gas Turbine Combustion of High Hydrogen Content Fuels." Presentation at the 2011 University Turbine Systems Research Workshop, NETL October 25-27, 2011, Columbus, Ohio.

2. Mansfield, A. and Wooldridge, M.S., "An Investigation of Syngas Ignition Phenomena," Conference Paper, Central States Meeting of the Combustion Institute, April 2012.

3. Mansfield, A. and Wooldridge, M.S., "An Investigation of Syngas Ignition Phenomena," Presentation at the Central States Meeting of the Combustion Institute, April 2012.

References

1. S.M. Walton, X. He, B.T. Zigler, and M.S. Wooldridge, "An Experimental Investigation of the Ignition Properties of Hydrogen and Carbon Monoxide Mixtures for Syngas Turbine Applications," *Proceedings of the Combustion Institute*, vol. 31, pp. 3147-3154 (2007).

2. A. Mansfield and M. S. Wooldridge, "An Investigation of Syngas Ignition Phenomena," Conference Paper, Central States Meeting of the Combustion Institute, April 2012.

3. S. Gupta, H.G. Im, and M. Valorani, "Classification of Ignition Regimes in HCCI Combustion Using Computational Singular Perturbation," *Proceedings of the Combustion Institute*, vol. 33, pp. 2991-2999 (2011).

4. S. Gupta, H.G. Im, and M. Valorani, "Analysis of N-Heptane Auto-Ignition Characteristics Using Computational Singular Perturbation," *Proceedings of the Combustion Institute,* vol. 34, accepted (2012).

V.B.9 Large Eddy Simulation Modeling of Flashback and Flame Stabilization in Hydrogen-Rich Gas Turbines Using a Hierarchical Validation Approach

Venkat Raman (Primary Contact), Noel Clemens
University of Texas at Austin
210, E. 24th Street
Austin, TX 78712
Phone: (512) 923-8713; Fax: (512) 471-3788
Email: v.raman@mail.utexas.edu

DOE Project Manager: Joseph Stoffa
Phone: (304) 285-0285
Email: Joseph.Stoffa@netl.doe.gov

Contract Number: FE0007107

Start Date: October 1, 2011
End Date: September 30, 2012

Fiscal Year (FY) 2012 Objectives

- Develop a design for lab-scale testing of key gas-turbine dynamics, focusing on the unsteady flashback dynamics that could lead to catastrophic failure of the combustor.
- Develop a large eddy simulation (LES) based combustion modeling framework suitable for modeling unsteady flame dynamics in high-pressure syngas-burning gas turbines.
- Begin setting up a methodology for transferring technology to industry using an open source platform.

FY 2012 Accomplishments

- A new premixed swirl flame burner to study flashback has been designed in collaboration with industry experts.
- A new technique for comparing LES results and experimental data has been evaluated using particle image velocimetry (PIV) data acquired in jet-flames-in-crossflow. This technique reveals the inadequacy of models for turbulent, intermittent quantities.
- A direct quadrature method of moments (DQMOM) approach has been developed for complex geometries and implemented in a highly parallel open source code. Preliminary simulations of canonical flow configurations show that the methodology is capable of accurately capturing flame evolution in turbulent flows. In particular, the methodology predicts the change in flame length and location as the hydrogen content in the fuel changes.
- Based on discussions with GE Company and Siemens Energy Corp., an open source platform called OpenFOAM® is being used for transferring the models. The first version of the DQMOM model has been shipped to Siemens under this framework.

Introduction

Hydrogen-enriched fuel gas synthesized from coal, among other means, is seen as a viable approach for limiting greenhouse gas emissions. However, currently available gas turbines are not capable of handling the large differences in the combustion characteristics and thermophysical properties of hydrogen as opposed to conventional fuels. Since hydrogen is readily combustible, it poses a significant safety hurdle. Apart from generating higher temperatures, hydrogen-rich fuel could also lead to flame flashback, where the reaction zone enters the fuel injection region leading to catastrophic failure. The availability of robust and predictive computational models will help overcome these engineering limitations. With this background, the goal of this work is to develop advanced computational tools validated using a suite of high-fidelity experimental data with the express interest of capturing flame flashback.

Approach

With the overall goal of predictively simulating gas turbine dynamics, three critical bottlenecks have been identified. First, there does not exist a comprehensive computational model that could describe the interaction of the flame with the turbulent flow. In particular, the evolution of the turbulent boundary layers in the fuel premixing region plays a critical role in the flashback process. The interaction of this boundary layer with the flame needs to be modeled. Second, there does not exist a high-fidelity, well-characterized experimental dataset for validating computational models. Without such complete validation, confidence in models cannot be built. Finally, even when such models are developed, the equipment manufacturers are unable to leverage these advances due

to the lack of a framework for transferring technology. Vast differences in the computational tools used in academia and industry, coupled with intellectual property problems, prevent a rapid transfer of technology. Here, these three issues are comprehensively addressed using a joint experimental/computational program.

The approach here is three-fold: (1) apply a hierarchical model validation approach, including developing a database for jet-flames-in-cross and flashback in a swirl combustor, (2) develop a comprehensive computational model using advanced combustion theory in order to describe flame-turbulence interactions, and (3) prepare an open source based computational framework that will ensure rapid transfer of technology.

Results

A flashback experiment has been designed. The solid computer aided design model is shown in exploded view in Figure 1a. Fuel is introduced through a central tube and is injected through holes in the swirl vanes (Figure 1b). The air is passed through the swirler and the fuel and air mix in the premix section. The gases then expand into the combustion section where they burn. Detailed mechanical drawings suitable for use by machinists have been made, and details are being worked out of the gas supply system.

Experiments are being run in the jet-flame-in-crossflow tunnel. To date, we have run a wide range of flames, using methane as the baseline, with increasing amounts of hydrogen to investigate stability limits. A sample image of a jet-flame-in-crossflow (with fuel 30% H_2 + 70% CH_4) at a jet Reynolds number of 7000 is shown in Figure 2a. Also shown in Figure 2b is the mean streamwise (crossflow direction) velocity and in Figure 2c the root mean square (RMS) streamwise velocity. The data, which were obtained with the PIV technique, are being used for validation of the LES models. These data are being used to investigate new ways to validate LES models with experimental data. In effect this process involves using the data to compute the same type of conditionally-averaged quantities that are computed by LES.

One of the critical requirements for computational models of gas turbines is the ability to describe the multiscale interactions between the turbulent flow and the combustion-related chemical reactions. In this project, a probabilistic approach, termed the probability density function (PDF) method, is used. This PDF describes the joint-scalar distribution as a spatially and temporally varying function. The PDF transport equation is high-dimensional and is typically solved using specialized numerical algorithms that rely on stochastic approaches. Since such strategies are computationally expensive, we have developed a novel Eulerian approach that could be implemented into existing computational software. This method, termed the direct quadrature method of moments (DQMOM), discretizes the PDF in composition space using a set of Dirac-delta functions. As a result, Eulerian transport equations for the position and strength (called weight) of these delta-peaks need to be solved in order to recover the moments of the PDF. This approach has been tested in canonical flow configurations as part of this project. In addition, simulations of a model combustor have been conducted to demonstrate the applicability in realistic flow configurations.

To facilitate transfer of technology, an open source platform (OpenFOAM®) has been adopted in this work. Two different research groups from GE Energy and Siemens Energy will collaborate with the University of Texas (UT) computational team in this part of the project. In this fiscal year, the UT team has worked extensively with the Siemens research team to formalize a framework for transfer. All research groups will use the open source platform for computational analysis. The UT team will deliver application packages that could be directly used with this platform. When necessary, graduate students working on this project will visit the industrial partners

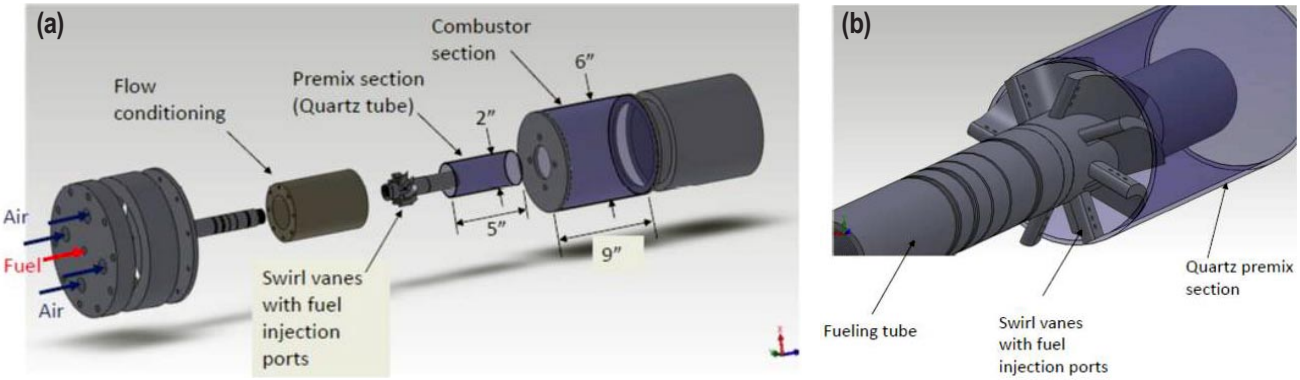

FIGURE 1. Solid model of the lean-premixed flashback rig (a) exploded view, and (b) close-up of the swirler with fuel-injection ports

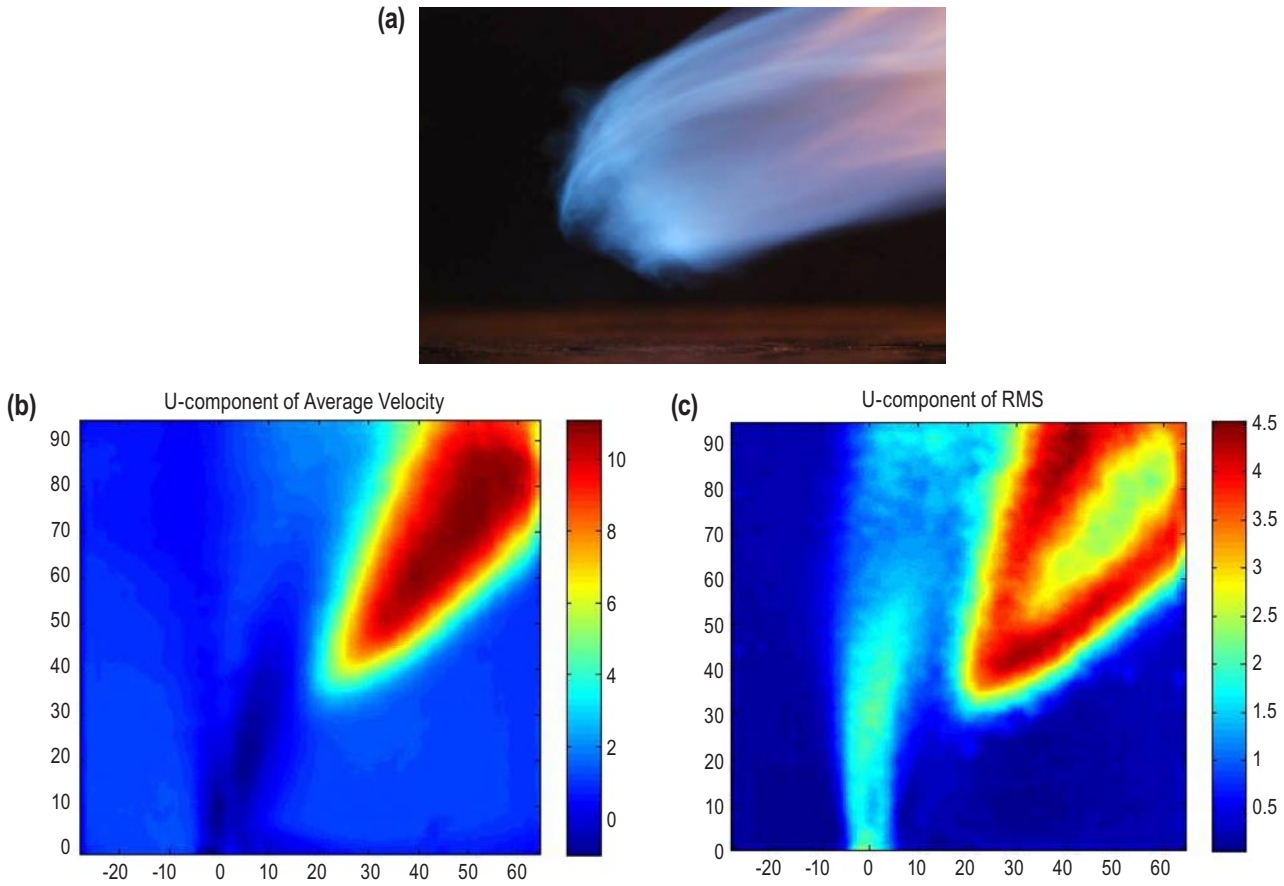

FIGURE 2. Jet-flame-in-crossflow (30% H_2 + 70% CH_4) at Reynolds number of 7,000 (a) Luminosity image, (b) Mean streamwise velocity, and (c) RMS streamwise velocity

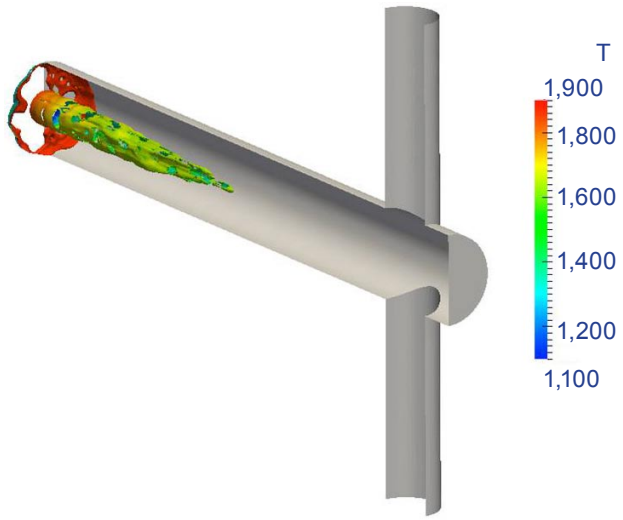

FIGURE 3. LES computation of a turbulent premixed burner; plot shows isosurface of OH mass fraction colored by temperature

to ensure that the models are being used correctly, and that the application packages have been installed without errors. In this year, we have supplied Siemens with basic combustion models to analyze gas turbine combustors. Figure 3 shows sample LES calculation of an experimental premixed burner using this open source software.

Conclusions and Future Directions

A new lean premixed swirl flame facility has been designed to study flashback dynamics. By the next reporting period, this facility will be operational and measurements made of the unsteady flame propagation by using high-speed imaging. In addition, jet-flames-in-crossflow are being used to provide validation data of complex flow-flame interactions. The next step will be to change the geometry by pitching the jet in the streamwise direction. Pitching the jet reduces the size of the recirculating flow and therefore changes the flameholding characteristics, which provides a severe challenge for the LES models. Planar laser-induced fluorescence of OH will be used in addition to the PIV measurements.

The models developed here require extensive validation, which is being carried out with the experimental program discussed above. In addition, the

effect of turbulent boundary layers on flame propagation needs to be studied. For this purpose, we have initiated collaboration with Dr. Jackie Chen at Sandia National Laboratories, who will provide high-resolution direct numerical simulation data of flame interaction with wall-bounded flows.

FY 2012 Publications/Presentations

1. C. Lietz, P. Donde, V. Raman, S. Martin, "Large Eddy Simulation/Eulerian Probability Density Function Approach for Simulating Hydrogen-Enriched Gas Turbine Combustors," Accepted for publication in the Proceedings of the ASME Turbo Expo, Copenhagen, Denmark, June 2012.

References

1. C. Lietz, P. Donde, V. Raman, S. Martin, "Large Eddy Simulation/Eulerian Probability Density Function Approach for Simulating Hydrogen-Enriched Gas Turbine Combustors," Accepted for publication in the Proceedings of the ASME Turbo Expo, Copenhagen, Denmark, June 2012.

V. UNIVERSITY TURBINE SYSTEMS RESEARCH

C. Materials

V.C.1 Computational Design and Experimental Validation of New Thermal Barrier Systems

Shengmin Guo
Louisiana State University and A&M College
Department of Mechanical Engineering
Baton Rouge, LA 70803
Phone: (225) 578-7619
Email: sguo2@lsu.edu

DOE Project Manager: Patcharin Burke
Phone: (412) 386-7378
Email: Patcharin.Burke@netl.doe.gov

Subcontractors:
Drs. Shizhong Yang and Ebrahim Khosravi
Southern University, Baton Rouge, LA

Contract Number: FE0004734

Start Date: October 1, 2010
End Date: September 30, 2013

Fiscal Year (FY) 2012 Objectives

- Cr-Y/Ta bond-coat potential building and computer simulation.
- Ta:YSZ top-coat potential building and computer simulation.
- Bond coat and top coat sample preparation.

FY 2012 Accomplishments

- Tested the potential code on Cr-Cr and Cr-Y systems and performed *ab initio* density functional theory (DFT) based simulation on dilute Cr-Y system under stress up to 36 GPa. The result shows that the evenly distributed Y-doped dilute Cr-Y alloy has a bulk modulus of 233 GPa, and the Y atom loses an average 0.3 electron to the nearest neighboring Cr atoms. Preliminary molecular dynamics (MD) simulation on Cr-Y system shows that at high temperature, other elements, for example Mo, may be needed to further improve the stability.
- *Ab initio* molecular dynamics simulation on the Ta doped YSZ (Ta :Y=1 :1) was performed. The system is found to be stable at a temperature as high as 1,350°C. The reflectivity at (111) direction is the highest with a value of 65% on the 10 eV position, increasing in the order of $n_{(100)} < n_{(110)} < n_{(111)}$.
- Design and fabrication of the thermal barrier coating (TBC) durability testing rig have been completed.
- Bond coat and top coat samples have been prepared, and hot corrosion tests on TBC samples have been performed.

Introduction

TBC systems are key components to safeguard modern gas turbine engines against significant temperature extremes and degradation. In order to develop reliable syngas-powered gas turbine power systems, such as integrated gasification combined cycle (IGCC) plants, robust TBCs must be developed to overcome material degradations (corrosion, erosion, and deposition) due to the usage of high hydrogen content syngas.

With current theoretical simulation tools and computer hardware power, material static and dynamic properties can only be investigated on very small scales (nano-size or smaller), thus not adequate for complicated high performance TBC design. The goal of this research project is to develop a novel TBC design tool, based on the integration of *ab initio* DFT method with classical MD method. Using high performance computing (HPC) simulation and experimental validation, we will demonstrate that new TBCs, which can withstand next IGCC environments, can be designed by using this novel computational material design tool. To support and validate the code development effort, experimental work on TBC samples will be performed.

Approach

Current studies on TBCs are usually performed by trial and error approach. By altering the bond coat and top coat compositions, new TBC materials can then be tested for mechanical, physical and chemical properties. As the trial and error process is usually very expensive and time consuming, in this proposal, we are developing a high performance TBC with enhanced top and bond coat through a reliable and efficient theoretical/computational approach, which can be used systematically to identify the promising TBC bond coat and top coat compositions. Using HPC simulations, an ab initio MD-based design method can screen and identify TBC systems with desired physical properties. We will demonstrate our new TBC systems experimentally under IGCC environments.

Results

We revised our atomic and solid *ab initio* quantum mechanical code to calculate the inter-atomic interaction energy terms in Shödinger equation. The performance of classical molecular dynamics packages/codes are tested in Louisiana Optical Network Initiative high performance computing facility. For dilute Y doped Cr-Y nanocrystal, we performed both *ab initio* DFT simulation and experimental tests under stress. The data measured from the synchrotron X-ray diffraction experiments show that the Cr-Y crystal structure is stable under a pressure up to 36 GPa when compressed. A fit to the Birch-Murnaghan equation of state yields the bulk modulus of 203 GPa. No Y peaks were found which means the yttrium and the chromium atoms have been fully mixed. The first principles DFT simulation shows that the evenly distributed Y-doped dilute Cr-Y alloy has a bulk modulus of 233 GPa. Charge density analysis shows that the Y atom loses an average 0.3 electron to the nearest neighboring Cr atoms. Density of states calculation indicates *dsp* hybridization between Y and Cr atoms. The full width at half maximum broadening at (211) shows a main plastic stain exists, while the data at (110) plane shows it is a slip plane. This study shows the capability of the computational materials code for material property predications.

For Ta and Y 1:1 doped YSZ system, we simulated the bulk phase of 1:1 Y and Ta doped cubic zirconia through *ab initio* MD simulation. In our DFT calculations, the electronic and optical properties of the ZrO_2-$YO_{1.5}$-$TaO_{2.5}$ system are implemented using local density approximation (LDA). We used the Vienna Ab-initio Simulation Package (VASP) with 350 eV as plane wave cutoff and frequency dependent dielectric matrix. The Ta-Y-ZrO_2 system is modeled using crystal containing up to total 108 atoms, 36 doped atoms (Ta and Y), and 24 zirconium atoms. The physical property of the system is analyzed and summarized. We found that the Ta-Y co-doped ZrO_2 is stable and the reflectivity at (111) direction reaches 65% at 10 eV.

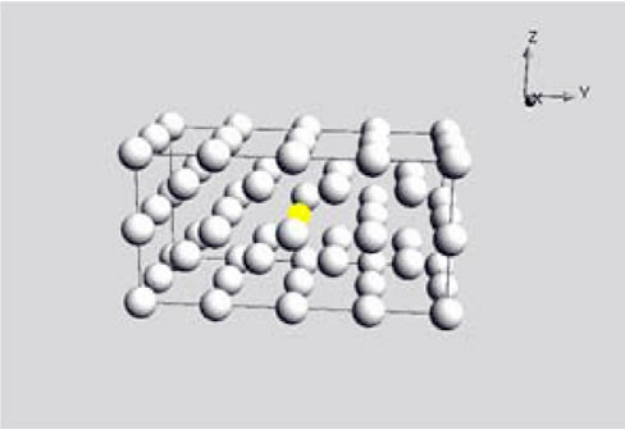

FIGURE 1. Model for simulation: the yellow ball stands for Y atom while the gray balls stand for Cr atoms

The construction of the TBC testing rig has been completed. Graduate assistants have been trained to operate our plasma spray system for preparing TBC samples, to conduct hot corrosion evaluations, and to perform material characterizations. For training purposes, nickel-based superalloy (Inconel 738) disks of Φ25×1.5 mm were employed as the substrates. TBCs with a ceramic top coating and a NiCrAlY bond coat (Amdry 9625, Sulzer Metco, particle size 45~75 μm) were deposited onto the superalloy substrates by the atmospheric plasma spray (APS) process. Three types of top coats, YSZ, 50 wt% YSZ + 50 wt% $Gd_2Zr_2O_7$, and $Gd_2Zr_2O_7$ were made using agglomerated powders. The plasma spraying was carried out using a Sulzer-Metco 9 MB plasma spray system with an Ar/H_2 gas mixture. To perform an accelerated high-temperature hot corrosion test on TBCs, a mixture of Na_2SO_4 + V_2O_5 deposit was spread onto the surfaces of the TBC specimens with a salt amount of 20 mg/cm^2. After each 4 hours of testing at 1,050°C, the samples were allowed to cool down, and then the coatings were inspected. The samples were then recoated with the Na_2SO_4 + V_2O_5 salt mixture and the heating profile was repeated until the failure of the coatings. After hot corrosion testing, detailed material characterizations were performed. The chemical interactions and the induced phase transformation are the primary factors for degradation and spallation of the conventional YSZ and $Gd_2Zr_2O_7$ coatings. Based on the degradation rate, the corrosive layer thickness, and the general status of the coating after hot corrosion, $Gd_2Zr_2O_7$ containing coatings have a better hot corrosion resistance at a temperature of 1,050°C than that of YSZ coatings.

Conclusions and Future Directions

In 2012 fiscal year, we updated our MedeA package and it is fully functional in our SUN server. The performance of several related classical MD codes are tested. We confirmed that Y can be efficiently mechanically alloyed with Cr metal and stable under a stress up to 36 GPa. A strong hybridization is found among the 4p orbitals of Cr, 4d orbitals and 5p orbitals of Y. At nano-scale, the plastic deformation is found at (211) face. In Ta and Y 1:1 doped YSZ simulation, it is found that the cubic lattice structure is stable at a high temperature up to 1,350°C.

In the next fiscal year, we will:

1. Continue to perform bond coat screening using MD method simulation to screen out the candidates.

2. Screen out the top coat that matches the bond coat and remains stable under high temperature.
3. Prepare and evaluate TBC systems identified in the simulation.

FY 2012 Publications/Presentations

1. Jialin Lei, Bin Chen, Shengmin Guo, Kaiyang Wang, Ebrahim Khosravi, Jinyuan Yuan, Selva Vennila Raju, and Shizhong Yang, "Stability and Stiffness of Dilute Yttrium Doped Chromium Crystal under Axial Stress," to be submitted to Physical Review Letters.

2. Lei Zhao, Shizhong Yang, Ebrahim Khosravi, and Shengmin Guo, "Cr Based Alloy Cr-Y Oxidation Study from First Principles Molecular Dynamics Simulation," *Materials Science & Technology* 2011.

3. Lei Zhao, Shizhong Yang, and Ebrahim Khosravi, "Cr based Alloy Cr-Y-Mo-W Oxidation Study from First Principles Molecular Dynamics Simulation," APS March 2012 Meeting, Boston, Massachusetts.

4. M.H. Habibi, Li Wang, and S.M. Guo, "Evolution of Hot Corrosion Resistance of YSZ, $Gd_2Zr_2O_7$, and $Gd_2Zr_2O_7$+YSZ Composite Thermal Barrier Coatings in $Na_2SO_4+V_2O_5$ at 1050°C," *Journal of the European Ceramic Society,* 10.1016/j.jeurceramsoc.2012.01.006

V.C.2 Advanced Thermal Barrier Coatings for Operation in High Hydrogen Content-Fueled Gas Turbines

Sanjay Sampath (Primary Contact),
Christopher Weyant
Stony Brook University
130 Heavy Engineering
Stony Brook, NY 11794
Phone: (631) 632-9512; Fax: (631) 632-7878
Email: Sanjay.Sampath@stonybrook.edu

DOE Project Manager: Briggs White
Phone: (304) 285-5437
Email: Briggs.White@netl.doe.gov

Contract Number: FE0004771

Start Date: October 1, 2010
End Date: September 30, 2013

Fiscal Year (FY) 2012 Objectives

- Development of optimum bond coat (BC) layer with adequate roughness to provide good adhesion with top coat.
- Start developing and evaluating the multi-layer top coat (TC) architecture for high temperature application.
- Development of erosion resistant Gd_2ZrO_7 (GDZ) top layer for multilayer thermal barrier coating (TBC) scheme.
- Development of gradient thermal conductivity model for plasma sprayed GDZ.
- Evaluation of GDZ coatings for their resistance to infiltration of lignite ash at high temperature.

FY 2012 Accomplishments

- An optimal BC deposition condition was successfully developed practicing two-layered BC deposition scheme. A thin (~50 µm) BC layer was deposited using a relatively coarse particle size powder on a dense BC layer deposited using a fine particle size powder. The post deposition roughness of the BC ranged from 7.9 to 8.5 Ra, which is significantly higher than the roughness achieved in previous trials of BC deposition. The new BC which is under evaluation for its adhesion requirement with TC.
- Demonstrated a successful bi-layer TC deposition of yttria-stabilized zirconia (YSZ) and GDZ coating utilizing coating compliance map for process parameter selection. The furnace cycle test (FCT) of three such bi-layer TC showed differences in coating spallation lives indicating that individual layer's porosity is a critical characteristic for overall bi-layer TC life.
- Completed the process parameters optimization for development of erosion-resistant GDZ coating for top layer. The erosion rate measured (ASTM G76) for this coating was 0.7 g/kg, which was significantly lower than standard YSZ layer (2.5 g/kg).
- Completed the development of one dimensional (1D) gradient thermal conductivity for plasma sprayed GDZ. The model demonstrates the increase (50°C) in BC-TC interface temperature with 100 hours exposure of a two layer (YSZ-GDZ) TC at 1,400°C. The model will be used to optimize the layer thickness for multilayer TBC architecture.
- Investigated the GDZ coatings' resistance against lignite ash environments at 1,200°C for three different coatings porosity cases. The results show that the lignite penetration depth was similar (~100 µm) for all the three coatings cases.

Introduction

The Center for Thermal Spray Research (CTSR) at Stony Brook University in partnership with its industrial Consortium for Thermal Spray Technology is investigating science and technology related to advanced thermally sprayed metallic alloy bond coats and ceramic TBCs for applications in the hot section of integrated gasified combined cycle (IGCC) turbine power systems. The current state of art with traditional TBCs will not likely be suitable in IGCCs due to demand of higher operating temperature, which not only will require lower sintering rate and phase stability but also will accelerate hot corrosion degradation phenomenon. Many solutions have been considered to meet the challenging performance objectives in the IGCC environments. Advanced coatings provide a solution to combat the several degradation challenges along with improvements in performance needed for higher temperature operating environments. Coatings are and have been an economic means to extend the life of expensive structural superalloys.

Great advances in process science and control, and relation of process to microstructure and properties

have been achieved in the last decade in particular for YSZ-based materials [1-14]. This achievement is an underlying reason for improved confidence in thermal spray coatings, and this science-based philosophy is taking root in industry. The current strategy to design a protective layer for substrate consists of development of a multilayer coating architecture, where the different layers will be optimized to withstand different environmental challenges for higher temperature. In conjunction with our original equipment manufacturer partners (GE and Siemens) and through a strategic partnership with Oak Ridge National Laboratory (ORNL) (materials degradation group and high temperature materials laboratory), a systems approach, considering all components of the TBC (multilayer ceramic top coat, metallic bond coat and superalloy substrate) is being taken during multi-layered coating design, process development and subsequent environmental testing. Recent advances in process science and advanced in situ thermal spray coating property measurement enabled within CTSR has been incorporated for full-field enhancement of coating and process reliability. TBCs developed in this project will enable increased temperatures in IGCC turbines contributing to the efficiency goals of the Hydrogen Turbine Program.

Approach

The current state-of-the-art of TBCs (YSZ) is limited for survival under the extreme temperature and environmental conditions in the hot section of IGCC engines. The goal of this project is to design a multilayer TBCs system which includes layers of YSZ along with some new potential TBC materials, known for their lower thermal conductivity (*K*), sintering and molten ash resistance. One part of this multilayer TBC design is to develop an oxidation resistant BC, which, specifically, withstands high H_2O content environment at high temperature with longer durability. The approach taken here is to first develop individual layers to meet different requirements, such as erosion, molten ash, BC compatible TC layer, BC with adequate roughness and overall mechanical compliance of the structure.

For development of multilayer TC to meet different requirements, it is important to develop a detailed understanding of individual layers. A process map approach has been utilized to produce such monolithic layers. In addition, a basic correlation between process and properties for YSZ and GDZ materials has been being established, which will guide the selection of an optimum coating microstructure for a particular coating. The next step towards multilayer coating is to investigate the mechanical and thermal compatibility of a YSZ-GDZ bi-layer coating. Based on the understanding of process-property relationships of YSZ and GDZ, the property of each monolithic coating can be individually improved by selecting an optimal process condition. However, compatibility for multilayer coatings remains an issue. Therefore, currently a batch of three bi-layer coatings with significantly different microstructures is being evaluated for their layers' compatibility. Based on the performance of these bi-layers under different characterization procedures, the processing conditions for each layer will be optimized.

Results

A key task for the program is to develop the process parameters for an optimum BC layer. Previous results suggest that for a long topcoat spallation life the adhesion between TC and BC is critical and can be improved by optimizing the BC surface roughness. Therefore, in order to provide adequate BC roughness, a new strategy of two layer bond coat deposition has been adopted, where the first layer (~100 µm) is deposited using fine powder on the substrate, and the second one (~50 µm) using coarse powder on the first layer (Figure 1a). Two process parameters, spray distance and plume enthalpy (fuel-to-oxygen ratio), were varied to produce the various combinations of the layers. The spray distance allows different particle dwell time in plume which controls the resultant melting and velocity of particle. On the other hand, the plume enthalpy controls the heat and momentum transfer from the plume to the particles. These two parameters are found to be sufficient to provide a wide range of coating microstructures. For all the two layer BCs, NiCoCrAlYHfSi composition (Sulzer Metco AMDRY 386-x) powder was used. Fine powder and coarse powder particle distributions (mean particle size 32.31 µm and 62.7 µm) were used to produce oxidation resistant dense BC and rough surface roughness respectively.

Figure 1b shows the optimum two-layer BC microstructure down-selected from various trials. As it can readily be observed that Layer 1 was sufficiently dense and Layer 2 produces a surface roughness (Ra) ranging from 7.9 µm to 8.5 µm, which is significantly higher than the roughness produced only by Layer 1 (3.1–4.5 µm). In addition, the microstructure also exhibits a good splat welding between Layer 1 and Layer 2, which is an implication of high quality bonding between the two layers. This optimized condition is being used for further characterizations such as oxidation behavior in dry and moist environments.

One of the many requirements for the multilayer TC structure is to develop an erosion resistant GDZ layer, which would be the top layer in the multilayer structure. GDZ has been reported for poor erosion resistant material as compared to traditional YSZ. The intrinsic

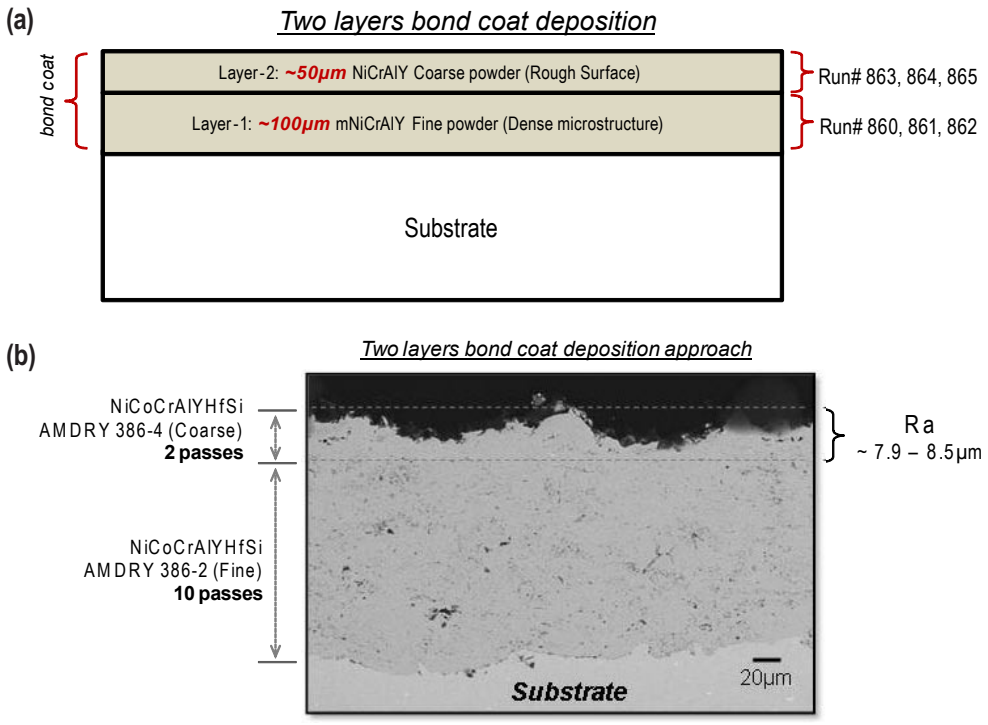

FIGURE 1. (a) The schematics showing two layer bond coat deposition scheme adapted to produce higher surface roughness for adequate topcoat-bond coat adhesion. (b) The optimal microstructure of a two layer bond coat. The surface roughness obtained was 7.9–8.5 µm Ra.

low fracture toughness of the material can be attributed to its poor performance against erosion. However, the performance of GDZ coating can be improved by modifying the coating microstructure via process control. Figure 2 shows the results of four GDZ coating along with a standard YSZ coating. The names low, med, high, and ultra high correspond to the plasma plume enthalpy conditions, with low being cooler and ultra high being the hottest plasma condition producing high and low coating porosity respectively.

Figure 2 shows the erosion test (American Society for Testing and Materials [ASTM] G76) results of the coatings. All the GDZ coatings sprayed using coarse powder with different plasma conditions exhibit poor erosion performance as compared to YSZ coatings. GDZ coating sprayed with high plasma condition shows better erosion resistance as compared to the low and med condition GDZ coatings; however it is still poorer than the YSZ coating. This suggests that the erosion properties of coatings can be modified by processing parameters. Interestingly, a GDZ coating sprayed with ultra high plasma condition using fine powder, which produces a very dense coating, exhibits the lowest erosion rate among all the coatings, including the YSZ coating. This can be attributed to the very good splat welding and high density of the coating. However, due to very high density, the coating does not meet the mechanical compliance requirement for TC. A new experimental design is being considered to explore and optimize a process condition which can produce a coating with high erosion resistance and sufficient compliance.

As a part of multilayer coating evaluation, a simple 1D thermal conductivity and sintering model has been developed to investigate increase in temperature at BC-TC interfaces. The model is based on heat flux balance through thickness of layer or coatings, and it utilizes Larson Miller parameter (LMP) to calculate the effective thermal conductivity (K) at different high temperature exposure time. The LMPs of different ceramic topcoat materials/microstructures have been calculated and reported previously in this program. If the TC surface and starting BC-TC interface temperatures (T_{sur} and T^{o}_{int}) are known, the model is able to predict the change (increase) in the interface temperature (T_{int}) for a given exposure time. The robustness of this model is still under evaluation; however some preliminary calculation are as follows.

For a constant thickness of coating and exposure condition at T_{sur} =1,400°C and T^{o}_{int} =1,100°C, T^{o}_{int} increases by ~30°C after 10 hours of exposure and remains almost constant for up to 100 hours of exposure. On the other hand, for the YSZ coating with similar thickness as compared to GDZ, the T^{o}_{int} keeps on rising by ~60°C, 90°C, and 100°C for 10, 50, and 100 hrs of

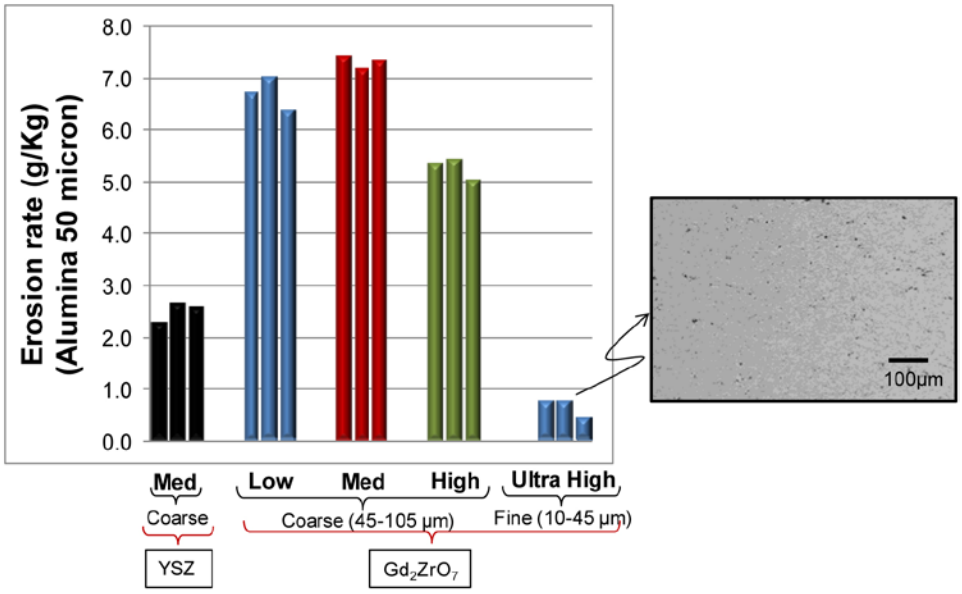

Figure 2. Erosion rates of GDZ coatings fabricated using different process conditions and powder particle size distributions. For reference the measurement on a standard YSZ coating is also shown. Coating sprayed using fine powder cut at very high plasma condition exhibited erosion performance better than the standard YSZ coating.

exposure respectively. It is very well known that GDZ has both lower sintering rate as well as *K*, which explains the lower increase in T_{int} with GDZ coating as compared to YSZ coating.

This 1D model can be extended to multilayer coating design as well. It has been calculated that for a bi-layer TC with identical layer thicknesses of GDZ and YSZ coatings, the T_{int} increases by ~50°C with 100 hrs of exposure with aforementioned conditions (Figure 3). In addition, the temperature at the layer interface can also be estimated.

Though the results obtained from this model are limited, they provide an opportunity to estimate the T_{int} for different coating architecture without having them sprayed. Currently, this model is being practiced to optimize layer thicknesses for our bi-layer TC coating developments. Further, the model will be applied for the multilayer coating architecture case with varying coating materials/microstructures.

One of the many challenges with a TC design for a higher operating temperature IGCC engine is the issue of dust/ash exposure on to TC. These foreign particles get ingested as the form of ground dust which get molten and remain stuck on the TC surface. Over a period of time at engine operating temperature, these melts reacts with and infiltrates into the TC leading to stiffening of coating, which results in coating spallation due to lack of compliance. Therefore, a parallel approach is being taken to investigate this issue in more detail, by exposing the GDZ coating to a simulated ash, lignite (provided by Prof. Nitin Padure at Brown University) at high temperatures (1,200°C). The composition of lignite ash is presented in the table below.

SiO_2	CaO	Fe_2O_3	Al_2O_3	Cr_2O_3	MgO	SO_3	TiO_2	SrO	MnO
29	25	16	14	5	3	2	1	1	1

The selection of GDZ material for this project was also made based on its excellent calcium magnesium alumina silicate (CMAS)/ash resistant characteristics reported in literature [15-16]. The material reacts with molten ash at early stages and forms a compound which stops further infiltration of molten ash. During this project, we have investigated the porosity dependent ash resistance of GDZ coatings. Figure 4 shows three GDZ-YSZ layer coatings, which were fabricated by spraying each layer at low, med and high plasma conditions to introduce different porosity levels in the coatings. A thin layer of the synthetic lignite ash was uniformly spread on each GDZ layers of the three coatings, and specimen was exposed to 1,200°C. It is surprising to observe that the infiltration/reaction zone depth was similar (~100 µm) for these three coatings with different porosities. This experimental result sheds light on two points: first is that the reaction zone doesn't seem to depend on the porosity, and second is that the minimum thickness required for GDZ layer should be ~100 µm in order to prevent any reactions with underneath layers. This information is being kept in mind for layer thicknesses optimization for future multilayer TC.

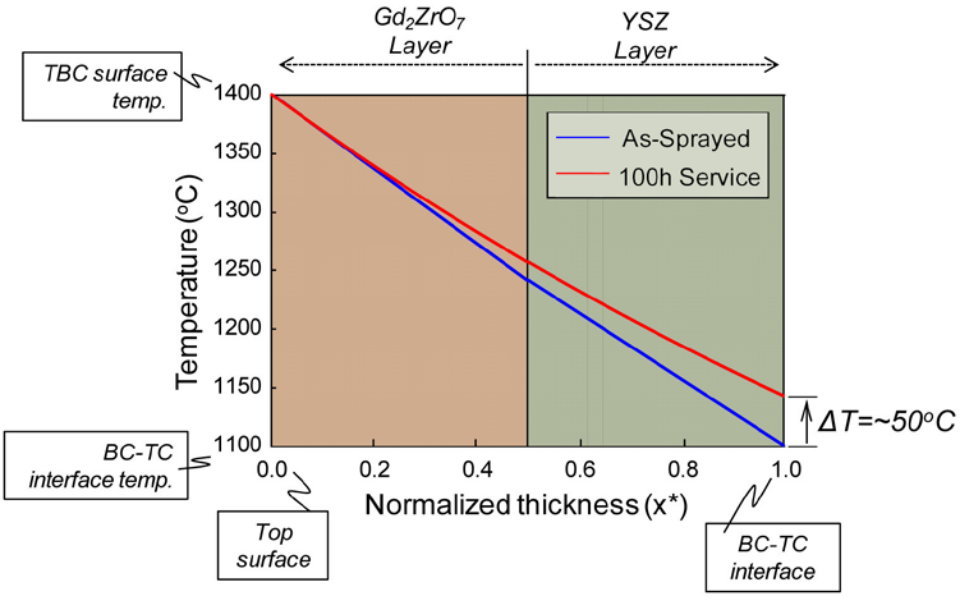

FIGURE 3. 1D thermal conductivity model to evaluate BC-TC interface temperature with 100 hrs of thermal exposure of a GDZ-YSZ bi-layer coating. The increase in the interface temperature is observed to be ~50°C.

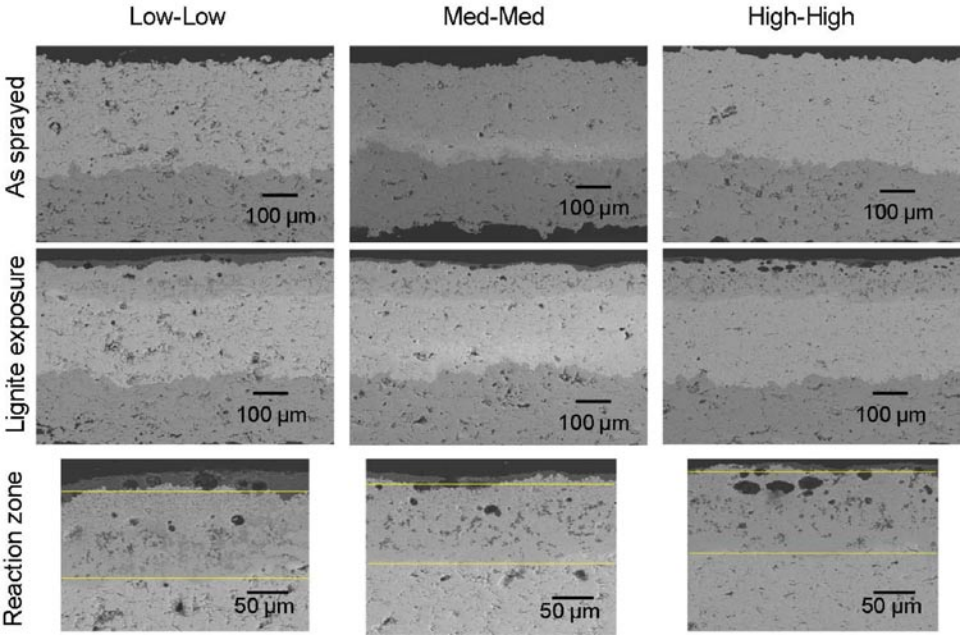

FIGURE 4. Lignite ash exposure of three bi-layers with different porosity levels for 24 hours at 1,200°C. The reaction zone depth is similar for all the three cases (~100 µm).

Conclusions and Future Directions

A two layer BC deposition scheme has been utilized to produce a BC with adequate surface roughness. The scheme consists of deposition of dense BC layer using fine NiCrAlYHfSi powder followed by a thin layer deposited using coarser powder. After several coating trails, an optimal BC coating has successfully been obtained with surface roughness of 7.9–8.5 µm Ra. The coating also exhibits limited porosity in its dense layer, which is important for good high temperature oxidation resistance of BC. The coating life of the TC deposited on this BC is being evaluated.

A study on GDZ coating shows that the erosion resistance of GDZ coating, in general, is lower than YSZ coatings; however a denser GDZ coating exhibits slightly improved erosion performance. It is also observed that changing feedstock powder to fine particle size helps improve the erosion resistance of GDZ coating significantly, primarily due to very high density produced by finer powder, although the mechanical compliance of such coating needs to be tailored by tuning the process parameters. Efforts are being made in this direction by developing a separate process map for fine GDZ powder similar to one developed for coarse GDZ powder.

An analytical model developed for estimating the BC-TC interface temperature has successfully been demonstrated and applied to monolithic GDZ and YSZ coatings. The model was able to capture the differences in interfacial temperature due to differences in coatings' thermal properties, such as *K* and sintering rate. As a preliminary attempt, the model has been applied for bi-layer coatings to evaluate its limitations and capabilities.

The lignite exposure of GDZ coatings with different porosity levels shows similar infiltration depth of molten ash in the coatings at high temperatures. The total reaction zone depth for these coatings is approximately 100 μm.

Lessons learned in past two fiscal years continued providing insights as well as possible solutions for the challenges with the development of new TBCs. Future work at CTSR under this project will include various system level testings such as a furnace cycle test at Siemens' facility, fracture toughness characterization of TC at ORNL's high temperature material testing facility, concurrent evaluation of BC oxidation at ORNL's material degradation group and at CTSR. In addition, other potential TBC materials, such as four different compositions of NASA co-doped zirconia, etc., will be explored as one of the layers of our proposed multilayer TC design.

FY 2012 Publications/Presentations

1. S. Sampath, "Advanced Thermal Barrier Coatings for Operation in High Hydrogen Content Fueled Gas Turbines," presentation at the University Turbine Systems Research Workshop, Ohio State Univeristy, October 26, 2011.

2. C. Weyant, G. Dwivedi, and S.Sampath, "Ceramic Coatings: Process to Performance, Advanced Thermal Barrier Coatings," presentation at the Consortium for Thermal Spray Technology bi-annual meeting, Stony Brook University, June 8, 2011.

3. S. Sampath, "Advanced Multilayer Thermal Barrier Coatings," presentation at the Consortium for Thermal Spray Technology bi-annual meeting, GE Learning Center, Cincinati, Ohio, November 17, 2011.

4. S. Sampath, "Multilayer Systems: Microstructure and Property Control by Thermal Spray," Winter Workshop on High Temperature Coatings , University of California , Santa Barbara, California, January 2012.

5. S. Sampath, "Ceramic Coatings: Processing to Performance, Part-1," presentation at the Consortium for Thermal Spray Technology bi-annual meeting, Stony Brook University, June 7, 2012.

6. G. Dwivedi, S. Sampath, "Ceramic Coatings: Processing to Performance, Part-2," presentation at the Consortium for Thermal Spray Technology bi-annual meeting, Stony Brook University, June 7, 2012.

References

1. L. Li, A. Vaidya, S. Sampath, H. Xiong, and L. Zheng, "Particle Characterization and Splat Formation of Plasma Sprayed Zirconia," *Journal of Thermal Spray and Technology*, 15, 97-105 (2006).

2. T. Streibl, A. Vaidya, M. Friis, V. Srinivasan, and S. Sampath, "A Critical Assessment of Particle Temperature Distributions During Plasma Spraying: Experimental Results for YSZ," *Plasma Chemistry and Plasma Processing*, 26, 73-102 (2006).

3. E. Turunen, T. Varis, S-P. Hannula, A. Kulkarni, J. Gutleber, A. Vaidya, S. Sampath, and H. Herman, "On the Role of Particle State and Deposition Procedure on Mechanical, Tribological and Dielectric Response of High Velocity Oxy-Fuel Sprayed Alumina Coatings," *Mater. Sci. & Eng.* A415, 1-11 (2006).

4. H.B. Xiong, L.L. Zheng, L. Li, and A. Vaidya, "Melting and Oxidation Behavior of In-Flight Particles in Plasma Spray Process," *Int. J. Heat and Mass Transfer*, 48, 5121-5133 (2005).

5. A. Vaidya, V. Srinivasan, T. Streibl, M. Friis, W. Chi, and S. Sampath, "Process Maps for Plasma Spraying of Yttria Stabilized Zirconia: An Integrated Approach to Design, Optimization and Reliability," *Mater. Sci. & Eng.* A497, 239-253 (2008).

6. S. Sampath, V. Srinivasan, A. Vaidya, A. Gouldstone, Y. Liu, and T. Nakamura, "Sensing, Control, and In situ Extraction of Coating Properties: An Integrated Approach towards Establishing Process Maps," *J. Thermal Spray Tech*. 18(2) 243-255 (2009).

7. A. Kulkarni, A. Vaidya, A. Goland, S. Sampath, and H. Herman, "Processing Effects on Porosity Property Correlations in Plasma Sprayed Yttria-Stabilized Zirconia Coating," *Mater. Sci. Eng.* A359, 100-111 (2003).

8. A.J. Allen, J. Ilavsky, G.G. Long, J.S. Wallace, C.C. Berndt, and H. Herman, "Microstructural Characterization of Yttria-Stabilized Zirconia Plasma-Sprayed Deposits Using Multiple Small-Angle Neutron Scattering," *Acta Mater.*, 49, 1661 (2001).

9. A. Kulkarni, Z. Wang, T. Nakamura, S. Sampath, A. Goland, H. Herman, A.J. Allen, J. Ilavsky, G. Long, J. Frahm, and R.W. Steinbrech, "Comprehensive Microstructural Characterization and Predictive Property Modeling of Plasma-Sprayed Zirconia Coatings," *Acta Mater.,* 51, 2457 (2003).

10. W. Chi, S. Sampath, and H. Wang, "Microstructure-Thermal Conductivity Relationships in Plasma Sprayed Yttria Stabilized Zirconia," *J. American Ceramic Society*, 91(8) 2636-2645 (2008).

11. Y. Liu, T. Nakamura, A. Valarezo, G. Dwivedi, and S.Sampath, "Anelastic Behavior of Plasma Sprayed Zirconia Coatings," *J. American Ceramic Society*, 91(12) 4036-4043 (2008).

12. J. Matejicek and S. Sampath, "In Situ Measurement of Residual Stresses and Elastic Moduli in Thermal Spray Coatings-Part 1: Apparatus and Analysis," *Acta Mater.*, 51, 863-872 (2003).

13. Y. Tan, J. Longtin, S. Sampath, and H. Wang, "Effect of Starting Microstructure on Thermal Properties of As-Sprayed and Thermally Exposed Plasma Sprayed YSZ Coatings," *J. American Ceramic Society*, 92(3) 710-716 (2009).

14. W.B. Choi, Y. Wu, S. Sampath, and A. Gouldstone, "Modified Indentation Technique to Probe Inelasticity in Ni-5%Al Coatings from Different Processes," *J. Thermal Spray Tech*. 18 (1) 65-74 (2009).

15. A. Aygun, A.L. Vasiliev, N.P. Padture, and X.Q. Ma, "Novel Thermal Barrier Coatings to High-Temperature Attack that are Resistant Glassy Deposits," *Acta Mater.* 55, 6734-6745, doi:DOI 10.1016/j.actamat.2007.08.028 (2007).

16. Xi Chen, "Calcium–Magnesium–Alumina–Silicate (CMAS) Delamination Mechanisms in EB-PVD Thermal Barrier," Coatings, Surface and Coatings Technology, Volume 200, Issue 11, March 15, 2006. Pages 3418-3427

V.C.3 An Alternative Low-Cost Process for Deposition of MCrAlY Bond Coats for Advanced Syngas/Hydrogen Turbine Applications

Ying Zhang
Department of Mechanical Engineering
Tennessee Technological University
TTU Box 5014, 115 W. 10th Street
Cookeville, TN 38505-0001
Phone: (931) 372-3265
Email: yzhang@tntech.edu

DOE Project Manager: Patcharin Burke
Phone: (412) 386-7378
Email: Patcharin.Burke@netl.doe.gov

Contract Number: FE0007332

Start Date: September 12, 2011
End Date: September 11, 2014

Fiscal Year (FY) 2012 Objectives

- Complete selection and procurement of substrate alloys and electro-codeposition supplies.
- Prepare the Cr-Al-Y alloy powder (via arc melting and subsequent ball milling) needed for electro-codeposition of MCrAlY coatings.
- Start electro-codeposition experiments to understand the effect of deposition parameters on coating composition/microstructure.
- Establish an electro-codeposition process to synthesize MCrAlY coatings.

FY 2012 Accomplishments

- Demonstrated that the arc melting process at Tennessee Tech was able to fabricate Cr-Al-Y alloys with accurate compositional control and extremely low impurity levels (e.g., S <1 ppmw, O <21 ppmw), which is a critical step in synthesis of Cr-Al-Y powder.
- Set up an electroplating system for initial coating deposition.
- Established pure Ni baseline coatings and observed that the coating thickness increased linearly with plating time at a fixed current density.
- Started electro-codeposition experiments with Cr-Al-Y powder added in the plating solution and observed the following effects of the plating parameters (1) a linear relationship existed between the coating thickness and current density for the same plating time and (2) the coating surface roughness appeared to increase with the increase of current density.

Introduction

One of material needs for the advancement of integrated gasification combined cycle (IGCC) power plants is the development of low-cost and effective manufacturing processes for application of coating architectures with enhanced performance and durability in syngas/hydrogen environments [1,2]. Thermal spray technologies such as air plasma spray (APS) and high-velocity oxy-fuel (HVOF) are currently used to fabricate thermal barrier coating (TBC) systems for large land-based turbine components [3]. The proposed research aims at developing MCrAlY (where M = Ni, Co or a mixture of Ni and Co) bond coats via an alternative low-cost electrolytic codeposition process. In contrast to thermal spray processes, the proposed process offers advantages such as non-line-of-sight and capability of producing dense and oxide-free coatings [4,5]. Pre-alloyed CrAlY-based powders will be codeposited into a metal matrix of Ni, Co or Ni-Co during the electroplating process, which is followed by a post-plating heat treatment to form the final MCrAlY coatings.

Specific research objectives include (1) exploring a sulfur-free plating solution (to replace conventional sulfate or sulfamate plating baths) with the aim of reducing the impurity levels (particularly S) in the MCrAlY coatings, which is expected to improve the oxidation resistance; (2) co-doping reactive elements (e.g., Y+Hf or Y+Zr) into the bond coats via engineering the composition of the CrAlY-based powders to further enhance their oxidation/corrosion performance; (3) optimizing the electro-codeposition parameters using a design-of-experiment (DoE) approach to provide a fundamental understanding of the synergistic effect of multiple variables on coating microstructure/composition and coating quality; and (4) evaluating the oxidation behavior of the new MCrAlY bond coats in H_2O-containing environments and understanding their failure mechanism.

Approach

Successful development of MCrAlY bond coats via electrolytic codeposition is dependent on three synergetic steps (i) synthesis of CrAlY-based powder

with well-controlled composition and particle size, (ii) incorporation of CrAlY particles in the Ni/Co-metal matrix during the electro-codeposition process, and (iii) post-plating heat treatment to convert the codeposited layer to the MCrAlY coating with desired composition and microstructure. Since the CrAlY-based powders have specific chemical compositions and particle sizes, the strategy is to use arc melting and subsequent ball milling to fabricate the powder at Tennessee Tech, and at the same time to communicate with commercial powder suppliers to seek commercial atomized alloy powders.

To understand the effect of electro-codeposition parameters, a laboratory electroplating system was set up, and pure Ni coatings were synthesized to establish a baseline coating. Directionally-solidified (DS) Ni-based superalloy René 80 (Ni-3.0Al-14.1Cr-9.3Co-4.0W-3.9Mo-5.1Ti-0.16C-0.016B-0.02Zr, in wt.%) and 142 (Ni-6.2Al-6.8Cr-12Co-6.35Ta-4.9W-1.5Mo-2.8Re-1.5Hf-0.12C-0.015B-0.02Zr, in wt.%) were selected as the substrate alloys for initial coating development due to relatively low cost as compared to single crystals such as CMSX-4 or CMSX-486 [6]. Disc coupons (16.5 mm in diameter x 1.7 mm thick) were electro-discharge machined. Prior to electroplating, the substrates were prepared by grinding to #600 grit, followed by grit-blasting with #220 Al_2O_3 grit and ultrasonic cleaning in hot water and acetone. The edges of the specimen were slightly rounded to minimize the possibility of coating cracking that might develop at sharp discontinuities of the substrate.

A schematic illustration of the electrodeposition setup is shown in Figure 1. Pure Ni plates were used as the anodes. The specimen (cathode) was placed with an anode-to-cathode distance of ~20 mm in the Watts bath [7], which consisted of 310 g/L of nickel sulfate, 50 g/L of nickel chloride and 40 g/L of boric acid, all mixed in deionized water to 600 mL solution in a glass beaker. Once a baseline pure Ni coating was established, Cr-Al-Y alloy powder (<20 μm of average particle size) was added to the plating bath at a particle loading of 30 g/L. The bath was magnetically stirred at a speed of ~220 rpm to maintain a fresh supply of the CrAlY powder and electrolyte at the cathode surface. Codeposition was performed with a power supply (Technic Inc, GPS-1830D) in constant current mode, and the current density was varied from 1.0 to 3.0 A/dm^2. The specimens were electroplated at ~50°C and the pH was maintained at 3.0–3.5. After plating, the coated specimen was removed from the bath and rinsed in deionized water.

The composition of the arc-melted Cr-Al-Y alloy was analyzed by inductively coupled plasma-optical emission (ICP-OE) at DIRATS Laboratories. The alloy was also characterized using scanning electron microscopy (SEM) equipped with energy dispersive spectroscopy (EDS), and X-ray diffraction (XRD). Initial characterization was carried out on the electro-codeposited coatings by SEM and EDS.

Results

In general, material losses during arc melting should be controlled to ~0.1% or less, so that the compositions can be taken as the nominal ones. However, a relatively high weight loss of ~4% was noticed in the initial Cr-Al-Y alloy fabrication. This was mainly due to the presence of brittle intermetallic phases in the alloy, which led to cracking and loss of material into the arc melter chamber during the turn-overs. Improvements were

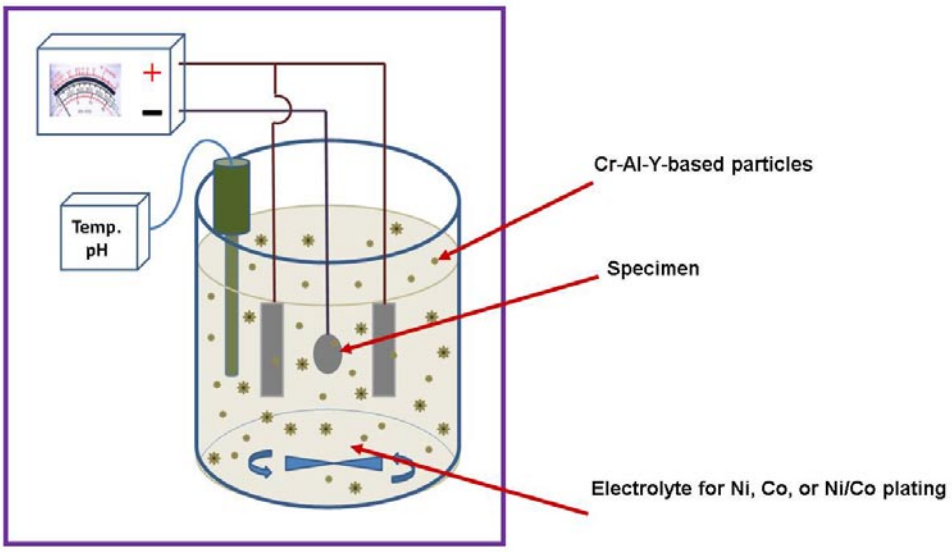

FIGURE 1. Schematic of the electro-codeposition setup

made focusing on careful control of the turn-over speed. Furthermore, after review of the Al-Y phase diagram [8], an Al-Y master alloy containing 66.7 wt.% Y was made to minimize Y oxidation and better control the Y content in the final alloy. The subsequent alloys (Table 1) showed much lower weight loss, indicating that a more accurate compositional control was achieved.

TABLE 1. Alloys synthesized using arc melting

Alloy	Measured total weight (g)		μw (g)	μw%
	Before melting	After melting		
#1	99.96	99.89	-0.07	-0.07%
#2	79.99	79.72	-0.27	-0.34%
#3	79.97	79.94	-0.03	-0.04%
#4	79.97	79.62	-0.35	-0.44%
#5	79.97	80.01	0.04	0.05%

Table 2 shows the chemical composition of a Cr-Al-Y alloy, analyzed by DIRATS Laboratories. The concentrations of the major alloying elements such as Cr, Al and Y were very close to the target composition. In addition, the levels of impurities (e.g., S and O) were extremely low due to the high purity of raw materials used in arc melting as well as the close control of the arc-melting environment.

TABLE 2. Chemical composition of the arc-melted Cr-Al-Y alloy

Elements	Target composition (wt.%)	Analysis by DIRATS (wt.%)
Cr	61.3	61.25
Al	37	37.07
Y	1.7	1.6
P	--	0.005
Fe	--	0.02
Si	--	0.02
W	--	0.02
C	--	0.0008
S	--	<0.0001
O	--	0.0021
N	--	0.0035

XRD analysis revealed that the Cr-37Al-1.7Y alloy consisted of the Cr_2Al, Cr_5Al_8 and YCr_4Al_8 phases. The SEM backscattered image and the X-ray maps of Cr, Al and Y are presented in Figure 2, further confirming the presence of three distinct phases. The phase constituents identified by XRD were consistent with the ternary Cr-Al-Y phase diagram [9].

Baseline pure Ni coatings were obtained first, using the Watts bath without the addition of Cr-Al-Y particles.

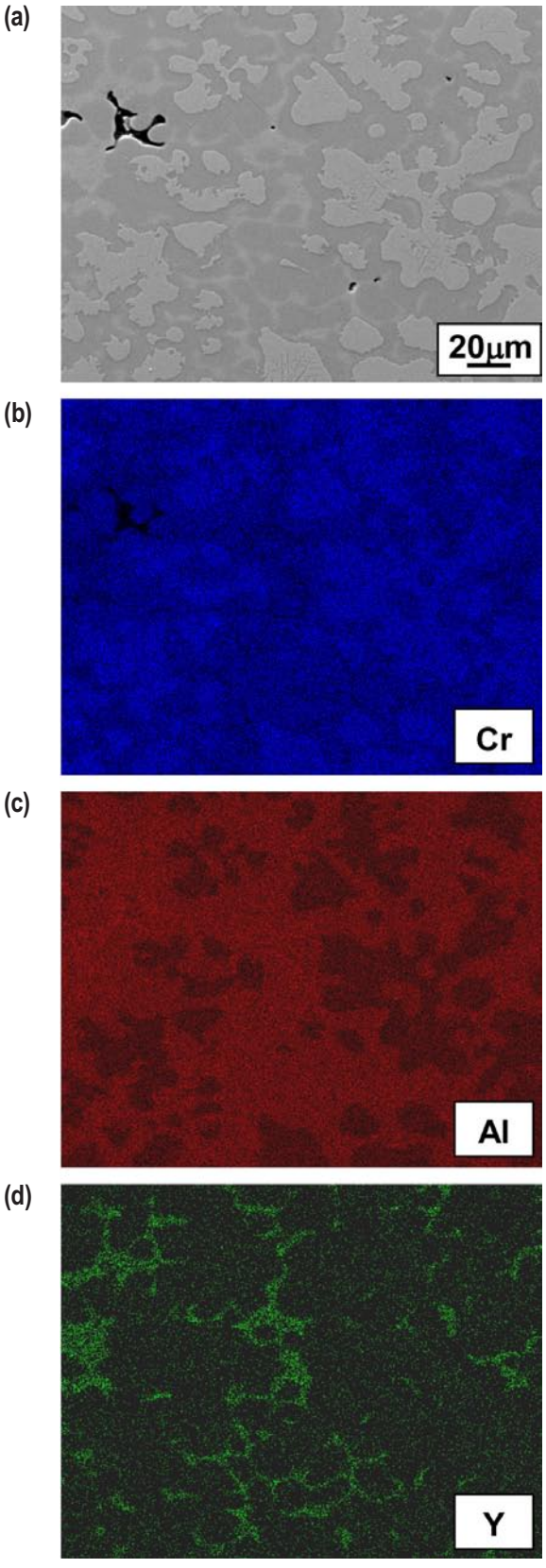

FIGURE 2. (a) Back-scattered electron image of the Cr-Al-Y alloy; (b)-(d) are SEM X-ray maps of Cr, Al, and Y, respectively

Figure 3a shows the relationship of the Ni coating thickness vs. electroplating time, with a current density of ~3.0 A/dm^2. A linear relationship was observed, and a ~45 µm thick coating was obtained after plating for 90 min.

After the baseline coating was established, electro-codeposition was conducted with the addition of Cr-Al-Y powder in the plating bath. The current density was varied from 1.0 to 3.0 A/dm^2 to investigate the effect of the current density. The coating thickness exhibited a linear increase with the increase of current density after the same plating time of 120 min (Figure 3b). Figures 4a–c show the surface morphologies of the electro-codeposited coatings plated at three different current density levels. Although the three coatings exhibited similar overall surface features, the roughness appeared to increase with the increase of current density.

Conclusions and Future Directions

Cr-Al-Y alloys with accurate compositional control and extremely low impurity levels were fabricated via arc melting, which is a critical step in synthesis of Cr-Al-Y powder, an important component used in electro-codeposition of MCrAlY coatings. XRD analysis showed that the present Cr-37Al-1.7Y alloy (in wt.%) consisted of three phases, i.e., Cr_2Al, Cr_5Al_8 and YCr_4Al_8. Pure Ni baseline coatings were established in a Watts bath, and the coating thickness increased linearly with the plating time when the current density was fixed. Initial electro-codeposition experiments were carried out with the addition of Cr-Al-Y powder in the plating bath. A linear relationship was observed between the thickness of codeposited coatings and the current density. The coating surface roughness appeared to increase with the increase of current density.

Future work on this project will include the following:

1. Optimizing the parameters of the electro-codeposition process.

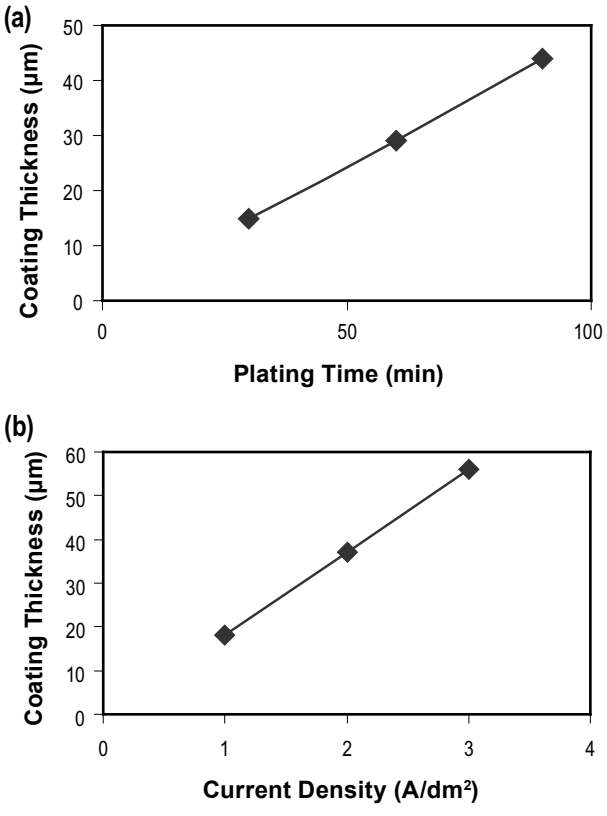

FIGURE 3. (a) Plot of pure Ni coating thickness versus plating time, without addition of Cr-Al-Y powder in the plating bath; (b) Plot of the thickness of electro-codeposited coating versus current density after 120-min plating

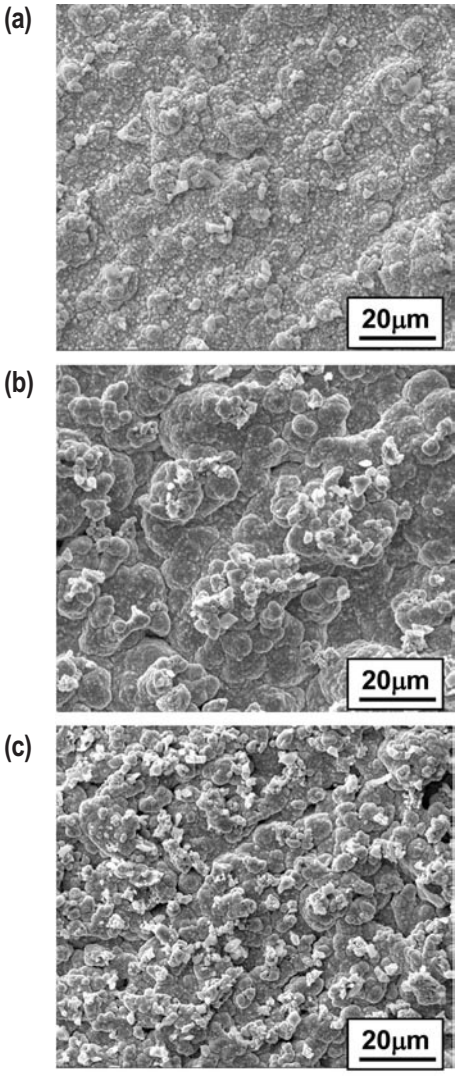

FIGURE 4. SEM surface morphology of the coatings plated at different current densities (a) 1.0 A/dm^2, (b) 2.0 A/dm^2, and (c) 3.0 A/dm^2

2. In-depth characterization of coating microstructure and surface roughness.
3. Development of the post-plating heat treatment process to produce the desired MCrAlY coating microstructure.
4. Conducting cost analysis to provide a cost comparison between the electro-codeposition process and state-of-the-art techniques such as APS and HVOF.
5. Evaluation of the oxidation performance of the electro-codeposited MCrAlY coatings.

References

1. M.A. Alvin, F. Pettit, G. Meier, M. Yanar, M. Helminiak, B. Kang, C. Feng, J.M. Tannebaum, R. Chen, B. Zhang, T. Fu, M. Chyu, S. Siw, W. Slaughter, V. Karaivanov, G. Richards, T. Sidwell, D. Straub, K. Casleton, and O. Dogan, "Materials and Component Development for Advanced Turbine Systems," The 22nd Annual Conference on Fossil Energy Materials, July 8–10, 2008, Pittsburgh, Pennsylvania.

2. T.B. Gibbons and I.G. Wright, "A Review of Materials for Gas Turbines Firing Syngas Fuels," Report #ORNL/TM-2009/137, Oak Ridge National Laboratory, Oak Ridge, Tennessee, 2009.

3. A. Feuerstein, J. Knapp, T. Taylor, A. Ashary, A. Bolcavage, and N. Hitchman, "Technical and Economical Aspects of Current Thermal Barrier Coating Systems for Gas Turbine Engines by Thermal Spray and EBPVD: a Review," *J. Therm. Spray Technol*., 17 (2008) 199.

4. J. Foster, B.P. Cameron, J.A. Carew, "The Production of Multi-Component Alloy Coatings by Particle Codeposition," *Trans. Inst. Met. Finish*, 63 (1985) 115.

5. F.J. Honey, E.C. Kedward, V. Wride, "The Development of Electrodeposits for High-Temeprature Oxidation/Corrosion Resistance," *J. Vac. Sci. Technol*., A 4 (1986) 2593.

6. K. Harris and J.B. Wahl, "Improved Single Crystal Superalloys, CMSX-4®(SLS)[La+Y] and CMSX-486®," in *Superalloys 2004*, K.A. Green, T.M. Pollock, H. Harada, T.E. Howson, R.C. Reed, J.J. Schirra, and S, Walston, eds. (TMS, 2004), pp. 45.

7. N.V. Parthasaradhy, in *Practical Electroplating Handbook*, Prentice Hall, 1989, pp. 183.

8. T.B. Massalski, H. Okamoto, P.R. Subramanian, and L. Kacprzak, eds., Binary Alloy Phase Diagrams, ASM, 1990.

9. "Aluminum-Chromium-Yttrium Ternary Alloy Phase Diagram," ASM Alloy Phase Diagrams Center, DOI: 10.1361/apd-al-cr-y-980313.

V.C.4 Low Thermal Conductivity, High Durability Thermal Barrier Coatings for IGCC Environments

Eric Jordan (Primary Contact), Maurice Gell
University of Connecticut
191 Auditorium Road
Storrs, CT 06269-3139
Phone: (860) 486-2371; Fax: (860) 486-5088
Email: Jordan@engr.uconn.edu

DOE Project Manager: Briggs White
Phone: (304) 285-5437
Email: Briggs.White@netl.doe.gov

Contract Number: FE0007382

Start Date: October 1, 2011
End Date: September 30, 2014

Fiscal Year (FY) 2012 Objectives

- Purchase precursor materials and receive bond coated superalloy specimens from Pratt & Whitney and Siemens Energy.
- Define critical processing variables enabling the deposition of yttria stabilized zirconia (YSZ) thermal barrier coatings (TBCs) with inter-pass boundaries (IPBs) for reduced thermal conductivity.
- Optimize the distribution and strength of IPBs by conducting a Taguchi Design of Experiments.
- Define a reliable, fast, inexpensive method of measuring the thermal conductivity of YSZ TBCs with IPBs.
- Define an optimized process for making low thermal conductivity YSZ TBCs with IPBs.

FY 2012 Accomplishments

- Procured materials for liquid precursor thermal spray and received 90 bond coated superalloy substrate from our industrial partners (Pratt & Whitney, Siemens Energy).
- Ran preliminary plasma spray trials to identify critical processing variables and appropriate ranges for these variables.
- Ran multiple designed (Taguchi) experimental spray trials to minimize thermal conductivity using inter-pass boundaries with over 75 different conditions investigated.
- Obtained the OOF finite element program from National Institute of Standards and Technology and successfully used it to calculate thermal conductivity from scanning electron microscopy (SEM) images of coating cross sections. We ran eight hypothetical microstructures to gain insight into what minimum thermal conductivity microstructures might look like. We also ran thermal conductivity calculations on six actual microstructures using SEM micrographs.
- Deduced that calculated conductivities might not be reliable. As a result, sought and found access to a laser flash conductivity measurement system on campus. Measurements to begin shortly.
- Used insights from the OOF simulations to determine the most important spray parameters for minimizing thermal conductivity which were (1) short spray distance, the distance between spray nozzle and the substrate (Figure 3); and (2) short raster scan step height, the distance between successive spray passes (Figure 4).

Introduction

Burning of coal by gasification with CO_2 separation and storage is a near-zero carbon footprint method of utilizing America's vast coal reserves. A key goal is to make this attractive option as economical as possible. Such plants use gas turbines and maximizing their efficiency and durability are key elements in making such plants economically attractive. Improved efficiency lowers the cost of electricity but requires higher firing temperatures. Higher temperatures are enabled by improved ceramic thermal barrier coatings (TBCs) used to protect the metal parts from high temperatures, and in addition, such coatings operating at higher temperatures need reduced thermal conductivity and improved resistance to chemical attack from contaminants that are especially aggressive at high temperatures. The purpose of this project is to use unique coating fabrication technology developed at the University of Connecticut to create coatings that have lower thermal conductivity, higher allowable operating temperature and better resistance to high temperature contaminants.

These improved coatings will be made using a new coating technology called solution precursor plasma spray (SPPS) that can create microstructures with unique features that reduce thermal conductivity. The first part of the program is designed to optimize these

features to minimize thermal conductivity. In the second part of the program the ability of the SPPS method to rapidly create new coating chemistries will be used to develop compositions with higher maximum operating temperatures and better contamination resistance. At every stage of the project, cyclic heating and cooling tests will be used to verify the improved properties and microscopy will be used to help understand the behavior and guide the parameter selection for the SPPS process. The expected result is improved thermal barrier coatings that will make these exciting green energy plants more economically attractive.

Approach

To develop improved coatings, the SPPS process will be used. This is a new process shown schematically in Figure 1. Chemicals in solution are injected into a plasma torch causing a chemical reaction leading to the formation of the desired ceramic which then melts and is deposited on the substrate. Standard methods inject a ceramic powder in place of precursors. This process can create unique pore structures which will be optimized through a series of spray trials in which the spray conditions are varied to create coatings with reduced thermal conductivity. Thermal conductivity is minimized by achieving a specific desired microstructure in which the porosity is arranged in sheets. Figure 2a shows an early coating with unstructured porosity, and Figure 2b shows the improved structure porosity with reduced thermal conductivity. The benefit of this pore arrangement is verified by computer calculations of thermal conductivity from various microstructures. The success of these trials is accessed by a combined use of measured thermal conductivities and thermal conductivities computed from microstructure photos. The goal is to reduce the thermal conductivity by a factor of two.

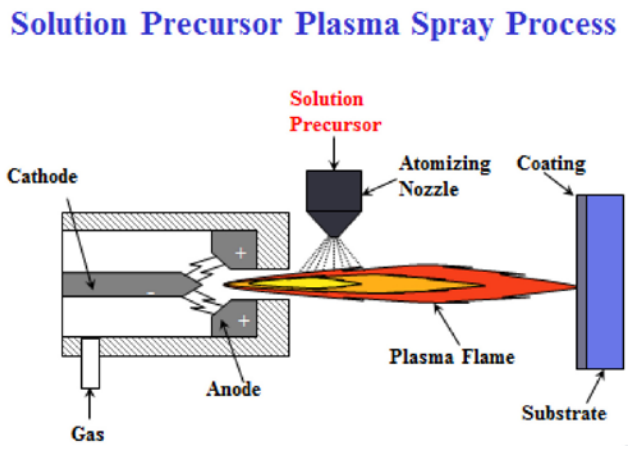

FIGURE 1. The SPPS process in which liquid precursors are injected into a plasma jet to create a coating

To develop coatings with improved maximum temperature capabilities, ceramics will be used that are known to have higher temperature capabilities. This class of ceramics is particularly expensive and as a result only the top hottest part on the coating will be made of these advanced ceramics. These ceramics also have improved contamination resistance. Additional contamination resistance will be achieved by adding aluminum oxide to the conventional ceramic underneath the expensive top layer. The SPPS process has the special trait that it can allow larger amounts of helpful aluminum in the coatings with less microstructure disruption. The improved high temperature capabilities of these coatings and contamination resistance will be verified by high temperature cyclic furnace testing. Mechanism of failure will be studied to generate insight for further improvements.

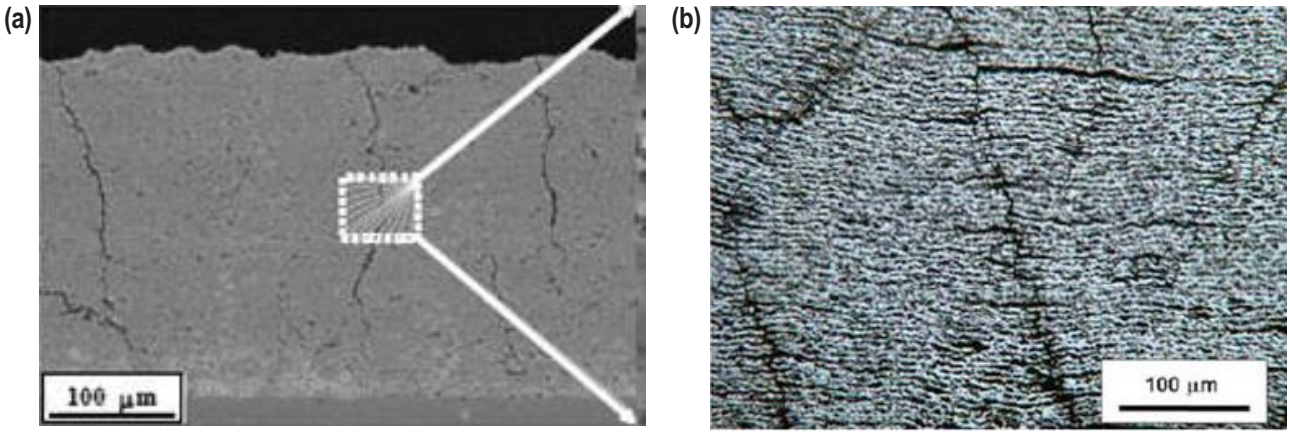

FIGURE 2. Microstructure of a SPPS TBC with vertical cracks (a) without thermal conductivity lowering horizontal layers porosity (IPBs) and (b) with IPBs

Results

In the first year of this program, over 75 different spray conditions have been investigated in an attempt to minimize thermal conductivity by creating structured porosity in the form of IPBs. Several important trends are shown in Figures 3 and 4. An improved understanding of how to create structured porosity has been gained and lower conductivity coatings have been created. It has been learned that in addition to the planned use of conductivity calculated from microstructure images it is important to have a significant number of measured values. We now have this measurement capability and will have even better information to direct our final experiments to create the desired low conductivity coating. In addition we have demonstrated the ability to deposit the higher temperature, higher cost, higher thermal resistance coating with our process ahead of schedule.

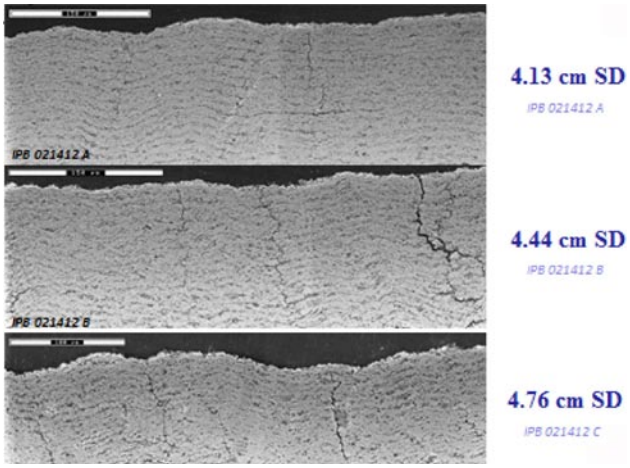

FIGURE 3. Effect of spray distance in IPB formation for SPPS TBCs

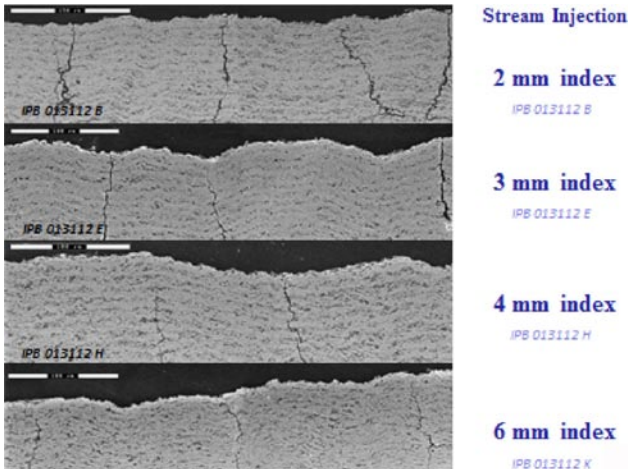

FIGURE 4. Effect of raster scan height on IPB formation in SPPS TBCs

Conclusions and Future Directions

The creation of IPBs (structured porosity) to reduce the thermal conductivity of TBCs has been demonstrated and is well on the way to being optimized. In the near future, this process will be complete and the program will then advance to adding a higher temperature, more contamination-resistant top layer and make compositional changes to the lower cost layer to dramatically improve contamination resistance. As an integral part of these efforts, verification testing will be conducted involving cycling the coatings at high temperatures with contaminants added to verify the improved durability. The result will be coatings with lower thermal conductivity providing superior thermal protection to turbine parts and coatings that allow higher surface temperatures with better contamination resistance. Such coatings will allow higher firing temperatures in gas turbines and, as a result, higher efficiency and lower cost electricity from these exciting new low-carbon-emission coal-fired plants.

FY 2012 Publications/Presentations

1. Maurice Gell, Eric H. Jordan, and Chen Jiang, "Progress In Depositing Solution Precursor Plasma Spray Thermal Barrier Coatings," International Conference on Metallurgical Coatings and Thin Films, San Diego, California, April 23–27, 2012.

2. Eric H. Jordan, Maurice Gell, and Chen Jiang, International Conference on Thermal Spray, Houston, Texas, May 20–24, 2012.

V.C.5 Preparation and Testing of Corrosion- and Spallation-Resistant Coatings

John P. Hurley (Primary Contact),
Matthew Cavalli
Energy & Environmental Research Center
University of North Dakota
15 North 23rd Street, Stop 9018
Grand Forks, ND 58202-9018
Phone: (701) 777-5159; Fax: (701) 777-5181
Email: jhurley@undeerc.org

DOE Project Manager: Briggs White
Phone: (304) 285-5437
Email: Briggs.White@netl.doe.gov

Contract Number: FE0007325

Start Date: October 1, 2011
End Date: September 30, 2014

Fiscal Year (FY) 2012 Objectives

- Prepare bonded rods of Kanthal advanced powder metallurgy technology (APMT) and nickel superalloys.
- Perform scanning electron microscopy (SEM) analyses of bonded parts to measure zinc diffusion rates.
- Model bond line pressures at temperature.
- Collect microcontaminants in combusted synthesis gas.
- Analyze captured microcontaminants.

FY 2012 Accomplishments (through May 2012)

- All materials, equipment, and clamps have been assembled for preparation of bonded parts in order to determine diffusion rates of zinc through the alloys.
- The equipment necessary to obtain alloy physical properties as functions of temperature has been purchased and assembled. The data are necessary in order to perform the modeling of bond line pressures.
- Microcontaminants in combusted synthesis gas have been collected during pilot-scale tests of an entrained-flow gasifier (EFG).

Introduction

The objective of this program is to take a recently developed method of bonding nickel superalloys with protective dispersion-strengthened FeCrAl layers closer to commercial use in syngas-fired turbines. The new bonding method developed by the Energy and Environmental Research Center (EERC) is known as evaporative metal bonding. The project is designed to determine if plating APMT, a highly oxidation-resistant oxide dispersion-strengthened FeCrAl alloy made by Kanthal, onto nickel-based superalloy turbine parts is a viable method for substantially improving the lifetimes and maximum use temperatures of the parts, both those with thermal barrier coatings and those without. If successful, the information will help move the protection process closer to demonstration testing. In addition, the team will characterize the microcontaminants in combusted synthesis gas. This information will be used to best simulate actual corrosion conditions but can also be used by other researchers studying deposition and gas flow in turbines.

Approach

In this program, we are testing the evaporative metal bonding method for joining single plates of APMT to actual turbine structures composed of the nickel-based superalloys Rene 80 and CM 247 LC. Working with Siemens Energy Inc., we will then measure the increase in performance or lifetime of the plated structures. This will involve optimizing the bonding process by determining diffusion rates of the bonding metal into and through the bonded structures and designing fixtures that apply uniform compressive force to the surfaces being bonded, while allowing the bonding alloy to vaporize from the structures. After bonding the plates of APMT to the surfaces of the superalloy parts, a thermal barrier coating will be applied to the surface of the APMT. Both coated and uncoated bonded pieces will be subjected to environmental testing such as determining high-temperature oxidation rates, spallation lifetime testing, and hot corrosion rates in atmospheres simulating those turbines firing syngas created from gasification of coal in an EFG.

To support the corrosion testing work, we will also collect and analyze the products of syngas combustion produced in EERC's pilot-scale coal-fired EFG, or

other gasifiers, in order to better understand realistic corrosion conditions inside a syngas-fired turbine. The information from the characterization of the products of syngas combustion, especially the size and composition distributions of particulates that are entrained in it (which are very different from gasifier fly ash), will be made available to other research groups modeling syngas combustion and gas flow and deposition within syngas-fired turbine systems. If successful, the overall impact of the work will be to greatly increase the lifetime and maximum use temperature of turbine parts made of nickel superalloys and to provide researchers with knowledge of the specific forms of microcontaminants present in combusted syngas.

Results

Two graduate students, Joshua Braband and Serges Tansinkou-Nguelo, have been working on the project. Both students are pursuing master's degrees in mechanical engineering. Joshua has been focusing on the diffusion-bonding, high-temperature property measurements and finite element modeling. Samples of the base metals to be joined as well as molybdenum plate for bonding jigs have been received, and Joshua has coordinated having them cut to shape via electrodischarge machining. Serges will help with the property measurements and has been focusing on characterizing the microcontaminants in the cleaned synthesis gas stream produced in the University of North Dakota EERC EFG.

The major equipment components have been received for the laboratory testing to be performed on the advanced alloys. They include a high-temperature furnace (Model 1608 FL, CM Furnaces), silicon carbide push rods (Applied Test Systems), and a high-temperature extensometer (Model 3548, Epsilon Technology). Joshua and Serges have assisted with the setup of the high-temperature equipment and the integration with the existing Bose Electroforce testing system. Necessary utility modifications (power and water) for the new equipment have been undertaken in the laboratory area. In addition, rods of Rene 80 and CM247LC were received from Siemens, and 3 mm thick APMT plate was received from Sandvik, located in Sweden, which owns Kanthal.

In addition to the laboratory testing, we have begun sampling activities to determine what types of trace contaminants may occur in cleaned syngas that could lead to corrosion issues in turbines firing syngas. EERC has several pilot-scale gasifiers that are continually used in a variety of test configurations. Sampling was done with the EFG. Funding for the EFG tests was provided from a separate project. The EFG fired a blend of Powder River Basin coal and ground wood. During those tests, we collected particulate and trace element samples from the thermal oxidizer used to burn the syngas produced. The sampling train used was designed for U.S. Environmental Protection Agency Method 29 sampling, although the typical glass fiber prefilter was replaced with a nucleopore polycarbonate membrane filter with etched 0.1 μm diameter pores. The thermal oxidizer contains a premixed air-syngas burner at the top of a refractory-lined chamber. The sampling occurs at the bottom of the downfired oxidizer. The gas being sampled is at approximately 750°C. It is quenched as it is pulled through the glass sampling tube to approximately 100°C before reaching the filter. Three sample sets were collected, two while firing the coal-biomass blend and one while no coal or biomass was fed into the EFG, but natural gas was fired in the thermal oxidizer. The Method 29 impinger samples will be analyzed during the next reporting period, and the filter samples will be analyzed by SEM this summer.

Figure 1 shows a cross-sectional view of the EFG. The EFG is a dry-feed, downfired system. The reactor tube is vertically housed in a pressure vessel approximately 24" in diameter and 7' in length. The EFG fires nominally 8 lb/h of coal and produces up to 20 scfm of fuel gas. The maximum allowable working pressure is 300 psig. The reactor has the capability to run in oxygen- or air-blown mode. The supplemental electrical heating system is capable of reaching a nominal temperature of 1,500°C (2,732°F) and is separated into four independent zones so that a consistent temperature can be maintained throughout the length of the furnace. The radially spaced heating elements provide the initial heat for the centrally located alumina reactor tube, and refractory walls outside the heating elements provide insulation. Type S thermocouples are used to monitor and control the temperatures of the heating zones and reactor tube. All of the gasification reactions occur inside the reactor tube, and slag is able to flow on the tube walls. Pressure inside the alumina reactor tube is balanced with a slightly positive nitrogen pressure outside of the alumina reactor tube.

Pulverized fuel is fed into the top of the furnace via a twin-screw feeder and scale contained in a pressurized vessel. A lock hopper is in place that allows the system to be refilled while running, thereby facilitating a continuous mode operation. Feed rates are calculated in real time. The feed system can be run in either volumetric mode or gravimetric mode. Nitrogen or syngas is used to convey the solid pulverized coal into the combustion zone.

Product gas exits at the bottom of the furnace tube and enters a reducing section that houses a quench system capable of injecting water, syngas, or nitrogen

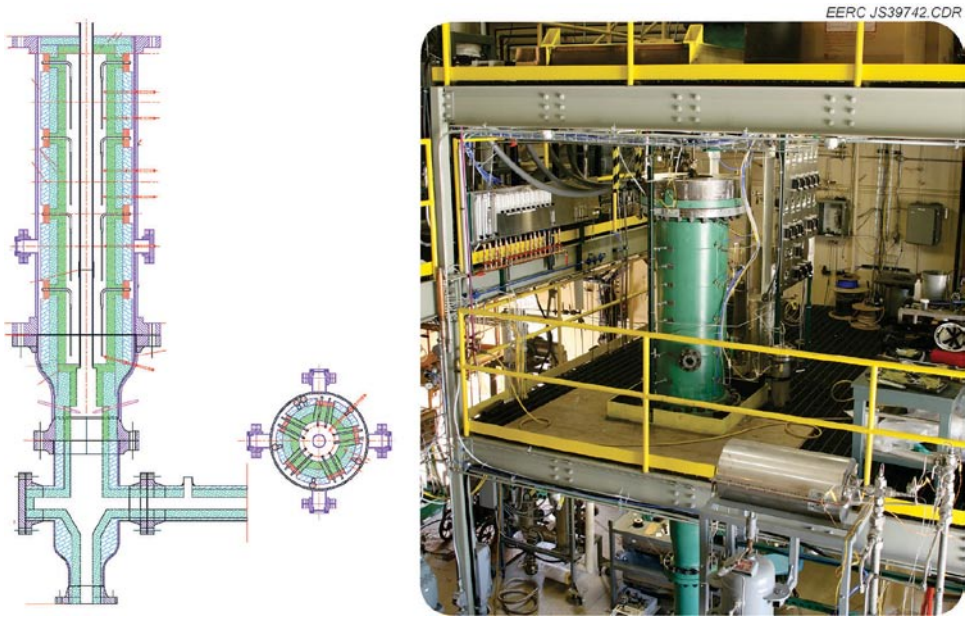

FIGURE 1. EERC EFG

as the quench fluid. The product gas then enters a cross, making a 90° turn, and then exits the main unit on its way to the back-end control devices. Slag, ash, and char drop through the cross and are collected in a refractory-lined slag trap. Fine particulate is able to flow with the gas through the 90° turn and is collected in a downstream filter. Slag is collected below the gasifier in a refractory-lined slag trap. Fly ash is captured in the hot-gas filter vessel that uses an iron aluminide candle filter, providing near-absolute filtration. The gas then passes through water-gas shift reactors that can shift sour gas (containing H_2S) to increase its H_2 concentration. A portion then goes through sulfur adsorbers and then to hydrogen separation membranes that were tested during this run. The portion not going to the separation membranes is quenched to remove moisture and any tars formed in the system. All gas streams, including the membrane raffinate and permeate streams, are then recombined before combusting them in the thermal oxidizer from which the Method 29 samples are collected.

Conclusions and Future Directions

Work has been proceeding as anticipated, but there are no conclusions to be drawn as yet. By the end of the fiscal year (September 30, 2012), all objectives for the year should be accomplished. In particular, measurements of bonding metal diffusion in the alloys of interest will be determined, and modeling of pressures at alloy bondlines during the bonding procedure should be completed. Also, sampling from the EERC pilot plant gasifiers should be completed so that we will have a much clearer idea of what microcontaminants are present in synthesis gas that is combusted in a turbine system.

FY 2012 Publications/Presentations

1. A presentation describing the project was given at the University Turbine Systems Research Conference in October of 2011.

V.C.6 Degradation of TBC Systems in Environments Relevant to Advanced Gas Turbines for IGCC Systems

Brian Gleeson (Primary Contact) and
Meltem Yanar
University of Pittsburgh
Department of Mechanical Engineering and
Materials Science
Pittsburgh, PA 15261
Phone: (412) 648-1185; Fax: (412) 624-4846
Email: bgleeson@pitt.edu; nmy4@pitt.edu

DOE Project Manager: Patcharin Burke
Phone: (412) 386-7378
Email: Patcharin.Burke@netl.doe.gov

Contract Number: FE0007271

Start Date: October 1, 2011
End Date: September 30, 2014

Fiscal Year (FY) 2012 Objectives

- Acquire and setup high-temperature testing apparatus that has the ability to achieve environments that have controlled steam and CO_2 contents.
- Acquire alloys and associated coated samples for testing. The thermal barrier coating (TBC) systems will be deposited by Praxair Surface Technologies (PST), an industry collaborator on this project.
- Test TBC systems in air, air + 20% H_2O, and 20% H_2O + 80% CO_2 at 900°C-1,100°C.

FY 2012 Accomplishments

- Hired a new graduate student specifically for this project.
- Completed setup of new testing apparatus. New furnace was setup, sample holders were fabricated, necessary equipment to establish steam and CO_2 environments was purchased.
- Preliminary tests were conducted and the results assessed.

Introduction

The large dependence on coal-derived fuels for power generation in the U.S. has led to technological innovations that can improve the efficiency and cleanliness of converting coal to electricity. One such innovation is the establishment of integrated gasification combined cycle (IGCC) power generation systems [1]. These systems offer increased efficiency over conventional coal-fired power generation systems and lower environmental emissions. The IGCC system converts coal or some combination of coal + biomass or waste into a synthetic gas (syngas) fuel that contains varying amounts of H_2 and CO, which is cleaned and then burned in a gas turbine combined cycle system to generate electricity. During this process, the presence of residual particulates comprised of calcia, magnesia, alumina, silica and iron compounds (i.e., ash) in the combustion gas stream, coupled with gaseous impurities such as alkalis (e.g., Na and K) can cause deposition and/or enhanced surface degradation of the turbine components.

The increased inlet temperature of turbines that has led to improved efficiencies has also led to the need for TBCs to protect components in the hot sections of turbines [2]. TBC systems typically consist of a bond coat, a thermally grown oxide (TGO), and a thermally insulating ceramic (topcoat). The bond coat is typically based on an MCrAlY (where M=Ni or NiCo) composition, the TGO results from oxidation of aluminum in the bond coat to form Al_2O_3, and the topcoat is typically zirconia (ZrO_2) stabilized with ~7 wt% yttria (Y_2O_3). A significant life-limiting feature of the TBC is the delamination of the ceramic topcoat, which tends to be exacerbated in the presence of deposits [3-5]. The environment in the IGCC systems, e.g., high steam levels from H_2 firing or high CO_2/steam mixtures in oxy fired systems, combined with gasifier-fuel-derived deposits, e.g., ash, and contaminants, e.g., alkali metals and sulfur, introduces complexities associated with TBC durability that are currently unresolved. These complexities include enhanced attack of the yttria stabilized zirconia (YSZ) by chemical reaction, physical damage of the topcoat by molten deposit penetration, and accelerated bond coat corrosion.

The overall goal of this project is to use lab-scale testing to systematically elucidate the interplay

between prototypical deposit chemistries, i.e., ash and its constituents, K_2SO_4 and FeS, and environmental oxidants, i.e., H_2O and CO_2, on the degradation behavior of advanced TBC systems.

Specific objectives are:

- To characterize and determine the main factors governing the degradation of a state-of-the-art nickel-cobalt-chromium-aluminum-yttrium (NiCoCrAlY) bond coat and three differently processed YSZ TBCs in gaseous atmospheres that are increasingly relevant to IGCC systems.
- Add the complexity due to the presence of a synthetic surface deposit based on coal fly ash, with particular emphasis on the fly-ash components calcium oxide and silicon dioxide.
- Establish an effective experimental procedure for assessing high-temperature, deposit-induced degradation in IGCC-relevant environments.
- Study the further complexity of adding K_2SO_4 or FeS to the synthetic ash deposit.

The fundamental relevance of these objectives lies in the need to better understand the chemical, physical, and kinetic factors that can lead to accelerated degradation of TBCs used in IGCC systems. The practical significance lies in the guidance provided for predicting TBC degradation behavior and for designing TBCs that exhibit adequate degradation resistance.

Approach

It is known that water vapor and carbon dioxide can adversely affect the oxidation resistance of alumina forming alloys and coatings. Water vapor can cause more extensive transient oxidation as well as increased cracking and spallation of the alumina. The potential effects of CO_2 on alumina scale formation and growth are neither well documented nor well understood, although, it is generally known that carbon in an alumina scale forming alloy can enhance scale spallation during thermal cycling. Additionally, the turbine components in IGCC process can be affected by coal fly ash deposits. The degradation mechanisms that result from IGCC-relevant environments containing H_2O, CO_2, and varying compositions of fly ash components will be systematically examined.

The specific environments to be tested will be air, air + 20% H_2O, and 20% H_2O + 80% CO_2 at temperatures of 900°C, 1,000°C, and 1,100°C. Tests will be carried out in these environments both with and without deposits based on fly ash and will consist of CaO, Al_2O_3, SiO_2, FeO_x. Such tests will also involve other deposits to assess the individual roles of CaO and SiO_2, as well as the influence of contaminants such as K_2SO_4 and FeS. The TBCs to be tested will consist of YSZ top coats deposited by an air plasma sprayed process (APS) and will be provided by PST. Additional testing will be done to simulate a thermal gradient to more precisely model actual operating conditions in a turbine.

Results

The first task in the project was to acquire and setup apparatus for the high-temperature testing to be conducted at the University of Pittsburgh. Figure 1 shows a schematic of the testing apparatus that has been built and that will be used for the duration of the project. The apparatus is capable of testing up to four samples at one time. A magnetic push/pull system is used to allow for the easy insertion of samples into complex environments and for the capability to conduct thermal cycling exposures. A typical test cycle will typically involve samples 45 minutes in the furnace followed by 15 minutes outside. This will continue for a range of cycles, depending on observed degradation behavior. New glassware has been prepared to accommodate the length of the furnace and allow for samples to travel a requisite distance to be considered out of the hot zone. The glassware will also allow for the appropriate connections to obtain steam- and CO_2-containing environments.

The steam content of the atmosphere will be set in accordance to temperatures prescribed by the steam tables, i.e., 60.3°C for 20% steam. Specifically, dry gas will first be bubbled through a water bath set at ~61–62°C and then passed through a condenser that is set at the targeted temperature of 60.3°C to achieve the desired steam content of 20%. After the gas is passed through the furnace, it will pass through a second bubbler to collect steam and then be expelled into a fume hood system.

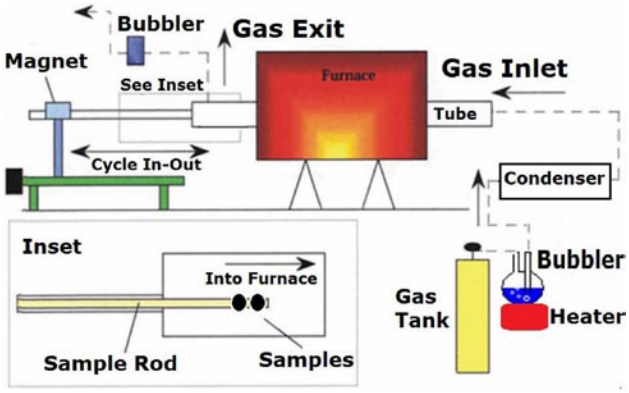

FIGURE 1. Schematic of testing apparatus that has been constructed for this project

Initial student training on relevant characterization equipment (mainly the scanning electron microscope and X-ray diffraction) has been conducted. These characterization techniques will be used throughout the study to analyze the as-received and thermally-exposed samples.

Several samples have been obtained from PST for preliminary testing. The next round of samples are expected to arrive by the end of July 2012. The TBC samples consist of a Ni-base superalloy substrate (Rene N5 or PWA1484), an argon shrouded plasma sprayed NiCoCrAlY overlay coating, and APS YSZ TBCs. The nominal compositions of the various layers are given in Table 1.

The first group of samples to be tested is high purity, low density (HP-LD) TBCs, which will be prepared from ultra-high purity YSZ powder that is known to have a remarkable combination of durability and resistance to phase transformation [6]. The next group of samples to be tested will be high purity, dense vertically cracked (DVC) YSZ TBCs. Table 2 provides a summary of the various systems to be tested.

Preliminary testing of the HP-LD YSZ TBC was performed at 1,100°C in 85% H_2O - 15% CO_2. Characterizations of an as-processed specimen together with the exposed specimen were completed. Figure 2 presents a cross-sectional micrograph from the NiCoCrAlY bond coat with HP-LD YSZ TBC in the as-processed condition. Oxide inclusions as well as some porosity, which are common for plasma sprayed coatings, are present throughout the coating. The microstructure consists of γ (Ni solid solution), β (NiAl) and Y- and/or Hf-rich phases. A thin layer of TGO, which is alumina, develops along the TBC/bond coat interface during TBC deposition. Figure 3 presents cross-sectional micrographs after 500 cycles of exposure at 1,100°C in 85% H_2O - 15% CO_2. The TGO is thicker and some cracks can be seen in the TGO and TBC, similar to observations made for dry-air exposures. However, the TBC is still intact. The preliminary results do not suggest a noticeable effect of the water vapor and carbon dioxide rich atmosphere on the durability of these TBCs.

Conclusions and Future Directions

The second year of the project will consist of:

- Continue testing of TBCs until failure in the three relevant environments (air, air + 20% H_2O, and 20% H_2O + 80% CO_2) at 900-1,100°C.
- Commence testing of TBC systems having a synthetic ash deposit and exposed to air + 20% H_2O and then 20% H_2O + 80% CO_2 at 900-1,100°C. Test selected TBC samples using individual fly-ash components (CaO and SiO_2).
- Commence testing of the TBC systems having a synthetic ash + 5 or 25% K_2SO_4 deposit and exposed to air and air + 30% H_2O at 900-1,100°C. Test selected TBC samples using individual fly-ash components (CaO and SiO_2). Commence testing of free-standing TBCs at 1,100°C and 1,300°C in air with and without deposits.

TABLE 1. Nominal compositions of the various constituents of the TBC systems to be studied

Nominal Composition of Materials (wt%)													
Layer	**Material**	**Ni**	**Co**	**Cr**	**Al**	**W**	**Mo**	**Ta**	**C**	**B**	**Re**	**Y**	**Hf**
Superalloy	**René N5+**	Bal	7.5	7	6.2	5	1.5	6.5	0.05	0.004	3	0.01	0.15
	PWA-1484	Bal	10	5	5.6	6	2	8.7			3		0.1
Bond Coat	**NiCoCrAlY**	**Ni**	**Co**	**Cr**	**Al**	**Y**							
		Base	22	16	13	0.5							
Topcoat	**YSZ**	**ZrO_2**	**Y_2O_3**	**Al_2O_3**	**CaO**	**Fe_2O_3**	**HfO_2**	**MgO**	**SiO_2**	**All Other**			
		Base	7.736	0. 011	0.003	0.007	1.69	<0.001	0.013	0.157			

TABLE 2. Summary of TBC systems that are being prepared by PST for this study

Specimen Group #	Substrate Alloy	Bond Coat Type	Bond Coat Thickness (mils)	TBC Powder	TBC Density (%T.D.)	TBC Thickness (mils)	Quantity
1a	René N5	Dual Layer NiCoCrAlY	7-8	High Purity YSZ	85	15	10
1b	PWA 1484	Dual Layer NiCoCrAlY	7-8	High Purity YSZ	85	15	13
2a	René N5	Dual Layer NiCoCrAlY	7-8	High Purity YSZ	92	15	10
2b	PWA 1484	Dual Layer NiCoCrAlY	7-8	High Purity YSZ	92	15	13

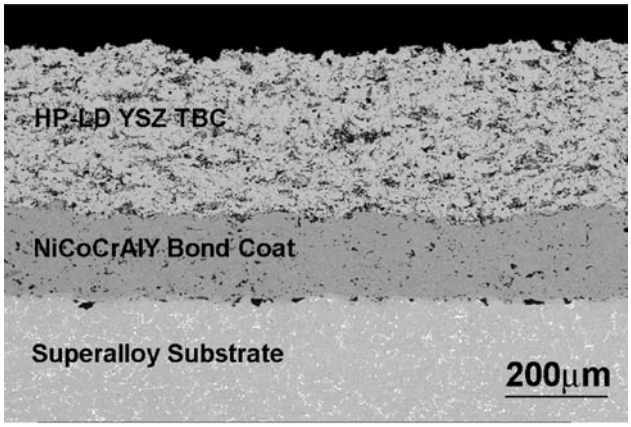

FIGURE 2. Cross-sectional micrograph of a NiCoCrAlY bond coat with HP-LD YSZ TBC in the as-processed condition

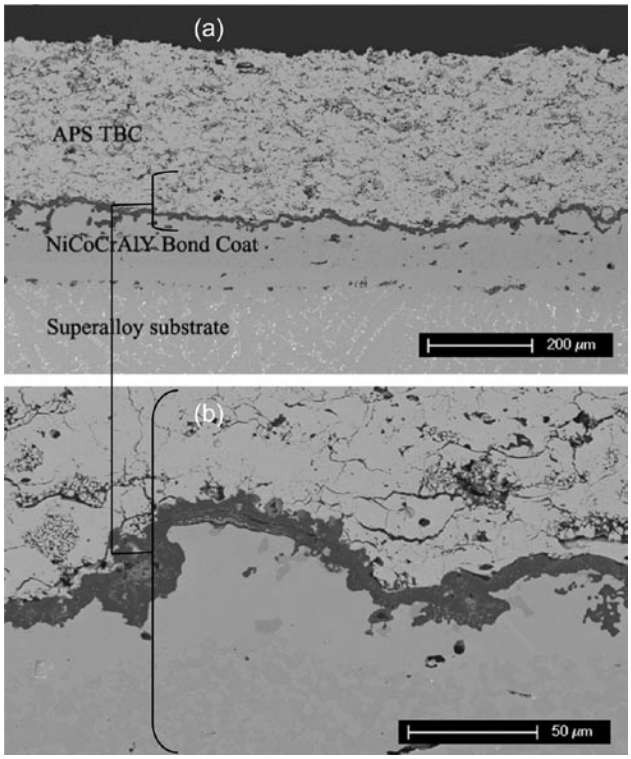

FIGURE 3. Cross-sectional micrographs of NiCoCrAlY bond coat with HP-LD TBC after 500 cycles of exposure at 1,100°C in 85% H_2O - 15% CO_2 at low (a) and high (b) magnifications

FY 2012 Publications/Presentations

1. Presentation: B. Gleeson, "Degradation of TBC Systems in Environments Relevant to Advanced Gas Turbines for IGCC Systems," 2011 University Turbine Systems Research Workshop, Columbus, Ohio, October 25, 2011.

References

1. N.J. Simms, P.J. Kilgallon and J.E. Oakey, "Fireside Issues in Advanced Power Generation Systems," *Energy Materials*, **2** (2007) 154-160.

2. W.P. Parks, E.E. Hoffman, W.Y. Lee and I.G. Wright, "Thermal Barrier Coatings Issues in Advanced Land-Based Gas Turbines," *Journal of Thermal Spray Technology*, **6** (1998) p187-192.

3. R.A. Miller, "Ceramic Thermal Barrier Coatings for Electric Utility Gas Turbine Engines," *NASA Technical Memorandum* 87288, National Aeronautics and Space Administration, Washington D.C., 1986.

4. B. Gleeson, "Thermal Barrier Coatings for Aeroengine Applications," *Journal of Propulsion and Power*, **22** (2006) 375-383.

5. R.L. Jones, "Some Aspects of the Hot Corrosion of Thermal Barrier Coatings," *Journal of Thermal Spray Technology*, **6** (1997) 77-84.

6. M.A. Helminiak, N.M. Yanar, F.S. Pettit, T.A. Taylor and G.H. Meier, "The Behavior of High-Purity, Low-Density Air Plasma Sprayed Thermal Barrier Coatings," Surface and Coatings Technology, 204, (2009), 793-796.

V.C.7 Hafnia-based Nanostructured Thermal Barrier Coatings for Advanced Hydrogen Turbine Technology

Chintalapalle V. Ramana
University of Texas at El Paso
500 W University Avenue
El Paso, TX 79968
Phone: (915) 747-8690; Fax: (915) 747-5019
Email: rvchintalapalle@utep.edu

DOE Project Manager: Briggs White
Phone: (304) 285-5437
Email: Briggs.White@netl.doe.gov

Contract Number: FE0000765

Start Date: October 1, 2009
End Date: September 30, 2012

Fiscal Year (FY) 2012 Objectives

- Investigation of thermal properties of the hafnia-based coatings.
- Detailed analysis of structure-property relationship.
- Evaluation of the coating's performance in the hot gas environment using laboratory scale combustor rig.

FY 2012 Accomplishments

- Thermal conductivity of the yttria stabilized hafnia (YSH) coating grown on various substrates has been investigated using photo-caustic technique. YSH coating showed lower thermal conductivity compared to pure HfO_2 or bulk YSH material.
- Effect of annealing on thermal conductivity has been investigated.
- Performance of YSH and yttria stabilized hafnia-zirconia (YSHZ) coating in hot gas environment has been evaluated in a laboratory scale combustor rig. Microstructural analysis has been performed after exposure to the hot gas. The material showed a complete stability in a hot gas environment.

Introduction

Thermal barrier coatings (TBCs) are the multifunctional thick film of low thermal conductivity ceramic refractory material. Among many other tasks, protecting the components from high temperature exposure is the key function of TBC materials. Thus, it allows for increasing the operating temperature and thereby improving the efficiency. Future generation gas turbine engines must tolerate fuel compositions ranging from natural gas to a broad range of syngas with high hydrogen contents, which require TBCs with a surface temperature tolerance much higher than the current standard materials. Currently TBCs are used predominantly in gas turbine applications. The current material of choice for TBC application is based on 7-8 wt% yttria stabilized zirconia (YSZ). However, YSZ TBC is limited to operating temperatures up to 1,200°C, above which phase transformation associated with a volume change leads to the formation of cracks in the coatings. This limits the application of YSZ TBC at elevated temperatures.

Among oxides with the fluorite structure that are suitable for TBCs, HfO_2 is the most promising candidate to meet the requirement of an advanced gas turbine system. The melting point of HfO_2 is higher than ZrO_2, and YSH exhibits durability to a temperature of 1,400°C [1]. From this viewpoint, it is important to understand the science and engineering of HfO_2-based TBCs. The goal of the proposed project is to develop the HfO_2-based coatings, namely YSH, gadolinia stabilized hafnia (GSH) and YSHZ for TBCs of advanced hydrogen turbines. This work is directed to investigate the novel hafnia based nanostructured TBCs to ensure the minimum 1,300°C surface temperature tolerance for long time operation. So, the research is focused on fabrications and deeper understanding of the growth behavior, ultra-microstructure, surface-interface interaction and stability, thermo-chemical and thermo-mechanical properties and durability of hafnia based TBCs. YSH, GSH and materials engineered from variable contents of hafnia (HfO_2) and zirconia (ZrO_2) stabilized by yttria (YSHZ) are being investigated. The goal of the research is to find alternate but ideal TBCs in order to meet the unique structural, thermo-chemical and thermo-mechanical performance required by advanced gas turbine engines.

Approach

The approach is to systematically vary the growth conditions and target/ingot materials to study their influence on the coatings' phase, microstructure, mechanical, thermal, chemical properties, and performance. We will derive qualitative and

quantitative models for failure mechanisms, life time and performance of the nanostructured YSH, GSH, and YSZH ceramic TBCs from all these studies. The models will be used to predict pathways to further improve the coating's microstructure (at the reduced nano-dimensionality), properties and ultimately the performance. The central theme of the microstructure evaluation and various characterizations is to provide feedback to fabrications so as produce materials with superior stability, high temperature tolerance, thermal durability and reliable sensitivity.

The specific approach in this project is to provide a large number of interconnected surface nano-grains while maintaining the columnar structure. This will lead to a large interfacial thermal resistance and extremely low thermal conductivity. There are several types of material structure improvements that will also be specifically addressed: morphology/geometric uniformity, crystal structure and phase, microstructure quality (nano-grain or nano-particle distribution, boundaries and linear defect densities), doping profiles (point defects) and material composition. In addition, fundamental thermo-mechanical and thermo-chemical properties and performance will be measured and correlated to the microstructure. The thermal conductivity and size-dependent surface reactivity of the ceramic coatings will be measured. Finally, laboratory experiments using accelerated test environments will be used to investigate the relative importance of various thermo-mechanical and thermo-chemical failure modes of TBCs. Effects of thermal stress cycling, oxidation degradation and their complex interaction on TBC failures will be evaluated using a static and cyclic experimental matrix of syngas combustor rig. The parametric relation between turbine environments of high hydrogen content fuels and thermo-mechanical cracking in the ceramic layer will be developed.

Results

Thermal Conductivity

Photo-acoustic (PA) method was used to measure thermal conductivity of the coatings. In the PA measurement, a laser beam operating at a wavelength of 0.8 mm was used as the heating source. The laser beam is periodically irradiated on the sample surface to get the sufficient heating. A 70 nm thick film of Ni is deposited on the top of the YSH coating by e-beam evaporation in order to absorb the laser beam. A least square fitting is employed to obtain thermal conductivity of the coatings [2-4]. Figure 1a shows the phase shift as a function of the modulation frequency for representative YSH coatings. The variation of thermal conductivity of YSH coatings (grown on Inconel-738 substrate) with growth temperature is shown in Figure 1b. The thermal conductivity of YSH coatings are found within the range from 0.89 ±0.03 to 1.3 ±0.04 W/m-K. The thermal conductivity measured for YSH coatings shows lower than that of pure hafnia or bulk YSH. It is evident that the thermal conductivity slightly increases with increasing the growth temperature. This behavior can be attributed to the increasing grain size with increasing growth temperature. Thermal diffusion through lattice vibrations in a solid can be affected by (a) phonon-phonon interactions, (b) imperfections, and (c) grain boundary scattering. The effective grain boundary decreases with increasing grain size leading to a decrease in phonon

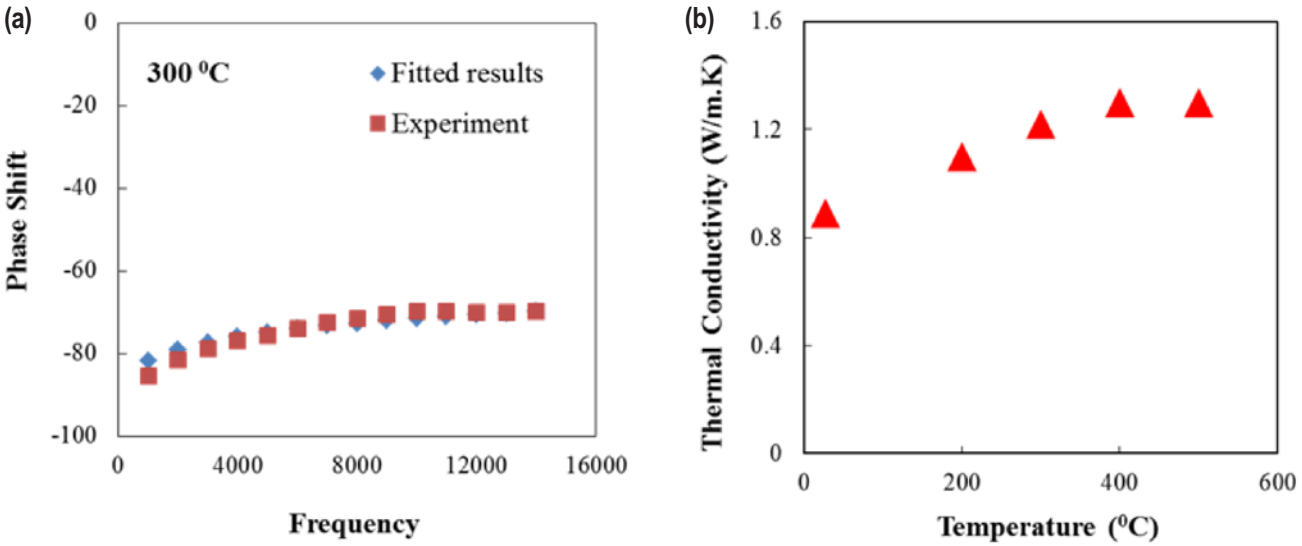

FIGURE 1. (a) Phase shift with respect to modulation frequency for YSH grown on Inconel-738 at 300°C and (b) the variation of thermal conductivity with growth temperature

scattering and, hence, resulting in the observed increase in thermal conductivity. Effective reduction in the thermal conductivity of the YSH coatings grown at room temperature can be attributed to an amorphous structure, where there exist only smaller particles occasionally. The thermal conductivity increase with increasing grain size has been reported for YSZ [5]. On the other hand, the observed thermal conductivity decrease in yttria stabilized hafnia can be attributed to the addition of yttria to hafnia. Furthermore, thermal conductivity of YSH is much lower than that of pure hafnia. The reason for YSH materials exhibiting lower thermal conductivity than pure hafnia is the introduction of oxygen vacancies. These are structural vacancies in the hafnia crystals due to charge compensation of Y^{+3} ions substituting for Hf^{+4} ions. As a result, phonon scattering from the vacancies decreases effective thermal transport.

Performance in Hot Gas Exposure

YSHZ and GSH coatings were exposed to hot gas to investigate the durability of the coatings in environments similar to practical turbines. A laboratory scale combustor rig was used to perform the experiments. Samples are exposed to the hot gases produced by the burning of methane with air. The experimental set up employed for the durability test by hot gas exposure is shown in Figure 2. X-ray diffraction (XRD) pattern of YSHZ coating (as a representative sample) before and after exposure to hot gases is shown in Figure 3. No significant microstructural change is observed from the XRD patterns. Little change in orientation is evident after nine hours exposure at 1,100°C. The coatings show stronger orientation toward (002) direction rather than (111) direction. The material does not show any change from the cubic crystal structure. Figure 4 shows the surface morphology of YSH coatings after exposure to hot gas. Again no significant change is visible from scanning electron microscopy (SEM) images; however, slight sintering is observed in the high magnified image (lowest panel of Figure 3b of the sample after nine hour exposures to hot gas at 1,100°C.

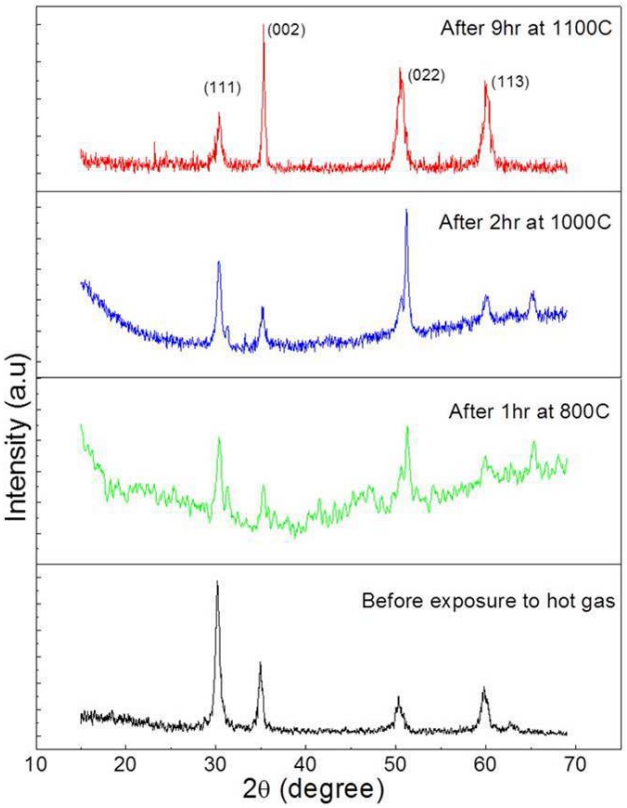

FIGURE 3. XRD patterns of YSHZ coating before and after exposure to hot gases

Conclusions and Future Directions

Structural, thermal and thermo-chemical investigation of the YSH and YSHZ samples grown using physical vapor deposition technique has been performed. Thermal analysis of YSH coatings indicate a lower thermal conductivity of YSH coating compared to HfO_2 or bulk YSH material. Both the YSH and YSHZ coatings demonstrated stability upon hot gas exposure. No significant change in microstructure or morphology was evident after exposure to a hot gas environment.

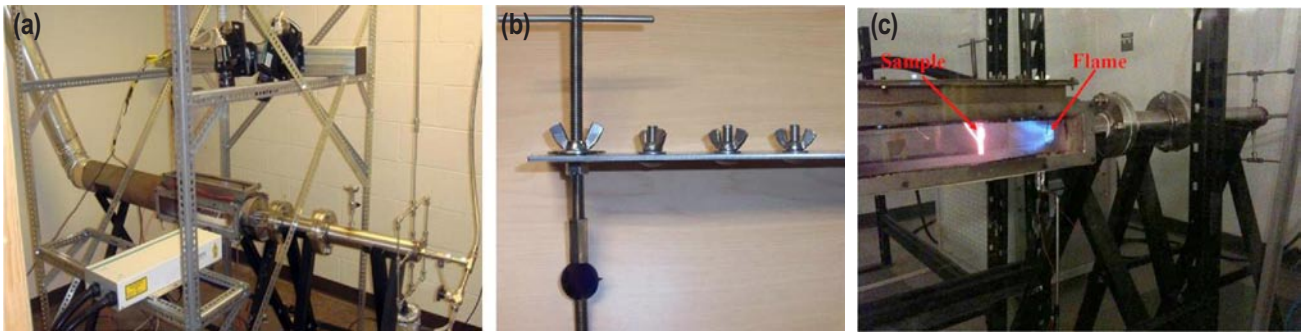

FIGURE 2. Experimental set up for durability under hot gas exposure

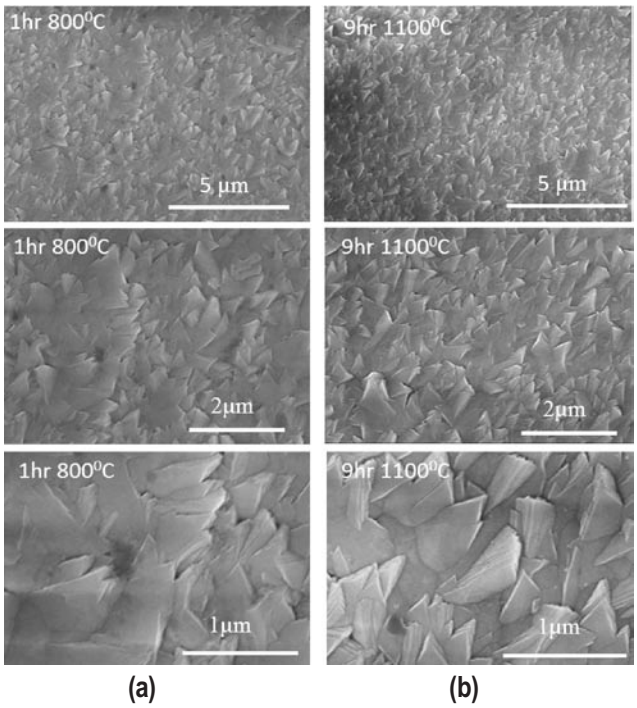

FIGURE 4. SEM images of YSH sample after exposure to hot gases

Selected compositions of YSH and YSHZ have been grown using electron beam physical vapor deposition (EB PVD). Investigation of microstructure, thermal properties thermo-mechanical and thermo-chemical analysis for EB deposited coatings are in process. Thermal analysis of the EB PVD coatings will be investigated in future experiments.

Special Recognitions & Awards/Patents Issued

Best Paper Award, "Thermal Conductivity of Ytrria-Stabilized Hafnia," American Society of Mechanical Engineers (ASME) and American Institute of Aeronautics and Astronautics (AIAA) joint symposium, Dayton Engineering and Sciences Symposium, Dayton, Ohio, October, 2011.

FY 2012 Publications/Presentations

1. M. Noor-A-Alam, A.R. Choudhuri, C.V. Ramana, "Effect of Composition on the Growth and Microstructure of Hafnia-Zirconia Based Coatings," *Surface & Coatings Technology*, 206 (2011) 1628–1633.

2. M. Noor-A-Alam**,** C.V. Ramana, "Structure and Thermal Conductivity of Yttria-Stabilized Hafnia Ceramic Coatings Grown on Nickel-Based Alloy," *Ceramics International*, 38 (2012) 2957–2961.

3. C.V. Ramana, M. Noor-A-Alam, Jamie J. Gengler, and John G. Jones, "Growth, Structure, and Thermal Conductivity of Yttria-Stabilized Hafnia Thin Films," *ACS Applied Materials and Interfaces*, 4 (2012) 200−204.

4. C.K. Roy, M. Noor-A-Alam, A.R. Choudhuri, C.V. Ramana, "Synthesis and Microstructure of Gd_2O_3-Doped HfO_2 Ceramics," *Ceramics International*, 38 (2012) 1801–1806.

5. M. Noor-A-Alam, C.V. Ramana ,and A.R. Choudhuri, "Analysis of Microstructure and Thermal Stability of Hafnia-Zirconia Based Thermal Barrier Coatings," Proceeding, 9th Annual International Energy Conversion Engineering Conference, July 31 – August 3, 2011, San Diego, California, USA.

6. M. Noor-A-Alam, A.R. Choudhuri, and C.V. Ramana, "Effect of Composition on the Growth and Microstructure of Hafnia-Zirconia Based Thermal Barrier Coatings," International Conference on Metallurgical Coatings and Thin Films, May 2–7, 2011, San Diego, California, USA. (Presented)

7. M. Noor-A-Alam, Chandan K. Roy, Christopher M. Bradely, A.R. Choudhuri, C.V. Ramana, "Development of Hafnia Based Thermal Barrier Coating and its Microstructural Analysis," 2011 TMS Annual Conference, Functional and Structural Nanomaterials: Fabrication, Properties, Applications and Implications symposium, San Diego, California, USA, February 27 – March 3, 2011. (Presented)

8. C.K. Roy, M. Noor-A-Alam, A.R. Choudhuri, C.V. Ramana, "Synthesis and Microstructure of Gd_2O_3-HfO_2 Thermal Barrier Coating," Southwest Energy Science and Engineering Symposium, April 16, 2011, El Paso, Texas, USA. (Presented)

References

1. Matsumoto K., Itoh Y., and Kameda T., 2003, "EB-PVD Process and Thermal Properties of Hafnia-Based Thermal Barrier Coating," *Sci. Technol. Adv. Mater.* 4, 153-158.

2. Wang X., Hu H., and Xu X., 2001, "Photo-Acoustic Measurement of Thermal Conductivity of Thin Films and Bulk Materials," *J. Heat Transfer*, 123, 138.

3. Rosencwaig A. and Gersho A., 1976, "Theory of the Photoacoustic Effect with Solids," *J. Appl. Phys.*, 47(1) 64–69.

4. Noor-A-Alam, M. and Ramana, C.V., 2012, "Structure and Thermal Conductivity of Yttria-Stabilized Hafnia Ceramic Coatings Grown on Nickel-Based Alloy," *Ceram. Int.*, 38, 2957-2961.

5. Soyez, G., Eastman, J.A., Thomson, L.J., Bai, G.R., Baldo, P.M., McCormick, A.W., DiMelfi, R.J., Elmustafa, A.A., Tambwe, M.F., and Stone, D.S., 2000, "Grain-Size-Dependent Thermal Conductivity of Nanocrystalline Yttria Stabilized Zirconia Films Grown by Metal-Organic Chemical Vapor Deposition," *Appl. Phys. Lett.* 77, 1155-1157.

VI. SMALL BUSINESS INNOVATION RESEARCH

A. Innovative Cooling Concepts

VI.A.1 High Temperature Capability and Innovative Cooling with a Spar and Shell Turbine Blade

James P. Downs
Florida Turbine Technologies, Inc.
1701 Military Trail, Suite 110
Jupiter, FL 33458-7101
Phone: (561) 427-6250; Fax: (561) 427-6190
Email: jdowns@fttinc.com

DOE Project Manager: Robin Ames
Phone: (304) 285-0978
Email: Robin.Ames@netl.doe.gov

Contract Number: ER84668

Start Date: June 20, 2007
End Date: May 31, 2012

Fiscal Year (FY) 2012 Objectives

- Develop a detailed mechanical design concept that can be manufactured for test within a follow-up program.
- Identify materials best optimized to the Spar-Shell™ turbine blade for use in specific environments.
- Define cooling system features required to produce high thermal efficiency.
- Identify manufacturing and fabrication requirements.
- Evaluate benefits and costs of this system.

FY 2012 Accomplishments

- Florida Turbine Technologies, Inc., (FTT) is nearing completion of the detailed design of a rotating Spar-Shell™ turbine blade.
- The feasibility of the mechanical design, cooling and structural aspects of this design are supported by engineering calculations and analysis.
- Manufacture and assembly of the Spar-Shell™ blade has been verified with the construction of prototype models.

Introduction

Current gas turbine systems already operate at temperature and pressure levels that are sufficiently high to require the use of advanced materials and cooling of the turbine components. The use of cooling in the turbine, although permitting turbine components to operate within an environment of high temperature and pressure, causes a parasitic efficiency debit to the turbine subsystem and overall power plant. Technology advances within the turbine systems therefore represent an excelled avenue for improving the overall power plant efficiency. In particular, technologies that permit turbines to operate at increased temperatures and pressures are desired to achieve the specific performance goals. Advances of both the materials and cooling systems are clearly required to extend the envelope for improved performance and efficiency in the future systems.

To meet future power generation needs, FTT is developing an innovative design approach to provide highly durable turbine components that increase efficiency by requiring the lowest cooling flow possible. The proposed gas turbine rotating blade design is constructed of an internal structurally supporting member (spar) and a separate external covering (shell) to provide the aerodynamic envelope. The so-called Spar-Shell™ system enables the use of advanced, high temperature materials that are not available based on current design philosophies and manufacturing approaches. In addition to providing higher temperature capabilities, features of this system resolve another well-known technical barrier which causes current turbine components to fail by cracking due to thermally-induced stresses. This barrier limits the capabilities of today's turbine components, particularly at the interface between the main airfoil body and the platform/attachment structure. Further, this architecture facilitates the cooling system to be optimized to the smallest possible cooling flow required by enabling the use of practical and robust near wall cooling features while minimizing the plugging risk of systems such as those associated with effusion and other porous media schemes. With this program, FTT has laid out a comprehensive plan for the design and development of this concept. Further, FTT has the full support and backing of a primary original equipment manufacturer, namely Siemens Energy with the expressed commitment to evaluate the design within the Siemens design review process and to test development hardware in an engine to permit design verification and validation data to be acquired.

Approach

FTT has proposed the development of a rotating Spar-Shell™ turbine blade system to realize the

future turbine system goals of reduced cooling flow consumption and increased efficiency. Development of the proposed Spar-Shell™ turbine component system offers several advantages relative to the current state-of-the-art. To realize these goals, several objectives, as delineated in the following paragraphs, must be pursued.

FTT recognizes the limitations of current turbine material and cooling systems and has been actively investigating alternatives to resolve the major issues. As a result, development of the Spar-Shell™ system has progressed to the point where detailed analytical and empirical verification was needed as a prerequisite to verification of the design concept in a test engine. One example of such a component is described in U.S patent #7080971, "Cooled Turbine Spar Shell Blade Construction," by Wilson and Brown (Figure 1). Development of the Spar-Shell™ system has proceeded beyond the fundamental details described in this patent, namely with respect to shell loading and attachment. As shown, this design approach utilizes an internal spar which is surrounded by an external shell. This fabrication approach has several advantages relative to the current state-of-the-art monolithic cast structures. First, the internal spar represents the primary framework of this concept. Since the shell protects this member from the hot working fluid passing around the airfoil, it can be maintained at a relatively low temperature very near that of the coolant. The spar material can therefore be optimized for very high strength at a moderate temperature level. Second, since the shell is structurally isolated from the spar, its material can be selected on the basis of high temperature capability.

Thermally induced stresses are a primary driver and limiter of existing cooled turbine components. The Spar-Shell™ turbine blade construction serves to mitigate the associated effects on low cycle fatigue and thermal mechanical fatigue distress through both thermal and mechanical isolation of the spar and shell. Further, other desirable thermal attributes, such as the ability to support high temperature and heat flux, can be considered as primary drivers in the shell material selection.

Results

Design and analysis of the Spar-Shell™ technology have been performed to support the feasibility of the concept. From a cooling perspective, the Spar-Shell™ blade may take many possible forms. However, to improve the performance of the cooling system while reducing the amount of cooling flow requires that the efficiency of the internal convection cooling system be increased while film cooling benefits are reduced with the reduction of overall cooling flow. To this end, a conceptual cooling circuitry has been defined to provide the required heat transfer characteristics. In addition, structural analyses have been performed within finite element models to verify the basic structural and vibration characteristics. Results from these analyses support the feasibility of the design and indicate the need for continued research to refine and optimize the design.

During the course of this program, a prototype model of one possible representation of the Spar-Shell™ system was developed and constructed using a three-dimensional printing process. The geometry selected for this demonstration was based on a spar which supports

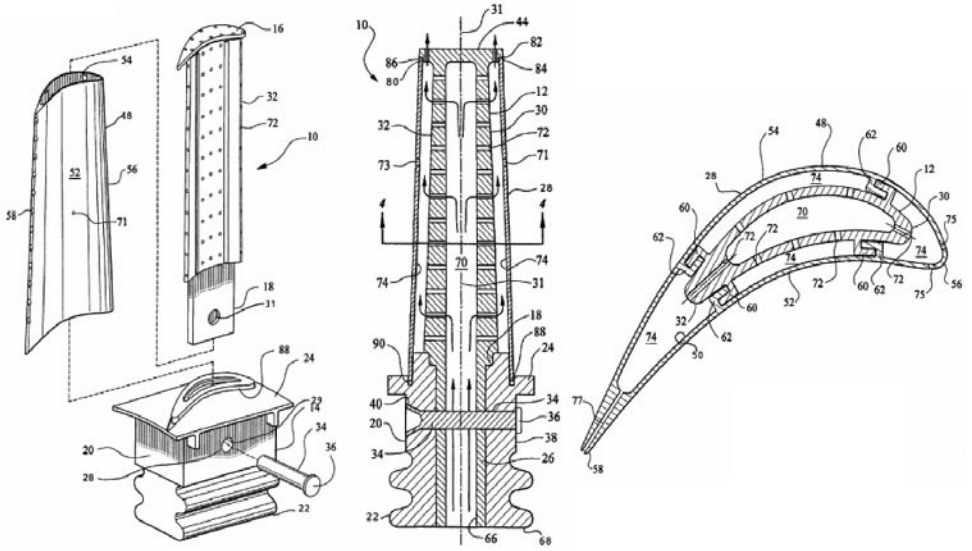

FIGURE 1. U.S. Patent #7080971, "Cooled Turbine Spar Shell Blade Construction"

the shell from the tip of the airfoil. In this construction, the spar must be inserted through the shell from the root of the airfoil with a mechanical attachment used to support the shell from the tip of the airfoil. For the purposes of this initial development, an airfoil having constant cross-sectional area was assumed, and wall thickness was set constant from the root of the airfoil to the tip. The entire system was modelled in the ProEngineer Computer-Aided-Design (CAD) system, and a physical model was constructed from this geometry definition (Figure 2).

Additional concept validation was performed under a complimentary U.S. Department of Energy program (DE-SC0003574) to demonstrate the manufacturing and fabrication feasibility. To facilitate this, actual spar and shell parts were produced in metal using the wire-slice electrical discharge machining method. Subsequent inspection and assembly of these parts verified the feasibility of the manufacturing and fabrication processes (Figure 3).

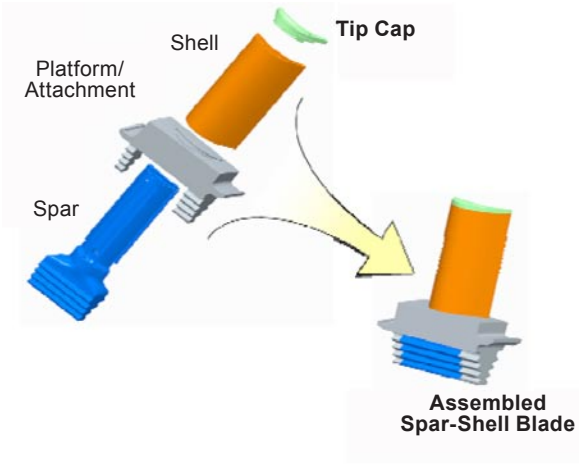

FIGURE 2. Spar-Shell blade prototype model

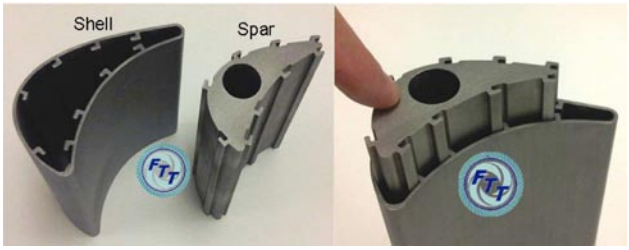

FIGURE 3. Spar-Shell™ blade manufacturing trial and fabrication feasibility

Conclusions and Future Directions

Results from conceptual design work performed during the initial Phase I Small Business Innovative Research (SBIR) grant supported continued development of the technology, and FTT was selected for a Phase II SBIR award to define a detailed design of a Spar-Shell™ turbine component. FTT has continued to work on this project through the support of a Phase II SBIR supplementary award. Work on the Phase II project has produced a viable design concept which continues to be developed within the detailed design phase.

Beyond the Phase II SBIR, development would continue to develop and optimize the design approach and to fabricate test articles based on a Phase III SBIR or other funding source. The development project plan culminates in a prototype demonstration of the technology. To facilitate this demonstration, an eventual test in an actual industrial gas turbine engine is recommended to:

i. Verify the feasibility of the spar-shell concept.
ii. Demonstrate thermally free platforms.
iii. Demonstrate thin-wall structures.
iv. Demonstrate increased manufacturing yields and lower cost with single crystal.
v. Evaluate advanced airfoil cooling.
vi. Evaluate advanced platform cooling.
vii. Test advanced materials.
viii. Evaluate advanced thermal barrier coatings.
ix. Evaluate fabricated blade and high speed machining capabilities.

Special Recognitions & Awards/Patents Issued

1. US8186953, "Multiple-Piece Turbine Blade," Keith D. Kimmel, May 29, 2012.

FY 2012 Publications/Presentations

1. James P. Downs, "Demonstration of Enabling Spar-Shell Cooling Technology in Gas Turbines," Presentation during University Turbine Systems Research (UTSR) workshop, October 27, 2011.

2. James P. Downs, "Perspectives on R&D Needs for Gas Turbine Power Generation," Presentation during University Turbine Systems Research (UTSR) workshop, October 26, 2011.

VI.A.2 Phase II SBIR: Advanced Cooling for IGCC Turbine Blades

Jill Klinger
Mikro Systems, Inc.
1180 Seminole Trail
Charlottesville, VA 22901
Phone: (434) 244-6480; Fax: (434) 244-6485
Email: klinger@mikrosystems.com

DOE Project Manager: Maria Reidpath
Phone: (304) 285-4140
Email: Maria.Reidpath@netl.doe.gov

Subcontractor:
Purdue University, West Lafayette, IN

Contract Number: SC0001359

Start Date: August 12, 2009
End Date: August 14, 2012

Fiscal Year (FY) 2012 Objectives

- Perform computational fluid dynamics (CFD) analysis on the most advanced TOMO^{SM} Lithographic Modeling (TOMO^{SM}) derived trailing edge (TE) coupons produced during FY 2011.
- Produce solid models that incorporate the results of the CFD and Global Inspection System (GIS) analysis, completed during FY 2011, for full size ceramic cores that include two TOMO^{SM} derived advanced TE geometries.
- Produce foundry ready ceramic cores that demonstrate the capability of TOMO^{SM} for advanced trailing edge designs for a Row 1 integrated gasification combined cycle blade (two designs).
- Conduct heat transfer testing of the metal cast Row 1 industrial gas turbine blades.

FY 2012 Accomplishments

- Purdue University conducted CFD analysis on the most advanced TOMO^{SM} derived TE coupon designs ("zigzag with turbulators" and "multi-mesh with hour-glass").
- Mikro Systems, Inc., completed solid models with advanced cooling geometries that enabled:
  - Siemens Energy, Inc., to perform CFD on the full-sized blades (part of the contribution-in-kind commitment from Siemens).
  - Mikro to produce TOMO^{SM} derived inserts that could be used in coordination with existing 8000H Mikro tooling.
- Mikro completed the TOMO^{SM} derived tooling inserts and has begun production of foundry ready ceramic cores.

Introduction

Turbine blade and vane survivability at higher operating temperatures is the key to improving turbine engine performance. Innovative cooling approaches are a critical enabling technology to meet this need. This project addressed two important aspects of the problem. First is the need to increase core manufacturing process capability (quality and reliability) to enable advanced cooling features to be incorporated in future turbines. Second is the need to rapidly and economically produce tools and prototype hardware whereby advanced designs can be empirically tested and optimized. Once these two aspects are realized, the design community is better enabled to test more radical cooling configurations through more complex, proven CFD analysis.

Approach

In order to improve heat transfer and lower cooling air requirements, the advanced blade designs will require more complex internal cooling passages that can be produced using current investment casting techniques. This is especially true when optimizing the cooling of the trailing edge region of the turbine blade where failures are a concern (both at metal casting and in the field). Mikro's approach to this problem has been to demonstrate that its patented TOMO^{SM} process could be used to manufacture advanced turbine blade trailing edge designs and incorporate these designs onto full-size foundry ready ceramic cores that provide improved internal cooling for IGCC turbine blades.

Purdue University applied CFD simulations to the trailing edge designs that were being produced by Mikro to model the heat transfer of the proposed trailing edge designs. Siemens Energy has developed a bench-top test to measure heat transfer empirically.

Additionally, National Energy Technology Laboratory-Regional University Alliance (NETL-RUA) has gained interest in testing the heat transfer performance of the FY 2011 coupons in both a low-

temperature test rig (University of Pittsburgh) as well as a high-temperature test rig (NETL, Morgantown).

Results

CFD Analysis

CFD simulations were used to study flow and heat transfer of the various cooling geometries. During FY 2012, Purdue University applied these simulations to two advanced geometries that were slight variations on the FY 2011 geometries. The results of the simulations for the two additional advanced designs (zigzag with turbulators and multi-mesh with hourglass) were compared to the simulations completed on the FY 2011 designs (plain zigzag and multi-mesh). These results are summarized in Figure 1. In the case of the zigzag, turbulators were added to the pressure and suction sides of the channel. This resulted in a larger temperature difference through the cooling channel (more heat transfer), and the turbulators caused the mass flow rate to be decreased (allowing the cooling air to reside in the channel longer). In the case of the multi-mesh, an hourglass profile was added to the shape of the cooling channel. The results indicated that this hourglass profile helped to eliminate some of the separation region that was seen on the original multi-mesh (better mixing), but the mass flow rate increased (causing the cooling air to move more quickly through the channel). The results of these simulations were used, in part, to optimize the designs being produced on the full-scale blade.

Bench Testing

Siemens Energy received the TE coupons produced during last year early on in FY 2012. The parts were mounted onto a fixture, where air was flowed through the cooling channels and then infrared images were taken of the external surface. Due to the limitations of the Siemens test rig, to date, there are still some unanswered questions about the results. Figure 2 demonstrates some of the problems in the experimental setup.

As an added program benefit, NETL-RUA has agreed to bench test the coupons in a low-temperature rig at the University of Pittsburg and then high-temperature rig at NETL-Morgantown. The coupons have been shipped to NETL-Pittsburgh for the low-temperature testing and then, if agreed to, the parts will be modified to fit into the high-temperature rig for testing. The results of these tests will help us better understand both the GIS testing as well as the CFD simulations.

Production 8000H Row 1 Ceramic Core

Mikro has completed the TOMO^{SM} derived insert that is being used in coordination with existing 8000H Row 1 ceramic core tooling. The modular tooling platform is being used to produce ceramic cores with two different advanced TE designs. The TE designs are adaptations of the geometries produced on the FY 2011 coupons (zigzag and multi-mesh) and are shown in Figure 3. The initial ceramic cores have been characterized using coordinate measuring machine (CMM) and are within foundry specifications for wax die

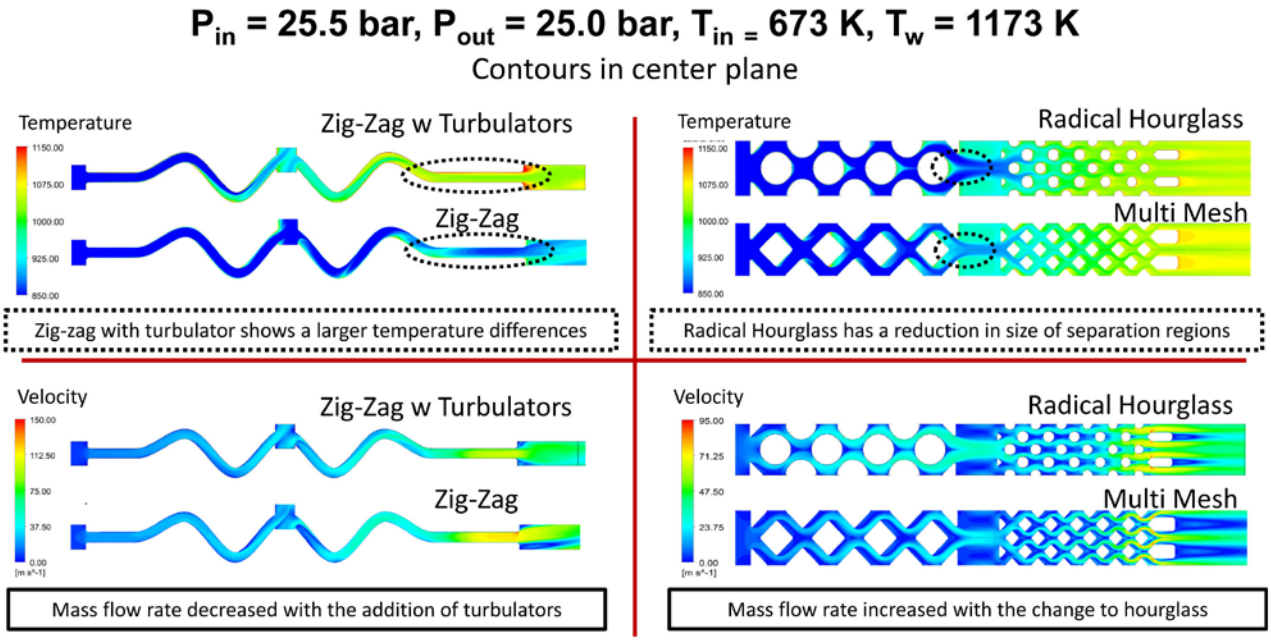

FIGURE 1. Results of CFD simulations for the two most advanced internal cooling geometries as compared to previous simulations

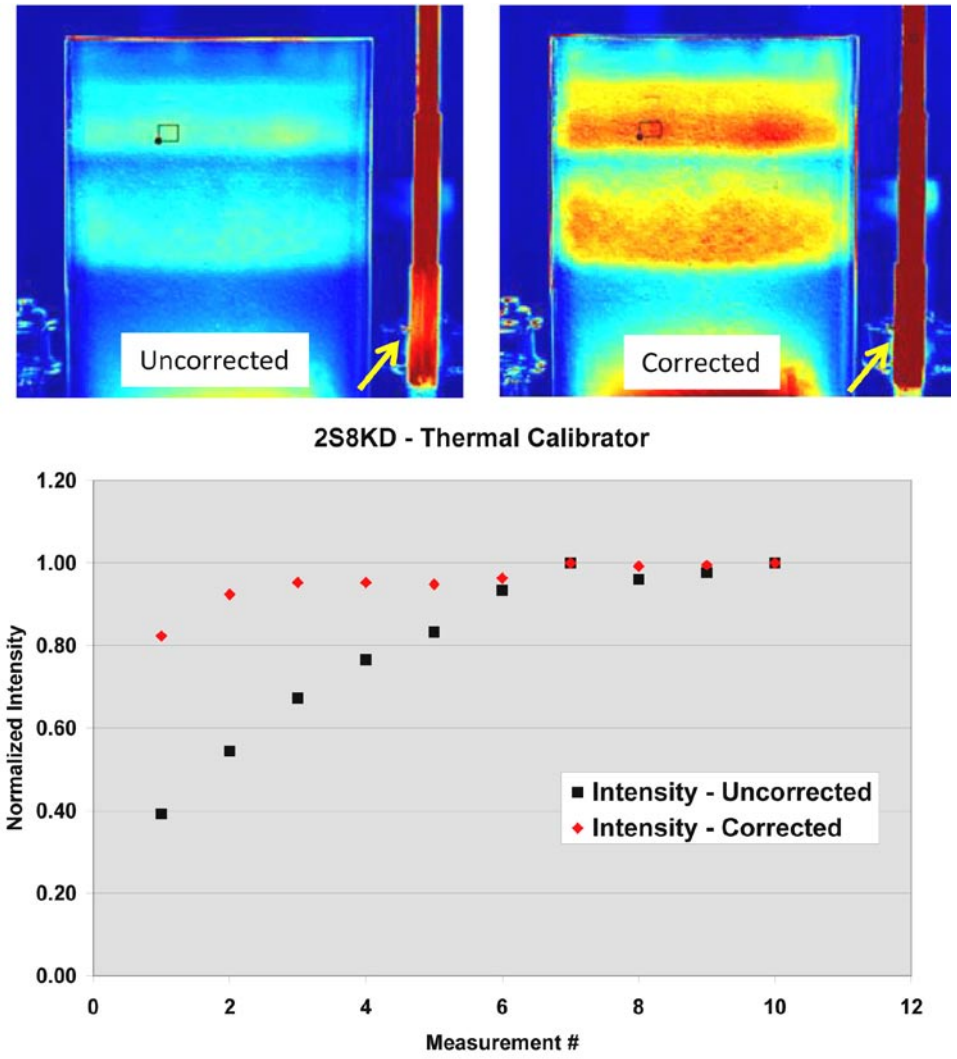

FIGURE 2. The GIS experimental results produced non-repeatable data. The variation in data was a function of how long the unit was running (thermal creep). The solution was to insert a thermal calibrator (hollow tube) into the measurement space to monitor the experimental conditions. The data was calibrated using this information.

FIGURE 3. Top: TOMO^{SM} derived tool insert (zigzag) in existing 8000H tooling; **Bottom-left**: Foundry-ready ceramic core with zigzag TE produced with TOMO^{SM} derived tooling; **Bottom-right**: Foundry-ready ceramic core with multi-mesh TE made with TOMO^{SM} derived tooling (multi-mesh tooling not shown for proprietary reasons).

fit (see CMM data in Figure 4). Mikro will be sending set-up pieces to the foundry (PCC Airfoils, LLC - Mentor, Ohio - Mentor) to verify these results.

Conclusions and Future Directions

The advantage of Mikro's TOMO^{SM} technology is not limited to the manufacturability of advanced designs for trailing edge cooling. The unique tooling approach allows designs to rapidly and cost-effectively fine-tune cooling geometries that can be tested in engine conditions. The approach developed during this Phase II contract has been recognized by industry leaders (both commercial and academic) as a powerful, and much needed, tool for pushing power generation technology in order to realize improved plant efficiency targets set by the U.S. Department of Energy.

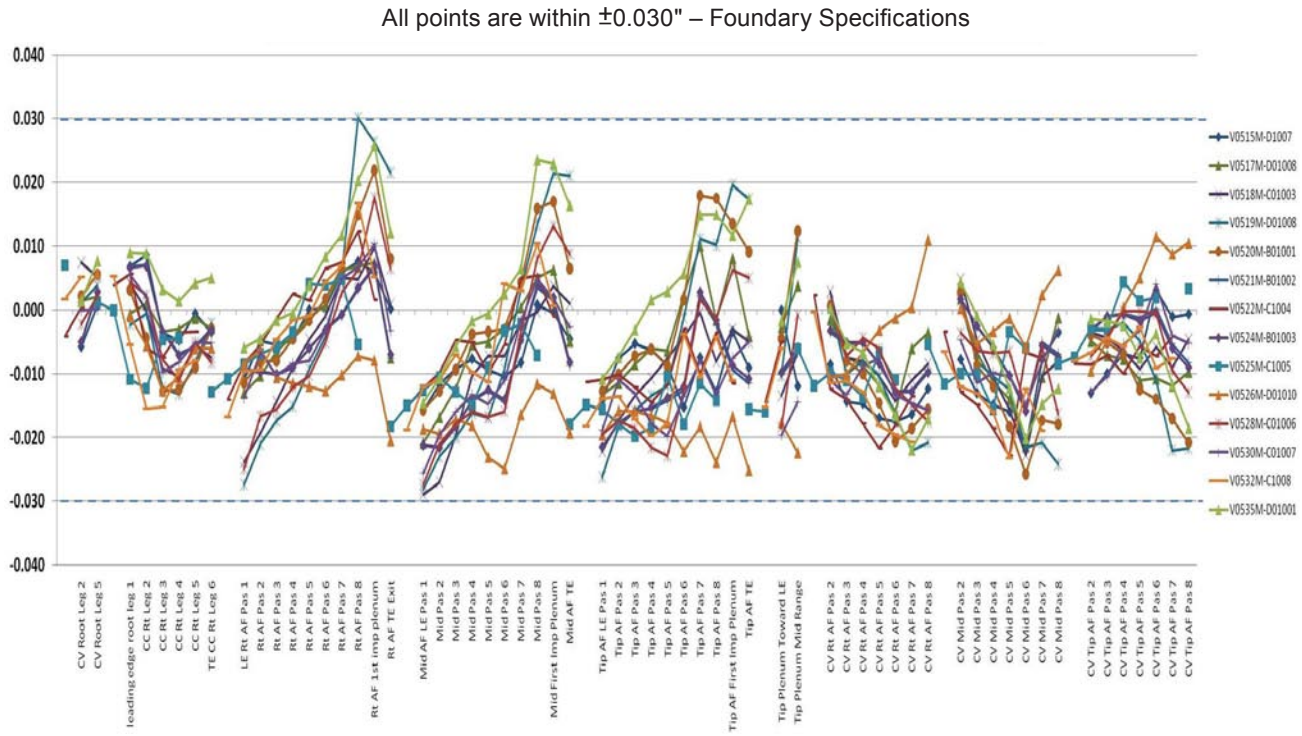

FIGURE 4. 8000H Row 1 ceramic core CMM data of the first 14 fired castings

The strong collaboration that has developed between Mikro, Purdue University, Siemens Energy and now NETL-RUA has supported the work being done in FY 2012, and Mikro predicts that the program will exceed the expectations of the initial goals as well as pave the way to future innovations in blade cooling and new turbine technology.

FY 2012 Publications/Presentations

1. Paper: Liu, J., Weaver, A., Lee, C.S., Shih, T.I-P., Klinger, J., Ames, R., and Dennis, R.A., "Flow and Heat Transfer in a Triple-Impingement Configuration for Trailing-Edge Cooling," ASME Paper GT-2012-70075, June 2012, Copenhagen, Denmark.

2. Talk: "Verification and Validation Issues in CFD Analysis of Turbine Cooling," 2011 University Turbine Systems Research Workshop, National Energy Technology Laboratory, Department of Energy, **Ohio State University,** October 25–27, 2011.

VI. SMALL BUSINESS INNOVATION RESEARCH

B. Manufacturing

VI.B.1 Advanced Laser Machining Techniques for Cooling Holes in Gas Turbines

Dr. John Steinbeck (Primary Contact),
Dr. Frederick Lauten
Physical Sciences Inc.
20 New England Business Center
Andover, MA 01810
Phone: (978) 738-8148; Fax: (978) 689-3232
Email: steinbeck@psicorp.com

DOE Project Manager: Patcharin Burke
Phone: (412) 386-7378
Email: Patcharin.Burke@netl.doe.gov

Contract Number: SC0003400

Start Date: December 7, 2009
End Date: November 30, 2012

Fiscal Year (FY) 2012 Objectives

- Successfully use water guided laser drilling to produce arrays of 0.020" cooling holes in Haynes 230 alloy with air flow variations less than ±2%. We will drill 0.020" hole arrays in ten 0.026" Haynes 230 alloy sheet at rates exceeding 1 hole/3 seconds and show that standard deviation of the air flow measured through arrays is less than 2% of the average air flow.
- Demonstrate that water guided laser drilling does not induce damage on the walls of holes; drill using water guided laser drilling. Completion verification method: We will use optical and electron microscopy to evaluate the surfaces of 0.020" holes drilled in 0.026" Haynes 230 alloy using water guided laser drilling. We will show that the surfaces contain no microcracks and that the composition of the material on the walls of the holes is the same as the bulk of the Haynes 230 alloy sheet.

FY 2012 Accomplishments

- Successfully demonstrated water guided laser drilling of holes between 0.10" and 0.030" using a YLS-3000 fiber laser system.
- Successfully drilled holes using water guided laser drilling in Inconel 718, 304 Stainless Steel and 0.026" Haynes alloy.

Introduction

The generation of a boundary layer to protect gas turbine components from hot combustion gases is critical to enable combustion gas temperatures to approach or exceed the melting temperature of the alloys used in gas turbine systems. The air used to create the boundary layer is supplied through cooling holes drilled into individual turbine components. Current methods for drilling cooling holes balance the cost of drilling with the air flow performance of the cooling holes. These methods currently produce cooling holes with air flow variations of ±10% so that more than the minimum number of cooling holes must be drilled into components to ensure that the gas turbine can meet its operational specifications. Physical Sciences, Inc., (PSI) is developing a reliable, low cost method for drilling the tens of thousands of holes needed in gas turbine systems with air flow variations ±2%. The improved flow performance of cooling holes drilled using PSI's water guided laser drilling technique will enable air previously needed for boundary layer cooling to be redirected through the flow path to increase the fuel efficiency of turbine systems.

PSI's water-guided laser drilling technology can be integrated onto existing laser machining platforms to enable rapid transition to gas turbine manufacturing. The method is applicable to all high temperature alloys used in gas turbine systems. Hole size may be adjusted by changing the size of the water stream for percussion (stationary) drilling or by adjusting the path of the beam for trepanning (circumscribed drilling).

Approach

Water guided laser drilling uses a high pressure stream of water as an optical waveguide to direct a high energy laser beam to the work piece to be drilled. A schematic is shown in Figure 1. The diameter of the water stream defines the diameter of the hole as all of the laser energy will be contained within the stream. The diameter of the water stream can be maintained for distances exceeding 100 mm, making the water guided laser drilling technique less sensitive to the absolute position of the work piece from the laser cutting head compared to laser drilling techniques that use lenses to focus the drilling laser. The high pressure water stream will be more effective than high pressure gas for purging debris

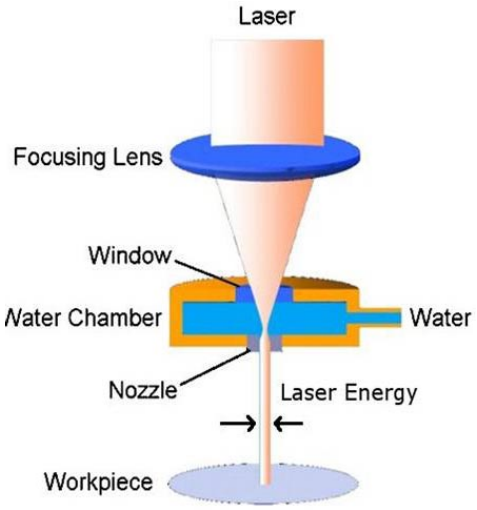

FIGURE 1. Schematic of the water guided laser drilling system. The module comprises the water chamber, window and nozzle assembly.

from the hole. In addition, water guided laser drilling will impede over drilling when drilling cooling holes in blades and vanes where the surface being drilled will be close to the backside of the part.

Results

During the second year of the Phase II project, PSI has focused on refining the water guided laser drilling process to improve the reliability of the hardware to deliver consistent drilling results for the thousands of holes that will be required in gas turbine combustor components. The second generation water guided laser drilling system shown in Figure 2 was used to perform drilling trials. We successfully demonstrated water guided laser drilling processes using both continuous wave and pulsed laser operation on stainless steel and Inconel 718 as shown in Figure 3 using water pressure of 2,000 psi at rates exceeding 1 hole/sec. Holes with diameters ranging from 0.010" to 0.030" were drilled in 0.050" Inconel 718 alloy, 304 Stainless Steel and 0.026" Haynes alloy at rates exceeding 3 sec/hole at normal incidence. The entry and exit sides of the first holes show excess material about their periphery compared to drilling processes using similar power density pulsed lasers and gas purging. Reduction of recast debris on the drilled hole is the primary goal for improving the predictability of cooling air flow through the cooling holes in a gas turbine system. Reduction of the recast can eliminate post drilling deburring processes that have been identified as an important contributor to air flow variation.

The primary difficulty being encountered is the lifetime of the sapphire orifice used to form the water stream. The number of holes that can be drilled with an orifice has been inconsistent and cannot be directly attributed to optical alignment or laser output power. We are currently investigating cavitation within the water

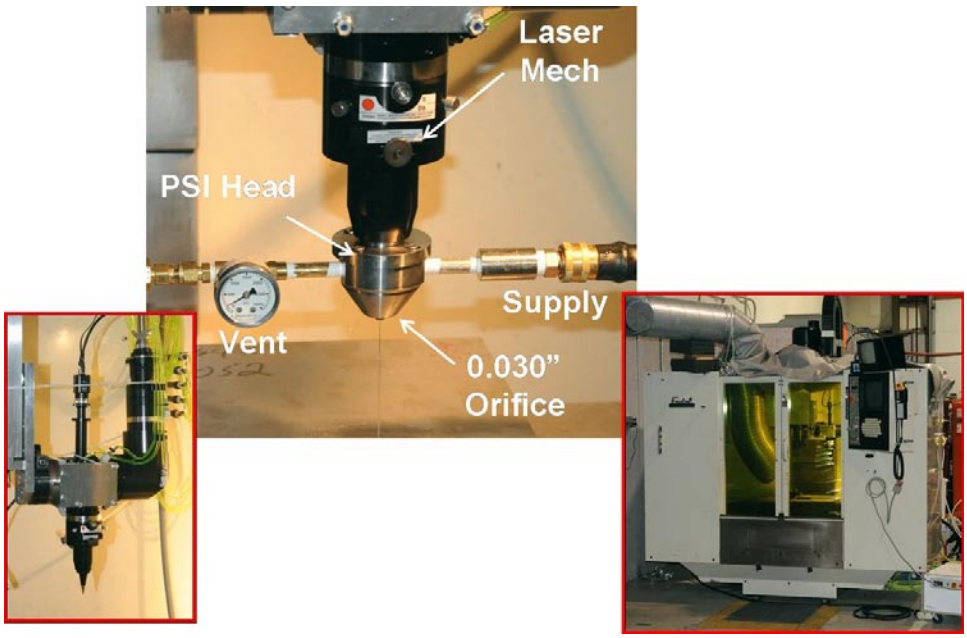

FIGURE 2. Second generation water guided laser drilling system built at PSI. The water guided laser drilling head is mounted on a Fadal 15 XCT machining system. Water is supplied to the head by a separate pumping and degassing system.

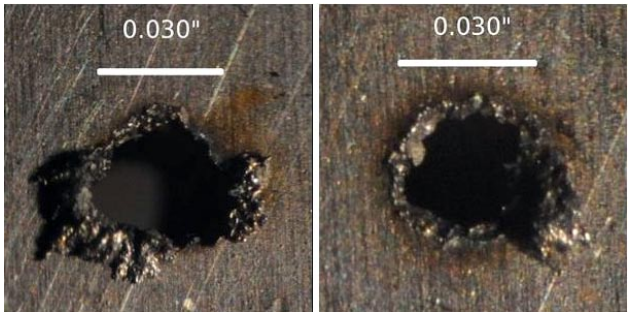

FIGURE 3. Successful hole drilling through 0.050" Inconel 718. (Left) Drilled using continuous wave exposure at 2,000 W for 3 sec. (Right) Drilled using a train of 1,000 W 10 ms pulses for 10 sec. Further process development is underway.

system as a bubble forming mechanism that causes random deflections of the drilling laser beam to cause orifice failure.

Conclusions and Future Directions

PSI continues to develop the water-guided laser drilling process by improving the hardware design. The second generation water guided laser drilling head developed during Phase II improves the coupling between the laser and the water stream and enables water pressures up to 3,000 psi to be used to clear drilling debris. Both the improved design and higher pressure operation will increase the rate at which holes can be drilled as well as expand the process envelope to reduce the debris remaining in and around the drilled holes.

The Phase II includes tasks to develop plans to transition the water guided laser drilling process to a commercial laser drilling system. We are currently engaged with a laser drilling system manufacturer to determine the best course for implementing water guided laser drilling on a drilling system used for the production of gas turbine components. System integration and water guided laser drilling trials on turbine components will be performed during a Phase III program.

VI. SMALL BUSINESS INNOVATION RESEARCH

C. Thermal Barrier Coatings

VI.C.1 Low Thermal Conductivity and Erosion Resistant Thermal Barrier Coatings Developed for High Temperature Applications

[1]Amarendra K. Rai (Primary Contact),
[1]Rabi S. Bhattacharya, [2]Dongming Zhu,
[3]Douglas E. Wolfe
[1]UES, Inc.
4401 Dayton-Xenia Road
Dayton, OH 45432
Phone: (937) 426-6900 ext. 127; Fax: (937) 426-5718
Email: arai@ues.com
[2]NASA John H. Glenn Research Center,
Cleveland, OH 44135
[3]Penn State University (PSU)
Applied Research Laboratory
P.O. Box 30
State College, PA 16804

DOE Project Manager: Patcharin Burke
Phone: (412) 386-7378
Email: Patcharin.Burke@netl.doe.gov

Contract Number: SC0004356

Start Date: August 15, 2011
End Date: August 14, 2013

Fiscal Year (FY) 2012 Objectives

The overall technical objective of this U.S. Department of Energy Small Business Technology Transfer (STTR) program is to develop novel thermal barrier coating (TBC) architectures that can provide high thermal insulation (low thermal conductivity) and high erosion resistance at higher turbine engine temperatures without sacrificing strain tolerance.

The specific goals of the first part of the Phase II STTR project (FY 2012) are:

1. Examine high temperature sintering resistance of TBCs fabricated with selected materials and multilayered coating architectures.
2. Examine high temperature erosion resistance of TBCs fabricated with selected materials and multilayered coating architectures.
3. Based on the results (from 1-2 above) fabricate additional TBCs and evaluate their relevant characteristics for further optimization.
4. Initiate development of low cost atmospheric pressure plasma spray (APS) process for the development of high temperature TBCs.

FY 2012 Accomplishments

1. Demonstrated better high temperature sintering characteristics of selected TBC materials and multilayered coating architectures compared to standard yttria stabilized zirconia (YSZ).
2. Trend in the erosion rate of the high temperature annealed TBCs was found to be similar to as-deposited TBCs. Even for annealed samples, multilayered TBC architecture was able to considerably reduce the erosion rate of gadolinium zirconate: $Gd_2Zr_2O_7$ (GZO).
3. Based on the data obtained in this program, additional TBCs were fabricated for further optimization.
4. Work was initiated to develop cost effective APS process for high temperature a TBCs.

Introduction

The durability of the gas turbine is primarily limited by the thermal stability of the metallic components operating in extreme environments such as high gas temperature and pressure. High gas temperature could lead to deleterious effects on the metallurgy and chemistry of the components, whereas high gas pressure together with particle impact could lead to erosive damage making the engine components less durable. Currently, the durability of the turbine engine components is achieved by the use of thermal barrier coating (TBC) consisting of yttria stabilized (6-8 wt%) zirconia (std. YSZ) and/or by internal/external cooling.

Higher operating temperature for the gas turbine engines used in integrated gasification combined cycle (IGCC) power plants is needed for enhanced efficiency, lower emission and increased performance goal. The current state-of-the-art TBCs (std. YSZ) are not adequate to provide the needed protection for the metallic components of the turbine engine operating at higher TBC surface temperature (>1,300ºC) with increased reliability. In the Phase I part of the STTR project, innovative TBC coating architectures of appropriate materials were developed for higher temperature applications, and the feasibility of their desired characteristics was demonstrated. It is expected that such TBCs would facilitate the operation of gas turbine

engines to operate at higher temperatures for enhanced efficiency and lower emission.

Approach

In this STTR program, two different thermal barrier coating materials, namely GZO and low k YSZ (std. YSZ doped with 1 mole% of Gd_2O_3 and 1 mole% Yb_2O_3) were selected for higher temperature applications. The overall technical approach of this program is focused on microstructural modifications/alternative design architecture for further enhancement of the relevant characteristics (reduction in thermal conductivity and erosion rate) of the selected pyrochlore oxide and doped YSZ (low k YSZ) TBC materials. The Phase I technical approach involved fabrication utilizing electron beam physical vapor deposition (EB PVD) technique, characterization, and performance evaluation (thermal conductivity, erosion resistance) of the different TBC architectures. Phase I results demonstrated the feasibility of the proposed approach.

Based on the Phase I results, the theme of the Phase II work is to modify the microstructure and compositions of the TBC architectures developed in Phase I for optimal thermal conductivity and erosion resistance at elevated temperatures. Phase II work also involves the development of low cost TBCs for higher temperature applications through the utilization of APS process.

In the Phase I program, the high temperature sintering characteristics of the fabricated TBC architectures of selected materials were not examined. Also in the Phase I work, erosion rate of TBCs was determined only in the as-deposited (as-fabricated) conditions. Since this program involves the development of TBCs for higher temperature applications, it is essential to examine the performance of the fabricated TBCs at higher temperatures. Conventionally, sintering characteristics of the TBC coatings are determined either by isothermal or by furnace cyclic tests. In such tests there is no deliberate thermal gradient between the TBC surface and the metallic substrate. In actual fielded operation, the TBC coated turbine engine parts, such as blades, are internally water cooled. Thus there is a thermal gradient between the high surface temperature of the TBC surface and the water cooled metallic super alloy.

In the thermal conductivity test conducted at NASA Glenn Research Center, the TBC surface temperature was maintained at 1,316°C for 20 hours through a constant heat flux from a 3.0 kW CO_2 laser while the back side of the metallic super alloy substrate was kept at 900°C-1,000°C by air cooling. Such experimental arrangement created a thermal gradient between the top TBC surface and the bottom super metallic alloy somewhat similar to the actual applications. Thus the thermal conductivity measurement under the said conditions would be very realistic for sintering study compared to isothermal aging test and could be used for design, development and life prediction for engine applications. In the Phase II project, the sintering characteristics of the TBCs fabricated in the Phase I project and subjected to the thermal conductivity test were examined. Also in the Phase II project, erosion rates of selected TBCs were determined after annealing the TBCs at higher temperatures. Based on the sintering and erosion rate data together with the Phase I results, TBCs with adequate microstructure and composition were fabricated for optimal thermal conductivity and erosion resistance.

Results

Surface and X-sectional scanning electron microscopy (X-SEM) as well as X-ray diffraction (XRD) techniques were used to determine the sintering characteristics of monolayered (std. YSZ, low k YSZ, and GZO) and multilayered low k YSZ-GZO TBCs after sintering for 20 hrs at 1316°C. Surface SEM analyses indicated that except on the GZO surface, surface cracks (commonly known as mud cracks) were observed on the surface of other TBCs. The cracks in std. YSZ were relatively wider than that in low k YSZ and multilayered low k YSZ-GZO). Thus it appears that rare earth oxide doping (low k YSZ) and multilayered design (low k YSZ-GZO) helps in lowering the extent of cracking. This observation reveals that by manipulating doping level and multilayered coating architecture/composition, the extent of sintering induced cracking can be mitigated. It should be emphasized that coating porosity also plays a role in sintering. Highly porous TBCs are expected to sinter more slowly compared to denser TBC.

Figure 1 (a,b,c,d) represent X-SEM micrographs, respectively, of monolayered std. YSZ, monolayered low k YSZ, monolayered GZO, and multilayered low k YSZ-GZO TBCs at various magnifications after sintering for 20 hrs. at 1,316°C. Relatively wider and longer cracks reaching to the TBC/thermally grown oxide at the bond coat/TBC) interface was observed in std. YSZ (Figure 1a). A considerable amount of column sintering close to the surface and inside the coating was also observed. In low k YSZ most cracks were shorter and terminated within the coatings (Figure 1b). Only a few long cracks were observed, and they did not appear to be as wide as those observed in the std. YSZ. Some sintering of the columns at the coating surface and inside the coating was observed. No cracks were observed in GZO (Figure 1c). Although some sintering of the closely spaced columns

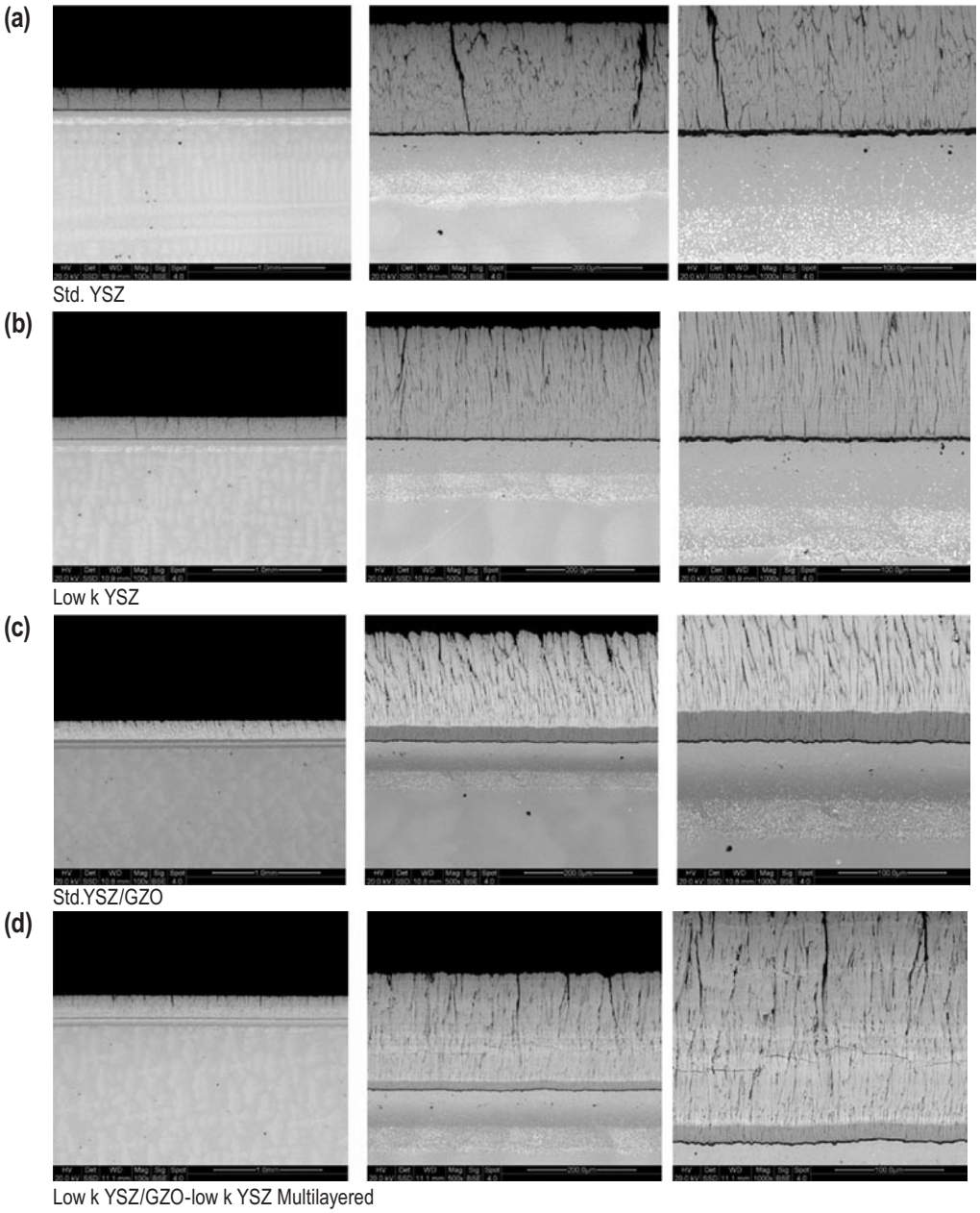

FIGURE 1. X-SEM micrographs of sintered (20 hours at 1,316°C) samples (a) Std. YSZ (b) Low k YSZ (c) GZO (d) Low k YSZ-GZO multilayer. A thin layer of std. YSZ and low k YSZ was deposited prior to GZO (Figure 1c) and multilayered TBC (Figure 1d).

was observed in GZO, relatively more inter-columnar gaps (porosity) were preserved compared to std. YSZ and low k YSZ. In the sintered multilayered low k YSZ-GZO sample, only shorter cracks that appeared to be terminated within the coating were observed (Figure 1d). Sintering of the columns close to the surface and inside the coating was observed. Non-continuous horizontal cracks were also observed at certain depths which could indicate deflection of vertical cracks and enhanced toughness in the multilayered TBC. Horizontal cracks could also be due to relatively less porous (denser) localized microstructures. Similar to the surface SEM observations, X-SEM observations also indicate that the rare earth oxide doped YSZ (low k YSZ) and multilayer (low k YSZ-GZO) TBCs are very effective in mitigating crack-propagation. Absence of cracks in GZO could be related to its intrinsically low sintering rate (coating chemistry/composition) and the presence of relatively higher porosity. These observations also suggest that the sintering induced cracking can be further minimized by manipulating the doping level, multilayered coating architecture/composition and porosity.

XRD technique did not reveal any obvious phase change in the sintered (20 hrs/1,316°C) TBCs (std. YSZ, low k YSZ and GZO); the XRD peak positions remained similar before and after sintering with no additional peaks observed after sintering. Although such observation suggests that the coatings were phase stable, it should be noted that due to the close peak position of the various phases (monoclinic, tetragonal, and cubic) for std. YSZ combined with the preferred orientation, it can be difficult to determine small volume changes. More work employing Raman analyses may be needed to further confirm coating phase stability. In the case of the multilayered low k YSZ-GZO sample, peak shifting was observed between 72°C-74°C. This observation could be due to strain in the coating and/or due to interfacial diffusion at the low k YSZ-GZO interface. Additional work is needed to clarify this observation.

The aforementioned work in conjunction with the Phase I results clearly validates the selected TBC materials and their coating architectures for higher temperature applications. It also points out the direction of future work which involves manipulation of doping level, multilayered coating composition and porosity to obtain optimal TBCs for higher temperature applications. Based on these findings, in the Phase II project additional TBC systems were fabricated with highly textured and porous coating microstructure. As an example, surface microstructure of low k YSZ fabricated in Phase I (Figure 2a) and low k YSZ fabricated in Phase II (Figure 2b) was compared. It is clear that the column tips of low k YSZ fabricated in Phase II are highly textured (faceted), and there is increased intercolumnar porosity (marked with arrows). The performance of the fabricated TBCs will be evaluated in terms of thermal conductivity and erosion resistance.

In the Phase I project, room temperature erosion resistance of the fabricated TBCs was determined. Among the fabricated TBCs, room temperature erosion rate of monolayered GZO was highest, whereas the erosion rates of monolayered low k YSZ and std. YSZ were found to be the lowest. In Phase I work, it was demonstrated that the erosion rate of GZO could be reduced considerably by utilizing multilayered (low k YSZ-GZO) architecture. The multilayered low k YSZ-GZO exhibited an intermediate erosion rate between that of GZO and low k YSZ.

In the Phase II project, erosion rates of monolayered std. YSZ, monolayered GZO and multilayered low k YSZ-GZO were isothermally annealed at 1,100°C for 20 hours. To protect the integrity of the metal substrate, higher temperature and/or longer time was not used. Trend in mass loss (erosion rate) of the annealed samples was found to be similar to that of the as-deposited samples. Annealed samples exhibited higher mass loss

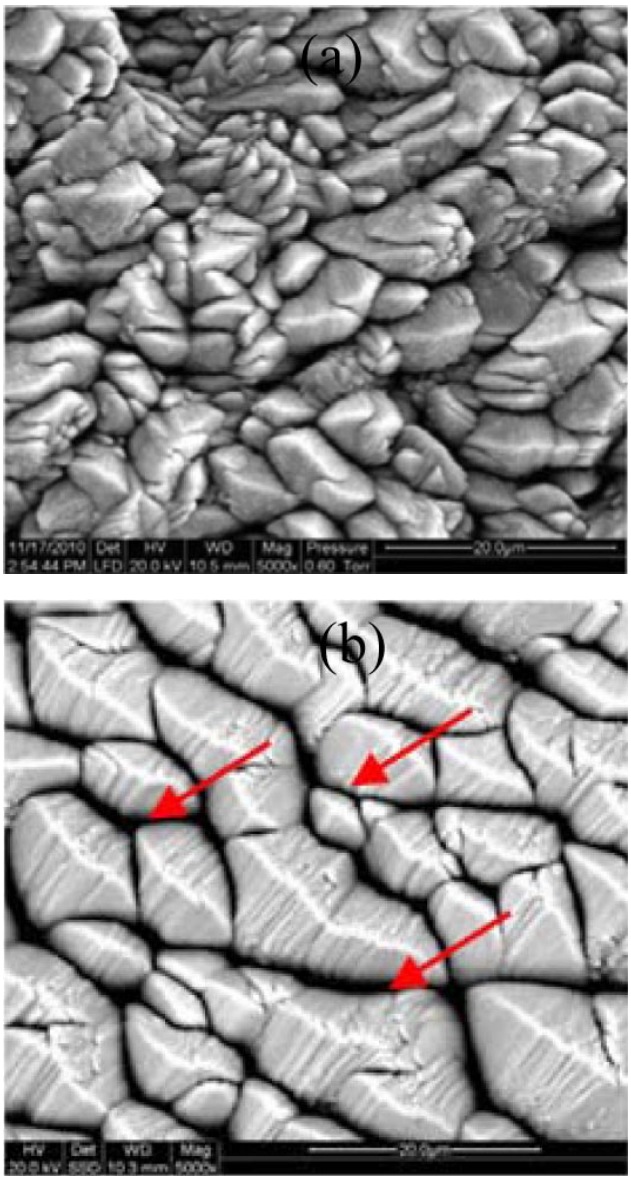

FIGURE 2. Microstructure comparison of monolayered low k YSZ (a) denser microstructure fabricated in Phase I and (b) more porous microstructure fabricated in Phase II. Some of the abundant inter-columnar pores are marked by arrows.

(erosion rate) compared to as-deposited samples. This is likely due to sintering induced densification of the TBCs. A considerable reduction in mass loss of annealed GZO was accomplished by incorporating the multilayered architecture design structure.

Conclusions

1. Higher temperature (1,316°C) sintering behavior of the TBCs fabricated for higher temperature applications was examined and compared with that of the currently used TBC (std. YSZ). It was

demonstrated that all the fabricated TBCs have better high temperature sintering resistance than the std. YSZ.

2. Erosion rates of the annealed TBCs were also determined and compared with that of the as-deposited (un-annealed) TBCs. It was found that the trend in the erosion rate of the annealed TBCs remained similar to that of the as-deposited TBCs. Even for the annealed samples, the multilayered TBC was able to considerably reduce the erosion rate of GZO. This observation demonstrated that the multilayered TBC maintains its erosion resistance capability even at elevated temperature.
3. High porosity TBCs were fabricated to further enhance their high temperature sintering resistance and reduce thermal conductivity.

Future Directions

1. Performance (thermal conductivity, sintering characteristics, erosion rate) evaluation of the TBCs fabricated with varied doping level, coating composition/design and porosity.
2. Further fabrication/characterization of TBCs (process optimization).
3. Development of cost effective atmospheric plasma spray process for higher temperature TBCs.

FY 2012 Publications/Presentations

1. In this report period a paper entitled, "Multilayered Thermal Barrier Coating Architectures for High Temperature Applications," by D.E. Wolfe, M.P. Schmitt, D. Zhu, A.K. Rai, and R.S. Bhattacharya was presented and accepted at 36th International Conference and Exposition on Advanced Ceramics and Composites, January 22–27, 2012, Daytona Beach, Florida.

2. The following website also reflects some of the results of this project http://www.netl.doe.gov/publications/factsheets/project/SC0004356.pdf.

VII. Acronyms and Abbreviations

-	Minus
#	Number
$	Dollar(s)
%	Percent
&	And
@	At
~	Approximately
“	Inches, minutes
+	Plus
<	Less than
=	Equals
>	Greater than
≈	Approximately equal
≤	Less than or equal to
≥	Greater than or equal to
°	Degree
°C	Degree(s) Celsius
°F	Degree(s) Fahrenheit
0D	Zero dimensional
1D	One dimensional
2D	Two dimensional
3D	Three dimensional
A	Area
ab initio	From the beginning
Adv.	Advanced
AIAA	American Institute of Aeronautics and Astronautics
Al	Aluminum
APMT	Advanced powder metallurgy technology
APS	Air plasma spray, atmospheric plasma spray
Ar	Argon
AR	Aspect ratio
ARMS	Armstrong Building
ARRA	American Recovery and Reinvestment Act
ASME	American Society of Mechanical Engineers
ASTM	American Society for Testing and Materials
at%	Atomic%
Atm	atmospheres
ATP	Advanced Turbine Program
ATS	Advanced Turbine Systems
AVS	American Vacuum Society
B	Boron
b/dj	Jet height-to-diameter ratio
BC	Bond Coat
BOP	balance of plant
BR	Blowing ratio
Btu	British thermal units
Btu/hr	British thermal units per hour
BYU	Brigham Young University
C	Carbon
C_2H_4	Ethylene
C_2H_6	Ethane
Ca	Calcium
CA	California
CAD	Computer aided design
CARS	Coherent anti-Stokes Raman scattering
CC	Combined cycle
CCD	Charge coupled device
CCS	Carbon capture and cequestration
Ceram.	Ceramics
CES	Clean Energy Systems
CFD	Computational fluid dynamics
CFI	Coatings for Industry
CFM56	A nozzle guide vane
CFX	A general-purpose computational fluid dynamics software suite
CH_4	Methane
cm	Centimeter(s)
cm^2	Square centimeter(s)
CMAS	Calcium magnesium alumina silicate
CMC	Ceramic matrix composite
CMM	Coordinate measuring machine
CMOS	Complementary metal oxide Cemiconductor
CMSX	A nickel-based alloy
CMSX-4®	Commercially available Y- and La-doped nickel alloy
CNC	Computer numerical control
Co	Cobalt
CO	Carbon monoxide
CO	Colorado
Co.	Company

CO_2	Carbon Dioxide
Coat.	Coating
COR	Coefficient of restitution
Cr	Chromium
CRC	Chemical Rubber Company
CrV	Chromium vanadium
CSP	Computational singular perturbation
CT	Connecticut
CTSR	Center for Thermal Spray Research
CVD	Chemical vapor deposition
dBA	Decibel A-weighting
DBC	Diffusion barrier coating
deg	Degree
DES	Detached-eddy simulation
DFT	Density functional theory
DLN	Dry low-NOx
DoE	Design-of-experiment
DOE	U.S. Department of Energy
DOE FE	U.S. Department of Energy Office of Fossil Energy
DQMOM	Direct quadrature method of moments
DR	Density ratio
Dr.	Doctor
DS	Directionally-solidified
DSC	Differential scanning calorimetry
DVC	Dense Vertically Cracked
e.g.	*Exempli gratia*: for example
EB PVD, EB-PVD	Electron beam physical vapor deposition
EBC	Environmental barrier coating
ECBM	Enhanced coalbed methane
ECP	Ex-situ coating property
ECY768	A cobalt-based alloy
ed.	Editor
EDAX	Energy dispersive X-ray analyses
EDS	Energy dispersive spectroscopy
eds.	Editors
EERC	Energy & Environmental Research Center
EEVP	Energy elastoviscoplasticity
EFG	Entrained-flow gasifier
EGR	Exhaust gas recirculation
Eng.	Engineering
ENO	Essentially non-oscillatory
EOR	Enhanced oil recovery
EPD	Electrophoretic deposition
EPMA	Electron Microprobe Analysis, electron probe microanalysis
et al.	*Et Alii*: and others
etc.	*Et cetera*: and so on
EVP	Elastoviscoplasticity
FCT	Furnace cycle test
Fe	Iron
FE	Fossil Energy (Office of the U.S. Department of Energy)
FFT	Fast Fourier transform
FIB	Focused ion beam
FL	Florida
FLUENT	A computational fluid dynamics code
FR	Flow regimes
ft	Feet
ft^3	Cubic feet
FTF	Flame transfer function
FTT	Florida Turbine Technologies
FWHM	Full width at half maximum
FY	Fiscal Year
GA	Georgia
Gd	Gadolinium
GdO_3	Gadolinia
GDZ	Gadolinia doped zirconia
GE	General Electric
GE E^3	General Electric Energy Efficient Engine program
Gen	Generation
GFY	Government Fiscal Year
GHG	Greenhouse gas
GIM	General instability model
GIS	Global Inspection System
GPa	Gigapascal(s)
gpm	Gallons per minute
GRC	Glenn Research Center
GRI	Gas Research Institute
GSH	Gadolinia stabilized hafnia
GT	Gas turbine
GTMC	Gas turbine model combustor
GZD	Gadolinium zirconate: $Gd_2Zr_2O_7$
GZO	Gadolinium zirconate
h	Heat transfer coefficient
h	Hour(s)
H	Height

H	Hydrogen
H/D	Height-to-diameter ratio
H_2	Diatomic hydrogen
H_2O	Water
Hf	Hafnium
HfO_2	Hafnium oxide, hafnia
HGIR	Hot Gas Ingestion Rig
HHC	High Hydrogen Content
HHF	High hydrogen fuel
HHV	Higher heating value
HP	Horsepower
HP	High pressure
HPC	High performance computing
HPC	High pressure compressor
HP-LD	High purity, low density
HPLFR	High pressure laminar flow reactor
HPT	High-pressure turbine
hr, hrs	Hour(s)
HTST	Harmonic transition state
HVOF	High-velocity oxy-fuel
HX	Heat exchanger
Hz	Hertz
i.e.	*id est*: that is
IA	Iowa
ICEPAG	International Colloquium on Environmentally Preferred Advanced Power Generation
ICP-OE	inductively coupled plasma-optical emission
IEC	Integrated Engineers and Contractors Co.
IEVP	Integration elastoviscoplasticity
IGCC	Integrated gasification combined cycle
IGT	Industrial gas turbine
IGTI	International Gas Turbine Institute
IMECE	International Mechanical Engineering Congress & Exposition
in	Inch
IN	Indiana
Inc.	Incorporated
Inst.	Institute
Int.	International
IP	Intermediate pressure
IPB	Inter-pass boundary
IPT	Intermediate Pressure Turbine
ISABE	International Society for Airbreathing Engines
ISEM	Innovative Science Engineering and Management
ITB	Interturbine burner
J.	Journal
JCPDS	Joint Committee on Powder Diffraction Standards
JSAE	Society of Automotive Engineers of Japan
K	Kelvin
K	Potassium
kg	Kilogram
kHz	Kilohertz
kW	Kilowatt
l	Length
La	Lanthanum
LA	Louisiana
lb	Pound(s)
LBNL	Lawrence Berkeley National Laboratory
LCF	Low cycle fatigue
LDA	Local density approximation
LDV	Laser Doppler velocimetry
LE, TE	Leading, trailing edge of the blade
LES	Large-eddy simulation
L_f	Length of flame
LLC	Limited liability company
LMP	Larson Miller Parameter
LP	Low pressure
LPPS	Low pressure plasma spray
LPT	Low-pressure turbine
LRIP	Low rate initial production
LSB	Low swirl burner
LSI	low-swirl injector
LSU	Louisiana State University
m	Meter(s)
m/s	Meters per second
MA	Massachusetts
Mat.	Materials
Mater.	Materials
MBA	Master of Business Administration
MCrAlY	M-chromium-aluminum-yttrium alloy, where M is one of several different metals
MD	Molecular dynamics
Meas.	Measurement
MFR	Mass flow ratio
mg	Milligram(s)
Mg	Magnesium

mil	Millimeter(s)
min	Minute(s)
ml	Milliliter(s)
ml/min	Milliliter(s) per minute
mm	Millimeter(s)
mol	Mole(s)
mol%	Mole percent
MPa	Megapascal
MW	Megawatt
mW	Milliwatt(s)
MW	Megawatt(s)
MW_e	Megawatt(s) electric
MW_t	Megawatt(s) thermal
N	Nitrogen
N_2	Diatomic nitrogen
N5	A nickel-based alloy
Na	Sodium
NASA	National Aeronautics and Space Administration
Nb	Niobium
ND	North Dakota
NETL	National Energy Technology Laboratory
NG	Natural gas
NGCC	Natural gas combined cycle
NGV	Nozzle guide vane
Ni	Nickel
NIST	National Institute of Standards and Technology
NJ	New Jersey
nm	Nanometer(s)
No.	Number
NO_x	Oxides of nitrogen
NSEMC	Near surface embedded micro-channel
Nu	Nusselt number
NY	New York
O	Oxygen
O_2	Diatomic oxygen
OEM	Original equipment manufacturer
O-F	Oxy-fuel
O-FRH	Oxy-fuel reheat
OFT	Oxy-fuel turbine
OFT-900	Oxy-fuel turbine based upon Siemens SGT-900
OH	Ohio
OH	Hydroxyl radical
OH-PLIF	Planar laser induced image velocimetry of hydroxyl radicals
OPPDIF	A computer simulation module
OR	Oregon
ORNL	Oak Ridge National Laboratory
OSU	Ohio State University
P	Pressure
p.	Page
P.O.	Post office
PA	Photo-acoustic
PA	Pennsylvania
PCC	Precision Castparts Corp. and PCC Airfoils, LLC, a division of Precision Castparts Corp.
PCI	Precision Combustion, Inc.
PDF	Probability density function
Penn State	Pennsylvania State University
PERC	Polyfunctional Emissions Reduction Catalyst
PI	Principal investigator
PIV	Particle image Velocimetry
PLC	Programmable logical controller
PLIF	Planar laser induced image velocimetry
PMP	Project Management Plan
PMT	Photomultiplier tube
POD	Proper Orthogonal Decomposition
pp.	Pages
ppm	Part(s) per million
ppma	Part(s) per million by atoms
ppmv	Part(s) per million by volume
ppmvd	Part(s) per million by volume diluted
PPQ	Pre-production qualification
Proc.	Proceedings
PSI	Physical Sciences, Inc.
psi	Pounds per square inch
psia	Pounds per square inch absolute
Psig	Pounds per square inch gauge
PSLS	
PSP	Pressure sensitive paints
PST	Praxair Surface Technologies
PSU	Pennsylvania State University
Pt	Platinum
Pts	Points
R&D	Research and development
RANS	Reynolds-averaged Navier-Stokes

RCF	Rapid compression facility
RCL®	Rich catalytic lean-burn
RCM	Rapid compression machine
Re	Reynolds number
Re	Rhenium
René N5	A nickel-based alloy
RH	reheat combustor or reheater
RI	Rayleigh Indices
RJIC	reacting jet in crossflow
RMS	Root mean square
RPM	Revolutions per minute
RSM	Reynolds stress model
RUA	Regional University Alliance
S	Sulphur
s	Second(s)
SBIR	Small Business Innovation Research
scfm	Standard cubic feet per minute
Sci.	Science
SCR	Selective Catalytic Reduction
sec	Second(s)
SEI	Siemens Energy, Inc
SEM	Scanning electron microscope, scanning electron microscopy
SGT	Siemens Gas Turbine
Si	Silicon
SiC	Silicon carbon
Soc.	Society
SOFC	Solid oxide fuel cell
SOTA	State-of-the-art
SPPS	Solution precursor plasma spray
SRZ	Secondary reaction zones
SS	Stainless steel
SST	Shear stress transport
St	Strouhal number
STP	Standard temperature and pressure
STTR	Small Business Technology Transfer Program
T	Temperature
Ta	Tantalum
TADF	Turbine Accelerated Deposition Facility
TAMU	Texas A&M University
TBC	Thermal barrier coating
TBC/BC	Thermal barrier coating-bond coat
TC	Top coat
TCLA	Turbine cooling and leakage air
TE	Trailing edge
TEM	Transmission electron microscope, transmission electron microscopy
TGO	Thermally grown oxide
Ti	Titanium
TIT	Turbine inlet temperature
TLC	Thermochromic liquid crystal
TMF	Thermal mechanical fatigue
TMS	The Minerals, Metals and Materials Society
TN	Tennessee
TOMO^{SM}	TOMO^{SM}-Lithographic Molding
TPC	Topologically closed packed
TPFL	Turbomachinery Performance and Flow Research Laboratory
T_{sur}	Surface Temperature
TTU	Tennessee Technological University
TuRFR	Turbine Reacting Flow Rig (OSU)
TX	Texas
U.S.	United States
UCI	University of California, Irvine
UM	University of Michigan
UND	University of North Dakota
URANS	Unsteady Reynolds averaged Navier-Stokes
URETI	University Research, Engineering, and Technology Institute
USA	United States of America
UT	University of Texas
UT	Utah
UTS	Ultimate tensile strength
UTSR	University Turbine Systems Research
V	Vanadium
V	Vector
V	Volt(s)
VA	Virginia
VASP	Vienna Ab-initio Simulation Package software
VKI	VonKarmann Institute Belgium
VLES	Very large eddy simulation
VOC	Volatile organic compound
vs.	Versus
VT	Virginia Polytechnic Institute
W	Tungsten
W	Watt(s)
W	West

W	Width
wt%	Weight percent
WV	West Virginia
WVU	West Virginia University
x, X	Times
XRD	X-ray diffraction
X-SEM	X-Scanning electron microscopy
Y	Yttrium
Y_2O_3	Yttria
Yb	Ytterbium
YSH	Yttria stabilized hafnia
YSHZ	Yttria stabilized hafnia-zirconia, ZrO_2-HfO_2
YSZ	Yttria stabilized zirconia
Zr	Zirconium
ZrO_2	Zirconia
β	Beta, second
Δ	Change, difference
λ	Conductivity
ρ	Density
Σ	Sigma, sum
Δ	Change (delta)
ϕ	Equivalence ratio
μm	Micrometer(s), micron(s)

VIII. Primary Contact Index

IX. Organization Index

X. Contract Number Index

National Energy Technology Laboratory

1450 Queen Avenue SW
Albany, OR 97321-2198
541-967-5892

2175 University Avenue South
Suite 201
Fairbanks, AK 99709
907-452-2559

3610 Collins Ferry Road
P.O. Box 880
Morgantown, WV 26507-0880
304-285-4764

626 Cochrans Mill Road
P.O. Box 10940
Pittsburgh, PA 15236-0940
412-386-4687

13131 Dairy Ashford, Suite 225
Sugar Land, TX 77478
281-494-2516

Richard A. Dennis
Technology Manager, Turbines
304-285-4515
richard.dennis@netl.doe.gov

Visit the NETL website at:
www.netl.doe.gov

Customer Service:
1-800-553-7681

DOE/NETL-2012/1587 October 2012

U.S. DEPARTMENT OF ENERGY | NETL